



Dergimize 4 dilde (Türkçe Tr, İngilizce En, Rusça Ru ve Ukraynaca Ua) yazı kabul etmekteyiz. Türkçe, Rusça ve Ukraynaca yazılarda İngilizce özet yazılması zorunludur.

ULUSLARARASI 3B YAZICI TEKNOLOJİLERİ VE DİJİTAL ENDÜSTRİ dergisi,

IJ3DPTDI, Endüstri 4.0 – dijital endüstri teknolojileri, 3B yazıcı teknolojileri, katmanlı-eklemeli imalat teknolojileri ve uygulamaları yani mühendislik, bilim, teknoloji gibi tüm disiplinlerle ilgili araştırmaların sonuçlarını yaymak için açık, hakemli, disiplinlerarası, uluslararası, bilimsel, akademik, online bir dergidir. IJ3DPTDI, Mühendislik, Teknoloji ve Bilimin Endüstri 4.0 daki uygulamaları, tüm araştırmaları, gözden geçirme makalelerini, kısa bilgi paylaşımlarını ve önemli ilerlemeleri sunan teknik notları online yayınlamak için yazarları davet eder.

Endüstri 4.0, Dijital Endüstri, 3B Yazıcılar üzerine tüm bilimsel mühendislik araştırma ve teknoloji alanı konuları;

- **3B baskı için tıbbi uygulamalar;** dokuların ve organların biyografik baskıları, 3B vaskülarize organların oluşturulmasında karşılaşılan zorluklar, özelleştirilmiş implantlar ve protezler, düşük maliyetli protez parçaları, cerrahi hazırlık için anatomik modeller, sentetik cilt, kafatası değişimi, tıbbi donatımı, kemik, özel üretilen sensörler, kişiselleştirilmiş ilaç dozu, benzersiz dozaj şekilleri, kompleks ilaç salınım profilleri v.d.
- **3B yazıcı uygulama alanları;** tıbbi ve diş hekimliği uygulamaları, diş hekimliği uygulamaları ve materyalleri, yumuşak robotik sistemleri, robot tutucu sistemler, bina uygulamaları, kalıp / kalıp uygulamaları, mimarlık uygulamaları, model uygulamaları, hızlı prototip uygulamaları, görsel sanat uygulamaları, tekstil uygulamaları, dijital fabrikalar, mimari model uygulamaları ve malzemeleri, endüstriyel uygulamaları ve malzemeler, gıda uygulamaları ve malzemeleri, sanatsal uygulamalar ve malzemeler, tarama yöntemleri ve modelleme v.d.
- Endüstri 4.0 ve dijital sanayi; büyük veri, yapay zeka, dijital yaşam döngüsü, sensör motorları, artırılmış gerçeklik, görselleştirme, sistem simülasyonu, kablosuz iletişim, BİT güvenlik, dijital iş, blok zinciri, veri Güvenliği, özerk robotlar, sistem entegrasyonu, nesnelerin interneti (IoTs), siber güvenlik, bulut bilişim, dijital fabrika v.d.
- **3B yazıcı tasarım, modelleme ve analiz;** 3D yazıcı tasarımı, ekstruder tasarımı, 3B baskı için ürün geliştirme, seramik sistemleri tasarımı, gıda sistemleri tasarımı, elektronik bileşenleri, mekanik parçalar, standart bileşenler v.d.
- **3B yazıcı malzeme ve mekanik özellikleri;** polimer malzemeler, esnek malzemeler, biyo malzemeler, metalik malzemeler, toz malzeme üretim yöntemleri, ağaç malzemeler, kompozit malzemeler v.d.
- **3B yazıcı program kontrol teknolojileri;** kontrol programları, tasarım programları, 3D tarama teknolojileri, DMLS teknolojileri, SLA teknolojileri, SLS teknolojileri, FDM teknolojileri, dijital üretim teknolojileri, diğer 3B yazıcı teknolojileri v.d.

IJ3DPTDI, online yayınlanan bir dergidir ve yılda 3 defa yayınlanır.

1.periyot Ocak-Nisan 2.periyot Mayıs-Ağustos 3.periyot Eylül-Aralık

ISSN 2602-3350

web-site : http://dergipark.gov.tr/ij3dptdi
e-mail : korayozsoy32@gmail.com

Print Turkey Org

Dear author,

Our Journal accepts articles in 4 languages (Turkish Tr, English En, Russian Ru and Ukrainian Ua). Articles in Turkish, Russian and Ukrainian must have an abstract in English.

International Journal of 3D Printing Technologies and Digital Industry

IJ3DPTDI, is an open access peer-reviewed, interdisciplinary international platform for disseminating results of relevant research related to all the disciplines of engineering, science, technology etc on Industry 4.0 - digital industry technologies, 3D printer technologies, additive manufacturing technologies and applications. IJ3DPTDI, invites all research, review articles, short communications & technical notes that describe significant advances research in the areas of Engineering, Technology, Science on Industry 4.0, Digital Industry, 3D Printers, additive manufacturing;

All scientific engineering research & technology area on Industry 4.0, Digital Industry and 3D printers;

Medical applications for 3D printing; bioprinting tissues and organs, challenges in building 3D vascularized organs, customized implants and prostheses, low—cost prosthetic parts, anatomical models for surgical preparation, synthetic skin, cranium replacement, medical equipment, bone, tailor-made sensors, personalized drug dosing, unique dosage forms, complex drug-release profiles ect.

Aplication fields; medical and dental applications, dental practices and materials, soft robotics systems, robot gripper systems, building applications, die/mold applications, architecture applications, models applications, rapid prototype applications, visual arts applications, textile applications, digital factories, architectural-model applications and materials, industrial applications and materials, food applications and materials, artistic practices and materials, scanning methods and modeling ect.

Digital industry; big data, artificial intelligence, digital life cycles, sensors actuators, augmented reality, visualization, system simulation, wireless communication, ICT security, digital business, block chain, data safety, autonomous robots, system integration, internet of things (IT's), cyber security, cloud computing, digital factory ect.

Design, modelling and analysis; 3D printer design, extruder design, product development, ceramic systems design, food systems design, table system design, electronics components, mechanic components, standard components ect.

Mechanical properties of filaments; polymer materials, flexible materials, bio materials, metallic materials, wood materials, composite materials ect.

Program – control technologies; control programs, design programs, 3D scanning technologies, DMLS technologies, SLA technologies, SLS technologies, FDM technologies, Digital production technologies, other 3D printer technologies ect.

IJ3DPTDI, Its publication frequency is 3 issues per year.

1.Period January-April
2.period May-August
3.period September-December
ISSN 2602-3350

Web-site: http://dergipark.gov.tr/ij3dptdi korayozsoy32@gmail.com



Уважаемый автор,

наш журнал принимает статьи на 4-х языках (турецком, английском, русском и украинском). Статьи на турецком, русском и украинском языках должны сопровождаться аннотацией на английском языке.

Международный журнал технологий 3D-печати и цифровой индустрии

IJ3DPTDI — это рецензируемое издание с открытым доступом, междисциплинарная международная платформа для обмена результатами исследований по инженерноконструкторским разработкам, теоретическим исследованиям, усовершенствованию технологий Индустрии 4.0, в том числе — технологий цифровой промышленности, 3D-печати, аддитивного производства и разработки приложений. **İJ3DPTDİ** принимает исследовательские статьи, обзорные статьи, краткие сообщения и технические заметки, которые описывают значимые результаты исследований в области машиностроения, технологии, теоретической основы индустрии 4.0, цифровой промышленности, 3D печати, производства многокомпонентных материалов.

Тематика журнала включает все научно-технические исследования и обзор технологий Индустрии 4.0, цифровой промышленности и 3D печати. Медицинские технологии 3D-печати: биопринтинг — воспроизведение объемных моделей тканей и органов, создание трехмерных васкуляризированных органов, индивидуализированных имплантатов и протезов, синтетической кожи, костей, замены частей черепа; удешевление технологии протезирования, разработка анатомических моделей для подготовки хирургов, тестовых хирургических операций, медицинского оборудования; изготовление датчиков с заданным набором характеристик, создание уникальных лекарственных препаратов с индивидуальными дозировками, сложных многокомпонентных лекарственных средств.

Области применения: материалы и оборудование для медицины и стоматологии, роботизированные системы на основе биологических прототипов, роботизированные захватные устройства, строительные материалы, пресс-формы, модели и прототипы в архитектуре, моделирование реальных объектов, прототипирование, сфера визуального искусства, текстильная промышленность, цифровые заводы, приложения и материалы для архитектурного моделирования, промышленные образцы и материалы, создание пищевых продуктов, технологии художественной обработки материалов, методы моделирования и сканирования и т.п.

Цифровая индустрия: большие данные, искусственный интеллект, жизненный цикл цифровых технологий, приводные механизмы датчиков, расширенная реальность, визуализация, моделирование систем, беспроводная связь, ИТ-безопасность, электронная коммерция, блокчейн технологии, безопасность данных, автономные роботы, системная интеграция, интернет вещей, кибербезопасность, облачные вычисления, цифровое производство.

Дизайн, моделирование и анализ: моделирование для 3D печати, экструдера; разработка разнообразных продуктов, проектирование систем керамического производства, усовершенствование технологии производства пищевых продуктов, проектирование предметов мебели, электронных компонентов, механических деталей, стандартных компонентов и т.п.

Механические свойства нитей: полимерные материалы, гибкие материалы, биоматериалы, изделия из металла и древесины, композиционные материалы.

Технологии управления приложениями: контрольные программы, проектные программы, технологии 3D-сканирования, технологии DMLS, SLA, SLS, FDM, цифровые технологии производства, другие технологии 3D-печати и т.п.Периодичность выхода журнала – 3 раза в год:

- 1-й выпуск январь-апрель;
- 2-й выпуск май-август;
- 3-й выпуск сентябрь-декабрь.

ISSN 2602-3350

Сайт журнала: http://dergipark.gov.tr/ij3dptdi
Электронная почта: korayozsoy32@gmail.com

Print Turkey Org

Шановний авторе,

наш журнал приймає статті на 4-х мовах (турецькою, англійською, російською та українською). Статті турецькою, російською та українською мовою повинні супроводжуватися анотацією англійською мовою.

Міжнародний журнал технологій 3D-друку і цифрової індустрії

IJ3DPTDI — це рецензоване видання з відкритим доступом, міждисциплінарна міжнародна платформа для обміну результатами досліджень з інженерно-конструкторських розробок, теоретичних досліджень, удосконалення технологій Індустрії 4.0, в тому числі — технологій цифрової промисловості, 3D-друку, адитивного виробництва і розробки додатків. **İJ3DPTDİ** приймає дослідні статті, оглядові статті, короткі повідомлення і технічні записки, які містять значущі результати досліджень в галузі машинобудування, технології, теоретичній основі індустрії 4.0, цифровій промисловості, 3D друку, виробництва багатокомпонентних матеріалів.

Тематика журналу охоплює всі науково-технічні дослідження та огляд технологій Індустрії 4.0, цифрової промисловості і 3D друку.

Медичні технології ЗD-друку: біопрінтінг — відтворення об'ємних моделей тканин і органів, створення тривимірних васкуляризованих органів, індивідуалізованих імплантатів і протезів, синтетичної шкіри, кісток, заміни частин черепа; здешевлення технології протезування, розроблення анатомічних моделей для підготовки хірургів, тестових хірургічних операцій, медичного обладнання; виготовлення датчиків із заданим набором характеристик, створення унікальних лікарських препаратів із індивідуальними дозуваннями; складних багатокомпонентних лікарських засобів.

Сфери застосування: матеріали та обладнання для медицини і стоматології, роботизовані системи на основі біологічних прототипів, роботизовані захватні пристрої, будівельні матеріали, прес-форми, моделі і прототипи в архітектурі, моделювання реальних об'єктів, прототипування, сфера візуального мистецтва, текстильна промисловість, цифрові заводи, додатки та матеріали для архітектурного моделювання, промислові зразки і матеріали, створення харчових продуктів, технології художньої обробки матеріалів, методи моделювання та сканування і т.п.

Цифрова індустрія: великі дані, штучний інтелект, життєвий цикл цифрових технологій, приводні механізми датчиків, розширена реальність, візуалізація, моделювання систем, бездротовий зв'язок, ІТ-безпека, електронна комерція, блокчейн технології, безпека даних, автономні роботи, системна інтеграція, інтернет речей , кібербезпека, хмарні обчислення, цифрове виробництво.

Дизайн, моделювання і аналіз: моделювання для 3D друку, екструдера; розробка різноманітних продуктів, проектування систем керамічного виробництва, удосконалення технології виробництва харчових продуктів, проектування предметів меблів, електронних компонентів, механічних деталей, стандартних компонентів і т.п.

Механічні властивості ниток: полімерні матеріали, гнучкі матеріали, біоматеріали, вироби з металу і деревини, композиційні матеріали.

Технології управління додатками: контрольні програми, проєктні програми, технології 3D-сканування, технології DMLS, SLA, SLS, FDM, цифрові технології виробництва, інші технології 3D-друку і т.п.

Періодичність виходу журналу – 3 рази на рік:

1-й випуск – січень-квітень;

2-й випуск – травень-серпень;

3-й випуск – вересень-грудень.

ISSN 2602-3350

Web-site: http://dergipark.gov.tr/ij3dptdi korayozsoy32@gmail.com



ULUSLARARASI 3B YAZICI TEKNOLOJİLERİ VE DİJİTAL ENDÜSTRİ **DERGISI**

Sayı: 2 Yıl: 2025 Cilt:9

INTERNATIONAL JOURNAL OF 3D PRINTING TECHNOLOGIES AND DIGITAL **INDUSTRY**

Volume: 9 Number: 2 Year: 2025

ISSN: 2602-3350

Yazıların tüm bilimsel sorumluluğu yazar(lar)a aittir. Editör, yardımcı editör ve yayıncı dergide yayınlanan yazılar için herhangi bir sorumluluk kabul etmez. Bu dergi, aşağıda listelenen veri tabanları tarafından taranmaktadır. All the scientific responsibilities of the manuscripts belong to the authors (s). The editor, assistant editor and publisher accept no responsibility for the articles published in the journal. The Journal is indexed by the following abstracting and indexing databases.

TR Dizin, Google Scholar, ResearchBib, Index Copernicus, Asos indeks









http://dergipark.gov.tr/ij3dptdi



Uluslararası 3B Yazıcı Teknolojileri ve Dijital Endüstri Dergisi / International Journal of 3D Printing Technologies and Digital Industry

Vol: 9, No:2 (2025) Cilt: 9, Sayı:2 (2025)

Editörler ve Kurullar / Editors and Boards

Yayın Kurulu Başkanı / Publication Board Manager

Dr. Kerim ÇETİNKAYA, Antalya BELEK Üniversitesi, Sanat ve Tasarım Fakültesi, TÜRKİYE

Baş Editörler / Editor(s)-in-Chief

Dr. Kerim ÇETİNKAYA, Antalya BELEK Üniversitesi, Sanat ve Tasarım Fakültesi, TÜRKİYE

Dr. Koray ÖZSOY, Isparta Uygulamalı Bilimler Üniversitesi, Isparta OSB MYO, Makine ve Metal Teknolojileri Bölümü, TÜRKİYE

Editörler Kurulu / Editorial Board

Dr. Burhan DUMAN, Isparta Uygulamalı Bilimler Üniversitesi, Teknoloji Fakültesi, Bilgisayar Mühendisliği Bölümü, TÜRKİYE

Dr. Ahu ÇELEBİ, Celal Bayar Üniversitesi, Mühendislik Fakültesi, Malzeme Mühendisliği Bölümü, TÜRKİYE

Dr. Hatice EVLEN, Karabük Üniversitesi, Teknoloji Fakültesi, Endüstriyel Tasarım Mühendisliği Bölümü, TÜRKİYE

Dr. Murat Aydın, Karabük Üniversitesi, Teknoloji Fakültesi, Endüstriyel Tasarım Mühendisliği Bölümü, TÜRKİYE

Dr. Hanane ZERMANE, Batna 2 Üniversitesi, Endüstri Mühendisliği Bölümü, CEZAYİR

Dr. Serhii Yevseiev, Simon Kuznets Kharkiv Ulusal Ekonomi Üniversitesi, Siber Güvenlik ve Bilgi Teknolojileri Bölümü, UKRAYNA

Dr. Pınar DEMİRCİOĞLU, Aydın Adnan Menderes Üniversitesi, Mühendislik Fakültesi, Makine Mühendisliği Bölümü, TÜRKİYE

Dr. Bekir AKSOY, Isparta Uygulamalı Bilimler Üniversitesi, Teknoloji Fakültesi, Mekatronik Mühendisliği Bölümü, TÜRKİYE

Dr. İshak ERTUĞRUL, Muş Alparslan Üniversitesi, Teknik Bilimler MYO, Mekatronik Programı, TÜRKİYE

Dr. Levent AYDIN, Kocaeli Üniversitesi, Sağlık Hizmetleri MYO, Sağlık Bakım Hizmetleri Bölümü, TÜRKİYE

Dr. Kıyas KAYAALP, Isparta Uygulamalı Bilimler Üniversitesi, Teknoloji Fakültesi, Bilgisayar Mühendisliği Bölümü, TÜRKİYE

Dr. İbrahim KARAAĞAÇ, İmalat Mühendisliği, Teknoloji Fakültesi, Gazi Üniversitesi, TÜRKİYE



Dr. Yasin HAMARAT, Biyoteknoloji, Kaunas University Of Technology, LİTVANYA

Dr. Binnur SAĞBAŞ, Yıldız Teknik Üniversitesi, Makine Fakültesi, Makine Mühendisliği Bölümü, TÜRKİYE

Dr. Heshham A. Hegazi, German University, Department of Design and Production Engineering, CAIRO

Mizanpaj Editörü/ Layout Editor

Mehmet YÜCEL, Isparta Uygulamalı Bilimler Üniversitesi, Teknoloji Fakültesi, Mekatronik Mühendisliği Bölümü, TÜRKİYE

Arda PAZARCIKCI, Isparta Uygulamalı Bilimler Üniversitesi, Teknoloji Fakültesi, Mekatronik Mühendisliği Bölümü, TÜRKİYE

Sema ÇAYIR, Isparta Uygulamalı Bilimler Üniversitesi, Teknoloji Fakültesi, Mekatronik Mühendisliği Bölümü, TÜRKİYE

Danışma Kurulu / Advisory Board

- Dr. M. Cengiz KAYACAN, SÜLEYMAN DEMİREL ÜNİVERSİTESİ, TR
- Dr. N. Nnamdi EKERE, WOLVERHAMPTON UNIVERSITY, UK
- Dr. Hüseyin Rıza BÖRKLÜ, GAZİ ÜNİVERSİTESİ, TR
- Dr. Cem SİNANOĞLU, ERCİYES ÜNİVERSİTESİ, TR
- Dr. Mustafa BOZDEMİR KIRIKKALE ÜNİVERSİTESİ, TR
- Dr. Savaş DİLİBAL, İSTANBUL GEDİK ÜNİVERSİTESİ, TR
- Dr. Cem Bülent ÜSTÜNDAĞ, YILDIZ TEKNİK ÜNİVERSİTESİ, TR
- Dr. Ahmet CAN, NECMETTİN ERBAKAN ÜNİVERSİTESİ, TR
- Dr. Fuat KARTAL, KASTAMONU ÜNİVERSİTESİ, TR
- Dr. İhsan TOKTAŞ, YILDIRIM BEYAZIT ÜNİVERSİTESİ, TR
- Dr. Okan ORAL, AKDENİZ ÜNİVERSİTESİ, TR
- Dr. Barış Berat BULDUM, MERSİN ÜNİVERSİTESİ, TR
- Dr. Serap ÇELEN, EGE ÜNİVERSİTESİ, TR
- Dr. Mustafa Aydın, KÜTAHYA DUMLUPINAR ÜNİVERSİTESİ, TR
- Dr. Serkan BÜRKEN, OSTİM TEKNİK ÜNİVERSİTESİ, TR
- Dr. Samsun M. BAŞARICI, AYDIN ADNAN MENDERES ÜNİVERSİTESİ, TR
- Dr. İsmail BÖĞREKCİ, AYDIN ADNAN MENDERES ÜNİVERSİTESİ, TR

ISSN 2602-3350



Vol:9, No:2 (2025)

Cilt:9, Sayı:2 (2025)

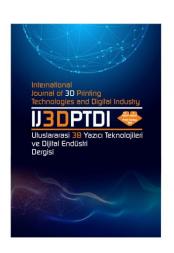
İçindekiler /Table of Contens	Sayfa /Pages
	T
Araştırma Makaleleri/Research Articles	
SUSTAINABLE RECYCLING PLA AND ABS MATERIALS IN	
ADDITIVE MANUFACTURING: EFFECTS ON STRENGTH,	142-154
THERMAL STABILITY, AND ENVIRONMENTAL IMPACT	142-134
Musa Yilmaz ^a D*	
OMEGA METAMATERYAL YAPISININ PENTA YAMA ANTENIN	
PERFORMANSINA ETKİSİ	155-163
Bülent Urul ^a (D*	
TRANSFORMING VIRTUAL REALITY TOURISM THROUGH THE	
CYBER ISPARTA YOUTH CENTER	164-170
Yasin Tekin ^a * Ebru Yılmaz İnce ^b	
FORECASTING CURRENT EXCHANGE AND GOLD RATES WITH	
HYBRID MODELS USING TIME SERIES AND DEEP LEARNING	171-182
ALGORITHMS	171 102
Gökalp Çınarer ^a	
316L PASLANMAZ ÇELİK TOZUNUN ARK İLE TEK ÇİZGİ	
ERGİTİLMESİNDE ELEKTROT MESAFESİNİN ETKİLERİNİN	183-193
ARAŞTIRILMASI	1
Arif Balcı ^a • CDICIH THE	
A BIBLIOMETRIC EVALUATION OF SMART AGRICULTURE	101.006
RESEARCH	194-206
Sara Naghib Zadeha, Dip*, Zümrüt Ecevit Saticip	
EXPERIMENTAL AND STATISTICAL ANALYSIS OF THE EFFECT OF 3D PRINTING PARAMETERS ON MECHANICAL	
OF 3D PRINTING PARAMETERS ON MECHANICAL PERFORMANCE	207-219
	-
Vahap Neccaroğlua **, İsmail Aykut Karamanlı ** OPTIMIZED MACHINE LEARNING METHODS FOR PREDICTION	
OF MARSHALL STABILITY VALUES	220-228
Remzi Gürfidan ^{a [D*} , Kemal Muhammet Erten ^{b [D]}	220-228
STRUCTURAL ANALYSIS OF MEDICAL IMAGES AND BACTERIAL	
POPULATIONS BY IMAGE PROCESSING AND ARTIFICIAL	
INTELLIGENCE	229-235
Mehmet Erhan Şahina D*	-
wennet eman şanın 💟	



HAFİF ELEKTRİKLİ ARAÇLAR İÇİN ARAÇ MODELİ VE SÜRÜŞ DÖNGÜSÜNE GÖRE ELEKTRİK MOTORU TASARIMI	236-246
Doğukan Ayhan ^a , Ali Bakbak ^a	200 210
PERFORMANCE COMPARISON OF VISION-LANGUAGE MODELS	
IN IMAGE CLASSIFICATION	247-262
Dogukan Ozeren ^a , Mehmet Erkan Yuksel ^a , Asım Sinan Yuksel ^b	
EVALUATION OF THE PROCESS PARAMETER AND	
PERFORMANCE OF L-DED SS316L-IN718 BIMETALLIC STRUCTURES	263-271
Mustafa Kaş ^a , Oğuzhan Yılmaz ^a	
COMPARISON OF MACHINE LEARNING MODELS IN HEART	
FAILURE PREDICTION AND THEIR INTEGRATION INTO	
CLINICAL DECISION SUPPORT SYSTEMS	272-282
Mustafa Çakır ^a D*	
AN INTELLIGENT SNOW REMOVAL ROBOTIC SYSTEM:	
TOPOLOGY BASED STRUCTURAL LIGHTWEIGHTING AND	283-293
POWER CONSUMPTION ANALYSIS	203-273
Hilmi Saygin Sucuoglu ^a **	
ELEKTRİKLİ ARAÇ BESLEME SİSTEMLERİNDE 3B BASKININ	
ÇEVRESEL ETKİLERİ VE MEVZUAT UYUMU	294-309
Zühre Aydın ^a De CEGG DADAMETERS ON THE	
THE EFFECT OF FDM PROCESS PARAMETERS ON THE	
MACHINABILITY OF PET-G MATERIAL: DELAMINATION	310-319
ANALYSIS USING THE TAGUCHI APPROACH	
Zihni Alp Çevik ** BODE: A BOUNDARY AWARE DIFFERENTIAL EVOLUTION BASED	
HYBRID OVERSAMPLING TECHNIQUE FOR IMBALANCED DATA	
CLASSIFICATION	320-330
Muhammed Abdulhamid Karabiyika **	
DIMENSIONALITY REDUCTION IN SMALLPOX	
HISTOPATHOLOGICAL IMAGES USING AUTOENCODER AND	221 242
KERNEL PCA	331-343
Nilgün Şengöz ^{a [D]*} , Emine Vargün ^{a [D]}	
DETECTION OF ARTIFICIAL DISCONTINUITIES LOCATED IN	
DIFFERENT LOCATIONS IN PLA SPECIMENS MANUFACTURED	
WITH MEX AT DIFFERENT LAYER THICKNESSES BY	344-351
ULTRASONIC INSPECTION	
Alperen Doğru ^a ************************************	
PREDICTION PERFORMANCE OF DECISION TREE INDUCERS ON	
AUGMENTED BACILLUS CEREUS GROWTH DATA	352-362
Hamit Armağan ^a D*	332-302



TASARIM EĞİTİMİNDE YAPAY ZEKÂ UYGULAMALARININ SOYUTLAMA VE YORUMLAMA EŞLİĞİNDE KULLANIMININ YARATICILIĞA ETKİSİ: ENDÜSTRİYEL TASARIM STÜDYO DENEYİMİ	363-394
Mahmut Celaleddin Kaleli ^a ** ** ** ** ** ** ** ** **	
WIND TURBINE POWER PREDICTION USING MACHINE LEARNING MODELS: A CASE STUDY WITH REAL FARM DATA	395-404
Abdullah Fatih Hocu ^a , Gul Fatma Turker ^a *	



ULUSLARARASI 3B YAZICI TEKNOLOJİLERİ VE DİJİTAL ENDÜSTRİ DERGİSİ

INTERNATIONAL JOURNAL OF 3D PRINTING TECHNOLOGIES AND DIGITAL INDUSTRY

ISSN:2602-3350 (Online)

URL: https://dergipark.org.tr/ij3dptdi

SUSTAINABLE RECYCLING PLA AND ABS MATERIALS IN ADDITIVE MANUFACTURING: EFFECTS ON STRENGTH, THERMAL STABILITY, AND ENVIRONMENTAL IMPACT

Yazarlar (Authors): Musa Yilmaz 10*

Bu makaleye şu şekilde atıfta bulunabilirsiniz (To cite to this article): Yilmaz M., "Sustainable Recycling PLA and ABS Materials In Additive Manufacturing: Effects On Strength, Thermal Stability, and Environmental Impact" Int. J. of 3D Printing Tech. Dig. Ind., 9(2): 142-154, (2025).

DOI: 10.46519/ij3dptdi.1591055

Araştırma Makale/ Research Article

SUSTAINABLE RECYCLING PLA AND ABS MATERIALS IN ADDITIVE MANUFACTURING: EFFECTS ON STRENGTH, THERMAL STABILITY, AND ENVIRONMENTAL IMPACT

Musa Yilmaz^a

^aNaci Topcuoğlu Vocational School, Gaziantep University, TÜRKİYE

* Corresponding Author: <u>msyilmaz@gantep.edu.tr</u>

(Received: 25.11.24; Revised: 28.03.25; Accepted: 03.06.25)

ABSTRACT

This study examines the impact of recycling on the thermal and mechanical properties of polylactic acid (PLA) and acrylonitrile butadiene styrene (ABS) filaments, as commonly used in additive manufacturing. Virgin and recycled PLA and ABS specimens were fabricated using an fused filament fabrication (FFF) type 3D printer. 3D printed specimens were evaluated using tensile and bending tests, as well as thermal analyses through differential scanning calorimetry (DSC) and scanning electron microscopy (SEM). Mechanical testing results showed minimal differences in tensile and bending strengths between virgin and recycled PLA samples, while in contrast recycled ABS demonstrated a more pronounced reduction in tensile strength. Thermal analysis revealed a slight decrease in the glass transition temperature for both materials, particularly in ABS, suggesting possible changes in layer bonding and structural stability. Overall, the recycled materials exhibited comparable mechanical properties to their virgin counterparts. This recycling approach not only lowers material costs but also enhances environmental sustainability within 3D printing applications. By reusing waste materials and reducing the dependency on virgin resources, this method supports a more sustainable manufacturing cycle, helping to reduce overall environmental impact in additive manufacturing.

Keywords: Additive Manufacturing, ABS Filaments, PLA Filaments, Recycling, Environmental Sustainability

1. INTRODUCTION

Plastics, synthetic polymers formed through the polymerization of monomers typically derived from petrochemicals, are widely used due to their lightweight nature, strength, durability, and versatile fabrication capabilities [1,2]. These properties and low manufacturing costs have made plastics integral to various sectors, including agriculture, construction, packaging, and medicine [3]. However, their short life cycle, especially in single-use products, has resulted in a significant accumulation of plastic waste in the environment. It is estimated that 6.3 billion tons of plastic waste were generated globally from 1950 to 2015, of which approximately 80% remains in natural ecosystems [4,5].

Plastic waste represents a significant environmental challenge because of its prolonged degradation period, which is estimated to range from 100 to 1000 years [6]. This has led to plastic fragmentation into macro, meso, micro, and nanoplastics, dispersed through various ecosystems, causing physical and chemical harm to numerous species [7,8]. Factors such as urbanization, economic growth, and population increase have contributed to the rise in plastic waste, which disproportionately affects developing regions that typically lack advanced waste management technologies and regulations [9,10].

As plastic waste continues to increase, the need for effective waste management and recycling strategies are becoming increasingly urgent. The management of plastic waste can be approached through reduced production, mindful consumption, and robust end-of-life processes, such as recycling [11]. However, recycling faces challenges due to high treatment costs and the complexities involved in

processing plastic waste without harming the environment [3,6]. Addressing these challenges is essential to reducing plastic's negative environmental impacts. Global organizations, such as the United Nations, have recognized plastic as a major environmental threat [12,13].

The challenges posed by plastic waste have driven global efforts to adopt sustainable practices in production, usage, and end-of-life management. In this context, the European Union (EU) has committed to advancing a circular economy model [14], with increased plastic recycling rates as a central goal. The EU's targets include recycling 50% of plastic packaging by 2025 and 55% by 2030, emphasizing the importance of innovative recycling methods alongside conventional approaches [15,16]. Achieving these targets would enable plastics to remain within the value chain longer, supporting their use in high-value applications and enhancing sustainability [17,18].

Additive manufacturing (AM) has grown rapidly in recent years, enabling quick and costeffective production without the need for traditional machining or tooling [19]. With advances in AM technologies, particularly FFF, the use of 3D-printed polymers like PLA and ABS continues to expand [20,21]. However, FFF generates significant waste, including failed prints, support structures, and disposable prototypes. PLA, a biodegradable polymer derived from renewable sources, can be managed through recycling, combustion, composting, or landfill disposal [22]. Among these, recycling is considered the most sustainable approach due to its minimal environmental impact, while composting and combustion present challenges related to process complexity and carbon emissions, respectively [23,24].

Given the increasing application of 3D printing in various industries and the environmental impact of plastic waste, exploring sustainable management of waste generated from AM, particularly in materials like PLA and ABS, has become vital. Recycling presents a promising solution to the reduction of the environmental footprint of FFF-generated waste, yet the effects of recycling on the mechanical and thermal properties of these polymers require further examination. An understanding of how

recycling impacts the performance durability of 3D-printed materials is critical to enabling sustainable practices without compromising the functional quality of printed parts. This study assesses the mechanical and thermal behaviours of recycled PLA and ABS filaments to evaluate their suitability for reuse in FFF-based 3D printing applications. The findings aim to support sustainable recycling practices in AM. Mechanical properties, including tensile and bending strength, along with thermal properties, were analysed for both virgin and recycled samples to identify any changes in performance resulting from the recycling process. Additionally, SEM analysis was conducted to examine fracture surfaces, offering insights into structural integrity and layer adhesion.

2. EXPERIMENTAL PROCEDURES

2.1. Materials

This study focuses on PLA and ABS in both their virgin and recycled forms. The recycled materials were sourced from previously used 3D printing waste. Test specimens were created using virgin and recycled filaments, each with a nominal diameter of 1.75 mm.

2.2. Methods

The test specimens were fabricated using a Creality K1C 3D printer with a maximum build volume of 220 x 220 x 250 mm. The 3D printer used for specimen fabrication, operating with FFF technology (Figure 1a), offers a printing accuracy of 100 ± 0.1 mm. The AM process was carried out with four distinct filament types: virgin PLA (v-PLA), recycled PLA (r-PLA), virgin ABS (v-ABS), and recycled ABS (r-ABS). In order to isolate the effects of the recycling process on the mechanical and thermal properties of the polymers, all 3D printing parameters—including layer height, print speed, nozzle temperature, and infill density—were kept constant for both virgin and recycled samples. To ensure optimal printing conditions, the printing temperature was set to 220°C for PLA filaments and 250°C for ABS filaments. Correspondingly, the temperature was set to 50°C for PLA and 100°C for ABS to promote adhesion throughout the process. Each specimen printing manufactured with a 100% infill density. The layer thickness was maintained at 0.28 mm, and the printing speed set to 50 mm/s. All other printing parameters, such as air gap, build

orientation, raster angle, printing velocity, contour width, and number of contours, followed the manufacturer's default settings and recommendations. All samples were fabricated using a flat build orientation along the XY plane to ensure a consistent printing direction throughout the study.

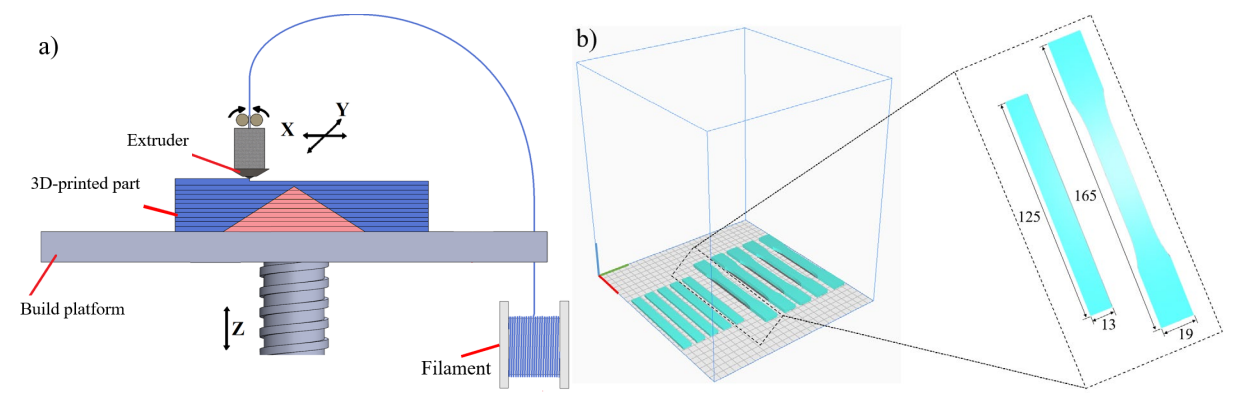


Figure 1. Schematic representation of (a) the FFF process and (b) the solid model of tensile/bending test samples with their building direction.

The recycling process for 3D printing materials begins with the collection of waste generated from previous 3D printing projects (Figure 2). These waste materials, often in the form of failed prints, support structures, or excess filament, are gathered and prepared for processing. The first step in the recycling workflow is the grinding phase, where the waste materials are fed into a grinder to be broken down into smaller particles or pellets. Once

ground, the particles undergo an extrusion process. The particles are heated to their melting point during extrusion, creating a homogeneous molten polymer. This molten material is then extruded through a nozzle to form a continuous filament, which is cooled and spooled for easy handling and storage. The recycled filament is then loaded into a 3D printer, where it can be used to create new objects.

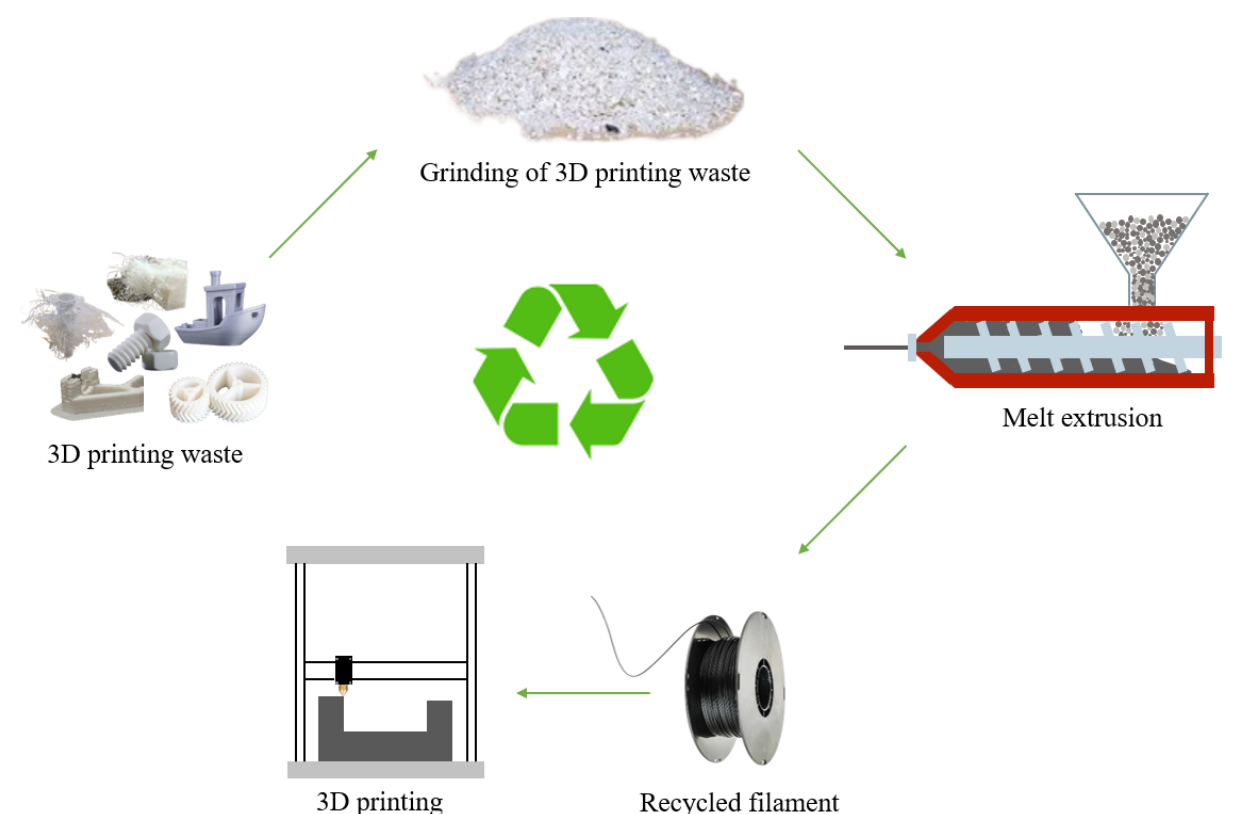
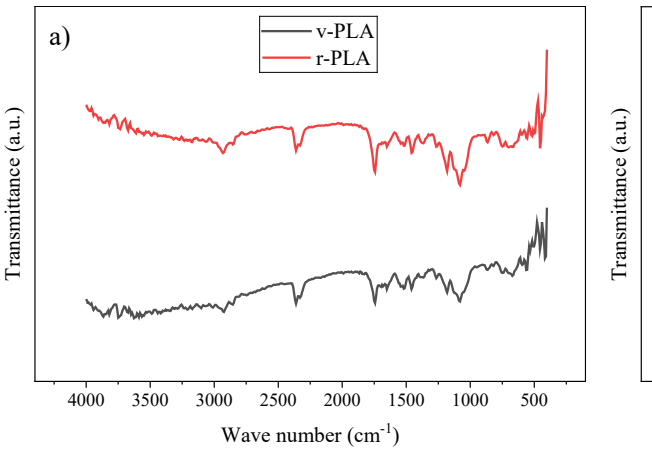


Figure 2. Recycling and filament production scheme for 3D printing materials



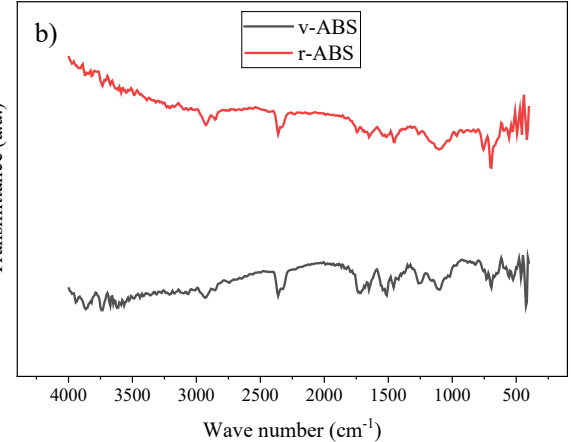


Figure 3. FTIR spectra of 3D-printed PLA and ABS samples

2.3. Characterization and Mechanical Testing

The chemical structure of the samples was analysed using fourier transform infrared (FTIR) spectroscopy using a Shimadzu IRTracer-100 spectrometer temperature. Spectral scans were conducted across the range of 4000 to 400 cm⁻¹, with a resolution of 4 cm⁻¹, for all specimens. DSC was used to analyse thermal transitions, including the glass transition and melting temperatures, with both heating and cooling rates set to 10°C/min on a Mettler-Toledo/700 DSC. Samples were placed in aluminium pans and initially heated from -50°C to 240°C at a rate of 10°C/min (first heating cycle). After reaching 240°C, the samples were again cooled to -50°C, then reheated from -50°C to 240°C at the same rate (second heating cycle). All measurements were performed in a nitrogen thermograms atmosphere. The obtained allowed for the identification of the glass transition temperature (Tg), cold crystallization temperature (Tcc), and melting temperature (Tm). SEM was used to capture detailed images of the surface morphology and microstructural characteristics of the specimens. A Zeiss Gemini 300 SEM was employed for sample preparation and imaging, with specimens coated in a thin layer of palladium/gold prior to analysis.

The mechanical properties were evaluated via tensile and bending tests following the ASTM D638 [25] and D790 [26] standards, respectively. Each test was conducted five times at room temperature using a Shimadzu AGX universal testing machine with a load capacity of 50 kN. The dimensions of the test samples are given in Figure 1b. The testing speeds were set

to 5 mm/min for tensile tests and 1.56 mm/min for bending tests.

3. RESULTS AND DISCUSSION 3.1. FTIR Results

The FTIR spectra of the PLA and ABS samples used in the study are presented in the spectral region in Figure 3a and Figure 3b, respectively. There are no apparent differences between samples printed with virgin and recycled filament for both PLA and ABS. The presence of identical peaks indicates that the recycling process did not lead to any chemical changes in the samples. Additionally, the chemical structures of all the samples align with IR spectra reported in the literature, as confirmed by the FTIR spectra shown in Figure 3 [27–29]. In the IR spectra of PLA, a strong CO stretching vibration is observed at 1757 cm⁻¹, while bands corresponding to the -CH₃ C-H stretching vibrations are observed at 2996 cm⁻¹ and 2945 cm⁻¹. Furthermore, bands associated with the characteristic absorption of ester CO stretching vibrations are observed at 1080 and 1187 cm⁻¹ [30].

In the FTIR spectra of ABS polymer, characteristic absorption bands corresponding to each of its main components -acrylonitrile, butadiene, and styrene- can be identified. Aromatic C-H stretching vibrations from the styrene component are observed in the range 3200–3000 cm⁻¹, while C-H bending vibrations in the benzene ring can be observed at approximately 700 cm⁻¹ and 760 cm⁻¹ [31]. The absorption at 1638 cm⁻¹ represents the stretching vibration of the C-C double bond from the butadiene units, while the stretching vibration of the aromatic ring from the styrene unit appears at 1495 cm⁻¹ [32]. The deformation

of C-H for hydrogen atoms attached to alkenic carbons is observed at 967 cm⁻¹ for 1,4butadiene units and 911 cm⁻¹ for 1,2-butadiene units [32]. These peaks confirm the presence and integrity of the ABS structure, and their alignment with equivalent spectra reported in the literature indicates that no significant chemical alteration has occurred to the samples due to processing.

3.2. DSC Results

The DSC analysis results for PLA samples, including heating and cooling cycles, are shown in Figure 4 and summarized in Table 1. Figure 4a and Figure 4b focus on the heating and

cooling cycles to highlight the consistent thermal behaviour of both v-PLA and r-PLA, with minimal influence from external factors like cooling rate. In the first heating cycle, there is no significant difference between v-PLA and r-PLA, as can be seen in Figure 4c, with both showing similar thermal patterns. During the second heating cycle, the Tg for v-PLA was 63.34°C, while for r-PLA, it is slightly lower at 61.13°C. This small drop (~2°C) in Tg for the recycled sample suggests some minor effect from the recycling process, but this difference is too small to impact the material's overall mechanical and/or thermal performance significantly.

Table 1. Table of DSC results after the second heating cycle of PLA and ABS samples						
Material	Tg - Glass transition (°C)	Tcc - Cold crystallization (°C)	Tm - Melting (°C)			
v-PLA	63.34	118.87	153.07			
r-PLA	61.13	117.99	149.88			
v-ABS	107.63	-	-			
r-ABS	103.68	-				

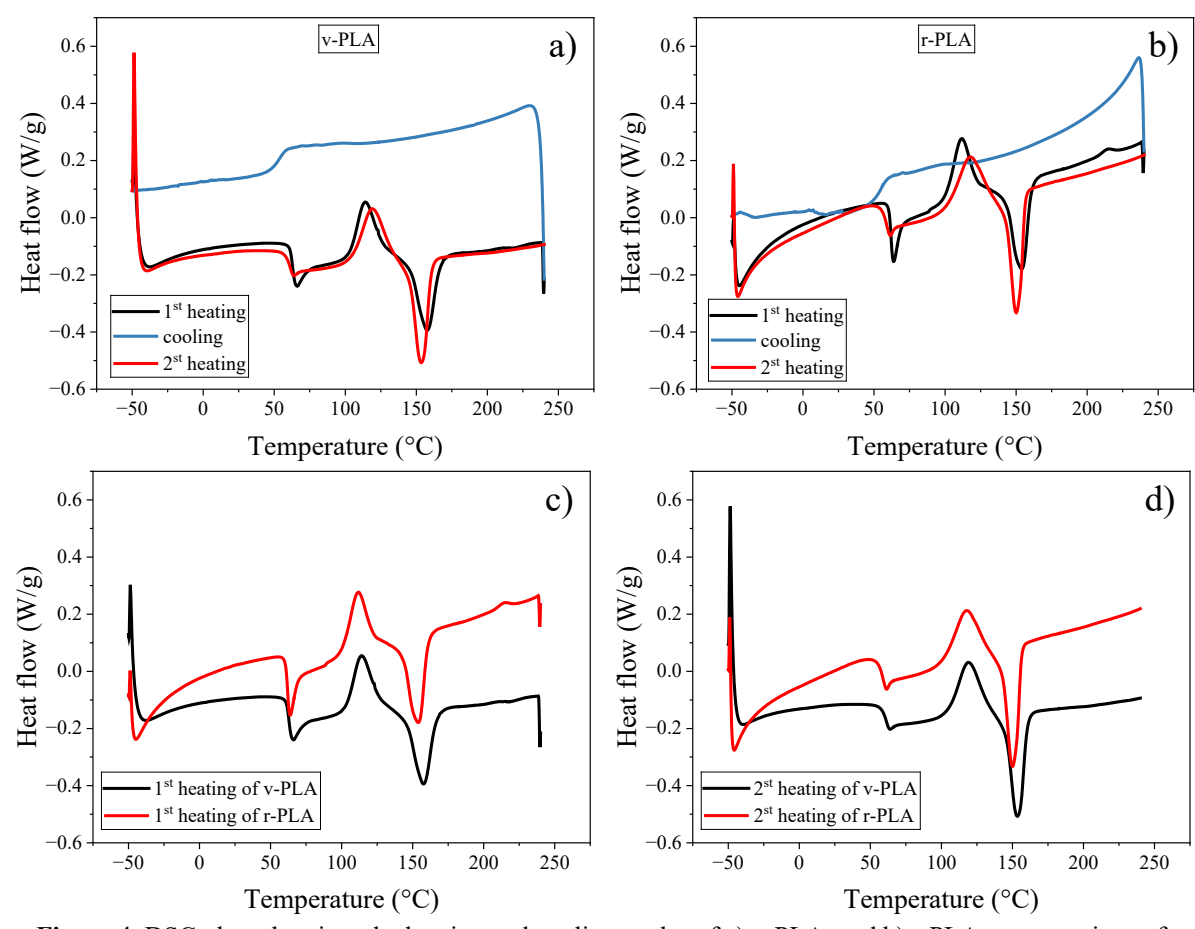


Figure 4. DSC plots showing: the heating and cooling cycles of a) v-PLA, and b) r-PLA, a comparison of c) first and d) second heating cycles

The cold crystallization temperature is also slightly lower for r-PLA, occurring at 117.99°C compared to 118.87°C for v-PLA. This indicates that r-PLA crystallizes just slightly earlier, but the difference (~1°C) is minimal and can be considered insignificant. Additionally, a decrease in melting temperature between the first and second heating cycles is noted for both materials, as shown in Figure 4c and Figure 4d. Therefore, the DSC results suggest that recycling causes only minor changes in the thermal properties of PLA. The recycled PLA maintains a similar thermal stability across both heating cycles, and the observed changes are very small, indicating that the recycling process has little effect on the polymer's stability.

The DSC analysis results for ABS samples, covering both heating and cooling cycles, are presented in Figure 5 and summarized in Table 1. Figure 5a and Figure 5b emphasize the heating and cooling cycles to demonstrate the stable thermal behaviour of both v-ABS and r-ABS, with minimal impact from external factors such as cooling rate. Due to the amorphous structure of ABS polymer, DSC

analysis generally provides information only on the glass transition temperature. In amorphous polymers, a lack of a regular crystalline structure means that thermal transitions such as crystallization or melting temperatures cannot be observed [33]. Consequently, in Table 1, only the Tg of ABS filaments can be reported. In the heating cycles, no significant difference is observed between v-ABS and r-ABS, as shown in Figure 5c and Figure 5d, with both displaying a similar thermal profile. In the second heating cycle, the Tg for v-ABS is 107.63°C, while for r-ABS it is slightly lower, at 103.68°C. The slight decrease in the Tg suggests that the recycling process can cause minor changes at the molecular level. This reduction may be due to chain scission, lower molecular weight, or increased free volume within the polymer, which can enhance chain mobility. Additionally, impurities introduced during recycling could act as plasticizers, further lowering Tg. Despite this small change, the thermal properties of r-ABS remain close to those of v-ABS, indicating that recycled ABS retains sufficient thermal stability for similar applications.

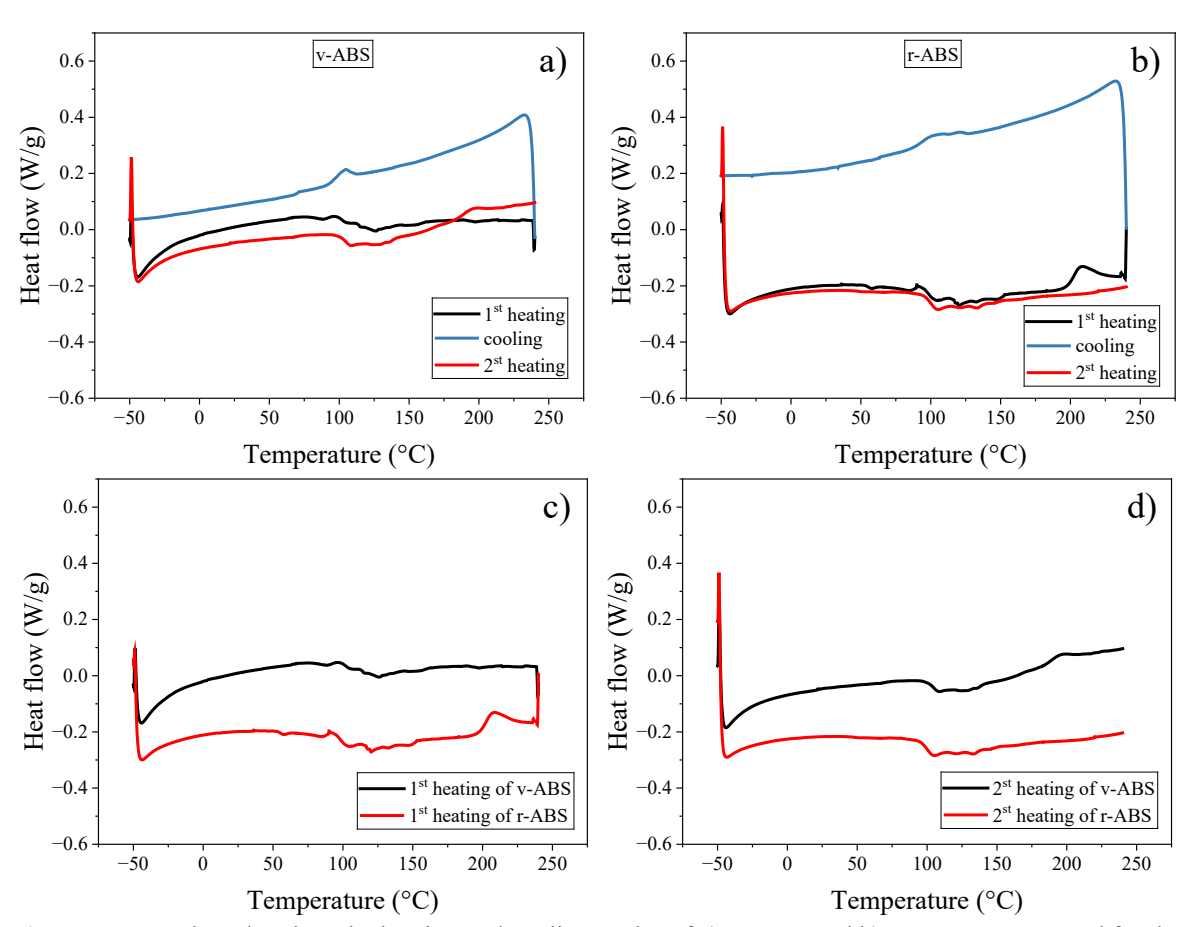


Figure 5. DSC plots showing: the heating and cooling cycles of a) v-ABS, and b) r-ABS, as compared for the c) first and d) second heating cycles

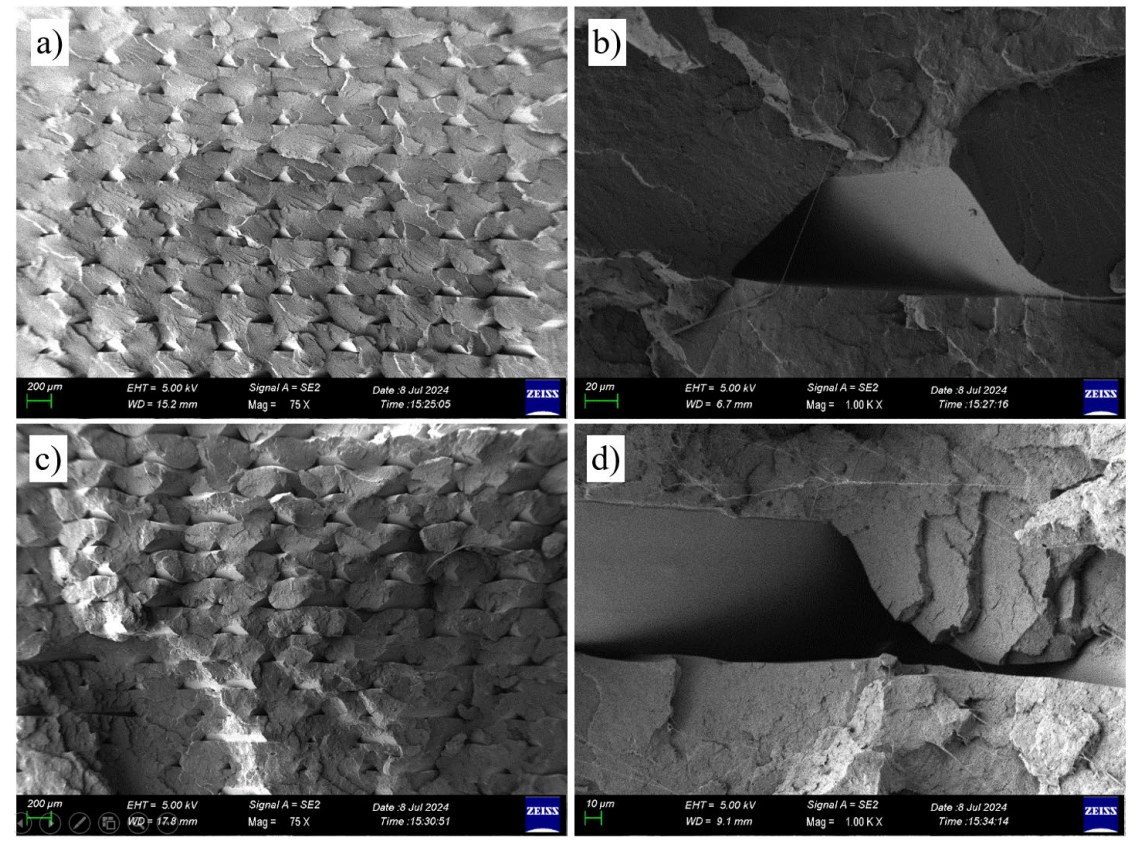


Figure 6. SEM images of the fractured surface of a) v-PLA at 75x, b) v-PLA at 1000x, c) r-PLA at 75x, and d) r-PLA at 1000x

3.3. SEM Results

In Figure 6 and Figure 7, SEM images illustrate the fracture surfaces of PLA and ABS samples, highlighting structural differences between the virgin and recycled materials. Figure 6a illustrates the fracture surface of the v-PLA sample, which shows a uniform appearance with the majority of fibres breaking along the fibre surfaces. In contrast, Figure 6c reveals that the r-PLA sample has a less uniform fracture surface, with more interfacial bond failure than seen in v-PLA. Additionally, the fibres in r-PLA appear to merge and smear each other, both at the interface and across individual fibre surfaces. This behaviour is thought to result from the reduction in Tg observed in the DSC analysis due to the recycling process. The lower Tg causes the recycled material to soften at a lower temperature, which may potentially allow fibres to bond more extensively. examining Figure 6b and Figure 6d, although there are slight differences in fracture patterns, the fracture surfaces of each of the samples appear quite similar. Thus, the recycling process does not seem to cause any significant changes in the microstructure or fracture surface of the material. At lower magnifications (Figure 7a

and Figure 7c), the v-ABS sample displays a smoother, more uniform surface, with fibres and layers distributed consistently across the structure. In contrast, the r-ABS sample shows clear smearing between layers, suggesting that the layers have bonded in a less uniform manner. Instead of fracturing evenly along each fibre, the r-ABS sample tends to break more along interlayer bond regions.

In Figure 7c and Figure 7d, a larger interlocking fibre structure can be observed in the recycled sample, where fibres merge and form a smeared structure. This increased smearing may result from the slight reduction in Tg, which causes the recycled material to soften earlier, potentially allowing the layers to bond more tightly. In Figure 7d, at higher magnifications, this smeared bonding between layers becomes even more apparent in r-ABS than it is in v-ABS.

For both the ABS and PLA samples, the SEM images revealed two main differences between virgin and recycled specimens. These differences include an increase in smearing and a higher rate of interfacial bond failure in the

recycled samples. Previous studies [21,34–36] have shown that an increase in interfacial bond failure generally reduces mechanical properties, as AM tends to produce stronger mechanical performance with fibre surface breakage, while interfacial regions are more likely to act as weak points. Therefore, the increased occurrence of interfacial bond failure in recycled samples is considered a negative outcome. However, the smearing observed between layers in the recycled samples may contribute to improved mechanical properties by creating a more integrated, cohesive structure. Provided that fibre smearing does not lead to dimensional shrinkage subsequent to production, it may enhance interfacial bonding and lead to more favourable mechanical properties.

3.4. Tensile Test Results

The stress-strain graphs obtained from the tensile test results for all samples are presented in Figure 8. These graphs show that there is generally little difference between the virgin and recycled samples, with the curves being quite close to each other and both samples for each material exhibiting similar tensile strengths. Furthermore, as stated in the literature, a comparison of the tensile strengths of PLA and ABS filaments reveals that PLA has the higher tensile strength. In accordance with ASTM standards, the repeated test results for each tensile test, along with their standard deviations, are presented in Table 2 and Table 3 for PLA and ABS, respectively, to allow for a more detailed analysis.

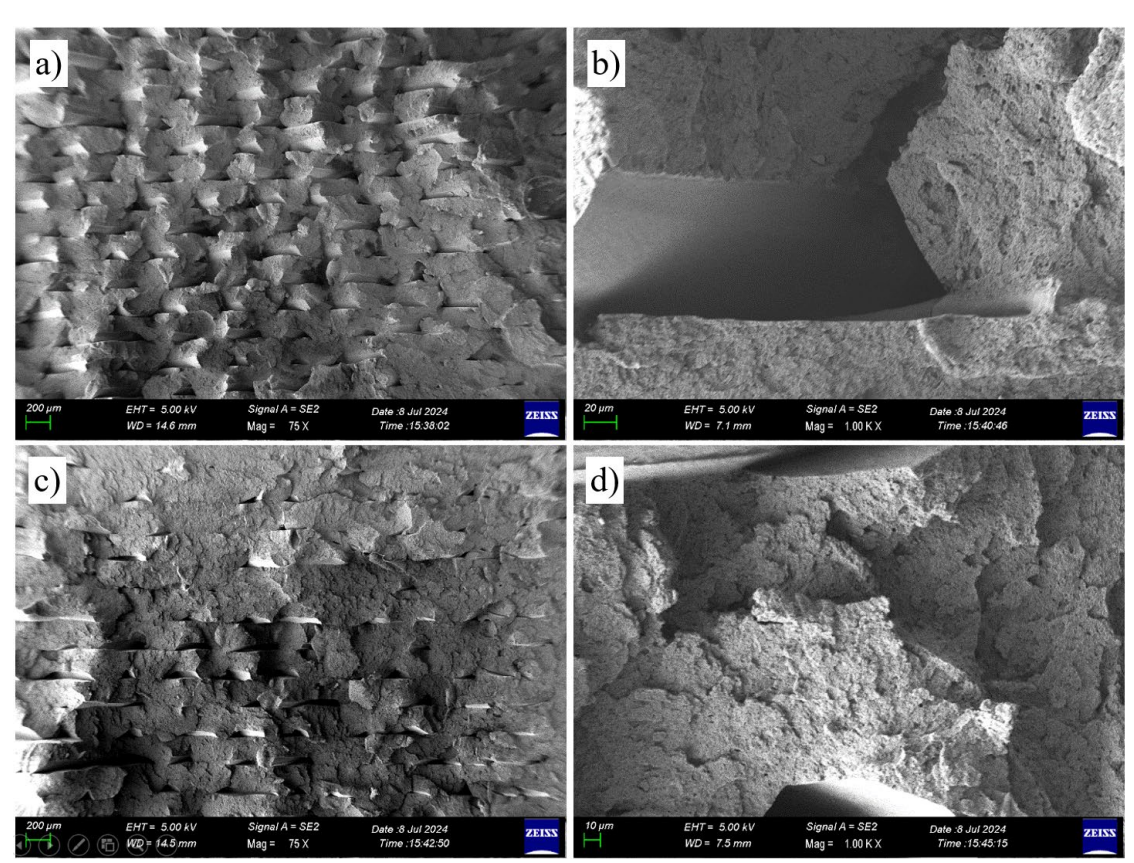


Figure 7. SEM images of the fractured surface of a) v-ABS at 75x, b) v-ABS at 1000x, c) r-ABS at 75x, and d) r-ABS at 1000x

Table 2. Results of tensile tests of samples produced with v-PLA and r-PLA

	14010 20 10000	THE CT COLLEGE	ests of summp.	res promotes .			
M. (1		Maximum stress (MPa)					
Material	1 st test	2 nd test	3 rd test	4 th test	5 th test	Mean	± S.D.
v-PLA	41.99	44.19	44.74	44.26	43.21	43.68	1.10
r-PLA	44.52	44.22	44.67	44.16	44.32	44.38	0.21
N (4 1				Strain (%)			
Material	1 st test	2 nd test	3 rd test	4 th test	5 th test	Mean	± S.D.
v-PLA	1.76	1.85	1.88	1.86	1.80	1.83	0.05
r-PLA	2.02	2.08	2.12	2.01	2.11	2.07	0.05

Table 3. Results of tensile tests of samples produced with v-ABS and r-ABS

M-4:1			Max	imum stress (MPa)		
Material	1st test	2 nd test	3 rd test	4 th test	5 th test	Mean	± S.D.
v-ABS	29.40	28.58	30.13	29.56	29.24	29.38	0.56
r-ABS	26.27	23.80	22.34	25.20	23.56	24.23	1.53

M-4:-1				Strain (%)			
Material	1st test	2 nd test	3 rd test	4 th test	5 th test	Mean	± S.D.
v-ABS	1.63	1.56	1.65	1.62	1.59	1.61	0.04
r-ABS	1.51	1.21	1.15	1.44	1.19	1.30	0.16

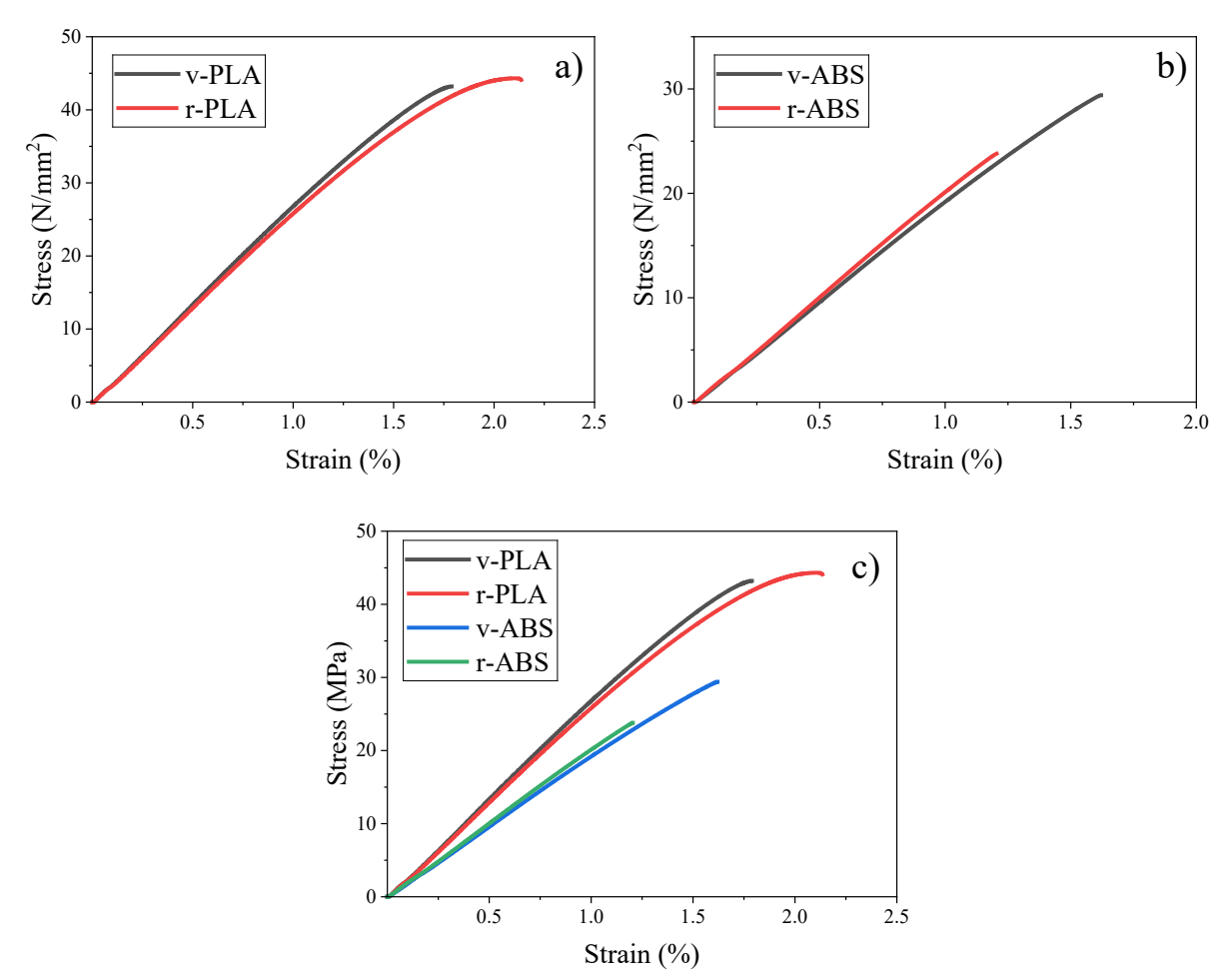


Figure 8. Stress-strain graphs of samples printed with; (a) PLA, (b) ABS, and (c) a comparison of the PLA and ABS samples

Table 2 shows that r-PLA samples had slightly higher tensile strengths. However, this difference is negligible, and cannot be considered significant when standard deviations are taken into account. The highest standard deviation, ±1.10 MPa, was observed for the v-PLA samples, which is sufficient to account for the strength difference between v-PLA and r-PLA. Therefore, it can be concluded that recycling does not have a significant effect on the tensile strength of PLA.

In Table 3, r-ABS samples show a relatively more pronounced decrease in tensile strength compared to PLA. v-ABS samples have a tensile strength of 29.38 MPa, while r-ABS samples exhibit an average tensile strength of 24.23 MPa. This indicates that ABS polymer is more strongly affected by the recycling process than PLA. Additionally, the low standard deviations observed for all samples suggest that production process for specimens manufactured via AM is stable and consistent across repeated analyses. The low standard deviations in the mechanical tests indicate that the production process for the specimens is stable and consistent, with the material properties showing a homogeneous structure and the test results being highly reliable. This suggests that the production parameters were themselves very consistent, thus minimizing environmental or measurement errors. Low standard deviation also implies that the material

3.5. Bending Test Results

Figure 9 presents the force-displacement curves obtained from the bending tests for all samples. Overall, the results indicate minimal differences between virgin and recycled specimens, with similar bending strengths observed across the groups. The curves are closely aligned, demonstrating comparable bending performance between samples. Detailed results for each bending test, following ASTM standards, as well as corresponding standard deviations, are listed in Table 4 and Table 5 for PLA and ABS samples, respectively, providing a comprehensive analysis.

is likely to perform predictably in terms of mechanical properties, such as tensile strength, and is unlikely to exhibit unexpected variations in application. Therefore, the low standard deviations obtained for the current test results support the stability of the production process and the reliability of the mechanical performance of the materials.

In Table 4, the bending force results show that v-PLA samples exhibit slightly higher bending forces than r-PLA samples. The average bending force for the v-PLA samples is 139.95 N, compared to 129.75 N for r-PLA. However, this difference remains relatively insignificant, particularly when standard deviations are considered. The highest standard deviation of ±13.37 N was recorded for v-PLA samples, which offsets the minor difference between v-PLA and r-PLA. Therefore, it can be inferred that recycling does not significantly impact the bending strength of PLA materials.

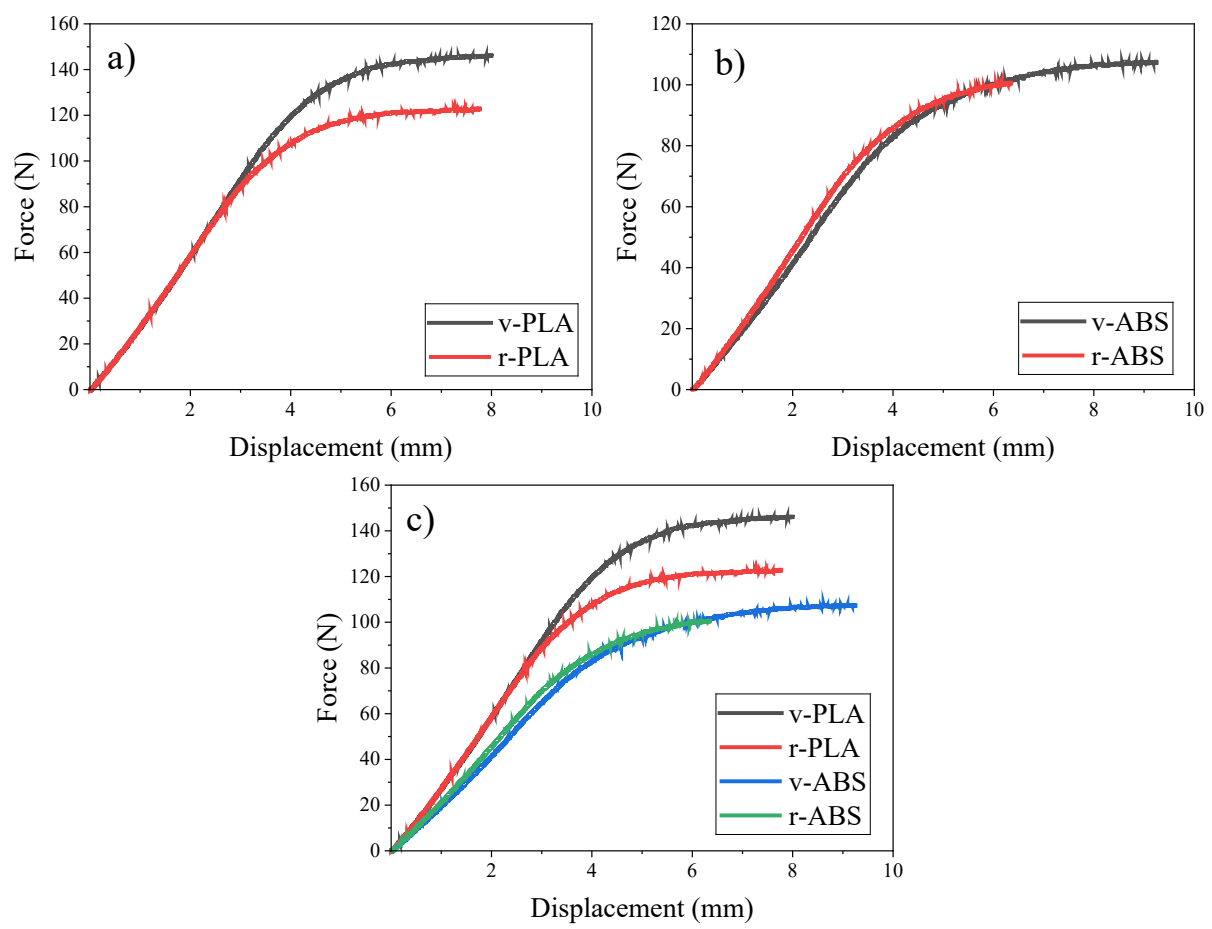


Figure 9. Bending force-displacement graphs of specimens produced with (a) PLA and (b) ABS, and (c) a comparison of PLA and ABS samples

Table 4. Results of bending test of samples produced with v-PLA and r-PLA

		Maxim	um bending fo	orce (N)		
1st test	2 nd test	3 rd test	4 th test	5 th test	Mean	± S.D.
152.92	128.22	123.12	146.25	149.25	139.95	13.37
137.19	133.32	129.70	122.98	125.55	129.75	5.74
		Maximu	ım displaceme	ent (mm)		
1st test	2 nd test	3 rd test	4 th test	5 th test	Mean	± S.D.
8.37	8.33	8.32	7.99	8.06	8.21	0.18
8.13	7.33	7.18	7.76	7.91	7.66	0.40
	152.92 137.19 1st test 8.37	152.92 128.22 137.19 133.32 1st test 2 nd test 8.37 8.33	1st test 2 nd test 3 rd test 152.92 128.22 123.12 137.19 133.32 129.70 Maximu 1st test 2 nd test 3 rd test 8.37 8.33 8.32	1st test 2 nd test 3 rd test 4 th test 152.92 128.22 123.12 146.25 137.19 133.32 129.70 122.98 Maximum displacement 1st test 2 nd test 3 rd test 4 th test 8.37 8.33 8.32 7.99	152.92 128.22 123.12 146.25 149.25 137.19 133.32 129.70 122.98 125.55 Maximum displacement (mm) 1st test 2 nd test 3 rd test 4 th test 5 th test 8.37 8.33 8.32 7.99 8.06	1st test 2 nd test 3 rd test 4 th test 5 th test Mean 152.92 128.22 123.12 146.25 149.25 139.95 137.19 133.32 129.70 122.98 125.55 129.75 Maximum displacement (mm) 1st test 2 nd test 3 rd test 4 th test 5 th test Mean 8.37 8.33 8.32 7.99 8.06 8.21

Table 5 Results of bending test of samples produced with v-ABS and r-ABS

M-4:-1			Maxim	um bending fo	orce (N)		
Material	1st test	2 nd test	3 rd test	4 th test	5 th test	Mean	± S.D.
v-ABS	110.10	107.58	106.86	103.81	102.76	106.22	2.96
r-ABS	103.33	98.37	95.18	100.71	104.76	100.47	3.84

M-4:-1			Maximu	ım displaceme	ent (mm)		
Material	1st test	2 nd test	3 rd test	4 th test	5 th test	Mean	± S.D.
v-ABS	9.37	9.24	9.62	8.45	8.74	9.08	0.48
r-ABS	6.88	6.32	6.62	6.34	6.57	6.55	0.23

As illustrated in Table 5, recycled ABS samples show a slightly reduced bending force compared to their virgin counterparts. The mean bending force for v-ABS is 106.22 N, whereas for r-ABS, it is 100.47 N, indicating a small reduction due to recycling. This suggests that ABS is relatively less impacted by the recycling process under bending loads compared to tensile loads, as seen in prior sections. The low standard deviations across all tests imply that the AM process was consistent and that the results are reliable. In terms of bending tests, the low standard deviations indicate that the material properties remain homogeneous and that the tests produced highly consistent results.

4. CONCLUSIONS

This study investigated the effects of recycling on the thermal and mechanical properties of PLA and ABS filaments, which are commonly used in AM. The results of mechanical tests, alongside thermal analyses, provided valuable observations regarding the structural stability and performance of virgin and recycled specimens. Thermal analysis showed a slight decrease in the Tg of both recycled PLA and ABS, which may facilitate increased layer bonding but could also influence their mechanical properties under stress. This reduction in Tg was more pronounced in recycled ABS, which aligns with its observed reduction in mechanical performance. The fracture surfaces revealed increased smearing and interfacial bond breaking in recycled

samples, especially for ABS, which supports the hypothesis that ABS is more significantly affected by recycling in terms of layer adhesion and structural integrity. Mechanical tests indicated a minimal impact of recycling on the performance of both PLA and ABS samples. The recycled materials demonstrated strengths comparable to their virgin counterparts, indicating that the recycling process did not significantly mechanical performance in either case. In the tensile tests, PLA showed only a 1.6% change, while ABS exhibited a greater decrease of 17.5%, indicating higher degradation susceptibility in the latter. Bending tests showed strength reductions of 7.3% in PLA and 5.4% in ABS, indicating a limited but more pronounced effect on ABS's properties. The similar mechanical strengths of recycled PLA and ABS suggest that recycled materials are suitable for applications where high strength is not critical, offering a cost-effective and sustainable alternative to the use of virgin materials. This closed-loop recycling system not only reduces waste but also minimizes the environmental impact associated with raw material production, enhancing the sustainability of 3D printing.

ACKNOWLEDGES

This work was supported by the Scientific Research Projects Unit (BAPYB) of Gaziantep University (Project numbers: NTMYO. HZP. 24. 02)

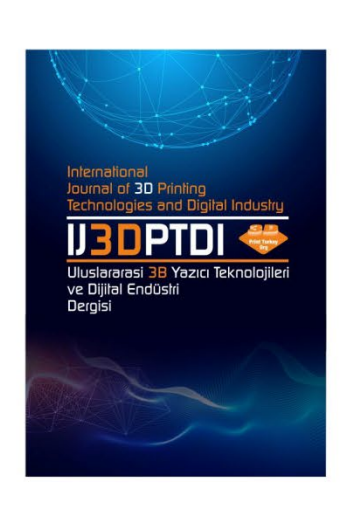
REFERENCES

- 1. Ilyas, M., Ahmad, W., Khan, H., Yousaf, S., Khan, K., and Nazir, S., "Plastic Waste as a Significant Threat to Environment–a Systematic Literature Review", Rev Environ Health, Vol. 33, Issue 4, Pages 383–406, 2018.
- 2. Torres-Agullo, A., Karanasiou, A., Moreno, T., and Lacorte, S., "Overview on the Occurrence of Microplastics in Air and Implications from the Use of Face Masks during the COVID-19 Pandemic", Science of the total environment, Vol. 800, Pages 149555, 2021.
- 3. Pan, D., Su, F., Liu, C., and Guo, Z., "Research Progress for Plastic Waste Management and Manufacture of Value-Added Products", Adv Compos Hybrid Mater, Vol. 3, Pages 443–461, 2020.
- 4. N.A. Welden, "The Environmental Impacts of Plastic Pollution", Plastic waste and recycling, Pages 195–222, 2020.
- 5. Liang, Y., Tan, Q., Song, Q., and Li, J., "An Analysis of the Plastic Waste Trade and Management in Asia", Waste Management, Vol. 119, Pages 242–253, 2021.
- 6. Pilapitiya P.G.C.N.T., and Ratnayake, A.S., "The World of Plastic Waste: A Review", Cleaner Materials, Pages 100220, 2024.
- 7. Hurley, R., Horton, A., Lusher, A., and Nizzetto, L., "Plastic Waste in the Terrestrial Environment, Plastic waste and recycling", Pages 163–193, 2020.
- 8. Gabbott, S., Key, S., Russell, C., Yonan, Y., and Zalasiewicz, J., "The Geography and Geology of Plastics: Their Environmental Distribution and Fate", Plastic Waste and Recycling, Pages 33–63, 2020.
- 9. Eze, W.U., Umunakwe, R., Obasi, H.C., Ugbaja, M.I., Uche, C.C., and Madufor, I.C., "Plastics Waste Management: A Review of Pyrolysis Technology", Clean Technol. Recycl, Vol. 1, Issue 1, Pages 50–69, 2021.
- 10. Amasuomo, E., and Baird, J., "The Concept of Waste and Waste Management", J. Mgmt. & Sustainability, Vol. 6, Pages 88, 2016.
- 11. Wichai-Utcha, N., and Chavalparit, O., "3Rs Policy and Plastic Waste Management in Thailand", J Mater Cycles Waste Manag, Vol. 21, Pages 10–22, 2019.

- 12. Borrelle, S.B., Ringma, J., Law, K.L., Monnahan, C.C., Lebreton, L., McGivern, A., Murphy, E., Jambeck, J., Leonard, G.H., and Hilleary, M.A., "Predicted Growth in Plastic Waste Exceeds Efforts to Mitigate Plastic Pollution", American Association for the Advancement of Science, Vol. 369, Issue 6510, Pages 1515–1518, 2020
- 13. Khan, F., Ahmed, W., and Najmi, A., "Understanding Consumers' Behavior Intentions towards Dealing with the Plastic Waste: Perspective of a Developping Country", Resour Conserv Recycl, Vol. 142, Pages 49–58, 2019.
- 14. Friant, M.C., Vermeulen, W.J., and Salomone, R., "Analysing European Union Circular Economy Policies: Words versus Actions", Sustain Prod Consum, Vol. 27, Pages 337–353, 2021.
- 15. Real, L.E.P., "Plastics Statistics: Production, Recycling, and Market Data, Recycled Materials for Construction Applications: Plastic Products and Composites", Pages 103–113, 2022.
- 16. Ludlow, P., "The European Commission, The New European Community", Routledge, Pages 85–132, 2018.
- 17. Thomas, J., Patil, R.S., Patil, M., and John, J., "Addressing the Sustainability Conundrums and Challenges within the Polymer Value Chain", Sustainability, Vol. 15, Issue 22, Pages 15758, 2023.
- 18. Rentizelas, A., Shpakova, A., and Mašek, O., "Designing an Optimised Supply Network for Sustainable Conversion of Waste Agricultural Plastics into Higher Value Products", J Clean Prod, Vol. 189, Pages 683–700, 2018.
- 19. Erdaş, M.U., Yıldız, B.S., and Yıldız, A.R., "Experimental Analysis of the Effects of Different Production Directions on the Mechanical Characteristics of ABS, PLA, and PETG Materials Produced by FDM", Materials Testing, Vol. 66, Issue 2, Pages 198–206, 2024.
- 20. Aksoz, Z.Y., Bogrekci, I., Demircioglu, P., and Tunc, K.M.M., "Thermo-Hydraulic Investigation of a Heat Exchanger Tube Equipped with 3D-Printed Swirl Flow Generators", Arab J Sci Eng, Vol. 50, Issue 4, Pages 2383–2408, 2024.
- 21. Yilmaz, M., Yilmaz, N.F., and Kalkan, M.F., "Rheology, Crystallinity, and Mechanical Investigation of Interlayer Adhesion Strength by Thermal Annealing of Polyetherimide (PEI/ULTEM 1010) Parts Produced by 3D Printing", J Mater Eng Perform, Vol. 31, Issue 12, Pages 9900-9909, 2022.

- 22. Anderson, I., "Mechanical Properties of Specimens 3D Printed with Virgin and Recycled Polylactic Acid", 3D Print Addit Manuf, Vol. 4, Issue 2, Pages 110–115, 2017.
- 23. Lanzotti, A., Martorelli, M., Maietta, S., Gerbino, S., Penta, F., and Gloria, A., "A Comparison between Mechanical Properties of Specimens 3D Printed with Virgin and Recycled PLA", Procedia CIRP, Vol. 79, Pages 143–146, 2019.
- 24. Thomson, A., Price, G.W., Arnold, P., Dixon, M., and Graham, T., "Review of the Potential for Recycling CO2 from Organic Waste Composting into Plant Production under Controlled Environment Agriculture", J Clean Prod, Vol. 333, Pages 130051, 2022.
- 25. A. D638-14, "ASTM International, Standard test method for tensile properties of plastics", 2014.
- 26. A. International, "ASTM D790- 17-Flexural Properties of Unreinforced and Reinforced Plastics and Electrical Insulating Materials", 2017.
- 27. Wu, C.-S., and Liao, H.-T., "A New Biodegradable Blends Prepared from Polylactide and Hyaluronic Acid, Polymer (Guildf)", Vol. 46, Issue 23, Pages 10017–10026, 2005.
- 28. Singla, P., Mehta, R., Berek, D., and Upadhyay, S.N., "Microwave Assisted Synthesis of Poly (Lactic Acid) and Its Characterization Using Size Exclusion Chromatography", Journal of Macromolecular Science, Part A, Vol. 49, Issue 11, Pages 963–970, 2012.
- 29. Yilmaz, M., Yilmaz, N.F., Kilic, A., and Mazi, H., "Investigation of Manufacturability of In-Situ Crosslinked Polylactic Acid (PLA) and Peroxide Composite in Additive Manufacturing", Journal of the Faculty of Engineering and Architecture of Gazi University, Vol. 39, Issue 2, Pages 859–867, 2024.

- 30. Chieng, B.W., Azowa, I.N., Yunus, W., Wan, M.D.Z., and Hussein, M.Z., "Effects of Graphene Nanopletelets on Poly (Lactic Acid)/Poly (Ethylene Glycol) Polymer Nanocomposites," Advanced Materials Research, Pages 136–139, 2014.
- 31. Neher, B., Gafur, M.A., Al-Mansur, M.A., Bhuiyan, M.M.R., Qadir, M.R., and Ahmed, F., "Investigation of the Surface Morphology and Structural Characterization of Palm Fiber Reinforced Acrylonitrile Butadiene Styrene (PF-ABS) Composites", Materials Sciences and Applications, 2014.
- 32. Li, J., Chen, F., Yang, L., Jiang, L., and Dan, Y., "FTIR Analysis on Aging Characteristics of ABS/PC Blend under UV-Irradiation in Air", Spectrochim Acta A Mol Biomol Spectrosc, Vol. 184, Pages 361–367, 2017.
- 33. Sorolla-Rosario, D., Llorca-Porcel, J., Pérez-Martínez, M., Lozano-Castello, D., and Bueno-Lopez, A., "Study of Microplastics with Semicrystalline and Amorphous Structure Identification by TGA and DSC", J Environ Chem Eng, Vol. 10, Issue 1, Pages 106886, 2022.
- 34. Yilmaz, M., and Yilmaz, N.F., "Effects of Raster Angle in Single-and Multi-Oriented Layers for the Production of Polyetherimide (PEI/ULTEM 1010) Parts with Fused Deposition Modelling", Materials Testing, Vol. 64, Issue 11, Pages 1651–1661, 2022.
- 35. Perez, D.B., Celik, E., and Karkkainen, R.L., "Investigation of Interlayer Interface Strength and Print Morphology Effects in Fused Deposition Modeling 3D-Printed PLA", 3D Print Addit Manuf, Vol. 8, Issue 1, Pages 23–32, 2021.
- 36. Li, Q., Zhao, W., Niu, B., Wang, Y., Wu, X., Ji, J., Li, Y., Zhao, T., Li, H., and Wang, G., "3D Printing High Interfacial Bonding Polyether Ether Ketone Components via Pyrolysis Reactions", Mater Des, Vol. 198, Pages 109333, 2021.



ULUSLARARASI 3B YAZICI TEKNOLOJİLERİ VE DİJİTAL ENDÜSTRİ DERGİSİ

INTERNATIONAL JOURNAL OF 3D PRINTING TECHNOLOGIES AND DIGITAL INDUSTRY

ISSN:2602-3350 (Online)

URL: https://dergipark.org.tr/ij3dptdi

OMEGA METAMATERYAL YAPISININ PENTA YAMA ANTENIN PERFORMANSINA ETKISI

THE EFFECT OF OMEGA METAMATERIAL STRUCTURE ON THE PERFORMANCE OF PENTAGONAL PATCH ANTENNA

Yazarlar (Authors): Bülent Urul (1914)

Bu makaleye şu şekilde atıfta bulunabilirsiniz (To cite to this article): Urul B., "Omega Metamateryal Yapısının Penta Yama Antenin Performansına Etkisi" Int. J. of 3D Printing Tech. Dig. Ind., 9(2): 155-163, (2025).

DOI: 10.46519/ij3dptdi.1598765

Araştırma Makale/ Research Article

OMEGA METAMATERYAL YAPISININ PENTA YAMA ANTENİN PERFORMANSINA ETKİSİ

Bülent Urul^a*

^aIsparta Uygulamalı Bilimler Üniversitesi, Teknik Bilimler Meslek Yüksekokulu, Elektronik ve Otomasyon Bölümü, TÜRKİYE

* Sorumlu Yazar: bulenturul@isparta.edu.tr

(Gelis/Received: 09.12.24; Düzeltme/Revised: 10.03.25; Kabul/Accepted: 12.06.25)

ÖZ

Bu çalışma, omega metamateryal yapılarının penta yama anten (PYA) performansına olan etkilerini incelemektedir. İlk olarak, 10.5 GHz merkez frekansı hedeflenerek PYA tasarlanmış ve CST yazılımı kullanılarak simüle edilmiştir. Referans antenin kazancı 3.042 dBi olarak elde edilmiştir. Daha sonra, çift negatif özelliklere sahip bir omega metamateryal tasarlanmış, elektriksel ve manyetik geçirgenlik değerleri belirlenmiş ve 9-13 GHz frekans aralığında negatif kırınım indisi gözlemlenmiştir. Bu özelliklerin metamateryalin etkin kullanımını mümkün kıldığı görülmüştür. Simülasyonlarda, omega metamateryal ile tek ve çift katmanlı lens tabakaları tasarlanmıştır. Tek katmanlı omega lens ile anten kazancında %30.51 artış sağlanmış ve kazanç değeri 3.97 dBi'ye ulaşmıştır. Çift katmanlı lens kullanımında ise lensler arası mesafe optimize edilerek 5.14 dBi kazanç elde edilmiş, bu değer referans anten kazancından %68.97 daha yüksek olmuştur. Bu bulgular, omega metamateryal yapılarının anten kazancını artırmada ve elektromanyetik yayılımın odaklanmasında önemli avantajlar sunduğunu göstermektedir. Sonuç olarak, bu çalışma metamateryal destekli anten tasarımında yenilikçi bir yaklaşım sunmakta ve uydu haberleşme gibi yüksek frekanslı uygulamalarda etkili çözümler önererek alanın ilerlemesine katkıda bulunmaktadır.

Anahtar Kelimeler: Penta Yama Anten, Metamateryal, Anten Kazancı

THE EFFECT OF OMEGA METAMATERIAL STRUCTURE ON THE PERFORMANCE OF PENTAGONAL PATCH ANTENNA

ABSTRACT

This study investigates the effects of omega metamaterial structures on the performance of pentagonal patch antennas (PPA). Initially, a PPA was designed targeting a central frequency of 10.5 GHz and simulated using CST software. The reference antenna achieved a gain of 3.042 dBi. Subsequently, an omega metamaterial with double-negative properties was designed, with its electrical and magnetic permeability values determined. A negative refractive index was observed in the 9-13 GHz frequency range, demonstrating the effective utilization potential of the metamaterial. In the simulations, single-and double-layer omega metamaterial lenses were designed. The single-layer omega lens resulted in a 30.51% increase in antenna gain, reaching a gain value of 3.97 dBi. For the double-layer lens configuration, optimizing the inter-layer distance yielded a gain of 5.14 dBi, which is 68.97% higher than the reference antenna's gain. These findings demonstrate that omega metamaterial structures offer significant advantages in enhancing antenna gain and focusing electromagnetic radiation. In conclusion, this study presents an innovative approach to metamaterial-supported antenna design and provides effective solutions for high-frequency applications, such as satellite communications, contributing to advancements in the field.

Keywords: Pentagonal Patch Antenna, Metamaterial, Antenna Gain.

1. GİRİS

Son yıllarda haberleşme teknolojilerinde yaşanan hızlı gelişmeler, daha etkili, yüksek performanslı ve kompakt antenlerin tasarımını zorunlu hale getirmiştir. Anten sistemlerinin performansını artırmak amacıyla kullanılan metamateryaller, bu alanda önemli bir yenilik olarak öne çıkmaktadır. Metamateryaller, doğal malzemelerde görülmeyen elektromanyetik özelliklere sahip yapay yapılar tanımlanır ve elektriksel (ɛ) ve manyetik geçirgenlik (μ) parametrelerinin negatif değerler alması gibi sıra dışı özellikler gösterebilirler. Bu özellikler, özellikle anten kazancı, yönlülük ve bant genişliği gibi performans metriklerini iyileştirme potansiyeline sahiptir [1-4].

Metamalzemeler ise elektromanyetik alanındaki çalışmalarda anten performansını arttırmak için sıklıkla kullanılan doğada kendiliğinden bulunmayan yapay bir malzemedir Özellikle [5]. mikrodalga çalışmalarında kullanılan mükemmel manyetik özellik gösteren ya da çoklu dielektrik katmanlara sahip frekans seçici yüzeyler olarak kullanılmaktadır [6-7]. Tasarım prosedürlerinde birim hücre geometrisi, dielektrik katmanların kalınlığı, kullanılan malzemelerin elektriksel ve manyetik özellikleri gibi kriterler önemlidir. Bu kriterler kullanılarak tasarım yoluyla elde edilen katmanın belirli bir frekans aralığında elektriksel ve manyetik geçirgenliğinin negatif olmasına çalışılır. Elde edilen yapının elektriksel ve manyetik geçirgenliklerinden bir tanesi bile istenen aralıkta negatif özellik gösteriyorsa yapı metamateryal bir yapı olarak adlandırılır [8-9].

oldukları Metamateryaller, sahip elektromanyetik özelliklere göre farklı kategorilere ayrılmaktadır. Negatif kırılma indisine metamatervaller. sahip elektromanyetik dalgaları olağan dışı yollarla vönlendirme yetenekleri nedeniyle anten ve dalga kılavuzu uygulamalarında kullanılır. Plazmonik metamateryaller, özellikle optik frekanslarda çalışarak ışığın manipülasyonunda önemli rol oynar [10]. Elektromanyetik band boşluklu (EBG) metamateryaller, belirli frekans bantlarında elektromanyetik dalgaların yayılmasını engelleyerek filtreleme ve gürültü azaltma uygulamalarında kullanılır [11].Ayrıca, programlanabilir ve yeniden yapılandırılabilir metamateryaller, dinamik olarak ayarlanabilir özellikleriyle 5G ve IoT uygulamalarında giderek daha fazla kullanılmaktadır [12]. Son yıllarda yapılan çalışmalar, bu yapıların yüksek kazançlı anten tasarımlarında ve elektromanyetik girişim azaltma uygulamalarında etkin bir şekilde kullanılabileceğini göstermektedir.

Khan 2013'te antenin genel boyutunda azalma sağlayan bir Koch beşgen fraktal yapısı kullanarak yeni bir küçültülmüş boyutta üç Koch Pentagonal fraktal sunulmustur [13]. Önerilen anten, temel fraktalizasyon için beşgen şekli kullanır ve ilk yinelemenin Koch fraktal deseniyle kazınmış iç tarafları ile birleştirerek antenin genel boyutunda küçülme sağlamıştır. Üçüncü yineleme önerilen fraktal anten için, ilk rezonans frekans bandında çalışan beşgen yama antenine kıyasla, ciddi bir oranda anten boyutunda küçültme elde etmiştir. Yine diğer bir çalışmada [14-15] fraktal yapılar için saçılma parametreleri incelenmiş ve Sierpinski vapısı için düsük geri saçılma parametresi elde edilebileceği ortaya konulmuştur.

Ramya 2017'dide metamateryal ile ilgili çalışmasında, ultra ince ve ultra geniş bant özelliklere sahip bir mikrodalga metamateryal emici tasarlamıstır. Bu yapı, 10.36–16.67 GHz %85'in üzerinde arasında absorpsiyon sağlayarak toplamda 6.31 GHz geniş bant absorpsiyon elde etmiştir. Asimetrik tasarım nedeniyle polarizasyon hassasiyeti gösterse de, geniş bant absorpsiyon normal ve eğik açılarda korunmuştur. Basit, kompakt ve yüksek performanslı bu tasarım, elektromanyetik girişim bastırma ve gizlilik uygulamaları için uygunluğunu, deneysel ve simülasyon sonuçları büyük ölçüde uyum göstererek ortaya koymuştur [16]. Yine 2017 yılında, Wu ve arkadaşları, ultra geniş bant (UWB) uvgulamaları için bir metamaterial mikroserit anten tasarlamış ve 2.9-33.7 GHz arasında %168.3 bant genisliği sağlamıstır. Anten, üstte düzensiz şekilli yuvalar ve altta ızgara desenli bir topraklama düzlemi kullanarak performansı artırmıştır. Ölçümler, maksimum %95.6 verimlilik ve 7.17 dB maksimum kazancı göstermiştir. Tasarım, yönlü radyasyon ve kompakt vapisivla UWB kablosuz iletisim sistemleri için uygun bir aday olarak öne çıkmıştır [17].

Yapılan diğer bir çalışmada omega şekilli metamateryal yapılarının mikroşerit anten performansı üzerindeki etkisi, Bilal Tütüncü ve arkadaşlarının çalışmasında kapsamlı şekilde ele alınmıştır. Çalışmada, bir omega şekilli metamateryal (OSM) lensin, Ku bandında çalışan referans bir mikroşerit anten üzerine yerleştirilmesiyle kazanç artışı sağlanmıştır. Tek katmanlı OSM lens kullanılarak 2.74 dB, çift katmanlı lens ile ise 4.08 dB kazanç artışı ölçülmüştür. Bu sonuçlar, metamateryallerin negatif kırınım indisi özelliklerinden faydalanarak elektromanyetik dalgaların odaklanması ve yönlülüğünün artırılabileceğini göstermektedir [18].

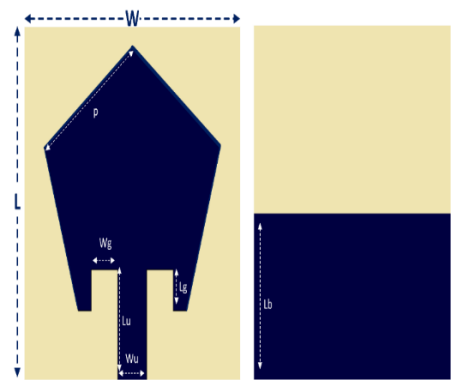
Bu çalışma ise penta fraktal yapısı kullanılarak elde edilen antenin önüne omega metamateryal yapısı lens olarak kullanılarak anten kazancı üzerine etkisi incelemeyi hedeflemektedir. Sonuç olarak, metamateryal teknolojisinin anten tasarımındaki potansiyeli, hem akademik de araştırmalarda hem endüstriyel uygulamalarda genis bir kullanım alanı bulmaktadır. Bu çalışmanın bulguları, anten performansının iyileştirilmesine yönelik yeni yaklaşımlar sunarak, haberleşme sistemlerinin daha verimli hale getirilmesine katkıda bulunmaktadır. Omega metamateryal yapılarının gelecekteki anten tasarımlarında yaygın olarak kullanılabileceği öngörülmektedir.

2. MATERYAL VE METOD

2.1 Anten Tasarımı ve Analizi

2.1.1 Penta Yama Anten Tasarımı

Bu çalısmada referans anten olarak Sekil 1'de görülen, tutarlı elektromanyetik yayılımı, tasarımının nispeten daha kolay olması nedeniyle penta yapısı (PYA) kullanılmıştır. Calışma frekansı olarak, 10.5 GHz merkez frekansı hedeflenmiştir.



Şekil 1. Referans anten (PYA) ön ve arka görünüşü

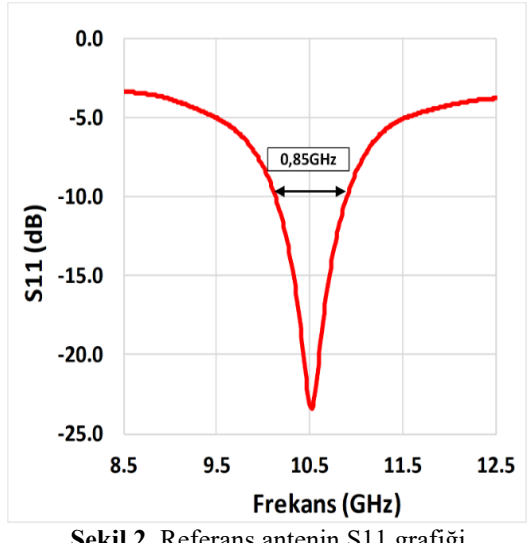
Tüm simülasyon işlemleri CST yazılımı kullanılarak yapılmıştır. PYA, FR4 madde özelliğine sahip bir alttaş üzerine tasarlanmıştır. Alttaşın boyutları 20 x 20 x 1.55 mm şeklindedir. FR4 alttaşın dielektrik sabiti Er = 4.3 ve tanjant kaybı tan $\delta = 0.025$ olarak alınmıştır. Antenin tasarım parametreleri Cizelge 1'de açıkça verilmiştir. Burada antenin yama kısmı ve arka kısmındaki metal kısım için bakır tercih edilmiştir.

Cizelge 1. PYA referans anten parametreleri

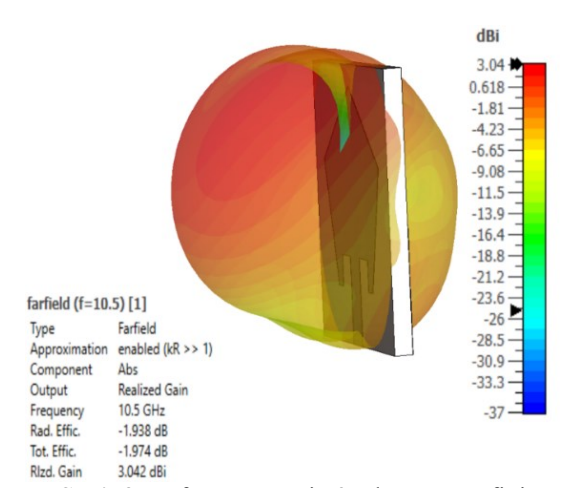
Parametreler	Değer(mm)
Anten Genişliği (W)	20
Anten Uzunluğu (L)	20
Penta Kenar uzunluğu (p)	9.41
Wg	2.3
Lu	6.3
Wu	2.5
Lg	2.27
Lb	9

Çizelge 1'deki anten parametrelerine göre elektromanyetik benzetim işlemleri elektromanyetik ölçüm programı olan CST programı ile 8.5 GHz ile 12.5 GHz frekans aralığında gerçekleştirilmiştir. Simülasyon işleminin sonuçlarına göre, antenin S11 grafiği

Şekil 2'de gösterildiği gibi ve kazanç grafiği de Şekil 3'te gösterildiği gibi elde edilmiştir. Şekil CMA'nın 2'de 10,5 GHz rezonans frekansındaki değeri -23,45 dB olduğu ve Şekil 3'de 3D anten kazancının 3,042 dBi olduğu görülmektedir. Antenin -10dB'deki band genişliği ise 0,85 GHz olarak elde edilmiştir.



Şekil 2. Referans antenin S11 grafiği



Şekil 3. Referans antenin 3D kazanç grafiği

2.2. Omega Şekli ile Metamateryal ve Lens Tasarımı

Bir hücrenin metamateryal olup olmadığını belirlemek için kırılım indisinin ϵ ve μ bağlı olarak negatif olması gerekmektedir. Burada 3 durum vardır; 1. Durumda sadece ε 'nun belirlenen frekans aralığında negatif olma durumu, 2.durum µ'nün negatif olma durumu ve 3. Durum ise her ikisinin de negatif olma durumudur. Bu üç durumdan birini sağlayan herhangi bir hücre için o hücrenin hangi frekans aralığında bu değerleri sağlıyorsa o frekans aralığı için metamaterval söylenebilmektedir. Bu ortam parametrelerinin hesaplanması için de literatürde Nicholson-Ross-Weir, Robust Metodu gibi birçok yöntem bulunmaktadır [19-20]. Genel olarak ortam parametreleri aşağıdaki şekilde elde edilebilmektedir.

Empedans (Z_e), kırılma indisi (N_e), S11 ve S21 arasındaki ilişki aşağıda verilen Denklem 1, 2, 3 ve 4 ile ifade edilebilir.

$$Z_e = \pm \sqrt{\frac{(1+S11)^2 - S_{21}^2}{(1-S11)^2 - S_{21}^2}} \tag{1}$$

$$e^{jN_ek_0d} = \frac{S_{21}}{1 - S_{11}\frac{Z_{e-1}}{I-J_{11}}} \tag{2}$$

Burada d etkin kalınlık, k0 ise dalga sayısıdır. Denklem 1'deki Ze empedansı için limit şartları $Re(Z_e) \ge 0$ ve $Im(Z_e) \ge 0$ olarak tanımlanabilir. Kırılma indisinin reel ve imajiner kısımları ise Denklem 3 ve Denklem 4 ile tanımlanır.

$$n_e = \frac{\text{Im}\left[\ln\left(\frac{S_{21}}{1 - S_{11}\frac{Z_e - 1}{Z_e + 1}}\right)\right]}{k_0 d} + \frac{2m\pi}{k_0 d}$$
(3)

$$k_e = \frac{-\operatorname{Re}[\ln{(e^{jN_e k_0 d})}]}{k_0 d} \tag{4}$$

Burada m, numunelerin etkin kalınlığına göre bir tam sayı olan faz periyodikliğini temsil eder ve m, bu makaledeki numune için 0 olarak alınabilir. Buna göre elektriksel ve manyetik geçirgenlik Denklem 5 ve 6'daki gibi ifade edilebilir [21].

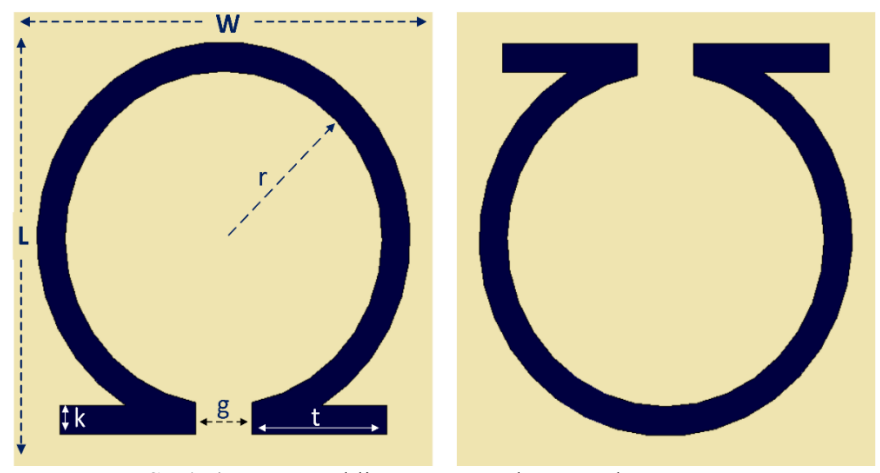
$$\mu_r = N_e Z_e \tag{5}$$

$$\varepsilon_r = \frac{N_e}{Z_e} \tag{6}$$

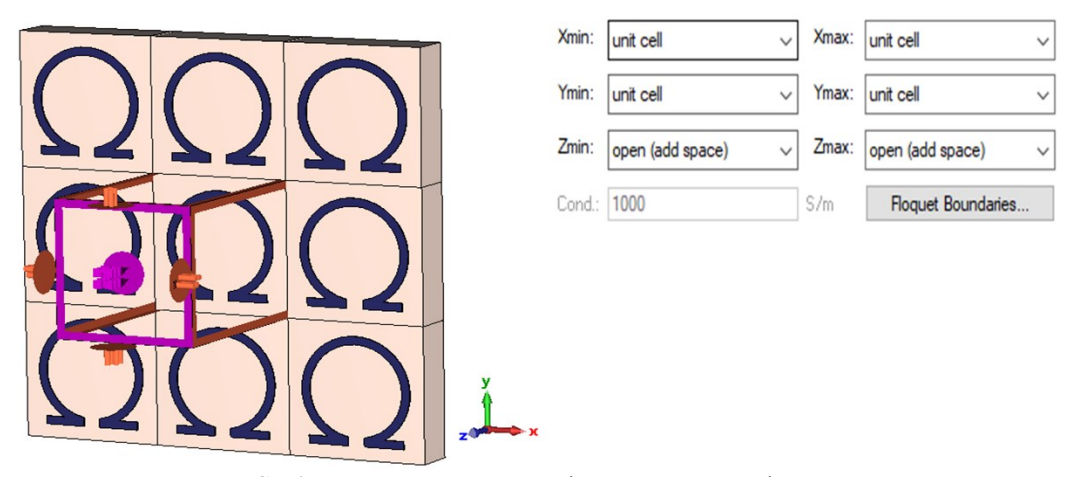
Bir hücrenin tasarım parametrelerine, kullanılan malzeme türüne göre şeklin ortam parametreleri belirlenebilmektedir. Bu amaçla Şekil 4'deki omega şekilli metamateryal hücresi tasarlanmıştır. Birim hücre oluşturmak için tasarım parametreleri Çizelge 2'de verildiği şekildedir. Birim hücre tasarımında periyodikliği sağlamak üzere sınır koşulları x ve y eksenleri için CST programında Şekil 5'de görüldüğü üzere unitcell olarak tercih edilmiştir. İstenilen frekans aralığında hücrenin negatif kırılım indeksine sahip olması için CST programının parameter sweep özelliği kullanılarak birçok denemeden sonra Şekil 6, 7 ve 8'de verilen sırasıyla μ , ε , ve n kırılım indisi grafikleri elde edilmiştir.

Çizelge 2. Omega metamateryal tasarım parametreleri

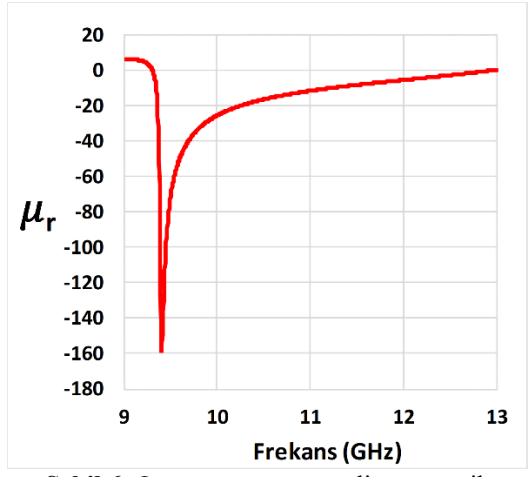
Parametreler	Değer(mm)
Alttaş Genişliği (W)	5
Alttaş Uzunluğu (L)	5
Yarıçap (r)	1.7
k	0.3
t	1.45
g	0.6



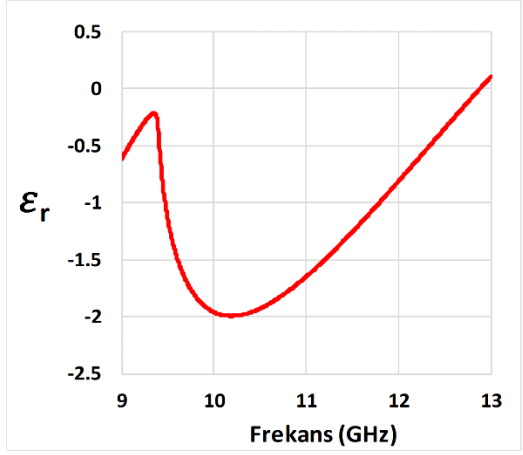
Şekil 4. Omega şekli metamateryal ön ve arka görünüş



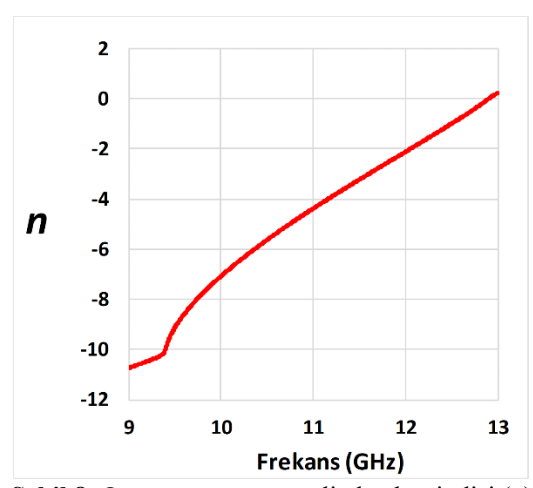
Şekil 5. Omega metamateryal tasarımı sınır şartları



Şekil 6. Omega metamateryalin manyetik geçirgenliği (μ_r)



Şekil 7. Omega metamateryalin elektriksel geçirgenliği (ε_r)



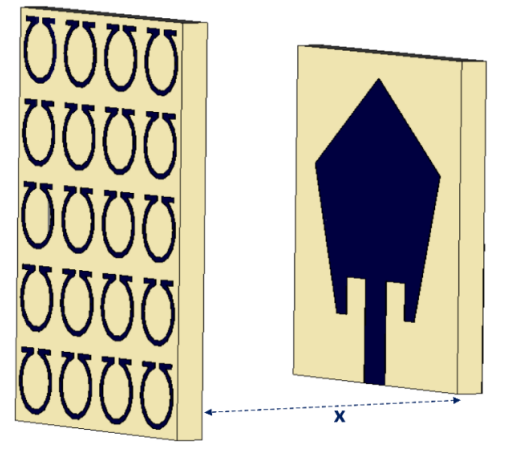
Şekil 8. Omega metamateryalin kırılım indisi (n)

Şekil 6 incelendiğinde tasarlanan omega hücresinin manyetik geçirgenliğinin 9.31 GHz ile 13 GHz arasında negatif olduğu ve Şekil 7 incelendiğinde ise 9 GHz ile 12.88 GHz aralığında negatif elektriksel geçirgenliğe sahip olduğu görülmektedir. Bu değerlere bağlı olarak ta Şekil 8'de görüldüğü üzere n kırılma indisin 9-12.9 GHz aralığında negatif olduğu görülmektedir. Bu değerlere göre 10.5 GHz merkez frekans olmak üzere omega birim hücresinin yaklaşık olarak 9-13 GHz aralığında double negatif metamateryal özelliği gösterdiği söylenebilir.

3. DENEYSEL BULGULAR

3.1. Omega Lens Tabakalarının Pya ile Kullanımı ve Sonuçları

Omega metamateryal yapısının PYA üzerine etkisini incelemek amacıyla 1.aşamada omega metamateryal yapısı 4x5'olmak üzere 20 adet olarak tek bir düzlem üzerinde antenin yayılım eksenini karşılamak üzere tasarlanmıştır. Daha sonra penta anteni önüne tek parça halinde eklenerek Şekil 9'daki yapı elde edilmiştir.



Şekil 9. Penta yama anten ve tek katman lens yapısı

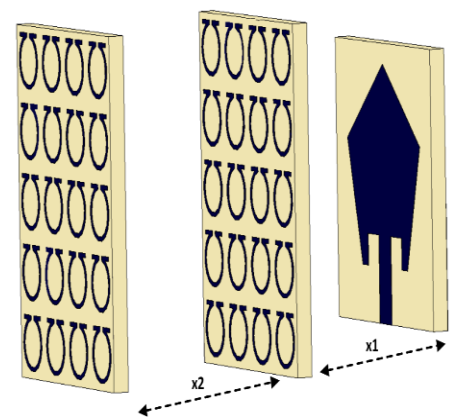
Daha sonra CST programı yardımıyla antenlens arası mesafe(x) 6-36 mm arasında 3mm aralıklarla değiştirilerek mesafeye bağlı olarak omega dizi lens tabakasının anten kazancına olan etkisi incelenmiş ve Çizelge 3 elde edilmiştir.

Çizelge 3. Tek katmanlı lens tabakasının anten uzaklığına göre kazanç değerleri

x (mm)	Kazanç(dBi)	Kazanç Artışı
6	2.48	-18.47%
9	1.92	-36.88%
12	2.56	-15.84%
15	3.21	5.52%
18	3.97	30.51%
21	3.22	5.85%
24	3.23	6.18%
27	3.42	12.43%
30	3.64	19.66%
33	3.72	22.29%
36	3.59	18.01%

Çizelge 3 incelendiğinde en iyi kazancın 3.97 dBi le 18 mm mesafede elde edildiği görülmektedir. Bu mesafe için tekli 4x5 omega lens tabakası ile yama anten üzerinde 30.51%'lik bir kazanç artışı elde edildiği görülmektedir.

2.aşamada omega lens tabakasından bir tane de daha tasarlanarak anten önüne Şekil 10'da görüldüğü üzere yerleştirilmiştir. Burada hem 1.lens tabakasının antenden uzaklığı, hem 1.lens tabakasının 2. Lens tabakasından uzaklığı önem kazanmaktadır. Bu nedenle bu iki aralık için CST programındaki parameter sweep özelliği kullanılarak 100'den fazla deneme yapılmıştır. Bunun için 1.lens tabakasının antenden uzaklığı ve 2. Lens tabakasının 1.lens tabakasından uzaklığı değiştirilerek Çizelge 4'deki anten kazanç değerleri elde edilmiştir.

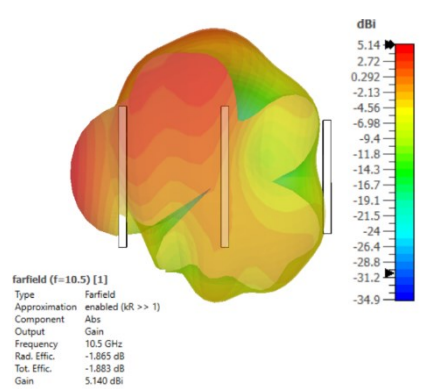


Şekil 10. Penta yama anten ve tek katman lens yapısı

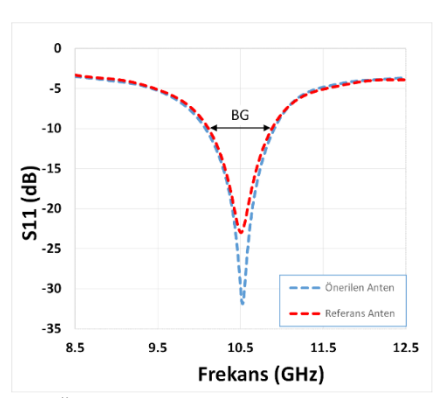
Çizelge 4. Çift katmanlı lens tabakasının anten uzaklığına göre kazanç değerleri

			. Çift katma								
<u>x1</u>	x2	Kazanç	Kazanç	x1	x2	Kazanç	Kazanç	x1	x2	Kazanç	Kazanç
(mm)	(mm)	(dBi)	Artış	(mm)	(mm)	(dBi)	Artış	(mm)	(mm)	(dBi)	Artış
6	6	0.58	-80.93%	15	36	3.6	18.34%	27	24	3.27	7.50%
6	9	0.12	-96.06%	15	39	3.27	7.50%	27	27	3.18	4.54%
6	12	-0.21	-106.90%	15	42	3.24	6.51%	27	30	3.21	5.52%
6	15	0.18	-94.08%	15	45	3.16	3.88%	27	33	3.46	13.74%
6	18	0.22	-92.77%	18	6	3.95	29.85%	27	36	3.67	20.64%
6	21	0.14	-95.40%	18	9	4	31.49%	27	39	3.51	15.38%
6	24	0.18	-94.08%	18	12	3.89	27.88%	27	42	3.46	13.74%
6	27	0.23	-92.44%	18	15	3.97	30.51%	27	45	3.46	13.74%
6	30	-0.29	-109.53%	18	18	3.89	27.88%	30	6	3.86	26.89%
6	33	0.24	-92.11%	18	21	3.42	12.43%	30	9	3.74	22.95%
6	36	0.45	-85.21%	18	24	4.42	45.30%	30	12	3.62	19.00%
6	39	0.38	-87.51%	18	27	3.71	21.96%	30	15	3.48	14.40%
6	42	0.11	-96.38%	18	30	4.15	36.42%	30	18	4.01	31.82%
6	45	0.45	-85.21%	18	33	4.69	54.17%	30	21	3.5	15.06%
9	6	1.81	-40.50%	18	36	4.72	55.16%	30	24	3.51	15.38%
9	9	2.13	-29.98%	18	39	4.32	42.01%	30	27	3.44	13.08%
9	12	2.37	-22.09%	18	42	4.15	36.42%	30	30	3.47	14.07%
9	15	2.54	-16.50%	18	45	4.34	42.67%	30	33	3.66	20.32%
9	18	3.55	16.70%	21	6	3.94	29.52%	30	36	3.78	24.26%
9	21	3.43	12.75%	21	9	3.68	20.97%	30	39	3.82	25.58%
9	24	1.94	-36.23%	21	12	3.49	14.73%	30	42	3.77	23.93%
9	27	2.17	-28.67%	21	15	3.25	6.84%	30	45	3.74	22.95%
9	30	2.35	-22.75%	21	18	4.5	47.93%	33	6	4.16	36.75%
9	33	3.08	1.25%	21	21	5.14	68.97%	33	9	4.04	32.81%
9	36	3.41	12.10%	21	24	3.88	27.55%	33	12	3.88	27.55%
9	39	2.17	-28.67%	21	27	3.24	6.51%	33	15	3.62	19.00%
9	42	2.09	-31.30%	21	30	3.44	13.08%	33	18	4.12	35.44%
9	45	2.25	-26.04%	21	33	4.34	42.67%	33	21	3.73	22.62%
12	6	2.48	-18.47%	21	36	5.12	68.31%	33	24	3.67	20.64%
12	9	2.67	-12.23%	21	39	3.54	16.37%	33	27	3.53	16.04%
12	12	2.82	-7.30%	21	42	3.82	25.58%	33	30	3.48	14.40%
12	15	2.86	-5.98%	21	45	3.77	23.93%	33	33	3.91	28.53%
12	18	2.93	-3.68%	24	6	3.51	15.38%	33	36	4.02	32.15%
12	21	2.88	-5.33%	24	9	3.34	9.80%	33	39	4.11	35.11%
12	24	2.31	-24.06%	24	12	3.22	5.85%	33	42	3.96	30.18%
12	27	2.37	-22.09%	24	15	3.08	1.25%	33	45	3.84	26.23%
12	30	2.51	-17.49%	24	18	3.98	30.83%	36	6	4.18	37.41%
12	33	3.17	4.21%	24	21	4.12	35.44%	36	9	3.91	28.53%
12	36	3.17	2.89%	24	24	3.14	3.22%	36	12	3.76	23.60%
12	39	2.52	-17.16%	24	27	2.98	-2.04%	36	15	3.5	15.06%
12	42	2.58	-15.19%	24	30	3.02	-0.72%	36	18	3.94	29.52%
12	45	2.54	-16.50%	24	33	3.61	18.67%	36	21	4.11	35.11%
15	6	3.23	6.18%	24	36	4.15	36.42%	36	24	3.62	19.00%
15	9	3.34	9.80%	24	39	3.49	14.73%	36	27	3.45	13.41%
15	12	3.42	12.43%	24	42	3.49	7.82%	36	30	3.43	9.47%
15	15	3.42	9.80%	24	45	3.24	6.51%	36	33	3.78	24.26%
15	18	3.34 4.5	9.80% 47.93%	2 4 27	6	3.24	17.36%	36	36	3.78 4.24	39.38%
15 15	21	3.23	6.18%	27	9	3.46	13.74%	36	39 42	3.93	29.19%
15	24	3.21	5.52%	27	12	3.35	10.12%	36	42	3.74	22.95%
15	27	3.2	5.19%	27	15	3.22	5.85%	36	45	3.64	19.66%
15	30	3.11	2.24%	27	18	3.84	26.23%				
15	33	3.93	29.19%	27	21	3.38	11.11%				

Cizelge 4 incelendiğinde en iyi uzaklık değerlerinin x1=21mm ve x2=21mm olduğu görülmektedir. Bu uzaklık değerleri için 10.5 GHz frekansındaki en yüksek kazanç değerinin 5.14 dBi olduğu ve bu değerin referans antenin kazancına göre 68,97% daha yüksek olduğu görülmektedir. Yine bu uzaklık değerlerine göre omega lensleriyle elde dilen yapının 3D kazanç grafiği Şekil 11'de verildiği şekildedir. Ayrıca simülasyon sonuçlarına göre elde edilen referans ve önerilen antenin S11 karşılaştırma grafiği Sekil 12'de verilmistir. Sekil 12 incelendiğinde önerilen antenin rezonans frekansında çok az bir kayma ile rezonans frekansı 10.51 GHz olmuş ve bu frekanstaki S11 değeri gelişim sağlayarak 32 dB olarak elde edilmiştir. Bununla birlikte referans antenin band genişliği 0.85 GHz iken önerilen antenin band genişliği 0.96 GHz'e yükselmiştir.



Şekil 11. Çift lensli anten yapısı 3D kazanç grafiği



Şekil 12. Önerilen ve referans anten S11 grafikleri

4. SONUC

Bu çalışmada omega metamateryal yapısının penta yama antenin (PYA) üzerine etkisi incelenmiştir. Bunun için ilk olarak bir PYA' i elektromanyetik programı yardımıyla tasarlanmış ve simüle edilmiştir. Simülasyon sonucunda anten kazancı bir uydu haberleşme frekansı olan 10.5 GHz için 3.042 dBi olarak elde edilmiştir. Daha sonra bir metamateryal

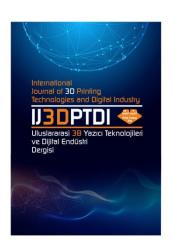
yapısı olan omega yapısı tasarlanmış ve belirlenen frekans aralığında elektriksel ve manyetik geçirgenlikleri elde edilmiştir. Bu değerlere göre 10.5 GHz frekansı için omega yapısının kırılım indeksi negatif olarak elde edilmis ve metamaterval olarak kullanılabileceği gösterilmiştir. Daha sonra omega metamateryal yapısıyla bir lens tabakası tasarlanmış ve PYA'i önüne eklenerek simüle edilmiştir. Simülasyon sonucunda 3.97 dBi anten kazancı elde edilerek referans antene göre anten kazancında 30.51% artıs elde edilmistir. Daha sonra ikinci bir lens tabakası yine omega metamateryal yapısıyla tasarlanarak referans anten önüne 2 tabaka halinde konulmuştur. Burada lens tabakaları arası mesafe ve lens tabakalarının referans antene olan mesafeleri ayarlanarak 100'den fazla simülasyon işlemi gerçekleştirilmiştir. Simülasyonların sonucuna göre çift lens tabakalı antenin kazancı 5.14 dBi elde edilmiştir. Bu kazanç değeri referans anten kazancına göre 68.97% daha fazladır. Bununla birlikte antenin band genişliği 13% oranında omega artmıştır. Bu değerlere göre metamateryal yapısının PYA yapısı ile birlikte kullanımında anten kazancında ciddi iyileştirilmeler elde edilebileceği ortaya konulmuştur.

KAYNAKLAR

- 1. Veselago, V.G., "The electrodynamics of substances with simultaneously negative values of ϵ and μ ", Usp. fiz. nauk, Vol. 92, Issue 3, Pages 517-526, 1967.
- 2. Smith, D.R., Pendry, J.B. and Wiltshire, M.C.K., "Metamaterials and negative refractive index", Science, Vol. 305, Issue 5685, Pages 788-792, 2004.
- 3. Pendry, J. B., Holden, A. J., Robbins, D. J. and Stewart, W. J., "Magnetism from conductors and enhanced nonlinear phenomena", IEEE transactions on microwave theory and techniques, Vol. 47, Issue 11, Pages 2075-2084, 1999.
- 4. Urul, B., "Fraktal yapılar ile yüksek kazançlı yansıtıcı dizi anten tasarımı", International Journal of 3D Printing Technologies and Digital Industry, Vol. 6, Issue 3, Pages 408-415, 2020.
- 5. Urul, B., "Gain enhancement of microstrip antenna with a novel DNG material", Microwave and Optical Technology Letters", Vol. 62, Issue 4, Pages 1824-1829, 2020.

- 6. Lanuzza, L., Monorchio, A. and Manara, G., "Synthesis of high-impedance FSSs using genetic algorithms", IEEE Antennas Prop. Soc Int. Symp 4, Pages 364-367, 2002.
- 7. Yuan, Y., Chan, C. H., Man, K. F. and Luk, K. M., "Metamaterial surface design using the hierarchical genetic algorithm", Microwave and Optical Technology Letters, Vol. 39, Issue 3, Pages 226-230, 2003.
- 8. Chan, C.H., "Analysis of frequency selective surfaces, Ch. 2, in Frequency selective surface and grid array", Wiley Inter-Science, New York, Pages 27-85, 1995.
- 9. Manara, G., Monorchio, A. and Mittra, R., "Frequency selective surface design based on genetic algorithm", Electron Lett Vol. 36, Pages 1400-1401, 1999.
- 10. Yılmaz M., "Nano Ölçekli Işık Manipülasyonu İçin Optik Nanoantenlerin İncelenmesi", Yüksek Lisans Tezi, Konya Teknik Üniversitesi, 2022.
- 11. Alam, M. S., Islam, M. T. and Misran, N., "Electromagnetic Band Gap Structure for Microstrip Antenna Gain *Enhancement at WLAN Band*", IEEE Asia-Pacific Conference on Applied Electromagnetics (APACE), Pages 1-4, 2020.
- 12. Tian, J., Cao, W., "Reconfigurable flexible metasurfaces: from fundamentals towards biomedical applications", PhotoniX , Vol 5, Issue 2, 2024.
- 13. Khan, O. M., Islam, Z. U., Rashid, I., Bhatti, F. A. and Islam, Q. U., "Novel miniaturized Koch pentagonal fractal antenna for multiband wireless applications", Progress in Electromagnetics Research, Vol. 141, Pages 693-710, 2013.

- 14. Yu, Z.W., Wang, G.M., Gao, X.J. and Lu, K., "A novel small-size single patch microstrip antenna based on Koch and Sierpinski fractal-shapes", Progress in Electromagnetics Research Letters, Vol. 17, Pages 95-103, 2010.
- 15. Li, D. and Mao, J.F., "Koch-like sided Sierpinski gasket multifractal dipole antenna", Progress in Electromagnetics Research, Vol. 126, Pages 399-427, 2012.
- 16. Ramya, S. and Rao, I. S., "A compact ultra-thin ultra-wideband microwave metamaterial absorber", Microwave and Optical Technology Letters, Vol 59, Issue 8, Pages 1837-1845, 2017.
- 17. Wu, W., Yuan, B., Guan, B. and Xiang, T., "A bandwidth enhancement for metamaterial microstrip antenna", Microwave and Optical Technology Letters, Vol. 59, Issue 12, Pages 3076-3082, 2017.
- 18. Tutuncu, B., Torpi, H. and İmeci, S. T., "Directivity improvement of microstrip antenna by inverse refraction metamaterial", Journal of Engineering Research, Vol. 7, Issue 4, Pages 151-164, 2019.
- 19. Shi, Y., Hao, T., Li, L. and Liang, C.H., "An improved NRW method to extract electromagnetic parameters of metamaterials", Microwave Optical Technology Letters, Vol. 58, Issue 3, Pages 647-652, 2016.
- 20. Shi, Y., Li, Z.Y., Li, L. and Liang, C.H., "An electromagnetic parameters extraction method for metamaterials based on phase unwrapping technique", Waves Random Complex Medium, Vol. 26, Issue 4, Pages 417-433, 2016.
- 21. Hu, D., Zhao, R., Du, L. and Wang, Y., "Design, simulation and measurement of an omega metamaterial at X band", In 2017 Sixth Asia-Pacific Conference on Antennas and Propagation, APCAP, IEEE, Pages 1-3, 2017.



ULUSLARARASI 3B YAZICI TEKNOLOJİLERİ VE DİJİTAL ENDÜSTRİ DERGİSİ

INTERNATIONAL JOURNAL OF 3D PRINTING TECHNOLOGIES AND DIGITAL INDUSTRY

ISSN:2602-3350 (Online)

URL: https://dergipark.org.tr/ij3dptdi

TRANSFORMING VIRTUAL REALITY TOURISM THROUGH THE CYBER ISPARTA YOUTH CENTER

Yazarlar (Authors): Yasin Tekin *, Ebru Yılmaz İnce

Bu makaleye şu şekilde atıfta bulunabilirsiniz (To cite to this article): Tekin Y., İnce Y. E., "Transforming Virtual Reality Tourism Through The Cyber Isparta Youth Center" Int. J. of 3D Printing Tech. Dig. Ind., 9(2): 164-170, (2025).

DOI: 10.46519/ij3dptdi.1616176

Araştırma Makale/ Research Article

Erişim Linki: (To link to this article): https://dergipark.org.tr/en/pub/ij3dptdi/archive

TRANSFORMING VIRTUAL REALITY TOURISM THROUGH THE CYBER ISPARTA YOUTH CENTER

Yasin Tekin^a, Ebru Yılmaz İnce^b

^aIsparta Municipality, TÜRKİYE ^bIsparta University of Applied Science, Computer Technologies Department, TÜRKİYE

* Corresponding Author: yasintekin32@gmail.com

(Received: 09.01.25; Revised: 25.04.25; Accepted: 26.06.25)

ABSTRACT

In recent years, virtual reality (VR) technology has transformed various sectors, and tourism is no exception. Virtual reality tourism offers an innovative way for people to experience the world without actually leaving their homes. In this research, the "Cyber Isparta Youth Center" project, supported by the Western Mediterranean Development Agency, implemented by the Isparta Municipality and in partnership with the Isparta University of Applied Sciences, will be discussed in terms of education and tourism. Within the scope of the project, a virtual reality tour of the Cyber Isparta Youth Center was developed. The developmental research strategy, a variant of the design-based research method, was used. Cyber Isparta Youth Center has been modeled in the Unity Game Engine. A semi-structured interview was conducted to examine the effects of the virtual tour. Participant opinions were categorized into three primary groups based on the content analysis: tourism & usability, technological experience, and educational value.

Keywords: Virtual reality, Tourism, Youth Center, Unity.

1. INTRODUCTION

In recent years, virtual reality (VR) technology has transformed various sectors, and tourism is no exception. Virtual reality tourism offers an innovative way for people to experience the world without actually leaving their homes. This article explores what virtual reality tourism entails, its benefits, current examples, and its future potential, accompanied by relevant references. Virtual reality tourism refers to the use of VR technology to create immersive travel experiences. This technology allows users to explore destinations in a simulated environment, providing a 360-degree view of landscapes, historical sites, and cultural landmarks. With VR headsets, users can walk through famous streets, visit museums, or even partake in activities such as skydiving or underwater diving, all from their living rooms [1].

One of the most significant advantages of virtual reality tourism is that it makes travel accessible to everyone. Individuals with physical disabilities, health issues, or financial constraints can explore destinations they may never have the chance to visit in real life [2]. Traveling can be expensive, considering accommodation, flights, food, and activities, but VR tourism eliminates these costs, allowing users to experience various destinations without the financial burden [3].

VR allows travelers to explore unfamiliar places without risk, as adventurous activities, like bungee jumping or hiking in remote areas, can be experienced safely in a virtual environment [4]. Experiencing a destination through VR can ignite a desire to visit in person, by providing a taste of what's available, virtual reality can promote actual travel plans [5]. Educational institutions can use VR to take students on virtual field trips, showcasing historical sites, natural wonders, or artistic masterpieces [6].

Several companies and organizations have started integrating VR experiences into their offerings. For instance, airlines and travel agencies now provide virtual tours of destinations to enhance booking experiences.

Museums and cultural institutions are also embracing VR by creating digital exhibits and virtual events [7]. Platforms like Oculus, HTC Vive, and Sony PlayStation VR host a variety of travel-related content, allowing users to explore locations such as Machu Picchu or the Great Barrier Reef. Additionally, tourism boards are increasingly employing VR in their marketing strategies to entice potential visitors [8].

In this research, the "Cyber Isparta Youth Center" project, supported by the Western Mediterranean Development Agency, implemented by the Isparta Municipality and in partnership with the Isparta University of Applied Sciences, will be discussed in terms of education and tourism. Within the scope of the project, a virtual reality tour of the Cyber Isparta Youth Center was developed.

2. METHODOLOGY

The developmental research strategy, a variant of the design-based research method, was used in this study. Design-based research is used to develop learning tools [9]. Product design and educational program development are the two types of developmental research product or program development [10]. In this study, using the developmental research product method, virtual reality material has been developed. Cyber Isparta Youth Center has been modeled in the Unity Game Engine. Software Development Kit (VR SDK) is configured for Oculus glasses.

The application development stages are presented below;

Stage and Camera Settings for VR: When using VR glasses, you need to use special VR cameras instead of traditional Unity cameras. The main camera was removed and a new VR camera prefab, OVRCameraRig prefab, was added to the scene depending on the targeted VR SDK.

Adding VR Glasses Controls: Appropriate controller prefabs were added to the scene to interact with VR controllers (hand levers, motion sensors, etc.). Oculus SDKs provide the necessary components to manage the inputs of VR controllers.

Interaction and Movement: Movement in the VR environment is usually done with a

"teleportation" (jumping) or "free movement" system to provide user movement. Ready-made movement scripts and teleportation systems were used with the Oculus SDK. Interactions were added using interactive objects colliders and raycast for the user to receive instructions in mission mode. The primary character performs tasks with interactions such as grabbing, picking up and throwing objects.

Testing and Editing:To connect and test the VR headset, the VR headset was connected to the computer and worked on in the Unity Editor to test the developed project. During the test, interactions in the scene were observed using the headset. For optimization, the frame rate was optimized to reach up to 90 fps. In addition, optimization techniques such as LOD (Level of Detail), occlusion culling, light baking and efficient asset management were applied.

Finalization and Publishing: While creating VR projects, the VR headset was selected as the target when making project settings for the target platform Oculus.

A semi-structured interview was conducted to examine the effects of the virtual tour in terms of education and tourism. 30 users were asked what they thought about the tour after the virtual tour experience. User opinions were presented in the form of category, code and frequency with content analysis.

3. FINDINGS

3.1. Cyber Isparta Youth Center

Isparta Municipality, in partnership with Isparta University of Applied Sciences, has put into service the Western Mediterranean Development Agency's 'Entrepreneurship Ecosystem Development Financial Support Program' under the name Cyber Isparta Youth Center for the development of young people (Figure 1).



Figure 1. Cyber Isparta Youth Center.

The center provided training in many areas such as cyber security, mobile and web-based application development, robotic coding, social media expertise, and digital assistance (Figure 2).



Figure 2. Course participants.

In addition to the trainings, Cyber Isparta Youth Center has pre-incubation rooms for students to develop projects in research and development classes (Figure 3).



Figure 3. Pre-incubation rooms.

3D printers and virtual reality glasses are provided to the users free of charge at the center for the project development of the company candidates (Figure 4). There have been many IT projects developed at the Cyber Isparta Youth Center, one of which is the virtual reality tourism project.



Figure 4. 3D printers and virtual reality glasses.

3.2. Virtual Reality Tourism: Cyber Isparta Youth Center

Cyber Isparta Youth Center virtual reality tourism project was developed for promotional purposes. It allows the center to be visited with virtual reality glasses. In fairs, the center aims to be visited with virtual reality technology and to attract visitors to the center (Figure 5).



Figure 5. Cyber Isparta Youth Center building exterior.

Cyber Isparta Youth Center Virtual Tour has been modeled in the Unity Game Engine and coded with C#. Visitors can view classrooms where training is given on informatics (Figure 6).



Figure 6. Classrooms.

In the Cyber Isparta Youth Center virtual reality tourism project, the center facilities are presented in a virtual environment. In the virtual tour, the visitor can tour the center as visitor wishes. Visitor can view the virtual universe classroom, robotics classroom and 3D printer facilities (Figure 7, Figure 8).



Figure 7. Virtual universe classroom



Figure 8. 3D printer.

In the virtual tour, visitors can also visit the "research and development halls" and the preincubation center. During the tour, information about the center is given by voice.



Figure 9. Research and development halls.

Also, the visitor can take part in the virtual tour and must follow the instructions to perform the task. For example, the tasks of starting the 3D printer and taking the virtual reality glasses to the instructor are presented in Figures 10 and 11.



Figure 10. Starting the 3D printer task.



Figure 11. Taking the virtual reality glasses to the instructor task.

3.3. Virtual Tour Participant Opinions

According to the content analysis, participant feedback was grouped under three main categories: Educational Value, Technological Experience, and Tourism & Usability. In the Educational Value category, the frequently mentioned theme was interaction, with a frequency of 9 (see Table 1). This was followed by attractiveness (7), learning (6), instructiveness (5), and encouragement to technology (5). Within the Technological Experience category, the most emphasized codes were use of technology (7) and realism (6), indicating participants' appreciation of the strong and immersive technological infrastructure. In the Tourism & Usability category, accessibility was highlighted most frequently (8), followed by promotion (5), touristic value (4), user-friendliness (4), multipurpose design (4), smooth navigation (3), and scalability (3). These findings indicate that the virtual tour is perceived as an effective tool in both educational and digital tourism contexts.

Table 1. Participants' opinions virtual reality tourism

Category	Code	F
	Attractiveness	7
Educational Value	Interaction	9
	Learning	6
	Instructiveness	5
	Encouragement to	5
	Technology	3
Technological	Realism	6
Experience	Use of Technology	7
	Accessibility	8
	Promotion	5
Tourism &	Touristic Value	4
10011011100	User-friendliness	4
Usability	Smooth Navigation	3
	Multi-purpose Design	4
	Scalability	3

Sentences quoted verbatim from the participants' virtual tour opinions:

Educational Value

"The virtual tour was very appealing and kept my interest throughout. The environment was engaging and visually captivating." (Attractiveness, f=7).

"I really enjoyed the interactive tasks in the VR tour. It wasn't just passive viewing; I could actively participate and complete tasks." (Interaction, f=9).

"I learned a lot about technology, robotics, and 3D printing. The virtual tour provided a great opportunity to understand these topics in depth." (Learning, f=6).

"The tasks in the virtual tour were very informative. I could easily understand the concepts being taught through the interactive components." (Instructiveness, f=5).

"This tour really inspired me to learn more about the technology behind virtual reality and robotics. It made me more interested in these fields." (Encouragement to Technology, f=5).

Technological Experience

"The sense of realism was incredible. It felt like I was actually there, interacting with the technology and machinery in the classes." (Realism, f=6).

"The use of technology was amazing. The VR setup, along with the robotics and 3D printing demonstrations, was a seamless experience that made everything feel cutting-edge." (Use of Technology,

Tourism & Usability

"The tour was very easy to access, and I had no trouble navigating through the virtual environment. It was user-friendly and available to anyone." (Accessibility, f=8).

"This virtual tour is a great promotional tool for the Isparta Youth Center. It allows people to explore the center without physically visiting it." (Promotion, f=5).

"For tourists, this is a great way to explore Isparta from a distance. It provides a unique experience that highlights the region's technological achievements." (Touristic Value, f=4).

"The interface was very intuitive, and I had no trouble finding my way through the different classes and tasks. It was simple yet effective." (User-friendliness, f=4).

"Navigation within the tour was very smooth. I never got lost and could easily move between

different areas of the center." (Smooth Navigation, f=3).

"I like how this virtual tour serves multiple purposes. It's not only educational, but also functions as a digital tourism tool, allowing both tourists and students to engage." (Multi-purpose Design, f=4).

"I believe this system could be scaled to reach even more people, which would be great for educational and tourism purposes in the future." (Scalability, f=3).

4. RESULTS AND DISCUSSION

Informatic literacy initiatives at youth centers continue to have a significant impact on closing the digital divide [11]. These initiatives level the playing field and provide equal chances for success by guaranteeing that all young people have access to the required resources and information. Another significant result is the promotion of creativity and innovation [12]. Young people are better equipped to create, develop, and make significant contributions to society as their informatics skills improve [13-14]. Young brains may turn ideas into reality when they are exposed to coding, digital design, and data science since these fields foster an imaginative mentality.

Youth development is revolutionized by the incorporation of informatics literacy programs into youth centers [15-16]. By utilizing these easily available educational tools, creating encouraging surroundings, putting successful programs into place, and tackling the digital divide, we lay the groundwork for a better, more technologically savvy future [17].

As technology continues to advance, the future of virtual reality tourism looks promising. Improvements in VR hardware and software will allow for even more immersive and realistic experiences. Integration with artificial intelligence (AI) could personalize experiences based on user preferences, while advancements in haptic technology could provide a tactile element to virtual tours [18]. Moreover, as global travel continues to face challenges such as pandemics and environmental concerns, virtual reality tourism may offer a sustainable alternative. Travelers can explore the world and its wonders without the carbon footprint that physical travel often incurs [19-20].

5. CONCLUSION

Virtual reality tourism is revolutionizing the way we think about travel. By making exploration accessible, cost-effective, and safe, VR opens up a world of possibilities for those eager to experience new places and cultures. As technology evolves, the virtual tourism landscape will expand, offering even more immersive experiences. Whether as a supplement to traditional travel or as a standalone experience, virtual reality tourism is here to stay, inviting everyone to explore the globe from the comfort of their homes.

VR is helping to transform the tourism sector by offering significant opportunities and innovative experiences. Some of the benefits of virtual reality in tourism are:

- •Virtual tours and promotions,
- •Cost and time savings,
- •Accessibility and inclusiveness,
- •Education and information,
- •Post-trip interaction,
- •New marketing and sales opportunities,
- •Facilitating travel decisions,
- •Individual experiences and needs.

Participant opinions were categorized into three primary groups based on the content analysis: Tourism & Usability, Technological Experience, and Educational Value. In terms of educational value, the most emphasized code was interaction (f=9). Participants highlighted not only passive viewing but also the importance of task completion and interactive learning processes. Regarding the technological experience, participants particularly emphasized the sense of realism and the effective use of technology. From the perspective of tourism and usability, the system's accessibility (f=8) and its potential for promotion were found to be significant. Additionally, the multi-purpose structure of the application, which appeals to both tourists and students, was particularly noteworthy.

As result, virtual reality offers great potential in the tourism sector for both travel companies and tourists. VR is used as a very important tool both in terms of marketing and in the decision-making processes of tourists. It also creates significant opportunities in terms of accessibility and inclusiveness.

ACKNOWLEDGES

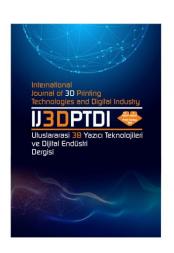
Project support was received within the scope of the Future is Future with Cyber in Isparta Project numbered TR61/22/GEG/0008, which is the Financial Support Program for the Development of Entrepreneurship Ecosystem of the Western Mediterranean Development Agency. The authors would like to thank the Western Mediterranean Development Agency for the financial support provided within the scope of the Project.

REFERENCES

- 1.Duziak, D., "Blockchain for Hospitality and Tourism: A Guide to the Future", Pages 87-113, Apress, Newyork, 2023.
- 2. Foggin, B., "Tourism in the leisure lives of people with disability". Buhalis D. and Darcy S. Editors, Accessible Tourism, Pages 98-122, Channel View Publications, Bristol, 2011.
- 3. Siddiqui, M. S., Syed, T. A., Nadeem, A., Nawaz, W., and Alkhodre, A., "Virtual tourism and digital heritage: an analysis of VR/AR technologies and applications", International Journal of Advanced Computer Science and Applications, Vol. 13 Issue 7, 2022.
- 4. Mallikarjuna, B., Sebastian, S., Chandra, R., Dadheech, P., and Sharma, M., "Virtual Reality in Tourism Industry within the Framework of Virtual Reality Markup Language", IEEE 3rd World Conference on Applied Intelligence and Computing (AIC), Gwalior, Pages 274-279, 2024.
- 5. Vinnakota, S., Mohan, M. D., Boda, M. J., Askarzai, W., Devkota, M. P., Shetty, M. S., and Choden, M. T., "Venturing into virtuality: exploring the evolution, technological underpinnings, and forward pathways of virtual tourism", Educational Research (IJMCER), Vol 5 Issue 6, Pages 08-49, 2023.
- 6. Asif, M., Mondal, A., Soumil, S., Das, A., & Sahoo, P., "Augmented Reality and Virtual Reality in Education: A Transformative Journey into Immersive Learning Environments", Kumar, R., Dhar, A., Banerjee, A. and Mahapatra, a. Editors, Advances in Computational Solutions, Pages 185-204, 2024.
- 7. Kamariotou, V., Kamariotou, M., and Kitsios, F., "Strategic planning for virtual exhibitions and visitors' experience: A multidisciplinary approach for museums in the digital age". Digital Applications in Archaeology and Cultural Heritage, Vol. 21, e00183, 2021.

- 8. Buhalis, D., Leung, D., and Lin, M., "Metaverse as a disruptive technology revolutionising tourism management and marketing", Tourism Management, Vol. 97, 104724, 2023.
- 9. Brown, A. L. "Design experiments: Theoretical and methodological challenges in creating complex interventions in classroom settings". Journal of the Learning Sciences, Vol. 2 Issue 2, Pages 141–178, 1992.
- 10. Richey, R.C., Klein, J.D. and Nelson, W. A., "Development research: Studies of instructional design and development", Jonassen D. H. Editor, Handbook of research for educational communications and technology, Mahwah, NJ: Lawrence Erlbaum Associates, Pages 141-150, 2013.
- 11. Detlor, B., Julien, H., La Rose, T., and Serenko, A., "Community-led digital literacy training: Toward a conceptual framework". Journal of the Association for Information Science and Technology, Vol. 73 Issue 10, Pages 1387-1400, 2022.
- 12. Rayna, T. and Striukova, L., "Fostering skills for the 21st century: The role of Fab labs and makerspaces", Technological Forecasting and Social Change, Vol. 164, 120391, 2021.
- 13. Stofkova, J., Poliakova, A., Stofkova, K. R., Malega, P., Krejnus, M., Binasova, V., and Daneshjo, N., "Digital skills as a significant factor of human resources development". Sustainability, Vol 14 Issue 20, 13117, 2022.

- 14. Li, L., "Reskilling and upskilling the futureready workforce for industry 4.0 and beyond", Information Systems Frontiers, Vol. 26, Pages 1694-1702, 2022.
- 15. Buchan, M. C., Bhawra, J., and Katapally, T. R., "Navigating the digital World: Development of an Evidence-Based Digital Literacy Program and Assessment Tool for Youth", Smart Learning Environments, Vol 11 Issue 1, Pages 1-24, 2024.
- 16. Özcan, B., "Impact of Demographic Characteristics on Information Management Attitudes Among Youth Center Directors. Journal of Education and Recreation Patterns", Vol. 5 Issue 2, Pages 265-284, 2024.
- 17. Kelly, K. and Zakrajsek, T. D., "Advancing online teaching: Creating equity-based digital learning environments", Taylor and Francis, Newyork, 2023.
- 18. Bhowmik, A. K., "Virtual and augmented reality: Human sensory-perceptual requirements and trends for immersive spatial computing experiences", Journal of the Society for Information Display, Vol. 32 Issue 8, Pages 605-646, 2024.
- 19. Siddiqui, S. and Sujood., "Promoting carbon neutrality: Indian tourists' intentions to adopt energy-saving behaviours", Current Issues in Tourism, Vol. 27 Issue 23, Pages 1-21, 2024.
- 20. Singh, B., "Assimilating Virtual Reality (VR) for Environmental Conservation in Tourist Spots". In Solutions for Managing Overtourism in Popular Destinations IGI Global Scientific Publishing. Pages 193-212, 2025.



ULUSLARARASI 3B YAZICI TEKNOLOJİLERİ VE DİJİTAL ENDÜSTRİ DERGİSİ

INTERNATIONAL JOURNAL OF 3D PRINTING TECHNOLOGIES AND DIGITAL INDUSTRY

ISSN:2602-3350 (Online)

URL: https://dergipark.org.tr/ij3dptdi

FORECASTING CURRENT EXCHANGE AND GOLD RATES WITH HYBRID MODELS USING TIME SERIES AND DEEP LEARNING ALGORITHMS

Yazarlar (Authors): Gökalp Çınarer •

Bu makaleye şu şekilde atıfta bulunabilirsiniz (To cite to this article): Çınarer G., "Forecasting Current Exchange and Gold Rates With Hybrid Models Using Time Series and Deep Learning Algorithms, Thermal Stability, and Environmental Impact" Int. J. of 3D Printing Tech. Dig. Ind., 9(2): 171-182, (2025).

DOI: 10.46519/ij3dptdi.1633193

Araştırma Makale/ Research Article

Erişim Linki: (To link to this article): https://dergipark.org.tr/en/pub/ij3dptdi/archive

FORECASTING CURRENT EXCHANGE AND GOLD RATES WITH HYBRID MODELS USING TIME SERIES AND DEEP LEARNING ALGORITHMS

Gökalp Çınarer^a

^aYozgat Bozok University, Engineering and Architecture Faculty, Computer Engineering Department, TURKEY

* Corresponding Author: gokalp.cinarer@bozok.edu.tr

(Received: 04.02.25; Revised: 25.03.25; Accepted: 09.07.25)

ABSTRACT

The flexibility and volatility experienced in exchange rates affect many financial activities in the world. In order to follow this situation, countries and multinational companies need to follow financial indicators in the world economy. There is a need for important decision systems that will follow all these systems with a reliable prediction model together with the developing technology. In this study, deep learning-based models that will accurately predict the movement of gold, dollar, and euro exchange rates are proposed. Time Series methods were used to analyze the data and make predictions. In addition to deep learning models such as LSTM, GRU, Bi-LSTM and RNN, hybrid models of these methods were also used to compare their prediction performances. The data set includes USD/TRY and EUR/TRY exchange rates and monthly prices of bullion gold in Turkish Lira. Data between the years 2000-2024 were included in the analyses, and a six-month future prediction of each rate was also made. In the study, the best results were obtained with a 98.39% f1 score in gold rate prediction with the GRU-RNN hybrid model. It was observed that hybrid models in particular provided higher accuracy in predictions in general. The findings show that optimizing model parameters has a significant impact on the success of financial forecasts.

Keywords: Deep Learning, Time Series Models, Artificial Intelligence, Foreign Exchange Prediction, Hybrid Models, Data Mining

1. INTRODUCTION

Exchange rates can be considered not only as an individual investment tool for companies that have close commercial relations with the outside world, but also as an important investment and economic indicator tool for the economies of countries. Countries multinational companies can use exchange rates as one of the most important financial indicators to maintain their economic relations with the outside world [1]. This could bring the global foreign exchange market to a significant position in the world, so that exchange rates can respond quickly to market conditions [2]. While the Dollar and Euro are among the most used foreign exchange types in international trade and borrowing in Turkey, gold can stand out as an important store of value for both individual investors and central bank reserves. Fluctuations in exchange rates are among the critical factors that directly affect inflation,

import and export balance in the Turkish economy. Gold is a widely preferred investment tool, but it also stands out as an asset that can be quickly affected by economic fluctuations and politics [3]. Gold, which has a wide range of uses in many industries such as electronics, aviation, medicine and jewelry, is considered a precious metal due to its properties as both a commodity and a monetary asset [4]. It also attracts great interest from individual investors, institutional investors and governments. As a result of changes in the exchange rate of a currency, the economy and trade are affected, inflation can increase, and the global economy is suppressed or stimulated.

The importance of disciplines such as machine learning (ML) and deep learning (DL) has been increasing over the years, and a lot of model inspired by these fields can supply solutions to today's complex problems as well as open the

doors to new research areas. The innovations provided by these technologies, especially in financial markets, can be quite remarkable. As mentioned before, the foreign exchange market is easily affected by external conditions such as trade. peopolitical situations, economic indicators and market sentiment. This situation causes exchange rates to generally exhibit complex and fluctuating structures, makes difficult to achieve best accuracy rates in forecasting processes [5]. However, machine learning-based models can be important to overcome these difficulties.

In this study, it is aimed to estimate the value of dollar (USD), euro (EUR) and gold against Turkish Lira (TL) by using deep learning based methods for time series analysis. In addition to DL models such as Long Short Term Memory (LSTM), Recurrent Neural Networks (RNN), Closed Recycled Units (GRU) and Bi-LSTM, hybrid models of these methods will be used and their prediction performances will be compared. This provides a comprehensive framework to understand the advantages and disadvantages of existing methods. In addition, gaps in the literature will be illuminated by determining which model or hybrid approach

performs better under which conditions. The lack of much information in the literature for performance of hybrid models provides a new reference point for this study. This study provides applicable results especially for market players, investors and financial analysts. The application of hybrid models in this study examines whether better results can be achieved compared to traditional approaches. The limited availability of information on the accuracy of hybrid models in the literature makes this study a new reference point. The findings of this research aim to provide practical insights, particularly for market participants, investors, and financial analysts.

1.1. Literature Review

Kilimci et al. [6] proposed to predict the final price of the BTC/USDT exchange rate in their study. Moreover, in addition they used statistical indicators, and considered data such as BB (Bollinger Band) and MA (Hourly Moving Average) as a feature set. Mohammad J. Hamayel et al [7] recommended three different RNN-based model to see the price of popular cryptocurrencies.

Table 1. Literature Review

Articles	Data	Method	Model	Rmse	Mae	Mape
[8]	USD	They proposed using sentiment analysis and time series analysis together.	ARIMA	-	0.0472	2.7144
[9]	GOLD	They proposed using time series analyzes.	LSTM Bi-LSTM GRU	61.728 76.711 87.425	48.85 61.53 71.24	3.48 4.24 4.91
[10]	VESTEL	They proposed using deep	RNN	0.3263	_	_
	(share)	learning methods.	CNN	0.086	-	-
[11]	ASELSAN	They proposed using deep	ARIMA	_	0,0836	_
	(share)	learning methods with time	LSTM	_	0,0213	_
		series algorithms.	GRU	-	0,0205	-
[11]	AKBANK	They proposed using deep	ARIMA	_	0,1066	_
	(share)	learning models.	LSTM	_	0,0317	_
			GRU	_	0,0257	_
[12]	GOLD	They proposed using time series	CNN	_	0,0850	4,9630
		methods based on sentiment	LSTM	_	0,1042	5,9920
		analysis.	CNN-	_	0,0969	5,5944
			LSTM		,	,
[13]	BIST100	They proposed using memory	LSTM	_	-	-
	(share)	based machine earning method.	GRU	-	-	-

[14]	USD	They proposed using a dual-layer LSTM.	SL- LSTM TLS- LSTM	0.007465 0.004251	0.00656 0.00336	
[15]	GOLD	They proposed using LSTM with time series.		-	-	0.4867
[16]	EUR	They proposed using LSTM.	LSTM	0.0015	-	0.12

2.MATERIAL AND METHOD

2.1. Time Series

Time series analysis is the process of examining and modeling data collected over a specific period of time [17]. Such data provides important clues for predicting future values using past observations. So that time series methods were used to analyze data and make predictions.

In time series analysis; Features such as trends, seasonal changes and random fluctuations in the data can be identified and future values can be predicted using these features.

2.2. Data Set

The data set was obtained through the Electronic Data Distribution System (EVDS) of the Central Bank of the Republic of Türkiye (CBRT) on November 15, 2024 [18]. The data set includes USD/TRY and EUR/TRY exchange rates and monthly prices of gold bullion in Turkish Lira. Data between 2000 and 2024 were included in the analysis and the data were recorded in Excel format.

Each data set contains 300 data points. During the data pre-processing phase, missing data were filled in using the linear interpolation method as it was suitable for the time series. USD/TRY data is visualized in Figure 1, EUR/TRY data is visualized in Figure 2, and gold price data is visualized in Figure 3



Figure 1. USD/TRY graph



Figure 2. EUR/TRY graph



Figure 3. GOLD/TRY Graph

The graphs shown in Figure 4 decompose the trend, seasonality, and residual components of the GOLD/TRY, EUR/TRY, and USD/TRY time series. When examining the graphs, the trend component exhibits a sharp increase after 2020. The seasonal components display

periodic fluctuations, reflecting the regular cycles in the foreign exchange market. The residual component represents minor deviations that the model cannot explain.

2.3. Deep Learning Models

In this study, deep learning models were used to analyze and predict dollar, euro and gold data. DL techniques such as LSTM, RNN and GRU were used in the predictions. The layer structure of each model was designed using the layer sequence shown in Figure 5. The efficiency of the models was evaluated with the Root Mean Square Error (RMSE), Mean Absolute Error (MAE) and Mean Absolute Percentage Error (MAPE) criteria.

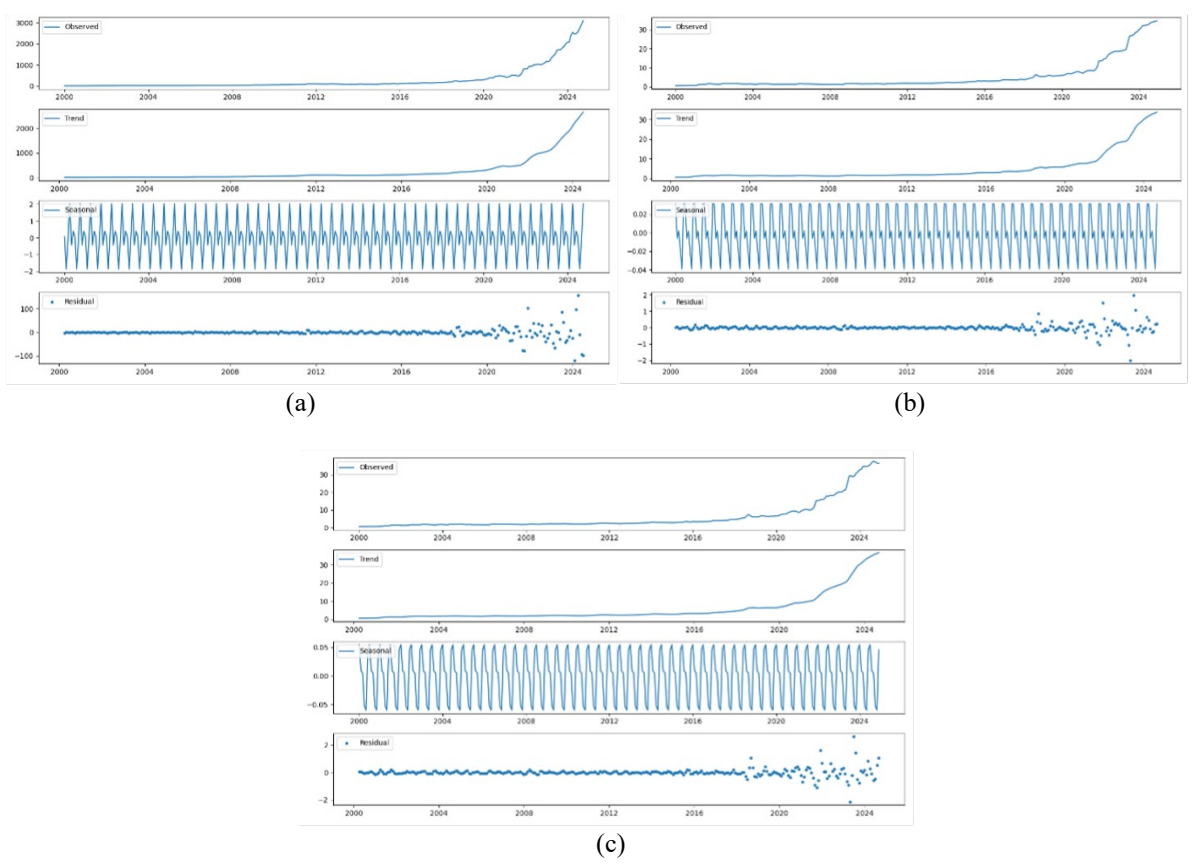


Figure 4. Trend, seasonality, and residual components of the Gold/TRY (a), USD/TRY (b) and EUR/TRY (c) time series

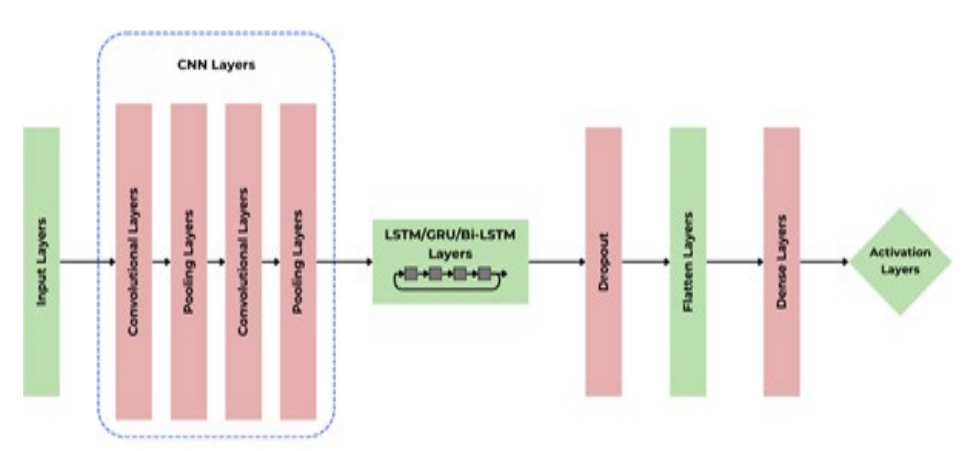


Figure 5. Model layers

The layers, parameters, optimization methods and functions used in this study are listed in Table 2. Adam was chosen as the optimizer within the scope of the study. The performance of each model was run for 100 epochs. In all

models, the Tanh activation function is preferred for the output layer. The Tanh function generally gives results in the basic output range between -1 and 1 and is especially suitable for normalized time series.

Table 2. Hyperparameter Values of Deep Learning Models

Layers	Activation Function	Epochs	Optımızer	Batch size	Loss Function
Lstm(64) dropout(0.2) Lstm(64) dropout(0.2) Flatten() dense(1)	Tanh	100	Adam	64	MSE
Bi-lstm(64) dropout(0.2) Bi-lstm(64) dropout(0.2)	Tanh	100	Adam	64	MSE
Flatten() dense(1) Gru(64) dropout(0.2) Gru(64) dropout(0.2) Flatten() dense(1)	Tanh	100	Adam	64	MSE
Rnn(64) dropout(0.2) Rnn(64) dropout(0.2) Flatten() dense(1)	Tanh	100	Adam	64	MSE
Lstm(64) dropout(0.2) Bi-lstm(64) dropout(0.2) Flatten() dense(1)	Tanh	100	Adam	64	MSE
Lstm(64) dropout(0.2) Gru(64) dropout(0.2) Flatten() dense(1)	Tanh	100	Adam	64	MSE
Lstm(64) dropout(0.2) Rnn(64) dropout(0.2) Flatten() dense(1)	Tanh	100	Adam	64	MSE
Bi-lstm(64) dropout(0.2) Rnn(64) dropout(0.2) Flatten() dense(1)	Tanh	100	Adam	64	MSE
Gru(64) dropout(0.2) Bi-lstm(64) dropout(0.2) Flatten() dense(1)	Tanh	100	Adam	64	MSE
Gru(64) dropout(0.2) Rnn(64) dropout(0.2) Flatten() dense(1)	Tanh	100	Adam	64	MSE

2.4. Deep Learning Time Series Models

In this study, LSTM networks, which are one of the most preferred recurrent architectures in the literature for the prediction of sequential data, were used. LSTM is a type of recursive neural network that has the capacity for learning longterm dependencies in time series data [19].

RNN were used to process sequential data. RNN is a type of artificial neural network designed for learning sequential dependencies in time series data [20]. These networks affect the out-put of the current step by processing information from previous steps and thus serve as a kind of memory. In general, it has an

architecture that evaluates the information from previous steps by processing inputs at each time step and produces outputs [21].

Gate Controlled Recurrent Unit (GRU) was used for periodic data processing. GRU has a similar structure to LSTM, but offers a simpler architecture and can be more computationally efficient. It is also frequently used with LSTM in the literature. GRU includes two basic mechanisms to control cell states: the update gate and the forget gate. As shown in Figure 6, the LSTM structure includes mechanisms such as input, forget and output gate.

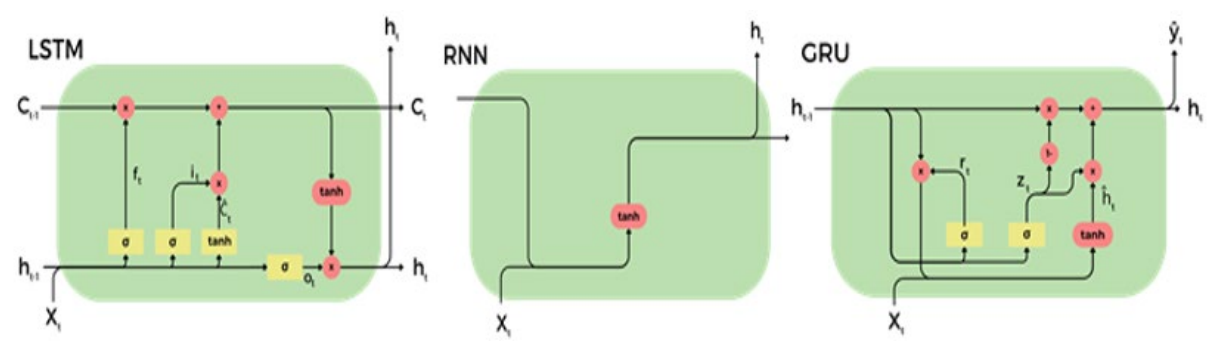


Figure 6. Basic structure of LSTM, RNN and GRU models.

Min-Max Normalization method was used to scale the data before model training. This method transforms each value in the data set into a certain range, ensuring that inputs at different scales are evaluated with equal importance by the model. Normalization contributes to the independent modeling of features and the stabilization of the learning process. Min-Max Normalization was performed by transforming each value according to the min and max value in the data set.

$$X' = \frac{X - X_{min}}{X_{max} - X_{min}} \tag{1}$$

RMSE metric was used for evaluation the model performance. RMSE is an error measurement criterion that is frequently used in the literature to measure the closeness of model predictions to the true values. With this metric, the square of the prediction errors is averaged and then the square root is calculated. The RMSE value indicates how much deviation there is in the model's predictions.

$$RMSE = \sqrt{\frac{1}{n} \sum_{i=1}^{n} (y_i - \hat{y}_i)^2}$$
 (2)

RMSE expresses the results depending on the scale of the dataset due to unit precision, and a low RMSE value means that the model's predictive performance is high. Using RMSE helps to understand full distribution of the errors [22].

MAE was used for evaluation as a metric the model's performance. MAE directly measures the magnitude of the prediction errors by averaging the absolute values of the differences between the model's predicted values and the actual values.

$$MAE = \frac{1}{n} \sum_{i=1}^{n} |y_i - \bar{y}_i|$$
 (3)

MAE shows the average error in the model's predictions in units and makes it easier to interpret the magnitude of the error. Another metric, In addition to this in this study MSE, selected to evaluate the performance of the models which is more sensitive metric to the outliers compared to the MAE [23].

MSE measures the magnitude of the prediction error by averaging the squared differences

between the model's predicted values and the actual values.

$$MSE = \frac{1}{n} \sum_{n=1}^{n} (y_i - \hat{y}_i)^2$$
 (4)

MSE shows the average error in the model's predictions in square units and is used as an effective metric to optimize model performance because it penalizes large errors.

In this study, the MAPE metric is used. MAPE calculates the percentage error rate of the model's predicted values compared to the actual values and expresses the results in percent units. This metric is widely used to measure prediction accuracy and compare error rates. Also, it is found to be commonly used in finance as profits and losses are relative terms [24].

$$MAPE = \frac{1}{n} \sum_{i=1}^{n} \left| \frac{y_i - \hat{y}_i}{y_i} \right| \times 100$$
 (5)

MAPE provides an advantage in comparing the results of different data sets, as it provides an error rate in percentage terms.

However, the results may become sensitive when the y_i values are close to zero.

In addition, F1 Score calculates the harmonic mean of the accuracy and recall values to measure the classification success of the model. This metric is an effective part of evaluating model performance even in imbalanced data sets.

$$F1 = 2 \cdot \frac{\text{Precision} \cdot \text{Recall}}{\text{Precision} + \text{Recall}}$$
 (6)

F1 Score can be especially useful in cases where it is important to correctly predict the positive class. It provides an advantage in summarizing the overall performance in model because it offers a balance between Precision and Recall.

3. RESULTS

In this study, LSTM, RNN, GRU, Bi-LSTM and hybrid models of these methods were used to estimate USD/TRY, EUR/TRY and bullion GOLD/TRY prices. While analyzing the performance of the models, 80% was separated as training and 20% as test data. In addition, a forward-looking forecast was made for each unit between 6 months.

When the graph of gold prices shown in Figure 7 is examined, it is seen that there is an increasing trend in gold prices in the 6-month forward forecast period. When the future forecasts of the GRU-RNN model, which showed the best performance, are examined, it is seen that it predicts gold prices as 3408,451 TRY at the end of the 6-month period.

The results of the GOLD/TRY data are presented in Table 3. According to the table, the best performance was obtained with the GRU-RNN hybrid model with an F1 score of 98.39%. The hybrid model closest to this result was the LSTM-GRU hybrid model.

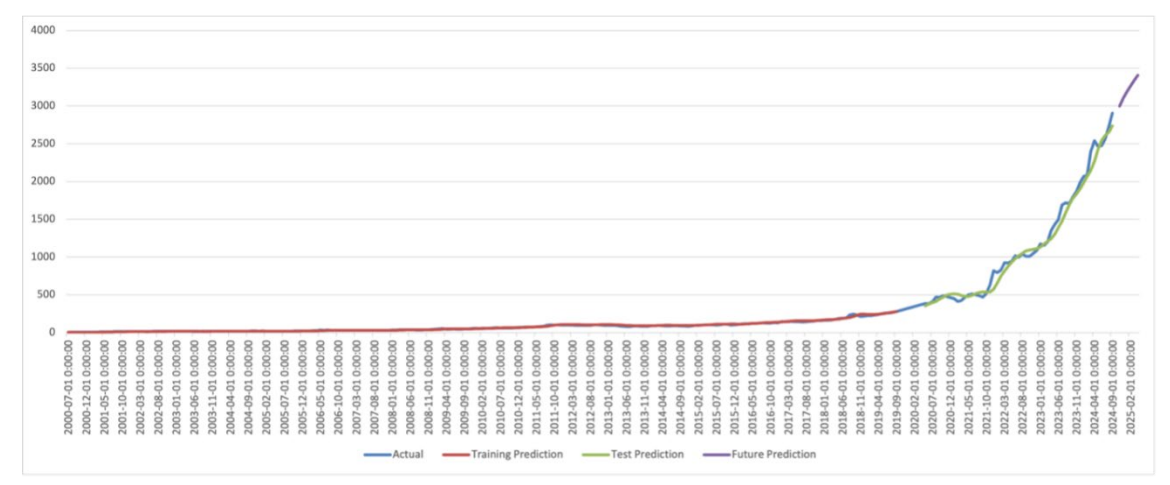


Figure 7. Gold/TRY test results.

Table 3. Gold/TRY test results

MODEL	RMSE	MSE	MAE	MAPE	F1
LSTM	0.0563	0.0032	0.0434	0.1146	0.9438
Bi-LSTM	0.0449	0.0020	0.0341	0.0931	0.9642
GRU	0.0427	0.0018	0.0318	0.0853	0.9677
RNN	0.0454	0.0021	0.0324	0.0801	0.9634
LSTM - GRU	0.0363	0.0013	0.0267	0.0809	0.9767
LSTM - RNN	0.0531	0.0028	0.0406	0.1067	0.9500
BiLSTM - RNN	0.0488	0.0024	0.0370	0.0974	0.9577
GRU - BiLSTM	0.0452	0.0020	0.0341	0.0942	0.9639
GRU - RNN	0.0301	0.0009	0.0220	0.0685	0.9839

The graph regarding dollar prices presented in Figure 8 reveals that there is a clear upward trend in dollar prices in the 6-month forecast period. According to the future data estimates obtained by the GRU-RNN model, the dollar exchange rate is predicted to be 37.33 TRY at the end of the 6-month period. The results of USD/TRY data are presented and evaluated in Table 4. According to the table, the best

performance was obtained with the GRU-RNN hybrid model. The closest result to this model was provided by the LSTM-GRU model. This clearly shows the superiority of the hybrid model when it comes to USD prediction. When the RMSE values are examined, it is seen that the GRU-RNN hybrid model achieved the best result with a value of 0.0363. And achieved the highest result with an F1 score of 98.26%.

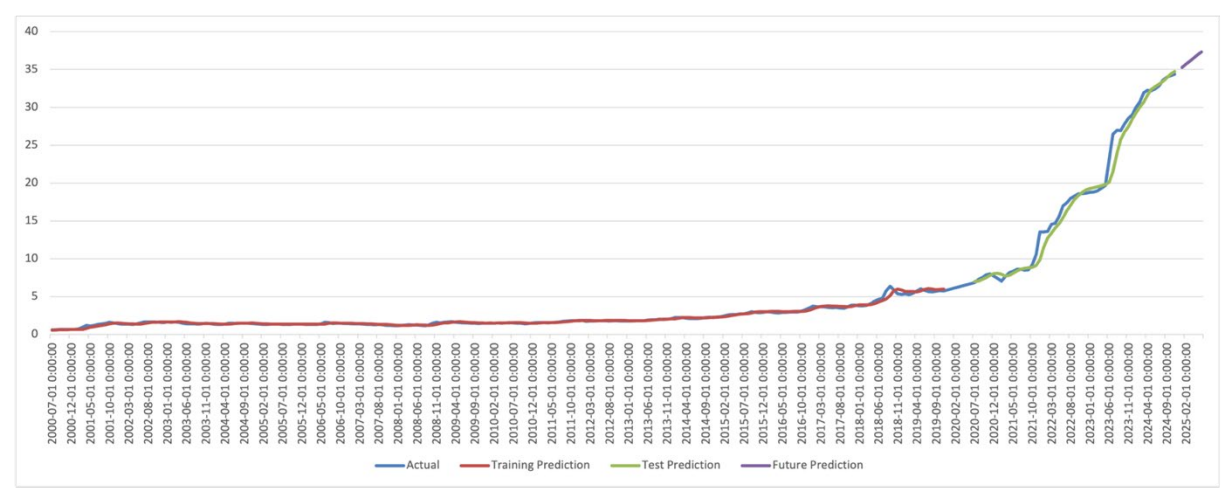


Figure 8. USD/TRY test results.

Table 4. USD/TRY test results.

MODEL	RMSE	MSE	MAE	MAPE	F1						
LSTM	0.0555	0.0031	0.0392	0.0760	0.9595						
Bi-LSTM	0.0643	0.0041	0.0497	0.0884	0.9456						
GRU	0.0443	0.0020	0.0300	0.0607	0.9741						
RNN	0.0666	0.0044	0.0542	0.0960	0.9417						
LSTM-GRU	0.0412	0.0017	0.0289	0.0595	0.9777						
LSTM-RNN	0.0565	0.0032	0.0421	0.0773	0.9581						
Bi-LSTM-RNN	0.0584	0.0034	0.0446	0.0807	0.9551						
GRU-Bi-LSTM	0.0612	0.0037	0.0460	0.0834	0.9507						
GRU-RNN	0.0363	0.0013	0.0234	0.0501	0.9826						

Figure 9 is examined, it is seen that the EUR/TRY results will tend to decrease in the future. Contrary to expectations, hybrid models generally performed worse than single models. The graph regarding euro prices presented in Figure 9 clearly reflects the downward trend in euro prices during the 6-month forecast period. According to these data obtained, the EURO price was estimated as 32.86 TRY according to the RNN model, which gave the best result at the end of the 6-month period. The estimates are especially important in terms of making predictions about the future direction of movements in the foreign exchange market.

The results of EUR/TRY data are presented and analyzed in Table 5. According to the analysis results, the best performance was obtained with the RNN model. The prediction success of the RNN model clearly shows its capacity to

effectively learn patterns in the data set. The closest performance to this model was provided by the Bi-LSTM model.

RNN gives best results among the single models with the lowest RMSE 0.0448 and MSE 0.0020 values on Table 5. It is also quite successful in the MAPE 0.0619 and MAE 0.0340 metrics. The F1 score was the highest among all models with 0.9718. This shows that RNN performs better than other models in financial prediction tasks. Although Bi-LSTM has slightly higher RMSE 0.0489 and MSE 0.0024 values than RNN, it has achieved more successful results than other models. When the Bi-LSTM results are examined, it gives better results than LSTM with MAPE 0.0630 and MAE 0.0340 values, while it shows a performance close to RNN. The performance of GRU is similar to LSTM, but it gives slightly weaker results.

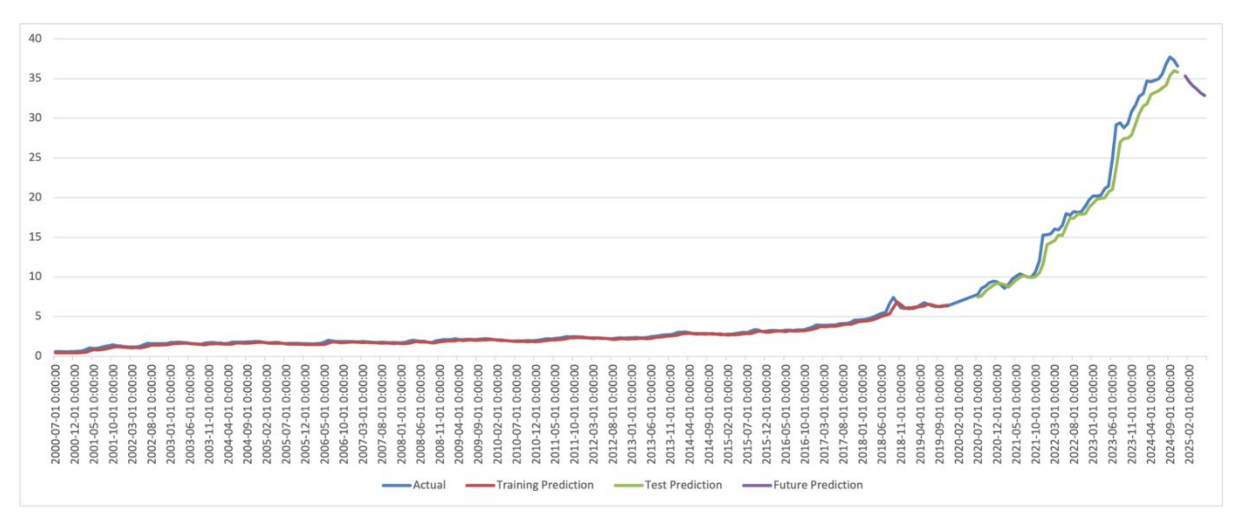


Figure 9. EUR/TRY test results.

Table 5. EUR/TRY test results.

MODEL	RMSE	MSE	MAE	MAPE	F1
LSTM	0.0517	0.0027	0.0346	0.0676	0.9625
BiLSTM	0.0489	0.0024	0.0340	0.0630	0.9665
GRU	0.0518	0.0027	0.0380	0.0736	0.9624
RNN	0.0448	0.0020	0.0340	0.0619	0.9718
LSTM-GRU	0.0599	0.0036	0.0449	0.0850	0.9497
LSTM-RNN	0.0593	0.0035	0.0442	0.0843	0.9508
BiLSTM-RNN	0.0690	0.0048	0.0553	0.0986	0.9333
GRU-Bi-LSTM	0.0629	0.0040	0.0478	0.0880	0.9445
GRU-RNN	0.0680	0.0046	0.0545	0.0985	0.9351

Today, the development of computers makes it possible to make future predictions in financial markets by processing large data sets. In this study; LSTM, RNN, GRU, Bi-LSTM and hybrid models of these methods were used to predict dollar, euro and gold prices.

4. DISCUSSION

Forecasting financial indicators such as exchange rates and precious metals is of great importance in determining economic policies worldwide, developing investment strategies and risk management policies. Therefore, there is an intense research interest in developing highly accurate artificial intelligence-supported forecasting systems. In recent years, deep learning-based time series models have come to the fore in this field. The application of hybrid models in this study shows whether better results can be obtained when compared to traditional approaches. There are different suggestions in the literature such as time series for forecasting gold prices [25,26], time series for USD/EUR exchange rate [27], models using LSTM and GRU Methods for Forecasting Gold Exchange Rate Against Dollar [28]. Since the main purpose of the studies in this field is high

accuracy and performance, hybrid models are more prominent. It is seen that the performance of the hybrid models reaches high accuracy values in USD/TRY and GOLD estimation. The performance of the models is evaluated with RMSE, MSE, MAE, MAPE and F1 Score metrics. In the study, the best results were obtained with the GRU-RNN hybrid model. It was observed that hybrid models in particular provide higher accuracy in estimates in general. The obtained findings show that optimizing the model parameters has a significant effect on the success of financial estimates. In the study conducted by Islam et al. using LSTM and GRU hybrid models to predict EUR/USD and GBP/USD currency pairs, MSE, RMSE and MAE results were reported as 0.00001, 0.00301 0.00224, respectively [29]. performance of the hybrid models used in this study on USD/TRY and EUR/TRY was similar to the results in the literature, and low error values were obtained. In addition they worked in a shorter time period. An accuracy of 0.948 was achieved in the study that determined the most advantageous time for investors' future EUR/USD transactions [30]. When the studies conducted are examined, it is seen that the data

sets only use time series methods and do not make future predictions. In this study, the MSE, MAE and RMSE values of the results obtained in the data set and the test set as well as the results of the lower rates in the future are also included. In the bitcoin price prediction study conducted by Buslim et al. [31], the GRU model gave the best result with the Grid Search method and a MAE value of 0.0594 was obtained. Similarly, in this study, the use of GRU and hybrid models provided high accuracy for gold, dollar and euro prices, and it was particularly noteworthy that GRU provided a low error rate in the test data. In this study, GRU achieved a very successful result in EURO prediction with a MAE value of 0.0380. While only Bitcoin data were analyzed in the study conducted by Buslim et al., this study evaluated more than one financial unit and made a wider evaluation. The effect of the selected hyperparameters on the prediction results while training LSTM models and hybrid models was analyzed comparatively. The 98.39% F1 score obtained in this study shows how effective the model in question can be in financial forecasting. It is seen that the presented study is compatible with the literature and supported by current approaches. In this context, the study contributes to the literature both methodologically and practically. In the literature, Wang et al. [32] achieved 98.8% R² in foreign exchange rate forecasting with CNN-LSTM hybrid model, for USD/CNY. Similarly, the finding in this study that hybrid models show higher success in many models compared to single models supports this literature. In the study [33] conducted to determine the future value of the Chinese Yuan (CNY) against the US dollar, LSTM models and machine learning models were analyzed as hybrids. In the study, LSTM and XGBoost algorithms were compared and the results obtained were analyzed. It was seen that the LSTM model gave better results in the study. Although the LSTM model gave a result below the average among deep learning models in this study, it has a very high performance among time series algorithms. Finally, hyperparameter optimization also seriously affects the model performance. Therefore, meticulous optimization of the model parameters proposed in this study increases the reliability of the results.

5. CONCLUSION

In this study, LSTM, GRU, RNN, Bi-LSTM, and hybrid models were used to forecast USD/TRY, EUR/TRY, and bullion gold prices. When the obtained results are compared with other studies in the literature, they show similarities and differences in terms of both the data sets used and accuracy measures. In this study, batch size, number of hidden layers and epoch number were also effective in measuring success. These parameters were specifically adjusted for the models as a result of experimental results. Parameter setting is very important for the performance of time series models, so the models were designed considering this. In the study, hybrid models were presented in addition to time series models and their performance values were analyzed comparatively. The limitations of the study are that the dataset only covers certain exchange rates. At the same time, future prediction time can be increased by making predictions over a wider time range. In future studies, longer-term prediction processes will be performed using different deep learning models. Performance results will be increased with large datasets and different hyperparameter combinations. This study is of a nature that will provide insight to investors with the future prediction results obtained by using recurrent neural network models.

REFERENCES

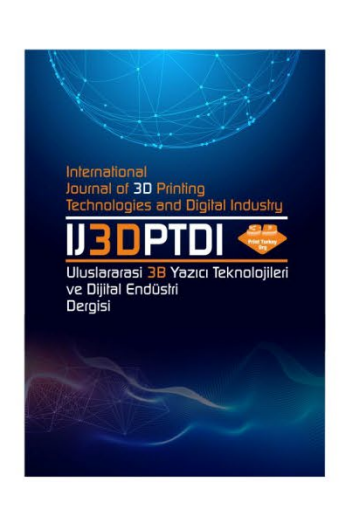
- 1. Yasar, H., and Kilimci, Z. H., "US dollar/Turkish lira exchange rate forecasting model based on deep learning methodologies and time series analysis", Symmetry, Vol. 12, Issue. 9, Pages 1553, 2020.
- 2. Duygulu, A. A., "Evaluation of Exchange Rate Stability in Terms of Economic Stability", Dokuz Eylul University Journal of Faculty of Economics and Administrative Sciences, Vol. 13, Issue. 1, Pages 105-116, 1998.
- 3. Elmastaş Gültekin, Ö., and Aktürk Hayat, E., "Analysis of Factors Affecting Gold Prices with VAR Model: 2005-2015 Period", Ege Academic Review, Vol. 16, Issue. 4, 2016.
- 4. Güney, S., and Ilgın, K. S., "Evaluation of the Impact of Investment Instruments on the BIST-100 Index", Erciyes University Journal of Faculty of Economics and Administrative Sciences, Issue. 53, Pages 226-245, 2019.

- 5. Manjula, K. A., and Karthikeyan, P., "Gold price prediction using ensemble based machine learning techniques", 2019 3rd International Conference on Trends in Electronics and Informatics (ICOEI), Pages 1360-1364, IEEE, April 2019.
- 6. Kilimci, H., Yıldırım, M., and Kilimci, Z. H., "The prediction of short-term bitcoin dollar rate (BTC/USDT) using deep and hybrid deep learning techniques", 2021 5th International Symposium on Multidisciplinary Studies and Innovative Technologies (ISMSIT), Pages 633-637, IEEE, October 2021.
- 7. Hamayel, M. J., and Owda, A. Y., "A novel cryptocurrency price prediction model using GRU, LSTM and bi-LSTM machine learning algorithms", AI, Vol. 2, Issue. 4, Pages 477-496, 2021.
- 8. Yasar, H., and Kilimci, Z. H., "US dollar/Turkish lira exchange rate forecasting model based on deep learning methodologies and time series analysis", Symmetry, Vol. 12, Issue. 9, Pages 1553, 2020.
- 9. Yurtsever, M., "Gold price forecasting using LSTM, Bi-LSTM and GRU", European Journal of Science and Technology, Issue. 31, Pages 341-347, 2021.
- 10. Çoban, Ç., and Hayat, E., "Comparison of Different Deep Neural Network Models in Stock Market Analysis", Adnan Menderes University Journal of Social Sciences Institute, Vol. 10, Issue. 2, Pages 120-139, 2023.
- 11. Albayrak, E., and Saran, N., "Stock Price Prediction Using Statistical and Deep Learning Models", Turkish Informatics Foundation Journal of Computer Science and Engineering, Vol. 16, Issue. 2, Pages 161-169, 2023.
- 12. Kantar, O., and Kilimci, Z., "Deep learning based hybrid gold index (XAU/USD) direction forecast model", Journal of the Faculty of Engineering and Architecture of Gazi University, Vol. 38, Issue. 2, 2023
- 13. Çelik, Y., "BIST100 Index Prediction Using Memory-Based LSTM and GRU Machine Learning Algorithms", Firat University Journal of Engineering Sciences, Vol. 36, Issue. 2, Pages 553-561, 2024.
- 14. Ayitey Junior, M., Appiahene, P., and Appiah, O., "Forex market forecasting with two-layer stacked Long Short-Term Memory neural network (LSTM) and correlation analysis", Journal of Electrical Systems and Information Technology, Vol. 9, Issue. 1, Pages 14, 2022.

- 15. Nurhambali, M. R., Angraini, Y., and Fitrianto, A., "Implementation of Long Short-Term Memory for Gold Prices Forecasting", Malaysian Journal of Mathematical Sciences, Vol. 18, Issue. 2, 2024.
- 16. Qi, L., Khushi, M., and Poon, J., "Event-driven LSTM for forex price prediction", 2020 IEEE Asia-Pacific Conference on Computer Science and Data Engineering (CSDE), Pages 1-6, IEEE, December 2020.
- 17. Velicer, W. F., and Fava, J. L., "Time Series Analysis", In Weiner IB et al. editors, Handbook of Psychology, Pages 581-606, John Wiley & Sons, Hoboken, 2003.
- 18. Central Bank of the Republic of Turkey (CBRT), "Electronic Data Distribution System (EDDS)", https://evds2.tcmb.gov.tr, 2024.
- 19. DiPietro, R., and Hager, G. D., "Deep learning: RNNs and LSTM", In Brunette DM, Tengvall P, Textor M et al. editors, Handbook of Medical Image Computing and Computer Assisted Intervention, Pages 503-519, Academic Press, San Diego, 2020.
- 20. Xiao, J., and Zhou, Z., "Research progress of RNN language model", 2020 IEEE International Conference on Artificial Intelligence and Computer Applications (ICAICA), Pages 1285-1288, IEEE, June 2020.
- 21. Zhang, J., and Man, K. F., "Time series prediction using RNN in multi-dimension embedding phase space", SMC'98 Conference Proceedings. 1998 IEEE International Conference on Systems, Man, and Cybernetics, Vol. 2, Pages 1868-1873, IEEE, October 1998.
- 22. Chai, T., and Draxler, R. R., "Root mean square error (RMSE) or mean absolute error (MAE)? Arguments against avoiding RMSE in the literature", Geoscientific Model Development, Vol. 7, Issue 3, Pages 1247-1250, 2014.
- 23. Chicco, D., Warrens, M. J., and Jurman, G., "The coefficient of determination R-squared is more informative than SMAPE, MAE, MAPE, MSE and RMSE in regression analysis evaluation", Scientific Reports, Vol. 11, Issue 1, Pages 1-10, 2021.
- 24. Myttenaere, A., Golden, B., Le Grand, B., and Rossi, F., "Mean Absolute Percentage Error for regression models", Neurocomputing, Vol. 192, Pages 38-48, 2016.
- 25. Salim, M., & Djunaidy, A., Development of a cnn-lstm approach with images as time-series data representation for predicting gold prices. Procedia Computer Science, Vol. 234, Pages 333-340, 2024.

- 26. Zangana, H. M., & Obeyd, S. R., "Deep Learning-based Gold Price Prediction: A Novel Approach using Time Series Analysis", Sistemasi: Jurnal Sistem Informasi, Vol. 13, Issue 6, Pages 2581-2591, 2024.
- 27. Marisetty, N., "Evaluating long-term and short-term relationships: Cointegration of NSE NIFTY with crude oil, gold, and USD/EUR currency pair. Gold, and USD/EUR Currency Pair", Asian Journal of Management and Commerce, Vol 5. Issue 2, Pages 395–405, 2024.
- 28. Bohovic, D., "Comparison of LSTM and GRU Methods for Predicting Gold Exchange Rate against US Dollar", International Journal Artificial Intelligent and Informatics, Vol. 3, Issue 1, Pages 24-29, 2025.
- 29. Islam, M. S., and Hossain, E., "Foreign exchange currency rate prediction using a GRU-LSTM hybrid network", Soft Computing Letters, Vol. 3, Pages 100009, 2021.

- 30. El Mahjouby, M., Bennani, M. T., Lamrini, M., El Far, M., Bossoufi, B., & Alghamdi, T. A., "Machine learning algorithms for forecasting and categorizing euro-to-dollar exchange rates", IEEE Access, Vol. 3, Pages 74211-74217, 2024.
- 31. Buslim, N., Rahmatullah, I. L., Setyawan, B. A., and Alamsyah, A., "Comparing bitcoin's prediction model using GRU, RNN, and LSTM by hyperparameter optimization grid search and random search", 2021 9th International Conference on Cyber and IT Service Management (CITSM), Pages 1-6, IEEE, September 2021.
- 32. Cao, W., Zhu, W., Wang, W., Demazeau, Y., & Zhang, C., A deep coupled LSTM approach for USD/CNY exchange rate forecasting. IEEE Intelligent Systems, Vol. 35, Issue 1, Pages 43-53, 2020.
- 33. Ullah, U., Rehman, D., Khan, S., Rashid, H., & Ullah, I., Forecasting Foreign Exchange Rate with Machine Learning Techniques Chinese Yuan to US Dollar Using XGboost and LSTM Model. iRASD Journal of Economics, Vol. 6, Issue 3, Pages 761-775, 2024.



ULUSLARARASI 3B YAZICI TEKNOLOJİLERİ VE DİJİTAL ENDÜSTRİ DERGİSİ

INTERNATIONAL JOURNAL OF 3D PRINTING TECHNOLOGIES AND DIGITAL INDUSTRY

ISSN:2602-3350 (Online)

URL: https://dergipark.org.tr/ij3dptdi

316L PASLANMAZ ÇELİK TOZUNUN ARK İLE TEK ÇİZGİ ERGİTİLMESİNDE ELEKTROT MESAFESİNİN ETKİLERİNİN ARAŞTIRILMASI

INVESTIGATION OF THE EFFECTS OF ELECTRODE DISTANCE ON SINGLE-TRACK MELTING OF 316L STAINLESS STEEL POWDER BY ARC

Yazarlar (Authors): Arif Balcı **

Bu makaleye şu şekilde atıfta bulunabilirsiniz (To cite to this article): Balcı A., "316L Paslanmaz Çelik Tozunun Ark ile Tek Çizgi Ergitilmesinde Elektrot Mesafesinin Etkilerinin Araştırılması" Int. J. of 3D Printing Tech. Dig. Ind., 9(2): 183-193, (2025).

DOI: 10.46519/ij3dptdi.1637693

Araştırma Makale/ Research Article

Erişim Linki: (To link to this article): https://dergipark.org.tr/en/pub/ij3dptdi/archive

316L PASLANMAZ ÇELİK TOZUNUN ARK İLE TEK ÇİZGİ ERGİTİLMESİNDE ELEKTROT MESAFESININ ETKİLERİNİN ARAŞTIRILMASI



^aKafkas Üniversitesi, Mühendislik Mimarlık Fakültesi, Makine Mühendisliği Bölümü. TÜRKİYE

* Sorumlu Yazar: <u>arifbalci@kafkas.edu.tr</u>

(Gelis/Received: 11.02.25; Düzeltme/Revised: 02.04.25; Kabul/Accepted: 01.05.25)

ÖZ

Eklemeli imalat yöntemleri, karmaşık geometrilerin ve prototip numunelerin üretimindeki avantajları nedeniyle yaygın olarak araştırılmaktadır. Toz yatakta birleştirmede, uygun ısı kaynağı ve işlem parametrelerinin belirlenmesi tek çizgi katılaşma ile başlamaktadır. Bu çalışmada, lazer ve elektron ışınına alternatif olarak ark kullanılarak, 316L paslanmaz çelik tozunun tek çizgi ergitilebilirliği incelenmiştir. Ergitmeler 0,4 mm kalınlığındaki toz yatakta, 17, 22 ve 27 amper akım değerleri ile gerçekleştirilmiş; ilerleme hızları 1 ve 2 mm/s, elektrot mesafeleri ise 0,7 ve 1 mm olarak belirlenmiştir. Farklı parametre kombinasyonları ile yapılan deneylerde katılaşma geometrisi, ısıl etkilenmiş bölge ve mikroyapı detaylı olarak değerlendirilmiştir. Elde edilen sonuçlar, düşük akım ve yüksek ilerleme hızlarında çizgisel katılaşma kabiliyetinin azaldığını; yüksek akım ve düşük ilerleme hızlarında ise daha geniş ve homojen katılaşma bölgelerinin oluştuğunu göstermektedir. Elektrot mesafesindeki artışın enerji yoğunluğunu azaltarak katılaşma genişliği ve tabla nüfuziyetini düşürdüğü belirlenmiştir. Çalışma, ark kullanımının lazer ve elektron ışınına alternatif olarak uygulanabilirliğini ortaya koymakta ve işlem parametrelerinin optimizasyonu için önemli bulgular sunmaktadır.

Anahtar Kelimeler: Eklemeli İmalat, Ark, Metal Tozu.

INVESTIGATION OF THE EFFECTS OF ELECTRODE DISTANCE ON SINGLE-TRACK MELTING OF 316L STAINLESS STEEL POWDER BY ARC

ABSTRACT

Additive manufacturing techniques are extensively studied nowadays because of their benefits in fabricating intricate geometries and prototype specimens. In powder bed fusion, the selection of the suitable heat source and process parameters initiates with single-line solidification. This study examined the single-line meltability of 316L stainless steel powder utilizing an arc as an alternative heat source to laser and electron beam methods. Melting was conducted on a 0,4 mm thick powder bed utilizing current values of 17, 22, and 27 amperes; travel speeds of 1 and 2 mm/s; and electrode distances of 0,7 and 1 mm. The experiments, performed with various parameter combinations, were assessed regarding solidification geometry, heat-affected zone, and microstructure. The findings indicated that linear solidification efficiency diminished at low current and elevated travel speeds, whereas broader and more uniform solidification areas were achieved at high current and reduced travel speeds. An increase in electrode distance was found to diminish energy density, resulting in a reduction of solidification width and substrate penetration. This study illustrates the viability of employing arc technology as a substitute for laser and electron beam methods in powder bed single-track melting, yielding significant insights for the optimization of process parameters.

Keywords: Additive Manufacturing, Arc, Metal Powder.

1. GİRİŞ

Eklemeli imalat yöntemleri karmaşık veya prototip numune geometrilerinin üretiminde önemli bir yöntemdir [1]. Toz yatakta ergitme ise bir eklemeli imalat metodu olup ergitme için gereken ısıl enerji genellikle lazer ve elektron ışınından sağlanmaktadır. Toz yatakta ergitme yöntemi için mevcut bu ısı kaynaklarına ek olarak araştırılacak yeni enerji kaynağının denenmesine lazer ve elektron yöntemlerinde olduğu gibi ilk adımda tek çizgi katılasmanın sağlanması ile baslanmaktadır [2]. Tek çizgi ergitme çalışmalarında ise belirlenen ilerleme hızı ve güç gibi parametrelerin enerji etkileyerek yoğunluğunu ergime havuzu boyutlarını, katılaşma geometrisini mikroyapı oluşumlarını doğrudan etkilediği bilinmektedir [3].

Toz yataklı ergitme yönteminde etkili olan parametrelerin anlaşılmasına yönelik yapılan literatür taramasında, lazerle gerçekleştirilen ergitme çalışmalarına ilişkin çok sayıda yayına rastlanmıştır. Nayak ve arkadaşları tarafından yapılan çalışmada, lazer gücünün etkileri araştırılmış olup 150 W ile 450 W arasında değişen güç değerleri ile ergitme yapılmıştır [4]. Yapılan çalışmada lazer gücündeki artışın ergime havuzunun genişliğini %40'a yakın iz stabilitesinin artırdığı ve geliştiği gözlenmiştir. Lazer gücünün 400 W üzerine çıkmasıyla %15 oranında porozite artışı tespit edilmiştir. İlerleme hızının etkilerinde ise Nayak ve arkadaşları, 0,02 m/s ile 0,08 m/s arasında değişen ilerleme hızlarının ergime havuzuna etkilerini araştırmışlardır. Artan ilerleme hızının lazer ile malzeme arasındaki etkileşim süresini %50 azalttığı ve ergime havuzu derinliğinde oransal olarak %30 azalma tespit edilmiştir [4]. İlerleme hızı ve gücün katılaşma geometrileri üzerindeki etkilerini inceleyen Yadroitsev ve Smurov tek çizgi ergitme calısması vapmıs olup cizgisel ergitmede kusur bölgelerini kararlılık, istikrarsızlık ve damla (toplaşma) bölgeleri olmak üzere üç bölgeye ayırmıştır [5]. Tespit edilen kusur bölgelerinde güç/ilerleme hızı oranı sırasıyla azalama göstermiştir. Tek çizgi ergitmede toz katmanın ergimesini inceleven bir diğer çalışmada Wang ve arkadaşları [6], yüksek lazer gücü ve düsük tarama hızının çizgisel ergimeyi desteklediği fakat ergime bölgesi etrafındaki tozları buharlastırarak uzaklaştırdığını ortaya koymuştur. Ayrıca ilerleme hızının artışı ile tek çizgi kabiliyeti

istikrarsızlaşmaya ve ergiyik metalin sürekliliğinin azalmasıyla toplaşma oluşmaya başladığını tespit edilmiştir [6].

Metal ergitmede enerji kaynakları arasında lazer, elektron ışını ve ark bulunmaktadır [7]. Eklemeli imalat yöntemlerinde ark kullanımı arastırıldığında tel formlu sistemlerin halihazırda araştırılmaya devam ettiği ve ticari olarak kullanıldığı görülmüştür [3]. Toz yatakta ergitme için lazer ve elektron ısınına alternatif olarak ark ile ergitme arastırılmaya baslanmıs olduğu ve parametrelerin etkileri hakkında literatürün yetersiz kaldığı tespit edilmiştir. Ark ile metal ergitmede ilerleme hızı ve kullanılan gücün ergiyik havuzu boyutlarına etkisi lazer ile benzer olup tungsten elektrot mesafesi ise bir diğer etken parametre olarak literatürde yer almaktadır [3,8]. Ark ile metal ergitmede amper büyüklüğünün etkisinin araştırıldığı Singh ve Agrawal tarafından yapılan çalışmada, lazer gücü etkisine benzer şekilde amper büyüklüğünün artması ergime havuzunun genisliği ve derinliğini artırmıştır [9]. Ark ile metal ergitmede ilerleme hızının etkilerine bakıldığında ise ilerleme hızındaki artışın ergime havuzu genişliğini azalttığı gözlenmiştir [10]. Ark ile metal ergitmede amper büyüklüğü ve ilerleme hızına ek olarak bir diğer etken parametre olan elektrot ile ergitme vapılacak yüzey arası mesafenin ergime havuzuna etkilerine bakıldığında elektrot mesafesindeki artışın ergime havuzu derinliğini düşürmüştür [11,12].Ayrıca elektrot mesafesinin azalmasıyla ark yolunun yoğunluğunun arttığı raporlanmıştır [13].

Eklemeli imalat yöntemlerinde katman kalınlığı parça kalitesini etkileyen önemli bir faktördür. Literatüre bakıldığında toz yatakta ergitme yapılan eklemeli imalat yöntemlerinde katman kalınlığının 150 mikron ve üstü değerler için [14–21] calısmaların var olduğu ve en fazla 400 mikron [22] katman kalınlığı kullanılarak ergitme yapıldığı tespit edilmiştir. Bu çalışmada literatür kaynaklarında yapılan araştırmalar sonucunda sınır değer olarak belirlenen 400 mikron katman kalınlığındaki 316L paslanmaz celik alasımından olusturulan toz yatakta lazer ve elektron ısınına alternatif olarak ark ile tek cizgi ergitilebilirlik arastırılmıstır. Tek cizgi ergitilebilirliğe etken parametreler olarak arkı oluşturan farklı amper değerleri, tek çizgi ergitme için ilerleme hızları ve elektrot seçilmiştir. mesafeleri Yapılan ergitme

deneyleri sonrası katılaşma görünümleri elde edilerek parametrelerin etkisi raporlanmıştır. Ayrıca ergitme yönüne dik kesitlerde alınan mikroyapı görünümlerinden tabla nüfuziyeti ve ergiyik yüksekliği araştırılmıştır.

2. MATERYAL VE METOT

Deney numunelerinin üretiminde kullanılan düzenek ve ekipmanların gösterimi Şekil 1 a)'da yer almaktadır. Yapılacak deneylerde kullanılacak güç kaynağı akım büyüklükleri 17,22 ve 27 amper olarak seçilmiştir. Belirlenen her bir amper değerinde 1 ve 2 mm/s ilerleme hızları için ayrı ayrı 0,7 ve 1 mm elektrot mesafelerinde ergitmeler yapılmıştır. Yapılan ergitme işleminde arkı oluşturan torcun uç kısmındaki lensli dağıtıcıdan 5 Lt/dak debide yüksek saflıktaki argon gazı ile koruyucu atmosfer oluşturulmuştur. Ergitmeler 10 x 30 mm boyutlarında 2 mm kalınlığındaki 316L paslanmaz celik sac altlıklar üzerinde yapılmıştır. Altlıklar toz yatak serimi sırasında konumlarının bozulmaması adına yine 2 mm derinliğinde ve 31 x 31mm boyutlarına sahip kare taban yüzeyli boşluklara üçer adet yerleştirilmiştir. Altlıkların tutucu tablaya yerleştirilmesi sonrası tabla üzerine getirilen sericinin toz haznesi tarafından gönderilen ışık ergitme tarafında ilk görünmez olduğu andaki tutucu tabla sevivesi üretim ekseninde sıfır konumda kabul edilmiştir. Sonrasında serici en yönlendirilmiş ve yükseltilen haznesinden aldığı ilk katman tozu sıfır konumdaki tabla üzerinde taşıyarak altlık yerleşimindeki boşlular toz ile doldurularak sıfırlama işlemi tamamlanmıştır. Tutucu tablaya verlestirilen altlıkların toz yatak serme islemi sonrası sıfırlanmış görünümü Şekil 1 b)'de gösterilmiştir. Sıfırlama işlemi sonrası serilen toz tabakasının görünümü ise Şekil 1 c)'de yer almaktadır.

Yapılan ergitmeler sonrası katılasma ve ara kesitlerden mikro görünümler elde edilmiştir. Elde edilen katılaşma görünümlerinden ısıl etkilenen bölge ve çizgisel katılaşma kalınlıklarına ulaşılmıştır. Yapılan çalışmada katılaşma görünümlerine ek olarak, üzerinde ergitme vapılan altlıklar orta bölgesinden hassas kesilmiştir. Hassas kesme sırasında kullanılan elmas kaplamalı disk dakikada 200 devir ile bir kısmı su icerisinde kalacak sekilde doldurulmustur. Bu sayede hem disk hem numune kesim sırasında ısınmamıştır. Mikroyapı görünümleri için hassas kesim ile elde edilen ergitme kesitleri zımpara ve keçe yardımıyla parlatılarak ergime nüfuziyetinin belirlenmesi için dağlanmıştır. Dağlama sıvısı olarak Viella solüsyonu, (5 ml HCl, 1 g pikrik asit ve 100 ml 95% ethanol) kullanılmıştır.

3. DENEYSEL BULGULAR

Yapılan çalışmada katılaşma geometrilerine dair incelemelerin araştırılması iki ana başlıkta yapılmıştır. Bu başlıklar katılaşma ve ara kesitlerin mikroyapısal görünümlerinin incelenmesi olup elde edilen bulgular aşağıdadır.

3.1. Katılaşma Görünümlerinin İncelenmesi

Ark ile farklı parametrelerde toz yatakta gerçekleştirilen çizgisel ergitme deneyleri sonucunda elde edilen katılasma görünümleri, sunulmustur. İncelemelerde, Sekil 2'de katılaşma bölgesinin hem ısıl etkilenmiş bölge dış sınırında hem de merkezinde bütünleşik olmayan ergiyik toplaşmalarının mevcut olduğu gözlenmiştir. Bu durum, enerji yoğunluğunun yeterli olmadığı ya da süreklilik arz etmediği koşullarda ergiyik katılaşmalarının düzensiz topaklanmalar halinde olustuğunu göstermektedir [23]. Enerji yoğunluğunun yeterli ve sürekli olduğu koşullarda ise daha düzenli bir çizgisel katılaşma gözlenmiştir. Akım şiddeti arttıkça ve özellikle düşük ilerleme hızlarında ark temas süresinin uzaması, ısı girdisini artırarak katılaşma genişliğini önemli ölçüde artırmıştır [5]. Bu bulgular, literatürdeki benzer çalışmalara paralel olarak, ark ile ergitme süreçlerinde enerji girdisinin ergime havuzu stabilitesi ve katılaşma formu üzerinde kritik bir rol oynadığını ortaya koymaktadır. Örneğin, TIG kaynağında enerji yoğunluğu ve ilerleme hızı gibi parametrelerin ergime havuzu geometrisini doğrudan etkilediği ve yetersiz enerji girdisinin düzensiz katılaşma veya mikro gözeneklere yol açabileceği çeşitli calısmalarda belirtilmistir [8,24].

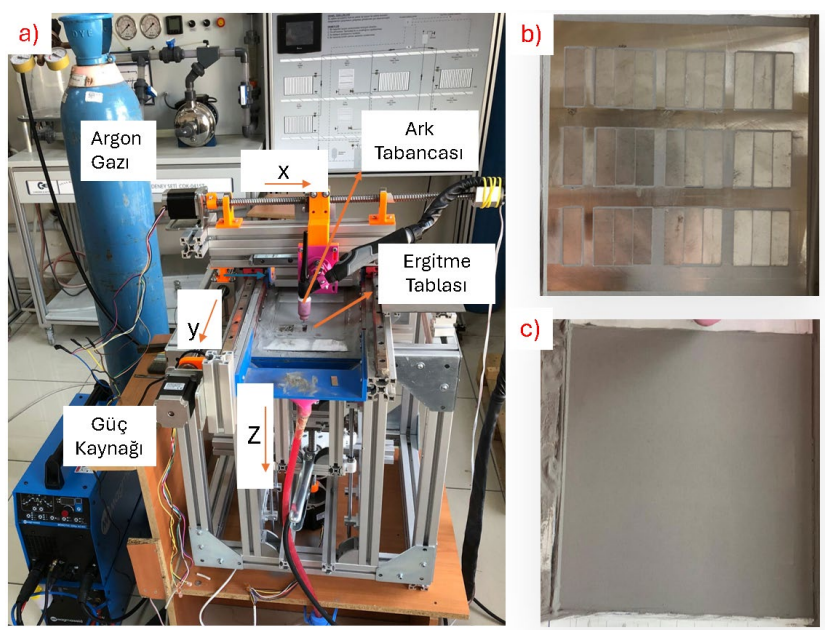
Katılaşma davranışının genel değişimine ait görünümler Şekil 2'de verilmiş olup, elde edilen ısıl etkilenen bölge ve çizgisel katılaşma genişlikleri sırasıyla Çizelge 1 ve Çizelge 2'de sunulmuştur. Isıl etkilenen bölge genişlikleri için yapılan incelemelerde, elektrot mesafesinin 0,7 mm'den 1 mm'ye çıkarılması durumunda ısıl etkilenen bölge genişliğinde azalma eğilimi gözlenmiştir. Ancak, bu durum akım ve ilerleme hızına bağlı olarak değişiklik göstermektedir. Düşük ilerleme hızında (1

mm/s) ve yüksek akım değerlerinde (örneğin, 27 amper) veya yüksek ilerleme hızında (2 mm/s) ve düşük akımda (örneğin, 17 amper), genişliğinde etkilenen bölge 1S1l kaydedilmistir. Orta yüksek ve değerlerinde ise ısıl etkilenen bölge genisliği genellikle azalmıştır. Elde edilen sonuçlar elektrot mesafesinin artışıyla birlikte enerji yoğunluğunun dağılım şeklinin değişmesi ve ergime bölgesine aktarılan ısıl enerjinin farklılaşmasıyla açıklanabilmektedir [25].

Varyasyon katsayısı (CV), ölçümlerin göre ne ortalamaya kadar değişkenlik belirler. CV %10'un altında gösterdiğini olduğunda düşük, %10-20 arasında orta, %20'nin üzerinde ise yüksek ve %40'ın çok yüksek [26] değişkenlik olarak kabul edilir. Isıl etkilenen bölge değişikliğinin belirlenmesinde çizgisel ergitme görünümlerinden en az 15

ölçüm alınmıştır Genel olarak Çizelge 1'de yer alan varyasyon katsayıları incelendiğinde %10'un altında olduğu ve ısıl etkilenen bölge genişliklerinin düzenli bir kalınlığa sahiptir. İsıl etkilenen bölge genişliklerinde en büyük varyasyon katsayısına sahip değerler incelendiğinde ark çanı sınırında oluşan ikincil ergime ve sinterleme karışımlarının çizgiselliği bozduğu tespit edilmiştir.

Çizelge 2'de verilen çizgisel katılaşma genişlikleri incelendiğinde, ilerleme hızı 1 mm/s ve akım 17 amper olduğunda 0,7 mm ve 1 mm elektrot mesafeleri için çizgisel katılaşma gözlenmemiştir. Aynı hız ve akım değerleri için çizgisel katılaşma genişliklerinde elektrot mesafesindeki artışın etkisi incelendiğinde, 22 amper için azalma (1,89 mm'den 1,58 mm'ye) ve 27 amper için artış (2,28 mm'den 2,44 mm'ye) görülmüştür.

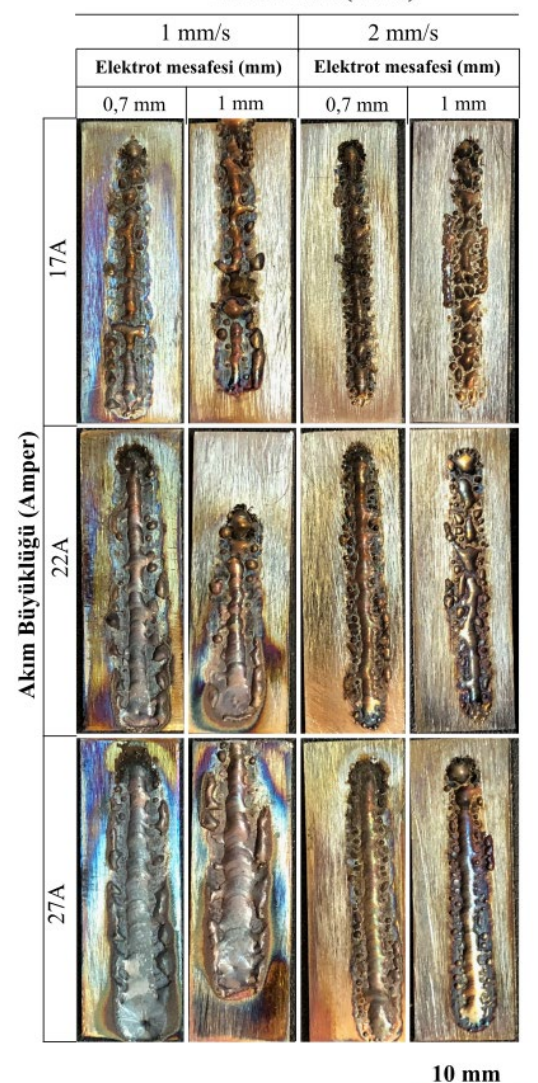


Şekil 1. Ergitmeler yapılırken kullanılan; a) Deney düzeneği, b) Sıfırlama işlemi sonrası altlıkların tutucu tablaya verlesimi ve c) Toz serimi sonrası oluşan görünüm

İlerleme hızı 2 mm/s olduğunda, düşük akımda (17 amper) yine çizgisel katılaşma gözlenmezken, 22 amper için 0,7 mm elektrot mesafesinde 1,29 mm sürekli çizgisel katılaşma elde edilmiş olup 1 mm elektrot mesafesi için sürekli çizgisel katılaşma elde edilememiştir. 27 amper için elektrot mesafesindeki artış ile çizgisel genişlikte azalma (1,63 mm'den 1,38 mm'ye) meydana gelmiştir. Genel olarak, elektrot mesafesi 0,7 mm'den 1 mm'ye çıktığında çizgisel katılaşmanın, akım ve

ilerleme hızına bağlı olarak farklılık gösterdiği tespit edilmistir. Düsük akım seviyelerinde cizgisel katılaşma oluşmazken, elektrot mesafesindeki artışla birlikte orta ve yüksek akımlarda aynı ilerleme hızlarında genellikle çizgisel katılaşma genişliğinde azalma eğilimi görülmüştür. Bu durum, elektrot mesafesi, akım ve ilerleme hızının birlikte kaynak sırasında enerji yoğunluğunu ve malzemenin katılaşma davranısını doğrudan etkilediğini göstermektedir [9,10].

İlerleme hızı (mm/s)



10 mm

Şekil 2. Farklı amper ve ilerleme hızları ile yapılan ergitmelere elektrot mesafesinin etkisi

Çizelge 1. Katılaşma görünümlerinden elde edilen ısıl etkilenen bölge genişlikleri

İlerleme Hızı (mm/s)		1 mm/s						2 mm/s					
Elektrot Mesafesi (mm)	0,7 mm			1 mm			0,7 mm			1 mm			
Akım Şiddeti (Amper)	17A	22A	27A	17A	22A	27A	17A	22A	27A	17A	22A	27A	
Ortalama (mm)	4,61	5,67	6,13	4,32	5,54	6,60	3,23	4,18	4,75	3,77	3,95	4,30	
Standart sapma	0,40	0,64	0,64	0,67	0,64	0,43	0,21	0,37	0,41	0,68	0,33	0,42	
Varyasyon katsayısı %	8,68	11,29	10,44	15,51	11,55	6,52	6,50	8,85	8,63	18,04	8,35	9,77	

Çizgisel katılaşmanın olmadığı durumlar genellikle düşük akım seviyelerinde ve yüksek ilerleme hızlarında enerji yoğunluğunun çizgisel katılaşma oluşturacak kadar yüksek olmadığını işaret etmektedir [17,19]. Buna karşılık, orta ve yüksek akımlarda enerji yoğunluğu yeterli olduğunda çizgisel katılaşma oluşmakta, ancak elektrot mesafesinin artışı ile katılaşma genişliğinde azalma görülmektedir [20]. Yüksek akım ve düşük ilerleme hızında

görülen artış eğilimi ise, daha uzun süreli bir enerji aktarımı ile ergime bölgesindeki termal birikimin artmasından kaynaklanmaktadır [19,20]. Literatürde, özellikle ark ile ergitme yöntemlerinde enerji yoğunluğu ve ilerleme hızının kaynak havuzu boyutları ve katılaşma davranışı üzerindeki etkileri detaylı şekilde incelenmiş ve benzer sonuçlar rapor edilmiştir [27–29].

Çizelge 2'de yer alan varyasyon katsayıları incelendiğinde, ilerleme hızının 1mm/s olduğu durumlarda genel olarak %20 ve üstü değerler görülürken ilerleme hızı 2 mm/s olduğunda değerler %15 ve altında elde edilmiştir. Elde

edilen bu sonuç ilerleme hızındaki artışın sürekli çizgisel katılaşmada genişlik dalgalanmalarını azalmaya sebep olduğunu göstermiştir.

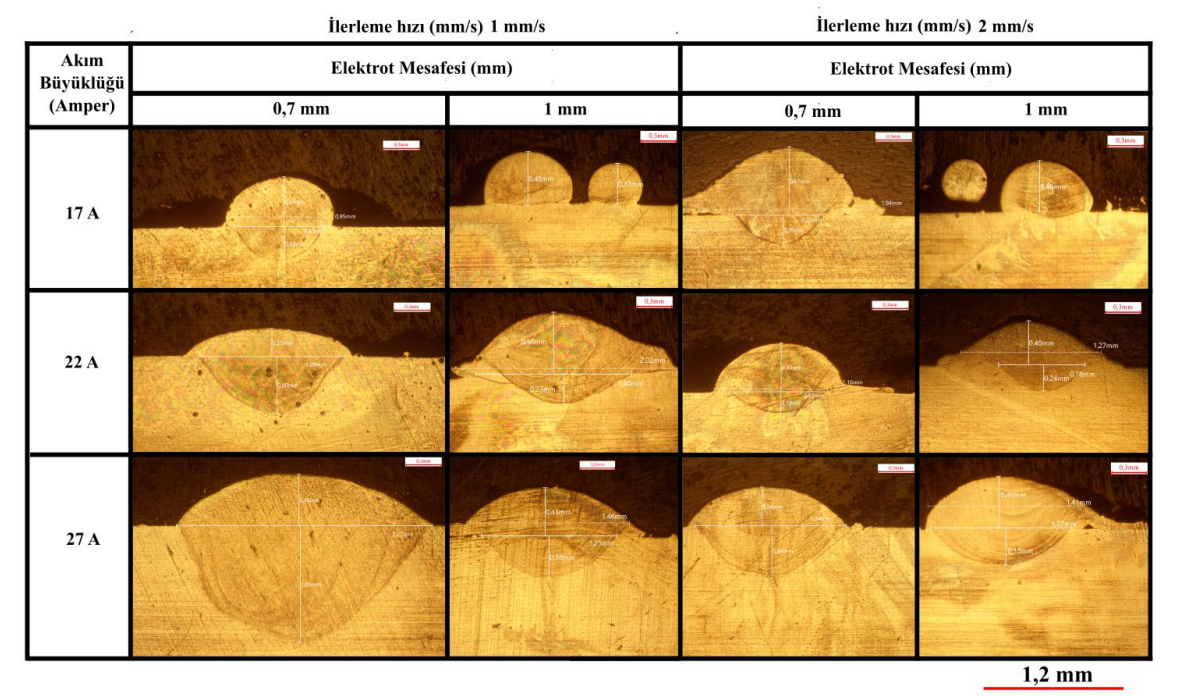
Cizelge 2. Katılaşma görünümlerinden elde edilen çizgisel katılaşma genişlikleri (SÇKY: Sürekli Çizgisel Katılasma Yok)

11													
İlerleme Hızı (mm/s)	1 mm/s						2 mm/s						
Elektrot Mesafesi (mm)	0,7 mm			1 mm			0,7 mm			1 mm			
Akım Şiddeti (Amper)	17 A	22A	27A	17A	22A	27A	17A	22A	27A	17A	22A	27A	
Ortalama (mm)	S	1,89	2,28		1,58	2,44		1,29	1,63			1,38	
Standart sapma	Ç	0,59	0,41	SÇK	0,36	0,69	SÇK	0,20	0,25	SÇK	SÇK	0,19	
Varyasyon katsayısı %	K Y	31,22	17,98	Y	22,78	28,28	Y	15,50	15,34	Y	Y	13,77	

3.2. Mikroyapı Geometrilerinin İncelenmesi

Yapılan ergitmeler sonrası tabla ve toz yatak katılaşmalarının durumunu gösteren mikro yapı görüntüleri Şekil 3'te yer almaktadır. Elde edilen mikroyapı görüntüleri incelendiğinde, ergitme tablası içerisinde ve üzerinde ergiyip katılaşan kısımlara ek olarak ergime alanına komşu sinterlenmiş toz bölgeleri tespit edilmiştir. Tespit edilen sinterlenmiş toz bölgelerinin oluşumunda enerji yoğunluğunun en etkin parametre olmasının yanı sıra malzeme özellikleri ve termal iletkenlik gibi faktörlerin etkin olduğu belirtilmiştir [5]. 17 amper ve 1

mm elektrot mesafesi ile yapılan deneylerde gözlemlenen yetersiz ergime ve nüfuziyet eksikliği, literatürde toplaşma etkisiyle ilişkilendirilmiştir [30]. Ancak, toplaşma yalnızca düşük enerji yoğunluğuna bağlı olmayıp, ısıl kaynağın hızı ve toz yatağın homojenliği ile de ilişkilidir [31]. Mikroyapı görünümlerinde gözlemlenen toplaşmanın yüzeysel ergime bölgelerinden alt tablaya yetersiz tutunması, ergime havuzunun tablaya edebilirliği hakkında ergitme nüfuziyet parametrelerinin kritik rolünü vurgulamaktadır [23].



Şekil 3. Farklı amper ve ilerleme hızları ile yapılan ergitmelere elektrot mesafesinin etkisi

Mikroyapı görünümlerinden elde edilen tabla nüfuziyet kalınlığı, tabla nüfuziyet genişliği, toz yatakta ergime sonucu oluşan katılaşma genişliği ve katılaşma yüksekliğine ait ölçümler için tanımlanan boyutların gösterimi Şekil 4'te yer almaktadır. Şekil 4'te tanımlanan boyutlar her bir mikroyapı için baz alınarak ölçülmüştür. Yapılan ölçümler Şekil 5'te grafikler halinde gösterilmiştir.



Şekil 4. Ergime bölgesine ait ölçümü yapılan geometrilerin gösterimi

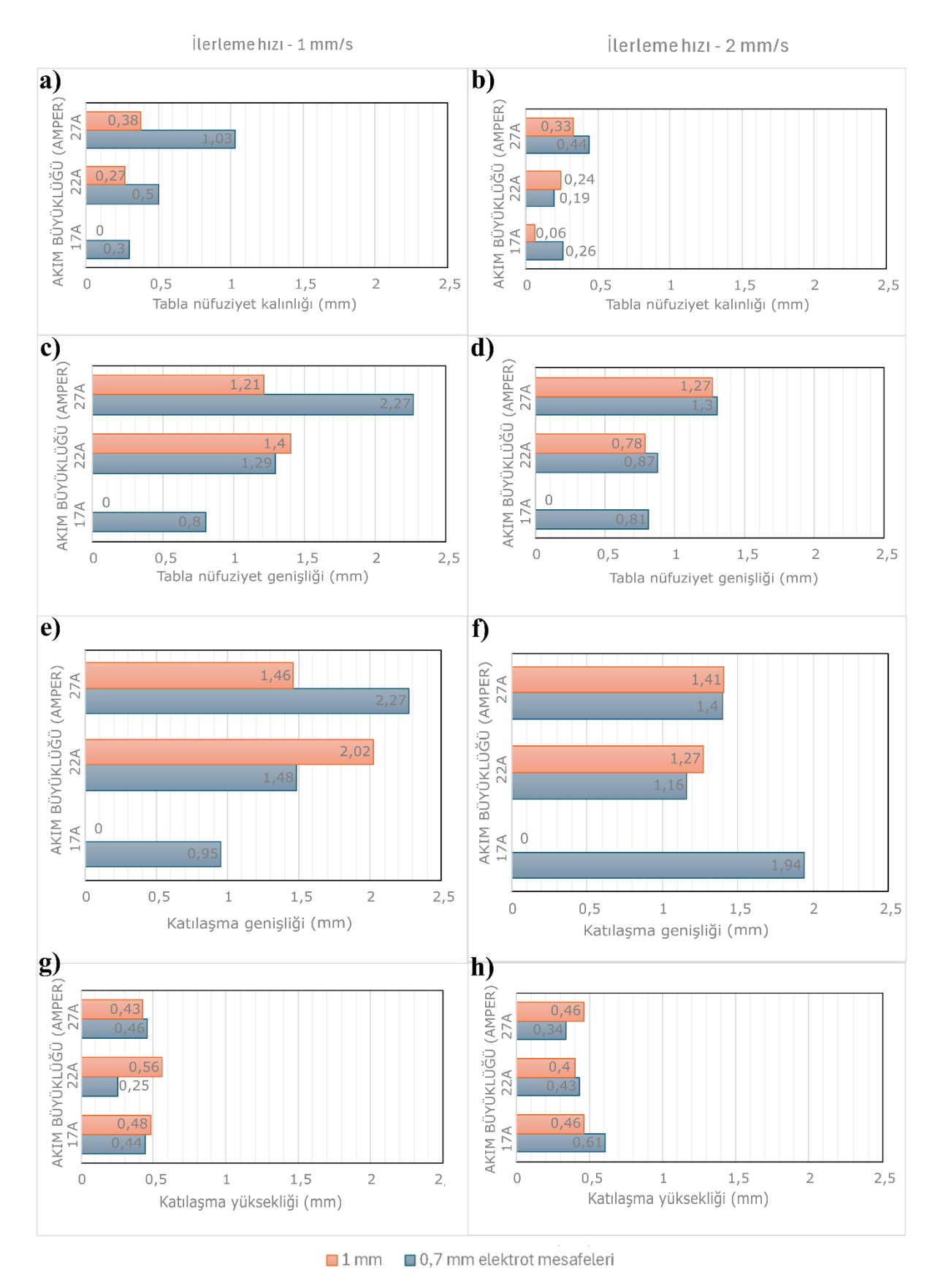
Farklı elektrot mesafesi (0,7 mm ve 1 mm) ve ilerleme hızlarının tabla nüfuziyet kalınlığı üzerindeki etkisi Şekil 5 a) ve b)'de gösterilmiştir. Elektrot mesafesi ve ilerleme hızına bağlı olarak nüfuzivet kalınlığının değiştiği gözlemlenmiş olup 0,7 mm elektrot mesafesi ile daha yüksek nüfuziyet kalınlığı değerleri elde edilmiş olup daha kısa elektrot mesafesi daha yüksek nüfuziyet değerleri sağlamıştır, ancak ilerleme hızındaki artışın bu etkivi dengelendiği görülmüstür [32]. İlerleme hızının artışı, nüfuziyet kalınlığını azaltıcı bir etki yaratmıstır, bu da düsük hızlarda malzemeye daha fazla ısının aktarılmasının enerji yoğunluğunu ve dolayısıyla ergimeyi artırdığını göstermektedir [27–29].

Şekil 5 c) ve d)'de elektrot mesafesi ve ilerleme hızının tabla nüfuziyet genişliği üzerindeki etkileri verilmiştir. 0,7 mm elektrot mesafesi ve 1 mm/s ilerleme hızıyla yapılan ölçümlerde, akımın artışıyla nüfuziyet genişliğinin tutarlı bir şekilde arttığı (0,8 mm'den 2,27 mm'ye) gözlenmistir. Elektrot mesafesi 1 mm'ye çıkarıldığında, düsük akımlarda ergime oluşmamıştır. Akım nüfuziyet artışı genişliğinde 1 mm/s için artış 2 mm/s için azalma şeklinde görülmüştür. Bu durumlar, elektrot mesafesindeki artısın enerji yoğunluğunu özellikle azaltarak düsük akımlarda ergimeyi engellediğini, ergime

genişliğini azalttığını ve düzensiz ergimeye sebep olduğunu göstermektedir [25,27,32].

Şekil 5 e) ve f)'de ise katılaşma genişliğine dair ölçümler verilmiştir. 0,7 mm elektrot mesafesi ile yapılan ölçümlerde, akımın artışıyla katılaşma genişliği belirgin bir şekilde artmıştır (örneğin, 1 mm/s hızda 0,95 mm'den 2,27 mm'ye). Buna karşın, 1 mm elektrot mesafesi kullanıldığında, düşük akımlarda (17 amper) ergime gözlenmezken, 1 mm/s ilerleme hızı için tabla nüfuziyet genişliğine benzer şekilde genişlik azalmıştır. İlerleme hızı 2 mm/s'ye çıkarıldığında, akım değişimlerinin etkisinin daha dengeli olduğu ve genişlik değerlerinde daha az dalgalanma gözlemlenmiştir.

Şekil 5 g) ve h)'de elde edilen tek çizgi ergitmelerin katılaşma yükseklikleri verilmistir. 2 mm/s ilerleme hızında 0,7 mm elektrot mesafesinde 17A, 22A ve 27A büyüklüklerinde katılaşma yükseklikleri 0,61 mm, 0,43 mm ve 0,34 mm olarak ölçülmüştür. Aynı ilerleme hızında elektrot mesafesi 1 mm've çıkarıldığında katılasma yüksekliklerinde 17A ve 22A için azalma ve 27 A için artış gözlenmiştir. İlerleme hızının 1 mm/s olduğu durumda 17 amperden 27 ampere akım artışında katılaşma yüksekliğinde önce akım siddetiyle artıs sonra ise azalma gözlenmiştir. Aynı ilerleme hızında 0,7 mm



Şekil 5. Farklı amper, ilerleme hızı ve elektrot mesafesi ile yapılan ergitmeler için mikroyapı unsurlarına ait ölçüm sonuçları (a), c), d) ve g) için ilerleme hızı 1 mm/s olup b), d), f) ve h) için ilerleme hızı 2 mm/s'dir.)

elektrot mesafesinde ise katılaşma yüksekliği önce azalmış sonra artmıştır. Yapılan katman kalınlığı katılaşma yüksekliği karşılaştırmasında özellikle Şekil 5 g)'de kırmızı ok ile gösterilmiş ergitme parametresi yapılacak üst üste katman ergitmelerinde katman kalınlığının toz yatak kalınlığının artarak yaklaşık 0,65 mm'ye çıkması sebebiyle ergitme için enerji yoğunluğu yetersiz kalacaktır. Ergitme için oluşan yetersiz enerji yoğunluğu ise toplaşma ve düşük alt katman nüfuziyeti sonuçlarına sebep olacaktır [5]. Tam tersi durum özellikle Sekil 5 h)'de mavi ok ile gösterilen ergitme parametreleri için geçerli olup artan katılaşma yüksekliği yeni katmanın kalınlığını azaltacağından enerji yoğunluğunun fazla olması sebebiyle kontrolsüz katılaşmalara sebep olacaktır [5].

Bu sonuçlar, elektrot mesafesi ve ilerleme hızının enerji yoğunluğu, ergime kalitesi ve katılaşma davranışı üzerindeki kritik rollerini vurgulamaktadır. Daha kısa elektrot mesafesi ve düşük ilerleme hızının genellikle daha iyi ergime sonuçları sağladığı, ancak yüksek hız ve mesafe koşullarının bu etkiyi sınırlayabileceği görülmüştür [32–34]

4. SONUÇLAR

316L paslanmaz çalışmada, alaşımından oluşturulan toz yatakta ark ile tek çizgi ergitilebilirlik incelenmiş ve ergitme parametrelerinin (elektrot mesafesi, akım ve ilerleme hızı) katılaşma davranışları mikroyapı üzerindeki değerlendirilmiştir. Elde edilen bulgular, işlem parametrelerinin ergitme performansı ve malzemenin katılaşma geometrisi üzerinde önemli bir etkiye sahip olduğunu ortaya koymuştur. Elektrot mesafesi arttıkça (0,7 mm'den 1 mm'ye) çizgisel katılaşma genislikleri ve 1511 etkilenmiş genisliklerinde azalma gözlenmis, ancak bu azalma eğiliminin akım ve ilerleme hızına bağlı olarak değişiklik gösterdiği belirlenmiştir. Düşük akım ve yüksek ilerleme hızlarında çizgisel katılaşma gözlenmezken, yüksek akım değerlerinde ve düşük ilerleme hızlarında daha genis katılasma bölgeleri elde edilmistir. mesafesinin Elektrot artısıyla enerji yoğunluğunun dağılım seklinin değismesi, düşük akım seviyelerinde ergimeyi engellerken akım sevivelerinde yüksek katılaşma genişliğinde azalmaya neden olmuştur.

Mikroyapı görünümleri incelendiğinde, elektrot mesafesi ve ilerleme hızlarının tabla nüfuziyet kalınlığı ve genişliği üzerinde belirgin bir etkiye sahip olduğu görülmüştür. Daha kısa elektrot mesafesi (0,7 mm) ve düsük ilerleme hızında (1 mm/s), daha yüksek nüfuziyet değerleri elde edilirken, yüksek ilerleme hızlarında ve büyük elektrot mesafelerinde enerji yoğunluğunun azalması sebebiyle ergime yetersiz kalmış ve sinterlenmiş toz bölgeleri ile yüzeysel topaklanmalar meydana gelmistir. Akım arttıkça genellikle tabla nüfuziyet genisliği ve kalınlığı artış göstermiş, ancak bu artış, elektrot mesafesine ve ilerleme hızına bağlı olarak farklılık göstermiştir.

Genel değerlendirmede, düşük ilerleme hızında ve kısa elektrot mesafesinde enerji aktarımı daha verimli gerçekleşmiş ve daha homojen katılasma geometrileri elde edilmistir. Elektrot mesafesi düzenli ergime için en etkili parametre olarak görülse de elektrot mesafesi arttıkça yoğunluğunun malzeme üzerinde homojen dağılımı bozulmus ve bu durum düsük akımlarda ergimeyi sınırlandırırken yüksek akımlarda katılaşma genişliğinde azalmaya yol açabilmiştir. Bu sonuçlar, toz yatakta ark ile tek çizgi ergitilebilirlik için işlem parametrelerinin enerji yoğunluğu, ergime geometrisi ve katılaşma özellikleri üzerindeki etkilerinin optimize edilmesi gerektiğini açıkça ortaya koymuş ve bu alanda yapılacak araştırmalar için yol gösterici olmuştur.

TESEKKÜR

Bu çalışma Kafkas Üniversitesi Bilimsel Araştırma Projeleri Koordinatörlüğü tarafından 2023-FM-40 nolu projesi ile desteklenmiştir.

KAYNAKLAR

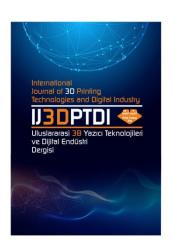
- 1. Babaev A., Promakhov V., Schulz N., Semenov A., Bakhmat V., Vorozhtsov A., "Processes of Physical Treatment of Stainless Steels Obtained by Additive Manufacturing", Metals, Vol. 12, Issue 9, Pages 1-18, 2022.
- 2. Liu, B., Fang, G., Lei, L., Yan, X. "Predicting the porosity defects in selective laser melting (SLM) by molten pool geometry", International Journal of Mechanical Sciences, Vol. 228, Issue 1, Pages 1-14, 2022.
- 3. DebRoy, T., Wei, H.L., Zuback, J.S., Mukherjee, T., Elmer, J.W., Milewski, J.O., Beese, A.M., Wilson-Heid, A., De, A., Zhang, W., "Additive manufacturing of metallic components Process,

- structure and properties", Progress in Materials Science, Vol. 92, Issue 1, Pages 112-224, 2018.
- 4. Nayak, S. K., Mishra, S. K., Paul, C. P., Jinoop, A. N., Bindra, K. S., "Effect of energy density on laser powder bed fusion built single tracks and thin wall structures with 100 μm preplaced powder layer thickness", Optics & Laser Technology, Vol. 125, Issue 1, Pages 112-224, 2018.
- 5. Yadroitsev, I., Smurov, I., "Selective laser melting technology: From the single laser melted track stability to 3D parts of complex shape", Physics Procedia, Vol. 5, Issue 1, Pages 551–560, 2010.
- 6. Di, W., Yongqiang, Y., Xubin, S., Yonghua, C., "Study on energy input and its influences on single-track, multi-track, and multi-layer in SLM", The International Journal of Advanced Manufacturing Technology, Vol. 58, Issue 1, Pages 1189–1199, 2012.
- 7. Cary, H. B., and Helzer, S. C., "Modern Welding Technology", Pages 271-292, Pearson/Prentice Hall, New Jersey, 2005.
- 8. Kutelu, B. J., Seidu, S. O., Eghabor, G. I., Ibitoye, A. I., "Review of GTAW welding parameters", Journal of Minerals and Materials Characterization and Engineering, Vol. 6, Issue 1, Pages 541-554, 2018.
- 9. Singh, R. P., Agrawal, M. K., "Effect of welding current on the dimensions of bead in tungsten inert gas welding process", Materials Today: Proceedings, Vol. 45, Issue 2, Pages 3235-3239, 2021.
- 10. Singh, L., Singh, D., Singh, P. "A Review: Parametric effect on mechanical properties and weld bead geometry of Aluminium alloy in GTAW", IOSR-JMCE, Vol 6, Issue 1, Pages 24-30, 2013.
- 11. Stenbacka, N., Choquet, I., Hurtig, K., "Review of arc efficiency values for gas tungsten arc welding", IIW Commission IV-XII-SG212 Intermediate Meeting, Pages 18-20, Berlin, 2012.
- 12. Mills, K.C., Keene, B.J., "Factors affecting variable weld penetration", International Materials Reviews, Vol. 35, Issue 1, Pages 185–216, 1990.
- 13. Shaoyong, C., Shixin, X., Jimei, W., & Xing, L., "Influence of gap distance on the arc modes transition of cup type AMF electrode", International Symposium on Discharges and Electrical Insulation in Vacuum, Pages 384-387, Matsue, 2016.
- 14. Schleifenbaum, H., Diatlov, A., Hinke, C., Bültmann, J., Voswinckel, H., "Direct photonic production: Towards high speed additive

- manufacturing of individualized goods", Production Engineering, Vol. 5, Issue 1, Pages 359-371, 2011.
- 15. Ma, M., Wang, Z., Gao, M., Zeng, X., "Layer thickness dependence of performance in high-power selective laser melting of 1Cr18Ni9Ti stainless steel", Journal of Materials Processing Technology, Vol. 215, Issue 1, Pages 142-150, 2015.
- 16. Shi, X., Ma, S., Liu, C., Chen, C., Wu, Q., Chen, X., Lu, J., "Performance of high layer thickness in selective laser melting of Ti6Al4V", Materials, Vol. 9, Issue 12, Pages 1-15, 2016.
- 17. Wang, S., Liu, Y., Shi, W., Qi, B., Yang, J., Zhang, F., Han, D., Ma, Y., "Research on high layer thickness fabricated of 316L by selective laser melting", Materials, Vol. 10, Issue 9, Pages 1-15, 2017.
- 18. Shi, W., Liu, Y., Shi, X., Hou, Y., Wang, P., Song, G., "Beam diameter dependence of performance in thick-layer and high-power selective laser melting of Ti-6Al-4V", Materials, Vol. 11, Issue 7, Pages 1-17, 2018.
- 19. Shi, W., Wang, P., Liu, Y., Hou, Y., Han, G., "Properties of 316L formed by a 400 W power laser Selective Laser Melting with 250 µm layer thickness", Powder Technology, Vol. 360, Issue 1, Pages 151-164, 2020.
- 20. Shi, X., Yan, C., Feng, W., Zhang, Y., Leng, Z., "Effect of high layer thickness on surface quality and defect behavior of Ti-6Al-4V fabricated by selective laser melting", Optics & Laser Technology, Vol. 132, Issue 1, Pages 1-11, 2020.
- 21. Brudler, S., Medvedev, A. E., Pandelidi, C., Piegert, S., Illston, T., Qian, M., Brandt, M., "Systematic investigation of performance and productivity in laser powder bed fusion of Ti6Al4V up to 300 μ m layer thickness", Journal of Materials Processing Technology, Vol. 330, Issue 1, Pages 1-18, 2024.
- 22. Aboulkhair, N. T., Maskery, I., Tuck, C., Ashcroft, I., & Everitt, N. M., "On the formation of AlSi10Mg single tracks and layers in selective laser melting: Microstructure and nano-mechanical properties", Journal of Materials Processing Technology, Vol. 230, Issue 1, Pages 88-98, 2016.
- 23. Yadroitsev, I., Krakhmalev, P., Yadroitsava, I., Johansson, S., Smurov, I., "Energy input effect on morphology and microstructure of selective laser melting single track from metallic powder", Journal of Materials Processing Technology, Vol. 213, Issue 4, Pages 606-613, 2013.

- 24. Singh, A. K., Dey, V., Rai, R. N., "Techniques to improveweld penetration in TIG welding (A review)", Materials Today: Proceedings, Vol. 4, Issue 2, Pages 1252-1259, 2017.
- 25. Anık S., Tülbentçi, K., Kaluç, E., "Örtülü Elektrot İle Elektrik Ark Kaynağı", Sayfa 16-83, Gedik Holding A.Ş., İstanbul, , 1991.
- 26. Abubakar, M.L., Ahmed, M.S., Abdussalam, A.F., Mohammed, S. "Meteorological drought and long-term trends and spatial variability of rainfall in the Niger River Basin", Nigeria. Environmental Science and Pollution Research, Vol. 32, Pages 5302–5319, 2025.
- 27. Samiuddin, M., Li, J. L., Taimoor, M., Siddiqui, M. N., Siddiqui, S. U., Xiong, J. T., "Investigation on the process parameters of TIG-welded aluminum alloy through mechanical and microstructural characterization", Defence Technology, Vol. 17, Issue 4, Pages 1234-1248, 2021.
- 28. Tseng, K. H., Chuang, K. J., "Application of iron-based powders in tungsten inert gas welding for 17Cr–10Ni–2Mo alloys", Powder technology, Vol. 228, Issue 1, Pages 36-46, 2012.
- 29. Singh, S.R., Khanna, P., "A-TIG (activated flux tungsten inert gas) welding: A review", Materials Today: Proceedings, Vol. 44, Issue 1, Pages 808–820, 2021.

- 30. Tang, C., Tan, J. L., Wong, C. H., "A numerical investigation on the physical mechanisms of single track defects in selective laser melting", International Journal of Heat and Mass Transfer, Vol. 126, Issue 1, Pages 957-968, 2018.
- 31. Gu, H., Wei, C., Li, L., Han, Q., Setchi, R., Ryan, M., & Li, Q., "Multi-physics modelling of molten pool development and track formation in multi-track, multi-layer and multi-material selective laser melting", International Journal of Heat and Mass Transfer, Vol. 151, Issue 1, Pages 1-16, 2020.
- 32. İpek, İ., "Nikel ve monel malzemelerin kaynağı", Yüksek Lisans Tezi, [Weldıng of nickel and monel materials], [Thesis in Turkish], Sakarya Üniversitesi, Sakarya, 2007.
- 33. Kou, S., "Welding metallurgy", John Wiley and Sons Inc., Hoboken N.J., 2003.
- 34. Coniglio, N., Cross, C. E., "Effect of weld travel speed on solidification cracking behavior. Part 2: testing conditions and metrics", The International Journal of Advanced Manufacturing Technology, Vol. 107, Issue 1, Pages 5025-5038, 2020.



ULUSLARARASI 3B YAZICI TEKNOLOJİLERİ VE DİJİTAL ENDÜSTRİ DERGİSİ

INTERNATIONAL JOURNAL OF 3D PRINTING TECHNOLOGIES AND DIGITAL INDUSTRY

ISSN:2602-3350 (Online)

URL: https://dergipark.org.tr/ij3dptdi

A BIBLIOMETRIC EVALUATION OF SMART AGRICULTURE RESEARCH

Yazarlar (Authors): Sara Naghib Zadeh **, Zümrüt Ecevit Sati**

Bu makaleye şu şekilde atıfta bulunabilirsiniz (To cite to this article): Zadeh S. N., Sati Z. E., "A Bibliometric Evaluation of Smart Agriculture Research" Int. J. of 3D Printing Tech. Dig. Ind., 9(2): 194-206, (2025).

DOI: 10.46519/ij3dptdi.1648618

Araştırma Makale/ Research Article

A BIBLIOMETRIC EVALUATION OF SMART AGRICULTURE RESEARCH

Sara Naghib Zadeh^{a,b}D*, Zümrüt Ecevit Sati

^aIstanbul University, Institute of Graduate Studies in Sciences, Department of Informatics, Türkiye. ^bHalic University, Vocational School, Istanbul, Department of Computer Programming, Türkiye. ^cIstanbul University, Faculty of Political Sciences, Department of Business Administration, Türkiye.

*Corresponding Author: sarazadeh@halic.edu.tr

(Received: 28.02.25; Revised: 26.05.25; Accepted: 25.07.25)

ABSTRACT

Smart agriculture, leveraging technologies such as the Internet of Things, machine learning, and artificial intelligence, offers innovative solutions to enhance productivity, minimize environmental impact, and support data-driven decision-making. This study aimed to perform a bibliometric analysis of research published in the field of smart agriculture from 2014 to 2024. Data were collected from two major databases, Web of Science and Scopus, and analyzed using VOSviewer software. Key indicators examined included annual publication trends, citation metrics, researcher co-authorship networks, and keyword co-occurrence patterns. The results reveal that the number of publications in this field has increased more than twelvefold over the past decade, with emerging technologies forming the core of the main conceptual clusters. Countries such as China, the United States, and India have been leading contributors to scientific output. Six major thematic clusters were identified: technology, resource management, sustainability, data analytics, policymaking, and economics. However, the involvement of social sciences and humanities remains relatively limited. Despite significant advances, challenges persist, including a lack of indigenous research from developing countries and insufficient integration of interdisciplinary data. The findings of this study provide valuable insights to inform innovative policymaking, guide investment in technological infrastructure, and shape future research directions in smart agriculture.

Keywords: Agriculture, Farming, Smart Agriculture, Smart Farming, Bibliometric Analysis

1. INTRODUCTION

The Food and Agriculture Organization (FAO) estimates that the global population will reach approximately 9.73 billion by 2050, leading to a significant increase in the demand for food, water, and natural resources. In response to this challenge, smart agriculture is emerging as a complementary or alternative approach to traditional farming systems [1]. This approach utilizes innovative technologies in the production and management of agricultural products with the aim of increasing productivity, reducing costs, and minimizing environmental impacts [2,3].

Smart agriculture leverages a range of advanced technologies such as the Internet of Things (IoT), Artificial Intelligence (AI), Machine Learning (ML), smart sensors, drones, and

robotics to enable precise monitoring and management of agricultural operations [1]. The evolution of agriculture can be historically categorized into four main stages:

- Agriculture 1.0, based on manual labor and animal power;
- Agriculture 2.0, characterized by the introduction of machinery and mechanization [4];
- Agriculture 3.0, marked by the integration of environmental sensing, data analytics, and digital monitoring systems [5,6];
- Agriculture 4.0 (smart agriculture), which incorporates sensor networks, robotics, cloud computing, and AI to optimize decision-making and improve crop performance [7,8].

Within this context, precision agriculture, as a subset of smart agriculture, focuses on the efficient use of resources through spatial management supported by information technologies. Agriculture 4.0 goes beyond operational precision by intelligently integrating technologies to enhance the resilience and sustainability of agricultural systems [9,10].

Understanding the research developments in this domain requires the application of methods such as bibliometric analysis—a quantitative approach to examining and evaluating the structure, evolution, and trends in a research field using indicators such as publication trends, citation rates, frequent keywords, and patterns of international collaboration [11–13]. The key advantage of bibliometric analysis lies in its ability to structure complex literature and identify gaps and opportunities for further research [14].

This study conducts a bibliometric analysis of smart agriculture research within the time frame of 2014 to 2024. This period was selected due to the rapid growth in scholarly publications, increased investment in digital agricultural technologies, and significant shifts in global agricultural policy.

The primary innovation of this study lies in its comprehensive and structured bibliometric evaluation of the smart agriculture research landscape. Unlike most previous studies that rely solely on either the Web of Science or Scopus database, this research integrates both sources, enhancing the accuracy and completeness of the Additionally, by focusing data. contemporary period (2014–2024), it provides a forward-looking perspective on scientific progress in this field. Another noteworthy contribution is the application of the VOSviewer software to generate visual science maps, illustrating the relationships between concepts, keywords, and authors and revealing hidden structures within the literature. The study also categorizes key concepts into major thematic clusters such as technology, management, sustainability, and agricultural economics, offering a clear framework for guiding future research. Finally, the analysis of contributing countries and academic disciplines provides a realistic depiction of global and interdisciplinary collaboration in advancing smart agriculture.

The main objectives of this research are as follows:

- To analyze research trends and patterns in smart agriculture using data from the Web of Science and Scopus databases.
- To identify and classify the main keywords, concepts, and emerging technologies such as IoT and machine learning within smart agriculture.
- To examine the relationships among key concepts and terms to reveal dominant patterns in smart agriculture research.
- To map the strategic development of smart agriculture research based on publication trends, geographic distribution, and citation metrics.
- To discover and categorize the major themes and concepts in smart agriculture research, with an emphasis on technological advancements and innovations.

2. MATERIAL AND METHOD

There are several sources available for collecting data on scientific publications, the most common of which include Web of Science (WoS), Scopus, Dimensions, Crossref, Microsoft Academic, and Google Scholar. Among these, WoS and Scopus are the two most widely used databases in bibliometric studies [15]. Historically, they were the only accessible options for publication analysis [16]. Due to their high data quality and comprehensive coverage across multiple dimensions, these two databases remain the primary choices for bibliometric research. Choosing between these databases can significantly influence the outcomes of the analysis (Wang & Waltman, 2016). Although Scopus offers broader coverage than WoS, it faces several issues, such as the lack of pre-processed reference lists, which leads to inconsistencies in citations and necessitates complex more bibliometric matching techniques. Additionally, Scopus provides more fragmented coverage, includes a higher number of duplicate citations, varies in source quality, has a shorter historical record, and its classification and indexing systems are less standardized. These factors can bibliometric analyses' accuracy and comprehensiveness [16,17].

In this study, both Web of Science and Scopus were used separately to collect data. Each database was considered an independent source, and no merging or matching of records between them was performed. To extract relevant

publications, a combination of keywords and commonly used terms in the field of smart agriculture was employed. Keywords such as "smart agriculture," "precision agriculture," "digital farming," "agriculture 4.0," and "smart farming" were selected using the OR operator. These keywords were further combined using the AND operator with thematic phrases such as "Smart agriculture" and "Climate change," "Smart agriculture" and "Smart farming," "Smart agriculture" and "Governance," "Smart agriculture" and "Technologies," agriculture" and "Agricultural policies," "Smart agriculture" and "Decision making," "Smart agriculture" and "Machine learning," and "Smart agriculture" and "Internet of Things." The search was conducted across all sections of the articles, including titles, abstracts, keywords, and full text.

A time filter was applied to include studies published between 2014 and 2024, ensuring the inclusion of research relevant to recent developments and emerging technologies in smart agriculture. Only English-language articles were included in the final analysis. However, this language restriction may introduce a bias by excluding research from non-English-speaking countries, particularly in regions such as Latin America, China, Russia, and the Middle East, which could influence the geographical and thematic diversity of the data. In the Web of Science database, the search was conducted across a broad range of indexes, including SCI-EXPANDED, SSCI, A&HCI, CPCI, and BKCI, to capture interdisciplinary dimensions. This approach ensured that articles addressing the social, technological, policyrelated, and conceptual aspects of smart agriculture were also included in the analysis.

3. EXPERIMENTAL FINDINGS3.1. The Analysis of Published Articles in Smart Agriculture

To conduct a more precise analysis of scientific publications in the field of smart agriculture, criteria were established to evaluate and select relevant keyword combinations. The data were extracted from the Web of Science database covering the period from 2014 to 2024. According to Table 1, keyword combinations with at least 1,000 articles and an average citation count above 25 were considered eligible for in-depth analysis, while those with fewer than 500 articles or an average citation count

below 20 were excluded. Additionally, the diversity of publication types—such as reviews, conference papers, and book chapters—was used as a supplementary criterion to ensure a more comprehensive evaluation.

As shown in Table 2, over the past decade, research in the field of smart agriculture has experienced significant growth. According to data extracted from the Web of Science database, more than 17,000 scientific articles containing the keyword "smart agriculture" were published between 2014 and 2024. This considerable volume of academic output reflects the growing global interest in technology- and data-driven solutions in agriculture. Among these, 2,277 are review articles (approximately 13.1% of the total), indicating a relative conceptual maturity of the field. Additionally, 3,570 are conference papers (about 20.5%), which highlights the dynamic nature of technologies emerging and their active dissemination through scientific forums.

In the keyword combination analysis, the pairing of "smart agriculture" and "technologies" yielded the highest number of publications, with 5,000 articles (around 28.8% of the sample). This reflects a strong research focus on modern technologies such as the Internet of Things (IoT), machine learning (ML), robotics, and remote sensing. The average citation per article in this category is approximately 26.3, underscoring its notable scientific impact.

The combination "smart agriculture" and "climate change" ranks second, with 2,962 articles (roughly 17%). This pairing underscores global environmental concerns and the need for climate-resilient agricultural systems. Notably, this category has the highest average citation count (approximately 29.7) among all combinations, indicating its high scientific relevance and interdisciplinary influence across agriculture, environmental science, and sustainable development.

The combination "smart agriculture" and "precision/smart farming", with 4,005 articles, also represents a significant portion of the literature. This co-occurrence reflects a conceptual overlap between the two terms, emphasizing technology-driven precision in agricultural management. However, the average citation rate in this group (21.2) is slightly lower than that of other technology-focused categories.

One noteworthy finding is the relatively low representation of governance and policy-related topics. The combination "smart agriculture" and "governance" appears in only 345 articles (around 1.9%) and has a comparatively lower citation average (17.4 citations per article), suggesting a research gap in institutional, legal, and ethical dimensions. In contrast, the combination "smart agriculture" "agricultural policies" shows a better presence 1.246 with articles. yet remains underrepresented compared to the more dominant technology-oriented themes.

Combinations related to data-driven decision-making and artificial intelligence, such as "decision making" (1,127 articles) and "machine learning" (1,416 articles), account for a substantial share of the research and report relatively high average citation rates (24.1 and 32.8, respectively). This highlights their crucial role in guiding modern agricultural processes. Similarly, the combination "Internet of Things", with 1,858 articles and an average citation rate

of 28.9, underscores its foundational role in enabling real-time communication and automation in smart farming.

In conclusion, the analysis reveals that research in smart agriculture is predominantly oriented toward technological innovation, data-centric approaches, and environmental sustainability, especially through themes such "technologies," "precision agriculture," and "IoT." However, the relatively limited focus on governance. policy, and equity-driven development points to a significant gap. Future research must adopt a more interdisciplinary perspective, with greater attention to the human, institutional, and social dimensions of smart agriculture. Moreover, the rapid growth in studies focused on "decision making" and "machine learning" reflects the increasing importance of data-driven strategies and advanced algorithms in optimizing agricultural systems, marking the evolution of this field into a multifaceted and intelligent discipline.

Table 1. Inclusion and Exclusion Criteria for Keyword Combinations in the Bibliometric Study of Smart Agriculture Research (2014–2024).

Criterion	Eligibility	Elimination
Total Articles	More than 1,000 articles	Fewer than 500 articles
Average Citations (Impact)	Citation average above 25	Citation average below 20
Tech Orientation	Use of emerging technologies (e.g., IoT, ML, AI)	Lack of technological relevance
Article Type Diversity	Includes reviews, conferences, book chapters	Limited to one type of publication
Social/Policy Relevance	Relevant to governance or policy-making	Low attention in policy-related research
Growth/Dynamism	Active in conferences and dynamic publications	Low growth or limited development
Environmental	Interdisciplinary topics like "Climate	Weak connection to global
Relevance	change" considered	environmental issues

Table 2. Distribution of Publications in Smart Agriculture Based on Keyword Combinations (Web of Science, 2014–2024).

Keyword Combination	Total	Review	Proceeding	Book
	Articles	Article	Paper	<u>Chapter</u>
"Smart agriculture"	17,356	2277	3570	369
"Smart agriculture" and "Climate change"	2,962	582	224	120
"Smart agriculture" and "Smart farming"	4,005	605	1,032	94
"Smart agriculture" and "Governance"	345	38	63	15
"Smart agriculture" and "Technologies"	5000	1199	1799	173
"Smart agriculture" and "Agricultural policies"	1,246	192	102	48
"Smart agriculture" and "Decision making"	1,127	151	289	19
"Smart agriculture" and "Machine learning"	1,416	235	359	12
"Smart agriculture" and "Internet of things"	1,858	368	921	47

3.2. Analysis of Published Articles in Smart Agriculture: Role and Impact of Various Scientific Disciplines

Based on data extracted from the Web of Science database, Figure 1 illustrates the distribution of published articles in the field of smart agriculture across various scientific disciplines between 2014 and 2024. The search was conducted using the keywords "smart agriculture" OR "precision agriculture" OR "digital farming" OR "agriculture 4.0" OR "smart farming," and included only publications in the English language.

As expected, the field of agriculture ranks first, with 5,652 published articles, underscoring its central role as the foundational domain of smart agriculture. However, what distinguishes smart agriculture from traditional farming is the strong presence and complementary contributions of interdisciplinary and technology-oriented fields. In second place is engineering, with 4,777 articles, highlighting the importance of engineering tools, systems, and equipment in advancing modern agricultural technologies. This includes subfields such as electrical. mechanical, mechatronics, and control engineering, which play essential roles in the development of agricultural robots, drones, automated irrigation systems, and smart harvesting equipment.

Computer science follows in third place with 4,520 articles. This field plays a key role in developing machine learning algorithms, big data processing, computer vision, and predictive analytics. Many decision-support systems, soil and crop monitoring platforms, and pest detection systems are built on algorithms derived from computer science. Environmental sciences and ecology, with 3,423 articles, rank fourth. These disciplines focus on monitoring climatic conditions. assessing environmental sustainability, and modeling the environmental impacts of agricultural technologies. Their connection with smart agriculture is particularly relevant in the context of climate-smart agriculture. Multidisciplinary science and technology fields, with 2,665 articles, reflect the increasing integration of research efforts across basic sciences, engineering, and the humanities. These areas contribute to the development of sensors, agricultural bioinformatics, and multipurpose analytical tools.

The field of chemistry, with 2,090 articles, has contributed to the design and production of pesticides, nanofertilizers, smart friendly environmentally compoundsespecially relevant in precision agriculture and efforts to reduce ecological harm. Plant sciences, with 1,637 articles, have explored the impact of smart technologies on crop growth, productivity, and resilience. This field is closely linked to genomics. phenotyping, and genetic improvement, which are being significantly enhanced bv data-driven technologies. **Telecommunications** information and technologies, with 1,534 articles, have played a key role in implementing Internet of Things (IoT) infrastructure, wireless sensor networks, and 5G-enabled systems in smart farm management. Additionally, materials science (1,293 articles) and food science and technology (1,354 articles) have contributed to innovations in agricultural equipment materials, smart packaging, cold chain logistics, and extending the shelf life of products.

This analysis clearly highlights the deeply interdisciplinary nature of smart agriculture. Its continued and sustainable development requires collaboration between technical. close biological, environmental, and social sciences. insights help These can researchers. policymakers, and investors better understand existing gaps and capacities, enabling more targeted investments and the formulation of forward-looking policies.

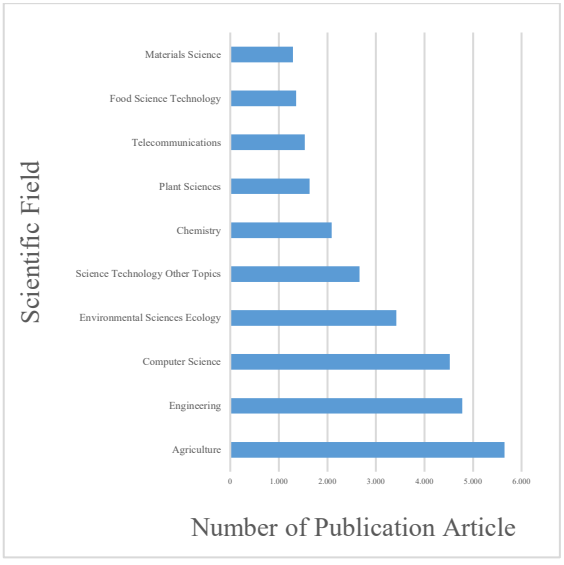


Figure 1. The spread of articles published in the domain of smart agriculture from 2014 to 2024 among different scientific field.

3.3. Analysis of Global Trends in Published Articles on Smart Agriculture (2014-2024)

The data analyzed in this section were extracted from the Web of Science (WoS) database, covering the period from 2014 to 2024. The search was conducted using the keywords "smart agriculture" OR "precision agriculture" OR "digital farming" OR "agriculture 4.0" OR "smart farming." Only English-language documents were included, comprising various types such as Articles, Proceeding Papers, Book Chapters, Review Articles, and Editorial Materials. The purpose of this analysis is to examine the annual growth trend of global publications in the field of smart agriculture and to identify shifts in scientific attention over the past decade.

According to Table 3, titled "Global Publication Trends in Smart Agriculture: Annual Growth and Statistics (2014-2024)," the number of publications increased from 380 in 2014 to 4,914 in 2024, indicating a more than twelvefold rise during this period. This remarkable growth reflects the increasing role of smart agriculture in addressing major global challenges such as food security, climate change, and resource efficiency. In certain years, such as 2016, the annual growth rate peaked at 57.08%, likely driven by technological breakthroughs and increased investment in research. However, in more recent years—specifically 2023 and 2024—the growth rate declined to 9.92% and 15.46%, respectively, which may suggest a saturation in some research areas or a shift in research priorities.

Overall, despite a slight decline in the growth rate in the later years, the general trend highlights the continuous dynamism and relevance of the smart agriculture domain. The high number of publications in 2024 further confirms its established and growing importance in scientific studies. This analysis indicates that smart agriculture remains not only a thriving area of research but also holds great potential for innovation and delivering sustainable solutions to global challenges.

Table 3. Global Publication Trends in Smart Agriculture: Annual Growth and Statistics (2014-2024).

Final Publication	Record	annual growth
Year	Count	quantity of
		publications
2014	380	35%
2015	438	15.26%
2016	688	57.08%
2017	881	28.05%
2018	1,173	33.14%
2019	1,622	38.28%
2020	2,256	39.09%
2021	3013	33.55%
2022	3,872	28.51%
2023	4,256	9.92%
2024	4,914	15.46%

3.4. Analysis of Article Distribution by Countries and Regions in the Area of Smart Agriculture

Based on data extracted from the Web of Science database, Figure 2 illustrates the distribution of scientific publications in the field of smart agriculture across various countries during the period 2014-2024. As shown in the chart, China leads by a significant margin, having published over 600 articles. This dominance is the result of multiple factors. including substantial government investments, technology-driven policies, advanced research infrastructure, and the high economic importance of agriculture within the country. Furthermore, through strategic initiatives such as the "Digital Agriculture 2035" program, China is actively pursuing a structural transformation of its agricultural production and supply chains[18].

In second place is the United States, with more than 350 publications, playing a crucial role in the advancement of agricultural technologies. Leveraging the capabilities of leading universities and research institutions, as well as strong industry collaboration, the U.S. has significantly contributed to the development of machine learning algorithms, land management systems, and agricultural robotics.

India ranks third, with approximately 270 articles. Its position is rooted in a vast agricultural market, a growing demand for efficient technologies, and government-led digital agriculture initiatives. Given challenges such as droughts, resource constraints, and population growth, smart agriculture research in India primarily focuses on productivity enhancement, optimized water usage, and intelligent crop monitoring.

South Korea and Italy occupy the fourth and fifth positions, respectively. These countries have made notable contributions to the scientific literature by capitalizing on advanced technologies and successful experiences in implementing precision agriculture. South Korea, in particular, has emphasized the development of environmental sensors, farm robots, and communication networks (e.g., 5G), playing a key role in enabling IoT-based agriculture.

Other notable contributors include Spain, Germany, Brazil, and Japan, each of which has conducted impactful research based on their unique economic, climatic, and technological contexts. These countries have made advances in areas such as sustainable agriculture, artificial intelligence, supply chain optimization, and climate modeling.

This geographical distribution highlights that scientific output in smart agriculture is closely linked to a country's technological development level, supportive policies, and the economic significance of its agricultural sector. Countries with robust research infrastructures or persistent agricultural challenges tend to show greater interest in innovation and the adoption of advanced technologies. Moreover, regional differences reflect localized priorities within the domain of smart agriculture. For example, North America and East Asia focus more on automation and data mining, while Europe prioritizes environmental sustainability, and South Asia emphasizes resource efficiency and food security.

This analysis can assist researchers, policymakers, and investors in identifying successful global models and designing appropriate research and development pathways tailored to their specific regional needs and conditions.

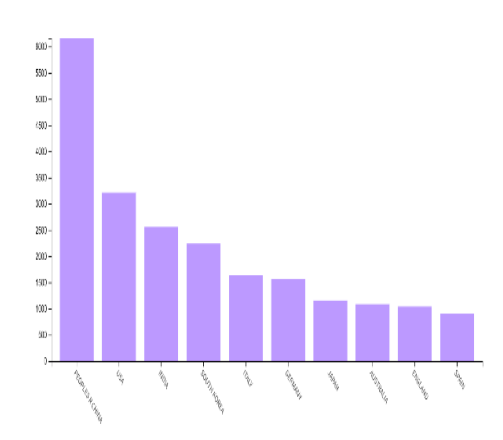


Figure 2. Article distribution across countries and region in the area of smart agriculture.

3.5. Evaluation of Web of Science Citation Indexes in Smart Agriculture

Figure 3 presents an analysis of the Web of Science citation indexes in the field of smart agriculture from 2014 to 2024. The data indicate that a substantial portion of research in this domain has been published in reputable scientific and technological journals. The SCI-Expanded index, with 16,258 records, holds the largest share among the Web of Science indexes. This dominance suggests that research on smart agriculture is primarily disseminated through high-impact journals in the fields of basic science and technology, underscoring the scientific and technological orientation of the discipline.

Furthermore, the CPCI-S index, with 3,460 records, highlights the significant role of conferences in the dissemination of innovative research in this field. The ESCI index, with 2,799 records, reflects the growing presence of emerging studies in newly established journals, signaling an increasing interest in smart agriculture among newer scientific publications. Similarly, the SSCI index, with 1,965 records, addresses the social, policy-related, economic, and sociological aspects of smart agriculture.

On the other hand, the publication of books and humanities-related research in the area of smart agriculture has remained relatively limited. The BKCI-S and BKCI-SSH indexes, with 323 and 160 records respectively, along with the CPCI-SSH index (308 records), indicate that books and the humanities have been less utilized as platforms for disseminating research in this field. This highlights an opportunity to expand

interdisciplinary studies, particularly by integrating the humanities and social sciences with technological approaches in smart agriculture.

Overall, the analysis of citation indexes indicates that research in the field of smart agriculture is predominantly scientific and technological in nature, with the majority of publications appearing in high-impact journals indexed in SCI-Expanded. In addition, conferences and emerging journals—reflected through indexes such as CPCI-S and ESCI-have played a significant role in disseminating innovative research in this domain. However, the relatively low representation of books and humanitiesrelated studies, as indicated by the BKCI and CPCI-SSH indexes, highlights a gap in interdisciplinary engagement. To fully harness the transformative potential of smart agriculture, future research should emphasize the integration of humanities and social sciences with scientific and technological approaches, paving the way for more balanced and sustainable development.

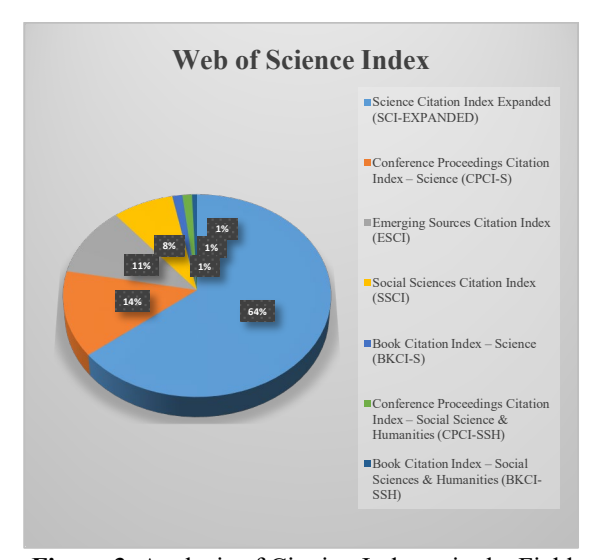


Figure 3. Analysis of Citation Indexes in the Field of Smart Agriculture.

3.6. Citation Analysis and Key Trends in Smart Agriculture Research

In a bibliometric analysis of leading research in the field of smart agriculture from 2014 to 2024, some highly cited articles were identified, focusing on emerging technologies such as the Internet of Things (IoT), machine learning, nanotechnology, and blockchain. Data were collected from the Web of Science database using the keywords: "smart agriculture," "precision agriculture," "digital farming,"

"agriculture 4.0," and "smart farming," combined with the OR operator and limited to the years 2014 to 2024. From the search results, articles were selected based on two criteria: publication in reputable journals under the publishers IEEE and Springer Nature, and receiving more than 400 citations. The selection of articles from the reputable publishers IEEE, Springer Nature, and Elsevier is based on their prominent role in disseminating high-quality research in the field of emerging agricultural technologies. These publishers contribute significantly to the most influential publications in areas such as the Internet of Things, machine learning, and smart agriculture, and their articles are widely cited in the academic community. Focusing on these sources ensures the scientific credibility of the analysis and enables the accurate identification of key research trends. Details of these influential publications are presented in Table 4.

One of the most prominent articles is a study published by Springer Nature in Nature Climate Change, titled "Climate-Smart Agriculture for Food Security". This work presents a conceptual framework for adapting agriculture to climate change and highlights the role of smart technologies in enhancing the resilience of farming systems against environmental variability.

In addition, articles published by IEEE emphasize the pivotal role of IoT in developing infrastructure for environmental monitoring, precision irrigation, and real-time data collection in agriculture. For instance, studies such as "IoT and Data Analytics in Agriculture" and "Survey on IoT in Smart Farming", featured in IEEE Access and the IEEE Internet of Things Journal, explore both the opportunities and challenges of implementing IoT in agricultural environments. These publications underline the benefits of sensor integration, real-time communication, and data analytics, while also addressing barriers such as infrastructure limitations and data security that must be overcome for successful digital agriculture deployment.

Beyond technology, several articles also investigate the social dimensions of smart agriculture. One notable example discusses interdisciplinary approaches to ethical concerns, data ownership, and farmer participation. These

types of studies, often published in Springer Nature journals, stress that technological advancement must be accompanied by consideration of human, social, and policy factors to ensure sustainable adoption within farming communities.

Finally, innovations such as blockchain and nanotechnology are also featured in the most cited articles. Blockchain is presented as a tool for improving transparency and traceability in agricultural supply chains, while nanoformulations are explored for their potential to reduce pesticide usage and enhance pest control efficiency. Overall, this analysis reveals that the convergence of digital technologies with agriculture outlines a promising path toward a more sustainable, data-driven, and climateresilient agricultural future.

Table 4. Most Cited Articles on Smart Agriculture Technologies (2014–2024) Published by IEEE, Springer Nature, and Elsevier (Source: Web of Science).

Title	Citations	Year	Journal	Key Topics	Conceptual Contribution
Climate-smart Agriculture for Food Security [19]	960	2014	Nature Climate Change (Springer Nature)	Climate Change	Establishes a framework linking food security, climate change, and smart agricultural technologies.
An Overview of Internet of Things (IoT) and Data Analytics in Agriculture: Benefits and Challenges [20]	646	2018	IEEE Internet of Things Journal	IoT, Data Analytics	Explores early applications of the Internet of Things in agriculture, highlighting benefits and infrastructure challenges.
IoT and Agricultural UAVs: Comprehensive Review[21]	370	2022	Internet of Things Journal (IEEE)	UAV, IoT	Reviews the combined applications of UAVs and sensors in advancing smart agriculture.
IoT-Based Smart Agriculture: Making the Fields Talk [22]	368	2019	IEEE Access	ІоТ	Focuses on developing communication infrastructure for smart agriculture through IoT.
A Survey on the Role of IoT in Agriculture for the Implementation of Smart Farming [23]	333	2019	IEEE Access	IoT	Offers a broad examination of the role of IoT in smart farming practices.
IoT for Smart Precision Agriculture in Rural Areas [24]	285	2018	IEEE Internet of Things Journal	IoT, Precision Agriculture	Discusses how IoT can enhance agricultural development in remote and rural regions.
UAVs in Smart Agriculture: Applications and Challenges [25]	283	2021	IEEE Sensors Journal	UAVs, Automation	Reviews the technical requirements and challenges of integrating UAVs in smart agriculture.
Internet of Things for the Future of Smart Agriculture: A Comprehensive Survey of Emerging Technologies [26]	236	2021	IEEE/CAA Journal of Automatica Sinica	IoT, Technology	Provides a comprehensive review of emerging IoT technologies for the future of smart agriculture.
Recent advancements and challenges of Internet of Things in smart agriculture: A survey [27]	212	2022	Future Generation Computer Systems (Elsevier)	IoT, Challenges	Surveys current and future challenges associated with implementing IoT in agricultural systems.

3.7. Visualizing Bibliometric Networks in **Smart Agriculture Research Using Vosviewer** Information visualization is an essential technique for understanding the structure and relationships within large sets of documents. To support this, specialized tools have been developed that allow for dynamic and intuitive representation of vast amounts of information. One such tool is VOSviewer, an open-source software designed specifically for creating and visualizing bibliometric networks. VOSviewer allows researchers to generate network maps and explore complex relationships in a visual format [28]. In this study, VOSviewer was also used to construct and display networks of co-authorship and country collaboration.

This study employed VOSviewer software to generate a strategic coordination map, enabling analysis in-depth of the complex interconnections among keywords and thematic areas within smart agriculture research. The selection of VOSviewer was based on its powerful capabilities in producing bibliometric maps and its user-friendly interface, which enhances clarity and accessibility for a broad range of users. Figure 4 presents a network diagram created using VOSviewer, visualizing the most influential publications on smart agriculture indexed in the Scopus database between 2014 and 2024. In this visualization, author-assigned keywords appear as nodes, where the size of each node indicates the frequency of the keyword's occurrence, and the links between nodes represent the co-occurrence relationships between keywords [45]. Only keywords appearing at least five times were included in the analysis, resulting in a total of 3,474 keywords, with 277 meeting the minimum threshold. After constructing the co-occurrence network, we analyzed the nodes and identified the most frequently co-occurring keywords. Based on a review of relevant literature in smart agriculture, we then classified the keywords into thematic clusters. Each cluster was labeled with a parent category reflecting its overarching research domain. Table 5 presents the most frequently used keywords in smart agriculture, organized into categories according to the primary themes that emerged from the network analysis.

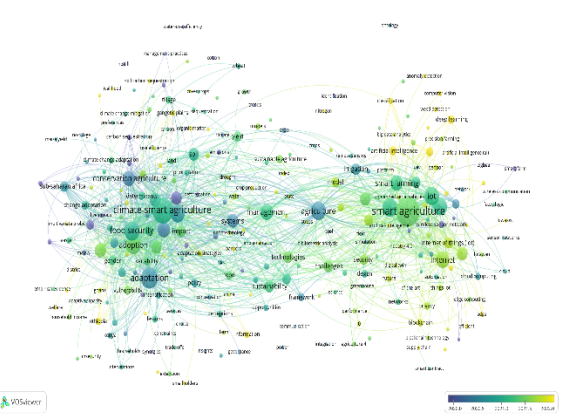


Figure 4. Keyword Co-occurrence networks.

Table 5. The key terms in the domain of smart

agriculture, separated by the main branches.					
Primary	Key Words				
Branches					
General	Smart Agriculture, Precision				
Keywords	Agriculture, Agricultural				
	Technology, Sustainable				
	Agriculture, Agricultural				
	Innovation				
Technology	IoT Applications in Agriculture,				
and	Big Data Utilization in				
Applications	Agriculture, Artificial				
	Intelligence in Agricultural				
	Practices, Machine Learning in				
	Agriculture, Agricultural				
	Drones, Remote Sensing in				
	Agriculture, Crop Monitoring,				
	Soil Monitoring, Smart				
	Irrigation, Variable Rate				
	Technology (VRT), GPS				
	Agriculture				
Agricultural	Farm Management Information				
Management	Systems (FMIS), Decision				
and	Support System, (DSS) in				
Strategies	Agriculture, Agricultural Supply				
	Chain Management, Yield				
	Mapping, Site-Specific Farming				
Sustainability	Climate-Smart Agriculture,				
and	Carbon Sequestration in				
Environment	Agriculture, Water-Efficient				
	Farming, Organic Farming				
	Technology				
Data and	Data Analytics in Agriculture,				
Analysis	Sensor Networks in Agriculture,				
	Agricultural Robotics,				
	Geospatial Analysis in				
	Agriculture				
Research and	Agricultural Research, Agri-				
Education	Tech Education, E-agriculture,				
	Digital Farming				
Economic	Agricultural Economics, Rural				
and Social	Development Technology, Agri-				
	Business Innovation				

Table 5 presents a review of key terms in the field of smart agriculture, categorizing them according to major thematic branches. General terms such as smart agriculture, precision agriculture, agricultural technology, sustainable agriculture are introduced foundational concepts. The technology and applications branch encompasses the use of technologies such as the Internet of Things (IoT), big data, artificial intelligence, machine learning, drones, sensors, smart irrigation, and other related tools in agricultural settings. The agricultural management and strategy branch includes terms such as farm management information systems, decision support systems, agricultural supply chain management, and localized agricultural technologies. sustainability and environment branch addresses concepts like climate-resilient agriculture, water optimization, and organic farming, emphasizing environmental adaptation and resource conservation. The data and analytics branch focuses on areas such as data analysis, sensor networks, agricultural robotics, and geospatial analytics.

The research and education branch covers terms related to agricultural research, agricultural technology education, and digital agriculture. Lastly, the economic and social aspects branch includes themes such as agricultural economics, rural development technologies, and innovation in agribusiness. This categorization offers a comprehensive overview of the core domains and terminology within smart agriculture.

Table 6 further introduces and defines key concepts in smart agriculture and illustrates the relationships among them. It explains terms such as climate-resilient agriculture, food security, water efficiency, and smart agriculture, highlighting their roles in improving agricultural productivity and sustainability. For each concept, the table provides a description of its function and interconnections. For instance, smart agriculture refers to the application of technologies like IoT and sensors to enhance efficiency and output, while water efficiency involves improved water management aimed at reducing environmental impacts. The table also identifies key conceptual linkages, such as the connection between food security and climate change, or between soil management and sustainability. This structure enables readers to grasp the multidimensional implications of each concept and understand their importance in driving forward smart agriculture.

4. RESULTS

This bibliometric study offers a comprehensive assessment of the evolution, conceptual structure, and scientific landscape of smart agriculture research from 2014 to 2024. Drawing on data from two reputable databases-Web of Science and Scopus—and utilizing visual analytical tools such as VOSviewer, the study presents a detailed overview of publication core research themes, and trends, technological developments in the field. The rapid increase in scholarly output, particularly in areas related to data-driven approaches and climate-resilient agriculture, reflects growing global interest in leveraging advanced technologies to address agricultural challenges. Further analysis revealed that scientific publications in smart agriculture grew more than twelvefold during the study period. The highest annual growth occurred in 2016, while the publication volume peaked in 2024, highlighting the dynamic nature and rising prominence of the field. Geographically, China, the United States, and India lead in scientific output, underlining influence of national policies investments agricultural technology. Moreover, disciplinary analysis shows that smart agriculture lies at the intersection of agricultural sciences, engineering, information technology, and environmental studies, demonstrating its inherently interdisciplinary character.

The conceptual analysis using VOSviewer identified six major thematic clusters centered on technologies such as the Internet of Things (IoT), big data, intelligent decision-making, and environmental sustainability. While these technologies dominate the current literature, citation analysis reveals limited engagement from the social sciences, humanities, and policy-related fields. This gap underscores the need for broader, more inclusive research perspectives that integrate human, institutional, and ethical dimensions alongside technical innovations.

In conclusion, the findings of this study suggest that the future of smart agriculture should focus on enhancing interdisciplinary collaboration, empowering smallholder farmers, advancing digital equity, and employing more sophisticated analytical tools. Additionally, developing open, data-driven infrastructures and evidence-based

policymaking will help guide the research and application of smart agriculture more effectively. Ultimately, smart agriculture

represents not only a technological imperative but also a critical pathway toward achieving global sustainability goals.

Table 6. Key terms and related concepts in smart agriculture.

		<u> </u>
Key Words	Definition	Links
Climate-smart	Agricultural methods designed to adjust to	Entails strong connections with food
Agriculture	climate variations and optimize the	security, adaptation, water management.
	utilization of climate-related resources.	
Smart	It aims to increase agricultural efficiency	Data-based decision making is linked to
Agriculture	by using technological innovations (IoT, sensors).	drive systems and automation.
Adaptation	Changing farming methods to respond to the effects of climate change.	Climate smart agriculture is associated with environmental sustainability; various strategies (e.g., plant species change).
Food Security	Ensuring that all have access to sufficient, safe and nutritious food.	Climate change interacts directly with agricultural productivity and social justice.
Water Efficiency	Better use of water resources and savings.	Irrigation is related to groundwater management and environmental impacts
Sustainability	Conserving resources by balancing economic, environmental and social conditions.	Linked to sustainable agricultural practices, renewable energy and natural resource management.
IoT (Internet of Things)	A system in which objects are connected to each other to collect data in agriculture.	Smart agriculture involves many connections with data analytics and automation.
Agricultural Practices	Methods of conducting agriculture; sustainable, traditional or modern practices.	Related to agricultural policies, food production impacts and environmental sustainability.
Technology Adoption	Incorporating new technologies into agricultural processes.	Links to education, policy development and financing.
Climate Resilience	Increasing resilience to climate change.	Adaptation approaches are related to environmental protection and healthy ecosystems.
Crop	Optimization of the growth processes of	Productivity is directly linked to adaptation
Management	agricultural products.	strategies to climatic conditions.
Soil Health	Preservation of soil structure and fertility.	Water management has an important relationship with agricultural practices and sustainability.

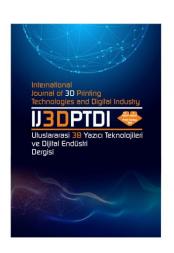
REFERENCES

- 1. Charoenkwan, P., Chotpatiwetchkul, W., Lee, V. S., Nantasenamat, C., Shoombuatong, W., "A novel sequence-based predictor for identifying and characterizing thermophilic proteins using estimated propensity scores of dipeptides", Scientific Reports, Vol. 11, Issue 1, Pages 1–15, 2021.
- 2. Abbasi, R., Martinez, P., Ahmad, R., "The digitization of agricultural industry a systematic literature review on agriculture 4.0", Smart Agricultural Technology, Vol. 2, Pages 100042, 2022.
- 3. Liu, D. M., et al., "Agriculture 4.0 as a new vector towards increasing the food security in Russia", IOP Conference Series: Earth and Environmental Science, Vol. 677, Issue 3, Pages 032016, 2021.

- 4. Xing, Z. P., et al., "Temperature and solar radiation utilization of rice for yield formation with different mechanized planting methods in the lower reaches of the Yangtze River, China", Journal of Integrative Agriculture, Vol. 16, Issue 9, Pages 1923–1935, 2017.
- 5. Domínguez-Niño, J. M., Oliver-Manera, J., Girona, J., Casadesús, J., "Differential irrigation scheduling by an automated algorithm of water balance tuned by capacitance-type soil moisture sensors", Agricultural Water Management, Vol. 228, Pages 105880, 2020.
- 6. Stambouli, T., Faci, J. M., Zapata, N., "Water and energy management in an automated irrigation district", Agricultural Water Management, Vol. 142, Pages 66–76, 2014.

- 7. Tetteh Quarshie, P., et al., "Myth or reality? The Digitalization of Climate-Smart Agriculture (DCSA) practices in smallholding agriculture in the Bono East Region of Ghana", Climate Risk Management, Vol. 42, Pages 100553, 2023.
- 8. Wakweya, R. B., "Challenges and prospects of adopting climate-smart agricultural practices and technologies: Implications for food security", Journal of Agricultural and Food Research, Vol. 14, Pages 100698, 2023.
- 9. Bacco, M., Barsocchi, P., Ferro, E., Gotta, A., and Ruggeri, M., "The Digitisation of Agriculture: a Survey of Research Activities on Smart Farming", Array, Vol. 3–4, Pages 100009, 2019.
- 10. Chiu, M. C., Yan, W. M., Bhat, S. A., and Huang, N. F., "Development of smart aquaculture farm management system using IoT and AI-based surrogate models," journal of Agriculture and Food Research, Vol. 9, Pages 100357, 2022.
- 11. Almas, K., Ahmad, S., Ur Rehman, S., Aljofi, F., and Siddiqi, A., "Mapping out the scientific literature on extraction and socket preservation: A Scopus based analysis (1968–2020)," The Saudi Dental Journal, Vol. 34, Issue 8, Pages 681–688, 2022.
- 12. Fauzi, M. A., "A bibliometric review on knowledge management in tourism and hospitality: past, present and future trends," International Journal of Contemporary Hospitality Management, Vol. 35, Issue 6, Pages 2178–2201, 2023.
- 13. Yan, S., Zhang, H., and Wang, J., "Trends and hot topics in radiology, nuclear medicine and medical imaging from 2011–2021: a bibliometric analysis of highly cited papers," Japanese Journal of Radiology, Vol. 40, Issue 8, Pages 847–856, 2022.
- 14. Fauzi, M. A., Zainal Abidin, N. H., Suki, N. M., and Budiea, A. M., "Residential rooftop solar panel adoption behavior: Bibliometric analysis of the past and future trends," Renewable Energy Focus, Vol. 45, Pages 1–9, 2023.
- 15. Waltman, L., and Larivière, V., "Special issue on bibliographic data sources," Quantitative Science Studies, Vol. 1, Issue 1, Pages 360–362, 2020.
- 16. Visser, M., van Eck, N. J., and Waltman, L., "Large-scale comparison of bibliographic data sources: Scopus, Web of Science, Dimensions, Crossref, and Microsoft Academic," Quantitative Science Studies, Vol. 2, Issue 1, Pages 20–41, 2021.
- 17. Waltman, L., "A review of the literature on citation impact indicators," Journal of informetrics, Vol. 10, Issue 2, Pages 365–391, 2016.

- 18. MacPherson, J., Voglhuber-Slavinsky, A., Olbrisch, M., Schöbel, P., Dönitz, E., Mouratiadou, I., & Helming, K., "Future agricultural systems and the role of digitalization for achieving sustainability goals. A review," Agronomy for Sustainable Development, Vol. 42, Issue 4, Pages 70, 2022.
- 19. Lipper, L., Thornton, P., Campbell, B., Baedeker, T., Braimoh, A., Bwalya, M., Caron, P., Cattaneo, A., "Climate-smart agriculture for food security," Nature Climate Change, Vol. 4, 2014.
- 20. Elijah, O., Rahman, T.A., Orikumhi, I., Leow, C.Y., Hindia, M.D.N., "An overview of Internet of Things (IoT) and data analytics in agriculture: Benefits and challenges," IEEE Internet of Things Journal, Vol. 5, Issue 5, 2018.
- 21. Boursianis, A. D., et al., "Internet of things (IoT) and agricultural unmanned aerial vehicles (UAVs) in smart farming: A comprehensive review," Internet of Things, Vol. 18, Pages 100187, 2022.
- 22. Ayaz, M., Ammad-Uddin, M., Sharif, Z., Mansour, A., & Aggoune, E. H. M., "Internet-of-Things (IoT)-based smart agriculture: Toward making the fields talk," IEEE, Vol. 7, Pages 129551-129583,2019.
- 23. Raliya, R., Saharan, V., Dimkpa, C., & Biswas, P., "Nanofertilizer for Precision and Sustainable Agriculture: Current State and Future Perspectives," Journal of Agricultural and Food Chemistry, Vol. 66, Issue 26, Pages 6487–6503, 2017.
- 24. Ahmed, N., De, D., & Hussain, I., "Internet of Things (IoT) for Smart Precision Agriculture and Farming in Rural Areas," IEEE Internet of Things Journal, Vol. 5, Issue 6, Pages 4890–4899, 2018.
- 25. Maddikunta, P. K. R., Hakak, S., Alazab, M., Bhattacharya, S., Gadekallu, T. R., Khan, W. Z., & Pham, Q. V., "Unmanned aerial vehicles in smart agriculture: Applications, requirements, and challenges," IEEE Sensors Journal, Vol. 21, Issue 16, Pages 17608-17619, 2021.
- 26. Friha, O., Ferrag, M. A., Shu, L., Maglaras, L., & Wang, X., "Internet of Things for the Future of Smart Agriculture: A Comprehensive Survey of Emerging Technologies," IEEE/CAA Journal of Automatica Sinica, vol. 8, Issue 4, Pages 718–752, 2021.
- 27. Sinha, B., Dhanalakshmi, R., "Recent advancements and challenges of Internet of Things in smart agriculture: A survey," Future Generation Computer Systems, Vol. 126, Pages 169-184, 2022.
- 28. Van Eck, N.J., & Waltman, L., "VOSviewer Manual," Leiden: Universiteit Leiden, Pages 1-53, 2013.



ULUSLARARASI 3B YAZICI TEKNOLOJİLERİ VE DİJİTAL ENDÜSTRİ DERGİSİ

INTERNATIONAL JOURNAL OF 3D PRINTING TECHNOLOGIES AND DIGITAL INDUSTRY

ISSN:2602-3350 (Online)

URL: https://dergipark.org.tr/ij3dptdi

EXPERIMENTAL AND STATISTICAL ANALYSIS OF THE EFFECT OF 3D PRINTING PARAMETERS ON MECHANICAL PERFORMANCE

Yazarlar (Authors): Vahap Neccaroğlu¹, İsmail Aykut Karamanlı 1

Bu makaleye şu şekilde atıfta bulunabilirsiniz (To cite to this article): Neccaroğlu V., Karamanlı İ. A., "Experimental and Statistical Analysis of The Effect of 3D Printing Parameters On Mechanical Performance" Int. J. of 3D Printing Tech. Dig. Ind., 9(2): 207-219, (2025).

DOI: 10.46519/ij3dptdi.1653336

Araştırma Makale/ Research Article

EXPERIMENTAL AND STATISTICAL ANALYSIS OF THE EFFECT OF 3D PRINTING PARAMETERS ON MECHANICAL PERFORMANCE

Vahap Neccaroğlu^a, İsmail Aykut Karamanlı^b

^aBartın University, Faculty of Engineering, Department of Mechanical Engineering, TÜRKİYE ^bYozgat Bozok University, Sorgun Vocational School, Department of Motor Vehicles and Transportation Technologies, TÜRKİYE

* Corresponding Author: <u>vahapneccaroglu@gmail.com</u>

(Received: 07.03.25; Revised: 31.05.25; Accepted: 12.06.25)

ABSTRACT

This study examines the influence of material type, layer height, and fill rate on the surface hardness, bending strength, and printing duration of specimens produced via Fused Deposition Modeling (FDM). Specimens made from PLA+ and ABS were fabricated using two distinct layer thicknesses (0.10 mm and 0.20 mm) and four varying fill rates (40%, 60%, 80%, and 100%). The mechanical properties of these specimens were assessed through three-point bending tests and Shore D hardness evaluations. The Taguchi optimization method was employed to identify optimal printing parameters that maximize bending strength and surface hardness while minimizing printing time. The findings revealed that PLA+ displayed superior bending strength compared to ABS, particularly at elevated infill densities. Furthermore, the fill rate predominantly affected the surface hardness, with higher densities correlating with improved hardness values. Statistical analysis conducted through ANOVA indicated that the material type significantly impacts bending strength, while the fill rate primarily influences surface hardness. In addition, the findings indicate that the print time is significantly affected by both material selection and filler density. The results obtained have been verified by producing control samples. According to the verification tests, the model was able to perform predictions with deviations changing between %3-16. This study highlights the essential trade-off between mechanical performance and production efficiency in 3D printing applications and suggests a different approach to optimizing manufacturing process parameters in order to improve part quality while reducing production costs.

Keywords: Fused Deposition Modeling, Bending Strength, Hardness, Taguchi Analysis.

1. INTRODUCTION

Additive Manufacturing (AM) manufacturing technique that, unlike traditional manufacturing methods, is based on the principle of layer-by-layer deposition of materials and allows complex dimensional (3D) structures to be produced with high precision and minimal material waste [1]. This technology has received a great deal of attention in recent years, especially due to its design flexibility, rapid prototyping and personalized production [2]. It is widely used in various industries such as aerospace, robotic healthcare, automotive. systems, consumer products and even architecture to produce lightweight and high-performance components [3-4].

Among additive manufacturing techniques, Fused Deposition Modeling (FDM) is one of the most widely preferred methods due to its low cost, ease of use and wide range of materials [5-6]. FDM is particularly suitable for thermoplastic materials such as polylactic acid (PLA) and acrylonitrile butadiene styrene (ABS) [7]. These materials are frequently preferred in industrial and academic studies due to their environmentally friendly properties and mechanical performance [8].

The FDM process is based on the principle of extruding a thermoplastic filament through a heated nozzle and depositing it layer by layer according to a predetermined pattern [9]. However, the mechanical performance of

components produced by this method is significantly affected by various parameters such as layer thickness, fill rate, build-up rate, print orientation, material composition and nozzle temperature [10-11]. Optimizing these parameters plays a critical role in improving the durability, surface quality and dimensional accuracy of the produced parts [12]. In the comparative optimization of the production parameters of ABS and PLA specimens, it was found that material type, fill rate and printing speed were effective on tensile strength and printing times [13]. In another study, it was reported that the bending and tensile strength of polyethylene terephthalate (PET) reinforced with PLA and thermoplastic polyurethane (TPU) decreased slightly compared to standard PET, but the impact strength increased significantly [14].

Popescu et al. [9] investigated the FDM process parameters that affect the mechanical properties through a literature review and reported that layer thickness, build-up rate and print orientation are critical factors. It was found that thin layer thickness and appropriate print orientation increased tensile and bending strength. Similarly, Sood et al. [15] performed ANOVA analysis on the experimental data by examining five basic process parameters (layer thickness, orientation, printing angle, printing width and air gap) and showed that layer thickness and printing angle are significant factors on tensile, bending and impact strength. Camargo et al. [16] found that layer thickness improves mechanical properties, but the fill parameter showed different results in different tests. It was observed that as the layer thickness increased, tensile and bending strength increased while impact energy decreased. Letcher et al. [17] Afrose et al. [18] investigated the effects of print orientation on fatigue strength and tensile strength, results showed that 45° orientation gave the best fatigue strength and tensile strength.

Signal-to-noise (S/N) ratio analysis by Taguchi method and analysis of variance (ANOVA) are widely used statistical techniques for optimization of experimental parameters and determination of their effects on mechanical

performance [19]. Travieso-Rodriguez et al. [20] investigated the effect of six different printing parameters (layer height, layer width, fill rate, layer orientation, print speed and fill pattern) on bending strength of PLA specimens using Taguchi and ANOVA and found that layer orientation is the most critical parameter. Zisopol et al. [21] performed experimental compare analyses to the mechanical performance of PLA and ABS materials and showed that PLA offers higher bending strength compared to ABS.

This study aims to investigate the effect on bending strength, surface hardness and printing time of PLA+ and ABS specimens printed by FDM for two different layer thicknesses and three different fill rates. In addition, using Taguchi optimization method, it is also aimed to determine the best parameters for the bending strength performance and surface hardness of ABS and PLA. In addition, printing time was added to the analysis to determine the optimum conditions for production costs.

2. MATERIALS AND METHODS

The specimens, investigated for bending strength and surface hardnesses within this study, were produced in additive manufacturing processes using a 3D printer (Creality K1) with Fused Deposition Modeling (FDM) method. The filament diameters are 1.75 mm and were produced with ESUN's PLA+ and ABS filaments. The infill pattern for all specimens is grid. The specimens were fabricated with four different fill rates (40%, 60%, 80% and 100%), two different layer thicknesses (0.10 mm and 0.20 mm) and two different materials (ABS, PLA). Specimen dimensions were selected according to ASTM D790 standard [22]. The dimensions of the specimen are presented in Figure 1. The CAD model of the specimen was created with the academic version SOLIDWORKS software. Then, the model was saved in STL format, sliced with Creality Print Software and G-codes were generated. For fabrication. the printing parameters recommended by ESUN for Creality K1 were utilized [23]. The mechanical properties and printing parameters of the filament are given in Table 1.

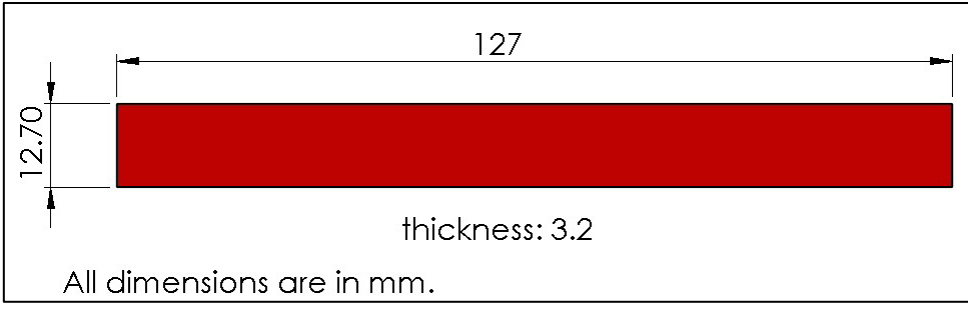


Figure 1. Bending specimen dimension according to ASTM 790 [22].

Table 1. Mechanical properties [24-25] and printing parameters [23] of ABS and PLA.

Material Type	Mechanical	Properties	Printing Parameters		
	Density	:1.04 g/cm ³	Printing Temperature	:240 °C	
	Flexural Modulus	:1177 MPA	Heating Table Temperature	:105 °C	
ABS	Tensile Strength	:43 MPa	Printing Speed	:50 mm/s	
	Bending Strength	:66 MPa			
	Elongation	:22 %			
	Density	$:1.23 \text{ g/cm}^3$	Printing Temperature	:220 °C	
	Flexural Modulus	:1973 MPA	Heating Table Temperature	:60 °C	
PLA	Tensile Strength	:60 MPa	Printing Speed	:300 mm/s	
	Bending Strength	:74 MPa			
	Elongation	:20 %			

In accordance with the aim of the study, Taguchi method was used for optimization of material type, layer thickness and fill rate according to bending strength, surface hardness and printing time. The Taguchi experimental design was performed according to L8 Taguchi's orthogonal array with Minitab software. The effect rates of input parameters on parameters and the output statistical significance of output parameters for the optimization model were determined by ANOVA. Taguchi L8 orthogonal array design given in Table 2. Where the input parameters are fill rate, layer height and material type. The output parameters are bending strength, surface hardness and printing time. The criteria used for Taguchi optimization are signal/noise (S/N) ratios [26]. The bending strength and surface hardness, which are the output parameters investigated in the study, were desired to be high and optimizations were made with the "larger is better" method. The related equation is given in Equation (1). The printing time is desired to be low to reduce production costs. For this, the optimization was done with the "smaller is better" method and the related equation is given in Equation (2).

$$S/N = -10\log[\frac{1}{n}(\sum \frac{1}{y^2})]$$
 (1)

$$S/N = -10\log[\frac{1}{n}(\sum Y^2)]$$
 (2)

Table 2. Taguchi L8 orthogonal array design.

1 44 10 10	 1 5 • 2	o orunogonur	array arrangin
	Material	Fill Rate	Layer
RUNs	Type	(%)	Height (mm)
RUN 1	ABS	40	0.10
RUN 2	PLA	40	0.20
RUN 3	ABS	60	0.10
RUN 4	PLA	60	0.20
RUN 5	ABS	80	0.20
RUN 6	PLA	80	0.10
RUN 7	ABS	100	0.20
RUN 8	PLA	100	0.10

Three specimens were produced from each specimen type. The production process is illustrated in Figure 2 (a) and the specimens are illustrated in Figure 2 (b). Hardness measurements were performed with a Shore D hardness gauge (Zwick R5LB041) by averaging the hardness values taken from five different points on the surface for each specimen. The hardness measuring gauge is presented in Figure 2 (c). The bending tests were then carried out in accordance with ASTM 790 using a UTEST UTM-0100AE model three-point bending machine at a speed of 5 mm/min [22]. The three-point bending machine and the test process are given in Figure 2 (d).



Figure 2. 3D printer used for specimen production (a), specimen fabrication (b), test specimens (c), shore D hardness gauge and measurement operation (d) and three-point bending test device and bending operation (e).

3. RESULTS AND DISCUSSION 3.1. Hardness

Figure 3 illustrates the Shore D hardness values achieved under varying production parameters. The results indicate the significant effects of infill density, material type, and layer thickness on hardness. The experimental data suggest that hardness values increase with elevated infill densities. The lowest recorded hardness value was 31.50 Shore D in RUN 2, while the highest was 85.50 Shore D in RUN 8. This trend indicates that the relationship between fill density and internal structural homogeneity directly reflects material hardness. Higher fill densities contribute to a more homogeneous and compact internal structure, thereby increasing the hardness of the material [27-28]. Similarly, in a study investigating the surface hardness of PLA samples produced at different fill rates, it

was found that an increase in the fill rate also increased the surface hardness [29]. In specimens with infill densities up to 60%, ABS exhibited superior hardness values compared to PLA. For example, RUN 3 demonstrated an ABS hardness of 52.81 Shore D, while RUN 4 showed a PLA hardness of 44.43 Shore D at the same infill density. However, when infill density surpassed 60%, PLA specimens exhibited higher hardness values. In RUN 6, the PLA specimen achieved a hardness of 77.57 Shore D. In contrast, the ABS specimen in RUN 5, featuring a similar infill density, recorded a hardness of 69.10 Shore D. This observation suggests that the inherent rigidity of PLA becomes increasingly pronounced at higher infill densities. Due to its superior molecular bonding characteristics, PLA typically exhibits a harder structure than ABS [30-31]. Portoacă

et al. [32] in their study comparing the wear performance of ABS and PLA, stated that PLA samples had higher surface hardness than ABS samples for the same filling ratios. This was explained by better surface quality and more homogeneous material accumulation. Additionally, specimens with reduced layer thickness displayed higher hardness values. Specifically, when comparing RUN 7 and RUN 8, the specimen with the thinner layer thickness (RUN 8) achieved a higher hardness value. Thinner layers facilitate uniform material deposition, enhancing hardness by minimizing internal voids and improving mechanical properties [33-34]. RUN 8, exhibiting the highest hardness value, underscores that a combination of 100% infill density and a layer thickness of 0.1 mm represents the optimal configuration for surface hardness.

Although these findings are consistent with some studies in literature, there are also some conflicting results. For example, some studies have reported a decrease in hardness when the filling ratio exceeds 75%. This can be explained by internal stresses caused by excessive pressure and micro voids that develop during cooling [35]. In the current study, all specimens were left on the printing plate until they reached room temperature. This prevented the formation of internal stress caused by heat changes.

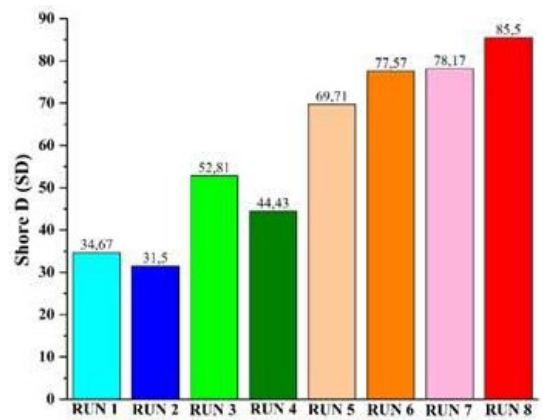


Figure 3. Shore D Hardness results for PLA and ABS materials considering different printing parameters.

3.2. Three-Point Bending Test

Force-displacement curves of bending specimens are given in Figure 4. ABS curves (Figure 4(a)) revealed that as the fill rate increased, the specimens were able to withstand larger forces and exhibited larger displacements. Notably, the bending strength of

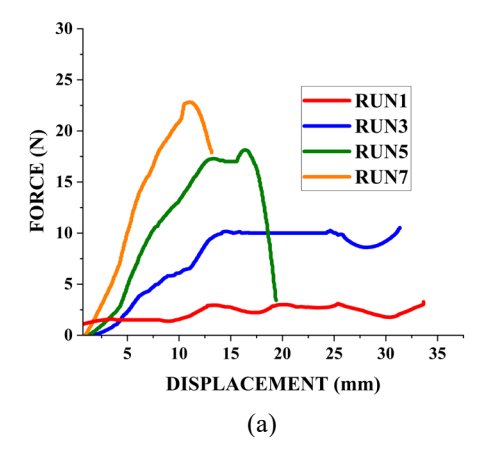
ABS significantly increases with higher fill rates. The specimen with a 40% fill rate demonstrated the lowest performance, achieving a maximum force of 6 N, whereas the specimen with a 100% fill rate reached a maximum force of 27 N. This improvement can be attributed to the enhanced homogeneity of the internal structure, which allows for more uniform stress distribution as the fill rate escalates [36-37]. Figure 4 (b) displays the force-displacement curves for PLA specimens. PLA consistently exhibited a substantially higher bending strength compared to ABS. The PLA specimen with a 40% fill rate recorded a maximum force of 13 N, while the 100% fill rate specimen attained a maximum force of 57 N. This superior performance of PLA is largely due to its rigid molecular structure and enhanced interlayer bond strength [38]. Additionally, PLA's lower thermal shrinkage relative to ABS improves interlayer adhesion, thereby augmenting mechanical strength.

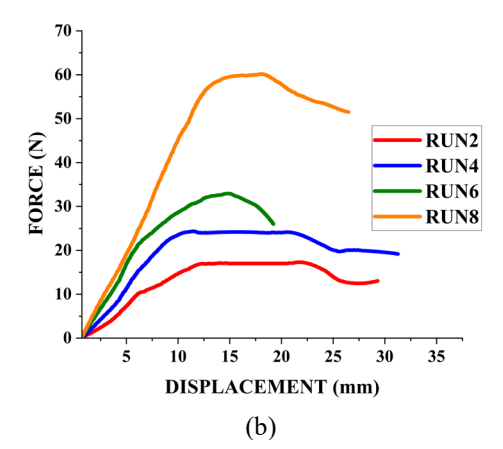
Current research supports these results. Zisopol et al. [21] noted that PLA exhibits higher bending strength than ABS, and that this difference is particularly pronounced at high filler ratios. In addition, Sudin et al. [39] reported that PLA has higher strength and stiffness values than ABS and nylon. These findings indicate that PLA is more resistant to bending loads due to its rigid structure, interlayer bond quality, and low internal void ratio. Azadi et al. [40] showed that PLA specimens outperformed ABS in high cycle bending fatigue tests, with PLA specimens exhibiting up to 11 times longer fatigue lifetimes at comparable stress levels. This was attributed to PLA's semi-crystalline structure and reduced interlayer voids, which also support our findings on its superior interlayer adhesion and rigidity. Similarly, Abeykoon et al., [41] demonstrated that optimized FDM parameters (100% infill density, 90 mm/s print and 215°C nozzle temperature) speed, maximized PLA's mechanical performance, with pure PLA achieving a flexural modulus 68% higher than ABS under identical printing conditions. Their SEM analysis further confirmed that PLA's superior interlayer adhesion and minimal porosity, linked to its linear infill pattern and optimal melt viscosity, contributed to its enhanced rigidity.

The advantages of PLA over ABS are particularly pronounced at higher fill rates for instance, whereas ABS reached 27 N at a 100% fill rate, PLA achieved 57 N, nearly double the strength of ABS.

Figure 4 (c) provides a comparative analysis of the bending strengths of both ABS and PLA specimens. PLA consistently exhibited higher bending strength at identical fill rates and layer thicknesses than ABS. For example, at a 40% fill rate, ABS recorded a maximum force of 6 N, while PLA reached 13 N. Similarly, at a 60% fill rate, ABS displayed 10 N, compared to PLA's 24 N. This disparity in performance can be attributed to the superior rigidity of PLA and its stronger interlayer bond strength [38]. The study's findings underscore that bending strength is significantly influenced by both the fill rate and the material type: higher fill rates yield increased strength for both ABS and PLA, with PLA outperforming ABS at every filling level. These results suggest that PLA is more suitable than ABS for applications necessitating high mechanical strength, highlighting the criticality of optimizing fill rates to attain maximum bending strength.

The analysis of printing times (Table 3) reveals that production duration increases with higher fill rates and layer thickness, particularly at elevated fill rates. For instance, a PLA specimen with a 40% fill rate (RUN 2) was produced in 4.5 minutes, while a 100% filled PLA specimen (RUN 8) required 12 minutes. In contrast, for ABS specimens, the RUN 1 specimen at a 40% fill rate took 21.5 minutes, compared to the RUN 7 specimen at a 100% fill rate, which was completed in 20.5 minutes. These findings indicate that while augmenting fill rates and layer thicknesses enhances the mechanical strength of the materials, it significantly extends production time. As such, finding a balance between mechanical performance production efficiency is crucial. Although PLA and high fill rates offer benefits for applications demanding high strength, careful consideration must also be given to production time and cost, particularly in mass production or timesensitive scenarios, where strategic selection of parameters such as fill rate and layer thickness is essential for optimizing both mechanical performance and production efficiency.





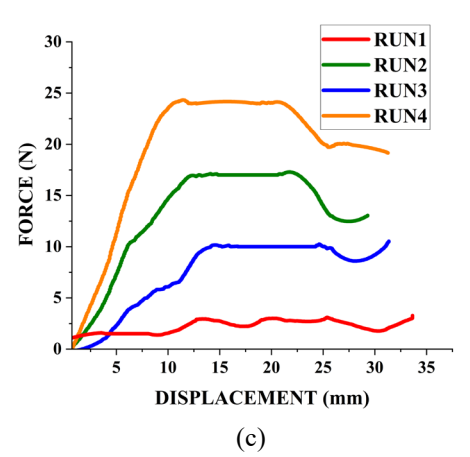


Figure 4. Force-Displacement Curves for ABS (a), PLA (b), and ABS vs. PLA (c) under Three-Point Bending Test

3.3. Statistical Results and Optimization with Taguchi

In this section, the results obtained by analyzing the experimental data with Taguchi and ANOVA were evaluated. All statistical analyses were performed for 95% confidence interval (p<0.05). Table 3 shows the experimental results. The model data and ANOVA results generated as a consequence of the analyses are presented in Table 4.

Accordingly, the R² of the model has values above 96%. This is an indication that the model could explain the results with great accuracy. The ANOVA results revealed that material type was found to be significant (p<0.05) for maximum force change. The effect of material type on the maximum force change was calculated as 43.05%. Similarly, Prajapati et al. reported that material type has an effect on bending strength [42]. The effects of fill rate and layer height on maximum force were found to be insignificant (p>0.05). Although the effect of fill rate on maximum force was found to be insignificant, the experimental demonstrate that fill rate has an effect on maximum force. The regression equation expressing the change in maximum force is given in equation (3).

Max Force = 24.84 - 14.75 x (%40 Fill Rate) - 6.09 x (%60 Fill Rate) + 2.49 x (%80 Fill Rate) + 18.34 x (%100 Fill Rate) - 11.40 x (ABS Material Type) + 11.40 x (PLA Material Type) + 3.50 x (0.1 mm Layer Height) - 3.50 x (0.2 mm Layer Height) (3)

Table 3. Experimental results.

Specimen No	Fill Rate (%)	Material Type	Layer Height (mm)	Maximum Force (N)	SEM	Hardness (SD)	SEM	Printing Time (min)
RUN 1	40	ABS	0.1	3.08 ± 0.17	0.09	37.67 ± 2.17	1.25	21.5
RUN 2	40	PLA	0.2	17.11 ± 2.11	1.22	31.50 ± 2.14	1.24	4.5
RUN 3	60	ABS	0.1	9.98 ± 0.98	0.57	52.81 ± 4.42	2.55	28.5
RUN 4	60	PLA	0.2	27.53 ± 3.57	2.06	44.43±3.32	1.92	5.5
RUN 5	80	ABS	0.2	16.89 ± 2.78	1.61	69.10±4.69	2.71	18
RUN 6	80	PLA	0.1	37.78 ± 4.11	2.37	77.57 ± 5.98	2.95	10.5
RUN 7	100	ABS	0.2	23.82 ± 3.56	2.06	78.17 ± 5.73	3.31	20.5
RUN 8	100	PLA	0.1	62.54 ± 5.78	3.34	85.50±6.24	3.60	12

The effective parameters on hardness were found to be fill rate and layer height. The effect of fill rate on hardness was calculated as 96.70% and the effect of layer height as 3%. Here, the great effect of fill rate on hardness change was remarkable. Material type was found to have no effect on the hardness change. The regression equation for hardness is given in equation (4). In support of the results, Varma et al. found that fill rate and layer height have an effect on hardness change [43]. Printing time is affected by the material type. recommended production speed of ABS is considerably lower than PLA. This is the reason for this difference. The related regression equation is given in equation (5).

```
Hardness = 59.22 -
26.13 \ x \ (\%40 \ Fill \ Rate) -
10.60 \ x \ (\%60 \ Fill \ Rate) +
14.12 \ x \ (\%80 \ Fill \ Rate) +
22.62 \ x \ (\%100 \ Fill \ Rate) -
0.53 \ x \ (ABS \ Material \ Type) +
0.53 \ x \ (PLA \ Material \ Type) +
3.42 \ x \ (0.1 \ mm \ Layer \ Height) -
3.42 \ x \ (0.2 \ mm \ Layer \ Height)
(4)
```

```
Printing Time = 15.13 - 2,12 \times (\%40 \text{ Fill Rate}) + 1.88 \times (\%60 \text{ Fill Rate}) - 0.88 \times (\%80 \text{ Fill Rate}) + 1.12 \times (\%100 \text{ Fill Rate}) + 7 \times (ABS \text{ Material Type}) - 7 \times (PLA \text{ Material Type}) + 3 \times (0.1 \text{ mm Layer Height}) - 3 \times (0.2 \text{ mm Layer Height})
(5)
```

			and ANOVA resul	ts.	
	Mo	del Summa			
	S	R	2	Adj. R ²	2
Maximum Force (N)	6.43	90	6.58%	88.03%	
Hardness (SD)	1.89	99	9.77%	99.20%	
Printing Time (min)	2.15	98	8.13%	93.44%)
	AN	OVA Resu	ılts		
	Source	DF	Contribution	F-Value	P-Value
Maximum Force (N)	Fill Rate	3	49.46%	9.64	0.095
	Material Type	1	43.05%	25.18	0.038
	Layer Height	1	4.07%	2.38	0.263
	Error	2	3.42%		
	Total	7	100%		
Hardness (SD)	Fill Rate	3	96.70%	282.40	0.004
	Material Type	1	0.07%	0.64	0.509
	Layer Height	1	3.00%	26.30	0.036
	Error	2	0.23%		
	Total	7	100%		
Printing Time (min)	Fill Rate	3	4.08%	1.45	0.433
	Material Type	1	79.45%	84.76	0.012
	Layer Height	1	14.59%	15.57	0.059
	Error	2	1.87%		
	Total	7	100%		
	Layer Height Error	1 2	14.59% 1.87%		

Figure 5 presents the SN ratios of the output parameters. According to the maximum force results (Figure 5 (a)), the maximum force increases with an increase in fill rate. With the increase in fill rate, the gaps between the layers of the specimens are filled and the material could exhibit properties closer to homogeneous [44]. Similarly, in the study where bending tests were applied to PLA specimens with different fill rates, it was found that the fill rate was the most effective parameter in bending strength [45]. In addition, PLA specimens have higher maximum force values than ABS specimens. Prajapati et al. reported that PLA was superior to ABS in terms of bending strength [38]. Layer height changes are not effective in the maximum force change, supporting the ANOVA results. When Figure 5 (b) is examined, again as in maximum force, there is an increase in surface hardness with an increase in fill rate. Şirin et al. also indicated in their study on PLA specimens that an increase in fill

rate leads to an increase in surface hardness [28]. The hardness increase is linearly increasing up to 80% fill rate. At 100% fill rates, there is a decrease in the amount of increase. Considering that increases in fill rates are accompanied by increases in production costs, it may indicate that 80% fill rate may provide sufficient surface hardnesses in applications produced with 3D manufacturing methods and where high surface hardness is required. The results indicated that material type had no significant effect on hardness change. It was found that the surface hardness decreased slightly with increasing layer height. As the layer height decreases, the number of layers increases and the micro gaps between the layers decrease and harder structures could be obtained [43]. According to Figure 5(c), decreasing the fill rate and increasing the layer height have the effect of decreasing the printing time. In addition, preferring PLA as material type also decreases the printing time.

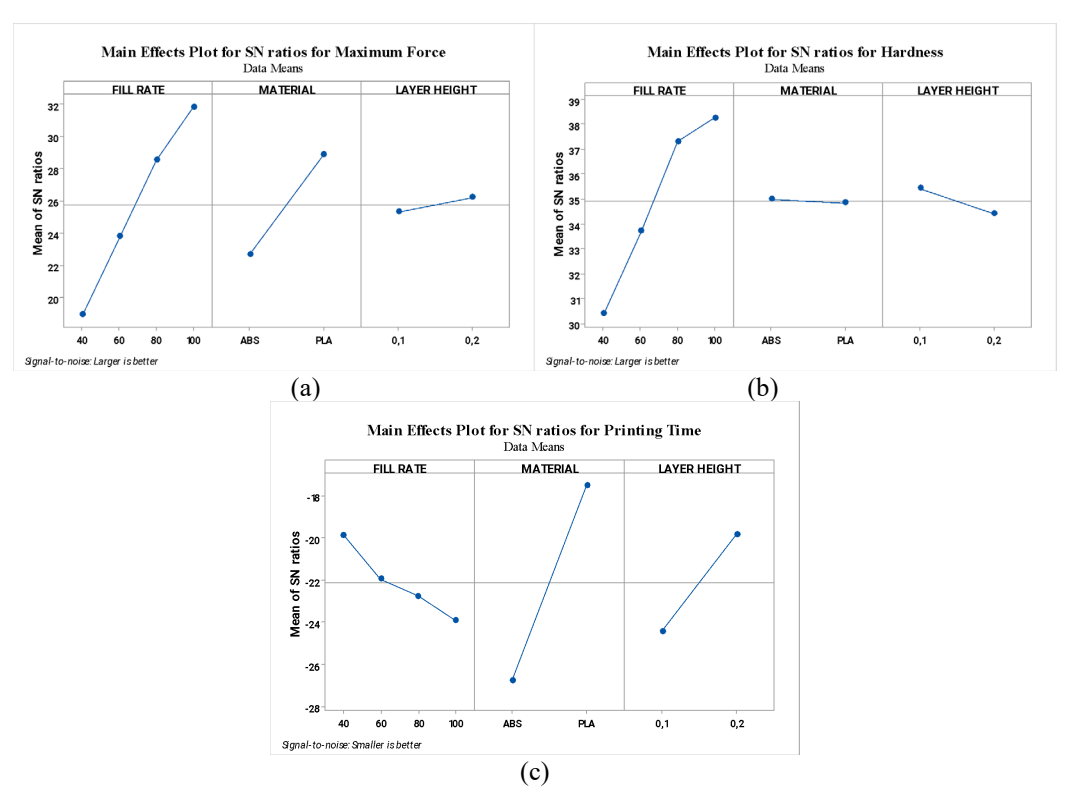


Figure 5. SN ratios of maximum force (a), hardness (b) and printing time (c)

Table 5. Regression and experimental results for control specimens.

Specimen Name		Control 1		Control 2		
	Regression Equation	Experimental Results	Error Rate (%)	Regression Equation	Experimental Results	Error Rate (%)
	Results			Results		
Max. Force (N)	51.08	59.13±3.42	13.61	35.48	34.45±1.63	-2.99
Hardness (SD)	78.95	75.67±1.31	-4.33	84.73	73.21+0.55	-15.74
Printing Time (min)	6.25	7	10.71	26.25	29	9.48

Control samples were fabricated to validate the established model. Three Control 1 specimens with 100% fill ratio and 0.2 mm layer thickness were fabricated for PLA. The purpose of selecting this specimen configuration is to compare it with the RUN 8 specimen, which yielded the best results, in order to reveal the effect of layer thickness changes on the results. For ABS, three specimens were produced from the Control 2 specimen with a layer thickness of 0.1 mm at 100% fill rate. The purpose of selecting this sample configuration for the verification tests is to obtain the best performance for ABS based on statistical analysis results. Hardness measurements were taken from at least five different points for each sample type, and bending tests were performed. In addition, estimated results were calculated using regression equations. The experimental data obtained and the values calculated using the regression equation are given in Table 5. According to this, the maximum force for

sample Control 1 was calculated as 51.08 N, while the experimental results were found to be 59.13 N. The hardness value was 78.95 SD according to the statistical model and 75.67 SD according to the experimental results. The error rate for maximum force was approximately 13.61%, while for hardness it was 4.33%. The model was able to predict the printing time with an error of 10.71% at 6.25 minutes. Additionally, the Control 1 specimens exhibited lower maximum force and hardness compared to RUN 8. These results confirm that a decrease in layer thickness increases maximum force and hardness.

For Control 2 specimens, the maximum force results were calculated as 35.48 N. In experimental tests, this value was found to be 34.45 N. The performance of the statistical model for maximum force was quite good, with an error rate of approximately 2.99%. Similarly, the model estimated the hardness of the Control 2 sample with an error rate of 15.74% and the

printing time with an error rate of 9.48%. Consistent with the Taguchi analysis, the highest maximum force and hardness values were obtained with these specimens.

According to Taguchi analyses, for applications where high strength and high surface hardness are required, parts made of PLA with a fill rate of 80% and above are preferable. However, the low deformation onset temperatures [13] limit the use of PLA, especially in applications with operating temperatures above 60 °C. ABS could be preferred for applications at higher temperatures. Although an increase in fill rate and decrease in layer height increases bending strength and surface hardness, it also increases production times and costs. For applications where strength and surface hardness are not important, lower fill rates and thicker layer heights may be preferred. Additionally, a positive correlation was observed between surface hardness and bending strength, particularly at higher infill densities. Specimens with increased hardness values generally exhibited enhanced bending resistance. suggesting that a denser internal structure and improved interlayer bonding not only enhance surface properties but also contribute significantly overall mechanical to performance. There are studies that confirm the results obtained. Turaka et al. [46] compared the mechanical properties of ABS and compositereinforced ABS samples produced at different fill rates and optimized them with Taguchi. According to the results obtained, the best bending strengths were observed in samples with fill rates of 60% and above. Another study stated that changes in layer height affect bending strength and that a decrease in layer height increases bending strength [47].

4. CONCLUSION

This study examined the effects of material type, layer height, and fill rate on surface hardness, bending strength, and printing time for FDM-printed PLA+ and ABS specimens. The Taguchi optimization method was utilized to ascertain the optimal parameters that enhance mechanical performance and production efficiency. Based on the experimental results and subsequent statistical analyses, the following conclusions were drawn:

- •Surface hardness for both PLA and ABS specimens significantly increased with elevated fill rates. The maximum hardness value of 85.50 Shore D was attained with PLA at a 100% fill rate and a layer thickness of 0.10 mm.
- •In bending strength, PLA demonstrated superior performance to ABS across all fill rates and layer thicknesses. For instance, at a 100% fill rate, PLA achieved a maximum force of 57 N, nearly double that of ABS, recorded at 27 N.
- •Layer thickness significantly influenced surface hardness, with thinner layers (0.10 mm) correlating with higher hardness values.
- •The fill rate emerged as the most potent parameter affecting bending strength, with increased fill rates resulting in heightened strength for both materials.
- •It was observed that printing time increased with higher fill rates and reduced layer heights. For example, a PLA specimen with a 100% fill rate and a layer height of 0.10 mm required 12 minutes to print, in contrast to 4.5 minutes for a specimen with a 40% fill rate and a layer height of 0.20 mm.
- •Statistical analysis employing ANOVA revealed that material type exerted the most substantial effect on bending strength, contributing 43.05%, while fill rate had the greatest influence on surface hardness, contributing 96.70%. Although less impactful, layer height still had a notable effect on hardness, contributing 3%.
- •The results from the Taguchi optimization suggest that for applications necessitating high strength and surface hardness, PLA with a fill rate of 80% or higher and a layer thickness of 0.10 mm is deemed optimal.
- Validation tests demonstrated that the optimization model could generate estimates with deviations of between 3% and 16%.

Future research could expand on this study by exploring the influence of alternative infill patterns, such as honeycomb or gyroid, to yield valuable insights into strength, surface hardness, and printing efficiency. Finally, assessing high-temperature behavior and impact resistance would provide a more comprehensive understanding of the industrial applicability of PLA and ABS materials.

REFERENCES

- 1. J. Go, S.N. Schiffres, A.G. Stevens, and A.J. Hart, "Rate limits of additive manufacturing by fused filament fabrication and guidelines for high-throughput system design", Addit Manuf, Vol. 16, Pages 1–11, 2017.
- 2. M.K. Thompson, G. Moroni, T.H. Vaneker, G. Fadel, R.I. Campbell, I. Gibson, A. Bernard, J. Schulz, P. Graf, B. Ahuja, and F. Martina, "Design for Additive Manufacturing: Trends, Opportunities, Considerations, and Constraints", Cirp Annals, Vol. 65, Issue 2, Pages 737–760, 2016.
- 3. A. Bagsik, V. Schöppner, and E. Klemp, "FDM part quality manufactured with Ultem* 9085",. 14th international scientific conference on polymeric materials. Pages. 307–315 (2010).
- 4. O. Arslan, Ö. Selvi, and O.H. Totuk, "Characterization Of 3d Printed Conductive Flexible Materials For Soft Robotic Applications", International Journal of 3D Printing Technologies and Digital Industry, Vol. 8, Issue 1, Pages 1–7, 2024.
- 5. P.K. Gurrala and S.P. Regalla, "Part strength evolution with bonding between filaments in fused deposition modelling", Virtual Phys Prototyp, Vol. 9, Issue 3, Pages 141–149, 2014.
- 6. Q. Sun, G. Rizvi, C.T. Bellehumeur, and P. Gu, "Effect of processing conditions on the bonding quality of FDM polymer filaments", Rapid Prototyp J, Vol. 14, Pages 72–80, 2008.
- 7. C. Bellehumeur, L. Li, Q. Sun, and P. Gu, "Modeling of Bond Formation Between Polymer Filaments in the Fused Deposition Modeling Process", J Manuf Process, Vol. 6, Issue 2, Pages 170–178, 2004.
- 8. B.M. Tymrak, M. Kreiger, and J.M. Pearce, "Mechanical properties of components fabricated with open-source 3-D printers under realistic environmental conditions", Mater Des, Vol. 58, Pages 242–246, 2014.
- 9. D. Popescu, A. Zapciu, C. Amza, F. Baciu, and R. Marinescu, "FDM process parameters influence over the mechanical properties of polymer specimens: A review", Polym Test, Vol. 69, Pages 157–166, 2018.
- 10. C.S. Lee, S.G. Kim, H.J. Kim, and S.H. Ahn, "Measurement of anisotropic compressive strength of rapid prototyping parts", J Mater Process Technol, Vol. 187–188, Pages 627–630, 2007.

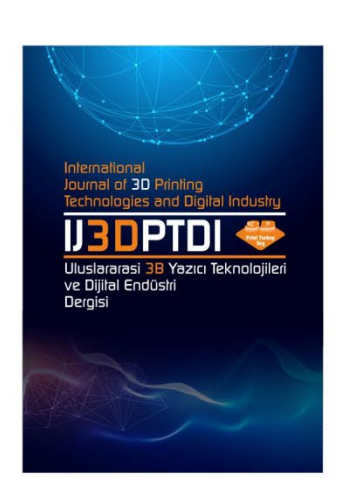
- 11. J. Torres, M. Cole, A. Owji, Z. DeMastry, and A.P. Gordon, "An approach for mechanical property optimization of fused deposition modeling with polylactic acid via design of experiments", Rapid Prototyp J, Vol. 22, Issue 2, Pages 387–404, 2016.
- 12. A. Dey and N. Yodo, "A Systematic Survey of FDM Process Parameter Optimization and Their Influence on Part Characteristics", Journal of Manufacturing and Materials Processing, Vol. 3, Issue 3, Pages 64, 2019.
- 13. İ.A. Karamanlı and K. Tahnal, "Optimization of Printing Parameters of PLA and ABS Produced by FFF", Journal of Materials and Mechatronics: A, Vol. 5, Issue 2, Pages 286–302, 2024.
- 14. K. Çava and M. Aslan, "Investigating Printability And Mechanical Performance Of 3d Printed Recycled Pet With Pla And Tpu Hybrid Additives", International Journal of 3D Printing Technologies and Digital Industry, Vol. 7, Issue 2, Pages 252–258, 2023.
- 15. A.K. Sood, R.K. Ohdar, and S.S. Mahapatra, "Parametric appraisal of mechanical property of fused deposition modelling processed parts", Mater Des, Vol. 31, Issue 1, Pages 287–295, 2010.
- 16. J.C. Camargo, Á.R. Machado, E.C. Almeida, and E.F.M.S. Silva, "Mechanical properties of PLA-graphene filament for FDM 3D printing", The International Journal of Advanced Manufacturing Technology, Vol. 103, Issue 5–8, Pages 2423–2443, 2019.
- 17. T. Letcher and M. Waytashek, "Material property testing of 3D-printed specimen in PLA on an entry-level 3D printer", ASME international mechanical engineering congress and exposition. Pages. V02AT02A014. *American Society of Mechanical Engineers* 2014.
- 18. M.F. Afrose, S.H. Masood, P. Iovenitti, M. Nikzad, and I. Sbarski, "Effects of part build orientations on fatigue behaviour of FDM-processed PLA material", Progress in Additive Manufacturing, Vol. 1, Issue 1–2, Pages 21–28, 2016.
- 19. T. Nancharaiah, D.R. Raju, and V.R. Raju, "An experimental investigation on surface quality and dimensional accuracy of FDM components", Int. J. Emerg. Technol, Vol. 1, Issue 2, Pages 106–111, 2010.

- 20. J.A. Travieso-Rodriguez, R. Jerez-Mesa, J. Llumà, O. Traver-Ramos, G. Gomez-Gras, and J.J. Roa Rovira, "Mechanical Properties of 3D-Printing Polylactic Acid Parts subjected to Bending Stress and Fatigue Testing", Materials, Vol. 12, Issue 23, Pages 3859, 2019.
- 21. D.G. Zisopol, I. Nae, A.I. Portoaca, and I. Ramadan, "A Statistical Approach of the Flexural Strength of PLA and ABS 3D Printed Parts", Engineering, Technology & Applied Science Research, Vol. 12, Issue 2, Pages 8248–8252, 2022.
- 22. ASTM, "ASTM 790-17 Standard Test Methods for Flexural Properties of Unreinforced and Reinforced Plastics and Electrical Insulating Materials", https://www.astm.org/d0790-17.html, (2017).
- 23. ESUN, "Recommended printing parameters for Creality K1", https://www.esun3d.com/uploads/eSUN-Fast-filaments-print-parameters.pdf, February 25, 2025
- 24. ESUN, "ESUN ABS Mechanical Properties", https://www.esun3d.com/abs-product/, February 25, 2025
- 25. ESUN, "ESUN PLA+ Mechanical Properties", https://www.esun3d.com/tr/pla-proproduct/, February 25, 2025.
- 26. S. Demir, A. Temiz, and F. Pehlivan, "The investigation of printing parameters effect on tensile characteristics for triply periodic minimal surface designs by <scp>Taguchi</scp>", Polym Eng Sci, Vol. 64, Issue 3, Pages 1209–1221, 2024.
- 27. P. Zhang, Z. Hu, H. Xie, G.-H. Lee, and C.-H. Lee, "Friction and wear characteristics of polylactic acid (PLA) for 3D printing under reciprocating sliding condition", Industrial Lubrication and Tribology, Vol. 72, Issue 4, Pages 533–539, 2020.
- 28. Ş. Şirin, E. Aslan, and G. Akincioğlu, "Effects of 3D-printed PLA material with different filling densities on coefficient of friction performance", Rapid Prototyp J, Vol. 29, Issue 1, Pages 157–165, 2023.
- 29. I. Bogrekci, P. Demircioglu, H. Sucuoglu, and O. Turhanlar, "The Effect of the Infill Type and Density on Hardness of 3D Printed Parts", International Journal of 3D Printing Technologies and Digital Industry, Vol. 3, Pages 212–219, 2019.

- 30. B. Bojović, Z. Golubović, L. Petrov, A. Milovanović, A. Sedmak, Ž. Mišković, and M. Milošević, "Comparative Mechanical Analysis of PLA and ABS Materials in Filament and Resin Form", In: Mitrovic, N., Mladenovic, G., and Mitrovic, A. (eds.) International Conference of Experimental and Numerical Investigations and New Technologies. Pages. 114–131. Springer Nature Switzerland, Cham 2024.
- 31. M. Ahmed Ramadan, Hassan. A. Sabour, and E. EL-Shenawy, "Tribological Properties of 3D Printed Polymers: PCL, ABS, PLA and Co Polyester", Tribology in Industry, Vol. 45, Issue 1, Pages 161–167, 2023.
- 32. A.I. Portoacă, R.G. Ripeanu, A. Diniță, and M. Tănase, "Optimization of 3D Printing Parameters for Enhanced Surface Quality and Wear Resistance", Polymers (Basel), Vol. 15, Issue 16, 2023.
- 33. N. Ayrilmis, "Effect of layer thickness on surface properties of 3D printed materials produced from wood flour/PLA filament", Polym Test, Vol. 71, Pages 163–166, 2018.
- 34.Y. Liu, W. Bai, X. Cheng, J. Tian, D. Wei, Y. Sun, and P. Di, "Effects of printing layer thickness on mechanical properties of 3D-printed custom trays", J Prosthet Dent, Vol. 126, Issue 5, Pages 671.e1–671.e7, 2021.
- 35. A.I. Portoacă and M. Tănase, "Exploring Shore D Hardness Variations Under Different Printing Conditions and Post-processing Treatments", Jordan Journal of Mechanical and Industrial Engineering, Vol. 18, Issue 2, Pages 421–429, 2024.
- 36. J.H. Porter, T.M. Cain, S.L. Fox, and P.S. Harvey, "Influence of infill properties on flexural rigidity of 3D-printed structural members", Virtual Phys Prototyp, Vol. 14, Issue 2, Pages 148–159, 2019.
- 37. A.S. Karad, P.D. Sonawwanay, M. Naik, and D.G. Thakur, "Experimental study of effect of infill density on tensile and flexural strength of 3D printed parts", Journal of Engineering and Applied Science, Vol. 70, Issue 1, Pages 104, 2023.
- 38. S.W. Ahmed, G. Hussain, K. Altaf, S. Ali, M. Alkahtani, M.H. Abidi, and A. Alzabidi, "On the Effects of Process Parameters and Optimization of Interlaminate Bond Strength in 3D Printed ABS/CF-PLA Composite", Polymers (Basel), Vol. 12, Issue 9, Pages 2155, 2020.

- 39. Sudin, M. N., N. M. Daud, and M. A. Yusuff, "A comparison of the flexural properties of PLA and ABS printed parts.", Journal of Engineering and Technology (JET) Vol. 13, Issue 2, Pages 53-65, 2022.
- 40. M. Azadi, A. Dadashi, S. Dezianian, M. Kianifar, S. Torkaman, and M. Chiyani, "High-cycle bending fatigue properties of additive-manufactured ABS and PLA polymers fabricated by fused deposition modeling 3D-printing", Forces in Mechanics, Vol. 3, Pages 100016, 2021.
- 41. C. Abeykoon, P. Sri-Amphorn, and A. Fernando, "Optimization of fused deposition modeling parameters for improved PLA and ABS 3D printed structures", International Journal of Lightweight Materials and Manufacture, Vol. 3, Issue 3, Pages 284–297, 2020.
- 42. S. Prajapati, J.K. Sharma, S. Kumar, S. Pandey, and M.K. Pandey, "A review on comparison of physical and mechanical properties of PLA, ABS, TPU, and PETG manufactured engineering components by using fused deposition modelling", Mater Today Proc, 2024.
- 43. K. Sandeep Varma, K. Lal Meena, and R.B.R. Chekuri, "Optimizing mechanical properties of 3D-printed aramid fiber-reinforced polyethylene terephthalate glycol composite: A systematic approach using BPNN and ANOVA", Engineering Science and Technology, an International Journal, Vol. 56, Pages 101785, 2024.

- 44. G. Atakok, M. Kam, and H.B. Koc, "Tensile, three-point bending and impact strength of 3D printed parts using PLA and recycled PLA filaments: A statistical investigation", Journal of Materials Research and Technology, Vol. 18, Pages 1542–1554, 2022.
- 45. M. Günay, "Modeling Of Tensile And Bending Strength For PLA Parts Produced By FDM TT Modeling Of Tensile And Bending Strength For Pla Parts Produced By FDM", International Journal of 3D Printing Technologies and Digital Industry, Vol. 3, Issue 3, Pages 204–211, 2019.
- 46. S. Turaka, V. Jagannati, B. Pappula, and S. Makgato, "Impact of infill density on morphology and mechanical properties of 3D printed ABS/CF-ABS composites using design of experiments", Heliyon, Vol. 10, Issue 9, 2024.
- 47. O. Tunçel, Ç. Kahya, and K. Tüfekci, "Optimization of Flexural Performance of PETG Samples Produced by Fused Filament Fabrication with Response Surface Method", Polymers (Basel), Vol. 16, Issue 14, 2024.



ULUSLARARASI 3B YAZICI TEKNOLOJİLERİ VE DİJİTAL ENDÜSTRİ DERGİSİ

INTERNATIONAL JOURNAL OF 3D PRINTING TECHNOLOGIES AND DIGITAL INDUSTRY

ISSN:2602-3350 (Online)

URL: https://dergipark.org.tr/ij3dptdi

OPTIMIZED MACHINE LEARNING METHODS FOR PREDICTION OF MARSHALL STABILITY VALUES

Yazarlar (Authors): Remzi Gürfidan **, Kemal Muhammet Erten **

Bu makaleye şu şekilde atıfta bulunabilirsiniz (To cite to this article): Gürfidan R., Erten K. M., "Optimized Machine Learning Methods for Prediction of Marshall Stability Values" Int. J. of 3D Printing Tech. Dig. Ind., 9(2): 220-228, (2025).

DOI: 10.46519/ij3dptdi.1660315

Araştırma Makale/ Research Article

Erişim Linki: (To link to this article): https://dergipark.org.tr/en/pub/ij3dptdi/archive

OPTIMIZED MACHINE LEARNING METHODS FOR PREDICTION OF MARSHALL STABILITY VALUES

Remzi Gürfidan^a, Kemal Muhammet Erten^b

a Isparta University of Applied Sciences, Yalvaç Vocational School of Technical Sciences, Computer Programming Department, TURKEY
Isparta University of Applied Sciences, Yalvaç Vocational School of Technical Sciences, Building Inspect

^b Isparta University of Applied Sciences, Yalvaç Vocational School of Technical Sciences, Building Inspection
Department, TURKEY

* Corresponding Author: remzigurfidan@isparta.edu.tr

(Received: 18.03.25; Revised: 29.03.25; Accepted: 23.07.25)

ABSTRACT

This study evaluates the performance of machine learning algorithms in predicting Marshall stability values to improve quality control processes in highway pavements. Coring is a costly, time-consuming and destructive method, which increases the need for alternative prediction models. In this context, Extra Trees, Random Forest, Gradient Boosting, K-Nearest Neighbours (KNN) and AdaBoost algorithms were used to predict the stability values obtained from core samples and error metrics were analyzed. In the study, the effects of hyperparameter optimization on model performance were examined in detail. The results show that the Extra Trees algorithm has the best prediction performance with an R² of 97.62% and an accuracy of 99.71%. Random Forest and Gradient Boosting algorithms also showed improvements after optimization, but their error rates remained higher compared to the Extra Trees model. The KNN model showed moderate success, while the AdaBoost model showed the lowest performance with an R² value of 58.87%. The findings reveal that machine learning algorithms can be used effectively in the prediction of stability values obtained from core samples and model performance can be improved by optimizing the right hyperparameters. The study shows that data-driven approaches can be less costly and time efficient in quality control processes.

Keywords: Machine Learning, Marshall Stability, Core Sample, Hyperparameter Optimization

1. INTRODUCTION

In recent years, machine learning (ML) gained prominence techniques have engineering due to their ability to reduce the cost and time associated with traditional testing methods. In pavement engineering, destructive and labor-intensive nature of Marshall stability tests has highlighted the need for data-driven alternatives. Supervised ML regression algorithms, models. and hyperparameter optimization have shown promise in accurately predicting stability values from core samples, offering a more efficient and reliable solution.

Although flexible pavements are manufactured to have properties such as flexibility, durability, fatigue resistance, stability and slip resistance, they lose these properties over time due to traffic and climatic conditions [1-4]. In order to

evaluate pavements, various tests are performed [5-6], one of the most important of which is coring the pavement, even though it is a destructive method, by extracting the core samples, it can be determined how the aggregate shows physical changes under the compaction processes and traffic load during construction phase and how the bitumen shows physical changes in the face of production and climatic factors [7-11]. Stability and yield checks can also be performed for core samples [12]. In this way, both material and stability properties of the pavement can be realistically determined. Marshall design method is a widely used method to evaluate the mechanical properties of bituminous mixtures [13-16]. As it is known, one of the most important evaluation criteria of the samples produced for design is stability [17-19]. Stability is also important as a control criterion for core samples taken from the

existing road. However, since the coring process is a destructive method for the road and requires labour and equipment, it is necessary to make predictive approaches on this subject, which is lacking in the literature. Phung, Thanh-Hai Le, Nguyen, Bang Ly, 2023, Marshall stability was predicted using machine learning for asphalt mixtures using basalt fiber. They emphasized that the use of artificial intelligence is promising in engineering problems [20]. Erten and Terzi, 2023, in their study for the reuse of these products by examining the condition of aggregate and bitumen after extraction of core samples taken from existing pavement, they emphasized the importance of asphalt recycling for sustainable transportation [21]. Köfteci, 2017, analyzed the performance of road aggregates that can be obtained from recycling by applying extraction to 20 core samples taken from the bituminous base layer. The author stated that although the aggregates lost some of their properties, they were reusable [8]. Kıyıldı, 2021, whose data are also used in our study, used the Marshall stability values of core samples taken during the construction of Niğde-Adana highway to predict the Marshall stability value with artificial neural networks. In the model with 4 inputs, 15 neurons in the 1st hidden layer, 15 neurons in the 2nd layer and 1 output network structure, it was stated that the prediction made by the ANN was largely consistent with the actual values [12].

2. DATASET AUGMENTATION

In our study, Bitumen as a percentage of the Aggregate by Weight, Bitumen Percentage in the Mixture, Bulk Specific Gravity, Void Percentage in the Mixture values of the core samples given in Kıyıdı, 2021 were used as input data for the developed model [12]. The stability values of the core samples were estimated with the developed models and compared with the estimated values found in Kıyıdı, 2021.

In this study, a data augmentation process was applied to a dataset consisting of continuous variables. Since SMOTE (Synthetic Minority Over-sampling Technique) is only applicable to classification problems, alternative techniques such as Gaussian jittering and sample-based interpolation, which are more suitable for this dataset, were utilized. SMOTE is a method designed for classification problems and cannot be directly applied to regression problems with

continuous variables. For this reason, data augmentation techniques such as Gaussian jittering and linear interpolation, which are more suitable for regression problems, are preferred in our study.

The Gaussian jittering method enhances the model's generalization capability introducing small-scale, normally distributed random noise to existing data points, thereby expanding the dataset. In this approach, minimum and maximum of all variables are determined, and random deviations are added based on a priori defined noise level such that newly generated data points maintain the original distribution. Although Gaussian jittering by itself is not enough to create sufficient diversity, additional techniques such as random sampling and linear interpolation employed achieve were to a more heterogeneous dataset augmentation. Through random sampling, slight modifications were applied to data points selected from the existing dataset, while interpolation was used to generate new points, filling gaps between observed values and promoting a more homogeneous distribution. The combined use of these methods increased the dataset's diversity while preserving its statistical properties, thus mitigating the risk of overfitting and enhancing the model's generalization performance. The results indicate that the augmented dataset largely retains the characteristics of the original data and provides a more stable foundation for training. The pseudocode representation of the data augmentation process is provided in Algorithm 1.

Algorithm 1 Synthetic Data Generation Pseudo Code

```
if additional samples needed > 0:
1:
2:
          additional data = []
3:
              for
                                                in
     range(additional samples needed):
4:
                 sample
     dataset.random sample(1)
                 jittered sample = sample.copy()
5:
6:
                             column
     dataset.numerical columns():
7:
                jittered sample[column]
                add jitter
                (jittered sample[column])
8:
     additional_data.append(jittered sample)
9:
            dataset = dataset.append(additional data)
     save_excel(dataset, "augmented_dataset.xlsx")
10:
```

The 63 rows of data in the existing dataset were increased to 200 rows using augmentation methods. Figure 1 shows the consistency and

correlation graphs of the distributions between the original and augmented data set.

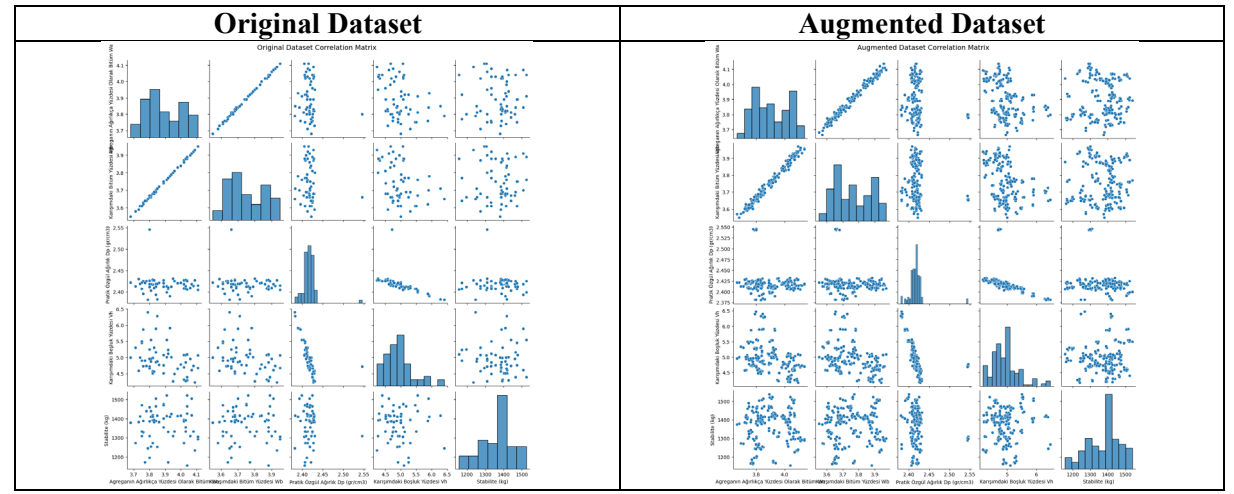


Figure 1. Marshall Core Dataset Augmentation and Correlation Graph

In order to assess the effectiveness of the data augmentation methods, an analysis was performed on the cross-relationship matrices (pair plot) presented above. In the original dataset, it is observed that the distribution between variables has a certain structure. Especially as seen from the histograms, there are intervals where certain variables are concentrated. In the data augmented dataset, the distribution of variables has become denser with the increase in the amount of data. However, it can be said that the overall distribution structure of the data points is quite similar to the original dataset. This shows that the data augmentation process preserved the characteristics of the original dataset to a large extent. Strong linear relationships are observed between certain pairs of variables in the original dataset. In particular, the relationship between "Bitumen Wa as Wt% of Aggregate" and "Bitumen Wb as Wt% of Mixture" shows an almost perfect linear

correlation. After data augmentation, this correlation is largely preserved. The data augmentation process was able to expand the data set without disturbing the existing This shows that the data relationships. augmentation method preserves statistical integrity. However, it was observed that the distribution between some variables was widened. In particular, it is observed that the distribution between the "Stability (kg)" variable and other variables has widened. As observed from the histogram graphs, the data augmentation process increased the data density in certain variable ranges. The addition of a small amount of random variation in the data augmentation process has added extra diversity to the data set. However, the general shape of the histograms is largely preserved. The PCA projection shown in Figure 2 shows that the augmented dataset is largely distributed in the same space as the original dataset.

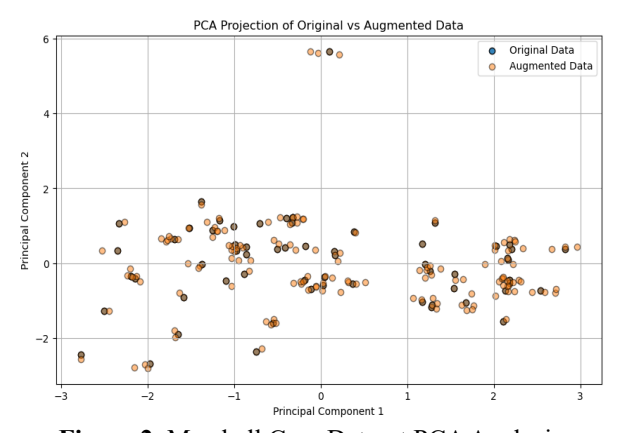


Figure 2. Marshall Core Dataset PCA Analysis

Dark coloured represent the original dataset before augmentation. Light orange points show the new, synthetically generated samples added through data augmentation techniques like Gaussian jittering and interpolation. When the regions where the data points are concentrated are compared, it is seen that the augmented dataset does not disturb the original data structure and preserves the general distribution. This shows that the data augmentation process ensures statistical integrity and extends the without changing dataset its general characteristics. However, the increased density in certain regions indicates that some samples were predominantly derived during the data augmentation process. In particular, new data derived by oversampling or small variations tend to cluster in certain regions. On the basis of principal components, the augmented dataset was found to have the same variance distribution as the original dataset. If the data augmentation process had deviated significantly from the principal components of the original dataset, the newly generated data points would have been collected in a different space. However, the situation observed here shows that the augmented data are appropriately distributed in the original data space and thus the model can reduce the risk of overfitting. In conclusion, the PCA analysis shows that the data augmentation process largely preserves the original data structure but increases the data density in certain regions.

3. ALGORITHMS AND METRICS

In this section, the success, error and prediction values obtained from the machine learning algorithms prepared for prediction will be shown both numerically and graphically. Each algorithm tested for training is analyzed under a separate heading. Each section contains basic and brief information about the algorithm and the results obtained.

The Extra Trees (Extremely Randomized Trees) algorithm is a machine learning method specifically used to solve classification and regression problems. Extra Trees is a method based on decision trees. It uses many trees similar to the Random Forest algorithm as a working logic. In addition, unlike Random Forest, Extra Trees takes more randomness into account when constructing trees [22-23]. $G(\theta)$ denotes the prediction function for a single tree, where θ is a random vector defining splits. All

trees are combined and averaged into a tree ensemble of G(x), which is generated using the Breiman [22] equation (Equation 1) [24].

$$G(x, \theta_1, \dots, \theta_2) = \frac{1}{2} \sum_{r=1}^R G(x, \theta_r)$$
 (1)

Random Forest builds an ensemble of decision trees using bootstrap samples of the data and selects the best split among a random subset of features. This method improves generalization by decorrelating trees and reduces variance through averaging. The prediction is obtained as Equation 2.

$$\nu = \frac{1}{T} \sum_{m=1}^{M} h_{t(x)} \tag{2}$$

where h_t is the output of each tree.

Gradient Boosting builds models sequentially, each new model trained to minimize the residuals (errors) of the previous ensemble. At each step, a weak learner $h_t(x)$ is fitted to the negative gradient of the loss function, improving overall accuracy. This calculation has made Equation 3.

$$F_{M(x)} = \sum_{m=1}^{M} \lambda_m h_{m(x)} \tag{3}$$

The final model is a weighted sum Equation 4 where λ_m is learning rate.

Error metrics used to determine the success of machine learning models are used to measure the model's performance. These metrics are used to measure the degree of fit of a model's predictions to the actual values and the capacity of the model to generalize. Table 1 shows the comparative results of R2, MSE, RMSE, MAPE, Accuracy, measurements of 5 different machine learning models.

Root means square error (RMSE) was employed in order to compare the prediction errors of different trained models. The closer the RMSE value is to 0, the better the predictive ability of the model in terms of its absolute deviation. The RMSE value is calculated by Equation 4 [24-25].

$$RMSE = \sqrt{\frac{1}{n} \sum_{r=1}^{n} (P_d^{r,m} - P_d^{r,c})^2}$$
 (4)

The coefficient of determination (R2) is used to estimate model efficiency and is calculated by Equation 5 [24].

$$R^{2} = 1 - \frac{\sum_{r=1}^{n} (P_{d}^{r,m} - P_{d}^{r,c})^{2}}{\sum_{r=1}^{n} (P_{d}^{r,m} - P_{d}^{-r,m})^{2}}$$
 (5)

MSE either assesses the quality of an estimator. The MSE metric is calculated by Equation 6.

$$MSE = \frac{1}{n} \sum_{r=1}^{n} (P_i - P_i')^2$$
 (6)

Mean Absolute Percentage Error (MAPE), or Mean Absolute Percentage Error, is a metric that measures the percentage error between predicted and actual values and is calculated by Equation 7.

$$MAPE = \frac{1}{n} \sum_{i=1}^{n} \left| \frac{A_i - F_i}{A_i} \right| x100 \tag{7}$$

In the equation n is total number of data points, A_i is the actual values, F_i is the predicted value.

4. FINDINGS AND DISCUSSIONS

Table 1 details the impact of hyperparameter optimization over five different regression models-Extra Trees, Random Forest, Gradient Boosting, K-Nearest Neighbours (KNN) and AdaBoost-on various error and accuracy metrics. After applying hyperparameter optimization, a significant performance improvement is observed in all algorithms.

In the study conducted by Kıyıdı, 2021, it was stated that the relationship between the ANN results and the test results separated for control purposes was $R^2 = 0.91201$.

In this study, Grid Search was employed to optimize the hyperparameters of each machine learning model. For each algorithm, a predefined grid of hyperparameter values was constructed (Table 1), and all possible parameter combinations were evaluated. The optimal configuration was selected based on performance metrics such as R² and MSE using cross-validation on the training set.

Table 1. Test results and error metric values of machine learning algorithms

	gorithm & Metric	ExtraTrees	Random Forest	GradientBoosti ng	KNN	AdaBoost
	\mathbb{R}^2	97.6187	90.4844	90.2832	93.7374	58.8713
ED	Accuracy	99.7141	98.5282	98.4713	99.0599	96.5564
ZIV	MSE	177.135	707.2400	722.1965	466.4547	3063.4103
OPTIMIZED	MAE	4.0588	20.03795	20.9395	13.2304	48.3017
OP	MAPE	0.0028	0.01471	0.01528	0.0094	0.03443
	RMSE	13.3092	26.5939	26.8737	21.5975	55.3480
OPTIMIZATION PROCESS	Parameters and Values for Hyper Parameter Optimizatio n	n_estimators: [50, 100, 200] max_depth: [None, 10, 20, 30] min_samples_sp lit: [2, 5, 10] min_samples_le af: [1, 2, 4]	n_estimators: [50,100,200] max_depth: [2, 4, 8, 16] min_samples_sp lit: [2,3,4] min_samples_le af: [2,3,4,8]	n_estimators: [50, 75, 100] max_depth: [2, 4, 8] min_samples_sp lit: [1,2,4] min_samples_le af: [1,2,8] learning rate: [0.05, 0.1, 0.5, 1]	n_neighbor s: [1, 2, 4, 8] p: [1,2,3,4]	n_estimators : [30, 50, 75, 100,200] learning rate : [0.05, 0.1, 0.5, 1, 2]
OPTIMIZA	Hyper Parameter Values	max_depth: 20 min_samples_le af: 1 min_samples_sp lit: 2 n_estimators: 200	max_depth: 16 min_samples_le af: 2 min_samples_sp lit: 2 n_estimators: 50	learning rate: 0.1 max_depth: 4 min_samples_le af: 8 min_samples_sp lit: 2 n_estimators: 100	n_neighbor s: 2 p: 1	learning rate: 2 n_estimators: 100

WITHOUT OPTIMIZATION	R ²	97.6170	86.2635	87.2378	80.6169	49.8340
	Accuracy	99.7165	98.2236	98.2823	97.7082	96.3632
	MSE	177.1125	1020.9568	948.5401	1443.7228	3736.5405
	MAE	4.0250	24.0883	23.5265	31.4891	51.3384
	MAPE	0.0028	0.0177	0.01717	0.0229	0.0363
	RMSE	13.3083	31.9524	30.7983	37.9963	61.1272

When evaluating the effects of optimization, R² (coefficient of determination) results are one of the most critical measures summarizing model performance. After optimization, the Extra Trees model stood out as the most successful model, offering the highest explanatory power with an R² value of 97.61873%. Random Forest, Gradient Boosting and KNN models also showed significant improvements, but the AdaBoost model performed poorly despite optimization. With an R² value of 58.87%, AdaBoost did not generalize well to the dataset. This indicates that the model has high variability and inconsistencies in its predictions. In terms of error metrics, Extra Trees was the model with the lowest error rates after optimization. MSE (Mean Squared Error) value was 177.14, RMSE (Root Mean Squared Error) value was 13.31, MAE (Mean Absolute Error) value was 4.0588 and MAPE (Mean Absolute Percentage Error) value was 0.00285. These results show that the Extra Trees model has the lowest prediction error and provides the best fit to the dataset.

Random Forest and Gradient Boosting models also yielded good results by reducing the error values significantly after optimization. Although there is some improvement in the KNN model, error values are greater than other models. The largest error values for the AdaBoost model (MSE = 3063.41, RMSE = 55.34) show that the model cannot generalize

well based on the dataset and also contains a very high margin of error. This is a measure of model precision, and the best model is Extra Trees with an accuracy rate of 99.71%. The two best-performing models were the KNN model with an accuracy rate of 99.06% and Random Forest model with an accuracy rate of 98.52%. The worst model was the AdaBoost model at an accuracy rate of 96.55%. The outcome tells us the error rate of the AdaBoost model is higher than other models while its accuracy rate is lower. The low performance of the AdaBoost model may be attributed to its sensitivity to noise and outliers, especially in small and moderately noisy datasets. Since AdaBoost fits regressors sequentially to minimize residuals, early-stage errors may compound, reducing generalization ability.

In summary, as evident, the optimization process influences the performance of the model greatly. Systematic hyperparameter optimization, specifically, has served to decrease the model's error rates, therefore its generalization ability and prediction accuracy. Of the models being considered, Extra Trees was found to be most effective, with Random Forest and Gradient Boosting presenting themselves as good alternatives. The AdaBoost model, however, was not highly successful even with optimization and needs more improvements.

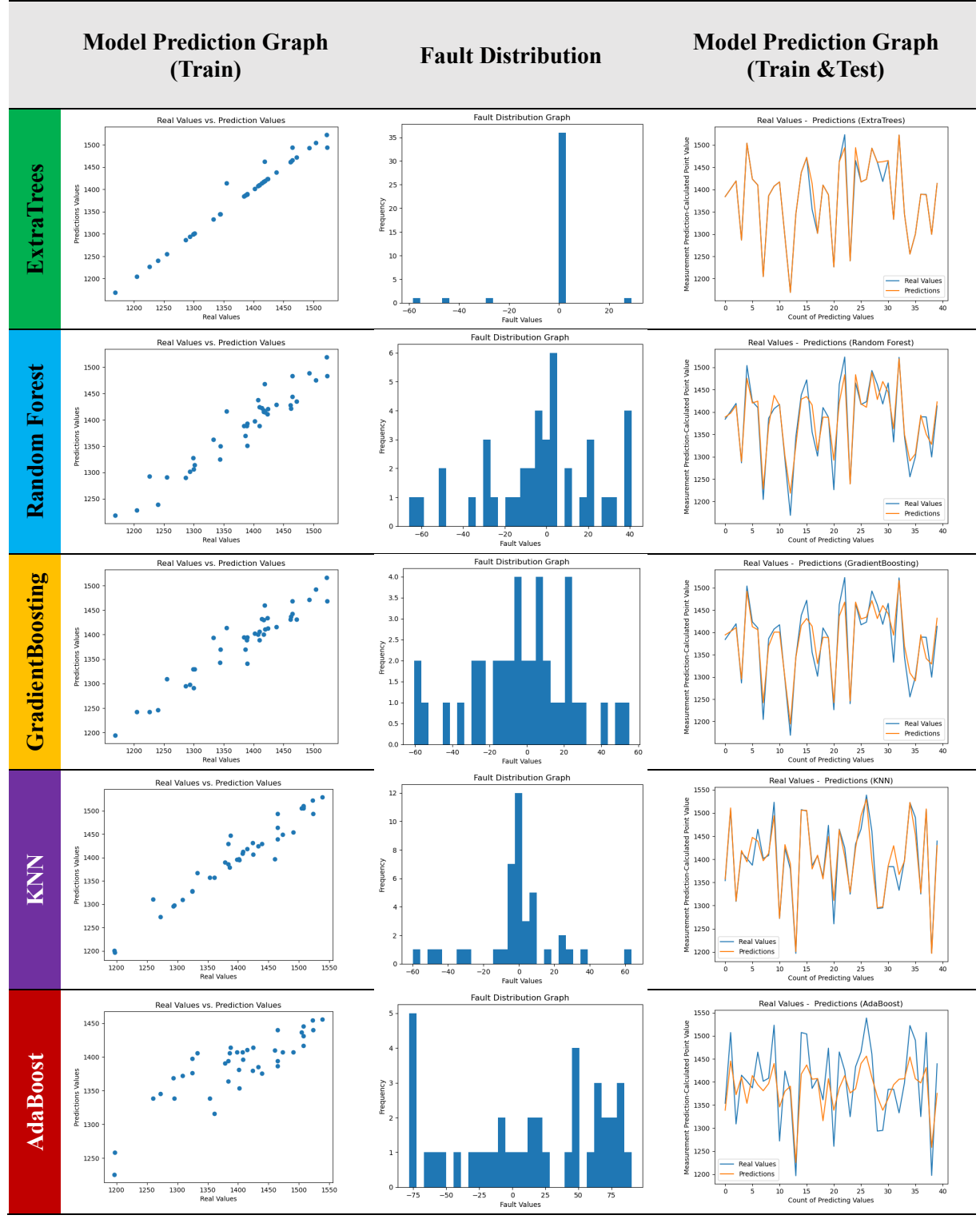


Table 2. Prediction and error scatter plots of all machine learning models

Table 2 provides a comparison of regression performance of five machine learning models (Extra Trees, Random Forest, Gradient Boosting, KNN and AdaBoost) and offers three important analyses per model: Model Prediction Graph - Train, Fault Distribution, and Model Prediction Graph - Train & Test. Training data prediction graphs in the first column investigate

whether actual and predicted values are linearly distributed. The Extra Trees, Random Forest and KNN model predictions are more spread towards the actual values, but Gradient Boosting and AdaBoost models are more deviated. This indicates that the first three models better fit the dataset, but Gradient Boosting and AdaBoost deviate more in the

predictions. The plots of error distribution in the second column compare the spread and frequency of errors in each forecast in the models. The Extra Trees and KNN models have minimal deviations in their error distributions, whereas the Random Forest and Gradient Boosting models have a broader error distribution. Surprisingly, the AdaBoost model has the largest variance of errors, indicating that its generalization ability is poorer than the other models. The third column presents the test and training data prediction plot, which is a time series of predicted versus actual values. Extra Trees and KNN models display more stable performance in their predictions compared to the test data, while the prediction errors for Gradient Boosting and AdaBoost models are more pronounced.

5. CONCLUSIONS

In this work, different machine learning models' performances were compared to predict Marshall stability values for quality control on highway pavements. More particularly, Extra Trees, Random Forest, Gradient Boosting, K-Nearest Neighbours (KNN) and AdaBoost algorithms were used to predict the stability values from core samples and their error measurements and accuracy percentages were compared. In the experiment, the before- and after-optimization performance of models is compared and the effect that optimizing hyperparameters have on model performance. From the results, the prediction accuracy of Extra Trees algorithm with R² being 97.62% and accuracy rate at 99.71% stands out as the highest. It has the least error measures indicating that the prediction values are quite close to actual values.

The Random Forest and Gradient Boosting algorithms also significantly improved after optimization, but their error rates were worse than the Extra Trees model. The KNN algorithm performed moderately, while the AdaBoost algorithm performed the worst with an R² of 58.87% and an accuracy of 96.55%. The increased error rates of AdaBoost suggest that the data set is not likely to be appropriate for this model or that other optimization methods are needed. Additionally, if the graphs of the error distribution are examined, it can be seen that the error distribution of Extra Trees and KNN models are more concentrated, while that of Gradient Boosting and AdaBoost are more

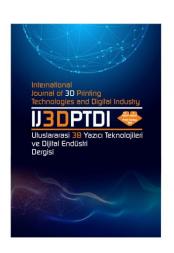
dispersed. This study demonstrates that machine learning algorithms can be used effectively to forecast core sample stability values and model performance can be significantly improved by hyperparameter tuning of the appropriate hyperparameters. The findings show how data-driven approaches as an alternative to traditional destructive testing methods can be made cost-effective and timeefficient in quality control processes. Future work will further improve model performance using different feature engineering techniques, deep learning architectures and larger data sets. Additionally, the model's generalization capability will be tested with different core samples of the field to provide a more generalized prediction mechanism for rating the condition of pavement.

REFERENCES

- 1. Llopis-Castelló, D., García-Segura, T., Montalbán-Domingo, L., Sanz-Benlloch, A., and Pellicer, E., "Influence of pavement structure, traffic, and weather on urban flexible pavement deterioration", Sustainability, Vol. 12, Issue 22, Pages 9717, 2020.
- 2. Haslett, K.E., Knott, J.F., Stoner, A.M., Sias, J.E., Dave, E.V., Jacobs, J.M., and Hayhoe, K., "Climate change impacts on flexible pavement design and rehabilitation practices", Road Materials and Pavement Design, Vol. 22, Issue 9, Pages 2098-2112, 2021.
- 3. Bhandari, S., Luo, X., and Wang, F., "Understanding the effects of structural factors and traffic loading on flexible pavement performance", International Journal of Transportation Science and Technology, Vol. 12, Issue 1, Pages 258-272, 2023.
- 4. Raffaniello, A., Bauer, M., Safiuddin, M., and El-Hakim, M., "Traffic and climate impacts on rutting and thermal cracking in flexible and composite pavements", Infrastructures, Vol. 7, Issue 8, Pages 100, 2022.
- 5. Deng, Y., Luo, X., Zhang, Y., and Lytton, R.L., "Evaluation of flexible pavement deterioration conditions using deflection profiles under moving loads", Transportation Geotechnics, Vol. 26, Pages 100434, 2021.
- 6. Özgan, E., "Determining the Stability of Asphalt Concrete at Varying Temperatures and Exposure Times Using Destructive and Non-Destructive Methods", Journal of Applied Sciences, Vol. 7, Issue 24, Pages 3870-3879, 2007.

- 7. İskender, E., "Asfalt kaplama kalınlığının karışım homojenitesi üzerindeki etkisi", Gümüşhane Üniversitesi Fen Bilimleri Dergisi, Vol. 9, Issue 4, Pages 681-690, 2019.
- 8. Köfteci, S., "Bitümlü sıcak karışımlardan geri dönüşüm yolu ile elde edilen agregaların performanslarının değerlendirilmesi: Deneysel bir çalışma", Niğde Ömer Halisdemir Üniversitesi Mühendislik Bilimleri Dergisi, Vol. 6, Issue 2, Pages 535-545, 2017.
- 9. Shaffie, E., Jaya, R.P., Ahmad, J., Arshad, A.K., Zihan, M.A., and Shiong, F., "Prediction model of the coring asphalt pavement performance through response surface methodology", Advances in Materials Science and Engineering, Vol. 2022, Issue 1, Pages 6723396, 2022.
- 10. Dan, H.C., Huang, Z., Lu, B., and Li, M., "Image-driven prediction system: Automatic extraction of aggregate gradation of pavement core samples integrating deep learning and interactive image processing framework", Construction and Building Materials, Vol. 453, Pages 139056, 2024.
- 11. Braham, A., Hossain, Z., Yang, S., and Chowdhury, N., "Evaluating performance of asphalt pavement based on data collected during IRP", Final Report for Arkansas State Highway and Transportation Department, TRC, Report No. 1404, Pages 1404, 2015.
- 12. Kıyıldı, R.K., "Yapay sinir ağları ile Marshall stabilite değerinin tahmini", Niğde Ömer Halisdemir Üniversitesi Mühendislik Bilimleri Dergisi, Vol. 10, Issue 2, Pages 627-633, 2021.
- 13. Yıldırım, Z.B., Karacasu, M., and Okur, V., "Optimisation of Marshall Design criteria with central composite design in asphalt concrete", International Journal of Pavement Engineering, Vol. 21, Issue 5, Pages 666-676, 2020.
- 14. Chen, H., Xu, Q., Chen, S., and Zhang, Z., "Evaluation and design of fiber-reinforced asphalt mixtures", Materials & Design, Vol. 30, Issue 7, Pages 2595-2603, 2009.
- 15. Xu, B., Chen, J., Zhou, C., and Wang, W., "Study on Marshall Design parameters of porous asphalt mixture using limestone as coarse aggregate", Construction and Building Materials, Vol. 124, Pages 846-854, 2016.
- 16. Heydari, S., Hajimohammadi, A., Javadi, N.H.S., and Khalili, N., "The use of plastic waste in asphalt: A critical review on asphalt mix design and

- Marshall properties", Construction and Building Materials, Vol. 309, Pages 125185, 2021.
- 17. Duran Aşkar, D., "Yapay Zeka Destekli Asfalt Performans Tahmini", Yüksek Lisans Tezi, İskenderun Teknik Üniversitesi, Fen Bilimleri Enstitüsü, Hatay, 2018.
- 18. Aljassar, A.H., Metwali, S., and Ali, M.A., "Effect of filler types on Marshall stability and retained strength of asphalt concrete", International Journal of Pavement Engineering, Vol. 5, Issue 1, Pages 47-51, 2004.
- 19. Changra, A., and Singh, E.G., "Comparison of Marshall Stability values of the different bitumen mixes with crumb rubber", IOP Conference Series: Earth and Environmental Science, Vol. 1110, No. 1, Pages 012034, 2023.
- 20. Phung, B.N., Le, T.H., Nguyen, M.K., Nguyen, T.A., and Ly, H.B., "Practical numerical tool for Marshall stability prediction based on machine learning: An application for asphalt concrete containing basalt fiber", Journal of Science and Transport Technology, Pages 26-43, 2023.
- 21. Erten, K.M., and Terzi, S., "Technical Investigation of the Usability for Foamed Bitumen Stabilized Materials in Asphalt Pavements", Journal of Engineering Research, Vol. 11, Issue 3, Pages 1-10, 2023.
- 22. Breiman, L., and Cutler, R.A., "Random forests machine learning", Journal of Clinical Microbiology, Vol. 2, Pages 199-228, 2001.
- 23. Geurts, P., Ernst, D., and Wehenkel, L., "Extremely randomized trees", Machine Learning, Vol. 63, Pages 3-42, 2006.
- 24. Hammed, M.M., AlOmar, M.K., Khaleel, F., and Al-Ansari, N., "An extra tree regression model for discharge coefficient prediction: Novel, practical applications in the hydraulic sector and future research directions", Mathematical Problems in Engineering, Vol. 2021, Pages 1-19, 2021.
- 25. Willmott, C., and Matsuura, K., "Advantages of the mean absolute error (MAE) over the root mean square error (RMSE) in assessing average model performance", Climate Research, Vol. 30, Pages 79–82, 2005.



ULUSLARARASI 3B YAZICI TEKNOLOJİLERİ VE DİJİTAL ENDÜSTRİ DERGİSİ

INTERNATIONAL JOURNAL OF 3D PRINTING TECHNOLOGIES AND DIGITAL INDUSTRY

ISSN:2602-3350 (Online)

URL: https://dergipark.org.tr/ij3dptdi

STRUCTURAL ANALYSIS OF MEDICAL IMAGES AND BACTERIAL POPULATIONS BY IMAGE PROCESSING AND ARTIFICIAL INTELLIGENCE

Yazarlar (Authors): Mehmet Erhan Şahin D*

Bu makaleye şu şekilde atıfta bulunabilirsiniz (To cite to this article): Şahin M. E., "Structural Analysis of Medical Images and Bacterial Populations By Image Processing and Artificial Intelligence" Int. J. of 3D Printing Tech. Dig. Ind., 9(2): 229-235, (2025).

DOI: 10.46519/ij3dptdi.1624544

Araştırma Makale/ Research Article

Erişim Linki: (To link to this article): https://dergipark.org.tr/en/pub/ij3dptdi/archive

STRUCTURAL ANALYSIS OF MEDICAL IMAGES AND BACTERIAL POPULATIONS BY IMAGE PROCESSING AND ARTIFICIAL INTELLIGENCE

Mehmet Erhan Şahin^a

^aIsparta Applied Science University, Vocational School of Technical Sciences, Biomedical Devices Technology Department, TÜRKİYE

*Corresponding Author: erhansahin@isparta.edu.tr

(Received: 21.01.25; Revised: 18.05.25; Accepted: 04.07.25)

ABSTRACT

This study was carried out to investigate the structural properties of medical images and bacterial populations using fractal analysis and lacunarity measurements. In the study, image processing techniques, fractal and lacunar analysis methods and artificial intelligence-based models were used together to determine the geometric complexity and irregularity levels of healthy and pathological conditions. Deep learning models such as convolutional neural networks (CNN) and U-Net have been successfully applied to the classification and segmentation of images. The results showed that fractal dimension and lacunarity measures are effective tools for detecting fibrotic changes in lung tissue and pathological growth patterns in bacterial colonies. Differences between healthy and diseased states were successfully discriminated by fractal dimension and lacunarity values. Artificial intelligence based models have attracted attention with their high accuracy and sensitivity rates in image processing. This study reveals that the integration of fractal and lacunar analysis with artificial intelligence offers a strong potential for developing fast, objective and accurate decision support systems in medical diagnosis and microbiological analysis. In the future, it is recommended to apply this method on larger data sets and different disease models.

Keywords: Convolutional Neural Networks (CNN), U-Net, Medical Imaging, Lung X-Ray Image, Image Processing, Decision Support Systems.

1. INTRODUCTION

Today, image processing techniques and artificial intelligence methods offer powerful tools for analysing complex structures in medical imaging and microbiological analysis. In particular, fractal analysis and lacunarity measurements play an important role in early diagnosis of diseases and detection of structural changes by quantitatively evaluating the geometric properties of tissues microorganism colonies [1]. This study aims to combine fractal analysis and lacunarity measurements with artificial intelligence-based image processing techniques to objectively evaluate healthy and pathological conditions.

Medical imaging (such as Computed Tomography [CT], Magnetic Resonance Imaging [MR], X-ray) methods are widely used in clinical diagnoses. However, directly

analysing these images is complex and may introduce experience-based errors. Image processing techniques enable preprocessing, noise reduction, segmentation and analysis of such images. Traditional image processing steps include grey-scale, thresholding, morphological operations and edge detection algorithms [2].

In recent years, deep learning methods, especially segmentation models such as Convolutional Neural Networks (CNN) and U-Net, have revolutionised medical image analysis. These methods provide clinicians with an important decision support mechanism by detecting pathological regions in complex images with high accuracy [3].

Fractal analysis is a method used to measure the geometric properties of irregular and complex structures. Fractal geometry, defined by Mandelbrot, mathematically expresses the self-similarity in nature [4]. Fractal dimension indicates how complex a structure is and can be calculated by counting boxes. A healthy tissue or colony of microorganisms grows in a specific fractal pattern, whereas under pathological conditions this structure is disrupted and the fractal dimension changes [5-6].

Lacunarity measurements express the degree of irregularity of the voids of a structure. An increase in the lacunarity value indicates that tissue homogeneity is disrupted and the void distribution is heterogenised [7]. In lung tissues, disruption of the alveolar structure during fibrotic diseases leads to an increase in fractal dimension and lacunarity values [8].

In medical images, fractal analysis is used to distinguish normal and pathological conditions of lung tissue. For example, while fractal dimension values in healthy lung tissue are within a certain range, this value increases in diseases such as fibrosis [9]. Lacunarity analyses provide information about the progression of the disease by numerically evaluating the irregularities in the alveolar spaces [10].

Similarly, fractal analysis and lacunarity measurements in microbiological images are used to examine changes in the growth patterns of bacterial colonies. While healthy colonies exhibit regular and homogeneous growth, growth patterns become complex and irregular under pathological conditions [11].

The aim of this study is to combine fractal analysis and lacunarity measurements with artificial intelligence-based image processing techniques to investigate the geometric structural changes of bacterial colonies in medical lung images. Quantitative comparison of healthy and pathological conditions will reveal how fractal and lacunar features can contribute to diagnostic processes. In this way, it is aimed to develop fast, objective and accurate decision support mechanisms in clinical diagnosis processes.

2. MATERIAL METHODS

2.1. Data Set

In this study, two different data sets were used: Medical Images: Computed tomography (CT) images including healthy and fibrotic lung tissues were used. These images were selected to analyse structural differences in lung tissue [12].

Bacterial Images: Microscopic images of healthy and diseased bacterial colonies were obtained. These images were used to analyse changes in bacterial growth patterns [13].

The dataset consists of a total of 400 images. The images are divided into two main groups: medical (CT) lung images and microscopic bacterial colony images. Each group includes two classes: healthy and pathological. Specifically, the medical image group contains 100 healthy and 100 fibrotic lung images, while the bacterial image group includes 100 healthy and 100 diseased colony images. The dataset was split into three subsets for deep learning model training: 70% for training, 15% for validation, and 15% for testing. This distribution ensures a balanced sampling across classes and allows for a fair evaluation of model performance.

2.2. Data Preprocessing

The following pre-processing steps were applied to make the images suitable for analysis:

- Grayscale: Colour images were converted to grayscale for ease of processing and analysis [14].
- Noise Reduction: Filtering methods such as Gaussian filter and median filter were used to reduce noise and unwanted signals in the images [15].
- Edge Detection: Sobel and Canny edge detection algorithms were applied to detect object boundaries in the images. This step enabled the structural features to be revealed more clearly [16].
- Segmentation: Two different techniques were used to segment the images into meaningful regions: Otsu thresholding method and U-Net model. U-Net is a deep learning model that provides successful results in biomedical image segmentation and is widely used in medical image analysis [17]. Figure 1 shows an example of segmentation with U-Net.

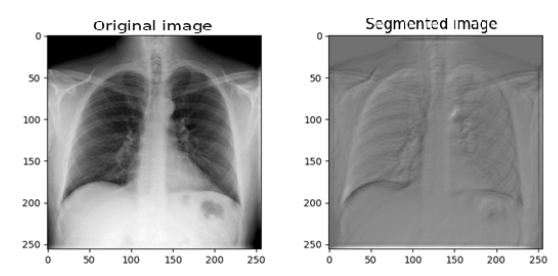


Figure 1. Segmentation of lung X-ray image using U-Net model

2.3. Fractal and Lacunar Analysis

Fractal Dimension (D): The box counting method was used to calculate the fractal dimension of the images. This method quantitatively measures the geometric complexity of a structure and is frequently used in the evaluation of biological images [18].

Lacunarity (Λ): Pixel intensity variance was used to quantify the degree of irregularity of gaps in the images. Lacunarity analysis is an effective method for assessing the homogeneity or heterogeneity of tissues [19].

2.4. Artificial Intelligence Methods

Deep Learning Models:

- Convolutional Neural Networks (CNN): CNN models were used for image classification and feature extraction. CNN has high accuracy rates on complex visual data such as medical image analysis [20].
- U-Net: The U-Net model used in segmentation processes is widely preferred especially in biomedical image analysis. U-Net offers successful results in detecting diseased regions with its segmentation performance [21].

Model Training and Evaluation:

- Data Partitioning: The data set is divided into three as training (70%), validation (15%) and testing (15%). This division is important to evaluate the generalisation ability of the model [22].
- Performance Measures: Metrics such as accuracy, precision, F1 score and ROC curve were used to evaluate the performance of the model. These metrics allow for a comprehensive analysis of classification and segmentation performance [23].

3. RESULTS

This section presents the findings obtained through fractal dimension analysis, lacunarity measurements, and deep learning-based image processing methods, applied to both medical and microbiological images. While fractal and lacunarity features were quantitatively analyzed to assess the geometric complexity and irregularity of healthy versus pathological structures, it remains important to note that these values were not integrated into the convolutional neural network (CNN) model as explicit input features. Instead, fractal and lacunarity metrics were independently and used for descriptive and comparative purposes to support the visual and statistical differentiation between the groups. The CNN and U-Net models were trained directly on raw image data, focusing on classification and segmentation performance without relying on manually extracted structural features.

3.1. Fractal Analysis Results

3.1.1. Lung Images

Significant differences were observed in the fractal analysis performed on healthy and fibrotic lung tissues. While the fractal dimension of healthy lung tissue was calculated as 1.9, this value increased to 2.3 in fibrotic lung tissue. This increase indicates that the complexity of the tissue structure increases and fibrotic processes disrupt the homogeneous structure of the lung tissue. Figure 2 compares the fractal analysis results obtained for healthy and fibrotic tissues.

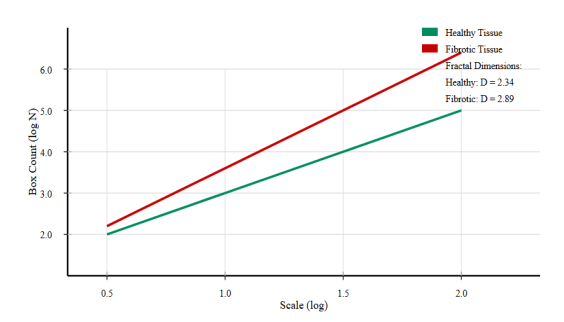


Figure 2. Fractal analysis results of healthy and fibrotic lung tissue.

3.1.2. Microbiological Images

In the fractal analysis performed on bacterial colonies, the fractal dimension of healthy colonies was calculated as 1.5. However, this value increased to 1.8 in diseased colonies. This

result indicates that the growth patterns of bacterial colonies under pathogenic conditions become more complex. Figure 3 provides a visual comparison of the fractal dimension in healthy and diseased bacterial colonies.

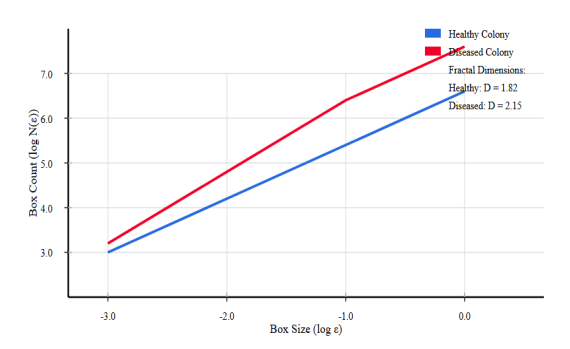


Figure 3. Fractal analysis results of healthy and diseased bacterial colonies.

Table 1 summarises the fractal dimension values in lung tissue and bacterial colonies for healthy and pathological conditions.

Table 1. Fractal dimension values in healthy, pathological lung tissue and bacterial colonies

Data Group	Fractal Dimension (D)
Healthy Lung Tissue	1.9
Fibrotic Lung Tissue	2.3
Healthy Bacterial Colony	1.5
Diseased Bacterial Colony	1.8

3.2. Lacunarity Analysis Results 3.2.1. Lung Images

Lacunarity values numerically express the rate of irregularity of tissues. While the lacunarity value was measured as 0.12 in healthy lung tissues, this value increased to 0.34 in fibrotic lung tissues. This increase in lacunarity values indicates that the spaces within the tissue lost their homogenous structure and became irregular with fibrotic processes.

3.2.2. Microbiological Images

While the lacunarity value was 0.08 in healthy bacterial colonies, this value was calculated as 0.27 in diseased colonies. This increase in diseased colonies indicates that the spaces within the colony are disorganised and form a complex structure.

Table 2 summarises the lacunarity values for healthy and pathological conditions:

Table 2. Lacunarity values in healthy, pathological lung tissue and bacterial colonies

Data Group	Lacunarity (Λ)
Healthy Lung Tissue	0.12
Fibrotic Lung Tissue	0.34
Healthy Bacterial Colony	0.08
Diseased Bacterial Colony	0.27

3.3. Artificial Intelligence Model Findings 3.3.1. CNN ve U-Net Performance

Classification and segmentation performance of deep learning models were compared. The CNN-based model provided 94.2% accuracy and 0.91 F1 score in lung tissue images. The U-Net model used in the segmentation process provided 96.5% accuracy and 0.93 sensitivity for the detection of fibrotic areas.

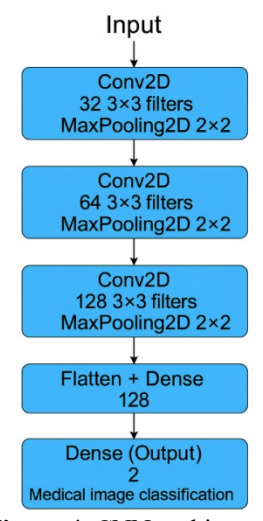


Figure 4. CNN architecture

The Figure 4 shows the CNN architecture. The model consists of three convolutional layers with increasing filter sizes (32, 64, 128), each followed by max pooling operations. These are followed by a fully connected dense layer for binary classification and a softmax output layer. ReLU activation is used in all hidden layers, while softmax is applied in the output. This architecture is widely adopted for grayscale CT images in medical diagnostics.

3.3.2. Visual Results

During the segmentation process, the U-Net model was able to distinguish fibrotic tissues and pathological areas with high precision. Figure 5 shows the segmentation results of lung tissues.

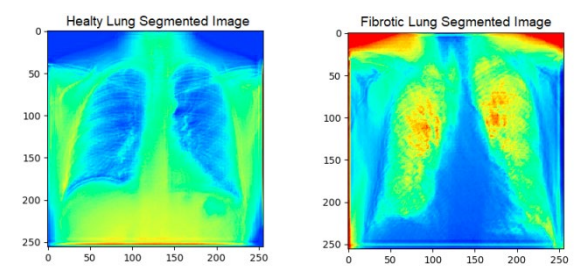


Figure 5. Segmentation results of healthy and fibrotic lung tissues with U-Net model.

The basic hyperparameters used in the model training process are based on values widely preferred in the literature. The learning rate was determined as 0.001 for the training of both models, and the training process was carried out for 50 epochs. In terms of processing efficiency and memory management, the batch size value was used as 32. For the optimization process, the Adam optimization algorithm, which offers adaptive learning rate, was preferred. Categorical crossentropy loss function was applied for the CNN model, and binary crossentropy loss function was applied for the U-Net model. While the ReLU (Rectified Linear Unit) function was used in the intermediate layers as the activation function, Softmax was preferred in the output layer of the CNN model, and Sigmoid activation function was preferred in the output of the U-Net model. These parameters enabled the model to show high accuracy and generalization performance in classification and segmentation tasks.

Table 3 shows the accuracy, Precision and F1 score performance values of CNN and U-Net models.

Table 3. Performance measures of CNN and U-Net models

Model	Accuracy (%)	Precision	F1 Score
CNN (Classification)	94.2	0.89	0.91
U-Net (Segmentation)	96.5	0.93	0.93

These findings show that fractal and lacunar analysis methods and artificial intelligence models are effective in distinguishing between healthy and pathological conditions. Fractal dimension and lacunarity measurements were able to successfully assess the geometric complexity and irregularity levels of tissue and microbial structures. Artificial intelligence

based models are promising with high accuracy rates in classification and segmentation processes.

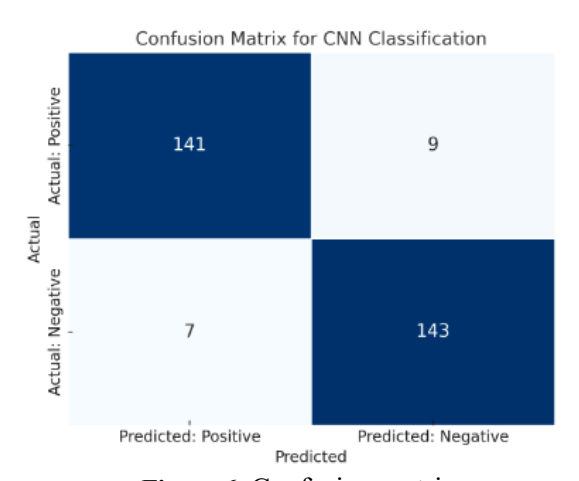


Figure 6. Confusion matrix

According to the confusion matrix in Figure 6, the model correctly classified 141 out of 150 diseased samples (True Positive) and correctly identified 143 out of 150 healthy samples (True Negative). The number of false positives (False Positive) is 9, and the number of false negatives (False Negative) is 7. This distribution shows that the model has high sensitivity and specificity values, especially in terms of disease detection.

4. CONCLUSION

In this study, fractal and lacunar analysis methods are combined with image processing techniques and artificial intelligence-based models to evaluate the results of analyses performed on medical images (lung tissue) and microbiological images (bacterial populations). The findings show that this approach is a powerful and effective method for both medical and microbiological analyses.

The results of fractal and lacunar analysis allowed the quantification of geometric and morphological differences between tissue and microbial structures. In particular, the effectiveness of these methods in the detection of fibrotic changes in lung tissue and pathological growth patterns in bacterial colonies has been demonstrated. The fractal dimension and lacunarity values between healthy and pathological conditions prove that complexity and disorder ratios provide important clues to disease processes.

At the same time, artificial intelligence-based models such as CNN and U-Net have come to the fore with high accuracy rates in the classification and segmentation of medical images. These models provide significant advantages in terms of precise evaluation of tissue complexity and detection of diseased regions. The superior success of the U-Net model in segmentation (96.5% accuracy and 0.93% precision) shows that such methods can be applied in clinical decision support systems.

This study shows that the integration of fractal and lacunar analyses with artificial intelligence-based methods has the potential to provide fast, objective and accurate decision support mechanisms in clinical diagnosis processes. Fractal and lacunar measurements provide a better understanding of pathological processes, especially in diseases that require early diagnosis. The importance of these analyses has been emphasised in the diagnosis of bacterial infections as well as lung pathologies.

In this context, the developed methods, unlike conventional imaging techniques: Provided higher sensitivity and accuracy, evaluated the complexity and irregularities of tissues more objectively, and saved time and resources in medical imaging and microbiological analysis.

The findings of this study show that the integration of fractal and lacunar analysis with artificial intelligence-based methods offers an effective approach in medical microbiological image analysis. However, further studies are needed to apply and validate the methods in a wider scope. In future research, the use of larger and more diverse datasets including different patient groups geographical regions may increase generalisability of the results obtained. In addition, the application of these analyses to different pathological conditions, such as tumour structures, neurological diseases or vascular disorders, may accelerate the transition of the method to clinical use. Considering the ongoing developments in the field of artificial intelligence, the use of Transformer-based models and hybrid artificial intelligence approaches can improve the accuracy and efficiency of fractal and lacunar analyses. Finally, testing and validation of these methods in real clinical settings with patient outcomes is critical to assess the applicability of the analyses

in the healthcare sector. In this context, it is suggested that future studies should focus on the aforementioned issues.

In conclusion, this study has demonstrated that fractal and lacunar analysis combined with artificial intelligence can provide an effective solution in medical imaging and microbiological analysis. This integration is considered as a promising approach that can make diagnostic processes in the health sector more efficient, fast and accurate in the future.

ACKNOWLEDGES

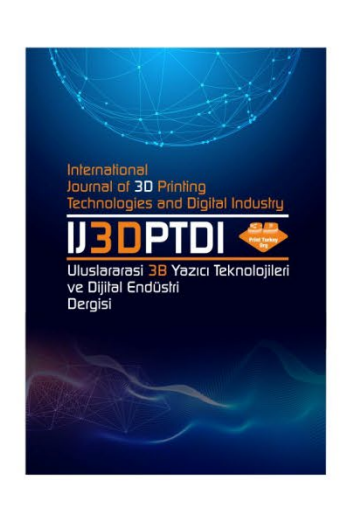
The author received no financial support for the research, authorship, and publication of this article.

REFERENCES

- 1. Smith, T. G., Lange, G. D., & Marks, W. B. "Fractal methods and results in cellular morphology—Dimensions, lacunarity, and multifractals", Journal of Neuroscience Methods, Vol. 69, Issue 2, Pages 123–136, 1996.
- 2. Gonzalez, R. C., & Woods, R. E. Digital Image Processing, Pearson Education, 2018.
- 3. Ronneberger, O., Fischer, P., & Brox, T. "U-Net: Convolutional Networks for Biomedical Image Segmentation", MICCAI, Pages 234–241, 2015.
- 4. Mandelbrot, B. The Fractal Geometry of Nature, W.H. Freeman, San Francisco, CA, 1982.
- 5. Losa, G.A., Merlini, D., Nonnenmacher, T.F., & Weibel, E.R. (Eds.) Fractals in Biology and Medicine (Vol. 4), Birkhäuser, Basel, Switzerland, 2005.
- 6. Di Ieva, A., Grizzi, F., Jelinek, H., Pellionisz, A.J., & Losa, G.A. "Fractals in the Neurosciences, Part I: General Principles and Basic Neurosciences", Neuroscientist, Vol. 20, Issue 4, Pages 403–417, 2014.
- 7. Karperien, A., Jelinek, H., & Milosevic, N. "Reviewing lacunarity analysis and classification of microglia in neuroscience", European Conference on Mathematical and Theoretical Biology, 2011.
- 8. Güleç, M., Taşsöker, M., & Şener, S. "Tıpta ve diş hekimliğinde fraktal analiz", Ege Üniversitesi Diş Hekimliği Fakültesi Dergisi, Vol. 40, Issue 1, Pages 17–31, 2019.

- 9. Arsan, E., Genç, A., Gözü, A., & Şahin, B. "Fractal analysis for differentiation of idiopathic pulmonary fibrosis and normal lung parenchyma", Digital Medicine, Vol. 3, Issue 2, Pages 61–66, 2017.
- 10. Bayrak, N., & Kırcı, M. "Fractal and lacunarity analysis of dental radiographs to detect periodontitis", Journal of X-Ray Science and Technology, Vol. 28, Issue 2, Pages 309–321, 2020.
- 11. Karthik, R., Menaka, R., & Singh, S. P. "Fractal Analysis of Bacterial Colony Images for Predicting the Effect of Nano-Ag on the Production of Extracellular Enzymes in Bacillus subtilis", Journal of Nanoscience and Nanotechnology, Vol. 19, Issue 7, Pages 3933–3941, 2019.
- 12. Yap, S.Y., Yeong, C.H., Ng, K.H., & Abdul Majid, Z. "Deep Learning Algorithms for Detection of Diabetic Retinopathy in Retinal Fundus Photographs: A Systematic Review and Meta-Analysis", Computer Methods and Programs in Biomedicine, Vol. 196, Page 105642, 2020.
- 13. Tang, Y., Zhang, Y., Chai, Y., Wang, Y., & He, X. "Fractal analysis of Actinobacillus pleuropneumoniae biofilm initial adhesion using box-counting method", Microbial Pathogenesis, Vol. 137, Page 103732, 2019.
- 14. Rafael, C., & Richard, E. Digital Image Processing, 2nd ed., Pearson Education, Upper Saddle River, NJ, 2008.
- 15. Tomasi, C., & Manduchi, R. "Bilateral Filtering for Gray and Color Images", Proceedings of the Sixth International Conference on Computer Vision, Pages 839–846, 1998.
- 16. Ziou, D., & Tabbone, S. "Edge Detection Techniques An Overview", Pattern Recognition and Image Analysis C/C of Raspoznavaniye Obrazov I Analiz Izobrazhenii, Vol. 8, Issue 4, Pages 537–559, 1998.

- 17. Zhang, Y., Brady, M., & Smith, S. "Segmentation of brain MR images through a hidden Markov random field model and the expectation-maximization algorithm", IEEE Transactions on Medical Imaging, Vol. 20, Issue 1, Pages 45–57, 2001.
- 18. Mureşan, R.C., Zaharie, D., & Zaharie, M. "Fractal Dimension for Data Mining", In: Roşu, A-L., Rebedea, T. (eds), Data Mining with Decision Trees. Intelligent Systems Reference Library, Vol. 81, Springer, Cham, Pages 81–91, 2016.
- 19. Losa, G.A., & Nonnenmacher, T.F. "Self-affinity and fractal dimension in the microarchitecture of human cancellous bone", European Journal of Morphology, Vol. 34, Issue 3, Pages 159–167, 1996.
- 20. LeCun, Y., Bengio, Y., & Hinton, G. "Deep learning", Nature, Vol. 521, Issue 7553, Pages 436–444, 2015.
- 21. Çiçek, Ö., Abdulkadir, A., Lienkamp, S.S., Brox, T., & Ronneberger, O. "3D U-Net: learning dense volumetric segmentation from sparse annotation", In: Proceedings of the International Conference on Medical Image Computing and Computer-Assisted Intervention (MICCAI), Pages 424–432, 2016.
- 22. Kohavi, R. "A study of cross-validation and bootstrap for accuracy estimation and model selection", In: Proceedings of the 14th International Joint Conference on Artificial Intelligence, Vol. 2, Pages 1137–1143, Montreal, Canada, Morgan Kaufmann Publishers Inc., 1995.
- 23. Saito, T., & Rehmsmeier, M. "The precision-recall plot is more informative than the ROC plot when evaluating binary classifiers on imbalanced datasets", PloS One, Vol. 10, Issue 3, Page e0118432, 2015.



ULUSLARARASI 3B YAZICI TEKNOLOJİLERİ VE DİJİTAL ENDÜSTRİ DERGİSİ

INTERNATIONAL JOURNAL OF 3D PRINTING TECHNOLOGIES AND DIGITAL INDUSTRY

ISSN:2602-3350 (Online)

URL: https://dergipark.org.tr/ij3dptdi

HAFİF ELEKTRİKLİ ARAÇLAR İÇİN ARAÇ MODELİ VE SÜRÜŞ DÖNGÜSÜNE GÖRE ELEKTRİK MOTORU TASARIMI

ELECTRIC MOTOR DESIGN BASED ON VEHICLE MODEL AND DRIVING CYCLE FOR LIGHT ELECTRIC VEHICLES

Yazarlar (Authors): Doğukan Ayhan[®], Ali Bakbak[®]

Bu makaleye şu şekilde atıfta bulunabilirsiniz (To cite to this article): Ayhan D., Bakbak A., "Hafif Elektrikli Araçlar İçin Araç Modeli ve Sürüş Döngüsüne Göre Elektrik Motoru Tasarımı" Int. J. of 3D Printing Tech. Dig. Ind., 9(2): 236-246, (2025).

DOI: 10.46519/ij3dptdi.1630021

Araştırma Makale/ Research Article

HAFİF ELEKTRİKLİ ARAÇLAR İÇİN ARAÇ MODELİ VE SÜRÜŞ DÖNGÜSÜNE GÖRE ELEKTRİK MOTORU TASARIMI

Doğukan Ayhan^a, Ali Bakbak^a

^aManisa Celal Bayar Üniversitesi, Mühendislik ve Doğa Bilimleri Fakültesi, Elektrik ve Elektronik Mühendisliği Bölümü, Türkiye

*Sorumlu yazar: ali.bakbak@cbu.edu.tr

(Geliş/Received: 30.01.25; Düzeltme/Revised: 23.04.25; Kabul/Accepted: 09.06.25)

ÖZ

Günümüzde elektrikli araçların yaygınlaşması, bu alanda yapılan araştırmaları hızlandırmıştır. Hafif elektrikli araçlar, sürüş döngüleri sırasında belirli bir hız-tork karakteristiğine sahip olmaları ve düşük hızlarda yüksek tork gereksinimleri nedeniyle, bu tür araçlara uygun elektrik motorlarının belirlenmesi, tasarımı ve analizi kritik bir öneme sahiptir. Bu çalışma, hafif elektrikli araçlar için dış rotorlu, yüzey montajlı, sabit mıknatıslı senkron motor (SMSM) tasarımı ve analizini kapsamaktadır. Motor tasarımına geçmeden önce, araç geometrisi ve fiziksel parametreleri ile sürüş döngüsü analiz edilmiştir. Araç modeline, pist koşullarına ve belirlenen sürüş döngüsüne göre motor tasarım gereksinimleri belirlenmiş ve bu doğrultuda optimizasyon yapılmıştır. Enerji verimliliği ve araç performansının ön planda olduğu hafif elektrikli araç yarışlarında kullanılmak üzere tasarlanan dış rotorlu SMSM, bu gereksinimlere göre optimize edilmiştir. Bu tasarım ve analiz süreci, motorun yüksek enerji verimliliği ve performansını sağlamayı hedeflemektedir.

Anahtar Kelimeler: Hafif Elektrikli Araçlar, Sürüş Döngüsü, Araç Modeli, Hafif Elektrikli Araç Yarışları, Dış Rotorlu PMSM, Motor Tasarımı.

ELECTRIC MOTOR DESIGN BASED ON VEHICLE MODEL AND DRIVING CYCLE FOR LIGHT ELECTRIC VEHICLES

ABSTRACT

The widespread adoption of electric vehicles has accelerated research in this field. Light electric vehicles, due to their specific speed-torque characteristics during driving cycles and their requirement for high torque at low speeds, necessitate the selection, design, and analysis of suitable electric motors. This study focuses on the design and analysis of an outer rotor, surface-mounted, permanent magnet synchronous motor (PMSM) for light electric vehicles. Before initiating the motor design process, vehicle geometry, physical parameters, and the driving cycle were analyzed. Motor design requirements were then determined based on the vehicle model, track conditions, and the specified driving cycle, and an optimization process was carried out accordingly. The outer rotor PMSM, developed for use in light electric vehicle competitions where energy efficiency and performance are critical, was optimized to meet these demands. This design and analysis process aims to ensure high energy efficiency and performance of the motor.

Keywords: Light Electric Vehicles, Driving Cycle, Vehicle Model, Outer Rotor PMSM, Motor Design.

1. GİRİŞ

Otomotiv sektöründe, konvansiyonel araçlar egzoz emisyonları ve iklim değişikliği gibi ekolojik dengeyi, yaşam koşullarını ve insan sağlığını etkileyen geniş kapsamlı çevresel sorunlara neden olmaktadır. Artan enerji verimliliği talepleriyle birlikte küresel çevresel düzenlemelere uyum sağlamak amacıyla elektrikli araçlar alanında geçtiğimiz son on yıl içerisinde dikkate değer teknolojik ilerlemeler kaydedilmistir. Birçok ülke ve otomotiv sürdürülebilirliğe sirketleri cevresel taahhütlerini daha da ileriye götürmek amacıyla toplumsal farkındalık kazanmıştır konvansiyonel araç satışlarını kademeli olarak sonlandırmak için zaman çizelgeleri belirlemişlerdir [1]. Avrupa Birliği'nin çevresel hedeflerinden biri, 2050 yılına kadar iklim nötrlüğünü sağlamaktır. Avrupa Parlamentosu verilerine göre, karayolu tasımacılığının en büyük paya (yaklaşık %72) sahip olduğu 2016 yılında küresel karbondioksit emisyonlarının %25'ini ulaşım emisyonları yaklaşık oluşturmaktadır [2]. Elektrikli araçlara olan ilgi arttıkça, sürüş döngüsü ve araç modeli tabanlı motor tasarımı çalışmaları da artış göstermiştir. Bu alandaki çalışmalar, elektrikli araçların daha da yaygınlaşması için önemli bir adım olarak görülmektedir [3].

Hafif elektrikli araçlar genel olarak enerji verimliliğinin temel amac olduğu uygulamalarda tercih edilirler. Literatürde, çeşitli motor topolojileri için sürüş döngüsü verimlilik analizlerine rastlanmaktadır [4]. [5] çalışmasında elektrikli arac performansının izlenmesi ve optimize edilmesinde dijital ikiz teknolojisi kullanılarak farklı motor tiplerinin enerji tüketimi ve hızlanma performanslarını gerçek zamanlı yol verilerine dayanarak karşılaştırmış ve SMSM motorun üstün performans sergilediğini ortaya koymustur. Sürüs döngüsü aracın gerçek dünya performansını modellemek için kullanılır ve aracın hızı, ivmesi, yokuş çıkma ve frenleme gibi faktörler ile araç motorunun tork ve hız gereksinimlerinin belirlenmesine olanak tanır. Diğer bir yandan, araç modeli aracın fiziksel özelliklerini ve performansını matematiksel olarak tanımlayan bir modeldir. Araç modeli, aracın hızı, ağırlığı, direnci, sürtünmesi, aerodinamik özellikleri vb. gibi faktörleri hesaba katarak aracın performansını ölçer. Bu sayede, daha verimli ve performanslı elektrik motorları tasarlanarak, hafif elektrikli araçların performansı maksimize edilir [6-11]. Bu çalışmada araç modelinden elde edilen veriler ve pist geometrik verileri ile birlikte araç için pist simülasyonu "Sürüş Döngüsü Çıkarılması ve Analizi" bölümünde gerçekleştirilmiştir.

Hafif elektrikli araç kategorisindeki araçların hareketini sağlayacak olan motor türünün belirlenmesi önem arz etmektedir. Çalışma [12]'de doğru akım, sabit mıknatıslı senkron, senkron relüktans ve asenkron motor gibi farklı topolojilerdeki makineler performans, güvenilirlik ve verim gibi parametreler açısından değerlendirilmiştir. Ancak motor seçimi, sürüş döngüsüne özgü gereksinimler dikkate alınarak yapılmalıdır. Özellikle bazı hafif elektrikli araç uygulamaları düşük hız bölgesinde çalışma yüksek tork etmektedirler. Çekiş uygulamalarında (traction applications) genellikle senkron motor kategorisi altındaki iç kalıcı mıknatıslı senkron motor (Interior permanent magnet synchronous-IPMSM) veya yüzey montajlı kalıcı mıknatıslı senkron motorlar (Surface mounted synchronous motor-SMPMSM) tercih edilmektedir. Cünkü senkron motorlar, nominal hız aralığında asenkron motorlara kıyasla daha yüksek güç yoğunluğu ve verimlilik sunar [3,13-15]. Bu uygulamada hafif elektrikli aracın hareketini sağlamak için dış rotorlu SMPMSM tercih edilmiştir. Dış rotorlu motorlar (hub motorlar), doğrudan tekerleklere entegre edilebilir olmaları sayesinde mekanik aktarma organlarına olan ihtiyacı ortadan kaldırır. Bu yapı, sistemin toplam kütlesini azaltır ve enerji kayıplarını minimize eder. Bu yapı, özellikle yarış araçlarında görülen düşük hız-yüksek tork gereksinimleri için verimli bir çözümdür [5]. Ayrıca araç güç aktarımında Şanzıman ve diferansiyel gibi mekanik aktarma organlarının ortadan kalkması, daha hafif ve sade bir yapı sağlar [2,16].

Pist simülasyonu sonucu elde edilen değerler ile motor tasarımı için isterler oluşturulmuştur. Motor isterlerine göre dış rotorlu SMSM elektromanyetik analizi sonlu elemanlar analizi (SEA) programlarıyla gerçekleştirilmiştir.

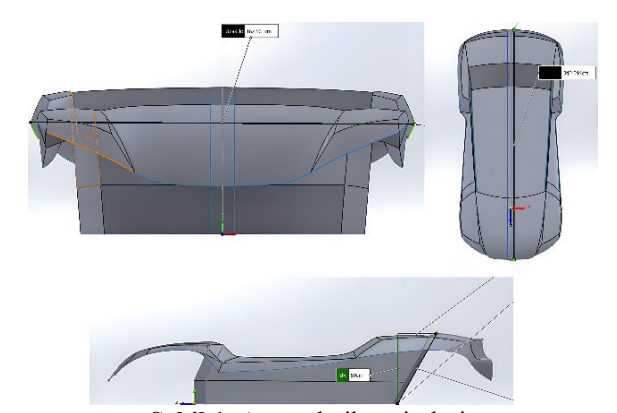
2. SÜRÜŞ DÖNGÜSÜ ÇIKARILMASI VE ANALİZİ

Motor isterlerinin belirlenmesi için pist gerçekleştirilmiştir. simülasyonu Pist simülasyonunun amacı; pistin bölümlere ayrılması, her bir bölüm için hız ve karakteristik araç parametrelerinin belirlenmesi ve bunlara gelen değerlerinin karşılık tork hesaplanmasıdır. Toplam araç ister kuvvet değerinin belirlenmesi ile birlikte, bu değer kullanılarak araç ister toplam tork değeri hesaplanmıştır. Gerçekleştirilen çalışmada pist viraj, frenleme ve hızlanma bölgeleri olarak üç farklı bölgeye ayrılmıştır. Virajlar ve düz yollar arasındaki hız değişimi, tork gereksinimlerinin neden farklılaşmasına olmaktadır. Hesaplamalarda fren mesafeleri ve süreleri de hesaba katılmıştır. Bu kuvvet hesaplarını yaparken araç ivme değeri 0,5 m/s² ve ortalama pist eğimi %1,4 değeri kullanılmış olup, frenleme noktalarında ise araç ivme değeri -0,5 m/s² olarak hesaba katılmıştır. Viraiların keskinliğine göre araç hız değerleri değişmektedir. Bununla birlikte düz yollarda araç hızı 36 km/h olarak alınmış olup, pist içerisindeki yük ve elektriksel torkunun hesaplanması için Denklem (1) kullanılmıştır [17].

$$T_E - T_L = J \frac{d\omega}{dt} \tag{1}$$

Buradaki T_E elektriksel torku, T_L yük torkunu, J eylemsizlik momenti ve ω açısal hızı temsil etmektedir.

Pist bilgileri ve pist için yapılan hesaplamalar Çizelge 1'de, sürüş döngüsü boyunca araç ister tork hesabının yapılabilmesi için gerekli olan araç geometrik ve aerodinamik parametreleri ve diğer parametreler Çizelge 2'de verilmiştir. Araç teknik resimleri Şekil 1'de mevcuttur.



Şekil 1. Araç teknik resimleri

Çizelge 1. Pist bilgileri

Özellik	Birim	Değer
Pist Tur Uzunluğu	m	1370
Pist Tur Sayısı	-	5
Pisti Bitirmek İçin Toplam Süre	S	900
Toplam Viraj Sayısı	-	8
Sağa Doğru Viraj Sayısı	-	5
Sağa Doğru Viraj Toplam Uzunluk	m	90
Sola Doğru Viraj Sayısı		3
Sola Doğru Viraj Toplam Uzunluk	m	115
Pist Ortalama Eğim	%	1,4
Görev Sayısı	-	3
Görev İçin Verilecek Ek Süre	-	90
Pisti Bitirmek İçin Ortalama Hız	km/h	28

Çizelge 1'de bulunan veriler TEKNOFEST "Uluslararası Efficiency Challenge Elektrikli Araç Yarışları" şartnamesinden alınmıştır [18].

Çizelge 2. Araç parametreleri

Özellik	Birim	Değer
Araç Kütlesi Sürücü İle		500
Birlikte(m)	kg	
Araç Hızlanma İvmesi(a)	m/s^2	0,5
Araç Yavaşlama İvmesi(a)	m/s^2	-0,5
Yerçekimi Sabiti(g)		9,81
	Nm^2/kg^2	
Hava Yoğunluğu(pa)	kg/m^3	1,23
Sürükleme Sabiti(Cd)	-	0,46
Yuvarlanma Direnci(Cr)	-	0,02
Araç Ön Alanı(A)	m^2	1,48
Araç Teker Yarıçapı	m	0,3
Araç Jant Dış Çapı	inç	17
Araç Jant İç Çapı	inç	10,79
Dişli Oranı	-	1
Tekerlek Ataleti	kg.m ²	22,5

Sürüş döngüsü boyunca araca çeşitli direnç kuvvetleri etki eder. Bu kuvvetler sırasıyla; Aerodinamik Direnç Kuvveti (Aerodynamic Resistance Force-Fa), Lastik Yuvarlanma Direnç Kuvveti (Tire Rolling Resistance Force-Fr), Gradyan Direnç Kuvveti (Gradient Resistance Force-Fg), Eylemsizlik Direnç Kuvveti(Inertia Resistance-F_A)'dir. Araç ister tork değerinin hesaplanması için Denklem (2), Denklem (3), Denklem (4), Denklem (5) ve Denklem (6) kullanılır [1,2,8,17,19].

$$F_a = m.a (2)$$

$$F_g = m.g.\sin(\alpha) + \frac{1}{2}$$
 (3)

$$F_{A} = \frac{1}{2} \cdot \rho_{a} \cdot C_{d} \cdot A_{v} \cdot (V_{w} + V_{v})^{2}$$
 (4)

$$F_r = m.g. C_r. cos(\alpha)$$
 (5)

$$F_T = F_a + F_g + F_A + F_r \tag{6}$$

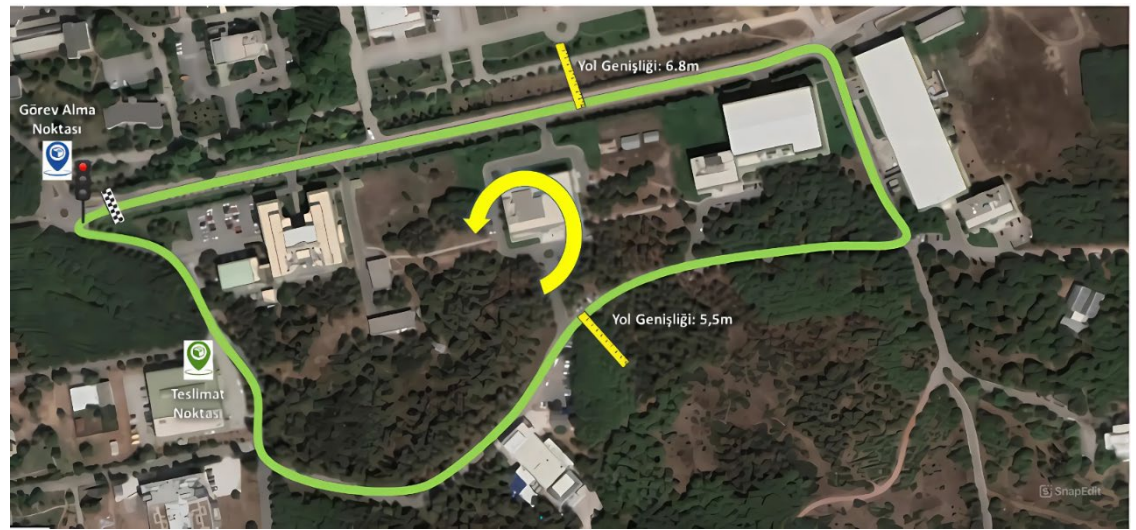
Buradaki denklemlerde sırasıyla; m araç kütlesini, a araç ivmesini, g yerçekimi ivmesini, α yol eğimi, ρ_a hava yoğunluğunu, C_d araç sürüklenme sabitini, A_v araç ön alanını, V_v araç

hızını, V_w rüzgar hızını, C_r araç yuvarlanma direncini temsil etmektedir [3,8,11]. Araç ister tork değeri hesaplanırken pist ortalama eğim değeri %1,4, rüzgar hızı 0 km/h olarak hesaba katılmıştır. Tekerlek ataleti ise Denklem (7) yardımıyla hesaplanmıştır.

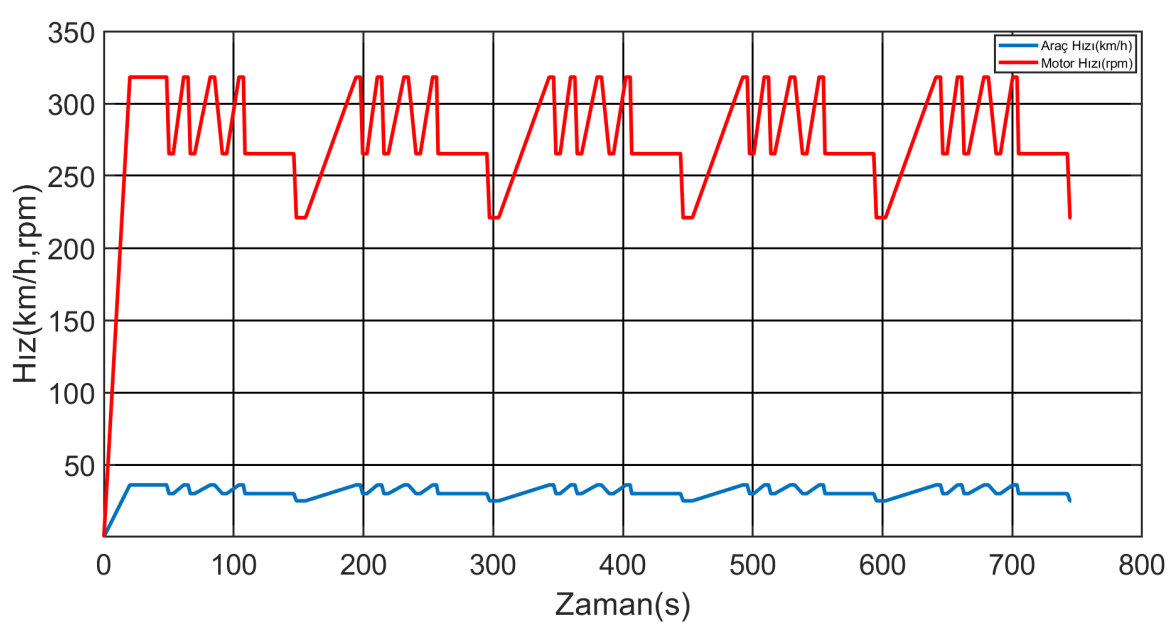
$$I = m. r^2 \tag{7}$$

Burada m tekerlek kütlesi ve r tekerlek yarıçapını temsil etmektedir.

Yarış pistinin Google Earth üzerinden elde edilen iki boyutlu görüntüsü Şekil 2'de sunulmuştur.



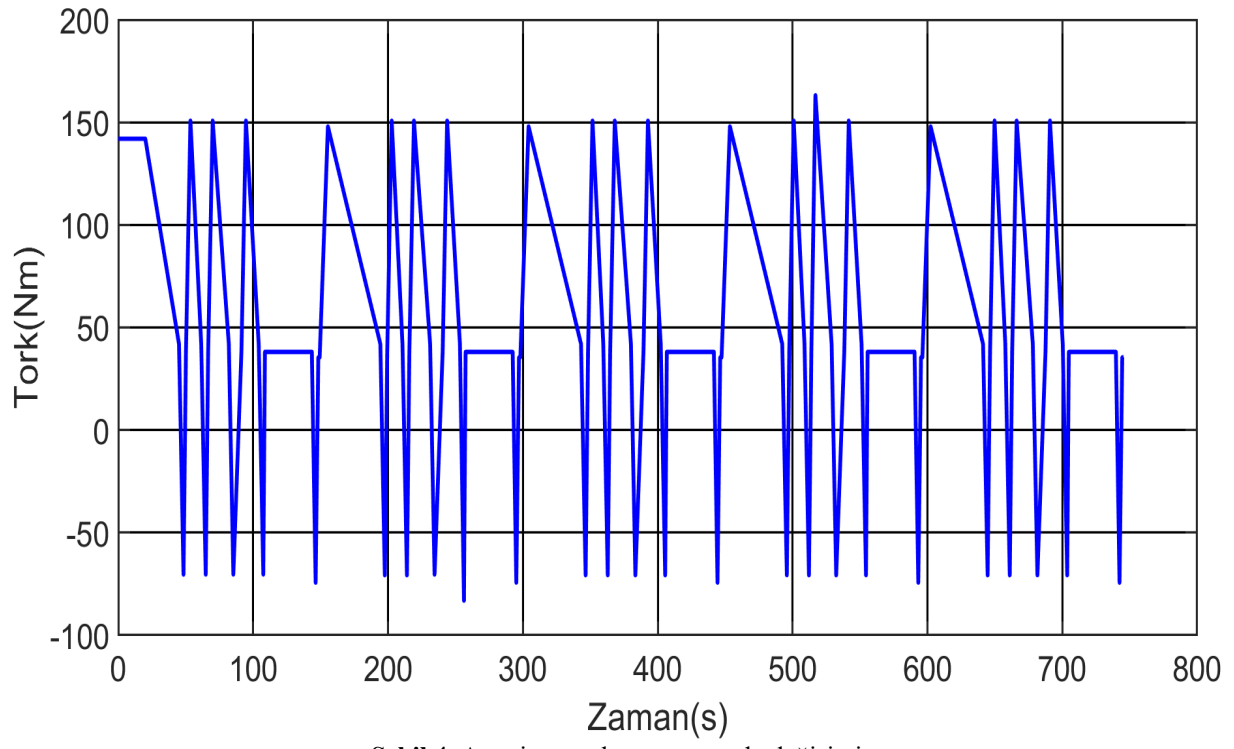
Şekil 2. TEKNOFEST "Uluslararası Efficiency Challange Elektrikli Araç Yarışları" yarış pisti [18]



Şekil 3. Araç hızı ve motor hızının bir döngüdeki değerleri

Sürüş döngüsü sonuçlarının elde edilebilmesi için araç geometrik ve aerodinamik parametrelerinin değerleri ile birlikte aracın pisti bitirmesi için süre, virajların ve düzlüklerin mesafeleri, virajlardaki araç hız değerleri ve düzlüklerde araç hız değerleri kullanılmıştır. Virajlarda araç hızının belirlenmesinden önce ortalama araç hızı pisti bitirme süresi ve toplam pist uzunluğu değerlerinden 28 km/h olarak

hesaplanmıştır. Hesaplamalar ve analizlerin sonucunda araç belirtilen hız değerleri ile yarışı 745,4 s'de tamamlamaktadır. Bu doğrultuda, araç hızı ve araç hızından elde edilmiş motor hızının zamana göre değişimi Şekil 3'de verilmiştir. Araç ister torku, sabit ivmeli hareket boyunca sürekli değişmekte; frenleme noktalarında ise negatif değerlere ulaşmaktadır (Şekil 4).



Şekil 4. Araç ister torkunun zamanla değişimi

3. MOTOR TASARIMI

Sürüş döngüsünde elde edilen maksimum tork ve hız değerlerine göre, aracın ihtiyaç duyduğu maksimum mekanik güç Denklem (8) ile 5026,16 W olarak hesaplanmıştır. Motor tasarımı için maksimum ve ortalama mekanik güç değeri referans alınmaktadır [20]. Sistemde iki motor kullanılacağından, her bir motor için 75,4 Nm tork ve 316,6 rpm hız değerleri esas alınarak yaklaşık 2500 W mekanik güç gereksinimi hesaplanmıştır.

3.1. Motor Boyutlandırması

Sürüş döngüsü içerisinde araç ister ortalama mekanik gücü ise Denklem (9) yardımıyla 1811,55 W olarak hesaplanmıştır. Sürüş döngüsü araç ister ortalama mekanik güç hesabı yapılırken, ortalama araç ister tork değeri ve ortalama motor hız değeri sırasıyla, 62.876 Nm ve 275.128 rpm olarak hesaba katılmıştır. [17,21-22].

$$P_{\rm m} = \omega_{\rm max}.\,T_{\rm max} \tag{8}$$

$$P_{\text{ort}} = \omega_{\text{ort}}.T_{\text{ort}} \tag{9}$$

Motor doğru akım bara gerilimi (VDC_{BUS}) 72V'dur. Uygulamada kullanılacak olan HUB motor jantı 274 mm değerine sahiptir. Motor temel boyut hesapları yapılırken birim hacim başına tork (Torque Ratio Per Volume - TRV) değeri belirleyici bir kriterdir. İstenen motor torku, rotor çapı ve TRV değerleri bilindiği için Denklem (10) yardımıyla motor uzunluğu hesaplanmıştır [21-22].

$$TRV = \frac{T}{V_{\text{rotor}}} = \frac{4.T}{\pi . L_{\text{stk}}.D^2}$$
 (10)

Burada T motor torkunu, V_{rotor} rotor hacmini, L_{stk} motor eksenel uzunluk, D rotor çapını temsil etmektedir. Yüksek enerjili sinterlenmiş NdFeB mıknatıs kullanılacağı için TRV değeri 40 kNm/m³ olarak hesaba katılmıştır [22]. Bu

değer, NdFeB mıknatısların sağladığı yüksek manyetik akı yoğunluğu ve daha önce benzer motor topolojilerinde elde edilen değerlerle uyumlu olduğu için tercih edilmiştir. Ayrıca, literatürde küçük hacimli dış rotorlu motorlarda TRV değeri genellikle $35-45~\mathrm{kNm/m^3}$ aralığında tanımlanmaktadır. Böylelikle Denklem (10) yardımıyla motor uzunluğu (L_{stk}) değeri $38,5~\mathrm{mm}$ olarak hesaplanmıştır.

Uygulamada kullanılacak olan HUB motor jantı, mıknatısların sabitleneceği yüzey için 6 mm rotor saç kalınlığı sabittir. Mıknatıs(kutup) boyutlandırması için Denklem (11), Denklem (12) ve Denklem (13) kullanılmıştır.

$$\lambda = \frac{L_{stk}}{\tau p} \tag{11}$$

$$e = \frac{\tau_{arc}}{\tau_p} \tag{12}$$

$$\tau_{p} = \frac{\pi.D_{rotor}}{p} \tag{13}$$

içerisindeki Bu denklemler sembollerin sırasıyla; L_{stk} motor anlamları eksenel uzunluğunu, τρ kutup adımını, τ_{arc} kutup yerleştirme açısını, D_{rotor} rotor çapını ve p ise kutup sayısını temsil etmektedir [22]. Motor rotor saç kalınlığı (rotor back iron thickness) 11 mm değerine, mıknatıs kalınlığı 5 mm değerine ve motor dış çapı 274 mm değerine sahip olduklarından dolayı rotor iç çapı 252 mm olarak hesaplanır. Mıknatıs kalınlığı 5 mm; üretim kısıtları nedeniyle hava aralığı ise 1 mm olarak belirlenmis ve bu değerlere göre analiz süreci başlatılmıştır. Bu durumda stator çapı 250 mm değerine sahiptir.

3.2. Oluk/Kutup Seçimi

Motor hızı ile kutup sayısı arasındaki ilişki Denklem (14)'de verilmiştir [21].

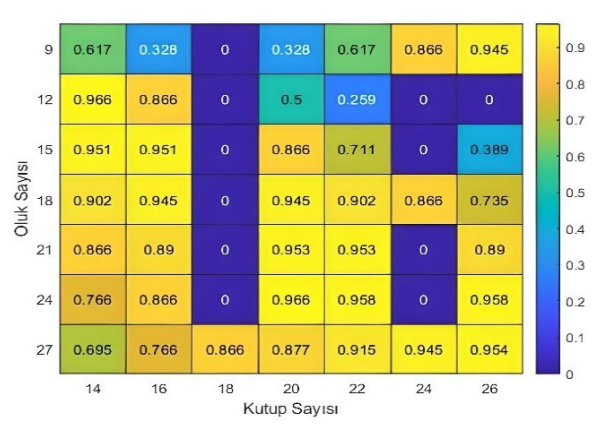
$$n = \frac{60.f_e}{p} \tag{14}$$

Bu eşitlikte n devir sayısını, f_e elektriksel frekansı, p kutup çifti sayısını temsil etmektedir. Motorun hesaplanan maksimum devir sayısında (316,6 rpm) çalışabilmesi için farklı kutup sayılarında gerekli olan elektriksel frekans değerleri Çizelge 3'de verilmiştir.

Çizelge 3. Kutup sayısı ve frekans ilişkisi

Kutup Çifti Sayısı	Elektriksel Frekans
1	5,28
2	10,55
3	15,83
4	21,11
5	26,38
6	31,66
7	36,94
8	42,21
9	47,49
10	52,77
11	58,04

Elektriksel frekansın fazla olmasının nüve kayıplarını artırma gibi dezavantajları vardır. Ancak çok düşük seçilmesi durumunda da modülasyon zorlukları olusacaktır. Bu sebeple kutup çifti sayısı(p) 10 ve 11 şebeke frekansına yakın değeriyle uygun olarak görülmektedir. Öte yandan motor kutup sayısının belirlenmesi için dikkat edilmesi gereken noktalardan bir diğeri de dengesiz manyetik kuvvetlerdir (Unbalanced Magnetic Forces-UMF). Kutup $say_1s_1(2p) = 3.k - 1$ olan makinelerde radyal ve çevresel gezici gerilimlere (radial circumference traveling stresses) bağlı iki bileşenli bir UMF ortaya çıkar. Buna karşın, 2p = 3k + 1 olan kutup sayılarında bu bileşenlerin etkisi kısmen azalır. Bu etkileşimler nedeniyle, aynı oluk sayısı için, kutup sayısı oluk sayısına göre daha küçük bir değere sahip olan makine, kutup/oluk sayıları bir farklı olduğunda daha büyük bir dengesiz manyetik kuvvet üretir. Diğer bir deyişle, aynı kutup sayısı için, kutup/oluk sayıları iki farklı olan makineler, kutup/oluk sayıları bir farklı olan makinelerden daha az dengesiz manyetik kuvvet üretir [23]. 22 kutuplu (11 çift) yapı, stator oluk sayısıyla birlikte belirli kutup/oluk oranlarında daha dengeli manyetik kuvvet dağılımı sağlar. 24 oluk ile birlikte 22 kutuplu yapı kullanıldığında sargı faktörü yüksek kalmakta ve UMF oluşumu minimuma inmektedir. Bu, özellikle düşük hızda çalışan ve yüksek tork gerektiren dış rotorlu motorlar için önemli bir avantajdır. Bu durumda 22 kutup sayısı(2p) ve 24 ve 21 oluk sayısı(S) için sargı faktörü (k_w) 0,958 ve 0,953 değerine sahiptir. Çeşitli kutup ve oluk sayısı kombinasyonlarına göre sargı faktörü hesaplama sonuçları Sekil 5'de verilmiştir. Çalışma kapsamında 22 kutup sayısı için 24 ve 21 stator oluk sayıları analiz edilmiş ve 24 stator oluk sayısına karar verilmiştir. Kutup sayısı 22 ve stator oluk sayısı 24 kombinasyonu için sargı faktörü 0.958 olarak, stator oluk sayısının her bir faza ve kutup sayısına oranı (q) ise 0,364 olarak hesaplanmıştır.



Şekil 5. Oluk kutup kombinasyonlarına karşılık gelen sargı faktörü değerleri

3.3. Sarım Sayısı Ve Oluk Geometrisi

Endüklenen faz gerilimi faz başına akı, faz başına sarım sayısı, toplam iletken sayısı, oluk başına iletken sayısı ve motor faz gerilimi değerleri Denklem (15-20) ile hesaplanır [24-26].

$$E = \frac{2.\pi}{k_w.w_a.Fe.\emptyset.\sqrt{2}}$$
 (15)

$$\emptyset = \frac{2}{\pi} \cdot (B_{\mathbf{g}} \cdot \tau_{\mathbf{p}} \cdot L) \tag{16}$$

$$W_{a} = \frac{E.\sqrt{2}}{2.\pi.k_{w}.Fe.\emptyset}$$
 (17)

$$Z = 2. \,\mathrm{m.} \,\mathrm{W_a}$$
 (18)

$$Z_0 = \frac{Z}{N_c} \tag{19}$$

$$V_{RMS} = \frac{VDC_{BUS}}{\sqrt{3}.\sqrt{2}}$$
 (20)

Burada E endüklenen faz gerilimini, kw sargı faktörünü, Wa faz başına sarım sayısını, Fe elektriksel frekansı, Ø manyetik akı miktarını, Z toplam iletken sayısını, m faz sayısını, Z₀ oluk başına iletken sayısını, Ns stator oluk sayısını, V_{RMS} motor faz RMS gerilimini temsil V_{RMS} değeri etmektedir. 29,39V olarak hesaplanmıştır. Sonrasında Denklem (17) kullanılarak başına akı kutup değeri hesaplanmıştır. Bu eşitlik içerisinde hava aralığı akı yoğunluğu(B_g) 0,8 T-0,85 T arasında bir değerde olacağı ön görülmüştür. Hesaplama için akı yoğunluğu 0,85 T olarak hesaba katılmıştır. Buna göre; kutup başına manyetik akı miktarı 1,63 mWb, faz başına sarım sayısı değeri 178,81 ve toplam iletken sayısı 1072,86 olarak bulunmuştur. Sonrasında, oluk başına iletken sayısı 44,7 olarak hesaplanmış olup, tam sayı gerekliliği nedeniyle iletken sayısı 46 olarak yuvarlanmıştır. Bu değer hem üretim kolaylığı hem de oluk doluluk oranının %60 sınırını aşmaması açısından uygundur. Ayrıca akım yoğunluğu 5 A/mm² seviyesinde tutularak kablo kesiti ısınma problemlerine karşı güvenli sınırlarda tutulmuştur. Bu durumda, her bir oluk için sarım sayısı 23 tur olarak belirlenmiştir. İletken kesit hesabı yapılırken motor verimi yaklaşık %85 olarak alındığı taktirde faz akımı RMS değeri 33,36 A olarak hesaplanır. Doğal soğutmalı sistemlerde termal güvenlik açısından akım yoğunluğunun 5 A/mm²'yi aşmaması gerektiği göz önünde bulundurulmuştur [22]. Bu sınır değer esas alınarak iletken kesit alanı ve kablo kalınlığı hesaplamaları yapılmış, motorun sürekli çalışma koşullarında aşırı ısınmasının önüne geçilmesi hedeflenmiştir. Bu durumda kablo kesit alanı 6,67 mm² olarak hesaplanmıştır. Kamaların bulunduğu oluklarda, düşük güçlü uygulamalar için %60 civarında doluluk oranı hedeflenir. Oluk alanı ise kablo kesit alanı, toplam iletken sayısı ve %60 oluk doluluk oranı göz önüne alındığında 255,76 mm² olarak hesaplanmıştır.

Stator boyutlandırmasında, oluk adımı temel bir parametredir. Bu değer Denklem (21) ile hesaplanabilir.

$$\tau_0 = \frac{D_{\text{stator}} \cdot \pi}{N_S} \tag{21}$$

Burada τ_0 stator oluk adımı değerini, Dstator stator çapını, Ns oluk sayısını temsil etmektedir. Buna göre Denklem (21) ile hesaplanan stator oluk adımı değeri 32,73 mm olarak elde edilmiştir. Stator diş genişliğinin (b_d) hesaplanması için oluk adımı, oluk akı yoğunluğu, stator çeliği sıkıştırma faktörü ve hava aralığı akı yoğunluğu değerleri kullanılır ve Denklem (22) ile hesaplanır.

$$b_d = \frac{\tau_0.B_g}{(k_{fe}.B_s)} \tag{22}$$

Burada b_d stator diş genişliğini, k_{fe} sıkıştırma faktörünü, B_s stator manyetik akı yoğunluğunu ve B_g ise hava aralığı manyetik akı yoğunluğunu temsil etmektedir. Oluk adımı değeri 32,73 mm, stator çeliği sıkıştırma faktörü

değeri 0,98, B_s değeri M470-50A materyali için 1,8 T ve B_g değeri 0,85 T olarak hesaba katıldığında b_d değeri 15,77 mm olarak hesaplanır. Oluk üst genişliği (b₀) ise Denklem (23) yardımıyla 16,96 mm olarak belirlenmiştir.

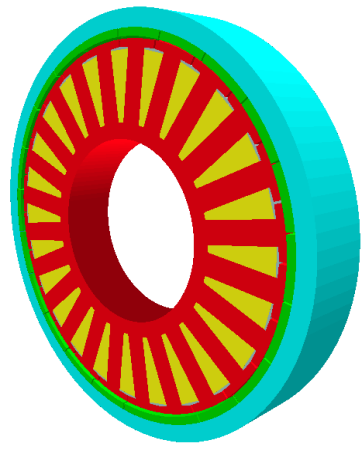
$$b_0 = \tau_0 - b_d \tag{23}$$

Gerekli oluk alanı bilindiğinden dolayı oluk uzunluğu 15,08 mm olarak hesaplanır.

4. ELEKTROMANYETİK SONLU ELEMANLAR ANALİZİ SONUÇLARI

Hesaplanan motor parametreleri, sonlu elemanlar analiz (SEA) yazılımına aktarılmıştır. Tasarlanan motorun üç boyutlu modeli Şekil 6'da sunulmuştur. Analizler, 72 V DC batarya gerilimi ve 45 A etkin faz akımı altında, motor 316,6 rpm hızla çalıştırılarak gerçekleştirilmiştir. Elde edilen sonuçlar Çizelge 4'te paylaşılmıştır.

Cizelge 4'te sunulan veriler, tasarlanan motorun hafif elektrikli araçlar için oldukça verimli ve performans dengeli bir sunduğunu göstermektedir. Motorun ortalama momenti 78,582 Nm, şafttan alınabilecek tork değeri ise 75,683 Nm olarak belirlenmistir. Bu değerler, aracın ihtiyaç duyduğu çekiş gücünü sağlayacak seviyede olup, moment dalgalılığının %11,96 seviyesinde olması motorun kararlılığını değerlendirmek açısından önemli bir göstergedir. Dalgalanma sevivesi kabul edilebilir aralıkta olmakla birlikte, daha stabil bir tork çıkısı elde etmek için ek optimizasyon çalışmaları düşünülebilir. Özellikle düşük hız aralığında çalışan motorlar için sürüş konforu açısından önem arz eden moment dalgalılığı, motor kontrol algoritmalarında yapılacak iyileştirmelerle daha da azaltılabilir.



Şekil 6. Dış Rotorlu SMPMSM

Cizelge 4. Elektromanyetik analiz sonuçları

Değişken	Değer	Birim
Ortalama Moment	78,582	Nm
Moment Dalgalılığı	9,3118	Nm
Moment Dalgalılığı [%]	11,963	%
Sabit Tork İçin Hız Limiti	350,01	rpm
Yüksüz Hız(No Load Speed)	425,98	rpm
Giriş Gücü	2778,6	Watts
Toplam Kayıplar (On Load)	269,4	Watts
Çıkış Gücü	2509,2	Watts
Verimlilik	90,305	%
Şafttan Alınabilecek Tork	75,683	Nm
Güç Faktörü	0,79606	
Güç Faktörü Açısı	37,245	EDeg
Faz Terminal Gerilimi (rms)	28,095	Volts

Motorun hız parametreleri incelendiğinde, sabit tork için hız limiti 350,01 rpm, yüksüz hızı ise 425,98 rpm olarak hesaplanmıştır. Bu değerler, motorun belirlenen sürüş döngüsüne uygun olarak tasarlandığını ve özellikle düşük hızlarda yüksek tork üreterek hafif elektrikli araçlar için gerekli performansı sağlayabileceğini göstermektedir.

Güç analizine bakıldığında, giriş gücü 2778,6 W, çıkış gücü 2509,2 W ve toplam kayıplar 269,4 W olarak hesaplanmıştır. Bu veriler doğrultusunda, motorun verimliliği %90,3 olarak elde edilmiştir ki bu, elektrik motorları için oldukça yüksek bir değer olup enerji düşük seviyede kayıplarının olduğunu göstermektedir. Yüksek verimlilik, batarya kapasitesinin daha etkin kullanılmasını sağlayarak aracın menzilini artıracaktır.

Elektriksel parametreler açısından incelendiğinde, motorun güç faktörü 0,79606 olarak hesaplanmış ve güç faktörü açısı 37,245° olarak belirlenmiştir. Güç faktörü 1'e ne kadar yakın olursa motorun şebekeden çektiği akımın o kadar verimli kullanıldığı anlamına gelir. Bu değer, motorun oldukça iyi bir seviyede çalıstığını gösterse de, belirli kontrol algoritmaları ve sürücü optimizasyonlarıyla daha da iyileştirilebilir.

Tasarlanan motorun ulaştığı %90,3 verimlilik, literatürde benzer dış rotorlu SMPMSM yapılarında elde edilen değerlere paralellik göstermektedir ve teorik anlamda manyetik kayıpların minimize edilerek yüksek enerji dönüşüm verimliliğinin sağlandığını ortaya

koymaktadır. Moment dalgalanması değeri olan %11.96 ise hafif elektrikli uygulamalarında kabul edilebilir sınırlar içerisinde yer almakta olup, düşük hızda çalışan sistemlerinde karsılasılan dalgalanma oranlarıyla örtüsmektedir [27]. Elde edilen bu sonuçlar, özellikle düsük hızda yüksek tork gerektiren yarış uygulamalarında, teorik beklentilerle uyumlu şekilde motorun kararlı ve verimli bir performans gösterebileceğini ortaya koymaktadır. Tasarımın dıs rotorlu yapıda ve doğrudan tekerlekle bütünleşik olması, pratikte şanzıman, diferansiyel gibi elemanlara olan ihtiyacı ortadan kaldırarak uygulama kolaylığı ve hafiflik sağlamaktadır.

Sonuç olarak, bu motor tasarımı hafif elektrikli araçlar için yüksek verimli bir çözüm sunmaktadır. Motorun düşük hızlarda yüksek tork üretme kapasitesi, yarış koşullarında ve enerji verimliliği odaklı uygulamalarda başarılı olabileceğini göstermektedir. Moment dalgalanmasının azaltılması ve güç faktörünün iyileştirilmesi, sistemin performansını daha da artırabilir. Genel olarak, motorun belirlenen tasarım gereksinimlerini büyük ölçüde karşıladığı ve hafif elektrikli araç yarışları gibi uygulamalarda etkin bir şekilde kullanılabileceği söylenebilir.

5. SONUC

Bu çalışma, dış rotorlu SMPMSM motor tasarımını sürüş döngüsü verilerine dayalı olarak doğrudan pist koşullarından türetilmiş hız ve tork profilleriyle optimize eden araç modeli tabanlı sistematik bir yaklasım önermektedir. Literatürde genel geçer test döngüleri kullanılarak yapılan analizlerinden farklı olarak, bu çalışmada gerçek pist geometrisi ve zamansal sürüş profilleriyle bütünleşmiş bir tasarım süreci yürütülmüştür. Bu yönüyle çalışma, benzerlerinden ayrılarak özel yarış pistlerine özgü senaryolara uyarlanabilir motor tasarımı yaklaşımı sunmaktadır. Çalışmanın başlangıç aşamasında, yarış pistine ait hız ve tork gereksinimleri belirlenmiş, sürüş döngüsüne bağlı olarak aracın ihtivac duyduğu performans hesaplanmıştır. kriterleri Araç ivmesi. aerodinamik direnc ve mekanik parametreler dikkate alınarak, sürüş sırasında ortaya çıkan tork talepleri kapsamlı bir şekilde analiz edilmiştir. Elde edilen veriler doğrultusunda, motorun tork ve hız gereksinimlerine uygun olacak şekilde tasarım kriterleri oluşturulmuştur.

Tasarım sürecinde, düşük hızlarda yüksek tork üretebilen ve enerji verimliliğini maksimize edebilecek bir motor topolojisi tercih edilmiştir. Bu kapsamda, dış rotorlu, yüzey montajlı kalıcı mıknatıslı senkron motor yapısının, hafif elektrikli araç uygulamaları için optimum çözüm sunduğu değerlendirilmiştir. Motorun boyutlandırılması ve manyetik tasarımı, belirlenen performans hedefleri doğrultusunda gerçeklestirilmis, akı yoğunluğu, oluk ve kutup yapısı optimize edilmiştir. Son aşamada, tasarlanan motor sonlu elemanlar analizi kullanılarak değerlendirilmiş ve elde edilen sonuçlar, motorun hem elektromanyetik hem de mekanik performans acısından belirlenen gereksinimleri karşıladığını ortaya koymuştur.

Bu çalışma, hafif elektrikli araçlara yönelik motor tasarımında sürüş döngüsü ve araç modeli tabanlı sistematik bir yaklaşım sunmaktadır. Elde edilen sonuçların, özellikle TEKNOFEST "Uluslararası Efficiency Challenge Elektrikli Araç Yarışları" gibi yarışmalara katılım sağlayacak ekipler ve hafif elektrikli araç teknolojileri üzerine çalışan araştırmacılar için yol gösterici olacağı düşünülmektedir.

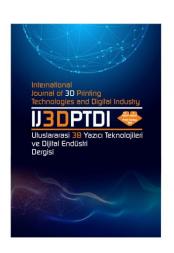
KAYNAKLAR

- 1. Cao, J., Chen, X., Qiu, R., Hou, S., "Electric vehicle industry sustainable development with a stakeholder engagement system", Technology in Society, Vol. 67, Pages 101771, 2021.
- 2. Pielecha, J., Skobiej, K., Kurtyka, K., "Exhaust Emissions and Energy Consumption Analysis of Conventional, Hybrid, and Electric Vehicles in Real Driving Cycles", Energies, Vol. 13, Issue 23, Pages 6423, Dec. 2020.
- 3. Kıyaklı, A. O., Solmaz, H., "Modeling of an Electric Vehicle with MATLAB/Simulink", International Journal of Automotive Science And Technology, Vol. 2, Issue 4, Pages 9-15, Dec. 2018.
- 4. Camargos, Pedro H., Ricardo E. Caetano., "A performance study of a high-torque induction motor designed for light electric vehicles applications.", Electrical Engineering, Vol. 104, Issue 2, Pages 797-805, 2022.

- 5. Polat, A.O, et al., "Light electric vehicle performance with digital twin technology: a comparison of motor types.", Arabian Journal for Science and Engineering, Vol. 49, Issue 5, Pages 7209-7222, 2024.
- 6. Krasopoulos, C. T., Beniakar, M. E., Kladas, A. G., "Multicriteria PM Motor Design Based on ANFIS Evaluation of EV Driving Cycle Efficiency", IEEE Transactions on Transportation Electrification, Vol. 4, Issue 2, Pages 525-535, June 2018.
- 7. Hu, X., Guo, H., Qian, H., Ding, X., Yang, Y., "Development of a high-power-density motor for formula SAE electric race car", IECON 2017 43rd Annual Conference of the IEEE Industrial Electronics Society, Beijing, China, Pages 6618-6622, 2017.
- 8. Targosz, M., Skarka, W., Przystałka, P., "Model-Based Optimization of Velocity Strategy for Lightweight Electric Racing Cars", Journal of Advanced Transportation, Vol. 2018, Article ID 3614025, Pages 20, 2018.
- 9. International Energy Agency (IEA), "Global EV outlook 2020", https://www.iea.org/reports/global-ev-outlook-2020, Februay 10, 2025.
- 10. Ballo, F., Stabile, P., Gobbi, M., Mastinu, G., "A Lightweight Ultra-Efficient Electric Vehicle Multi-Physics Modeling and Driving Strategy Optimization", IEEE Transactions on Vehicular Technology, Vol. 71, Issue 8, Pages 8089-8103, Aug. 2022.
- 11. Pusztai, Z., Kőrös, P., Szauter, F., Friedler, F., "Vehicle Model-Based Driving Strategy Optimization for Lightweight Vehicle", Energies, Vol. 15, Issue 10, Pages 3631, May 2022.
- 12. Bolvashenkov, I., Kammermann, J., Herzog, H.-G., "Methodology for selecting electric traction motors and its application to vehicle propulsion systems", 2016 International Symposium on Power Electronics, Electrical Drives, Automation and Motion (SPEEDAM), Pages 1214-1219, Capri, Italy, 2016.
- 13. Hashemnia, N., Asaei, B., "Comparative study of using different electric motors in the electric vehicles", 2008 18th International Conference on Electrical Machines, Pages 1-5, Vilamoura, Portugal, 2008.
- 14. Hadraoui, H., et al., "A multi-criteria analysis and trends of electric motors for electric vehicles.", World Electric Vehicle Journal, Vol. 13, Issue 4, Pages 65, 2022.

- 15. Yilmaz, M., "Limitations/capabilities of electric machine technologies and modeling approaches for electric motor design and analysis in plug-in electric vehicle applications", Renewable and Sustainable Energy Reviews, Vol. 52, Pages 80-99, 2015.
- 16. Sun, Y., Li, M., Liao, C., "Analysis of wheel hub motor drive application in electric vehicles", MATEC Web of Conferences, Vol. 100, Pages 01004, 2017.
- 17. Kumar, A., Chandekar, A., Deshmukh, P. W., Ugale, R. T., "Development of electric vehicle with permanent magnet synchronous motor and its analysis with drive cycles in MATLAB/Simulink", Materials Today: Proceedings, Vol. 72, Issue 3, Pages 643-651, 2023.
- 18. TEKNOFEST, "Uluslarası Efficiency Challange Elektrikli Araç Yarışları Şartnamesi", https://www.teknofest.org/tr/competitions/competiti on/44, April 1, 2023.
- 19. Vidhya, S. D., Balaji, M., "Modelling, design and control of a light electric vehicle with hybrid energy storage system for Indian driving cycle", Measurement and Control, Vol. 52, Issue 9-10, Pages 1420-1433, 2019.
- 20. Cardoso, J. F., Chillet, C., Gerbaud, L., Belhaj, L. A., "Electrical Machine Design by optimization for E-motor Application: a Drive Cycle Approach", 2020 International Conference on Electrical Machines (ICEM), Pages 2514-2519, Gothenburg, Sweden, 2020.
- 21. Canseven, H. T., Altıntaş, M., Bakbak, A., Ayaz, M., Meşe, E. and Pyrhönen, J., "Maintaining Synchronous Operation of a Damperless Dual-Port Tooth-Coil-Winding PMSG", IEEE Transactions on Industry Applications, Vol. 60, Issue 1, Pages 112-122, 2024.
- 22. Rosu, M., Zhou, P., Lin, D., Popescu, M., Rallabandi, V., Staton, D., Blaabjerg, F., Ionel, D. M., "Multiphysics simulation by design for Electrical Machines, Power Electronics, and drives", IEEE Press, Pages 8-9, 2018.
- 23. Zhu, Z. Q., Jamil, M. L. M., Wu, L. J., "Influence of Slot and Pole Number Combinations on Unbalanced Magnetic Force in PM Machines With Diametrically Asymmetric Windings", IEEE Transactions on Industry Applications, Vol. 49, Issue 1, Pages 19-30, 2013.
- 24. Levent, A., Lordoglu, A., Aydeniz, M., "Design and Optimization of Permanent Magnet Synchronous Motor for Electric Vehicle Applications", GPECOM, Pages 148-151, 2020.

- 25. Choi, G., Jahns, T. M., "Design of electric machines for electric vehicles based on driving schedules", 2013 International Electric Machines & Drives Conference, Chicago, IL, USA, Pages 54-61, 2013.
- 26. Bakbak, A., et al., "PMSG-Based Dual-Port Wind-Energy Conversion System With Reduced Converter Size", IEEE Access, Vol. 9, Pages 118953-118967, 2021.
- 27. Jang, G., Sehwan K., Gilsu C., "Design and Optimization of an Outer-Rotor PMSM for Torque Ripple Minimization.", 2024 27th International Conference on Electrical Machines and Systems (ICEMS). IEEE, 2024.



ULUSLARARASI 3B YAZICI TEKNOLOJİLERİ VE DİJİTAL ENDÜSTRİ DERGİSİ

INTERNATIONAL JOURNAL OF 3D PRINTING TECHNOLOGIES AND DIGITAL INDUSTRY

ISSN:2602-3350 (Online)

URL: https://dergipark.org.tr/ij3dptdi

PERFORMANCE COMPARISON OF VISION-LANGUAGE MODELS IN IMAGE CLASSIFICATION

Yazarlar (Authors): Dogukan Ozeren , Mehmet Erkan Yuksel, Asım Sinan Yuksel

Bu makaleye şu şekilde atıfta bulunabilirsiniz (To cite to this article): Ozeren D., Yuksel M. E., Yuksel A. S., "Performance Comparison of Vision-Language Models In Image Classification" Int. J. of 3D Printing Tech. Dig. Ind., 9(2): 247-262, (2025).

DOI: 10.46519/ij3dptdi.1693015

Araştırma Makale/ Research Article

PERFORMANCE COMPARISON OF VISION-LANGUAGE MODELS IN IMAGE CLASSIFICATION

Dogukan Ozeren^a, Mehmet Erkan Yuksel^a, Asım Sinan Yuksel^b

^aBurdur Mehmet Akif Ersoy University, Engineering and Architecture Faculty, Computer Engineering Department, TÜRKİYE

^bSüleyman Demirel University, Engineering and Natural Sciences Faculty, Computer Engineering Department, TÜRKİYE

* Corresponding Author: erkanyuksel@mehmetakif.edu.tr

(Received: 06.05.25; Revised: 20.06.25; Accepted: 28.06.25)

ABSTRACT

Vision-Language Models (VLMs) have introduced a new paradigm shift in image classification by integrating visual and textual modalities. While these models have demonstrated strong performance on multimodal tasks, their effectiveness in purely visual classification remains underexplored. This study presents a comprehensive, metric-driven comparative analysis of eight state-of-the-art VLMs—GPT-40-latest, GPT-40-mini, Gemini-flash-1.5-8b, LLaMA-3.2-90B-vision-instruct, Grok-2-vision-1212, Qwen2.5-vl-7b-instruct, Claude-3.5-sonnet, and Pixtral-large-2411—across four datasets: CIFAR-10, ImageNet, COCO, and the domain-specific New Plant Diseases dataset. Model performance was evaluated using accuracy, precision, recall, F1-score, and robustness under zero-shot and few-shot settings. Quantitative results indicate that GPT-40-latest consistently achieves the highest performance on typical benchmarks (accuracy: 0.91, F1-score: 0.91 on CIFAR-10), substantially surpassing lightweight models such as Pixtral-large-2411 (accuracy: 0.13, F1-score: 0.13). Near-perfect results on ImageNet and COCO likely reflect pre-training overlap, whereas notable performance degradation on the New Plant Diseases dataset underscores domain adaptation challenges. Our findings emphasize the need for robust, parameter-efficient, and domain-adaptive fine-tuning strategies to advance VLMs in real-world image classification.

Keywords: Vision-Language Models, Image Classification, Multimodal Learning, Zero-Shot Classification, Few-Shot Learning, Model Generalization.

1. INTRODUCTION

The field of computer vision has advanced rapidly, driven by breakthroughs in deep learning, resulting in outstanding achievements in tasks such as object detection, segmentation, and classification. Traditionally, Convolutional Neural Networks (CNNs) have dominated image classification, using hierarchical feature extraction to achieve high accuracy across diverse datasets [1-4]. In recent years, Vision Transformers (ViTs) have emerged, utilizing self-attention mechanism to capture long-range dependencies and enhance robustness to complex visual patterns [5]. These architectures have established new benchmarks on various datasets such as CIFAR-10 [6], ImageNet [7], MNIST [8], CelebA [9], and COCO [10],

solidifying their position as the standard for image classification tasks.

The emergence of VLMs marks a significant paradigm shift by integrating both visual and textual modalities, thereby offering a novel approach to image understanding. Trained on large-scale datasets comprising image-text pairs, these models utilize cross-modal learning to generate enriched semantic representations. Unlike traditional vision-only architectures, VLMs augment visual information with linguistic context, enabling enhanced reasoning in multimodal tasks such as image captioning, visual question answering (VQA), and scene understanding. However, their effectiveness in pure image classification—where explicit

textual context is absent—remains an open research question [11-14].

Despite their potential, VLMs encounter several challenges when applied to image classification tasks. Unlike CNNs and ViTs, which are optimized for extracting discriminative features from visual inputs, VLMs often rely on multimodal embeddings that may not be fully utilized in vision-only tasks. Typically, VLMs exhibit higher computational and memory requirements, resulting in increased inference latency compared to deep learning models, raising concerns about their efficiency for highperformance classification tasks. In addition, their reliance on pretraining corpora comprising image-text pairs poses risks of biases, domain dependencies, and reduced generalization when applied to vision-only tasks. Therefore, rigorous comparative analyses of VLMs and unimodal vision models are crucial to understand their advantages and limitations in image classification.

Traditional image classification models operate exclusively within the visual domain, extracting features from pixel-level data to identify patterns, textures, and object structures. CNNbased architectures, such as VGG [15], Inception [16], ResNet [17], DenseNet [18-20], and EfficientNet [21], have demonstrated remarkable success in large-scale image classification due to their use of local receptive fields, parameter sharing, and deep hierarchical structures. ViTs have further advanced the field by leveraging the self-attention mechanism that allow models to capture long-range dependencies and improve feature learning across entire images, achieving significant performance on diverse benchmark datasets and proving their robustness in various real-world applications [22-33]. In contrast, VLMs use a fundamentally different method by integrating both visual and textual inputs to learn multimodal representations [34-37]. Prominent examples include GPT-4V (OpenAI), Gemini 1.5 (Google DeepMind), LLaVA-Next (Meta), Claude 3 (Anthropic), and Qwen-VL (Alibaba Cloud), all of which have achieved notable success in multimodal tasks such as image captioning, VOA, and cross-modal retrieval. Despite their advantages in semantic reasoning, the application of VLMs to classification tasks that lack explicit textual context remains a critical area of research. Unlike tasks that

require joint vision-language understanding, image classification relies primarily on intrinsic visual characteristics, such as color, shape, texture, and spatial relationships, raising the critical questions about whether VLMs can outperform (or even match) established singlemodality models without fully leveraging their linguistic capabilities. While VLMs present advantages such as zero-shot classification, transfer learning, and improved generalization, they also pose notable challenges. Their reliance on large-scale multimodal pretraining corpora increases the risk of domain biases, limiting their effectiveness in exclusively visual tasks. Additionally, VLMs require substantial computational resources, making them less efficient and scalable compared to traditional CNNs and ViTs for high-throughput image classification scenarios. Consequently, evaluating their performance on standard and domain-specific classification benchmarks is crucial to understanding the feasibility and limitations of VLMs in vision-centric applications.

In this study, we address the following research questions:

- How do VLMs perform in terms of classification accuracy, precision, recall, and F1-score across diverse datasets?
- Can VLMs generalize effectively to visual domains without textual context, or do they exhibit limitations in such settings?
- What computational trade-offs arise when using VLMs for large-scale classification tasks?
- How robust are these models to data variations, including domain shifts and input noise?

To answer these questions, we conduct extensive evaluations on eight state-of-the-art VLMs—GPT-40-latest, GPT-40-mini, Gemini-flash-1.5-8b, LLaMA-3.2-90B-vision-instruct, Grok-2-vision-1212, Qwen2.5-vl-7b-instruct, Claude-3.5-sonnet, and Pixtral-large-2411—across four benchmark datasets: CIFAR-10, ImageNet, COCO, and New Plant Diseases [38] (as a domain-specific dataset). Our comparative analysis focuses on performance metrics such as accuracy, precision, recall, F1-score, robustness, and computational efficiency in zero-shot and few-shot classification settings.

In summary, this study presents a comprehensive and quantitative benchmarking analysis of various VLMs across multiple standard and domain-specific image classification datasets. The key contributions of this research are as follows:

- Comprehensive Benchmarking of VLMs: We systematically evaluate eight state-of-the-art VLMs across four diverse datasets under both zero-shot and few-shot settings. This extensive analysis offers valuable insights into the generalization capabilities of VLMs across domains with varying levels of complexity.
- Novel Analysis of Prompting Strategies: We investigate the impact of zero-shot and few-shot prompting strategies on VLM performance, providing a detailed understanding of how prompt engineering shapes classification outcomes across different contexts.
- Domain-Specific Dataset Evaluation: We use the New Plant Diseases dataset to assess VLM performance on fine-grained, domain-specific classification tasks, addressing an area that remains largely unexplored in the existing literature.

2. RELATED WORK

Traditional Deep Learning Approaches: Over the past decade, image classification has experienced substantial advancement, driven predominantly by advances in deep learning. CNNs have become the cornerstone of modern computer vision, demonstrating remarkable performance in tasks such as object detection, segmentation, and classification. Their strength lies in their capacity to learn hierarchical representations of visual data, effectively capturing both low-level features, such as edges and textures, as well as high-level semantic information [39-41]. However, their inherently unimodal architecture limits their ability to incorporate external information, such as textual cues, thereby constraining their effectiveness in tasks that require contextual reasoning. Successive architectures, including VGG, Inception, ResNet, DenseNet, and EfficientNet consolidated CNNs as dominant method for image classification.

Emergence of Multimodal Models: To overcome the limitations of unimodal models, multimodal learning approaches have gained traction. CLIP introduced contrastive learning

on large-scale image-text datasets, enabling zero-shot generalization [32]. ALIGN further scaled this paradigm, improving robustness and cross-domain transfer ability via vast, noisy data [12]. These models demonstrate the potential of large-scale multimodal pretraining to generalize across diverse vision tasks, including classification, detection, and style transfer, without requiring task-specific supervision [22-37].

The transformative impact of transformer architectures in natural language processing (NLP) has catalyzed their widespread adoption in vision tasks. Pioneering models such as VisualBERT [23], LXMERT [24], and ViLT [30] have substantially advanced unified visuallinguistic modeling by effectively integrating multimodal data, thereby achieving state-ofthe-art performance across a range of multimodal task. However, these models are typically computationally intensive demonstrate limitations in scenarios where textual information is limited or absent, as in traditional image classification tasks.

The introduction of the Vision Transformer (ViT) [28], which encodes images as sequences of fixed-size patches, marked a paradigm shift by enabling the efficient modeling of longrange dependencies within visual data. This approach effectively challenged the longstanding dominance of CNNs in image classification. This transformer-based approach inspired subsequent developments multimodal learning. Models like ViLT, VisualBERT, and LXMERT integrate vision and language employing unified transformer architectures, fusing modalities via crossattention and joint token processing. They achieved competitive results across tasks such as image classification, visual question answering, and image captioning. However, these models pose substantial challenges in terms of scalability and efficiency. Their high number of parameters and reliance on large training corpora require significant computational resources. Methods such as knowledge distillation, pruning, lightweight transformer design, and efficient fine-tuning have been proposed to reduce the computational load and improve model scalability [42-49].

While multimodal models such as CLIP and ALIGN have achieved remarkable performance on a range of benchmark datasets (e.g., ImageNet, COCO), their applicability to specialized domains warrants further examination. In practical scenarios—such as medical diagnosis or agricultural disease detection—visual distinctions are often subtle and may not be represented in generic benchmark datasets. Multimodal models tailored to specific domains, when fine-tuned on specialized data, can surpass the performance of general-purpose models like CLIP. This underscores the critical role of domain adaptation in ensuring robust and accurate outcomes in specialized contexts [50-53]. Another key challenge is model robustness. Although multimodal models exhibit high accuracy under standard testing conditions, they are frequently vulnerable to adversarial perturbations, distributional shifts, and noisy inputs. Such brittleness significantly constrains their suitability for safety-critical applications. To address these challenges, recent research has focused on robust training methodologies that incorporate adversarial data augmentation, uncertainty quantification, and distributionaware loss optimization [54–56].

As VLMs continue to evolve, several promising research directions have emerged that aim to enhance their effectiveness, efficiency, and robustness, particularly in the context of complex multimodal tasks such as image classification. These directions reflect the field's growing demand for models that are not only powerful but also adaptable, scalable, and resilient in real-world deployments.

- Efficiency Optimization: Reducing the resource demands of transformer-based multimodal architectures pose substantial barriers to their practical use, particularly in latency-sensitive or resource-constrained environments. To mitigate these limitations, recent efforts have focused on techniques such as sparse attention, quantization, adapter-based fine-tuning, efficient pretraining, knowledge distillation, and lightweight transformer architecture design.
- Domain Adaptation and Transfer Learning: Pretrained VLMs often struggle with distribution shifts in domain-specific applications. Emerging methods, including

adapter-based modular tuning, prompt-based adaptation, multi-stage domain-specific pretraining, seek to adapt these models to specialized domains like medical imaging, remote sensing, and agriculture, where data is typically limited and imbalanced. Moreover, the integration of auxiliary supervision signals, such as domain ontologies or metadata, can further refine the model's representations to align with the statistical and conceptual structure of the target domain.

-Robustness and Reliability: Despite high accuracy on benchmark datasets, many VLMs remain vulnerable to input noise and adversarial manipulation. Researchers have proposed incorporating adversarial training, uncertainty modeling, and robustness certification frameworks to enhance model stability under real-world conditions.

These directions point toward a future where VLMs are not only accurate, but also efficient. generalizable, and trustworthy—traits necessary for their successful integration into specialized applications. real-world summary, the integration of visual linguistic modalities has demonstrated considerable promise in image classification. While models like CLIP and ALIGN have set benchmarks in zero-shot generalization. challenges related to robustness, efficiency, and domain-specific adaptation remain. Addressing these limitations is critical for realizing the full potential of VLMs in both research and industry.

3. MATERIAL AND METHOD

We outline the experimental design to evaluate the performance of VLMs in image classification. The methodology includes model selection, dataset preparation, preprocessing protocols, prompt strategy (zero-shot and few-shot), and system configuration to ensure fair comparisons across models.

3.1. Model Selection

Eight VLMs were selected based on three criteria: (1) demonstrated performance in existing benchmarks, (2) capability to process multimodal inputs with prompt-based classification, and (3) availability through open-source implementations or public APIs. The analysis encompasses both closed (proprietary)

and open-source models, spanning the spectrum from large-scale semantic reasoners to lightweight, deployable systems. The use of closed models (e.g., GPT-40-latest, Claude 3.5) is acknowledged as a limitation to reproducibility and interpretability, as internal

architectures and processing protocols are not transparent. Table 1 list the models we evaluated. These models represent diverse design philosophies and serve as proxies for evaluating trade-offs between performance, scalability, and computational efficiency.

Table 1. Examined VLMs and their architectural characteristics.

Model Name	Developer	r Architecture Type			
GPT-4o-latest	OpenAI	Transformer architecture with specific enhancements for multimodal capabilities (handling both text and images), autoregressive generation, and potentially Sparse Mixture of Experts for efficiency.			
GPT-40-mini	OpenAI	Fransformer-based autoregressive model designed to be smaller and more computationally efficient than its larger counterpart, GPT-4.			
Gemini-flash-1.5	Google	Transformer-based architecture that integrates multimodal capabilities for both text and image processing.			
LLaMA-3.2-90B- vision-instruct	Meta	Multimodal transformer-based model that combines the LLaMA architecture with advanced vision processing capabilities. It benefits from large-scale pretraining with 90 billion parameters, cross-modal learning, and potential optimizations like sparse attention or Mixture of Experts (MoE).			
Grok-2-vision-1212	xAI	Multimodal VLM based on the transformer architecture.			
Qwen-2-VL-7B-instruct	Alibaba	Transformer-based multimodal model that integrates both text and image inputs.			
Claude-3.5-sonnet	Anthropic	Transformer-based language model focused on creative text generation tasks.			
Pixtral-large-2411 Mistral		Sophisticated transformer-based architecture, combining a large multimodal decoder with a dedicated vision encoder and an extensive context window			

Table 1. Examined VLMs and their architectural characteristics (cont.).

Model Name	Features	Characteristics			
	Multimodal capabilities: Text, image, audio, video.Advanced image captioning and interpretation.	Designed for versatile real-time content generation and			
GPT-4o-latest	- Supports real-time speech interaction and multimedia processing.	interaction across various formats, while reducing hallucinations.			
GPT-4o-mini	 Smaller, more efficient variant of GPT-4. Cost-effective with reduced memory and computation requirements. Excellent for text and image tasks. Efficient vision-text alignment. 	Focuses on reducing computational overhead while maintaining strong performance across NLP and VLM tasks.			
Gemini-flash- 1.5	 Optimized for speed and quality. Integrates advanced multimodal reasoning. Supports large-scale image captioning, processing, and QA tasks. Faster inference, better image-text coherence. 	Designed to increase processing speed and reduce latency, providing a robust solution for VL tasks.			
LLaMA-3.2- 90B-vision- instruct	 90B parameters with a VL instruction-following focus. Utilizes cross-attention layers for effective image processing and captioning. Large-scale model for fine-grained classification. Capable of processing both text and image data, making it suitable for a wide range of vision-language tasks such as image captioning, VQA, and instruction-based visual tasks. 	Highly capable of handling multimodal tasks such as VQA and document processing.			
Grok-2-vision- 1212	High-resolution image processing.Designed for daptive image classification and fine-grained visual	Focuses on vision-based processing, particularly suited for large and complex visual datasets.			
Qwen-2-VL-7B-instruct	 Specialized in multimodal tasks involving images and text. Capable of resolving dynamic image resolutions. Optimized for instruction-following in multimodal tasks. Low-computation multimodal learning. 	Features dynamic resolution processing to enable scalable VLM deployment.			

Claude-3.5-	- Fast and affordable version of Claude.	Aims for high safety levels and			
	- Uses dynamic token generation and advanced contextualization for	reduced hallucinations, designed			
	multimodal content.	for robust and safe			
sonnet	- Safety-focused and interpretable.	conversational AI.			
	- Strong context-aware reasoning in vision.				
	- High-performing model designed for visual reasoning tasks.	Specializes in integrating visual			
Pixtral-large-	- Optimized for image captioning and visual content understanding.	understanding with text-based			
2411	- Large-scale image processing.	queries, enhancing interactive			
	- Specializes in high-resolution image classification.	visual tasks.			

3.2. Dataset Preparation

To conduct a comprehensive evaluation of VLMs across different visual recognition scenarios, we utilized four publicly available datasets: CIFAR-10, ImageNet, COCO, and New Plant Diseases dataset. These datasets were selected based on their diversity in image resolution, domain complexity, multimodal richness, and relevance to both general-purpose

and domain-specific classification tasks. By employing these datasets under zero-shot and few-shot configurations, we were able to systematically investigate how VLMs leverage pretrained multimodal knowledge to perform classification in both standard and specialized domains without extensive retraining. Table 2 provides a summary of the datasets we used.

Table 2. Benchmark datasets.

Dataset	Domain	Number of Classes	Number of Samples	Characteristics
CIFAR-10	General object recognition	10	60K	Low-resolution, simple images, basic objects
ImageNet	Large-scale object classification	1000	1.2M	High-resolution, complex real-world images
COCO	Multimodal scene understanding	80	124K	Complex scenes, multiple objects per image, caption annotations
New Plant Diseases	Agricultural disease classifciation	38	55K	Fine-grained domain-specific classification, subtle visual differences

The selection of these datasets was carefully made to cover different aspects of classification and multimodal reasoning:

- -CIFAR-10: It is a low-resolution dataset used for benchmarking and rapid prototyping. It enables evaluation of performance on low-resolution, small-sized images, providing insights into the robustness of VLMs under constrained visual input conditions.
- ImageNet: It is a large-scale database of annotated images used for image classification, object detection, and object localization. It is the de facto standard for large-scale object recognition and offers a benchmark for evaluating VLMs' generalization ability on high-resolution natural images.
- COCO: It is a large-scale image recognition dataset for object detection, segmentation, and captioning tasks. It introduces

multimodal complexity through images with multiple objects and rich textual descriptions, allowing us to assess VLMs' capacity for reasoning in complex visual scenes.

- New Plant Diseases: It is a domain-specific agricultural dataset designed to address the challenges fine-grained of classification. It focuses on distinguishing subtle visual differences between healthy and diseased plant specimens, presenting a rigorous test of the domain adaptation capabilities of VLMs. By requiring models to detect nuanced patterns across closely related classes, this dataset serves as a valuable benchmark for evaluating the robustness and generalization performance of VLMs in specialized, real-world scenarios beyond traditional image classification domains.

This diverse selection enables an extensive analysis of VLMs across different visual domains and levels of task difficulty, ensuring that both generalist and specialist scenarios are rigorously evaluated.

3.3. Preprocessing

To ensure methodological consistency and preserve the integrity of performance comparisons across models, we adopt a model-specific preprocessing strategy tailored to the architectural and training specifications of each model under evaluation. The selected models represent a diverse range of architectures and visual tokenization mechanisms. Therefore, standardized preprocessing is neither feasible nor methodologically sound.

- Image Format and Quality Control: All images are first converted to high-quality RGB format (PNG or high-resolution JPEG) to maintain fidelity. The sRGB color space is enforced across the dataset to ensure consistency with the visual encoders' training environments.
- Normalization: For closed-source models (GPT-40, Gemini, Claude, Grok), normalization was handled internally by the API or runtime environment. No external pixel scaling or transformation is applied. For open-source models (LLaMA-3.2, Qwen2.5-vl, Pixtral), normalization was applied using model-specific routines.
- Prompt Engineering: Prompt design plays a critical role in determining **VLM** performance. particularly in few-shot settings. For zero-shot classification, prompts consisted of simple class lists or concise descriptions. In few-shot scenarios, the prompts incorporated either 5 or 10 classlabeled exemplars following a consistent template. Although contrastive learning is frequently cited as the foundation for prompt design in CLIP-like settings, in this study's few-shot configuration, we enhanced incontext prompting by providing explicit class examples without introducing additional contrastive objectives beyond those inherent to the original models. All text prompts were tokenized using each model's native tokenizer. For open-source models, we official implementations employed the available through Hugging Face or GitHub repositories. For proprietary models, prompts were formatted as plain text and submitted alongside the corresponding image via the respective API. Prompt templates were rigorously standardized across models to ensure consistent semantic intent in both fewshot and zero-shot evaluations.

-Inference Protocols: For open-source models, inference was performed using either default configurations or recommended settings specified in the official repositories (e.g., greedy decoding). For closed, API-based models, default parameter values (e.g., temperature and topwere adopted unless the official documentation explicitly required alternative specifications. It is important to acknowledge that, due to proprietary restrictions, access to or modification of the full set of inference parameters was not always possible for these closed APIs. Runtime latency was monitored in a qualitative manner. The practical aspects of all inference protocols were evaluated to the extent permitted by the transparency limitations of each API.

3.4. Experimental Setup

Input-Output Structure and Classification Flow: For all datasets, each VLM takes as input

Flow: For all datasets, each VLM takes as input an image accompanied by a text prompt designed to guide the model in performing the classification task. The output generated by the model is a predicted class label, selected from the set of true class labels corresponding to the respective dataset (CIFAR-10, COCO, ImageNet, or New Plant Diseases). The true class labels serve as the ground truth for the evaluation. Fig. 1 provides an overview of the general processing pipeline employed in the classification experiments. The predicted label is compared against the ground truth to evaluate performance metrics.

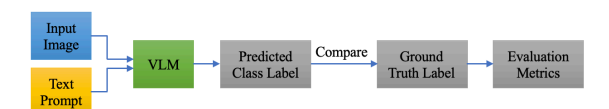


Figure 1. General classification pipeline for VLMs.

Fig. 2 illustrates the input-output structure of two prompting strategies applied in image classification tasks. In zero-shot prompting (left), the model receives an input image and a prompt specifying a set of categories, returning a predicted class in JSON format. In few-shot prompting (right), the prompt additionally includes category descriptions and example pairs to guide the model's prediction. Both strategies produce outputs in a consistent structured format, enabling direct comparison of performance across different prompting conditions.

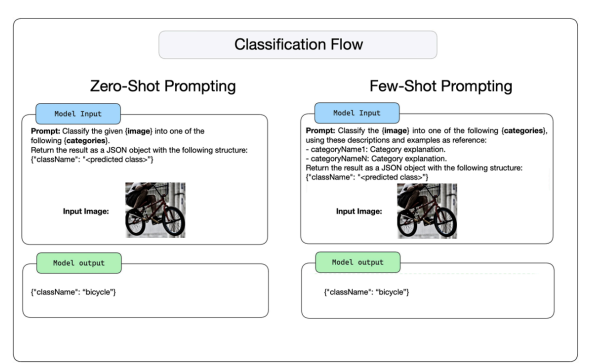


Figure 2. Classification flow for zero-shot and few-shot prompting in VLM.

To evaluate the classification capabilities of VLMs, we designed two experimental scenarios: zero-shot classification and few-shot classification.

Zero-Shot Classification: Models perform classification without access to any task-specific labeled examples. They leverage their pretrained visual and linguistic representations to infer class labels based on textual prompts. Each model receives a set of descriptive prompts corresponding to candidate classes and selects the most semantically relevant label based on its internal reasoning. Fig. 3 shows a zero-shot prompt template.

Figure 3. Zero-shot prompt template.

Few-Shot Classification: To evaluate the models' adaptability to low-resource settings, we used labeled exemplars. Fig. 4 shows a few-shot prompt template.

- •5-shot: Each class is represented by five labeled examples.
- ■10-shot: Each class is represented by ten labeled examples.

Figure 4. Few-shot prompt template.

These exemplars are incorporated into the input prompt in a structured in-context learning format. When supported by the model, contrastive learning techniques are employed to enhance inter-class discrimination. This setup is designed to evaluate each model's capacity to generalize from limited supervision, thereby simulating real-world scenarios in which labeled data is scarce or expensive to obtain.

3.5. Hardware Configuration

Experiments were conducted on a highperformance computing platform equipped with 64 GB of RAM, a 1 TB SSD, a 16-core CPU, a 40-core GPU, and a 16-core Neural Engine. The software environment comprised PyTorch 2.1, TensorFlow 2.10, and the Hugging Face Transformers library, ensuring full compatibility with open-source model architectures. Proprietary models were accessed through their respective public APIs.

3.6. Evaluation Metrics

Model performance was evaluated using standard classification metrics:

- Accuracy: Proportion of correctly classified images.
- Precision: Proportion of true positives among predicted positives.
- Recall: Proportion of true positives among actual positives.
- -F1 score: Harmonic mean of precision and recall, providing a balanced metric under class imbalance.

These metrics were calculated for each modeldataset pair and macro-averaged across all classes for comparative evaluation.

4. FINDINGS

We present a comparative analysis of eight state-of-the-art VLMs for image classification: Qwen2.5-vl-7b-instruct, Gemini-flash-1.5-8b, Grok-2-vision-1212, Pixtral-large-2411, GPT-4o-latest, GPT-4o-mini, Claude-3.5-sonnet, and LLaMA-3.2-90B-vision-instruct. These models were evaluated on four benchmark datasets—CIFAR-10, ImageNet, COCO, and New Plant Diseases— under both zero-shot and few-shot settings. Performance was assessed based on accuracy, precision, recall, and F1 score. Quantitative results are shown in Tables 3-6.

Results on CIFAR-10 Dataset: Table 3 reveals substantial variability in performance across the

evaluated models. GPT-40-latest achieved the highest scores, with an accuracy and F1-score of 0.91, followed closely by GPT-4o-mini, which attained an F1-score of 0.89. Geminiand flash-1.5-8b LLaMA-3.2-90B-visioninstruct also demonstrated competitive results, with F1-scores of 0.80 and 0.78, respectively. In contrast, Pixtral-large-2411 exhibited markedly poor performance, with both accuracy and F1score at 0.13. These results indicate that while large-scale VLMs effectively exploit advanced semantic reasoning capabilities, lightweight models may compromise classification performance in favor of computational efficiency.

Table 3. Results on CIFAR-10.

	Accuracy		Precision		Recall		F1 Score	
Model	Zero-	Few-	Zero-	Few-	Zero-	Few-	Zero-	Few-
	shot	shot	shot	shot	shot	shot	shot	shot
Qwen2.5-vl-7b-instruct	0.76	0.66	0.82	0.84	0.76	0.66	0.79	0.74
Gemini-flash-1.5-8b	0.70	0.77	0.87	0.83	0.70	0.77	0.78	0.80
Grok-2-vision-1212	0.65	0.68	0.73	0.74	0.65	0.68	0.69	0.71
Pixtral-large-2411	0.11	0.13	0.17	0.13	0.11	0.13	0.13	0.13
Claude-3.5-sonet	0.57	0.56	0.63	0.59	0.57	0.56	0.60	0.58
GPT-4o-latest	0.92	0.91	0.92	0.91	0.92	0.91	0.92	0.91
GPT-4o-mini	0.90	0.87	0.91	0.90	0.90	0.87	0.90	0.89
LLaMA-3.2-90B-vision-instruct	0.75	0.75	0.81	0.81	0.75	0.75	0.78	0.78

Results on ImageNet Dataset: Table 4 shows that most models achieved near-perfect performance, with accuracies and F1-scores of 0.99 or 1.00. An exception was LLaMA-3.2-90B-vision-instruct, which exhibited substantially lower performance, with an accuracy of 0.57 and an F1-score of 0.64. The

consistently high scores across models suggest significant overlap between the ImageNet dataset and the models' pretraining corpora, which may artificially inflate their measured capabilities on this benchmark. These findings highlight the need for caution when interpreting such results as evidence of true generalization.

 Table 4. Results on ImageNet.

	Accuracy		Precision		Recall		F1 Score	
Model	Zero-	Few-	Zero-	Few-	Zero-	Few-	Zero-	Few-
	shot	shot	shot	shot	shot	shot	shot	shot
Qwen2.5-vl-7b-instruct	0.99	0.98	0.99	0.99	0.99	0.98	0.99	0.99
Gemini-flash-1.5-8b	1.00	1.00	1.00	1.00	1.00	1.00	1.00	1.00
Grok-2-vision-1212	1.00	1.00	1.00	1.00	1.00	1.00	1.00	1.00
Pixtral-large-2411	0.98	0.99	0.99	0.99	0.98	0.99	0.98	0.99
Claude-3.5-sonet	0.99	0.99	0.99	0.99	0.99	0.99	0.99	0.99
GPT-4o-latest	1.00	1.00	1.00	1.00	1.00	1.00	1.00	1.00
GPT-4o-mini	1.00	1.00	1.00	1.00	1.00	1.00	1.00	1.00
LLaMA-3.2-90B-vision-instruct	0.98	0.57	0.98	0.71	0.98	0.57	0.98	0.64

Results on COCO Dataset: As seen in Table 5, all models achieved near-perfect classification performance (F1-scores≈1.00). It is important to note, however, that COCO, primarily an object detection and captioning

dataset, was adapted for classification by assigning a dominant label to each image. This methodological simplification likely reduced task complexity, which may explain the models' uniformly high scores.

Table 5. Results on COCO.

	Accuracy		Precision		Recall		F1 Score	
Model	Zero	Few-	Zero-	Few-	Zero-	Few-	Zero-	Few-
	-shot	shot	shot	shot	shot	shot	shot	shot
Qwen2.5-vl-7b-instruct	1.00	0.99	1.00	1.00	1.00	0.99	1.00	1.00
Gemini-flash-1.5-8b	1.00	1.00	1.00	1.00	1.00	1.00	1.00	1.00
Grok-2-vision-1212	0.99	1.00	0.99	1.00	0.99	1.00	0.99	1.00
Pixtral-large-2411	1.00	1.00	1.00	1.00	1.00	1.00	1.00	1.00
Claude-3.5-sonet	1.00	1.00	1.00	1.00	1.00	1.00	1.00	1.00
GPT-4o-latest	1.00	1.00	1.00	1.00	1.00	1.00	1.00	1.00
GPT-4o-mini	0.99	1.00	0.99	1.00	0.99	1.00	0.99	1.00
LLaMA-3.2-90B-vision-instruct	0.97	1.00	0.98	1.00	0.97	1.00	0.97	1.00

Results on New Plant Diseases Dataset: Table 6 reveals considerable performance degradation on the domain-specific New Plant Diseases dataset. GPT-40-latest again demonstrated the strongest performance (accuracy: 0.64, F1-score: 0.66). In contrast, Qwen2.5-vl-7B-instruct and Pixtral-large-2411 performed poorly, with F1-scores of 0.20 and 0.29, respectively. Several models, such as Gemini-

flash-1.5-8b and LLaMA-3.2-90B-vision-instruct, exhibited high precision but markedly low recall, indicating a conservative classification bias that favors precision at the cost of missing positive cases. This behavior is particularly concerning in high-stakes domains such as agriculture and healthcare.

Table 6. Results on New Plant Diseases.

	Accu	Accuracy		Precision		Recall		F1 Score	
Model	Zero-	Few-	Zero-	Few-	Zero-	Few-	Zero-	Few-	
	shot	shot	shot	shot	shot	shot	shot	shot	
Qwen2.5-vl-7b-instruct	0.28	0.20	0.39	0.20	0.28	0.20	0.33	0.20	
Gemini-flash-1.5-8b	0.57	0.50	0.61	0.64	0.57	0.50	0.59	0.57	
Grok-2-vision-1212	0.49	0.49	0.61	0.54	0.49	0.49	0.54	0.52	
Pixtral-large-2411	0.39	0.26	0.40	0.31	0.39	0.26	0.39	0.29	
Claude-3.5-sonet	0.46	0.46	0.50	0.47	0.46	0.46	0.48	0.47	
GPT-4o-latest	0.62	0.64	0.66	0.68	0.62	0.64	0.64	0.66	
GPT-4o-mini	0.49	0.46	0.52	0.55	0.49	0.46	0.50	0.50	
LLaMA-3.2-90B-vision-instruct	0.24	0.45	0.42	0.64	0.24	0.45	0.30	0.53	

4.1. Key Observations

Model Scale vs. Efficiency: Large-scale models (e.g., GPT-4o-latest) demonstrated superior performance across general and specialized datasets but incurred significant computational costs. Lightweight models (e.g., GPT-4o-mini, Qwen2.5-vl-7b-instruct) offered a more favorable balance between efficiency and moderate classification accuracy.

- Dataset Bias: The exceptionally high scores on ImageNet and COCO indicate possible overlaps with pretraining datasets, warranting further evaluations on out-of-distribution (OOD) benchmarks.
- Domain Adaptation Challenges: The substantial performance drop on New Plant Diseases dataset underscores the importance of domain adaptation (and the potential of

prompt engineering or fine-tuning), especially in specialized domains where fine-grained visual details are critical.

- Precision-Recall Imbalance: Models like LLaMA-3.2-90B-vision-instruct exhibited high precision but poor recall on domain-specific datasets, an imbalance that could lead to critical misclassifications in sensitive applications.
- Overall Best Performer: GPT-40-latest consistently achieved the highest or near-highest scores across all datasets and settings, demonstrating superior visual-text alignment, generalization, and robustness, especially in zero-shot and few-shot settings. This reinforces the effectiveness of large-scale multimodal training in zero-shot and few-shot settings.

5. DISCUSSION

We provided a comprehensive analysis of the observed results, discussing the strengths and limitations of each model across four critical dimensions: classification performance, generalization capability, computational efficiency, and robustness to data variations.

- Classification Performance: Large-scale VLMs such as GPT-4o-latest, LLaMA-3.2-90B-vision-instruct, and Claude-3.5-sonnet consistently exhibited strong classification performance, particularly under zero-shot settings. Their robust semantic alignment between visual inputs and textual prompts contributed significantly to high accuracy and F1-scores. GPT-40-latest, in particular, demonstrated exceptional adaptability across both general-purpose (CIFAR-10, ImageNet) and domain-specific (New Plant Diseases) datasets, outperforming other models in most settings. This highlights the advantage of large-scale, multimodal pretraining for crossdomain image classification Conversely, models such as Pixtral-large-2411 consistently underperformed across benchmarks. Despite architectural strengths for high-resolution visual reasoning, its poor results in standard classification tasks suggest that architectural specialization alone does not guarantee competitive generalpurpose performance. In few-shot settings (5shot and 10-shot), most models demonstrated performance improvements, suggesting that even a limited number of labeled examples can significantly enhance the classification abilities of VLMs. Nonetheless, lightweight models like GPT-4o-mini and Owen2.5-vl-7b-instruct maintained a trade-off between moderate classification accuracy operational efficiency.
- -Generalization Across Domains: While nearly all models achieved near-perfect scores on ImageNet and COCO, these results interpreted cautiously. must be likelihood of pretraining data overlap introduces a confounding factor that limits the interpretation of these scores as indicators of true generalization. In contrast, the performance on the New Plant Diseases dataset revealed critical weaknesses. Several models-including Grok-2-vision-1212 and Claude-3.5-sonnet—exhibited performance drops, highlighting limited

generalization when faced with specialized domains characterized by fine-grained visual distinctions and domain-specific patterns. GPT-40-latest demonstrated the highest cross-domain robustness, maintaining relatively strong performance even under domain shifts. This suggests that extensive multimodal pretraining with diverse datasets can, to some extent, confer improved transferability. However, even the bestperforming models displayed vulnerabilities, emphasizing the ongoing need for taskspecific calibration, domain-adaptive finetuning, and improved prompt design strategies to ensure reliable performance across varied real-world applications.

- Computational Efficiency and Scalability: A clear trade-off emerged between model scale and computational efficiency. Large models like GPT-40-latest and LLaMA-3.2-90B-vision-instruct, while achieving superior performance, impose significant computational burdens, potentially limiting their deployment in resource-constrained environments. In contrast, lightweight models such as GPT-4o-mini and Qwen2.5vl-7b-instruct offered lower computational costs with only a moderate reduction in classification performance. These models represent practical alternatives applications requiring real-time inference or deployment on edge devices. The findings reinforce the importance of model compression, parameter-efficient tuning, and adaptive architectures in future research to balance accuracy with scalability and

- Robustness to Data Variations: Robustness testing indicated that models with extensive multimodal pretraining—particularly GPT-40-latest—demonstrated greater stability under noisy or perturbed inputs. These models maintained consistent performance across minor adversarial attacks distributional shifts. However, several lightweight and specialized models (e.g., Pixtral-large-2411, Grok-2-vision-1212) higher sensitivity exhibited such variations, leading to degraded performance. The observed precision-recall imbalances, particularly on the New Plant Diseases dataset, further highlight the fragility of some domain-specific models under

resource demands.

imbalanced class distributions. High precision coupled with low recall indicates conservative decision thresholds, which, while minimizing false positives, increase the of critical misclassifications—an unacceptable trade-off high-risk applications like healthcare diagnostics or agricultural monitoring. Robustness. therefore, remains a critical research frontier. Future work should incorporate adversarial training, uncertainty modeling, and formal robustness certification into the VLM development pipeline.

5.1. Implications for Future Research

The findings of this study point to several key directions for advancing VLM-based image classification:

- Enhanced Multimodal Architectures: Future models must better balance visual and textual processing, ensuring that unimodal tasks like image classification are not disadvantaged by excessive reliance on language inputs.
- Parameter-Efficient Fine-Tuning: Methods such as Low-Rank Adaptation (LoRA), prompt tuning, and adapter modules offer promising avenues for adapting large VLMs to domain-specific tasks without prohibitive computational overheads.
- Robustness Optimization: Addressing sensitivity to distributional shifts, adversarial perturbations, and input noise is paramount. Techniques such as distributionally robust optimization and adversarial data augmentation should be incorporated into training regimes.
- Domain Adaptation Strategies: Tailoring VLMs for specialized domains will require sophisticated fine-tuning techniques that minimize catastrophic forgetting while enhancing domain-specific feature extraction.

Collectively, these research directions aim to build VLMs that are not only accurate and generalizable but also efficient, scalable, and resilient, thereby unlocking their full potential for real-world deployment.

6. CONCLUSION

This study presents a comprehensive comparative evaluation of eight state-of-the-art VLMs across diverse image classification benchmarks and data regimes (zero-shot, few-shot). The findings reveal that significant trade-

offs exist between accuracy, cross-domain generalization, and computational efficiency. Large-scale **VLMs** demonstrate performance, underscoring the benefits of large-scale multimodal pretraining for robust semantic understanding and cross-domain adaptability. However, reliability concerns remain due to inconsistencies on specialized datasets and susceptibility to distribution shifts. Near-perfect results on datasets like ImageNet and COCO raise concerns about overlap with pretraining corpora, emphasizing the need for rigorous out-of-distribution (OOD) evaluations to accurately assess model generalization. Performance gaps on domain-specific datasets (e.g., New Plant Diseases) further exposed limitations in domain adaptability, while precision-recall imbalances in several models highlighted reliability concerns for critical applications.

On the other hand, Lightweight VLMs offer improved efficiency but lagged in accuracy and robustness, reinforcing the persistent trade-off and scale between model operational practicality. Notably, **VLMs** could not consistently outperform unimodal vision models, suggesting that multimodal integration alone is insufficient for all classification tasks. To bridge the gaps we identified in our experiments, future research should focus on enhancing robustness to distributional shift via adversarial training and uncertainty modeling, employing advanced domain adaptation and parameter-efficient strategies, fine-tuning improving computational scalability, and explicitly evaluating models on benchmarks for realistic deployment scenarios. Transparent reporting and open protocols are crucial for reproducibility, particularly given the limitations of closed-source models. These directions are critical for the evolution of VLMs into reliable, efficient, and generalizable systems suitable for real-world deployment across diverse domains.

ACKNOWLEDGEMENTS

This research was supported by The Scientific and Technological Research Council of Türkiye (TÜBİTAK) through the 1005-National New Ideas and Products Research Support Program (Project No: 124E769). The study was conducted within the framework of this project, aligned with its technological scope and objectives. This work is based on the Master's

thesis titled "Performance Comparison of Vision-Language Models in Image Classification" completed at the Department of Computer Engineering, Institute of Science and Technology, Burdur Mehmet Akif Ersoy University, Türkiye.

FINANCIAL DISCLOSURE

The authors report no financial support for the research, authorship or publication of this study.

CONFLICT OF INTEREST

The authors declare no conflict of interest.

ETHICS STATEMENT

No ethical approval was required for this study.

REFERENCES

- 1. LeCun, Y., Bengio, Y., and Hinton, G. "Deep learning", Nature, Vol. 521, Issue 7553, Pages 436-444, 2015.
- 2. Yao, G., Lei, T., and Zhong, J. "A review of convolutional-neural-network-based action recognition", Pattern Recognition Letters, Vol. 118, Pages 14-22, 2019.
- 3. Goodfellow, I., Pouget-Abadie, J., Mirza, M., Xu, B., Warde-Farley, D., Ozair, S., ... and Bengio, Y. "Generative adversarial networks", Communications of the ACM, Vol. 63, Issue 11, Pages 139-144, 2020.
- 4. Alzubaidi, L., Zhang, J., Humaidi, A.J., Al-Dujaili, A., Duan, Y., ... and Farhan, L. "Review of deep learning: concepts, CNN architectures, challenges, applications, future directions", Journal of Big Data, Vol. 8, Issue 53, 2021.
- 5. Vaswani, A., Shazeer, N., Parmar, N., Uszkoreit, J., Jones, L., Gomez, A. N., ... and Polosukhin, I. "Attention is all you need", arXiv preprint arXiv: 1706.03762v7.
- 6. Krizhevsky, A., and Hinton, G. "Learning multiple layers of features from tiny images", https://www.cs.toronto.edu/~kriz/cifar.html, 2009.
- 7. Deng, J., Dong, W., Socher, R., Li, L. J., Li, K., and Fei-Fei, L. "Imagenet: A large-scale hierarchical image database", IEEE Conference on Computer Vision and Pattern Recognition, 248-255, 2009.

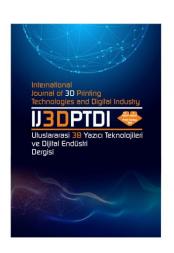
- 8. LeCun, Y., Bottou, L., Bengio, Y. and Haffner, P. "Gradient-based learning applied to document recognition", Proceedings of the IEEE, Vol. 86, Issue 11, Pages 2278-2324, 1998.
- 9. Liu, Z., Luo, P., Wang, X., and Tang, X. "Deep learning face attributes in the wild," IEEE International Conference on Computer Vision, Pages 3730-3738, 2015.
- 10. Lin, T. Y., Maire, M., Belongie, S., Hays, J., Perona, P., Ramanan, D., ... and Dollar, P. "Microsoft COCO: Common objects in context", arXiv preprint arXiv: 1405.0312v3, 2014.
- 11. Radford, A., Kim, J. W., Hallacy, C., Ramesh, A., ... and Sutskever, I. "Learning transferable visual models from natural language supervision", arXiv preprint arXiv: 2103.00020, 2021.
- 12. Jia, C., Yang, Y., Xia, Y., Chen, Y. T., Parekh, Z., Pham, H., ... and Duerig, T. "Scaling up visual and vision-language representation learning with noisy text supervision", arXiv preprint arXiv: 2102.05918v2, 2021.
- 13. Lai, Z., Saveris, V., Chen, C., Chen, H. Y., Zhang, H., ... and Yang Y. "Revisit large-scale image-caption data in pre-training multimodal foundation models", arXiv preprint arXiv: 2410.02740v1, 2024.
- 14. Alayrac, J. B., Donahue, J., Luc, P., Miech, A., Barr, I., Hasson, Y., ... and Simonyan, K. "Flamingo: A visual language model for fewshot learning", arXiv preprint arXiv: 2204.14198v2, 2022.
- 15. Simonyan, K. and Zisserman, A. "Very deep convolutional networks for large-scale image recognition", arXiv preprint arXiv: 1409.1556v6, 2015.
- 16. Szegedy, C., Liu, W., Jia, Y., Sermanet, P., Reed, S., Anguelov, D., ... and Rabinovich, A. "Going deeper with convolutions", arXiv preprint arXiv: 1409.4842v1 2015.
- 17. He, K., Zhang, X., Ren, S., and Sun, J. "Deep residual learning for image recognition", arXiv preprint arXiv: 1512.03385v1, 2016.

- 18. Huang, G., Liu, Z., Van Der Maaten, L., and Weinberger, K. Q. "Densely connected convolutional networks", arXiv preprint arXiv: 1608.06993v5, 2017.
- 19. Wang, Z., Lu, Y., Li, W., Wang, S., Wang, X., and Chen, X. "Single image superresolution with attention-based densely connected modüle", Neurocomputing, Vol. 453, Pages, 876-884, 2021.
- 20. Yildiz, E., Yuksel, M. E., and Sevgen, S. "A single-image GAN model using self-attention mechanism and DenseNets", Neurocomputing, Vol. 596, Issue, 127873, 2024.
- 21. Tan, M. and Le, Q. V. "EfficientNet: Rethinking model scaling for convolutional neural networks", arXiv preprint arXiv: 1905.11946v5, 2019.
- 22. Lu, J., Batra, D., Parikh, D., and Lee, S. "ViLBERT: Pretraining task-agnostic visiolinguistic representations for vision-and-language tasks", arXiv preprint arXiv: 1908.02265v1, 2019.
- 23. Li, L. H., Yatskar, M., Yin, D., Hsieh, C. J., and Chang, K. W. "VisualBERT: A simple and performant baseline for vision and language", arXiv preprint arXiv: 1908.03557v1, 2019
- 24. Tan, H. and Bansal, M. "LXMERT: Learning cross-modality encoder representations from transformers", arXiv preprint arXiv: 1908.07490v3, 2019.
- 25. Chen, Y. C., Li, L., Yu, L., Kholy, A. E., Ahmed, F., and Liu, J. "UNITER: Universal image-text representation learning", arXiv preprint arXiv: 1909.11740v3, 2020.
- 26. Li, X., Yin, X., Li, C., Zhang, P., Hu, X., ... and Gao, J. "Oscar: Object-semantics aligned pre-training for vision-language tasks", arXiv preprint arXiv: 2004.06165v5, 2020.
- 27. Li, J., Selvaraju, R. R., Gotmare, A. D., ... and Hoi, S. "Align before fuse: Vision and language representation learning with momentum distillation", arXiv preprint arXiv: 2107.07651v2, 2021.

- 28. Dosovitskiy, A., Beyer, L., Kolesnikov, A., Weissenborn, D., Zhai, X., Unterthiner, T., ... and Houlsby, N. "An image is worth 16x16 words: Transformers for image recognition at scale", arXiv preprint arXiv: 2010.11929v2, 2021.
- 29. Liu, Z., Lin, Y., Cao, Y., Hu, H., Wei, Y., ... and Guo, B. "Swin Transformer: Hierarchical vision transformer using shifted windows", arXiv preprint arXiv: 2103.14030v2, 2021.
- 30. Kim, W., Son, B., and Kim, I. "ViLT: Vision-and-Language Transformer without Convolution or Region Supervision", arXiv preprint arXiv: 2102.03334v2, 2021.
- 31. Touvron, H., Cord, M., Douze, M., Massa, F., Sablayrolles, A., and Jégou, H. "Training data-efficient image transformers & distillation through attention", arXiv preprint arXiv: 2012.12877v2, 2021.
- 32. Shen, S., Li, L. H., Tan, H., Bansal, M., Rohrbach, A., ..., and Keutzer, K., "How much can CLIP benefit vision-and-language tasks?", arXiv preprint arXiv: 2107.06383, 2021.
- 33. Li, J., Li, D., Xie, S., and Li, F. F. "BLIP: Bootstrapping language-image pre-training for unified vision-language understanding and generation", arXiv preprint arXiv: 2201.12086v2, 2022.
- 34. Caffagni, D., Cocchi, F., Barsellotti, L., Moratelli, N., Sarto, S., ... and Cucchiara, R. "The revolution of multimodal large language models: a survey", arXiv preprint arXiv: 2402.12451v2, 2024.
- 35. Fu, C., Chen, P., Shen, Y., Qin, Y., Zhang, M., ... and Ji, R. "MME: A comprehensive evaluation benchmark for multimodal large language models", arXiv preprint arXiv: 2306.13394v4, 2024.
- 36. Gong, T., Lyu, C., Zhang, S., Wang, Y., Zheng, M., ... and Chen, K. "MultiModal-GPT: A vision and language model for dialogue with humans", arXiv preprint arXiv: 2305.04790v3, 2023.

- 37. Bai, J., Bai, S., Yang, S., Wang, S., Tan, S., ... and Zhou, J. "Qwen-VL: A versatile vision-language model for understanding, localization, text reading, and beyond." arXiv preprint arXiv: 2308.12966v3, 2023.
- 38. Mohanty, S. P., Hughes, D. P., and Salathé, M. "Using deep learning for image-based plant disease detection", Frontiers In Plant Science, Vol. 7, Issue 215232, 2016.
- 39. Dosovitskiy, A. and Brox, T., "Discriminative unsupervised feature learning with exemplar convolutional neural networks", arXiv preprint arXiv: 1406.6909v2, 2015.
- 40. Chollet, F. "Xception: Deep Learning with Depthwise Separable Convolutions", arXiv preprint arXiv: 1610.02357v3, 2017.
- 41. Zeiler, M. D. and Fergus, R. "Visualizing and understanding convolutional networks", arXiv preprint arXiv: 1311.2901v3, 2014.
- 42. Chen, F., Zhang, D., Han, M., Chen, X., ... and Xu, B. "VLP: A survey on vision-language pre-training", arXiv preprint arXiv: 2202.09061v4, 2022.
- 43. Long, S., Cao, F., Han, S. C., and Yang, H. "Vision-and-language pretrained models: A survey", arXiv preprint arXiv: 2204.07356v5, 2022.
- 44. Gao, P., Geng, S., Zhang, R., Ma, T., ... and Qiao, Y. "CLIP-adapter: Better vision-language models with feature adapters", arXiv preprint arXiv: 2110.04544v2, 2025.
- 45. Gou, J., Yu, B., Maybank, S. J., and Tao, D. "Knowledge distillation: A survey", International Journal of Computer Vision, vol. 129, Pages. 1789-1819, 2021.
- 46. Sanh, V., Debut, L., Chaumond, J., and Wolf, T. "DistilBERT, a distilled version of BERT: smaller, faster, cheaper and lighter", arXiv preprint arXiv: 1910.01108v4, 2020.

- 47. Sanh, V., Wolf, T., and Ruder, S. "Movement pruning: Adaptive sparsity by finetuning", arXiv preprint arXiv: 2005.07683v2, 2020.
- 48. Zhou, K., Yang, J., Loy, C. C., and Liu, Z. "Conditional prompt learning for vision-language models", arXiv preprint arXiv: 2203.05557v2, 2022.
- 49. Yu, J., Wang, Z., Vasudevan, V., Yeung, L., ... and Wu, Y. "CoCa: Contrastive captioners are image-text foundation models", arXiv preprint arXiv: 2205.01917v2, 2022.
- 50. Liu, M., Li, B., and Yu, Y. "Fully fine-tuned CLIP models are efficient few-shot learners", arXiv preprint arXiv: 2407.04003v1, 2024.
- 51. Wang, S., Wang, J., Wang, G., Zhang, B., Zhou, K., and Wei, H., "Open-vocabulary calibration for fine-tuned CLIP", arXiv preprint arXiv: 2402.04655v4, 2024.
- 52. Chen, J., Yang, D., Jiang, Y., Li, M., ... and Zhang, L. "Efficiency in focus: LayerNorm as a catalyst for fine-tuning medical visual language pre-trained models", arXiv preprint arXiv: 2404.16385v1, 2024.
- 53. Duan, Z., Cheng, H., Xu, D., Wu, X., Zhang, X., ... and Xie, Z. "CityLLaVA: Efficient fine-tuning for VLMs in city scenario", arXiv preprint arXiv: 2405.03194v1, 2024.
- 54. Zhao, Y., Pang, T., Du, C., Yang, X., Li, C., Cheung, N. M. M., and Lin, M. "On evaluating adversarial robustness of large vision-language models", arXiv preprint arXiv: 2305.16934v2, 2023.
- 55. Zhou, W., Bai, S., Mandic, D. P., Zhao, Q., and Chen, B. "Revisiting the adversarial robustness of vision language models: a multimodal perspective. arXiv preprint arXiv: 2404.19287, 2024.
- 56. Li, L., Guan, H., Qiu, J., and Spratling, M. "One prompt word is enough to boost adversarial robustness for pre-trained vision-language models", arXiv preprint arXiv: 403.01849v1, 2024.



ULUSLARARASI 3B YAZICI TEKNOLOJİLERİ VE DİJİTAL ENDÜSTRİ DERGİSİ

INTERNATIONAL JOURNAL OF 3D PRINTING TECHNOLOGIES AND DIGITAL INDUSTRY

ISSN:2602-3350 (Online)

URL: https://dergipark.org.tr/ij3dptdi

EVALUATION OF THE PROCESS PARAMETER AND PERFORMANCE OF L-DED SS316L-IN718 BIMETALLIC STRUCTURES

Yazarlar (Authors): Mustafa Kaş D*, Oğuzhan Yılmaz

Bu makaleye şu şekilde atıfta bulunabilirsiniz (To cite to this article): Kaş M., Yılmaz O., "Evaluation of the Process Parameter and Performance of L-DED SS316L-In718 Bimetallic Structures" Int. J. of 3D Printing Tech. Dig. Ind., 9(2): 263-271, (2025).

DOI: 10.46519/ij3dptdi.1700837

Araştırma Makale/ Research Article

EVALUATION OF THE PROCESS PARAMETER AND PERFORMANCE OF L-DED SS316L-IN718 BIMETALLIC STRUCTURES

Mustafa Kaş^a *, Oğuzhan Yılmaz

^a Advanced Manufacturing Technologies Research Group (AMTRG), Mechanical Engineering Department, Faculty of Engineering, Gazi University, TURKEY

* Corresponding Author: <u>mustafakas@gazi.edu.tr</u>

(Received: 16.05.25; Revised: 11.06.25; Accepted: 01.07.25)

ABSTRACT

Laser Direct Energy Deposition (L-DED) is a promising additive manufacturing technique with potential application in joining two dissimilar materials to fabricate bi-metallic components. The quality and functionality of the bonding interfaces are of great significance and rely heavily on the process parameters. In this work, we first deposited IN718 on a wrought SS316L substrate to create a bimetallic interface. Different energy density values, ranging from 71.43 to 127.7 J/mm, were used through various combinations of laser power and scanning speed for deposition. The bimetallic interface quality in terms of interface geometry, morphology, and dilution values was investigated for every energy density. Geometric analyses and dilution measurements revealed that the optimum bimetallic fabrication was achieved with an energy density of 90-100 J/mm. To deposit bimetallic SS316L-IN718 blocks for mechanical testing, the laser power and scan speed were set to 1400 W and 14 mm/s, respectively. Line EDS measurements revealed a transition zone across the bimetallic interface within a 4 mm distance, avoiding abrupt chemical discontinuities. Micro-hardness testing using Vickers revealed a smooth hardness transition between the SS316L (~210 HV) and IN718 (~300 HV) sides without any defect formation, suggesting successful joining. The bimetallic structure exhibited yield strength of 268.88 ± 20 MPa, tensile strength of 462 \pm 12 MPa, and elongation of 19.6 \pm 0.8%, in good agreement with SS316L. The fracture occurred on the SS316L side with noticeable necking and ductile behavior, demonstrating good interfacial bonding. These findings demonstrate the potential of L-DED in the fabrication of bimetallic structures for structural applications.

Keywords: L-DED, Bi-Metal, SS316L, IN718

1. INTRODUCTION

The demand for complex and multi-functional materials has been increasing as technology advances. This need has driven the exploration of multi-material structures that synergistically combine the properties of dissimilar alloys. When there are different requirements for specific applications, bimetallic materials are used rather than a single material. Bimetallic materials, which integrate two different materials, offer a compelling solution by combining each material's excellent properties. For example, wear- and corrosion-resistant stainless steel can be combined with copper to enhance the heat conductivity of power plant boiler and gas turbine components [1]. In another application, SS316L-Ti64 bimetallic

structures can have very hard materials in the outer layers, providing excellent resistance, and inner material with excellent ductility and high toughness, where the parts are subjected to different load conditions [2]. Traditional joining and coating methods, such as welding [3], cold-sprayed coatings [4], thermally spraying [5], powder metallurgy [6], soldering, and interface diffusion [7], offer limited solutions with basic geometries to create bimetals. Moreover, these methods face significant challenges in joining different materials due to their distinct thermal expansion coefficients, chemical incompatibility, and susceptibility to intermetallic phase formation at the interface [8-9]. Unlike the methods mentioned above, additive manufacturing techniques have the unique capability of fabricating precisely controlled bimetallic components at complex geometry. Gurok et al. created bimetallic cutting tools using an additive manufacturing process with stainless steel and hard-facing materials, exhibiting good interfacial bonding, desirable microstructural features, and hardness gradient for wear-resistant applications [10].

Laser Directed Energy Deposition (L-DED) stands out as a leading additive manufacturing technology, offering the production of such complex multi-material systems [11]. In the L-DED process, a laser is employed to melt powder material as it is deposited onto a substrate. The powder material is fed through a nozzle, and the laser beam precisely melts and fuses it onto the substrate. L-DED exhibits versatility, as it can simultaneously use more than one raw material as feedstock, including metals, alloys, and ceramics. The selection of process parameters directly affecting the energy density delivered to the deposited material is crucial in L-DED. Improperly selected process parameters can lead to adverse thermally induced effects, such as lack of fusion, undesirable phase transformation, excessive dilution [12]. Dilution, defined as the melting of the underlying material during deposition. can significantly influence interfacial integrity and mechanical properties. High energy densities can lead to a larger melt pool, potentially causing issues such as increased dilution and undesirable phase transformations due to excessive heat input, particularly in alloy systems prone to such effects [10]. Conversely, too low an energy density may result in insufficient melting of the material, manifesting as lack of fusion defects that can severely degrade the mechanical integrity of the build [13].

One of the most promising bimetallic structures is the combination of austenitic stainless steel SS316L and nickel-based superalloy IN718 [14-15]. SS316L offers excellent ductility, corrosion resistance, and cost-effectiveness [16], while IN718 exhibits high strength, hardness, and oxidation resistance at elevated temperatures [17]. The superior mechanical performance of IN718 is attributed to the solid solution-strengthening effects of elements such as Mo and Nb [18]. Despite the advantages of IN718, its higher cost motivates efforts to

selectively apply it only where high performance is required while using SS316L in less critical regions. Both alloys share a face-centered cubic (FCC) matrix structure (γ phase), predominantly alloyed with Fe, Cr, and Ni, facilitating their compatibility in layered deposition.

In this study, IN718 powder was deposited on SS316L substrates through L-DED in six different process conditions to examine the effect of energy density on interface geometry dilution. The best combination of parameters was selected and utilized to build vertically deposited blocks of bimetallic SS316L-IN718 as well monolithic SS316L, monolithic IN718. The bimetallic samples were examined by line-EDS and Vickers microhardness profiling for determining composition and hardness transition at the interface. Finally, we compared the tensile properties of monolithic alloys and bimetallic sample to evaluate bonding quality of the bimetal. The objective of this study is to establish a uniform process window for fabricating defect-free bimetallic components and to gain fundamental understanding for future mechanical performance evaluation.

2. MATERIAL AND METHOD

In this study, spherical IN718 and SS316L powder (45-153) produced via gas atomization was used as the feedstock material for L-DED processes. The chemical composition of the IN718 and SS316L powders is provided in Table 1. The deposition was fabricated using Erlaser Hard+Clad L-DED system, which has a diode laser (maximum power output of 4 kW) and a 6-axis Kuka robotic arm. Argon gas was used as both the shielding gas during the L-DED process to protect the molten material from oxidation and as a feeding gas. The focal length between the laser head and the part was maintained at 13 mm, resulting in a laser beam spot diameter of approximately 3.5 mm. The powder feed rate of 30 gr/min and the carrier gas flow of 15 L/min were kept constant during deposition. The study was conducted in two main stages. In the first stage, single wall bimetallic production was done by depositing IN718 powder over the wrought SS316L substrate under six different process parameter sets, as shown schematically in Figure 1 (a). In this stage, deposition was carried out in a singletrack, multilayer configuration. Six wall

depositions were fabricated using varying combinations of laser power (1000, 1300, 1400W) and scan speed (11, 14 mm/s) to investigate the influence of energy density, calculated by Equation (1), on wall geometry, dilution at the interfacial zone, and deposition quality. The images of the produced single walls and the values of the parameters used for the process are shown in Figures 1(b) and (c), respectively. The ranges of parameters used for this stage were based on results from our preliminary tests. The linear energy density was calculated using the following expression:

Energy density
$$(J/mm) = \frac{P}{V}$$
 (1)

where P is laser power (W), and V is scan speed (mm/s). The optimal parameter set was identified based on optical microscope inspection. Before inspection, the samples were ground using SiC papers of 240-2500 grit size and polished using 6, 3, and 1 µm diamond solutions. Optical microscopy was employed to observe bonding geometry, microstructural features, and the presence of any defects such as porosity or cracks. The parametric set that exhibited optimal dilution [10] and stable geometries with no defect formation was selected as the optimum [19,20].

In the second stage of the study, bimetallic blocks were deposited entirely using L-DED, starting with SS316L powder and followed by IN718 powder. All blocks produced in this stage were fabricated with the same parameter set, which was selected as the optimal parameter set from single-wall productions. These blocks were used to investigate the bonding quality of SS316L-IN718 bimetallic interfaces through mechanical tests. **Energy-Dispersive** Spectroscopy (EDS) was utilized to verify bimetallic production through line elemental composition measurements. Vicker's microhardness measurements were performed using a 100 g force and a dwell time of 10 seconds with an AMH 55 (Leco Corporation, USA). In addition to bimetallic SS316L-IN718 blocks, monolithic form of SS316L and IN718 were produced to compare the tensile properties. Each block consisted of three vertically aligned tensile bars, fabricated with 110 layers to reach a total height of 82.5 mm, with a wall thickness of 6 mm and width of 50 mm, as shown in Figure 2. The geometries of the tensile specimens conformed to ASTM E8 standards, with a gauge length of 33 mm and a thickness of 2 mm (Figure 3). The tensile test was conducted at a constant strain rate of 0.015 mm/min using a Shimadzu Autograph 100 kN tensile test machine.

Table 1. Chemical composition (wt. %) of IN718 and SS316L powder

Material	Fe	Cr	Ni	Mn	Mo	Nb	Si	C	Co	Ti
SS316L	Bal.	17	12	2	2	_	0.1	0.03	-	_
IN718	Bal.	19	54	0.35	3	5	0.15	0.05	0.06	1

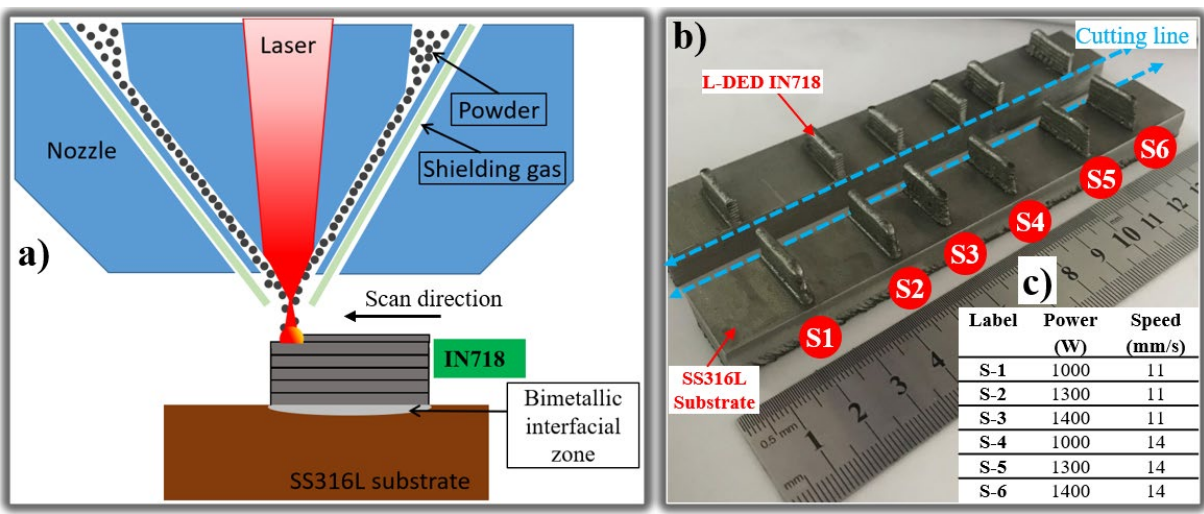


Figure 1. Single wall fabrication of IN718 on wrought SS316L substrate to form bimetallic interface via L-DED: (a) Schematic view of bimetal fabrication by IN718 deposition on wrought SS316L substrate, (b) Single wall depositions with different sets of parameters, which are cut with Electrical Discharge Machine (EDM) to inspect cross-section geometry, c) the process parameter matrix used for single wall depositions.

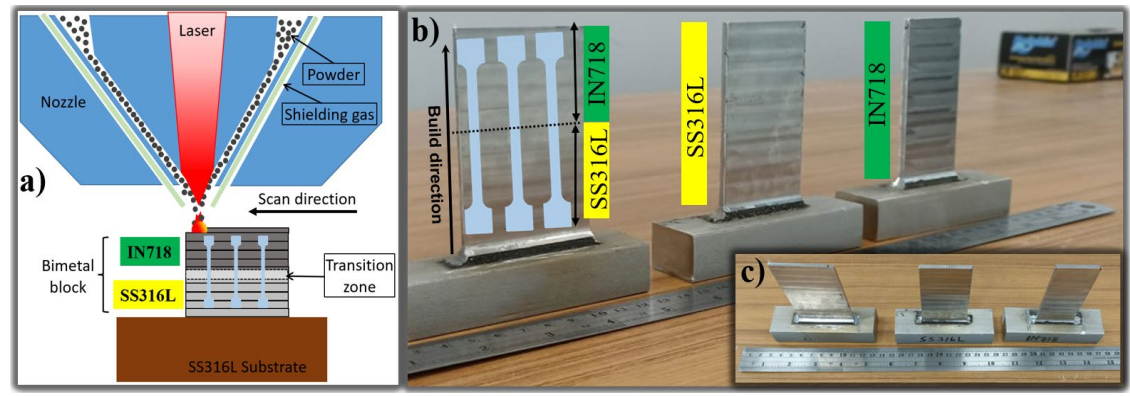


Figure 2. Vertical blocks fabrication in the form of IN718-SS316L bimetals via L-DED (a) Schematic view of bimetallic fabrication by IN718 deposition on L-DEDed SS316L, (b) front view of SS316L-IN718 bimetallic, and monolithic SS316L, IN718, (c) top view of SS316L-IN718 bimetallic, and monolithic SS316L, IN718.

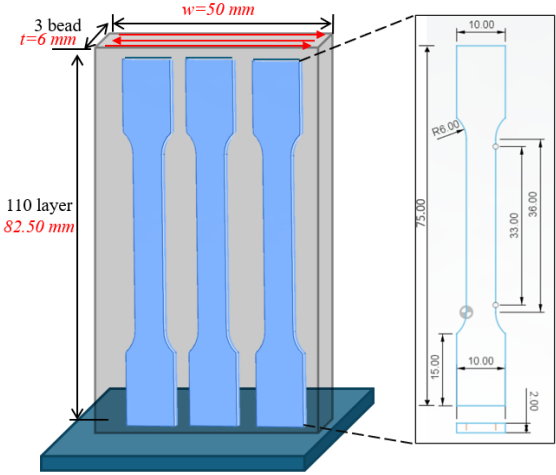


Figure 3. Schematic illustration of the vertical block fabricated via L-DED used for tensile specimen subtraction and test specimen geometry

3. RESULTS AND DISCUSSION3.1. Single Wall Deposition

To investigate the effect of energy density on the interfacial quality and wall geometry of IN718 deposition on wrought SS316L substrate, single-wall depositions performed using six different combinations of laser power and scan speed. The resulting energy densities ranged from 71.43 to 127.27 J/mm, as shown in Table 2. Cross-sectional views of the walls, including the interface area IN718 deposition between and SS316L substrate, were obtained by sectioning the samples perpendicular to the scanning direction. The penetration depth and width of the SS316L and IN718 interfaces were measured using ImageJ software applied to micrographs obtained from the microscope. The dilution ratio, which is a parameter that determines intermixing of materials at the interface, was calculated using Equation (2).

$$Dilution = \frac{D}{D+H} \tag{2}$$

where D is the penetration depth into the SS316L substrate and H is the height of the first layer of deposited IN718 above the substrate.

As depicted in Figure 4, the interface geometries were affected by the energy density values, leading to distinct dilution ratios. Higher energy density resulted in greater melting of the base material (SS316L), leading to increased mixing with the deposited material (IN718). The maximum dilution of 38.3% was observed in sample S-3, which had the highest energy density (127.27 J/mm), indicating significant substrate melting and mixing. In addition to increased dilution, excessively high energy densities can cause over melting, leading to unwanted changes in material properties and the vaporization of alloying elements [21]. Conversely, a lower energy density contributed to reduced dilution, resulting in less mixing of the composition and properties between the base and deposited materials. The lowest dilution of 16.3% occurred in sample S-4, which had the lowest energy density (71.43 J/mm). However, relatively low energy density could result in insufficient fusion and the presence of unmelted powder near the interface, as shown in samples S-4 and S-5. This inadequate fusion increases the risk of defects, such as pores, which can have a detrimental impact on the mechanical properties and longterm performance of components. Maintaining a balanced energy density is essential for preventing both over-melting and lack of fusion defects. The energy density values between 90-100 J/mm resulted in an optimal balance

between dilution values of 18–20%, and defectfree deposition in agreement with the previous study by Kas et al. [22]. These values produced clean fusion zones without excessive melting of the base material, thereby preserving compositional gradients and minimizing the occurrence of fusion-induced fabrication defects.

In addition to dilution, the wall height and width of the IN718 deposition were evaluated to assess deposition quality, as shown in the optical microscope images in Figure 5. The highest wall height (8.96 mm) was achieved at sample S-1 with energy density of 90.91 J/mm,

producing a stable wall with good geometric integrity. The widest wall (2.8 mm) was achieved at sample S-3 with energy density of 127.27 J/mm. Although higher energy densities led to wider depositions, they also introduced potential issues such as melt pool instability and over-broadening of the deposited path [23]. The sample S-6 exhibited a good compromise between build height, dilution, and structural integrity. In particular, it resulted in a height of 8.3 mm, a width of 2.6 mm, and a dilution of 20.2%, with no signs of unmelted powder or porosity, demonstrating that it is the best parameter.

Table 2. Process parameters, energy density, wall height, width, and dilution results for single-wall depositions.

"	Power (W)	Speed (mm/s)	Energy Density	Height (mm)	Width (mm)	Dilution (%)
			(J/mm)			
S-1	1000	11	90.91	8.96	2.65	18.4
S-2	1300	11	118.18	8.8	2.7	34
S-3	1400	11	127.27	8.7	2.8	38.3
S-4	1000	14	71.43	7.6	2.5	16.3
S-5	1300	14	92.86	7.9	2.55	19.3
S-6	1400	14	100	8.3	2.6	20.2

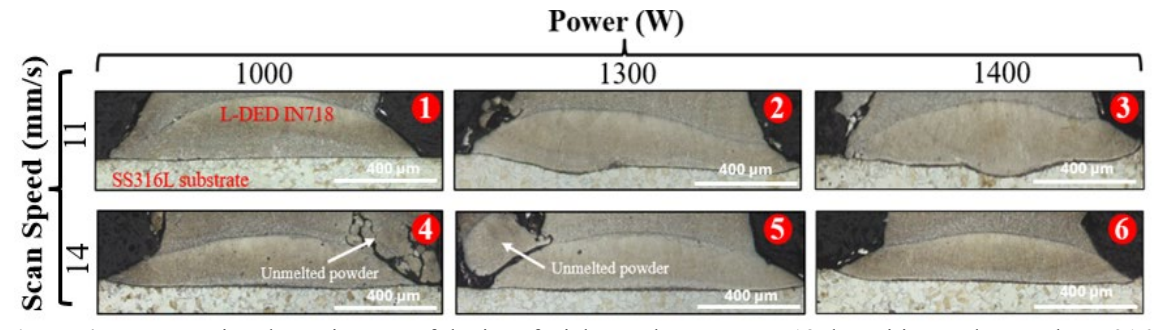


Figure 4. Cross-sectional OM images of the interfacial zone between IN718 deposition and wrought SS316L substrate were obtained at varying scan speeds and laser powers.

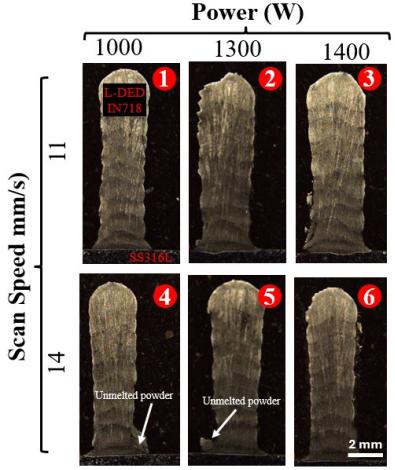


Figure 5. OM images of IN718 single-wall deposition fabricated on wrought SS316L substrate via L-DED, using varying scan speed and laser power.

3.2. Bimetallic Block Deposition

mechanical microstructural The and characterizations investigated in this section were performed on bimetallic and monolithic blocks fabricated using the process parameter set of sample S-6 (1400 W, 14 mm/s, 100 J/mm), which was identified as the optimal parameter set, as discussed in Section 3.1. The other parameter sets were excluded from further block fabrication due to observed issues such as excessive dilution, melt pool instability, or the presence of unmelted powder to save time and cost by prioritizing the most promising parameter set. Hence, further mechanical tests were conducted only for the optimal parameter set.

To investigate the composition change and elemental diffusion, the line EDS measurement was done on bimetallic SS316L-IN718 block. The line EDS result revealed a transition zone between the SS316L and IN718 materials, as shown in Figure 6. Specifically, a progressive decrease in Fe concentrations was observed in this region. Simultaneously, Ni, Nb, and Mo contents increased consistently, reflecting the compositional shift toward the IN718 alloy. spanned This region nearly corresponding to 5 to 6 deposited layers based on the layer thickness of 0.75 mm. Similarly, Grandhi et al. reported comparable elemental interdiffusion in cobalt-nickel bimetallic interfaces fabricated via L-DED, attributing this to convective flow within the melt pool [24]. The gradient structure between SS316L and IN718 is attributed not only to melt pool mixing and dilution during deposition but also potentially to the residual SS316L powder within the powder convey line, which was fed during the early stages of IN718 deposition.

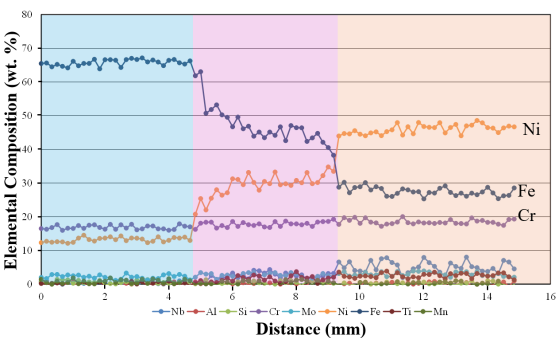


Figure 6. Elemental composition profile of the SS316L-IN718 bimetallic sample, which was obtained across the build direction.

Micro-hardness testing was performed across the interfaces from the SS316L region to the IN718 region to evaluate the hardness variations resulting from the composition change. The hardness profile along the cross-sections of the SS316L-IN718 interfaces was given in Figure 7. The hardness of the SS316L-IN718 bimetal exhibited a gradual increase across the interface, indicating that, despite the nominally abrupt change in material composition, substantial elemental interdiffusion took place at the interface during the deposition process. Ji et al. reported that a compositional diffusion across the interface facilitates a smoother transition. effectively minimizing concentrations that could otherwise degrade mechanical integrity interfacial and

performance [25]. The SS316L region exhibited hardness of 200-220 HV, consistent with its single-phase austenitic matrix. As the transition zone approached, a noticeable increase in hardness was observed, reflecting the change in composition. Within the transition zone, hardness values increased to 260-280 HV, highlighting the influence of alloying element interdiffusion and potential formation of fine secondary phases. The absence of abrupt hardness fluctuations across the transition zone suggests that the thermal profile induced by the selected process parameter set enabled gradual elemental diffusion while suppressing the formation of brittle intermetallic phases. The IN718 region exhibited the highest hardness values, ranging from 260 to 300 HV, which is typical for the as-deposited IN718 alloy due to solid solution and precipitation hardening of secondary phases.

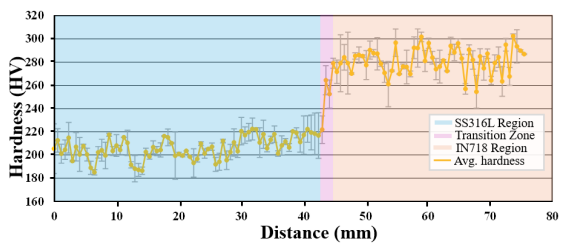


Figure 7. Hardness profile along the cross-section of the SS316L-IN718 bimetallic sample.

The mechanical properties of the SS316L-IN718 bimetallic interface were evaluated through tensile testing, and the results are presented in Figure 8. The monolithic counterparts of bimetal were also tested to compare the results.

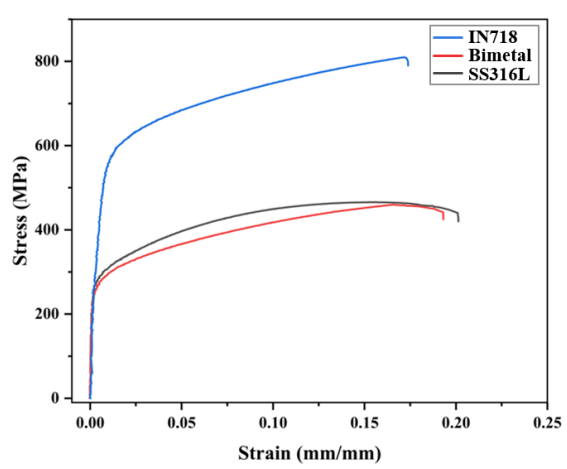


Figure 8. Stress–strain curves of SS316L, IN718, and SS316L-IN718 bimetallic specimens.

As shown in Table 3, the bimetallic sample exhibited a yield strength of 268.88 ± 20 MPa, a tensile strength of 462 ± 12 MPa, and an elongation of $19.6 \pm 0.8\%$. These values fall between those of SS316L and IN718, confirming the successful integration of the two dissimilar materials. Mechanical properties of the bimetallic sample were comparable to SS316L in terms of yield and ultimate strength, but with lower total elongation. The cause of the decrease in ductility was that half of the gauge length consisted of IN718, which has less inherent elongation capability compared to SS316L. The study by Lu et al. also showed elongation values between 16% and 21% for L-DED fabricated SS316L/IN718 functionally graded materials in the as-built and heat-treated conditions [26]. The necking and fracture occurred in the SS316L part of the bimetallic sample, indicating that the interface was stronger than the SS316L base alloy. The reason for the strong bonding between the parent alloys could be attributed to the gradual hardness the absence of transition and compositional changes, which minimizes stress concentration at the interface. A ductile fracture mode was observed, with no signs of interfacial delamination or premature failure, validating the mechanical integrity of the bonding zone.

Table 3. Tensile properties of the bimetallic SS316L-IN718 sample and its parent alloy counterparts.

Sample	Yield Strength (MPa)	Tensile Strength (MPa)	Elong. (%)
Bimetal	268.88 ± 20	462 ± 12	19.6 ± 0.8
SS316L	280.5 ± 18	465 ± 15	20.8 ± 0.5
IN718	547.5 ± 13	820 ± 14	17.3 ± 0.7

4. CONCLUSION

In this study, SS316L-IN718 bimetallic structures were fabricated using L-DED by depositing IN718 on wrought SS316L and fully deposited SS316L-IN718 blocks. The effects of processing parameters on the interfacial quality and the mechanical performance of the bimetallic interface were investigated. In the first stage of the study, single wall depositions of IN718 on wrought SS316L were performed with various combinations of laser power and scan speed. The experimental results revealed that both dilution ratio at the interface and wall

geometry were significantly dominated by energy density. An optimum energy density range of 90-100 J/mm was established to achieve steady deposition with good bonding, regulated dilution (~18-20%), and least geometric distortion. In the second stage of the study, vertically built blocks were fabricated by using the parameter set of sample S-6 to inspect mechanical integrity and compare tensile properties of bimetallic samples with their monolithic counterparts. EDS line scanning along the SS316L-IN718 interface confirmed a smooth elemental transition over a 4 mm region. Micro-hardness measurements revealed a continuous transition from a hardness of ~210 HV in the SS316L region to a hardness of ~300 HV in the IN718 region without the presence of any defect-related degradation at the interface zone. Tensile testing revealed that the yield strength and ultimate strength of the bimetallic sample are 268.88 ± 20 MPa and 462 ± 12 MPa, respectively, in good agreement with SS316L. Elongation of bimetal is lower than SS316L but higher than IN718, and the fracture occurred on the SS316L side with noticeable necking and ductile behavior, demonstrating good interfacial bonding. The uniform hardness profile, absence of interface defects, and robust mechanical integrity confirm that the L-DED process can be used to fabricate functional SS316L-IN718 bimetallic components for structural applications.

ACKNOWLEDGES

This study was supported by the Scientific Research Projects Coordination Unit of Gazi University within the scope of the Priority Area Research Project, with the project number FOA-2023-8507.

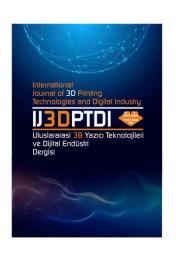
REFERENCES

- 1. Kar, J., Roy, S.K., Roy, G.G., "Effect of beam oscillation on electron beam welding of copper with AISI-304 stainless steel", Journal of Material Processing Technology, Vol. 223, Pages 174-185, 2016.
- 2. Alontseva, D., Yavuz, H.İ., Azamatov, B., Khoshnaw, F., Safarova, Y., Dogadkin, D., Avcu, E., Yamanoglu, R., "Improving corrosion and wear resistance of 316L stainless steel via in situ pure Ti and Ti6Al4V coatings: tribocorrosion and electrochemical analysis", Materials, Vol. 18, Issue 3, Pages 553, 2025.

- 3. Sherpa, B.B., Rani, R., "Advancements in explosive welding process for bimetallic material joining: A review", Journal of Alloys and Metallurgical Systems, Vol. 6, 2024.
- 4. Wu H., Xie, X., Liu, S., Xie, S., Huang, R., Verdy, C., Liu, M., Liao, H., Deng, S., Xie, Y., "Bonding behavior of bi-metal-deposits produced by hybrid cold spray additive manufacturing", Journal of Materials Processing Technology, Vol. 299, 2022.
- 5. Singh, S., Berndt, C.C., Singh Raman, R.K., Singh, H., Ang, A.S.M., "Applications and developments of thermal spray coatings for the iron and steel industry", Materials, Vol. 16, Issue 2, Page 516, 2023.
- 6. Chauhan, P. K., Khan, S., "Microstructural examination of aluminum-copper functionally graded material developed by powder metallurgy route", Materials Today: Proceedings, Vol. 25, Issue 4, 2020.
- 7. Yilmaz, O., Çelik, H., "Electrical and thermal properties of the interface at diffusion-bonded and soldered 304 stainless steel and copper bimetal", Journal of Materials Processing Technology, Vol. 141, Issue 1, Pages 67-76, 2003,
- 8. Wang, D., Liu, L., Deng, G., Deng, C., Bai, Y., Yang, Y., Han, C., "Recent progress on additive manufacturing of multi-material structures with laser powder bed fusion", Virtual and Physical Prototyping, Vol. 17, Issue 2, Pages 329–365, 2022.
- 9. Bandyopadhyay, A., Zhang, Y., Onuike, B., "Additive manufacturing of bimetallic structures", Virtual and Physical Prototyping, Vol. 17, Issue 2, Pages 256–294, 2022.
- 10. Dass, A., Moridi, A., "State of the art in directed energy deposition: From additive manufacturing to materials design", Coatings, Vol. 9, Pages 415, 2019.
- 11. Gürol U., Dilibal S., Turgut B., Baykal H., Kümek H., Koçak M., "Manufacturing and characterization of WAAM-based bimetallic cutting equipment", International Journal of 3D Printing Technologies and Digital Industry, Vol. 6, Issue 3, Pages 548-555, 2022.
- 12. Tan, Z. E., Pang, J. H. L., Kaminski, J., Pepin, H., "Characterization of porosity, density, and microstructure of directed energy deposited stainless steel AISI 316L", Additive Manufacturing, Vol. 25, Pages 286-296, 2019.

- 13. Benarji, K., Kumar, Y., Paul, C., Jinoop, A., Bindra, K., "Parametric investigation and characterization on SS316 built by laser-assisted directed energy deposition", Proceedings of the Institution of Mechanical Engineers Part L Journal of Materials Design and Applications, Vol. 234, Issue 3, Pages 452-466, 2019.
- 14. Mahmud, A., Ayers, N., Huynh, T., Sohn, Y., "Additive manufacturing of SS316l/IN718 bimetallic structure via laser powder bed fusion", Materials, Vol. 16, Issue 19, Page 6527, 2023.
- 15. Singh, S. P., Aggarwal, A., Upadhyay, R. K., Kumar, A., "Processing of IN718-SS316L bimetallic-structure using laser powder bed fusion technique", Materials and Manufacturing Processes, Vol. 36, Issue 9, Pages 1028-1039, 2021.
- 16. Nouri, A., Wen, C., "Stainless steels in orthopedics", In Structural Biomaterials, Pages 67-101, 2021.
- 17. Zhou, C., Wang, J., Hu, S., Tao, H., Fang, B., Long, L., Zhang, L., "Enhanced corrosion resistance of additively manufactured 316L stainless steel after heat treatment", Journal of the Electrochemical Society, Vol. 167, Issue 14, Page 141504, 2020.
- 18. Vikram, R., Kirchner, A., Klöden, B., Suwas, S., "Optimized heat treatment for electron beam powder bed fusion processed IN718: correlating microstructure, texture, and mechanical properties", Advanced Engineering Materials, Vol. 27, Issue 9, 2025.
- 19. Xu, J., Wu, Z., Niu, J., Song, Y., Liang, C., Yang, K., Chen, Y., Liu, Y., "Effect of laser energy density on the microstructure and microhardness of inconel 718 alloy fabricated by selective laser melting", Crystals, Vol.12, Issue 9, Pages 2022.
- 20. Chen, Z., Sun, W., Huang, Y., Zhou, H., Yang, K., Lu, J., "The effect of laser energy density on microstructural evolution and mechanical properties of laser clad 316L stainless steel for repair", Surface and Coatings Technology, Vol. 448, 2022.
- 21. Saboori, A., Aversa, A., Marchese, G., Biamino, S., Lombardi, M., Fino, P., "Application of directed energy deposition-based additive manufacturing in repair", Applied Sciences Vol. 9, Issue 16, Page 3316, 2019.
- 22. Kas, M., Muslim, T., Yilmaz, O. Karagoz, T., Turedi, E., Gumus. S., Bayram, A., "Directed energy deposition of PH 13–8 Mo stainless steel: microstructure and mechanical property analysis", International Journal Advanced Manufacturing Technology, Vol. 132, Pages 701–715, 2024.

- 23. Sampson, R., Lancaster, R., Sutcliffe, M., Carswell, D., Hauser, C., Barras, J., "The influence of key process parameters on melt pool geometry in direct energy deposition additive manufacturing systems", Optics & Laser Technology, Vol. 134, 2021.
- 24. Grandhi, M., Nagaraj, A., Khosravi, H., Liu, Z., Min, S., "Mechanical and microstructural profiling of additively manufactured cobalt–nickel functional gradient structure", Manufacturing Letters, Vol. 41, 2024.
- 25. Ji, C., Li, K., Zhan, J., Bai, S., Jiang, B., Murr, L. E., "The effects and utility of homogenization and thermodynamic modeling on microstructure and mechanical properties of SS316/IN718 functionally graded materials fabricated by laser-based directed energy deposition", Journal of Materials Processing Technology, Vol. 319, 2023.
- 26. Lu, J., Li, W., "Improvement of tensile properties of laser directed energy deposited IN718/316L functionally graded material via different heat treatments", Materials Science and Engineering: A, Vol. 866, 2023.



ULUSLARARASI 3B YAZICI TEKNOLOJİLERİ VE DİJİTAL ENDÜSTRİ DERGİSİ

INTERNATIONAL JOURNAL OF 3D PRINTING TECHNOLOGIES AND DIGITAL INDUSTRY

ISSN:2602-3350 (Online)

URL: https://dergipark.org.tr/ij3dptdi

COMPARISON OF MACHINE LEARNING MODELS IN HEART FAILURE PREDICTION AND THEIR INTEGRATION INTO CLINICAL DECISION SUPPORT SYSTEMS

Yazarlar (Authors): Mustafa Çakır •

Bu makaleye şu şekilde atıfta bulunabilirsiniz (To cite to this article): Çakır M., "Comparison of Machine Learning Models In Heart Failure Prediction and Their Integration Into Clinical Decision Support Systems" Int. J. of 3D Printing Tech. Dig. Ind., 9(2): 272-282, (2025).

DOI: 10.46519/ij3dptdi.1724620

Araştırma Makale/ Research Article

Erişim Linki: (To link to this article): https://dergipark.org.tr/en/pub/ij3dptdi/archive

COMPARISON OF MACHINE LEARNING MODELS IN HEART FAILURE PREDICTION AND THEIR INTEGRATION INTO CLINICAL DECISION SUPPORT SYSTEMS

Mustafa Çakır^a*

^aIskenderun Technical University, Iskenderun Vocational School of Higher Education, Electronics and Automation Department, TÜRKİYE

* Corresponding Author: <u>mustafa.cakir@iste.edu.tr</u>

(Received: 21.06.25; Revised: 23.07.25; Accepted: 08.08.25)

ABSTRACT

Heart failure remains a leading cause of morbidity and mortality worldwide, necessitating advanced tools for early risk prediction. This study presents an interactive, machine learning-driven web application designed to predict heart failure outcomes using clinical data. Leveraging the heart failure clinical records dataset (n=299), the application integrates a comprehensive suite of fifteen diverse predictive models, encompassing traditional/statistical-based algorithms, instance-based and probabilistic methods, various tree-based and ensemble techniques, and neural networks within an intuitive Shiny framework. Key features include exploratory data analysis (correlation matrices, feature importance), model training, and real-time risk prediction with customizable patient parameters. The system employs stratified cross-validation (10-fold) for robust evaluation and achieves impressive performance, with top-performing models exhibiting test set Area Under Curve values exceeding 0.85, alongside high scores in accuracy, sensitivity, specificity, and F1-score. By combining clinical variables such as ejection fraction, serum creatinine, and follow-up time, the tool demonstrates how interactive machine learning platforms can enhance clinical decision-making. The open-source R-Shiny implementation provides immediate visual feedback, model interpretability features, and a template for extending predictive analytics to other medical domains. This work bridges the gap between statistical modeling and clinical application, offering both a prognostic tool and an educational resource for datadriven cardiology.

Keywords: Heart Failure Prediction, Machine Learning, Clinical Decision Support, R-Shiny.

1. INTRODUCTION

Heart-failure (HF) is a chronic and progressive cardiovascular disease where the heart is unable to pump enough blood to meet the body's needs [1]. Affecting millions globally, HF represents a significant health challenge associated with high morbidity and mortality rates, severely diminishing patients' quality of life and imposing a substantial burden on healthcare systems [2]. Early diagnosis, accurate prognosis prediction, and the determination of effective treatment strategies are critically important in managing HF patients. However, the complex pathophysiology of HF and the variability of the disease among individuals can make precise diagnosis and prognosis challenging using traditional clinical methods.

In-recent years, the increasing availability of large datasets in medicine and advancements in computing technologies have opened up significant opportunities for applying machine learning (ML) techniques in healthcare. ML algorithms can analyse complex medical data, such as clinical findings, laboratory results, and imaging data, to uncover hidden patterns and relationships, providing valuable insights for tasks like disease diagnosis, predicting patient prognosis, and identifying risk factors that may influence disease progression. Particularly in the field of HF, ML models hold the potential to analyze patient data to predict the presence of disease, forecast patient survival probability, and pinpoint risk factors.

A review of the literature clearly indicates a significant increase in the number of scientific publications addressing both ML and HF over the years. As illustrated in Figure 1, research interest in this area has grown considerably, especially in recent years. This trend vividly demonstrates the increasing acceptance and potential of ML techniques in HF research.

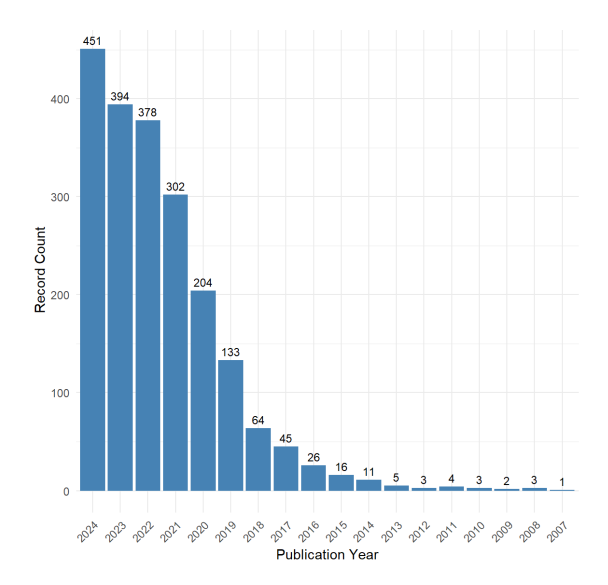


Figure 1. Trend of publications in HF and ML research

The literature frequently reveals the use of various ML algorithms for different prediction and classification tasks related to HF. These algorithms play a significant role in understanding, diagnosing, and predicting the prognosis of the disease.

A substantial portion of ML studies related to HF has focused on predicting the presence of the disease or forecasting patients' survival probability. For instance, [3] predicted the risk of death in HF patients using RF and Binary Particle Swarm Intelligence methods. [4], on the other hand, analysed the performance of Ensemble ML methods for predicting the survival of patients diagnosed with HF. Similarly, [5] proposed an ML-based approach to detect the survival status of HF patients. [6] application using also conducted an classification-based MLalgorithms predicting the survival of HF patients. Among more recent work, [7] developed time-adaptive ML models to predict the severity of HF with Reduced Ejection Fraction.

Researchers have employed a variety of ML algorithms in HF studies, including Linear Regression (LR) [4], [8-10], Support Vector Machine (SVM) [6, 7, 11], Decision Tree (DT) [12], Random Forest (RF) [13], Artificial Neural Network (ANN) [14-15], and Naïve Bayes (NB) [16]. The performance of these algorithms is typically evaluated using standard metrics such as accuracy, precision, recall, F1score, and Area Under the Curve (AUC) [7], [10], [17-19]. Some studies have aimed to compare the performance of different algorithms on the same dataset. For example, [9], [20] conducted a comparison of different ML classification algorithms for cardiovascular [10] examined the disease prediction. performance comparison of various algorithms in the early diagnosis of HF. [21] presented a comprehensive study evaluating the performance of different types of ML methods categorized into Tree, Meta, and Function categories for HF prediction. The use of webbased analytical tools [22] and ML applications shows significant potential not only in heart failure prediction but also in other health domains, such as estimating COVID-19 mortality [23] in Turkey.

While the datasets used vary, many studies have preferred publicly available datasets such as the Kaggle or University of California Irvine ML Repository. Nevertheless, some research has been conducted on specific clinical datasets.

Studies within the existing literature clearly demonstrate the strong potential of ML in the field of HF. However, the relative performance of different algorithms on specific datasets and their potential for clinical application remain an active area of research.

This study aims to contribute to the field by deeply analyzing the performance of various ML models, including or in comparison with previously used algorithms, on a specific dataset. In particular, comparing the strengths and weaknesses of different model types can help in making more informed choices for the development of future clinical decision support systems. Therefore, specifically aims to compare the performance of different ML models in predicting heart failure outcomes and to evaluate their potential for integration into clinical decision support systems. Utilizing a relevant and up-to-date dataset, we will train,

test, and compare various ML algorithms based on established performance metrics. The findings from this research are expected to contribute to the development of ML-based decision support systems [24], thereby facilitating more effective management of HF patients.

2. MATERIAL AND METHOD

In this study, ML models were used to predict the occurrence of deaths in patients with HF. Details of the dataset used, algorithms applied, and the developed R-Shiny platform are described below.

2.1. Dataset

The Heart Failure Clinical Records Dataset comprises clinical information from 299 patients with HF. It contains 12 clinical features and the target variable, "DEATH EVENT". The features included in the dataset are; age, (anaemia), creatinine anaemia status phosphokinase level (creatinine phosphokinase), diabetes status (diabetes), left ventricular ejection fraction (ejection fraction), high blood pressure status (high blood pressure), platelet count (platelets), creatinine serum level (serum creatinine), serum sodium level (serum sodium), sex, smoking status (smoking), and follow-up time (time). The target variable, DEATH EVENT, is a binary variable (yes/no) indicating whether the patient passed away during the follow-up period.

Prior to model development, a comprehensive exploratory data analysis was conducted to understand the distribution of each feature and the relationships between them. As part of this analysis, the pairwise Pearson correlation coefficients among all independent clinical features were calculated and are presented as a heatmap in Figure 2. This visualization allowed for the identification of potential linear relationships between variables, which is crucial for understanding the underlying structure of the dataset and for addressing issues such as multicollinearity in subsequent predictive modeling. For instance, the Figure highlights a notable moderate positive correlation between "sex" and "smoking" (r=0.45), suggesting a potential gender-specific association with smoking status within this patient cohort. Other weaker correlations, such as the slight positive association between 'age'

and "serum_creatinine" (r=0.16) or the weak negative correlation between "age" and "time" (r=-0.22), were also observed. While these correlations do not imply causation, they provide valuable insights into the interdependencies of the clinical parameters and informed the subsequent stages of feature selection and model building, ensuring robustness and interpretability of the derived models.

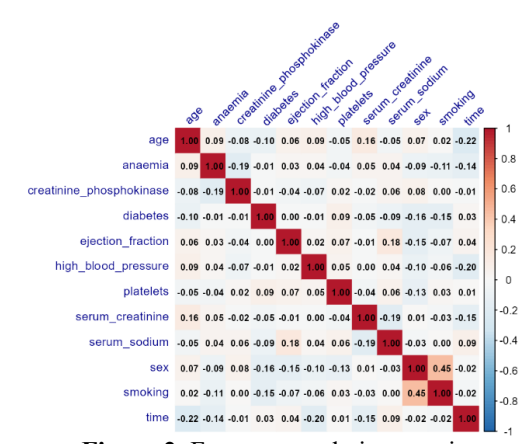


Figure 2. Feature correlation matrix

As illustrated in Figure 3, the RF feature importance analysis highlights time as the most influential predictor of death events in HF patients, with an importance score that markedly exceeds all other variables. This finding suggests that the duration of patient follow-up is a critical determinant of mortality risk, likely reflecting survival time as a proxy for event occurrence. Serum creatinine and ejection fraction emerge as the second and third most important predictors, reinforcing their established roles as indicators of renal dvsfunction and cardiac performance. respectively, both of which are key prognostic factors in HF. Variables such as age, platelets, creatinine phosphokinase, and serum sodium show moderate predictive value, implying their supplementary relevance. Conversely, features including high blood pressure, anaemia, smoking, sex, and diabetes contribute minimally, indicating limited independent prognostic utility after controlling for more dominant clinical factors. Thus, the Figure provides a data-driven hierarchy of risk factors that corroborates clinical expectations and enhances our understanding of variable importance in HF prognosis.

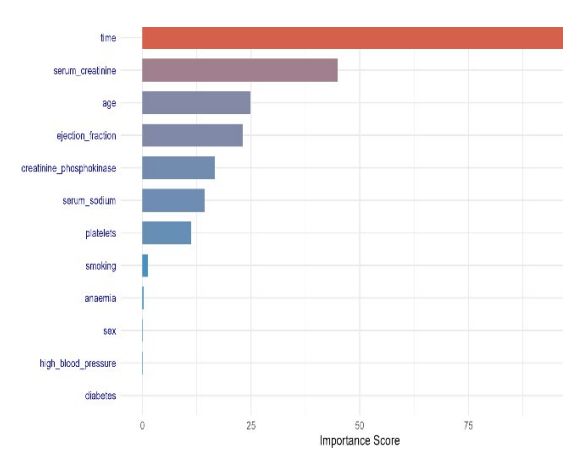


Figure 3. RF feature importance graph

2.2. Machine Learning Algorithms

In this study, various ML algorithms were compared to predict death events due to HF. The selected algorithms represent different learning approaches. The 15 different ML algorithms evaluated are listed below:

LR was introduced by David Cox in 1958 as a method to model binary outcomes using the logistic function, building on earlier work by Joseph Berkson in the 1940s who coined the term "logit" [25]. It models the log-odds of a binary response as a linear function of predictor variables, and it remains foundational in epidemiology and biomedical sciences.

Linear Discriminant Analysis (LDA) was developed by Ronald A. Fisher in 1936 as a method to find a linear combination of features that best separates two or more classes. It is widely used in pattern recognition and statistics for dimensionality reduction and classification [26].

QDA is an extension of LDA that emerged later as statisticians generalized discriminant analysis to relax the assumption of equal covariance matrices [27].

K-Nearest Neighbor (KNN) was first described by Evelyn Fix and Joseph Hodges in 1951 as a non-parametric method for pattern classification [28]. It gained prominence after Thomas Cover and Peter Hart formalized its statistical properties in 1967 [29].

NB classifiers stem from Bayes' Theorem proposed by Thomas Bayes in the 18th century. The "naive" assumption of conditional independence was formalized and applied in pattern recognition and information retrieval

starting in the 1950s, with early notable applications in text classification by Maron in 1961 [30].

DT gained traction through the Classification and Regression Trees (CART) framework developed by Leo Breiman, Jerome Friedman, Richard Olshen, and Charles Stone [31]. The CART methodology popularized recursive partitioning for classification and regression tasks.

RF was introduced by Leo Breiman in 2001 as an ensemble learning method that aggregates predictions of multiple decision trees to improve accuracy and reduce overfitting [32].

BT Bagging, short for Bootstrap Aggregating, was introduced by Leo Breiman in 1996 as a method that enhances the stability and predictive accuracy of ML algorithms by reducing variance through the aggregation of multiple bootstrapped models. This ensemble technique is particularly effective when applied to high-variance models such as decision trees because it combines the predictions of several models trained on different subsets of the data to improve overall performance and mitigate overfitting [33].

Fast Random Forest (FRF) is a fast implementation of RF introduced by Marvin N. Wright and Andreas Ziegler in 2017, optimized for high-dimensional data and genome-wide association studies [34].

Gradient Boosting Machine (GBM), the concept of boosting was introduced by [35] and further advanced by [36]. The specific formulation of gradient boosting was developed by [37], which generalized boosting algorithms using gradient descent techniques.

SVM was developed by Vladimir Vapnik and Alexey Chervonenkis in the 1960s, and popularized in the 1990s through Vapnik's extensive work [38]. The introduction of kernel functions, including the Radial Basis Function, extended its applicability to non-linear problems.

ANN, the foundational idea of artificial neural networks was introduced by Warren McCulloch and Walter Pitts in 1943. The modern, multilayer perceptron model and backpropagation algorithm were popularized by [39].

XGBoost, short for "Extreme Gradient Boosting" was introduced by Tianqi Chen and Carlos Guestrin in 2016 as a scalable and

regularized gradient boosting framework optimized for efficiency and predictive performance [40].

GLMNET was introduced by Hui Zou and Trevor Hastie in 2005 as a regularization technique that combines the strengths of L1 (Lasso) and L2 (Ridge) penalties to handle correlated predictors [41].

trics

Metric	Definition	Formula
Accuracy	The ratio of correctly classified instances (both positive	TP + TN
•	and negative) to the total number of instances.	$\overline{TP + TN + FP + FN}$
Sensitivity (Recall)	The proportion of actual positive cases (patients who	TP
• , ,	passed away) that were correctly identified by the model.	$\overline{TP + FN}$
Specificity	The proportion of actual negative cases (patients who did	TN
	not pass away) that were correctly identified by the model.	$\overline{TN + FP}$
Precision	The proportion of predicted positive cases that are actually	TP
	positive.	$\overline{TP + FP}$
F1 Score	The harmonic mean of Precision and Sensitivity, serving	2 * Precision * Sensitivity
	as a balanced measure of model performance, especially in	$^{2*}\overline{Precision + Sensitivity}$
	imbalanced datasets.	

2.3. R-Shiny Application Description

The structure and workflow of the R-Shiny-based application are illustrated in Figure 4. As depicted, the system initiates with dataset loading and preprocessing, and then branches into multiple functional tabs, each dedicated to a specific aspect of the machine learning pipeline, including data exploration, model training, evaluation, prediction, and interpretability.

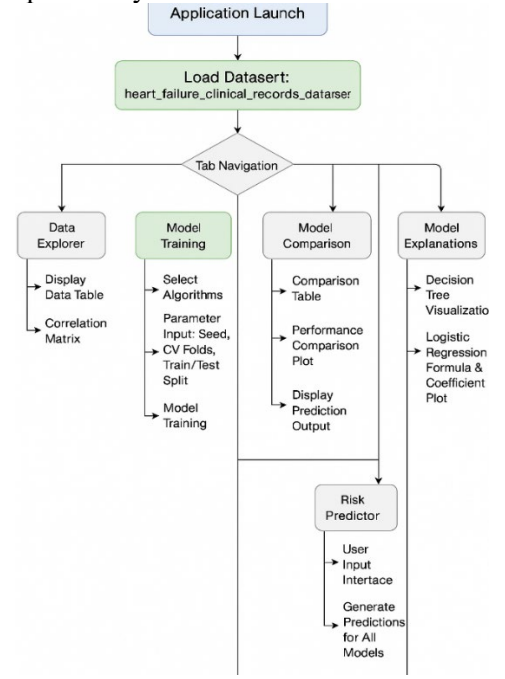


Figure 4. Workflow of R-Shiny based application

3. RESULTS AND DISCUSSION

For model training and performance evaluation, the dataset was split into two parts: 90% for training and 10% for testing. This split ensures that the models are tested on an independent dataset they have not seen during training, allowing for a more accurate estimation of their generalization capabilities. A fixed random seed value was used to reduce variations in results caused by randomness in data splitting and model training.

During the model training phase, 10-fold cross-validation was applied to estimate model performance more reliably and to optimize the algorithms' tuning parameters. In cross-validation, the training portion of the dataset was divided into 10 equal parts; in each iteration, one part was held out for validation while the remaining nine parts were used for training. This process was repeated 10 times, and the average performance was recorded. The optimal tuning parameters for the models were determined by selecting the combination that yielded the highest Area Under the ROC Curve (AUC) value from the cross-validation results.

The performance of the trained ML models was evaluated on the independent test dataset using various metrics. These metrics provide information about the models' prediction accuracy and classification abilities:

Upon analyzing the experimental results, it is evident that the ML models exhibited varying levels of success in predicting the HF death event. The evaluation conducted on the independent test dataset (Table 2) revealed that several models demonstrated superior overall performance. Specifically, GLM, LDA, GBM, SVM Linear, and GLMNET achieved the highest overall performance metrics, with Accuracy (96.6%) and F1_Score (97.6%) reaching and, respectively.

Table 2. Performance Evaluation Of Different Ml Models

Algorithm	Accuracy	Sensitivity	Specificity	F1_score
LR	0.966	1	0.889	0.976
LDA	0.966	1	0.889	0.976
GLMNET	0.966	1	0.889	0.976
GBM	0.966	1	0.889	0.976
SVM Linear	0.966	1	0.889	0.976
XGBoost	0.931	1	0.778	0.952
RF	0.931	1	0.778	0.952
FRF	0.931	1	0.778	0.952
SVM Radial	0.897	0.95	0.778	0.927
BT	0.897	0.95	0.778	0.927
DT	0.862	0.85	0.889	0.895
NB	0.828	0.95	0.556	0.884
NN	0.828	0.75	1	0.857
QDA	0.793	0.95	0.444	0.864
KNN	0.586	0.8	0.111	0.727

A particularly significant finding for these topperforming models is their Sensitivity value of 1.00 on the test set, indicating that they correctly identified

all the death cases in the test dataset. This highlights their substantial potential for identifying high-risk patients in a clinical setting. Other robust models, such as RF, FRF, and XGBoost, also performed strongly, with Accuracy (93.1%) and F1_Score 95.2%. These models also achieved a Sensitivity of 1.00, though their Specificity (77.8%) was slightly lower than that of the leading group.

The interpretable nature of the LR model, as shown by its equation (Equation 1) and coefficient plot (Figure 5), provided clear insights into the direction and magnitude of the relationship between individual clinical factors and the log-odds of death, largely aligning with clinical understanding of HF prognostic indicators.

The LR Coefficients plot:

$$Logit(p) = 9.23 + 0.041 * age - 0.05 * anaemia + 0.206 * diabetes - 0.077 * ejection_fraction - 0.003 * high_blood_pressure + 0.667 * serum_creatinine - 0.058 * serum_sodium + -0.485 * sex - 0.041 * smoking - 0.019 * time (1)$$

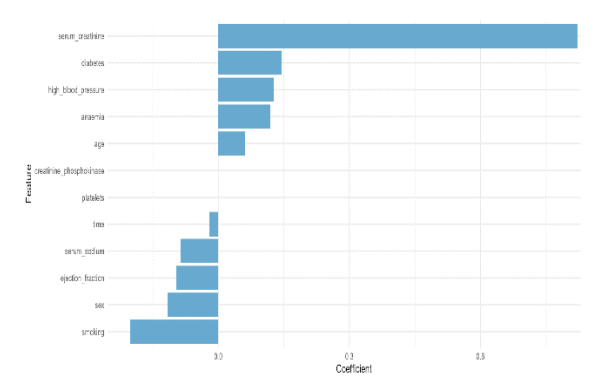


Figure 5. LR coefficient plot

This plot scientifically visualizes the estimated coefficients of the LR model, quantifying the linear association between each clinical feature and the log-odds of the HF death event, holding other variables constant. Features with positive coefficients, represented by bars extending to the right (notably serum creatinine and diabetes), indicate an increased log-odds, and thus an increased probability, of mortality as their values increase. Conversely, features with negative coefficients, shown by bars extending to the left (such as sex and ejection fraction), suggest a decreased log-odds of death with increasing values or different categories, highlighting their protective or inverse relationship with mortality risk in this model. Features with coefficients close to zero, indicated by bars near the central axis, demonstrate a minimal linear impact on the logodds of death when considered alongside other predictors in the model. This representation is crucial for interpreting the model's internal structure, revealing which clinical factors are most strongly associated with the outcome and in what direction, thereby contributing to the scientific understanding of feature-outcome relationships within this specific linear framework.

Figure 6 illustrates the constructed DT model, which clearly identifies key clinical features and their respective thresholds in predicting patient outcome. The tree's root node initiates with "time", indicating that patients with a follow-up time less than 74 days (time<74) enter a distinct risk pathway. Within this subgroup, "ejection fraction" emerges as the next crucial patients predictor: "ejection fraction>=33" exhibit a remarkably low mortality rate of 6% (representing 54% of the total dataset), suggesting this as the lowestrisk cohort. Conversely, for those with "ejection fraction<33", the "serum creatinine" level becomes decisive; patients "serum creatinine>=1.4" face a high mortality rate of 65% (comprising 9% of the dataset), identifying this as a particularly high-risk group characterized by shorter follow-up, reduced ejection fraction, and elevated serum creatinine. Intriguingly, patients with a follow-up time of 74 days or more (time>=74), constituting 26% of the dataset, show a high mortality rate of 81%. This highly interpretable structure allows clinicians to rapidly identify specific patient subgroups based on these key clinical

parameters and their thresholds, facilitating more informed prognostic assessments.

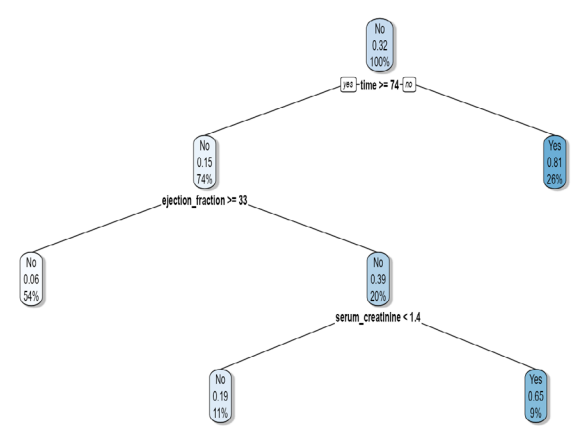


Figure 6. Visual representation of the DT model for predicting death event

Regarding computational efficiency, the training duration analysis (Figure 7) showed that ensemble methods like XGBoost, Ranger, and RF generally required longer training times compared to simpler models such as LR, LDA, and KNN. This suggests a trade-off between model complexity/training time and performance, which is a crucial consideration for practical deployment.

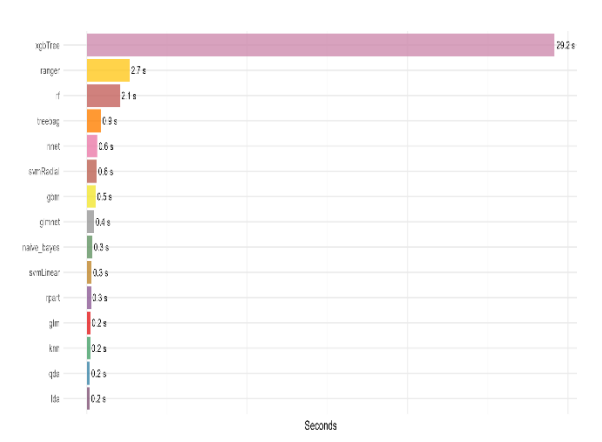


Figure 7. Model training duration

The developed R-Shiny application serves as a practical tool to leverage these trained models in a clinical context. Figure 8 provides an overview of the R-Shiny application's user interface, specifically showcasing the "Data Explorer" tab which facilitates initial data inspection and preliminary feature review. Beyond data exploration, the application integrates various functionalities such as model training, detailed model analytics, and model comparison. The "Risk Predictor" functionality, for instance, allows users to input specific patient clinical data and obtain instantaneous

risk predictions from multiple models. This feature demonstrates the potential of integrating these ML models into a clinical decision support system, offering healthcare professionals an additional resource to aid in risk assessment and decision-making by providing predictions based on diverse algorithmic perspectives.

Heart Failure Predictive Analytics Dashboard Data Explorer Model Training Model Analytics Model Comparison Risk Predictor Model Explanations age anaemia creatinine_phosphokinase diabetes ejection_fraction high_blood_pressure 582 7861 38 20 146 47 40 246 15 315 0 157 10 80 123

Figure 8. R-Shiny application user interface

4. CONCLUSION

This study successfully demonstrated the robust potential of various ML models in predicting heart failure outcomes, particularly death events, by leveraging the Heart Failure Clinical Records Dataset. My interactive, ML-driven web application, developed within the intuitive R-Shiny framework, served as a comprehensive platform for evaluating fifteen diverse predictive algorithms, encompassing traditional/statistical-based methods, instance-based and probabilistic methods, various tree-based and ensemble techniques, and neural networks.

The experimental results revealed that several models, including GLM, LDA, GBM, SVM Linear, and GLMNET, exhibited superior overall performance on the independent test dataset, achieving an Accuracy of 96.6% and an F1_Score of 97.6%. A particularly significant finding was the Sensitivity of 1.00 for these topperforming models, indicating their exceptional ability to correctly identify all death cases within the test set. This highlights their substantial promise for pinpointing high-risk patients in clinical environments. Other robust models like RF, Ranger, and XGBoost also showed strong performance with 93.1%

Accuracy and 95.2% F1_Score, alongside perfect Sensitivity.

The application's key features, such as exploratory data analysis (including correlation matrices and feature importance), model training, and real-time risk prediction, illustrate the practical utility of integrating these models into clinical decision support systems. The interpretability provided by models like LR and DT offers valuable insights into the relationships between clinical factors and mortality risk, corroborating existing medical understanding.

In conclusion, this work bridges the gap between statistical modeling and clinical application, providing both a prognostic tool and an educational resource for data-driven cardiology. The findings from this research are expected to contribute to the development of ML-based decision support systems, thereby facilitating more effective management of HF patients.

For future studies on this research topic, several key areas warrant further investigation. From a quantitative research perspective, future work should involve validating these models on larger and more diverse datasets, ideally from multiple institutions or different geographic regions, to enhance their generalizability and external validity. This expansion would provide more robust evidence of model performance across varied patient populations. Conducting prospective studies in actual clinical settings will also be crucial to evaluate the real-world impact and effectiveness of this interactive ML platform in improving patient outcomes and aiding healthcare professionals in their decision-making processes, which involves integrating the tool into clinical workflows and assessing its utility in a live environment. Additionally, quantitative research could focus on the economic impact of using such decision support systems, evaluating potential cost savings related to early prediction and optimized treatment strategies, and exploring the integration of real-time data from wearable health devices or continuous monitoring systems to enhance predictive accuracy and enable more dynamic risk assessments. Conversely, qualitative research is also vital. This includes understanding the perspectives of healthcare professionals regarding the usability, trustworthiness, and overall acceptability of

ML-based clinical decision support tools through interviews and focus groups, which could explore barriers and facilitators to adoption. Further qualitative research could delve into the ethical considerations surrounding the deployment of AI in clinical settings, particularly concerning data privacy, algorithmic bias, and accountability in decisionmaking. Finally, understanding the specific training and educational requirements for clinicians to effectively utilize and interpret ML model outputs is another crucial qualitative research area. By addressing these quantitative and qualitative research avenues, the field can further advance the integration of ML into realworld clinical practice for heart failure management.

ACKNOWLEDGES

This work was presented at the 7th International Scientific Mediterranean Research Innovation Congress. The author expresses their gratitude to the UCI Machine Learning Repository for providing access to the Heart Failure Clinical Records Dataset, which was fundamental to this study. The author also acknowledges the open-source community and developers of the R-Shiny framework, whose accessible and powerful tools enabled the development of the interactive analytical application central to this research. The code used in this study has been shared as openthe repository source in GitHub (https://github.com/ckrmustafa/HeartDiseasePr ediction).

REFERENCES

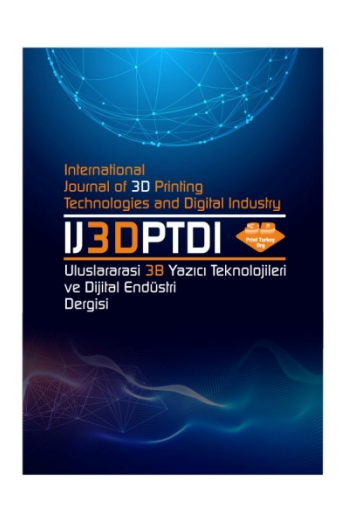
- 1. McDonagh, T. A. et al., "2021 ESC Guidelines for the diagnosis and treatment of acute and chronic heart failure," Eur. Heart J., Vol. 42, Issue. 36, Pages. 3599–3726, 2021.
- 2. L. S. Ranard, S. A. Parikh, and A. J. Kirtane, "COVID-19–Specific Strategies for the Treatment of ST-Segment Elevation Myocardial Infarction in China," J. Am. Coll. Cardiol., Vol. 76, Issue. 11, Pages. 1325–1327, 2020.
- 3. Salman, O. K. M. and Aksoy, B. "Rasgele Orman Ve İkili Parçacik Sürü Zekâsi Yöntemiyle Kalp Yetmezliği Hastalığındaki Ölüm Riskinin Tahminlenmesi," Int. J. 3D Print. Technol. Digit. Ind., Vol. 6, Issue. 3, Pages. 416–428, 2022.

- 4. Yapıcı, İ. Ş., Arslan, R. U., and Erkaymaz, O. "Kalp Yetmezliği Tanılı Hastaların Hayatta Kalma Tahmininde Topluluk Makine Öğrenme Yöntemlerinin Performans Analizi," Karaelmas Fen ve Mühendislik Derg., Vol. 14, Issue. 1, Pages. 59–69, 2024.
- 5. Erdaş, B., and Ölçer, D., "Kalp Yetmezliği Hastalarının Hayatta Kalma Tespiti İçin Makine Öğrenmesi Tabanlı Bir Yaklaşım," Pages. 16–19, 2020.
- 6. Keser, S. B., and Keskin, K., "Kalp Yetmezliği Hastalarının Sağ Kalım Tahmini: Sınıflandırmaya Dayalı Makine Öğrenmesi Algoritmalarının Bir Uygulaması," Afyon Kocatepe Univ. J. Sci. Eng., Vol. 23, Issue. 2, Pages. 362–369, 2023.
- 7. Winger, T., Ozdemir, C., Narasimhan, S. L. and Srivastava, J., "Time-Adaptive Machine Learning Models for Predicting the Severity of Heart Failure with Reduced Ejection Fraction," Diagnostics, Vol. 15, Issue. 6, Pages. 1–11, 2025.
- 8. Aydemir, M., Çakir, M., Oral, O., and Yilmaz, M., "Diagnosis of Cushing's syndrome with generalized linear model and development of mobile application," Medicine (Baltimore)., Vol. 104, Issue. 25, Pages. e42910, 2025.
- 9. Kaba G., and Kalkan, S. B., "Kardiyovasküler Hastalık Tahmininde Makine Öğrenmesi Sınıflandırma Algoritmalarının Karşılaştırılması," İstanbul Ticaret Üniversitesi Fen Bilim. Derg., Vol. 21, Issue. 42, Pages. 183–193, 2022.
- 10. Gürgen, G., and Serttaş, S., "Kalp Yetmezliği Hastalığının Erken Teşhisinde Makine Öğrenimi Algoritmalarının Performans Karşılaştırması," Euroasia J. Math. Eng. Nat. Med. Sci., Vol. 10, Pages. 165–174, 2023.
- 11. Nasution, N., Nasution, F. B., and Hasan, M. A., "Predicting Heart Disease Using Machine Learning: An Evaluation of Logistic Regression, Random Forest, SVM, and KNN Models on the UCI Heart Disease Dataset," IT J. Res. Dev., Vol. 9, Issue. 2, Pages. 140–150, 2025.
- 12. Yang, M., Zhang, X., Fang, W., Zhang, Y., and Fan, X., "Trajectories and Predictors of Frailty in Patients with Heart Failure: A Longitudinal Study," J. Clin. Nurs., Vol. 0, Pages. 1–14, 2025.
- 13. Ribeiro, E. G. et al., "Effect of Telemedicine Interventions on Heart Failure Hospitalizations: A Randomized Trial," J. Am. Heart Assoc., Vol. 14, Issue. 6, p. e036241, 2025.

- 14. Qureshi, M., Ishaq, K., Daniyal, M., Iftikhar, H., Rehman, M. Z., and Salar, S. A. A., "Forecasting cardiovascular disease mortality using artificial neural networks in Sindh, Pakistan," Springer, Vol. 25, Issue 1, 2025.
- 15. Mondal, S., Maity, R., Reports, A. N.-S., "An efficient artificial neural network-based optimization techniques for the early prediction of coronary heart disease: comprehensive analysis," nature.com, Vol. 15, Issue. 4827, Pages. 1–24, 2025.
- 16. Escobar, D. A. C., and Rivera, M. M., "Prediction of Heart Disease Using a Pattern Recognition Approach with Feature Selection and Naïve Bayesian Classifier," Springer, Pages. 347–363, 2025.
- 17. Chitta, S., Chandu, S., Chaitanya, K., Katha, Sundar Junapudi, S., Kumar Yata, V. and Junapudi, S., "Clinical and demographic predictors of heart failure outcomes: A machine learning perspective," Eurasian J. Med. Oncol., Vol. 9, Issue. 1, Page. 133, Jan. 2025.
- 18. Chulde-Fernández, B., et al., "Classification of Heart Failure Using Machine Learning: A Comparative Study," MDPI:Life, Vol. 15, Issue. 3, Pages. 1–18, 2025.
- 19. Khalid Hussain, M., Wani, S., and Abubakar, A., "Examining Mortality Risk Prediction Using Machine Learning in Heart Failure Patients," Int. J. Perceptive Cogn. Comput., Vol. 11, Issue. 1, Pages. 81–87, Jan. 2025.
- 20. Akbulut, B., Çakır, M., Görkem Sarıkaya, M., Oral, O., Yılmaz, M., and Aykal, G., "Artificial intelligence to predict biomarkers for new-onset atrial fibrillation after coronary artery bypass grafting," Turkish J. Thorac. Cardiovasc. Surg., Vol. 33, Issue. 2, Pages. 144–153, Apr. 2025.
- 21. Atacak, İ., "Kalp Yetmezliği Tahmininin Kategorik Olarak Farklı Tip Makine Öğrenmesi Yöntemleri ile Uygulanmasına Yönelik Bir Değerlendirme Çalışması," EMO Bilim. Dergi, Vol. 14, Issue. 1, Pages. 73–95, 2024.
- 22. Yigit, T., Isik, A. H., and Ince, M., "Web-based learning object selection software using analytical hierarchy process," IET Softw., Vol. 8, Issue. 4, Pages. 174–183, 2014.
- 23. Turan, T., Turan, G., and Köse, U., "Uyarlamalı Ağ Tabanlı Bulanık Mantık Çıkarım Sistemi ve Yapay Sinir Ağları ile Türkiye'deki COVID-19 Vefat Sayısının Tahmin Edilmesi," Bilişim Teknol. Derg. Vol. 15, Issue. 2, Pages. 97–105, 2022.

- 24. Almazroi, A. A., Aldhahri, E. A., Bashir, S., and Ashfaq, S., "A Clinical Decision Support System for Heart Disease Prediction Using Deep Learning," IEEE Access, Vol. 11, Issue June, Pages. 61646–61659, 2023.
- 25. Cox, D. R., "The Regression Analysis of Binary Sequences," J. R. Stat. Soc. Ser. B Stat. Methodol., Vol. 20, Issue. 2, Pages. 215–232, 1958.
- 26. Fisher, R. A., "The Use of Multiple Measurements in Taxonomic Problems," Ann. Eugen., Vol. 7, Issue. 2, Pages. 179–188, 1936.
- 27. Hastie, T., Tibshirani, R., and Friedman, J., The Elements of Statistical Learning. New York, NY: Springer New York, 2009.
- 28. Fix E., and Hodges, J. L., "Discriminatory analysis. Nonparametric discrimination: Small sample performance," 1951.
- 29. Cover T., and Hart, P., "Nearest neighbor pattern classification," IEEE Trans. Inf. Theory, Vol. 13, Issue. 1, Pages. 21–27, 1967.
- 30. Maron, M. E., "Automatic Indexing: An Experimental Inquiry," J. ACM, Vol. 8, Issue. 3, Pages. 404–417, 1961.
- 31. Breiman, L., Friedman, J. H., Olshen, R. A. and Stone, C. J., Classification And Regression Trees. Routledge, 2017.
- 32. Breiman, L., "Random forests," Mach. Learn., Vol. 45, Issue. 1, Pages. 5–32, 2001.
- 33. Breiman, L., "Bagging predictors," Mach. Learn., Vol. 24, Issue. 2, Pages. 123–140, Aug. 1996.
- 34. Wright, M. N., and Ziegler, A., "ranger: A Fast Implementation of Random Forests for High Dimensional Data in C++ and R," J. Stat. Softw., Vol. 77, Issue. 1, 2017.
- 35. Schapire, R. E., "The strength of weak learnability," Mach. Learn., Vol. 5, Issue. 2, Pages. 197–227, Jun. 1990.
- 36. Freund, Y., and Schapire, R. E., "A Decision-Theoretic Generalization of On-Line Learning and an Application to Boosting," J. Comput. Syst. Sci., Vol. 55, Issue. 1, Pages. 119–139, Aug. 1997.
- 37. Friedman, J. H., "Greedy function approximation: A gradient boosting machine," Ann. Stat., Vol. 29, Issue. 5, Oct. 2001.

- 38. Vapnik, V. N., The Nature of Statistical Learning Theory. New York, NY: Springer New York, 1995.
- 39. Rumelhart, D. E., Hinton, G. E., and Williams, R. J., "Learning representations by back-propagating errors," Nature, Vol. 323, Issue. 6088, Pages. 533–536, Oct. 1986.
- 40. Chen, T., and Guestrin, C., "XGBoost," in Proceedings of the 22nd ACM SIGKDD International Conference on Knowledge Discovery and Data Mining, 2016, Vol. 13-17-Augu, Pages. 785–794.
- 41. Zou, H., and Hastie, T., "Regularization and variable selection via the elastic net," J. R. Stat. Soc. Ser. B Stat. Methodol., Vol. 67, Issue. 2, Pages. 301–320, 2005.



ULUSLARARASI 3B YAZICI TEKNOLOJİLERİ VE DİJİTAL ENDÜSTRİ DERGİSİ

INTERNATIONAL JOURNAL OF 3D PRINTING TECHNOLOGIES AND DIGITAL INDUSTRY

ISSN:2602-3350 (Online)

URL: https://dergipark.org.tr/ij3dptdi

AN INTELLIGENT SNOW REMOVAL ROBOTIC SYSTEM: TOPOLOGY BASED STRUCTURAL LIGHTWEIGHTING AND POWER CONSUMPTION ANALYSIS

Yazarlar (Authors): Hilmi Saygin Sucuoglu D*

Bu makaleye şu şekilde atıfta bulunabilirsiniz (To cite to this article): Sucuoglu H. S., "An Intelligent Snow Removal Robotic System: Topology Based Structural Lightweighting and Power Consumption Analysis" Int. J. of 3D Printing Tech. Dig. Ind., 9(2): 283-293, (2025).

DOI: 10.46519/ij3dptdi.1733596

Araştırma Makale/ Research Article

Erişim Linki: (To link to this article): https://dergipark.org.tr/en/pub/ij3dptdi/archive

AN INTELLIGENT SNOW REMOVAL ROBOTIC SYSTEM: TOPOLOGY BASED STRUCTURAL LIGHTWEIGHTING AND POWER CONSUMPTION ANALYSIS

Hilmi Saygin Sucuoglu^a*

^aAydin Adnan Menderes University, Faculty of Engineering, Department of Mechanical Engineering, TURKEY

* Corresponding Author: hilmisucuoglu@adu.edu.tr

(Received: 03.07.25; Revised: 23.07.25; Accepted: 08.08.25)

ABSTRACT

This study involves a thorough investigation encompassing the comprehensive design, development, topology optimization and power analysis of a mobile snow removal robotic system. The creation of all subcomponents and assembly models was undertaken using Computer-Aided Design (CAD) tools. The electronic hardware, including components such as batteries, Raspberry Pi, and motor drivers, were selected. The assembly of these parts was then conducted, with the objective of integrating them into the overall structure. Finite element analyses (FEA) were performed to evaluate the system's structural strength and stability. The objective of topology optimization was to minimize the weight and energy consumption of the mobile robot. As a result, an optimized structure achieving a 7% weight reduction and 9% energy savings was developed. A novel feature of this study is the integration of a custom-designed Python-based power analysis tool, enabling precise energy consumption comparison between optimized and non-optimized structures. These combined methods demonstrate a significant improvement over the existing snow removal robotic system.

Keywords: CAD-based Snow Removal Robot, Energy-Efficient Mobile Robot, FEA Simulation, Power Consumption Analysis, Structural Lightweighting, Topology Optimization.

1. INTRODUCTION

There is no universally accepted definition of a robot. However, there are certain characteristics and qualities that can be used to determine whether a device or machine can be considered a robotic system. It is imperative that a robot be capable of environmental awareness, mobility, and energy source utilization. If circumstances require, it is important that the subject has the intelligence to meet the necessary requirements [1-2]. Mobile robots have the capacity to execute a wide range of tasks that are typically undertaken by humans. These tasks may include surveillance, reconnaissance, patrol, firefighting, search and rescue operations, internal security, care work, and entertainment [3-4]. Motion of robotic systems is highly dependent on the planned operating environment. These operating environments can be categorized as air, water and terrestrial. While propellers and screws are generally more useful for operation in aquatic and aerial environments, wheels, tracks, legs and their

combinations can be chosen for terrestrial conditions. In addition to conventional locomotion mechanisms, an additional apparatus has been developed for biologically inspired robots, namely adaptive legs [5-7].

In the context of ground mobile robotic systems, a range of mechanical structures and mechanical architectures have been put forward for both academic and industrial research. The classification of these structures is based on three primary categories: W (wheeled), T (tracked), and L (legged). In addition, four hybrids have been derived from the network, namely LW (leg-wheel), LT (leg-track), WT (wheel-track) and LWT (leg-wheel-track) [8-10].

Nowadays, computer-based and machine learning tools have a pivotal role in the design, analysis and optimization of structures. Solid modelling, utilizing CAD (Computer Aided Design) methodologies, enables designers to

define assemblies, components and subsequently employing the geometry for simulations, analyses and prototyping. Computer-aided engineering (CAE) methodologies encompass virtual prototype simulations and static, kinematic and dynamic analyses [11-13].

Topology optimization is a commonly used practice in product design processes including the automotive and aerospace sectors. The aim of topology optimization is to optimize material distribution within a specified design space; The objectives are to maximize the strength and natural frequencies of the design while decreasing the weight. In the optimization process, the designed volume is divided into smaller elements, a finite element analysis (FEA) model is created, and boundary conditions are respectively applied to perform the FEA. During the analysis process, it is observed that the elements show intermediate density values. The values examined converge to 1 or 0 through a penalization process where the power law is used to penalize elements with higher density [14-17]. The general process diagram of topology optimization is presented in Figure 1.

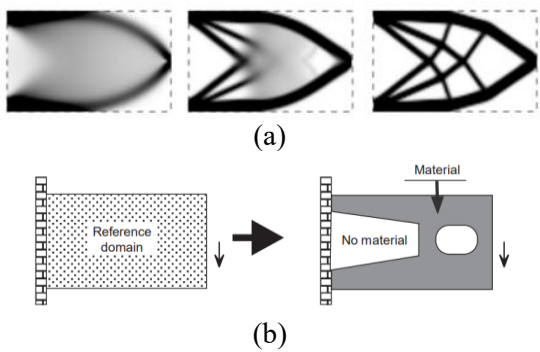


Figure 1. (a) Interpolation (b) The general scheme [13].

Two widely preferred methods for determining the distribution of elements in topology optimization are the Solid Isotropic Material Penalization (SIMP) and the Evolutionary Structural Optimization Technique (ESO).

The SIMP method calculates an optimum material distribution within a given design space for specific load cases, boundary conditions, manufacturing constraints and performance requirements. The density distribution of the material within a design space, denoted by ρ , is discrete and each element is assigned a binary value. For each

element, the assigned relative density may vary between a minimum value, denoted by pmin, and 1, thus allowing intermediate densities to be allocated for elements characterized as porous elements. It has been established that, due to the perpetual nature of the material's relative density, the material's Young's modulus in each element is concomitant with continuous change. The relationship between each element e and the material's relative density factor, denoted as pe, as well as the isotropic model's Young's modulus of elasticity, denoted by E₀, is calculated by means of a power law [14-15,18].

$$E(\rho_e) = \rho_e^{\rho} E_0 \tag{1}$$

Where:

ρ: The density distribution of material ρe: For each element "e" the relation between the material relative density factor

E₀: Young modulus of elasticity of the isotropic material

The stress-based ESO method is typically characterized by the utilization of von Mises stress for the extraction process. Initially, a piece of material of sufficient size to cover the designated area of the final design is divided into a fine mesh of finite elements. The application of loads and boundary conditions is a fundamental aspect of the analysis, which involves the execution of a stress analysis utilizing a finite element program. Given that the structure is composed of numerous minute components, the extraction of material can be readily illustrated by any available method. The stress level at each point can be measured by calculating the average of all stress components. In this context, the von Mises stress is one of the most frequently used criteria for isotropic materials. The von Mises stress is defined as follows in the context of plane stress problems:

$$\sigma^{vm} = \sqrt{\sigma x^2 + \sigma y^2 + \sigma x \sigma y + 3\tau^2 x y}$$
 (2)

In the context of the given problem, σx and σy are defined as the normal stresses in the x and y directions, respectively, and τ_{xy} is represented as the shear stress. The stress level of each element is determined by comparing the von Mises stress of σ_e^{vm} element with the maximum von Mises stress of the whole structure σ_{max}^{vm} . At the conclusion of each finite element

analysis, elements that satisfy the following condition are eliminated from the model:

$$\frac{\sigma_{\rm e}^{\rm vm}}{\sigma_{\rm max}^{\rm vm}} < RRi \tag{3}$$

RRi is the current rejection rate (RR). The commonly accepted limit value for RR is 25 %. The finite element analysis and element removal cycle is iterated using the same RRi value until a steady state is attained. This indicates that no additional elements are being removed during the current iteration. At this stage, the evolutionary rate (ER) is introduced and added to the rejection rate. As the rejection rate increases, it becomes evident that the finite element analysis and element removal cycle are reinitiated until a new steady state is attained [19-20].

Given its proven effectiveness in reducing weight and improving mechanical performance, topology optimization is highly relevant for mobile robotic systems that operate under dynamic and energy-demanding conditions. For snow removal robots reducing structural weight enhances maneuverability on slippery and uneven snow-covered terrain, which directly impacts operational stability and control. Additionally, minimizing energy consumption is critical for ensuring sustained functionality in cold environments, where power supply options are limited and batteries suffer from decreased efficiency. These factors make energy-aware structural design a necessity rather than a preference in such applications. Therefore, applying topology-based methods in the structural design of snow removal robots can lead to lighter, more energy-efficient, and costeffective solutions.

The optimization techniques discussed such as the Solid Isotropic Material Penalization (SIMP) and Evolutionary Structural Optimization (ESO) methods not only provide a theoretical basis for optimal material distribution but also serve as a practical guide to achieving the key design goals of our system: weight reduction, power savings, and structural safety under real-world loads.

Sreeramoju et al. [21] conducted an optimization study. They made a comparison between three different materials. The objective of this study was to provide a selection guide for the material of the drone chassis.

The composition of aluminum A356 T6, aluminum 6061 and ABS plastic materials were analyzed. The results showed that a 35% reduction was gained through optimization. Sobocki et al. [22] concentrated on an industrial application example of topology optimization for a spray tank bracket. The solid isotropic punishing material (SIMP) method was employed under static loads. The integration of finite element analysis (FEA) and topology optimization methodologies resulted in the development of a structure that was both lightweight and durable.

Yao et al. [23] demonstrated a static structural analysis of load-bearing frames. In addition, topology optimization processes were employed to improve the frame design for the parameters of deformation and uniform stress distribution. The results demonstrated that the total mass, deformation and stress were 8.7%, 88.2% and11.7%, respectively.

Snow removal vehicles boast a wide array of applications, along with the ability to swiftly exhibit remove snow and exceptional maneuverability [24]. The most common vehicle used for snow removal is the snow blower. In recent years, there has been a significant increase in the use of robotic systems. This development has led to the of mobile creation systems designed specifically for snow removal. The most prominent product on the market for snow removal is Snowbot. It is an autonomous snow removal robotic system developed by Hanyang Robotics [25].

Despite the growing interest in autonomous snow removal systems, most existing solutions rely on conventional structural designs without optimization for weight or energy efficiency. There is a lack of integrated approaches that combine CAD modeling, finite element analysis, topology-based structural refinement, and power consumption evaluation in a unified framework. This study addresses this gap by proposing a holistic design and evaluation methodology for a snow removal robot, incorporating both structural optimization and a novel energy analysis tool for real-time design feedback and improvement. The present work is a research study for the design and development of a snow removal robot system. The creation of the sub-assemblies and the assembly model was conducted using Computer Aided Design (CAD) tools. Finite element analyses (FEA) were used to evaluate the structural integrity and stability of the system. Then, topology optimization was applied to reduce the weight and energy consumption of the snow removal robot system. A power analysis tool was also proposed to calculate and to compare the energy consumption of structures.

2. MATERIALS AND METHODS

2.1. Design of the Snow Robotic System

In this section, the robotic structure was designed using Fusion 360 software. The components of the assembly, such as the bottom frame, the brush cover module, and the crawler structure, have all been created and assembled correctly. The integration of hardware layouts into the structure is a crucial aspect of the process. The materials of the bottom-frame and brush cover have been selected to be aluminum 6061. The structure was designed to be modular, facilitating ease of assembly. The assembled structure of the snow removal robotic system is illustrated in Figure 2

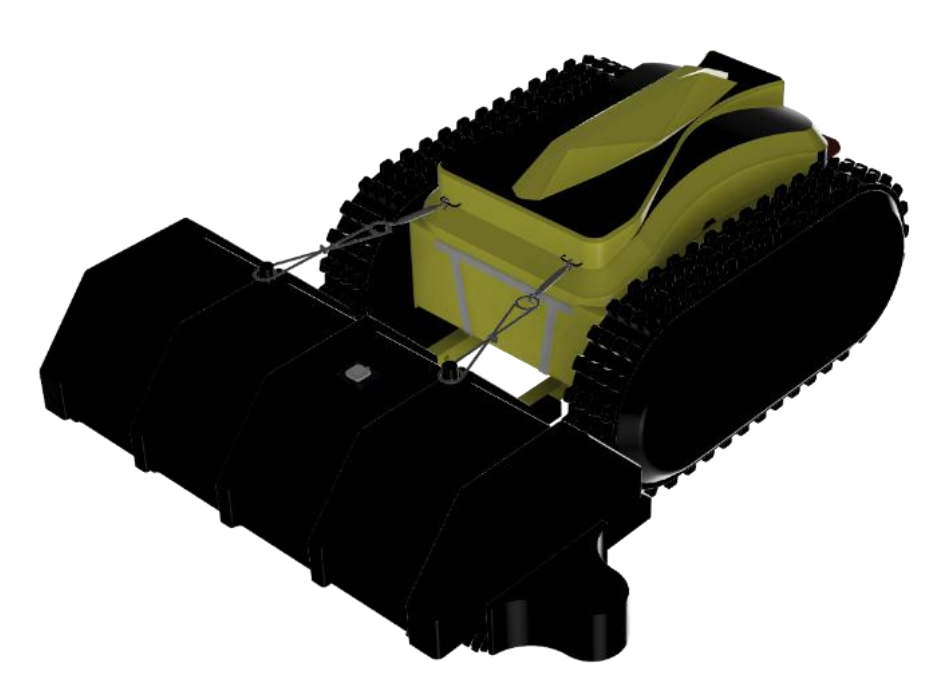


Figure 2. The assembled structure of the snow removal robotic system.

Following the 3D design process, engineering drawing documents including part list and exploded view, and an overall dimension were produced. Those documents were useful for identifying and sourcing the required parts and hardware. Two DC wiper motors of 24V, 20A, 8 Nm torque and 60 rpm were selected to move the robotic system. An appropriate assembly and layout of the crawler modules was designed. The motion control unit was designed with two motor driver boards with a maximum current source of 30 Amperes, Raspberry pi 5,

and Arduino Mega 2560. Two 24 V, 4A compact induction motors (CIMs) were integrated to rotate the snow brush. Five proximity motion sensors and a compass module were used to control the movement of the robotic system. A 24V 40 Ah lithium battery was chosen as the power source for the system. The part list exploded view and overall dimensions of the snow removal robot system structure are shown in Figures 3 and 4, respectively.

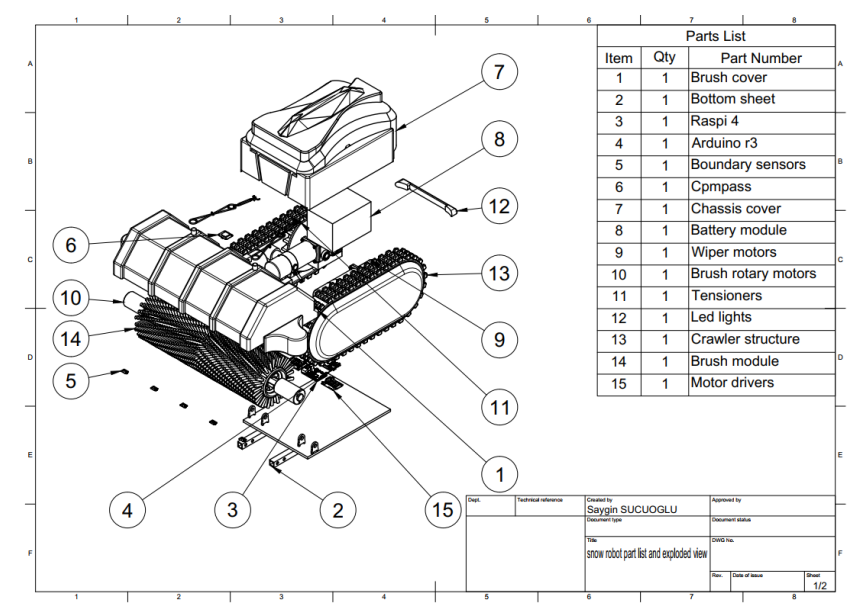


Figure 3. Part list and exploded view.

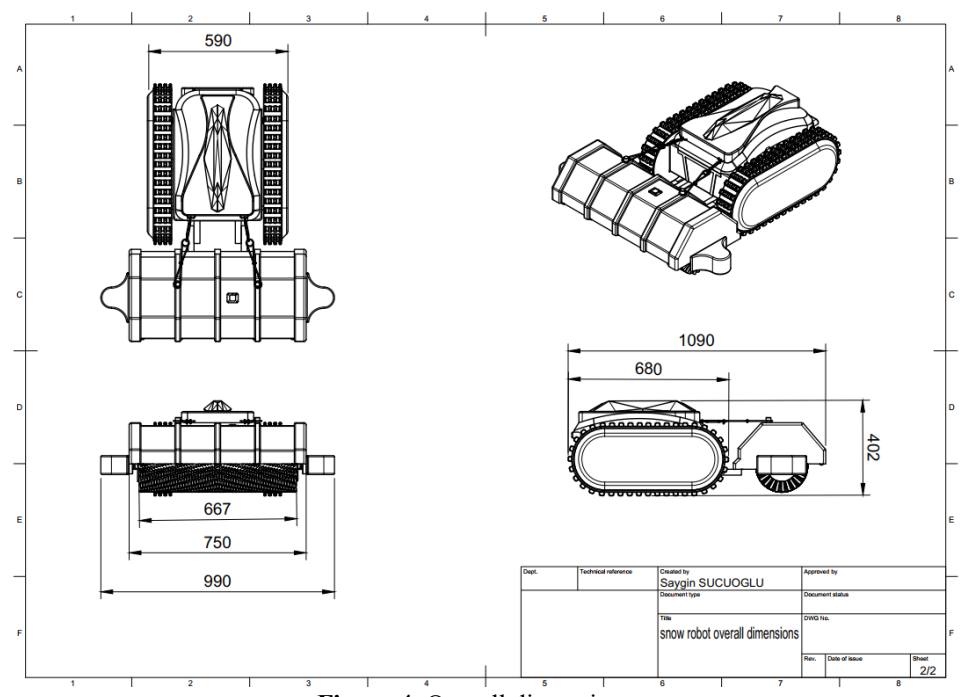


Figure 4. Overall dimensions.

2.2. Engineering Analysis of Preliminary Structure

Engineering analyses were performed using finite element analysis (FEA) to ascertain the structural integrity and stability of the mechanical structure. A significant rationale underlying this approach pertains to the necessity of ascertaining the viability of the topology optimization process. In the case of these models, the materials assigned to the brush cover and chassis cover were aluminum 6061. The application of loads served to verify the resulting safety factor and stress values. The creation of engineering analysis sets was

facilitated within the Ansys Workbench 2024 Static Structural Environment. These analyses were applied separately to the brush and chassis covers. The applied loads are presented in Figures 5 and 6, respectively. The loads were calculated as the sum of the forces due to the actuators, the weights of the structure and the snow load. For the chassis cover, 150 and 750 N forces resulting from the movement of the entire structure and weights were applied. For the brush cover, 720,200 and 400 N forces and 22Nm moment loads caused from the rotation of the brush rotary motors and snow brush and weights were applied.

The finite element models of both components were discretized using tetrahedral elements with a target mesh size of approximately 2 mm. The brush cover model contained nearly 180,000 elements, while the chassis cover model comprised approximately 250,000 elements. A mesh sensitivity analysis was performed to ensure that further refinement had no significant effect on the stress or safety factor results.

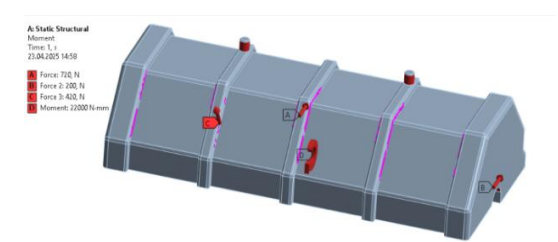


Figure 5. Loads of brush cover.

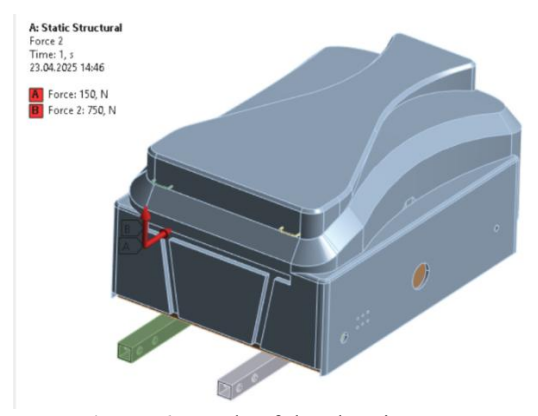


Figure 6. Loads of the chassis cover.

2.3. Topology Optimization

The topology optimization processes were executed utilizing the Ansys Structural Optimization tool. The load conditions employed in this study were consistent with those utilized in preliminary structural optimization engineering analyses. The definitions were selected as topology density, with a threshold value of 60%. Connection zones were designated as preserved areas. which excluded from the optimization processes. The objective function was defined to minimize structural compliance (maximize stiffness) under the applied loads. A total of 30 optimization iterations were performed, with convergence assessed based on density change across the mesh. Manufacturing constraints such as minimum member size were applied to ensure fabrication feasibility. New, optimized structure proposals were obtained through multiple iterations. Utilizing the collated data and the design file output, new optimized structures were created. These newly generated

models are demonstrated in Figures 7 and 8, respectively.



Figure 7. Optimized brush cover.



Figure 8. Optimized chassis cover.

2.4. Power Analysis Tool

The tool has been developed for the purpose of facilitating energy consumption and weight analysis for a snow removal robot system, by means of creating an intuitive graphical user interface (GUI) using Python's tkinter library. The application was utilized for the purpose of conducting comparative power analysis of two robotic de-signs, a process which involves the processing of parts lists detailing components such as motors, batteries, sensors, and coating materials (Figure 9). The tool is utilized by users through the entry of component properties, including voltage, current, quantity, and weight. These properties directly reflect the data present in the parts list. The component entries are added to a cumulative list in a systematic manner, thereby facilitating an iterative and comprehensive analysis. The tool facilitates real-time design evaluation and optimization through the dynamic calculation of total power consumption and total weight. It is notable that the tool incorporates a significant feature in the form of its image visualization capability, which enables users to load and subsequently view component images directly within the GUI. This enhancement in clarity facilitates a more integrated approach to system design, correlating visual representations with numerical analysis.

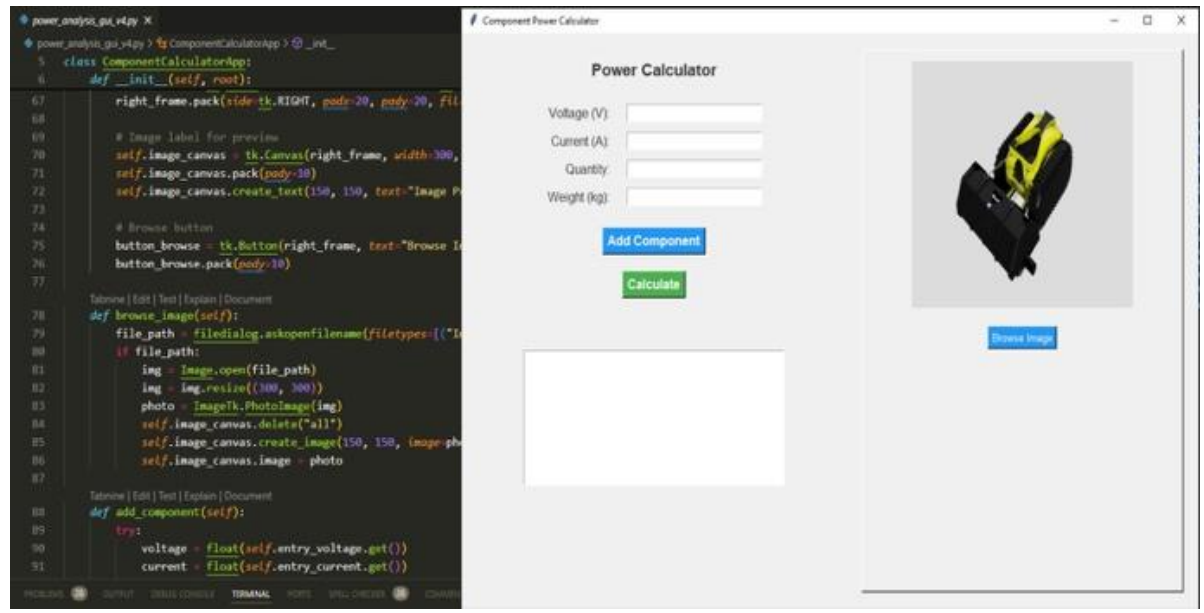


Figure 9. Design of power analysis tool.

In the analysis of the two robotic structures (preliminary and optimized), the tool facilitated the calculation of the total energy requirements and weight distribution based on the parts lists provided. This approach contributed to the identification of design efficiencies, including reduced power consumption and the adoption of lighter chassis configurations. The tool's capacity to execute critical calculations and to visualize components was conducive to the iterative design process and to the improvement of documentation for engineering reports

(Figure 10). Although formal experimental validation of the tool has not yet been completed, the outputs were manually cross-checked with conventional electrical formulas and verified component specifications. This ensured consistency and reliability within the scope of the study. For future work, hardware-based power measurements are planned to further validate and calibrate the tool under actual operating conditions.

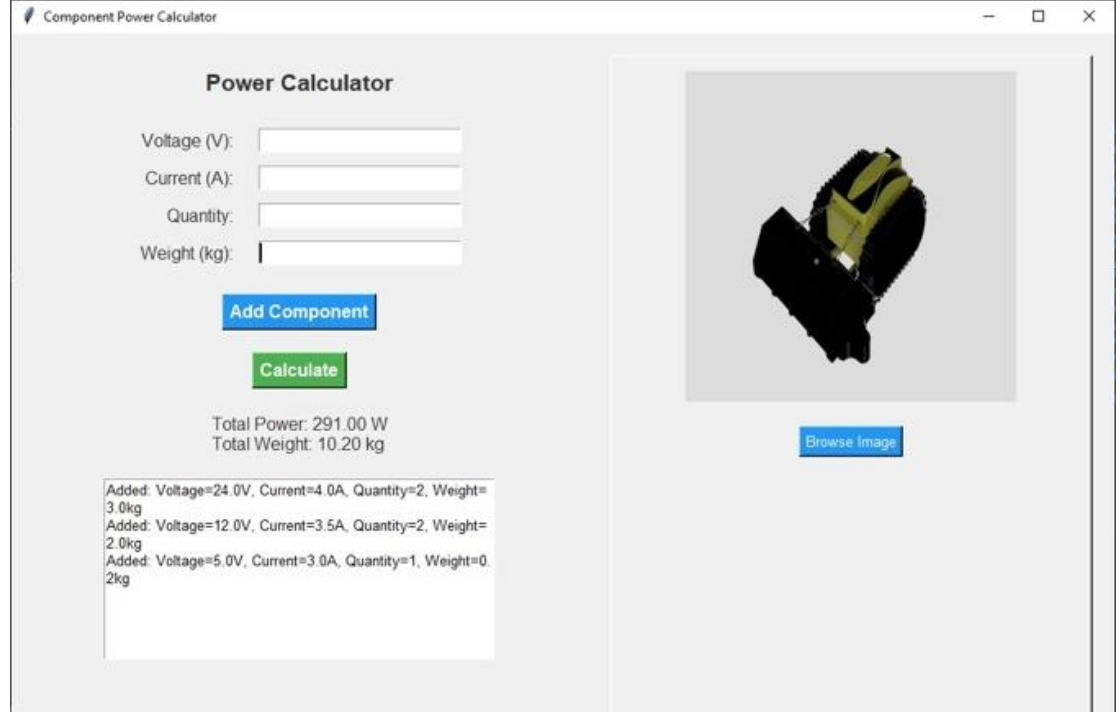


Figure 10. Calculations with power analysis tool.

2.5. Optimized Snow Robotic System

In this section of the study, a new assembly model was devised through the utilization of the optimized covers (Figure 11). The integration of all parts and hardware has been achieved, and the new, optimized structure has been prepared for power analysis.



Figure 11. Optimized snow robotic system.

3. RESULTS AND DISCUSSION

The results of the analysis studies are examined to verify the necessity of the topology optimization study. Preliminary structure calculations indicated that the weights of the brush and chassis covers were approximately 9.5 and 16 kilograms, respectively. The safety factors have been calculated to be in the range of approximately 13.5 and 5.7, which was more than sufficient. The resulting von Mises stresses were also observed to be approximately 7.5 and 15 MPa. The findings of this study indicated implementation of optimization was viable in terms of reducing both the weight and energy consumption of the snow removal robot system. The obtained factor of safety and von Mises stresses values of the brush cover are represented in Figures 12 and 13.

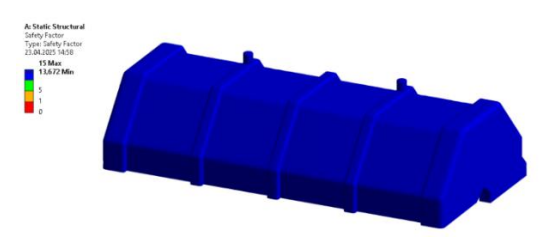


Figure 12. Factor of safety distribution in the preliminary design of the brush cover.



Figure 13. von Mises stress distribution in the preliminary brush cover design.

As demonstrated by the engineering analysis of the optimized structures, the safety factor values for the brush and chassis covers were approximately 2.2 and 5.4, respectively. Furthermore. von Mises stresses approximately 16 and 47 MPa. The analysis results of the optimized brush cover are presented in Figures 14 and 15. The ensuing results demonstrated that the safety factor values remain valid, and the von Mises stresses continue to be within safe limits. Consequently, it is hypothesized that snow robotic system structure can be established using new optimized structures to ensure reduced energy consumption and long-term use.

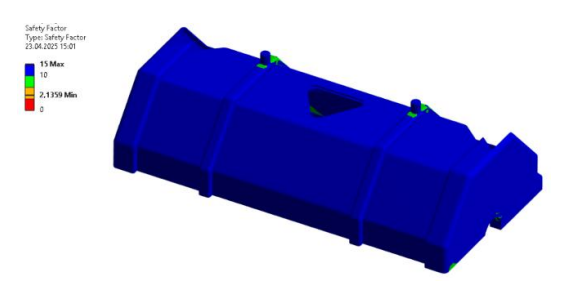


Figure 14. Factor of safety distribution in the optimized brush cover design. The minimum safety factor remains above 2, confirming structural integrity after material reduction.



Figure 15. von Mises stress distribution in the optimized brush cover design, with peak stresses reaching 47 MPa. Stress remains within the allowable limits for aluminum 6061.

The power analysis of the snow robotic system was performed to evaluate the energy efficiency and overall performance of the optimized structure in comparison to the preliminary version. The objective of this analysis was to

quantify the improvements achieved through topology optimization, with a particular focus on reductions in weight, power consumption and energy requirements.

In power analysis standard electrical and energy calculation formulas were used, including:

- a. Power (P) = Voltage (V) \times Current (I)
- b. Total Energy (E) = Power (P) \times Time (t)
- c. Total Power Consumption = \sum (Power consumption of individual components)
- d. Weight comparison = \sum (weights of all components in each design)

Comparison between the optimized and preliminary structures are given in Table 1.

Table 1. Comparison table between preliminary and optimized structure.

and optimized structure.					
Results	Preliminary	Optimized			
	Structure	Structure			
von Mises					
stresses of brush	7.5	16			
cover (MPa)					
von Mises					
stresses of	15	47			
chassis cover	13	7			
(MPa)					
Weight of the	9.5	7.5			
brush cover (kg)	9.3				
Weight of the					
chassis cover	16	10			
(kg)					
Weight of the					
entire system	116	108			
(kg)					
Energy					
consumption	446	405			
(Wh)					

The results showed that the optimized design achieved a 7% reduction in weight, which directly contributed to a decrease in energy consumption and an increase in efficiency. The total energy consumption of the optimized robot was almost 41 Wh lower than that of the preliminary structure, corresponding to a 9% reduction. This enhancement supported longer operational duration without increasing battery capacity. Furthermore, the optimized design's reduced energy consumption indicated the possibility of utilizing smaller or fewer battery modules, which could lead to a reduction in overall system cost and weight. emphasized the pivotal function of design optimization in the advancement of energyefficient robotic systems.

Although the safety factors in the optimized components decreased compared to the preliminary design, the values remained within acceptable engineering limits (2.2 for the brush cover and 5.4 for the chassis cover), indicating sufficient strength for operational loading conditions.

When compared with similar studies, our results are in line with reported trends. For example, Sreeramoju and Rao [20] reported a 35% weight reduction in drone chassis, while Sobocki et al. [21] achieved structural improvement using the SIMP method. Our 7% and 9% energy reductions are considered effective outcomes for a full-scale mobile robotic system.

4. CONCLUSION

In this study, a comprehensive design and analysis workflow was presented for a mobile snow removal robotic system, integrating CAD modeling, finite element analysis, topology optimization, and a Python-based power evaluation tool. The results showed that the proposed optimization strategy successfully reduced the structural weight of the robot by 7% and its energy consumption by 9%, without compromising mechanical safety. outcomes confirm the relevance of topology optimization in enhancing the energy efficiency and structural performance of robotic systems operating in snow-covered environments. This study also introduced a practical power analysis interface that enables designers to assess and compare energy usage during earlystage development. In future work, we aim to construct a physical prototype of the optimized system and conduct experimental validation of the power consumption predictions under realworld operating conditions.

Author Contributions

The percentages of the author(s) contributions are presented below. The author(s) reviewed and approved the final version of the manuscript.

	H. S. S
С	100
D	100
S	100
DCP	100
DAI	100
L	100
W	100
CR	100
SR	100
PM	100
FA	100

C=Concept, D= design, S= supervision, DCP= data collection and/or processing, DAI= data analysis and/or interpretation, L= literature search, W= writing, CR= critical review, SR= submission and revision, PM= project management, FA= funding acquisition.

Conflict of Interest

The author(s) declared that there is no conflict of interest.

Ethical Consideration

Ethics committee approval was not required for this study because there was no study on animals or humans.

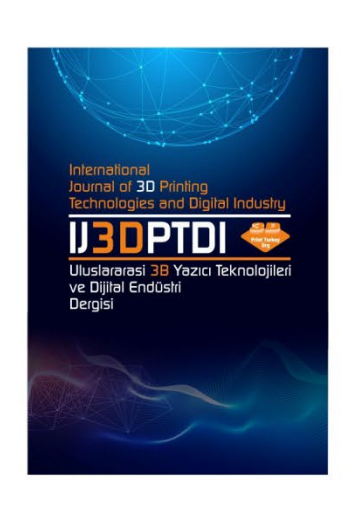
REFERENCES

- 1. Nourbakhsh, I.R. and Siegwart, R., Introduction to Autonomous Mobile Robots, 2004.
- 2. Silva, M.F. and Tenreiro Machado, J.A.T., "A historical perspective of legged robots", Journal of Vibration and Control, Vol. 13, Issues 9–10, Pages 1447–1486, 2007.
- 3. Chen, X., Chen, Y.Q. and Chase, J.G., "Mobile robots—state of the art in land, sea, air, and collaborative missions", 2009.
- 4. Tajti, F., Szayer, G., Kovács, B., Dániel, B. and Korondi, P., "CRM TC covering paper—Robotics trends", IECON 2013 39th Annual Conference of the IEEE Industrial Electronics Society, Pages 48–53, 2013.
- 5. Hahnel, D., Triebel, R., Burgard, W. and Thrun, S., "Map building with mobile robots in dynamic environments", Proceedings of the 2003 IEEE

- International Conference on Robotics and Automation, Pages 1557–1563, 2003.
- 6. Garcia, E., Jimenez, M.A., De Santos, P.G. and Armada, M., "The evolution of robotics research", IEEE Robotics & Automation Magazine, Vol. 14, Issue 1, Pages 90–103, 2007.
- 7. Patnaik, S. and Patnaik, S., "Cybernetic view of robot cognition and perception", Robot Cognition and Navigation: An Experiment with Mobile Robots, Pages 1–20, 2007.
- 8. Behnke, S., "Humanoid robots—from fiction to reality", Künstliche Intelligenz, Vol. 22, Issue 4, Pages 5–9, 2008.
- 9. Durán, B. and Thill, S., "Rob's robot: Current and future challenges for humanoid robots", The Future of Humanoid Robots Research and Applications, Pages 279–300, 2012.
- 10. Valgren, C., Duckett, T. and Lilienthal, A., "Incremental spectral clustering and its application to topological mapping", Proceedings of the 2007 IEEE International Conference on Robotics and Automation, Pages 4283–4288, 2007.
- 11. Sucuoglu, H.S., Bogrekci, I., Demircioglu, P. and Turhanlar, O., "Design & FEA and multi-body system analysis of human rescue robot arm", Advanced Mechatronics Solutions, Pages 651–656, Springer International Publishing, 2016.
- 12. Demir, N., Sucuoglu, H.S., Bogrekci, I. and Demircioglu, P., "Topology optimization of mobile transportation robot", International Journal of 3D Printing Technologies and Digital Industry, Vol. 5, Issue 2, Pages 210–219, 2021.
- 13. O. Yildiz, "Açık Radyo Erişim Ağı Üzerine Sistematik Bir İnceleme: Bileşenler, Uygulamalar ve Gelecek Perspektifleri", *BSJ Eng. Sci.*, Vol. 8, Issue. 4, Pages. 1235–1244, 2025.
- 14. Bendsøe, M.P. and Kikuchi, N., "Generating optimal topologies in structural design using a homogenization method", Computer Methods in Applied Mechanics and Engineering, Vol. 71, Issue 2, Pages 197–224, 1988.
- 15. Zhu, J.H., Zhang, W.H. and Xia, L., "Topology optimization in aircraft and aerospace structures design", Archives of Computational Methods in Engineering, Vol. 23, Pages 595–622, 2016.
- 16. Das, R., Jones, R. and Xie, Y.M., "Design of structures for optimal static strength using ESO", Engineering Failure Analysis, Vol. 12, Issue 1, Pages 61–80, 2005.

- 17. Abolbashari, M.H. and Keshavarzmanesh, S., "On various aspects of application of the evolutionary structural optimization method for 2D and 3D continuum structures", Finite Elements in Analysis and Design, Vol. 42, Issue 6, Pages 478–491, 2006.
- 18. Rozvany, G.I.N., "Exact analytical solutions for some popular benchmark problems in topology optimization", Structural Optimization, Vol. 15, Pages 42–48, 1998.
- 19. Ozkal, F.M. and Uysal, H., "Determination of the best topology for deep beams with web opening by the evolutionary method", 8th International Congress on Advances in Civil Engineering, Gazi Mağusa, North Cyprus, 2008.
- 20. Yurdem, H., Degirmencioglu, A., Cakir, E. and Gulsoylu, E., "Measurement of strains induced on a three-bottom moldboard plough under load and comparisons with finite element simulations", Measurement, Vol. 136, Pages 594–602, 2019.
- 21. Sreeramoju, S. and Rao, M.S., "Design and analysis of quad copter chassis using shape optimization technique", International Journal for Research in Applied Science and Engineering Technology, Vol. 11, Issue 3, 2023.

- 22. Sobocki, S., Legutko, S., Wojciechowski, J. and Szymczyk, S., "Topology optimization as a design tool—An industrial example of spray tank bracket", Acta Technica Napocensis Series: Applied Mathematics, Mechanics, and Engineering, Vol. 65, Issue 4s, 2023.
- 23. Yao, M.A., Wei, S.U., Lai, Q., Yu, Q. and Wan, Y., "Finite element analysis and topology optimization design of lightweight Panax notoginseng transplanting machine frame", Journal of Intelligent Agricultural Mechanization, Vol. 5, Issue 2, Pages 51–60, 2024.
- 24. Zhao, W., Wang, L., Zhang, Y., Cao, X., Wang, W., Liu, Y. and Li, B., "Snow melting on a road unit as affected by thermal fluids in different embedded pipes", Sustainable Energy Technologies and Assessments, Vol. 46, 101221, 2021.
- 25. Zonta, T., Selvanathan, J., Patel, J., Wilson, K., Kaura, H., Berry, C. and Barari, A., "Autonomous snowblower utilizes internet for minimal power consumption", 2021 14th IEEE International Conference on Industry Applications, Pages 686–693, 2021.



ULUSLARARASI 3B YAZICI TEKNOLOJİLERİ VE DİJİTAL ENDÜSTRİ DERGİSİ

INTERNATIONAL JOURNAL OF 3D PRINTING TECHNOLOGIES AND DIGITAL INDUSTRY

ISSN:2602-3350 (Online)

URL: https://dergipark.org.tr/ij3dptdi

ELEKTRİKLİ ARAÇ BESLEME SİSTEMLERİNDE 3B BASKININ ÇEVRESEL ETKİLERİ VE MEVZUAT UYUMU

ENVIRONMENTAL IMPACTS AND REGULATORY COMPLIANCE OF 3D PRINTING IN ELECTRIC VEHICLE SUPPLY EQUIPMENT

Yazarlar (Authors): Zühre Aydın 100*

Bu makaleye şu şekilde atıfta bulunabilirsiniz (To cite to this article): Aydın Z., "Elektrikli Araç Besleme Sistemlerinde 3B Baskının Çevresel Etkileri ve Mevzuat Uyumu" Int. J. of 3D Printing Tech. Dig. Ind., 9(2): 294-309, (2025).

DOI: 10.46519/ij3dptdi.1715813

Araştırma Makale/ Research Article

ELEKTRİKLİ ARAÇ BESLEME SİSTEMLERİNDE 3B BASKININ ÇEVRESEL ETKİLERİ VE MEVZUAT UYUMU

Zühre Aydına **

^aEnerji Piyasası Düzenleme Kurumu, TÜRKİYE

* Sorumlu Yazar: <u>zaydin@epdk.gov.tr</u>

(Geliş/Received: 07.06.25; Düzeltme/Revised: 14.07.25; Kabul/Accepted: 15.07.25)

ÖZ

Elektrikli araçların yaygınlaşması, karbon nötrlüğü hedefleri doğrultusunda sadece araçların kendisiyle değil, aynı zamanda şarj altyapısının çevresel etkileriyle de doğrudan ilişkilidir. Bu çalışma, 3B baskı teknolojilerinin elektrikli araç şarj altyapısında kullanılan bileşenlerdeki ve elektrikli araç besleme donanımındaki karbon ayak izine etkisini değerlendirmekte ve söz konusu bileşenlerin çevresel mevzuatlara uygunluğunu analiz etmektedir. Literatürde nadiren karşılaşılan şekilde, karbon salımı, mevzuat uyumu, üretim maliyeti, yapısal dayanıklılık ve üretim süresi gibi çoklu kriterler bir arada ele alınmıştır. Çok kriterli karar verme yöntemleri kullanılarak, üç boyutlu baskı yoluyla üretilen bileşenlerin geleneksel yöntemlerle üretilenlere kıyasla çevresel etki, maliyet ve mevzuat açısından uygunlukları değerlendirilmiştir. Monte Carlo tabanlı Analitik Hiyerarşi Süreci ile belirlenen kriter ağırlıkları doğrultusunda, İdeal Çözüme Benzerliğe Göre Sıralama Tekniği ile geleneksel ve üç boyutlu baskı üretim yöntemlerinin çevresel ve yapısal uygunlukları karşılaştırılmıştır. Bulgular, üç boyutlu baskı ile üretilmiş bileşenlerin karbon salımında daha düşük üretim kaynaklı karbon emisyonu sunduğunu, ancak bu etkinin sürdürülebilir olması için mevzuatla entegre tasarım kriterlerinin gözetilmesi gerektiğini ortaya koymuştur. Çalışma, sürdürülebilir dijital üretim teknolojilerinin enerji altyapısına entegrasyonu konusunda özgün bir hesaplama metodolojisi çerçevesinde katkı sunmaktadır.

Anahtar Kelimeler: Elektrikli Araç, 3B Baskı, Karbon Ayak İzi, Monte Carlo AHP, TOPSIS, Çok Kriterli Karar Verme, Dijital Üretim, Elektrikli Araç Besleme Donanımı

ENVIRONMENTAL IMPACTS AND REGULATORY COMPLIANCE OF 3D PRINTING IN ELECTRIC VEHICLE SUPPLY EQUIPMENT

ABSTRACT

The widespread adoption of electric vehicles is directly linked not only to the vehicles themselves but also to the environmental impacts of the associated charging infrastructure, in alignment with carbon neutrality targets. This study evaluates the carbon footprint of components used in electric vehicle charging infrastructure and electric vehicle supply equipment through 3D printing technologies while also analyzing them. It also analyzes their compliance with relevant environmental regulations. Unlike most studies in the literature, this research simultaneously considers multiple criteria including carbon emissions, regulatory compliance, production cost, structural durability, and production time. Using multi criteria decision-making methods, the environmental impact, cost efficiency, and regulatory alignment of 3D printed components are compared to those produced by conventional methods. Based on criterion weights determined through a Monte Carlo based Analytic Hierarchy Process, the Technique for Order Preference by Similarity to Ideal Solution is employed to rank conventional and additive manufacturing technologies according to their environmental and structural suitability. The findings reveal that 3D printed components

offer lower production related carbon emissions; however, for this advantage to be sustainable, integration with regulatory compliant design principles is essential. This study provides an original methodological framework for evaluating the integration of sustainable digital manufacturing technologies into energy infrastructure systems.

Keywords: Electric Vehicle, 3D Printing, Carbon Footprint, Monte Carlo AHP, TOPSIS, Multi-Criteria Decision Making, Digital Manufacturing, Electric Vehicle Supply Equipment

1. GİRİŞ

Elektrikli araç (EA) Şarj Ekipmanları/Elektrikli Araç Besleme Donanımı (Electric Vehicle Supply Equipment, EVSE) üretiminde üç boyutlu (3B) baskı teknolojisinin benimsenmesi, ulasım sektörünün karbonsuzlastırılmasında önemli bir potansiyel göstermektedir. Curran vd. [1], yeni nesil araçlarda enerji aktarma bileşenlerinin hızlı 3B baskı yoluyla üretilen prototiplemesi için Büyük Ölçekli Eklemeli Üretim (Big Area Additive Manufacturing, BAAM)'in uygulanabilirliğini göstererek, geleneksel yöntemlere kıyasla geliştirme süresinde bataryalı elektrikli aktarma bileşeninin entegrasyonunu gerçekleştirmiştir. Bilgisayar Destekli Tasarım (Computer Aided Design, CAD) 'dan fiziksel parçaya uzanan bu entegre süreç, geleneksel şasi geliştirme yöntemlerine kıyasla önemli ölçüde zaman tasarrufu sağlamış ve prototipleme süreçlerini hızlandırmadaki potansiyelini ortaya koymuştur. Kang vd. [2], büyük veri analitiğini kullanarak enerji tüketim desenlerini optimize eden akıllı şarj sistemleri geliştirmiş ve bu sayede yoğun talep dönemlerinde şebeke üzerindeki vükü azaltmıstır. Hachey [3], EA üretimi için mikro-fabrika modelini inceleyerek, dağıtılmıs 3B baskı tesislerinin tedarik zinciri emisyonlarını %35'e kadar azaltabileceğini ve kitlesel özelleştirmeyi mümkün kılabileceğini ortaya koymuştur. Moon vd. [4], veri odaklı üretim sistemlerinin gerçek zamanlı kaynak optimizasyonu yoluyla sürdürülebilir üretimi nasıl desteklediğini vurgulamıştır. Tseng ve Li [5], özelleştirilmiş EA bileşenleri için optimal 3B baskı parametrelerini seçmek üzere Analitik Ağ Süreci (Analytical Network Process, ANP) ve İdeal Çözüme Benzerliğe Göre Sıralama Tekniği (Technique for Order Preference by Similarity to Ideal Solution, TOPSIS) yöntemlerini kullanan bir karar verme çerçevesi sunmus ve malzeme verimliliğinde %22'lik bir iyileşme sağlamıştır.

Bu yaklaşımlar, EVSE gelişiminin hem teknik hem de çevresel yönlerini ele almaktadır.

EA şarj altyapısında standardizasyon çabaları önemli bir rol oynamıştır. Pallander [6], araçtan sebekeye (Vehicle to Grid, V2G) iletişim için HomePlug Green PHY standardını uygulamış, Serohi [7] ise 3B baskının kesintiler sırasında tedarik zinciri dayanıklılığını nasıl artırdığını belgeleyerek bu alana katkıda bulunmuştur. Elavarasan vd. [8], akıllı şarjın 2030 yılına kadar AB ulaşım sektörü emisyonlarını %18 ile %25 oranında azaltabileceğini gösteren kapsamlı karbonsuzlaşma stratejileri analizi sunmuştur. Zhang ve Ran [9], lityum iyon (LIB) ve sodyum iyon (SIB) bataryalarında yük/iyon tasınımını yönelik ivilestirmeye 3B karbon elektrotların tasarım stratejilerini incelemeyi amaclamıstır. Calışmada, elektrot mimarilerinin iyon ve elektron iletimi üzerindeki etkilerini optimize etmek amacıyla çeşitli malzeme mühendisliği teknikleri, nano/mikro yapılar ve gözenekli tasarım yaklaşımları değerlendirilmiştir. Yöntem olarak literatürdeki güncel calısmalar derinlemesine analiz edilmis; elektrot geometrisinin, elektriksel iletkenliğin ve iyon difüzyon yollarının performans üzerindeki etkileri sistematik olarak sınıflandırılmıştır. Sonuç olarak, 3B karbon bazlı elektrotların enerji yoğunluğu, döngü kararlılığı ve iletkenlik açısından önemli avantajlar sunduğu gösterilmiş, gelecekteki batarya teknolojileri için yüksek performanslı elektrot tasarımı açısından yönlendirici ilkeler ortaya konulmuştur.

Malzeme bilimi ve üretim alanındaki son gelişmeler ilerlemeyi daha da hızlandırmıştır. Tarancón vd. [10], enerji depolama ve dönüşüm sistemlerinde 3B baskılı enerji bileşenlerinin EA sistemlerinde de %30 ağırlık azaltımı sağlayabileceğini belirtmiştir. Jovanović vd. [11], eklemeli olarak üretilmiş otonom araç

bileşenlerinin %23 daha düşük karbon ayak izine sahip olduğunu raporlamıştır. Rosado vd. [12], şarj verimliliğini izlemek için düşük maliyetli enerji sayaçları geliştirerek veri odaklı optimizasyona olanak tanımıştır. Rabih vd. ile Hussein vd. [13-14], sürdürülebilir EA gelişimi çerçevesinde sırasıyla kablosuz şarj ve araç modelleme çerçevelerini ilerleterek teknik performans ve emisyon azaltımı arasında sinerji yaratmıştır.

Sürdürülebilir EA gelişimi için Çok Kriterli Karar Verme (ÇKKV) önemli bir metodoloji haline gelmiştir. Kumar vd. [15], 12 teknik ve çevresel parametreyi kullanarak motor seciminde optimizasyon yapmış, Kumar ve Farhan [16] ise şebeke güvenilirliğini %19 artıran optimal şarj istasyonu yerleşim algoritmaları geliştirmiştir. Prasittisopin [17], 3B baskının akıllı şehir gelişimine katkısını %28 daha hızlı altyapı yayılımı gösteren vaka çalışmalarıyla ortaya [18], koymuştur. batarya Sama yoğunluğunu %40 artırabilecek güçlendirilmiş malzemeleri tanıtarak EA menzili ve sari sıklığı üzerinde önemli bir etki yaratmıştır.

Dijital üretim ve döngüsel ekonomi ilkelerinin kesisimi kapsamında; Singh ve Sehgal [19], 3B ömrünü baskının kullanım tamamlamıs bileşenlerin yeniden üretimini nasıl mümkün kıldığını ve malzeme atıklarını %65'e kadar azaltabileceğini belgeleyerek bu alana katkıda bulunmuştur. Shuker [20], elektromekanik sistemler için gelişmiş yeniden üretim teknikleri gelistirerek genisletmistir. bu arastırmayı Marinkovic [21], EA gövde ağırlığını %30 azaltabilecek sürdürülebilir kompozit malzemeleri tanımlamış ve Owen ile Hayes [22], bu yeniliklerin yenilenebilir enerji entegrasyonu ile birleştirildiğinde 2030 yılına kadar üretim emisyonlarını %50 azaltabileceğini öngörmüştür. Jaller vd. [23], sıfır ve sıfıra yakın emisyonlu araçların benimsenmesini etkileyen faktörleri değerlendirmeyi amaçlamıştır. Araç türleri olarak hibrit elektrikli, batarya elektrikli ve hidrojen yakıt hücreli sistemler ele alınmıştır. Düşük anket katılımı nedeniyle uzman görüşlerine dayalı Küresel Bulanık Analitik Hiyerarşi Süreci (AHP) ve TOPSIS yöntemiyle çok kriterli karar analizi gerçekleştirilmiştir. Sonuçlar, ekonomik, çevresel ve altyapısal açılardan bataryalı EA' ların kısa

mesafelerde daha avantajlı olduğunu göstermiştir. Sonuçlar, sıfir emisyonlu araçların benimsenmesinin önündeki temel engellerin altyapı eksikliği, menzil kaygısı ve maliyet yapısı olduğunu ortaya koyarken; politika teşvikleri, filo dönüşüm planları ve teknolojik gelişmelerin bu araçların yaygınlaşmasında kritik rol oynayacağını göstermiştir.

EVSE bileşenlerinin 3B baskı teknolojisiyle üretilmesi, üretim süreçlerinin dijitalleşmesini sağlarken aynı zamanda karbon nötrlüğü hedefleri doğrultusunda çevresel ve teknik düzenlemelere yüksek düzeyde uyum gerektirir. EA şarj istasvonlarında kullanılan 3B baskı teknolojileriyle üretilen parçaların güvenli, dayanıklı ve standartlara uygun olması için belirli teknik düzenlemelere uyulması önemlidir. Bu kapsamda, üretimde kullanılan malzemelerin toksik içeriğe sahip olmaması için Zararlı Maddelerin Kısıtlanması Direktifi (Restriction of Hazardous Substances, RoHS) ve Kimvasalların Kaydı, Değerlendirilmesi, İzni ve Kısıtlanması Tüzüğü (Registration, Evaluation, Authorisation and Restriction of Chemicals, REACH) gibi düzenlemeler doğrultusunda kimyasal güvenlik süreçlerinin sağlanmalıdır. Üretim sürdürülebilirliğini güvence altına almak amacıyla, Çevre Yönetim Sistemi Standardı (Environmental Management System, ISO 14001) ile kurumsal çevre politikalarının uygulanması ve ürünlerin çevresel etkilerinin yaşam döngüsü boyunca sistematik şekilde analiz edilmesini sağlayan Yaşam Döngüsü Değerlendirmesi Standartları (Life Cvcle Assessment Standards, ISO 14040 / ISO 14044) dikkate alınmalıdır [24-27]. Avrupa Birliği (AB) pazarına sunulacak ürünler için CE (Conformité Européenne) işareti kapsamında temel sağlık, güvenlik ve çevre gerekliliklerine uygunluk belgelenmeli, ayrıca Elektrikli ve Elektronik Atık Yönetimi Direktifi (Waste of Electrical and Equipment Electronic Directive, WEEE) çerçevesinde geri dönüştürülebilirlik tasarım sürecine entegre edilmelidir. 3B baskıya özgü standartlar ise özellikle ISO/ASTM 52900 serisi altında tanımlanmakta olup; parça tasarımı (ISO/ASTM 52910), eklemeli üretimde dosya formatı uyumluluğu (ISO/ASTM 52915) ve tedarik edilen parçalar için kalite gereksinimleri (ISO/ASTM 52901) gibi temel teknik ilkeleri

Bu standartlar. kapsamaktadır. **EVSE** bileşenlerinin TS EN IEC 62196 gibi elektriksel bilesen güvenlik normları ve yukarıda belirtilen cevresel regülasyonlarla birlikte değerlendirilmesine olanak tanıyarak, sürdürülebilir üretim zincirinde izlenebilirlik ve teknik güvenliği bütüncül biçimde sağlamaktadır [28-34]. Türkiye'de EA şari sistemleri özelinde TS EN IEC 61851-1 standardı kapsamında şarj ünitelerinin teknik performans, güvenlik ve haberleşme protokolleri tanımlanmakta; ayrıca EA şarj istasyonları için güvenlik kurallarını, muayene, deney ve yeterliliğin gereklerini belirtleven TS 13912 standardı, ekipmanlarında kullanılacak bileşenlerin çevresel ve elektriksel güvenlik kriterlerini içermektedir. Bu bağlamda, EVSE bileşenlerinin 3B baskı ile üretiminde **TSE** onaylı standartların entegrasyonu, yerel regülasyonlara uygunluk açısından kritik önemdedir [35-36]. TS EN IEC 61439-7 standardı, elektrikli araç şarj istasyonları gibi özel uygulamalar için alçak gerilim güvenlik ve performans panolarının gerekliliklerini tanımlar; 3B baskılı panoların hafif tasarım, özellestirilebilirlik ve hızlı prototipleme avantajları, bu standart kapsamında edilerek uygunluk sağlayabilir Standartlara uyum, EVSE sistemlerinin 3B baskı teknolojisi ile üretilen parçaları için yalnızca çevresel fayda sağlamakla kalmayıp aynı zamanda kullanıcı güvenliği ve uluslararası pazar erisimi acısından da önemlidir.

Dünyada mevzuat ve uygulama yaklaşımları doğal olarak farklılık gösterse de AB, EA araçlar konusunda, özellikle mevzuat gelistirme ve destekleyici politika çerçevesi oluşturma açısından öncü olmuştur. Bu kapsamda Yeşil Mutabakat (Green Deal) gibi stratejik belgelerle bu süreci yapılandırmıştır [38]. Bununla birlikte, AB, EA'ların ticarileştirilmesi ve düzenlenmesi konusunda Cin ve ABD'den farklı, kendi normatif yapısına özgü bir yol izlemekte, özellikle veri yönetimi, dijital hizmetler ve güvenlik politikaları gibi alanlarda Dijital Hizmetler Yasası (Digital Services Act, DSA), Genel Veri Koruma Tüzüğü (General Data Protection Regulation, GDPR) gibi düzenleyici mekanizmalar çerçevesinde politika üretmektedir [39-40]. Bu bağlamda, EA şarj altyapısında düşük atık üretim avantajına sahip 3B baskı

teknolojilerini benimsemesi, yalnızca karbon salımını azaltan sürdürülebilir üretim stratejilerine katkı sunmakla kalmamakta, aynı zamanda yerli üretim kapasitesinin artırılması ve teknoloji tabanlı sanayi politikalarının uygulanmasına da doğrudan hizmet etmektedir. Bölgesel farklılıkları dikkate alan çok katmanlı bir değerlendirme perspektifi, hem uygulayıcılar hem de politika yapıcılar açısından anlamlı sonuçlar üretmektedir. EA şarj altyapısında ve genel otomotiv üretiminde düşük atık üretim avantaiına sahip baskı teknolojilerini 3B benimsemesi, yalnızca karbon emisyonlarını azaltan sürdürülebilir üretim stratejilerine katkı sunmakla kalmamakta, aynı zamanda yerli üretim kabiliyetini artırarak sanayide dijitallesme ve döngüsel ekonomi hedeflerine hizmet etmektedir [41-42].

3B baskı teknolojilerinin EA bileşenlerinin üretiminde sunduğu çevresel avantajlara rağmen, özellikle seri üretim ölceğinde maliyet etkinliği konusu literatürde sınırlı incelenmiştir. 3B baskı döngüsel ekonomi ve düşük karbon emisyonu hedeflerine katkıda bulunmaktadır ancak yüksek üretim süresi ve malzeme maliyetleri nedeniyle bu teknolojinin geleneksel vöntemlerle rekabetçiliğinin detaylı analizi literatürde yer almamaktadır. Bu çalışma, bu literatür boşluğunu dikkate alarak, 3B baskı teknolojilerinin çevresel kriterli modelivle etkilerini cok karar değerlendirirken, maliyet boyutunu da sınırlılıklar kapsamında ele almaktadır.

Bu çalışmanın amacı, EA şarj ekipmanları ve diğer bilesenlerinin üretiminde kullanılan 3B baskı gibi farklı imalat teknolojilerinin, karbon salımı, mevzuat uyumu, üretim maliyeti, yapısal dayanıklılık ve üretim süresi parametreleri çerçevesinde; karbon ayak izi, enerji verimliliği ve çevresel sürdürülebilirlik hedeflerine katkısını çok kriterli karar analizi ile değerlendirmektir. Bu kapsamda kriter ağırlıkları, karar kriterlerindeki belirsizlikleri ve varyasyonları istatistiksel olarak modelleyerek daha güvenilir ve sağlam ağırlık değerleri elde eden Monte Carlo tabanlı Analitik Hiyerarşi Süreci (MC-AHP) ile belirlenmiş, alternatif üretim yöntemleri ise her alternatifin ideal çözüme olan göreli yakınlığını ölçerek çok kriterli karar problemlerinde en uygun seçeneği belirleyen TOPSIS yöntemiyle karşılaştırılmıştır.

2. METODOLOJİ: KARBON NÖTR HEDEFLER DOĞRULTUSUNDA EVSE ÜRETİMİNDE 3B BASKI TEKNOLOJİSİ VE ÇOK KRİTERLİ KARAR VERME YAKLASIMI

Çalışmada önerilen yöntem ile AHP kriter seçiminde belirsizlik Monte Carlo simülasyonu ile modellenmiş, TOPSIS ile ideal çözüme göre sistematik sıralama imkanı sunulmuştur.

Bu çalısma, EVSE üretiminde 3B baskı teknolojilerinin uygulanabilirliğini sürdürülebilirlik etkisini ÇKKV yaklaşımıyla değerlendirmeyi amaçlamaktadır. Temel amaç, geleneksel **EVSE** üretiminde imalat karşılaştırıldığında 3B baskı yöntemleriyle teknolojisinin karbon nötrlüğü hedeflerine katkısını teknik, çevresel ve düzenleyici kriterler açısından sayısal olarak analiz etmektir. Bu doğrultuda, MC-AHP ve TOPSIS entegre edilerek hibrit bir karar destek metodolojisi olusturulmustur. Calısmada karar verici konumundaki enerji sektörü yöneticilerinin, alternatif üretim teknolojileri arasından en uvgulanabilir sürdürülebilir ve vöntemi seçebilmelerine olanak sağlayan MC-AHP ile TOPSIS yöntemlerinin birlikte kullanıldığı entegre bir ÇKKV modeli geliştirilmiştir.

MC-AHP, karar vericinin öznel yargılarından kaynaklanan belirsizlikleri istatistiksel olarak modellemek ve kriter ağırlıklarını daha güvenilir bir şekilde elde etmek amacıyla bu çalışmada tercih edilmiştir. Bu yöntem, klasik AHP'nin deterministik doğasını genişleterek, özellikle karbon salımı, mevzuat uyumu ve üretim süresi gibi çevresel ve teknik kriterlerin ağırlıklandırılmasında stokastik varyasyonları dikkate almayı mümkün kılmaktadır. MC-AHP kullanım amacı ve gerekçesi, hem belirsizlik içeren karar ortamlarında daha güvenilir kriter ağırlıkları üretmek, hem de geleneksel AHP'nin karar verici öznelliğine dayalı deterministik yapısını istatistiksel yaklaşımlarla desteklemektir [43-44].

Çalışmada MC-AHP ile kriter ağırlıkları belirlenmiş, bu ağırlıklar TOPSIS yöntemine entegre edilerek her üretim yönteminin ideal çözüme yakınlığı hesaplanmıştır. TOPSIS yöntemi, her bir alternatifin pozitif ideal (en iyi)

ve negatif ideal (en kötü) çözümlere olan Öklidven uzaklığını esas alarak, alternatiflerin çok kriterli bir yapıda sıralanmasını sağlar. Bu yöntemin tercih edilme nedeni, karbon ayak izi, mevzuat uyumu, maliyet, üretim süresi ve yapısal bütünlük gibi farklı ölçüm türlerine sahip kriterleri normalize ederek tek bir skorla karşılaştırma imkânı sunmasıdır. Böylece, sürdürülebilirlik temelli karar verme süreci hem istatistiksel hem de analitik olarak sağlamlaştırılmıştır [45-47].

Bu çalışmada kullanılan kriterler ve üretim teknolojisi alternatifleri, tematik analiz temelli bir literatür tarama süreciyle yapılandırılmıştır. İlk olarak, Google Scholar, Scopus ve Web of Science veri tabanlarında, karbon ayak izi, mevzuat uyumu, maliyet, üretim süresi ve yapısal dayanıklılık anahtar kelimeleri kullanılarak, 2020 sonrası yayımlanan 3B baskı teknolojilerine ilişkin Yaşam Döngüsü Değerlendirmesi (Life Cycle Assessment, LCA) temelli akademik yayınlar incelenmiştir. Bu literatür taramasında yer alan çalışmalarda, çevresel ve yapısal performans göstergeleri sistematik olarak kodlanmıs ve tematik analiz yöntemiyle gruplanarak çalışmada kullanılan kriter seti oluşturulmuştur. Üretim teknolojilerine ilişkin alternatifler ise, yine literatürden elde edilen çevresel etki karşılaştırmalarına ve Çevresel Ürün Beyanı (Environmental Product Declaration, EPD) veri tabanlarından alınan nicel göstergelere dayalı olarak belirlenmiştir. Bu kapsamda; enjeksiyon kalıplama (Injection Molding), metal döküm (Metal Casting), polilaktik asit (Polylactic Acid, PLA) ile 3B baskı, akrilonitril bütadien stiren (Acrylonitrile Butadiene Styrene, ABS) ile 3B baskı ve geri dönüştürülmüş PLA/ABS filamentler ile 3B baskı gibi üretim alternatifleri, çevresel metrikler açısından karsılastırmalı olarak değerlendirilmiş ve EVSE bileşen üretimi bağlamında sınıflandırılmıştır. Böylece çalışmada ver alan kriter ve alternatifler, bilimsel geçerliliğe ve uygulama bağlamına dayalı, analitik ve karsılastırılabilir bir biçimde tanımlanmıştır [48-49].

Bu çalışmada kullanılan Ecoinvent ve GaBi veri tabanlarının seçimi, LCA uygulamalarında metodolojik tutarlılık ve sonuç güvenilirliği açısından önem arz etmektedir. Herrmann ve

Moltesen, SimaPro ve GaBi gibi farklı LCA araçlarının aynı süreç verileri üzerinde nasıl değişken sonuçlar üretebildiğini karşılaştırmalı olarak incelemiş ve veri tabanı seçiminin çevresel çıktıların doğruluğunu doğrudan etkilediğini vurgulamıstır. Öte yandan, 3B baskı tabanlı üretim süreçlerinin yaşam döngüsü perspektifinden değerlendirilmesinde, Tinoco vd., çevresel sürdürülebilirliği etkileyen temel değişkenlerin malzeme kompozisyonu, üretim yöntemi ve bölgesel veri farklılıkları olduğunu sistematik bir literatür taramasıyla ortaya koymustur. Bu kapsamda, çalısmada kullanılan Ecoinvent v3.9 ve GaBi Professional 10 sürümlerine ait süreç verileri, hem uluslararası karşılaştırılabilirliği sağlamak hem de karbon ayak izi analizini teknik yönden sağlam temellere oturtmak amacıyla tercih edilmiştir [50-57].

Yürütülen tematik analiz kapsamında, her üretim alternatifi; enjeksiyon kalıplama, metal döküm, 3B baskı, PLA, ABS, geri dönüştürülmüş PLA/ABS, bes temel kriter doğrultusunda sistematik biçimde eşleştirilmiştir. Karbon ayak izi (C1) kriteri, LCA tabanlı çalışmalar ve EPD veri setlerinden elde edilen birim basına CO2 üzerinden hesaplanmıstır. salımı değerleri Mevzuat uyumu (C2) kriteri, RoHS, ISO 14001 ve çevresel etiketleme standartlarına uygunluk durumuna göre değerlendirilmiştir. Üretim maliyeti (C3), literatürde raporlanan birim maliyet analizleri ve düsük hacimli üretimlerde 3B baskının sağladığı maliyet avantajları temel alınarak tanımlanmıştır. Yapısal dayanıklılık (C4), malzeme mukavemeti, sıcaklık ve mekanik yük dayanımı gibi niteliksel ve niceliksel göstergelerle ölçülmüştür. Üretim süresi (C5) ise her teknolojide birim üretim süresi ve esnek kapasitesine üretim iliskin verilerle karşılaştırmalı olacak şekilde tasarlanmıştır [58-60].

Bu eşleştirme süreci, her alternatifin kriterler karşısındaki performansını somut verilerle ilişkilendirmiş; karar matrisine entegre edilmeden önce bilimsel geçerliliğe sahip ölçütlere dayalı olarak yapılandırılmıştır. Böylece, alternatifler ile kriterler arasında metodolojik olarak izlenebilir ve objektif temelli bir bağ kurulmuş, çok kriterli karar analizi sürecinin doğruluğu ve güvenilirliği artırılmıştır.

Bu metodoloji, belirsizlikleri MC-AHP ile minimize ederken, TOPSIS ile objektif bir sıralama sağlanmıştır. Çalışma sonuçlarının, politika belirleme süreçlerine bilimsel destek sunacağı düşünülmektedir. Bu çerçevede çalışmanın metodolojisi, aşağıda yer alan adımlardan oluşmaktadır:

Adım 1. Problemin Tanımı

Üretim sürecinde düşük karbon salımı, çevresel mevzuat uyumu, yapısal bütünlük, maliyet etkinliği ve üretim süresi gibi çoklu kriterler göz önüne alınarak alternatif üretim teknolojilerinin, özellikle 3B baskı yöntemlerinin, değerlendirilmesi gerekmektedir.

Adım 2. Kriterlerin Belirlenmesi

Kriterler, EA bileşen üretiminde çevresel ve yapısal performansı belirleyen faktörler olarak literatür taraması ve sektörel regülasyonlara göre tanımlanmış; karbon ayak izi, mevzuat uyumu, maliyet, üretim süresi ve yapısal dayanıklılık olmak üzere beş temel kriter belirlenmiştir. MC-AHP yöntemiyle bu kriterler arasında yapılan ikili karşılaştırmalar üzerinden istatistiksel güvenilirlik içeren ağırlıklar elde edilmiştir.

Adımlar:

1.Kriterlerin Belirlenmesi:

Literatür taraması ve çevresel performans odaklı tematik analizle belirlenen beş kriter (karbon ayak izi, mevzuat uyumu, maliyet, üretim süresi, dayanıklılık) karar problemine temel teşkil etmiştir.

2.İkili Karşılaştırma Matrislerinin Oluşturulması:

Kriterler arası öncelik ilişkileri, uzman görüşleriyle ikili karşılaştırma matrislerine dönüştürülmüştür.

3.Monte Carlo Tabanlı Ağırlık Hesaplaması:

10.000 iterasyonla rastgele varyasyonlar uygulanmış; her iterasyonda tutarlılık oranı ($CR \le 0,1$) sağlanmıştır.

4.İstatistiksel Ağırlıkların Elde Edilmesi: Her kriter için dağılım üzerinden medyan, ortalama ve %90 güven aralığı ile ağırlık değerleri hesaplanmıştır.

5. Sonuçların Görselleştirilmesi:

Kriter ağırlıklarının dağılımları Boxplot ve istatistiksel tablolarla sunulmuş, karar verme sürecine belirsizlik uyarlaması entegre edilmiştir.

Adım 3. Alternatiflerin Belirlenmesi

Bu çalışmada, EVSE bileşenlerinin üretiminde kullanılan beş farklı yöntem alternatif olarak belirlenmiştir: enjeksiyon kalıplama, metal döküm, PLA (Polylactic Acid) ile 3B baskı, ABS (Acrylonitrile Butadiene Styrene) ile 3B baskı ve geri dönüştürülmüş PLA/ABS ile 3B baskı. Alternatiflerin seçimi, 2020 sonrası tematik analiz için literatür taramaları ve çalışmada yer alan standart ve reegülasyonlara uygunluk temelinde yapılmıştır.

Adım 4. Karar Matrisinin Oluşturulması Alternatiflerin kriterler karşısındaki performans değerleri bir matris (1) şeklinde gösterilir.

$$X = \begin{vmatrix} x_{11} & x_{12} \dots & x_{1n} \\ x_{21} & x_{22} \dots & x_{2n} \\ x_{m1} & x_{m2} \dots & x_{mn} \end{vmatrix}$$
 (1)

Adım 5. MC-AHP ile Ağırlıklandırma

Geleneksel AHP yöntemi, uzmanların ikili karşılaştırmalarına dayalı ağırlık hesaplar. Ancak belirsizlikleri modellemek için MC-AHP kullanılır:

- Kriterler arası ikili karsılastırmalar yapılır.
- Tutarlılık indeksi ($CR \le 0,1$) kontrol edilir.
- Ağırlıklar, rassal varyasyonlarla simüle edilerek daha güvenilir sonuçlar elde edilir.

Adım 6. TOPSIS ile İdeal Çözüme Yakınlık Sıralaması

TOPSIS yöntemi, alternatifleri ideal çözüme yakınlığına göre sıralar.

Adımlar:

1.Normalizasyon: Karar matrisi normalize edilir.

2. Ağırlıklandırılmış Matris: MC-AHP'den gelen ağırlıklar uygulanır.

- 3.İdeal ve Negatif İdeal Çözümler Belirlenir:
 - A+: Her kriter için en iyi değer
 - A-: Her kriter için en kötü değer

4.Uzaklık Hesaplama:

- D_i⁺: Alternatifin ideal çözüme uzaklığı
- D_i⁻: Alternatifin negatif ideal çözüme uzaklığı

5. Göreceli Yakınlık Katsayısı:
$$C_i = D_i^- / (D_i^+ + D_i^-)$$

Adım 7. Sonuçların Yorumlanması ve Politik Öneriler: TOPSIS sonuçlarına göre en iyi alternatif belirlenir. Politika yapıcılar için öneriler sunulur.

2.1. Kriterlerin Belirlenmesi ve MC-AHP Uygulaması

Kriter belirleme aşamasında, literatüre dayalı olarak karbon salımı, çevresel mevzuat uyumu, üretim maliyeti, yapısal dayanıklılık ve üretim süresi gibi enerji altyapısında kritik kabul edilen beş temel kriter tanımlanmıştır. Karbon salımı, üretim sürecinde ortaya çıkan toplam sera gazı emisyonunu yansıtmakta; mevzuat uyumu ise RoHS ve ISO 14001 düzenleyici standartlarla teknik uyumluluğu temsil etmektedir. Üretim maliyeti ve süresi, operasyonel verimliliği; yapısal dayanıklılık ise bileşenin yaşam döngüsü ve güvenlik gereksinimlerine uyumunu ölemektedir.

Önerilen model, 3B baskının geleneksel üretim yöntemlerine kıyasla karbon salımı, çevresel mevzuat uyumu, üretim maliyeti, yapısal dayanıklılık ve üretim süresi gibi kritik kriterlerdeki performansını sayısal olarak değerlendirmeyi mümkün kılmaktadır.

Kriterler, sistematik literatür taramasına dayalı tematik analiz ile belirlenmiştir:

- C1: Karbon Ayak İzi (kg CO2-eq)
- C2: Regülasyon Uygunluğu (RoHS, ISO 14001)
- C3: Üretim Maliyeti (DOLAR/kg)
- C4: Yapısal Dayanıklılık (dayanım test puanı)
- C5: Üretim Süresi (dk/adet)

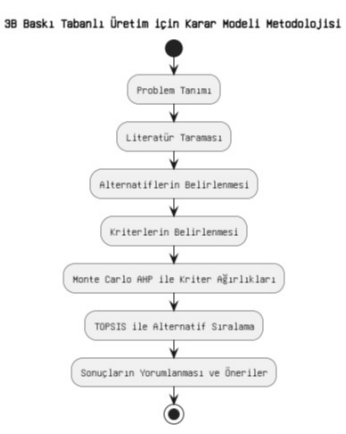
2.2. Monte Carlo Tabanlı AHP Kriterlerinin Ağırlıklandırması

Bu çalısmada, karar verme sürecinin nesnelliğini artırmak ve uzman tabanlı öznellikleri ortadan kaldırmak amacıyla AHP yöntemine Monte Carlo edilmistir. simülasyonu entegre Bövlece geleneksel AHP yönteminin temelinde yer alan ikili karşılaştırmalar bu çalışmada doğrudan uzman görüşleri yerine parametrik dağılımlardan türetilmiştir. Her kriter çifti için, sektörel teknik dökümanlar ve literatürdeki ampirik veriler referans alınarak uniform veya üçgen dağılımlar tanımlanmıs; örneğin karbon ayak izi ile üretim maliyeti kriterleri arasındaki karşılaştırma oranı aralığında uniform dağılımla modellenmiştir. Bu vaklasım. karar matrisinin türetilmesinde herhangi bir bireysel uzman önyargısını dışlamış, bunun yerine çok sayıda simülasyon yoluyla istatistiksel güvenilirlik sağlanmıştır.

Bu çalışmada kullanılan Monte Carlo tabanlı AHP yaklaşımında, ağırlıkların belirsizliğini değerlendirmek amacıyla uniform dağılım esas alınarak her bir kriter çifti için 10.000 iterasyon gerçekleştirilmiştir. Örnekleme yöntemi olarak basit random sampling değil, Latin Hypercube Sampling (LHS) uygulanmış ve bu sayede tüm olasılık aralığı daha dengeli bicimde kapsanmıştır. Tutarlılık İndeksi (CI), her iterasyonda Saaty'nin orijinal AHP tutarlılık oranı metoduna göre hesaplanmış ve tüm iterasvonlar icin ortalama CI değeri < 0.1 olacak sekilde kabul edilmiştir.

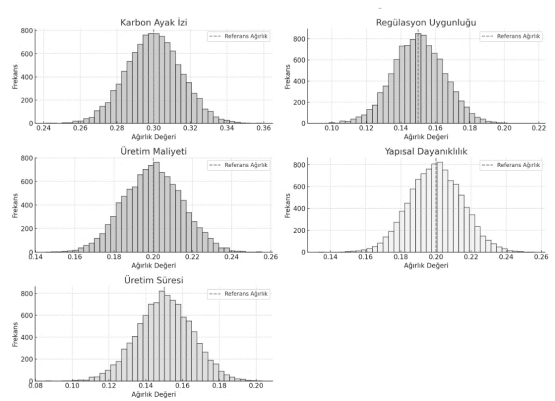
AHP'de Tutarlılık İndeksi (Consistency Index, CI) ve Tutarlılık Oranı (Consistency Ratio, CR), karar vericinin yaptığı ikili karşılaştırmaların tutarlılığını ölçmek için kullanılır. Ancak Monte Simülasyonu ile stokastik uygulandığında, CI ve CR tek bir deterministik matristen değil, binlerce simüle edilmiş ikili karsılastırma matrisinden elde edilir. Monte Carlo entegrasyonu kapsamında, her simülasyon iterasyonunda rastgele seçilen ikili karsılastırmalarla olusturulan AHP karar matrislerinin tutarlılık oranı (CR < 0,1) sağlanana kadar 10.000 tekrar yapılmıştır. Bu süreç sonunda elde edilen her bir kriterin ağırlığı, bir dağılım fonksiyonu tanımlanmıs olarak dağılımlardan elde edilen ortalama ağırlıklar TOPSIS analizinde kullanılmıştır. Ayrıca,

ağırlıkların %95 güven aralıkları hesaplanmış ve sıralama tutarlılığı Spearman korelasyon katsayısı ile test edilmiştir ($\rho=0.91,\ p<0.01$). Böylece, AHP'nin deterministik yapısı yerine stokastik, esnek ve belirsizliği yöneten bir karar destek mekanizması geliştirilmiştir. Bu yöntem, özellikle çevresel ve üretim teknolojileri gibi karmaşık sistemlerde karar verme süreçlerinin güvenilirliğini artırmak amacıyla literatüre özgün bir katkı sunmaktadır. Şekil 1, 3B baskı tabanlı üretim için çalışmada takip edilen karar modeli akışını sunmaktadır.



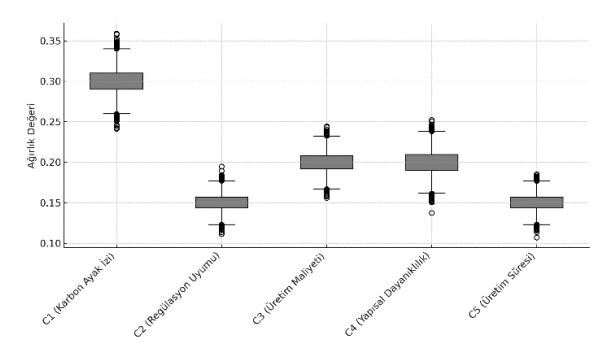
Şekil 1. 3B baskı tabanlı üretim için karar modeli akısı

Saaty'nin 1–9 önem skalasına göre uzman görüşleriyle oluşturulan ikili karşılaştırma matrisi kullanılarak [46], Monte Carlo tabanlı Analitik Hiyerarşi Süreci (MC-AHP) ile kriter ağırlıkları hesaplanmıştır. Bu kapsamda, karbon ayak izi (C1) için 0,30, mevzuat uyumu (C2) için 0,15, üretim maliyeti (C3) için 0,20, yapısal dayanıklılık (C4) için 0,20 ve üretim süresi (C5) için 0,15 ağırlıkları elde edilmiştir. Hesaplamalar sonucunda elde edilen tutarlılık oranı (CR = 0,064), < 0,1 koşulunu sağladığı için karar matrisinin tutarlı olduğu kabul edilmiştir. Böylece, kriter ağırlıkları istatistiksel güvenilirlik sağlayacak şekilde belirlenmiş ve normalize edilmiş ağırlıklar, TOPSIS analizine aktarılmıştır. Sekil 2. Monte Carlo simülasyonu ile elde edilen kriter ağırlıklarının dağılımını göstermektedir. Her bir histogram, ilgili kriterin (örneğin karbon ayak izi, üretim maliyeti, regülasyon uyumu, yapısal dayanıklılık, üretim süresi) 10.000 iterasyonda elde edilen ağırlık değerlerinin frekans dağılımını sunmaktadır. Şekil 2'de görüldüğü üzere, tüm kriterlerin ağırlıkları simetrik ve çan eğrisi şeklinde dağılım göstermekte olup, bu durum simülasyonun istatistiksel olarak dengeli ve güvenilir sonuçlar ürettiğini ortaya koymaktadır. Her dağılımın üzerine eklenen kesikli dikey çizgi, AHP süreciyle hesaplanan referans ağırlığına karşılık gelmekte; bu referans değerlerin dağılımların medyanına yakın olduğu görülmektedir. Bu durum, klasik AHP ile elde edilen değerlerin Monte Carlo simülasyonu ile doğrulandığını ve karar ağırlıklarının belirsizlik altında bile kararlı kaldığını göstermektedir.



Şekil 2. Monte Carlo simülasyonu ile elde edilen ağırlıkların dağılımı

Şekil 3, Monte Carlo AHP yöntemiyle elde edilen beş karar kriterine ait ağırlıkların dağılımını kutu grafiği (boxplot) ile sunmakta olup, özellikle karbon ayak izi (C1) kriterinin en yüksek medyan değere ve daha düşük dağılım genişliğine sahip olduğunu, böylece karar sürecinde baskın ve tutarlı bir parametre olduğunu göstermektedir.



Şekil 3. Monte Carlo simülasyonu ile AHP kriter ağırlıkları değerleri

Özetle Çizelge 1, MC-AHP sonucunda her bir kriter için elde edilen ağırlıkların temel

istatistiksel ölçütlerini sunmaktadır. karbon ayak izi (C1) kriteri hem en yüksek ortalama ve medyan değeriyle öncelikli kriter olduğunu göstermekte, hem de standart sapma ve çeyrekler arası aralık değerlerinin görece düşük olması sayesinde istatistiksel olarak kararlı bir yapıya sahiptir. Diğer kriterlerdeki daha düşük ortalama ağırlıklar, çevresel önceliğin karar sürecinde baskın olduğunu desteklemektedir. Bu dağılım özellikleri, belirsizliğin dikkate alındığı modellerde dahi kararların çevresel etkiler üzerinden şekillendiğini ortaya koymaktadır.

Çizelge 1. Kriter ağırlıklarına ilişkin temel istatistikler

Kriter	Ort. Ağırlık	Medyan	Std Sapma	Çeyrekler Arası
C1 (Karbon Ayak İzi)	0,35	0,35	0,04	0,07
C2 (Enerji Tüketimi)	0,20	0,20	0,03	0,06
C3 (Üretim Maliyeti)	0,15	0,15	0,02	0,04
C4 (Mevzuat Uyumu)	0,15	0,15	0,03	0,05
C5 (Üretim Süresi)	0,15	0,15	0,03	0,05

2.3. Alternatiflerin Tanımlanması

Çalışmada, EA şarj ekipmanı üretiminde değerlendirilen alternatif teknolojiler; cevresel etki, mevzuat uyumu ve teknik uygunluk temelinde seçilmiştir. 2020-2024 dönemine ait indirgenmis 56 akademik yayın ile LCA ve EPD veri tabanları taranarak üretim yöntemlerine ilişkin karbon salımı, enerji tüketimi, üretim süresi ve geri dönüşüm oranı gibi veriler tematik olarak kodlanmıştır. Seçilen beş üretim yöntemi, **EVSE** bileşeni bir muhafaza üzerinden karsılaştırmalı analiz için standartlara uygun bicimde sayısallastırılmış ve çalışma kapsamında önerilen MC-AHP, TOPSIS çok kriterli karar modelinde kullanılmak üzere karar matrisine dönüstürülmüstür.

Bu süreç, analizde kullanılan alternatif ve kriterlerin uygulama bağlamına dayalı, geçerli ve bütüncül bir yapıda tanımlanmasını sağlamıştır.

Çizelge 2'de sunulan karar matrisi, EA şarj ekipmanı üretiminde değerlendirilen beş alternatif teknolojinin; karbon ayak izi, mevzuat uyumu, üretim maliyeti, yapısal dayanıklılık ve

kriterleri üretim süresi açısından nicel performanslarını göstermektedir. **TOPSIS** yöntemi bu çalışmada, söz konusu kriterler doğrultusunda alternatiflerin çevresel ve teknik uygunluk düzeyine göre sıralanmasını sağlamak amacıyla uygulanmıştır. İlk aşamada, ölçüm birimlerinin heterojen yapısı nedeniyle karar matrisi vektör normu yöntemiyle normalize edilmiştir (Çizelge 3). Normalizasyon, klasik vektör tabanlı yöntemle yapılmış olup daha sonra AHP ile elde edilen ağırlıklar, normalize matrisin her bir sütunuyla çarpılarak ağırlıklı karar matrisi elde edilmistir (Cizelge 4). İkinci asamada, her bir kriter değeri MC-AHP ağırlıklarıyla çarpılarak ağırlıklı karar matrisi elde edilmiştir. Ardından, ideal ve negatif ideal çözüm noktaları tanımlanmış ve her alternatifin bu noktalara olan Öklidyen uzaklıkları hesaplanmıştır (Çizelge 5). Son aşamada, her alternatif için göreli yakınlık katsayısı (C_i) hesaplanarak, alternatiflerin çok kriterli bir yapıda ideal çözüme olan yakınlıkları belirlenmiştir. Karar matrisi verileri; örneğin A5 için 0.85 kgCO₂, 0.92 regülasyon uyumu, 65 dolar maliyet, 65 yapı dayanımı, 11 dakika üretim süresi gibi min-max normalizasyon yöntemiyle ölçeklendirilmis, ardından MC-AHP ile elde edilen kriter ağırlıklarıyla çarpılarak her çok boyutlu alternatifin performansi hesaplanmıştır. Bu süreç sonucunda üretim alternatifleri çevresel ve teknik uygunluk düzeylerine göre sıralanmıştır (Çizelge 6). TOPSIS vöntemi bu bağlamda, belirsizlik altında elde edilen istatistiksel ağırlıklarla entegre edilmiş, çevresel etki ve teknik uygulanabilirlik kriterlerini birlikte değerlendiren bütüncül bir sıralama çerçevesi sunmustur. Elde edilen sonuçlar, karar vericilerin karbon nötr hedeflerle uyumlu, mevzuat temelli ve üretim verimliliğini gözeten stratejik tercihler yapmasına olanak sağlamaktadır.

Çizelge 2. Karar matrisi

Alternatif	C1	C2	С3	C4	C5
ler	(kgCO2)		(dolar)		(dk)
A1	1,02	0,90	100	90	20
A2	2,00	0,85	120	95	25
A3	1,18	0,88	60	70	10
A4	2,10	0,86	70	75	12
A5	0,85	0,92	65	65	11

Çizelge 3. Normalize karar matrisi

Altern	C1	C2	C3	C4	C5
atifler	(kgCO2)		(dolar)		(dk)
A1	0,29	0,45	0,51	0,50	0,53
A2	0,58	0,43	0,62	0,53	0,67
A3	0,34	0,44	0,31	0,39	0,26
A4	0,61	0,43	0,36	0,42	0,32
A5	0,24	0,46	0,33	0,36	0,29

Çizelge 4. Ağırlıklı karar matrisi

Altern	C1	C2	C3	C4	C5
atifler	(kgCO2		(dola		(dk)
)		r)		
A1	0,10	0,06	0,10	0,05	0,11
A2	0,20	0,06	0,12	0,05	0,13
A3	0,12	0,06	0,06	0,04	0,05
A4	0,21	0,06	0,07	0,04	0,06
A5	0,08	0,07	0,07	0,04	0,06

Cizelge 5. İdeal ve anti-ideal çözüm noktaları

C1	C2	C3	C4	C5 (dk)
(kgCO2)		(dolar)		
0,2161	0,0699	0,1246	0,0532	0,1341
0,0875	0,0646	0,0623	0,0364	0,0536

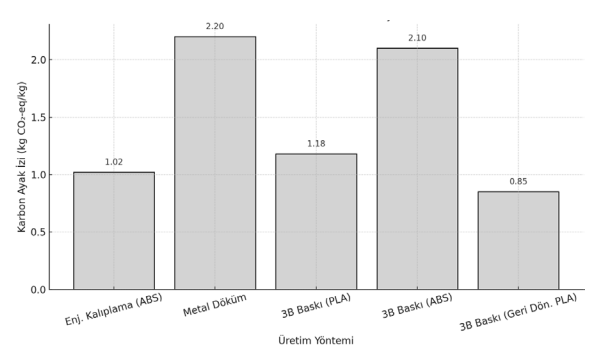
Cizelge 6. TOPSIS skorları ve sıralama

Alternatifler	TOPSIS Skoru	Sıralama
A5	0,799395	1
A3	0,745924	2
A1	0,477239	3
A4	0,396643	4
A2	0,388920	5

Cizelge 6, değerlendirmeye alınan beş üretim alternatifinin TOPSIS yöntemiyle elde edilen göreli yakınlık skorlarını ve bu skorlar doğrultusunda yapılan sıralamayı göstermektedir. En yüksek skoru elde eden A5 alternatifi (geri dönüştürülmüş PLA/ABS ile 3B baskı), çok kriterli değerlendirme kapsamında en uygun seçenek olarak belirlenmiştir. Bunu sırasıyla A3 (PLA ile 3B baskı), A1 (enjeksiyon kalıplama), A4 (ABS ile 3B baskı) ve A2 (metal döküm) takip etmektedir. Bu sonuçlar, düşük karbon ayak izi ve çevresel uyumluluğun öncelikli olduğu karar ortamlarında, 3B temelli baskı üretim alternatiflerinin sürdürülebilirlik açısından daha avantajlı olduğunu ortaya koymaktadır.

3. BULGULAR VE DEĞERLENDİRME

calısmada değerlendirilen bes üretim alternatifine ait karbon ayak izi değerleri, çevresel sürdürülebilirlik açısından belirgin farklılıklar sergilemistir. Geri dönüstürülmüs PLA ile üretilen 3B baskı yöntemi, 0,85 kg CO2-eq/kg ile en düsük emisyon değerine ulasarak karbonsuzlaşma hedefleriyle en yüksek uyumu göstermiştir. Buna karşılık, metal döküm (2,20 kg CO2-eq/kg) ve ABS ile 3B baskı (2,10 kg CO2eq/kg) yöntemleri, karbon emisyonu açısından en olumsuz performansı sergileyerek geleneksel ve petrol türevi tekniklerin çevresel dezavantajlarını ortaya koymuştur. Orta düzey emisyon sunan PLA ile 3B baskı (1,18 kg CO₂-eq/kg) ve enjeksiyon kalıplama (1,02 kg CO₂-eq/kg) ise görece daha az çevresel etki göstermektedir (Şekil 4). Bu dağılım, üretim yöntemlerinin karbon nötrlüğü politikalarıyla teknik uyum düzeyini net biçimde yansıtmaktadır.



Şekil 4. Üretim yöntemine göre karbon ayak izi değişimi

TOPSIS analizinde en yüksek skoru alan alternatifin geri dönüstürülmüs PLA ile 3B baskı (C = 0,799) olması, düşük karbonlu ve döngüsel üretim çözümlerinin çevresel ve teknik açıdan bütünleşik avantaj sunduğunu doğrulamaktadır. Diğer 3B baskı seçenekleri (örneğin PLA filament, $C^* = 0.746$), hem maliyet hem de üretim esnekliği açısından rekabetçi seviyelerde konumlanmıştır. Mevzuat uyumu açısından, enjeksiyon kalıplama yöntemi halen RoHS ve ISO 14001 gibi çevresel standartlara en yüksek düzeyde uyum gösteren yöntem olarak öne çıkarken, geri dönüştürülmüş filamentlerin bu alandaki eksiklikleri nedeniyle genel skoru görece sınırlanmıştır. Ancak bu eksikliklerin giderilmesi, çevresel regülasyonlarla tam uyumlu karbon nötr üretim için stratejik bir fırsat sunmaktadır.

Normalize karar matrisi üzerinden yapılan kriter bazlı hassasivet analizi, özellikle C1 (Karbon Ayak İzi) ve C3 (Üretim Maliyeti) kriterlerinin karar modeline etkisinin yüksek olduğunu göstermistir. C2 (Mevzuat Uyumu) kriterinde ise geleneksel enjeksiyon kalıplama yöntemi en yüksek uygunluk skorunu alırken. dönüştürülmüş filament tabanlı 3B baskı sistemlerinin RoHS ve ISO 14001 gibi çevresel regülasyonlarla kısmen uyumsuz olduğu görülmüştür. Bu durum, alternatifin çevresel avantajina rağmen genel TOPSIS skorunu düsürmüstür. Ancak bu regülasyonel eksikliklerin giderilmesi durumunda, 3B baskı tabanlı döngüsel üretim yapıları, çevresel ve teknik açılardan ideal çözüme en yakın seçenekler olarak öne çıkmaktadır. MC-AHP ve TOPSIS'in entegre kullanımı, teknik ve çevresel değişkenleri istatistiksel güvenilirlikle modelleyerek, karar vericilere sürdürülebilir enerji altyapılarında uygulanabilir, karşılaştırılabilir ve politika uyumlu bir karar destek çerçevesi sunmaktadır.

4. TARTIŞMA VE SINIRLILIKLAR

Bu çalışmada değerlendirilen PLA ve ABS gibi yaygın polimer malzemeler, EA besleme sistemlerinde kullanılan bilesenlerin çevresel etkilerinin analizinde temel alınmıştır. Bununla birlikte, son yıllarda literatürde öne çıkan karbon takviyeli polimerler fiber (Carbon Fiber Reinforced Polymer, CFRP) dönüstürülmüs hibrit kompozitler, özellikle 3B baskı teknolojileriyle entegre kullanıldığında hem dayanım mekanik hem de cevresel sürdürülebilirlik açısından önemli avantajlar sunmaktadır. CFRP gibi malzemeler, yüksek mukavemet/ağırlık oranı sayesinde taşıyıcı parçalarda daha ince ve hafif yapıların tasarlanmasına tanırken. olanak geri dönüstürülmüs iceriklerin kullanımıyla da döngüsel ekonomi hedeflerine katkı sağlayabilmektedir. Ancak bu malzemelere ilişkin LCA verilerinin ve üretim sürecine ait sayısal girdilerin sınırlı oluşu, karar modeline bütüncül entegrasyonlarını kısıtlamaktadır. Bu malzemelere ilişkin yeterli LCA verisi ve üretim parametresi bulunmadığından, mevcut entegrasyonu kriterli karar modeline yapılamamıstır. İlerleyen çalısmalarda bu tür ileri kompozitlerin değerlendirilmesi önerilmektedir.

Bu çalışmada üretim maliyeti kriteri çok kriterli karar modeline dâhil edilmiş olsa da 3B baskı teknolojilerinin seri üretim ölçeğinde maliyet etkinliğine ilişkin kapsamlı yaşam döngüsü verileri ve teknik/ekonomik analizler literatürde sınırlı düzeydedir. Bu nedenle, maliyet parametresi daha çok özelleştirilmiş düşük hacimli üretim bağlamında değerlendirilmiştir [58].

Literatürde, 3B baskı teknolojilerinin EA uygulamalarında baskı hızı, kalite kontrol süreçlerinin standardizasyonu ve uzun vadeli çevresel dayanıklılık gibi operasyonel zorluklar taşıdığı vurgulanmaktadır [59]. Ancak Türkiye bağlamında, bu teknolojilerin hâlen prototipleme ve düşük hacimli üretim düzeyinde uygulanması ve şarj altyapısı bileşenlerinde endüstriyel seri üretim düzeyine geçilmemiş olması nedeniyle, bu çalışmada söz konusu mühendislik sınırlılıklar öncelikli değerlendirme kapsamına alınmamıştır.

Ayrıca, literatürde 3B baskı teknolojilerinin elektrikli araç uygulamalarında yaygınlaşmasının önünde bazı yapısal zorluklar bulunduğu da belirtilmektedir. Özellikle üretim hızının düsük olması, kalite kontrol süreclerinin otomatiklestirilememesi ve üretim çıktılarının uzun vadeli dayanıklılık açısından sınırlı saha verisine dayanması gibi etkenler, bu teknolojinin üretim ölçeğinde uygulanabilirliğini azaltmaktadır. Bununla birlikte. döngüsel ekonomi ilkeleri doğrultusunda hurda plastik parçaların geri kazanımı ve 3B baskı yoluyla veniden değerlendirilmesi, sürdürülebilir üretim stratejileri açısından gelecek vadeden bir yaklaşım olarak değerlendirilmektedir. yandan, batarya ve güç elektroniği sistemlerinin yeniden kullanımı ve parça bazlı üretimle entegre edilmesi gibi alternatif döngüsel çözümler de elektrikli araç teknolojilerinin sürdürülebilirliği acısından tamamlayıcı potansiyel sunmaktadır [59-60].

5. SONUÇ VE ÖNERİLER

Çalışma, elektrikli araç besleme sistemlerine yönelik üretim teknolojilerinde yalnızca çevresel etkilerin değil, aynı zamanda teknik uygunluk, ekonomik sürdürülebilirlik ve mevzuat uyumunun birlikte değerlendirilmesi gerektiğini ortaya koymaktadır. Karar destek sürecine

entegre edilen LCA tabanlı karbon ayak izi verileri, üretim alternatifleri arasında önemli farklılıkları ortaya koymuş; özellikle geri dönüştürülmüş PLA ile 3B baskı yöntemi, en düşük karbon salımı (0,85 kg CO₂-eq/kg) ile sürdürülebilir üretim adına en yüksek uyumu göstermiştir. Buna karşın, metal döküm (2,20 kg CO₂-eq/kg) ve ABS ile 3B baskı (2,10 kg CO₂-eq/kg) gibi yüksek emisyonlu yöntemler, geleneksel tekniklerin çevresel dezavantajlarını açıkça ortaya koymuştur. Enjeksiyon kalıplama ve PLA bazlı 3B baskı ise orta düzeyde emisyon sunarak çevresel sürdürülebilirlik açısından alternatif çözümler olarak konumlanmıştır.

TOPSIS analizinde, en yüksek skoru alan alternatifin geri dönüştürülmüş PLA ile 3B baskı (C = 0,799) olması, düşük karbonlu ve döngüsel üretim çözümlerinin teknik ve çevresel açılardan bütünleşik avantaj sunduğunu doğrulamaktadır. uyumu bakımından enjeksiyon kalıplama yöntemi, RoHS ve ISO 14001 gibi çevresel standartlara en yüksek uygunluk gösteren alternatif olarak öne çıkmış; buna karşın, geri dönüştürülmüş filamentlerin henüz tam mevzuat uyumu sağlayamaması, bu seçeneğin genel skorunu sınırlamıstır. Bununla birlikte, çevresel regülasyonlarla uyum eksikliklerinin giderilmesi durumunda, 3B baskı tabanlı döngüsel üretim çözümleri, teknik ve çevresel kriterleri en yüksek düzeyde karşılayan stratejik secenekler haline gelecektir.

Normalize karar matrisi üzerinden yapılan kriter bazlı hassasiyet analizleri, özellikle karbon ayak izi (C1) ve üretim maliyeti (C3) kriterlerinin karar modeli üzerindeki etkisinin yüksek olduğunu MC-AHP göstermiştir. ile belirsizlikleri minimize edilen kriter ağırlıkları ve TOPSIS ile belirlenen sıralamaları. alternatif enerji dijital üretim teknolojilerinin altyapısında seçiminde karar vericilere sistematik, istatistiksel geçirilebilir temelli ve uygulamaya yönlendirmeler sunmaktadır.

Politika önerileri, çalışmada ulaşılan bulgularla bütüncül biçimde uyumludur. Özellikle düşük karbon salımı sağlayan üretim alternatifleri arasında yer alan geri dönüştürülmüş PLA ve ABS filament kullanan yerli üreticilerin, stratejik üretim destek programlarına öncelikli olarak dahil

edilmesi gerekmektedir. Ayrıca, EPD tabanlı karbon etiketleme uygulamalarının EVSE tedarik zincirinde zorunlu hale getirilmesi, çevresel şeffaflığı artırarak Avrupa Yeşil Mutabakatı ve Türkiye'nin 2053 Net Sıfır Emisyon hedefleri ile yapısal uyumu güçlendirecektir. Düşük karbon ayak izine sahip üretim tekniklerinin sanayi destek mekanizmalarında öncelikli kriter olarak değerlendirilmesi ve 3B baskı tabanlı üretim altyapılarının yeşil kamu alımları ve stratejik yatırım teşvikleri kapsamında kurumsal düzeyde yaygınlastırılması önem arz etmektedir. Bu doğrultuda önerilen çok kriterli karar destek yapısı, Avrupa Yeşil Mutabakatı, Türkiye'nin İklim Kanunu ve 2053 net sıfır emisyon hedefleriyle doğrudan uyumlu bir çerçevede kurgulanmıştır. Model; çevresel sürdürülebilirlik, döngüsel ekonomi ilkeleri, karbon ayak izinin azaltımı, üretim süreçlerinin mevzuatlara uygunluğu ve enerji verimliliği gibi çok boyutlu politika hedeflerini birlikte ele alabilen entegre bir karar mekanizması sunmaktadır. Bu çok kriterli yaklaşım, üretim teknolojileri bağlamında sadece çevresel etkileri değil, aynı zamanda ekonomik uygulanabilirlik, yapısal dayanıklılık ve düzenleyici uygunluk gibi parametreleri sayısallaştırarak politika yapıcılar için nesnel bir önceliklendirme ve senaryo analizi aracı islevi görmektedir. Dolayısıyla önerilen model, hem sanayi aktörleri açısından sürdürülebilir üretim dönüşümüne yönelik teknik yol haritası olusturmakta hem de kamu otoritelerine vönelik stratejik planlama ve mevzuat uyumluluğu için veri temelli bir karar altyapısı sağlamaktadır.

KAYNAKLAR

- 1. Curran, S., Chambon, P., Lind, R., Love, L., Wagner, R., Whitted, S., Keller, M. "Big area additive manufacturing and hardware-in-the-loop for rapid vehicle powertrain prototyping: A case study on the development of a 3-D-printed Shelby Cobra", SAE Technical Paper, 2016-01-0328, 2016.
- 2. Kang, H. C., Kang, K. B., Ahn, H. K., Lee, S. H., Ahn, T. H., Jwa, J. W. "The smart EV charging system based on the big data analysis of the power consumption patterns", International Journal of Internet, Broadcasting and Communication, Cilt 9, Sayı 2, Sayfa 1-10, 2017.

- 3. Hachey, S. Q. "Prospects for sustainable microfactory retailing in Canada: A case study of 3D printed electric vehicles" (Master's thesis, McMaster University). McMaster University Institutional Repository.2017.
- 4. Moon, I., Lee, G. M., Park, J., Kiritsis, D., von Cieminski, G. (Eds.). "Advances in production management systems. Production management for data-driven, intelligent, collaborative, and sustainable manufacturing: IFIP WG 5.7 International Conference, Proceedings, Part I", Cilt 535, Springer, 2018.
- 5. Tseng, T., Li, D. "Use of ANP and TOPSIS for the 3D printing on customized electrical vehicles", 2020 The 6th International Conference on E-Business and Applications, Sayfa 128-132, 2020.
- 6. Pallander, R. "Implementation of HomePlug Green Phy standard (ISO15118) into Electric Vehicle Supply Equipment", 2021.
- 7. Serohi, A. "Impact of 3-D printing technology in manufacturing supply lines to improve resilience during black swan events", International Journal of Supplementary Chain Management, Cilt 10, Sayfa 88, 2021.
- 8. Elavarasan, R. M., Pugazhendhi, R., Irfan, M., Mihet-Popa, L., Khan, I. A., Campana, P. E. "State-of-the-art sustainable approaches for deeper decarbonization in Europe- An endowment to climate neutral vision", Renewable and Sustainable Energy Reviews, Cilt 159, Sayfa 112204, 2021.
- 9. Zhang, T., Ran, F. "Design strategies of 3D carbon-based electrodes for charge/ion transport in lithium ion battery and sodium ion battery", Advanced Functional Materials, Cilt 31, Sayı 17, Sayfa 2010041, 2021.
- 10. Tarancón, A., Esposito, V., Torrell, M., Di Vece, M., Son, J. S., Norby, P., Pedersen, D. B. "2022 roadmap on 3D printing for energy", Journal of Physics: Energy, Cilt 4, Sayı 1, Sayfa 011501, 2022.
- 11. Jovanović, M., Mateo Sanguino, T. D. J., Damjanović, M., Đukanović, M., Thomopoulos, N. "Driving sustainability: Carbon footprint, 3D printing, and legislation concerning electric and autonomous vehicles", Sensors, Cilt 23, Sayı 22, Sayfa 9104, 2023.
- 12. Rosado, J., Cardoso, F., Silva, M. "A low cost and highly parameterizable energy meter", 2023 3rd International Conference on Electrical, Computer, Communications and Mechatronics Engineering (ICECCME), Sayfa 1-6, 2023.

- 13. Rabih, M., Takruri, M., Al-Hattab, M., Alnuaimi, A. A., Bin Thaleth, M. R. "Wireless charging for electric vehicles: A survey and comprehensive guide", World Electric Vehicle Journal, Cilt 15, Sayı 3, Sayfa 118, 2024.
- 14. Hussein, H. M., Ibrahim, A. M., Taha, R. A., Rafin, S. S. H., Abdelrahman, M. S., Kharchouf, I., Mohammed, O. A. "State-of-the-art electric vehicle modeling: Architectures, control, and regulations", Electronics, Cilt 13, Sayı 17, Sayfa 3578, 2024.
- 15. Kumar, P., Channi, H. K., Kumar, R., Stević, Ž., Singh, S., Bhattacherjee, A., Bhowmik, A. "Optimizing electric mobility: A multi-criteria decision-making approach for sustainable future of electric vehicles through smart motor choices", Journal Européen des Systèmes Automatisés, Cilt 57, Sayı 6, Sayfa 1825, 2024.
- 16. Kumar, B. V., Farhan, A. "Optimal simultaneous allocation of electric vehicle charging stations and capacitors in radial distribution network considering reliability", Journal of Modern Power Systems and Clean Energy, Cilt 12, Sayı 5, Sayfa 1584-1595, 2024.
- 17. Prasittisopin, L. "How 3D printing technology makes cities smarter: A review, thematic analysis, and perspectives", Smart Cities, Cilt 7, Sayı 6, Sayfa 3458-3488, 2024.
- 18. Sama, A. "Introducing graphene-enhanced technologies to the regulated market to mitigate carbon emissions", Environmental Progress Sustainable Energy, Cilt 43, Sayı 1, Sayfa e14338, 2024.
- 19. Singh, B. J., Sehgal, R. "Applications of 3D printing, rapid prototyping, and digital manufacturing for low carbon development", Sustainability in smart manufacturing, Sayfa 37-60, CRC Press, 2024.
- 20. Shuker, S. "The role of emerging advanced technologies in facilitating the remanufacture and upgrade of end-of-use electro-mechanical and mechanical equipment, tooling and assets" [Doktora Tezi], University of Wales Trinity Saint David, 2024.
- 21. Marinkovic, D. "Sustainable composite materials for electric vehicle applications: A comprehensive review", Facta Universitatis, Series: Mechanical Engineering, 2025.
- 22. Owen, A., Hayes, D. "Technological innovations in EV manufacturing", 2025.

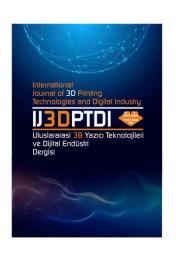
- 23. Jaller, M., Pineda, L., Gueldas, Y., Alemi, F., Otay, I. "Fostering the use of zero and near zero emission vehicles in freight operations", 2020.
- 24. Avrupa Parlamentosu. "Elektrikli ve elektronik ekipmanlarda belirli tehlikeli maddelerin kullanımının kısıtlanmasına ilişkin 2011/65/AB Direktifi (RoHS 2)", Avrupa Birliği Resmi Gazetesi, L 174, Sayfa 88-110, 2011.
- 25. Avrupa Kimyasallar Ajansı. "Kimyasalların Kaydı, Değerlendirilmesi, İzni ve Kısıtlanması hakkında (EC) No 1907/2006 Tüzük (REACH)", Avrupa Birliği Resmi Gazetesi, L 396, Sayfa 1-849, 2010.
- 26. Avrupa Parlamentosu. "Atık elektrikli ve elektronik ekipmanlara ilişkin 2012/19/AB Direktifi (WEEE)", Avrupa Birliği Resmi Gazetesi, L 197, Sayfa 38-71, 2010.
- 27. Uluslararası Standardizasyon Örgütü. "ISO 14001:2015 Çevre yönetim sistemleri, Kullanım kılavuzlu şartlar", 2015.
- 28. Uluslararası Standardizasyon Örgütü. "ISO 14040:2006 Çevre yönetimi Yaşam döngüsü değerlendirmesi, Prensipler ve çerçeve", 2006.
- 29. Uluslararası Standardizasyon Örgütü. "ISO 14044:2006 Çevre yönetimi Yaşam döngüsü değerlendirmesi, Şartlar ve kılavuzlar", 2006.
- 30. Uluslararası Standardizasyon Örgütü ve ASTM International. "ISO/ASTM 52900:2021 Eklemeli imalat, Genel prensipler, Temeller ve terminoloji", 2021.
- 31. Uluslararası Standardizasyon Örgütü ve ASTM International. "ISO/ASTM 52910:2019 Eklemeli imalat, Tasarım, Şartlar, kılavuzlar ve öneriler", 2019.
- 32. Uluslararası Standardizasyon Örgütü ve ASTM International. "ISO/ASTM 52915:2020 Eklemeli imalat dosya formatı (AMF) şartnamesi", 2020.
- 33. Uluslararası Standardizasyon Örgütü ve ASTM International. "ISO/ASTM 52901:2017 Eklemeli imalat, Genel prensipler, Satın alınan AM parçaları için şartlar", 2017.
- 34. Türk Standardları Enstitüsü. "TS EN 62196-1:2022 Elektrikli araçlar için fişler, prizler ve araç konnektörleri-Bölüm 1: Genel kurallar", 2022.

- 35. Türk Standardları Enstitüsü. "TS EN IEC 61851-1: Elektrikli araçlar için iletken (kablolu) şarj sistemi", 2023.
- 36. Türk Standardları Enstitüsü. "TS 13912: Elektrikli araç şarj istasyonları için güvenlik kuralları Muayene, deney ve yeterliliğin değerlendirilmesi", 2022.
- 37. Türk Standardları Enstitüsü. "TS EN IEC 61439-7: Alçak gerilim anahtarlama düzeni ve kontrol düzeni panoları Bölüm 7: Marinalar, kamp alanları, pazar yerleri ve elektrikli araç şarj istasyonları gibi özel uygulamalar için panolar", 2023.
- 38. Avrupa Komisyonu. "Avrupa Yeşil Mutabakatı", Sayfa 1-24, 2019.
- 39. "Sayısal Hizmetler için Tek Pazar ve 2000/31/EC Direktifinin Değiştirilmesi Hakkında (AB) 2022/2065 Tüzük (Sayısal Hizmetler Yasası)", AB Resmi Gazetesi L277/1, 19 Ekim 2022.
- 40. "Doğal kişilerin kişisel verilerinin işlenmesi ve bu verilerin serbest dolaşımı hakkında ve 95/46/EC Direktifinin yürürlükten kaldırılmasına ilişkin (AB) 2016/679 Tüzük (Genel Veri Koruma Tüzüğü)", AB Resmi Gazetesi L119/1, 27 Nisan 2016.
- 41. Kanyilmaz, A., Demir, A. G., Chierici, M., Berto, F., Gardner, L., Kandukuri, S. Y., Razavi, N. "Role of metal 3D printing to increase quality and resource-efficiency in the construction sector", Additive Manufacturing, Cilt 50, Sayfa 102541, 2022.
- 42. Barzaghi, L. "Sensors' Architecture Definition for Energy Consumption Reduction in Urban Battery Electric Vehicles" [Doktora Tezi], Politecnico di Torino, 2023.
- 43. Ataei, M., Shahsavany, H., Mikaeil, R. "Monte Carlo Analytic Hierarchy Process (MAHP) approach to selection of optimum mining method", International Journal of Mining Science and Technology, Cilt 23, Sayı 4, Sayfa 573-578, 2013.
- 44. Jing, L., Chen, B., Zhang, B., Li, P., Zheng, J. "Monte Carlo simulation-aided analytic hierarchy process approach: case study of assessing preferred non-point-source pollution control best management practices", Journal of environmental engineering, Cilt 139, Sayı 5, Sayfa 618-626, 2013.

- 45. Díaz, H., Teixeira, A. P., Soares, C. G. "Application of Monte Carlo and Fuzzy Analytic Hierarchy Processes for ranking floating wind farm locations", Ocean Engineering, Cilt 245, Sayfa 110453, 2022.
- 46. Saaty, T. L. "The analytic hierarchy process (AHP)", The Journal of the Operational Research Society, Cilt 41, Say1 11, Sayfa 1073-1076, 1980.
- 47. Hwang, C. L., Yoon, K. "Multiple attribute decision making: Methods and applications", Springer, 1981.
- 48. Jovanović, M., Mateo Sanguino, T. D. J., Damjanović, M., Đukanović, M., Thomopoulos, N. "Driving sustainability: carbon footprint, 3D printing, and legislation concerning electric and autonomous vehicles", Sensors, Cilt 23, Sayı 22, Sayfa 9104, 2023.
- 49. Prasittisopin, L. "A Review and Thematic Analysis of How 3D Printing Technology Makes a City Smarter", 2024.
- 50. Herrmann, I. T., Moltesen, A. "Does it matter which Life Cycle Assessment (LCA) tool you choose?
 a comparative assessment of SimaPro and GaBi",
 Journal of Cleaner Production, Cilt 86, Sayfa 163-169,
 2015.
- 51. Olanrewaju, O. "Data Quality Assurance in Construction Environmental Product Declarations for Whole Building Life Cycle Assessment" [Doktora Tezi], Open Access Te Herenga Waka-Victoria University of Wellington, 2025.
- 52. Ansah, N. B., Adinyira, E., Agyekum, K., Aidoo, I. "Systematic Review of Environmental Product Declarations (EPDs) Towards Construction Emission Mitigation in the African Region", International Conference on Infrastructure Development in Africa, Sayfa 41-54, 2023.
- 53. Benke, K. K., Steel, J. L., Weiss, J. E. "Risk assessment models for invasive species: uncertainty in rankings from multi-criteria analysis", Biological Invasions, Cilt 13, Sayfa 239-253, 2011.
- 54. Akaa, O. U. "Balancing stakeholder goals in structural fire design of steel-framed buildings" [Doktora Tezi], University of Canterbury, 2017.
- 55. Jalao, E. R., Wu, T., Shunk, D. "A stochastic AHP decision making methodology for imprecise preferences", Information Sciences, Cilt 270, Sayfa 192-203, 2017.

- 56. Banzon, M. J. R., Bacudio, L. R., Promentilla, M. A. B. "Application of Monte Carlo analytic hierarchical process (MCAHP) in the prioritization of theme park service quality elements", 2016 International Conference on Industrial Engineering and Operations Management, Sayfa 1241-1252, 2016.
- 57. Tinoco, M. P., de Mendonça, É. M., Fernandez, L. I. C., Caldas, L. R., Reales, O. A. M., Toledo Filho, R. D. "Life cycle assessment (LCA) and environmental sustainability of cementitious materials for 3D concrete printing: A systematic literature review", Journal of building engineering, Cilt 52, Sayfa 104456, 2022.
- 58. Choudhuri, B., Uddin, M. F., Sen, R. "Review on 3D printing technology in automotive industry and electric vehicle". Proceedings of the Institution of Mechanical Engineers, Part D: Journal of Automobile Engineering, 09544070251337273, 2025.

- 59. Ruiz, L.E.; Pinho, A.C.; Resende, D.N. "3D Printing as a Disruptive Technology for the Circular Economy of Plastic Components of End-of-Life Vehicles: A Systematic Review". Sustainability 14, 13256., 2022.
- 60. Fereydoonian, M., Lee, K., Kiriella, C., Moon, J., Lee, W. "Closing the Loop on Circular Economy in Transportation Electrification: Reuse, Repurposing, and Recycling of Batteries, Power Electronics, and Electric Machines". IEEE Journal of Emerging and Selected Topics in Industrial Electronics, 2025



ULUSLARARASI 3B YAZICI TEKNOLOJİLERİ VE DİJİTAL ENDÜSTRİ DERGİSİ

INTERNATIONAL JOURNAL OF 3D PRINTING TECHNOLOGIES AND DIGITAL INDUSTRY

ISSN:2602-3350 (Online)

URL: https://dergipark.org.tr/ij3dptdi

THE EFFECT OF FDM PROCESS PARAMETERS ON THE MACHINABILITY OF PET-G MATERIAL: DELAMINATION ANALYSIS USING THE TAGUCHI APPROACH

Yazarlar (Authors): Zihni Alp Çevik D*

Bu makaleye şu şekilde atıfta bulunabilirsiniz (To cite to this article): Çevik Z. A., "The Effect Of FDM Process Parameters On The Machinability Of PET-G Material: Delamination Analysis Using The Taguchi Approach" Int. J. of 3D Printing Tech. Dig. Ind., 9(2): 310-319, (2025).

DOI: 10.46519/ij3dptdi.1704399

Araştırma Makale/ Research Article

THE EFFECT OF FDM PROCESS PARAMETERS ON THE MACHINABILITY OF PET-G MATERIAL: DELAMINATION ANALYSIS USING THE TAGUCHI APPROACH

Zihni Alp Çevik ^a

^aAdıyaman University, Besni Vocational School, Department of Mechatronics, TÜRKIYE

*Corresponding Author: <u>zcevik@adiyaman.edu.tr</u>

(Received: 22.05.25; Revised: 03.07.25; Accepted: 08.07.25)

ABSTRACT

In this study, the machinability of PET-G (Polyethylene Terephthalate Glycol) material produced by Fused Deposition Modeling (FDM) was experimentally investigated under various manufacturing and machining parameters. The effects of key parameters influencing delamination—namely infill percentage, layer thickness, spindle speed, and feed rate—were specifically examined. Statistical data were obtained using the Taguchi method, and the results were analyzed in terms of both mean values and Signal-to-Noise (S/N) ratios. The findings revealed that infill percentage has a significant effect on delamination. The lowest delamination values were observed at a 100% infill level, while the highest delamination occurred at a 33% infill ratio. When layer thickness was increased from 1 mm to 2 mm, a reduction in delamination tendency was observed. An increase in spindle speed resulted in a notable rise in delamination, particularly at high rotational speeds (4500 rpm), where elevated cutting forces and temperature led to structural damage and delamination. The influence of feed rate on delamination was relatively minor. This study presents a comprehensive experimental analysis of both production parameters (infill percentage and layer thickness) and machining parameters (spindle speed and feed rate) for PET-G material. It is concluded that, for optimal machinability of PET-G manufactured via the FDM method, an infill percentage of 100% and a layer thickness of 2 mm are recommended. This work provides valuable guidance for quality control and parameter optimization in post-additive manufacturing machining processes.

Keywords: FDM, PET-G, Machinability, Delamination, Taguchi Method, Parameter Optimization

1. INTRODUCTION

Additive Manufacturing (AM), commonly known as 3D printing, has become a preferred technology in various industrial fields such as defense, automotive, and medical sectors. It is increasingly favored over traditional manufacturing methods due to its cost-effectiveness, rapid prototyping capabilities, and minimal material waste [1-2].

The classical manufacturing method based on melting and shaping plastic is known as Fused Deposition Modeling (FDM). These 3D printers, which have become integrated into daily life, enable the rapid production of commonly used items such as household tools and toys, as well as components used in sectors like defense, automotive, and home appliances.

In FDM, the production process is carried out by a system where the extruder nozzle of a 3D printer moves along the x, y, and z axes [3]. The material to be produced is modeled in CAD software and converted to an STL file. Then, CAM codes are generated and sent to the 3D printer. Production is based on the principle of layer-by-layer deposition of molten material [4]. A wide variety of polymers can be used in this process. Among them, Polyethylene Terephthalate Glycol (PET-G) is one of the most commonly used materials due to its glossy finish, impact resistance, toughness, and machinability [5].

After FDM production, secondary machining processes such as threading, drilling, surface finishing, and edge trimming are often

necessary to facilitate assembly and integration [6].

However, due to the non-homogeneous structure of the printed materials, delamination may occur, leading to structural failure [7]. Therefore, machinability studies are essential to characterize the behavior of FDM-manufactured materials during machining. The literature contains numerous studies on the production and mechanical properties of PET-G material.

For instance, Basurto-Vázquez and colleagues investigated the energy absorption capacities of honeycomb structures made from PET-G under different infill percentages (30%, 70%, 100%) and printing orientations (horizontal, vertical, flat). According to the results, printing parameters significantly influenced both delamination tendency and energy absorption behavior. The best performance was observed in the structure printed vertically with a 100% infill ratio [8].

Lozrt et al. applied post-processing treatments (chemical smoothing, heat treatment, epoxy and water-based coatings) to samples made of recycled PET-G (rPET-G). Heat treatment was found effective not only in improving mechanical properties but also in reducing moisture absorption. These findings highlight the importance of post-processing techniques in enhancing the durability of PET-G materials [9].

Menderes et al. investigated the relationship between surface roughness, infill percentage, pattern type, and certain mechanical properties of PET-G produced via 3D printing. They used a nozzle temperature of 240 $^{\circ}\mathrm{C}$ and a wall thickness of 0.2 mm, with Ra values ranging from 10.38 to 14.02 μm [10].

Santana et al. employed a Taguchi experimental design to examine the effects of process parameters in printing PLA and PETG materials. They found that filament diameter, viscosity, and deposition speed significantly influenced material properties [11].

Guo et al. worked to improve the surface quality of FDM-fabricated amorphous PEEK and carbon fiber-reinforced PEEK composites through dry milling. They investigated the interplay between printing parameters (layer thickness, raster angle) and milling parameters (cutting depth, spindle speed, feed rate). It was demonstrated that a +45°/-45° raster angle and small layer thickness improved surface quality [12].

Xu et al. evaluated the machinability of carbon fiber-reinforced polyimide (PI) and PEEK composites in terms of cutting forces, temperature rise, delamination damage, surface morphology, and tool wear during drilling. It was determined that carbon/PEEK composites exhibited higher drilling forces and wear tendencies, yet achieved better surface quality due to continuous chip formation [13].

Kumar et al. fabricated carbon fiber-reinforced PETG using FDM and analyzed tensile strength, flexural strength, and hardness to optimize machine parameters [14]. Khoran et al. studied the effects of cryogenic cooling (carbon dioxide snow) on the grinding of Polyether Ether Ketone (PEEK), showing that it reduced tool loading and improved surface quality and tool life [15].

El Magri et al. optimized printing parameters to enhance the mechanical and thermal performance of 3D-printed PEEK parts. Nozzle temperature was identified as the most significant parameter affecting tensile properties and crystallinity. Annealing further improved performance by relieving residual stresses and increasing crystallinity [16].

Kartal et al. conducted cutting tool operations on 100% infill rate PLA material produced via 3D printing to determine optimal machining parameters [17]. Ergene et al. theoretically investigated the effects of conical angle and boundary conditions on the natural frequency values of PET-G material beams fabricated by FDM, validated their results using ANSYS software, and subsequently performed tensile tests [18].

Karaca et al. utilized PLA material manufactured via FDM and conducted pressure and compression tests [19]. Peduk et al. produced a NiTi shape memory alloy via Electron Beam Melting (EBM), employing a high-energy electron beam in the additive manufacturing process, and subsequently

machined the material using Wire Electrical Discharge Machining (WEDM) [20].

Doğru et al. experimentally and numerically investigated the impact strength, interlayer delamination defects, and bending stress effects of PET material produced by additive manufacturing [21]. Çevik et al. studied optimal cutting parameters for 316L stainless steel manufactured through additive manufacturing techniques [22].

Mercado-Colmenero et al. examined the mechanical characterization of PET-G material produced by FDM under uniaxial compressive loading conditions [23]. Özen et al. conducted a study on the modeling of mechanical properties of FDM-fabricated PET-G material using the finite element method [24].

As understood from the literature, there are limited studies on the machinability of PET-G materials produced via FDM. In particular, systematic investigations that simultaneously consider production parameters (such as infill percentage and layer thickness) and machining parameters (such as spindle speed and feed rate) are lacking. This study aims to evaluate the delamination behavior of PET-G materials after CNC machining following FDM production, Taguchi experimental design using the approach. Thus, it is intended to contribute the first comprehensive experimental study that jointly examines both production and machining parameters for PET-G in the literature.

2. MATERIALS AND METHODS

2.1. Materials

In this study, the specimen used was produced using the FDM (Fused Deposition Modeling) method and is commonly referred to as PET-G (Polyethylene Terephthalate Glycol). This composite material is widely used due to its high strength-to-weight ratio, hardness, and excellent thermal stability, which are among its superior mechanical properties. The PET-G filament used in this study has a diameter of 1.75 mm and is a standard material for Fused Deposition Modeling (FDM) 3D printing processes.

The technical specifications of the 3D printer used in the FDM process are presented in Table 1

Table 1. Technical specifications of the 3D printer used in FDM production

usea m i biii	used in 1 Bivi production			
Bambu Lab X-Carbon	Bambu Lab X-Carbon Fused Deposition			
Model	ing			
Maximum speed of	500 mm/s			
moving head part				
Maximum speed of	20 m/s^2			
moving head part				
Nozzle Diameter	0.4 mm			
(Included)				
Filament Diameter	1.75 mm			
Max Hot End Flow	Temperature: 280			
Recommended PETG, vb.				
Filament				

2.2. Specimen Fabrication

The specimens were fabricated using an FDM-based 3D printer. The printer was equipped with a heated build plate and an extruder capable of processing high-temperature materials such as PET-G. A systematic experimental design was implemented to

investigate the effects of various processing parameters on the delamination behavior of the printed parts. The primary processing parameters included infill percentage (iF), layer thickness (LT), spindle speed (n), and feed rate (F). These parameters were varied at multiple levels, as detailed below. The parameters are presented in Table 2.

Table 2. Production and processability parameters

	Parameter					
Infill	Layer	Feed rate	spindle			
percentage	thickness	(F)	speed (n)			
(iF) %	(LT) (mm)	mm/min.	rpm			
100	1	100	1500			
66	1,5	150	3000			
33	2	200	4500			

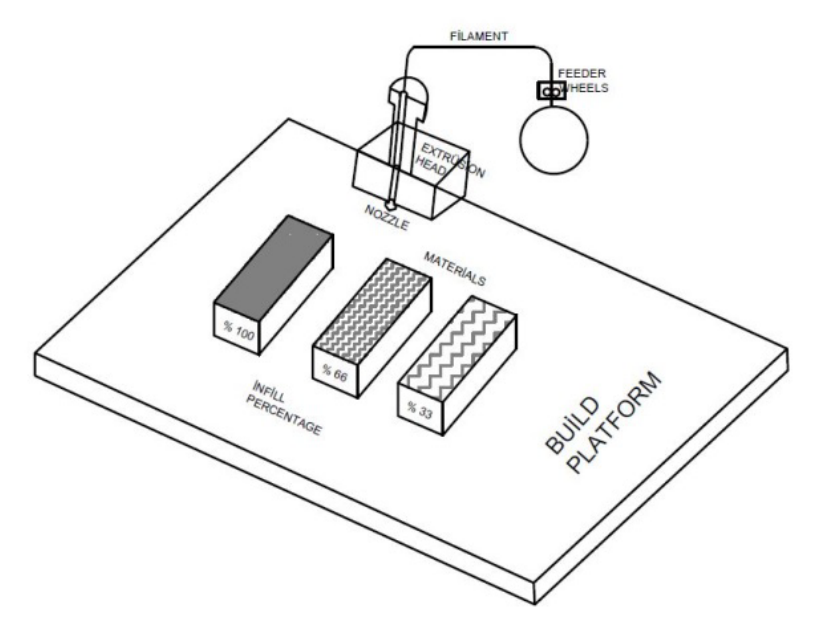


Figure 1. Schematic representation of materials produced in different categories during production

For this experimental study, materials were produced for processability study with different infill percentages and wall thicknesses under constant printing speed and extruder temperature (240°C). Figure 1 illustrates the schematic representation of the production process. In Figure 2, the printed samples' infill percentages and wall thicknesses are clearly shown.

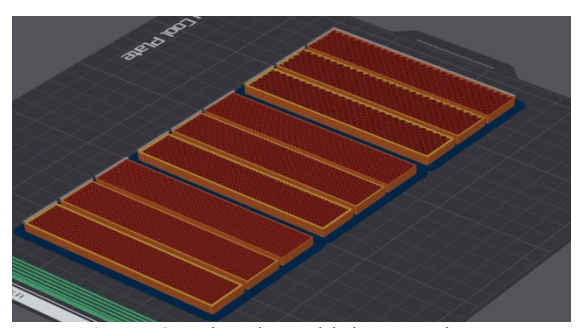


Figure 2. Printed Machining Specimens

The PETG specimens produced by FDM were fabricated using three different levels of Infill Percentage (iF) (%33, %66, %100) and three different levels of Layer Thickness (LT) (1 mm, 1.5 mm, 2 mm), resulting in a total of 9 specimens. These parameter levels were combined to produce a total of 9 samples. Each was sample printed under controlled environmental conditions to minimize external effects such as temperature and humidity variations. The printing and machining parameters, along with their corresponding category levels (1, 2, and 3), are presented in Table 3.

Table 3. Printing and Machining Parameters Corresponding to Categories 1, 2, and 3.

	Infill percentage (iF) %	Layer thickness (LT) (mm)	Feed rate (F) mm/min	Spindle speed (n) rpm
Category 1	100	1	100	1500
Category 2	66	1,5	150	3000
Category 3	33	2	200	4500

2.3. Experimental Setup

The experimental setup was designed to evaluate the delamination behavior of PETG specimens. Delamination, defined as the separation between layers within the printed part, was measured in millimeters (mm) and recorded for each combination of processing parameters. Measurements were taken using a high-precision instrument to ensure accuracy and repeatability.

PETG samples were produced with the FDM method in the dimensions of 100 mm x 20 mm x 6 mm (Figure 2). Testing operations were carried out on PETG samples produced with the FDM method on a Tezaymak brand 3-axis high-speed CNC milling machine (Figure 3b). The maximum spindle speed of this CNC machine is 10,000 rpm and the machining precision is 1 µm. A 4 mm diameter coated carbide end milling cutter (Figure 3a) was used as the cutting tool for machining. The machinability test setup is shown in Figure 3.



Figure 3. Machining system

2.4. Taguchi and Delamination

To investigate the machinability parameters of PET-G material produced via Fused Deposition Modeling (FDM), the Taguchi orthogonal array design, will be employed. This method is used method, a systematic Design of Experiments (DOE) approach such as full factorial design or Box-Behnken to evaluate the effect of multiple input variables on a single output variable and provides a systematic approach for accurately characterizing the response surface and determining optimal parameters [25-26].

The Taguchi method helps identify the factors that significantly influence the machining performance, enhances the robustness of the process at optimal levels, and reveals the effective parameters with minimal experimental effort. For this purpose, XLSTAT, an add-on tool for Microsoft Excel, was utilized. Graphs representing mean values, Signal-to-Noise (S/N) ratios, and other tools were employed to analyze variability in the process and minimize the output responses.

In this study, four different parameters—namely infill percentage, layer thickness, feed rate, and spindle speed—were considered. A total of eighty-one machining operations were carried out by assigning each parameter to a separate channel. Measurements were taken

from two different regions within each channel using precision calipers. Since minimal delamination during machining is desired, the "smaller-the-better" category was selected as the response criterion in this study.

Delamination occurring during machining was quantified using the delamination factor, defined as the ratio of WMax/W. Here, WMax represents the maximum width reached by the damage zone, while W denotes the diameter of the cutting tool's tip.

3. RESULTS

In this study, the machinability of PET-G material produced using the Fused Deposition Modeling (FDM) method was investigated under different manufacturing parameters such as infill percentage, layer thickness, spindle speed, and feed rate. The effects of certain parameters on delamination were systematically evaluated and supported with Taguchi plots.

For four different parameters, infill percentage, layer thickness, feed rate and spindle speed, three different categories were considered. Three different values were used in three different categories for the four different parameters used and are shown in Table 4. In this way, eighty-one data inputs were taken and eighty-one delamination output values were found. These values were made according to the larger is better principle in the Taguchi method Signal to noise ratios graph and are shown in Figure 4. In addition, delamination output values (according to mean values) were plotted according to the smaller is better principle. This graph is shown in Figure 5.

The results obtained using the Taguchi experimental design approach showed that the infill percentage among the production parameters had the most significant effect on delamination. While the lowest delamination values were obtained especially at 100% infill ratio, it is thought that this situation can be explained by the denser structure between the layers. In similar studies conducted in the literature, it has been observed that the infill ratio plays an important role on the mechanical and structural properties.

Table 4. Signal-to-Noise ratio values presented across three categories.

Signal to Noise ratios:

	İnfill percentage	Layer thickness	Spindle speed	Feed rate (F)
	(iF) %	(LT) (mm)	(n) rpm	mm/min.
Category 1	15,458	17,503	17,661	18,140
Category 2	18,199	17,939	17,968	17,989
Category 3	20,248	18,462	18,276	17,776

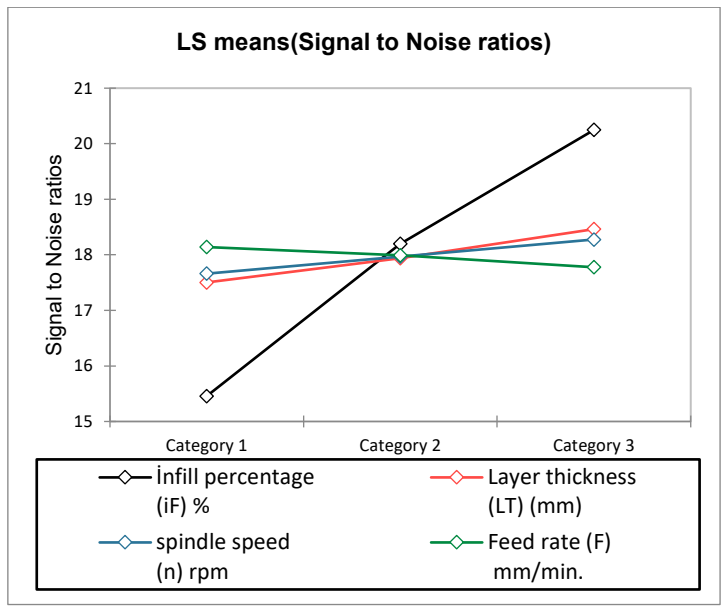


Figure 4. Taguchi Signal to Noise ratios graph

Table 5. Display of delamination (mm) values in 3 categories.

0,130

0,122

İnfill percentage

(iF) %

0,169

0,124

0,097

Category 1

Category 2

Category 3

Micans.		
Layer thickness	spindle speed	Feed rate (F)
(LT) (mm)	(n) rpm	mm/min.
0,137	0,135	0,127

0,130

0,125

0,130

0,133

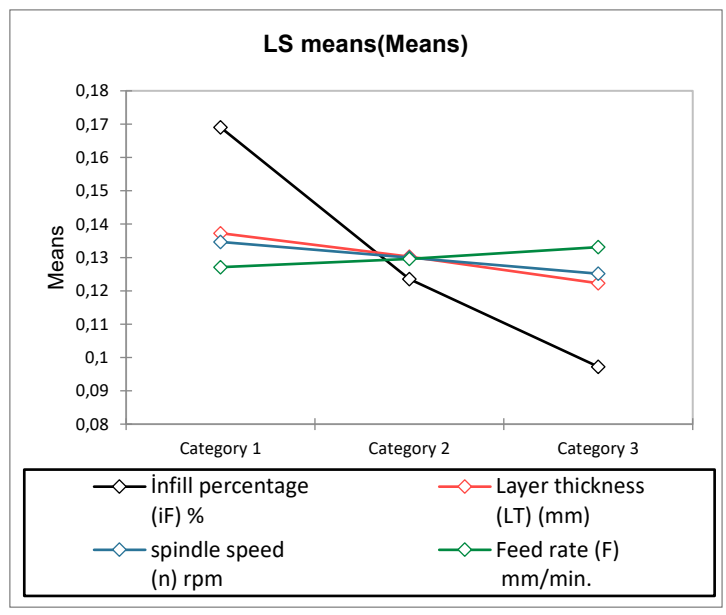


Figure 5. Taguchi Delamination graph

In the graph, the horizontal axis is divided into three categories. The vertical axis represents the Signal-to-Noise (S/N) ratios. The central bar lines indicate different parameters (infill percentage, layer thickness, spindle speed, and feed rate). The entire graph compares the delamination amount corresponding to three different categories using the Signal-to-Noise (S/N) ratios. It is observed in Table 4 and Table 5 that the delamination tendency decreases with increasing the layer thickness (from 1 mm to 2 mm). This result can be interpreted as the thicker layers exhibit relatively homogeneous behavior during the material removal process and reduce the number of operations at weak points. This situation here is also consistent with the result of the study conducted by Mercado-Colmenero et al. [23] that the mechanical behavior of the

PET-G material changes depending on the layer thickness.

3.1. Delamination

Delamination can be defined as the formation of undesirable conditions such as layer separation or expansion in the processing area during the removal process of a material after production. This problem is particularly important for additively manufactured materials, as it affects the surface quality and structural integrity of the part. According to the results obtained from the graphical analysis, the degree of delamination varies depending on parameters such as infill percentage, layer thickness, spindle speed and feed rate. This change is shown in Figure 4 and Figure 5.

In general, an increase in infill percentage results in a decrease in delamination. The lowest delamination values, ranging between 0.102 mm and 0.987 mm, were observed at 100% infill, while the highest delamination values, between 0.147 mm and 0.197 mm, occurred at 33% infill. This suggests that a higher infill percentage leads to a more compact internal structure, thereby increasing the bonding strength between layers.

An increase in wall thickness also showed a tendency to reduce delamination. It was observed that samples with a layer thickness increased from 1 mm to 2 mm exhibited reduced delamination. This can be attributed to the fact that thicker layers have fewer weak points

during the machining process and display a more homogeneous behavior during cutting operations.

An increase in spindle speed led to a significant rise in delamination. Especially when the spindle speed was increased from 1500 rpm to 4500 rpm, more pronounced delamination was observed in samples with 100% infill. This indicates that high cutting speeds at higher spindle speeds can damage the structure of the material.

During the processing of the material, high speed processing generates thermal heat, which leads to deterioration in the material and therefore delamination.

Although a slight reduction in delamination was observed with an increase in feed rate, the effect was not found to be statistically significant.

According to literature, machinability studies on FDM-produced thermoplastic materials are generally focused on a single parameter or material type. However, this study presents a comprehensive experimental investigation on PET-G material, for the first time, where both production parameters (infill percentage and layer thickness) and machining parameters (spindle speed and feed rate) are evaluated together.

Due to the layered structure of PET-G materials produced via FDM, significant challenges are encountered during machining. Optimizing the results obtained with the parameters used in this study enables the minimization of delamination. It was concluded that using a 2 mm layer thickness and 100% infill percentage produces specimens with high strength and good machinability.

It has been observed that the increase in spindle speed causes a significant increase in the amount of delamination, especially at high speeds (4500 rpm). The reason for this situation can be considered as the damage to the material structure caused by the increased temperature and cutting forces that occur at high cutting speeds.

Although delamination tends to decrease slightly with the increase in feed rate, no statistically significant difference was found. In

this case, it is thought that the effect of the feed rate on the layered structure of the PET-G material is limited. It is consistent with the statement that there are only small mechanical changes depending on the feed rate in the study conducted by El Magri et al. [16].

4. DISCUSSION

According to the studies in the literature, it has been observed that the machinability studies of thermoplastic materials produced with FDM generally focus on a single parameter or materials.

However, in this study, for the first time, a comprehensive experimental study was conducted in PET-G material, where the production parameters (fill ratio and layer thickness) and the machinability parameters (spindle speed and feed rate) were evaluated together.

Due to the layered structure of this PET-G material produced with FDM, great difficulties are encountered during processing. Optimizing the results found with the parameters used here ensures that delamination is minimized. It was concluded that samples with high strength and good machinability can be produced, especially by preferring 2 mm layer thickness and 100% fill ratio.

5. CONCLUSION

In this study, the machinability of PET-G material produced via Fused Deposition Modeling (FDM) was investigated with respect to both printing parameters (infill percentage and layer thickness) and machining parameters (spindle speed and feed rate). Delamination emerged as one of the critical issues during tool-based machining operations. The influence of these parameters on delamination was analyzed using the Taguchi design of experiment methodology. Based on the analysis, the following conclusions were drawn:

An increase in infill percentage resulted in a decrease in delamination. The lowest delamination values were achieved at 100% infill density. This can be attributed to the fact that higher infill percentages lead to a denser material structure and improved interlayer bonding strength. Conversely, the highest delamination was observed at the 33% infill level.

From the perspective of wall thickness, an increase from 1 mm to 2 mm led to a reduction in delamination tendency. This improvement may be explained by the more homogeneous behavior of the material during the machining process and a corresponding decrease in weak zones.

An increase in spindle speed caused a noticeable rise in delamination. As the spindle speed increased from 1500 to 4500 rpm, cutting forces and temperature increased, leading to structural damage in the material and promoting delamination. Therefore, it is recommended to use moderate spindle speeds during machining for better performance.

Although a slight decreasing trend in delamination was observed with increasing feed rate, the effect was not found to be statistically significant. Thus, the influence of feed rate on delamination remains limited.

In conclusion, for optimizing the machinability of PET-G material produced via the FDM method, a 100% infill level and 2 mm layer thickness are recommended as the most favorable parameters. This study provides valuable guidance for parameter optimization in additive manufacturing processes and subsequent machining operations.

REFERENCES

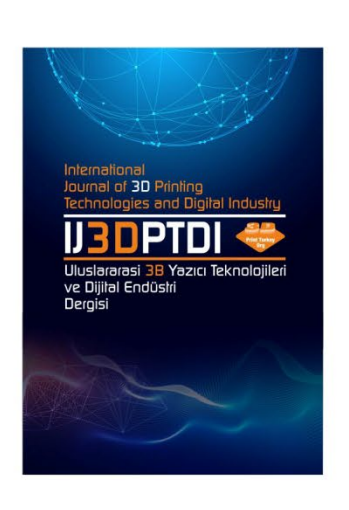
- 1. Wang, X., Jiang, M., Zhou, Z., Gou, J., & Hui, D. 3D printing of polymer matrix composites: A review and prospective. Composites Part B: Engineering, Vol.110, Pages 442-458, 2017.
- 2. Levy, G. N., Schindel, R., & Kruth, J. P. Rapid manufacturing and rapid tooling with layer manufacturing (LM) technologies, state of the art and future perspectives. CIRP annals, Vol. 52 Issue 2, Pages 589-609, 2003.
- 3. Özsoy, K., Erçetin, A., & Çevik, Z. A. Comparison of mechanical properties of PLA and ABS based structures produced by fused deposition modelling additive manufacturing. Avrupa Bilim ve Teknoloji Dergisi, Vol. 27, Pages 802-809, 2021.
- 4. Bruni, C., Gianangeli, C., Mancia, T., Greco, L., & Pieralisi, M.. Improving dimensional and surface quality of additive manufactured parts. In Journal of Physics: Conference Series, IOP Publishing, Vol. 1507, Issue 4, Pages 042003, 2020.

- 5. Cianci, C., Pappalettera, G., Renna, G., Casavola, C., Laurenziello, M., Battista, G., ... & Ciavarella, D. Mechanical behavior of PET-G tooth aligners under cyclic loading. Frontiers in Materials, Vol. 7, Pages 104, 2020.
- 6. Karataş, M. A., & Gökkaya, H. A review on machinability of carbon fiber reinforced polymer (CFRP) and glass fiber reinforced polymer (GFRP) composite materials. Defence Technology, Vol. 14 Issue 4, Pages 318-326, 2018.
- 7. Boschetto, A., Bottini, L., & Veniali, F. Finishing of fused deposition modeling parts by CNC machining. Robotics and Computer-Integrated Manufacturing, Vol. 41, Pages 92-101, 2016.
- 8. Basurto-Vázquez, O., Sánchez-Rodríguez, E. P., McShane, G. J., & Medina, D. I. Load distribution on PET-G 3D prints of honeycomb cellular structures under compression load. Polymers, Vol. 13, Issue 12, Pages 1983, 2021.
- 9. Lozrt, J., Votava, J., Henzl, R., Kumbár, V., Dostál, P., & Čupera, J. Analysis of the Changes in the Mechanical Properties of the 3D Printed Polymer rPET-G with Different Types of Post-Processing Treatments. Applied Sciences, Vol. 13, Issue 16, Pages 9234, 2023.
- 10. Kam, M., İpekçi, A., & Saruhan, H. Investigation of 3d printing filling structures effect on mechanical properties and surface roughness of PET-G material products. Gaziosmanpaşa Bilimsel Araştırma Dergisi, 6(Özel Sayı (ISMSIT2017)), Pages 114-121, 2017.
- 11. Santana, L., Lino Alves, J., & Da Costa Sabino Netto, A. Dimensional analysis of pla and petg parts built by open source extrusion-based 3d printing. In Proceedings of the 10° Congresso Brasileiro de Engenharia de Fabricação, São Carlos, SP, Brazil, Pages 5-7, 2019.
- 12. Guo, C., Liu, X., & Liu, G. Surface finishing of fdm-fabricated amorphous polyetheretherketone and its carbon-fiber-reinforced composite by dry milling. Polymers, Vol. 13, Issue 13, Pages 2175, 2021.
- 13. Xu, J., Huang, X., Davim, J. P., Ji, M., & Chen, M. On the machining behavior of carbon fiber reinforced polyimide and PEEK thermoplastic composites. Polymer Composites, Vol. 41, Issue 9, Pages 3649-3663, 2020.

- 14. Kumar, M. A., Khan, M. S., & Mishra, S. B. Effect of machine parameters on strength and hardness of FDM printed carbon fiber reinforced PETG thermoplastics. Materials Today: Proceedings, Vol. 27, Pages 975-983. (2020).
- 15. Khoran, M., Amirabadi, H., & Azarhoushang, B. The effects of cryogenic cooling on the grinding process of polyether ether ketone (PEEK). Journal of manufacturing processes, Vol. 56, Pages 1075-1087. 2020.
- 16. El Magri, A., El Mabrouk, K., Vaudreuil, S., Chibane, H., & Touhami, M. E. Optimization of printing parameters for improvement of mechanical and thermal performances of 3D printed poly (ether ether ketone) parts. Journal of Applied Polymer Science, Vol. 137, Issue 37, Pages 49087, 2020.
- 17. Kartal, F., & Kaptan, A. Experimental determination of the optimum cutting tool for CNC milling of 3D printed PLA parts. International Journal of 3D Printing Technologies and Digital Industry, Vol. 7, Issue 2, Pages 150-160, 2023
- 18. Ergene, B., Atlıhan, G., & Pınar, A. Investigation of the effect of taper angle and boundary condition on natural frequency of the 3D printed PET-G beams. International Journal of 3D Printing Technologies and Digital Industry, Vol. 6, Issue 1, Pages 31-39, 2022.
- 19. Karaca, M. M., Ekinci, İ., & Ali, D. Effect of geometric modifications on the compressive strength and mechanical performance of gyroid-based bone scaffolds. International Journal of 3D Printing Technologies and Digital Industry, Vol. 9, Issue 1, Pages 63-72, 2025.
- 20. Peduk, G. S. A., Dilibal, S., & Gürol, U. Effect of wire electrical discharge machining on the surface of ebm-additive manufactured NiTi alloys. International Journal of 3D Printing Technologies and Digital Industry, Vol. 5, Issue 3, Pages 606-613, 2021.
- 21. Doğru, A., Sözen, A., Neşer, G., & Seydibeyoğlu, M. Ö. Numerical and experimental investigation of the effect of delamination defect at materials of polyethylene terephthalate (PET) produced by additive manufacturing on flexural resistance. International Journal of 3D Printing Technologies and Digital Industry, Vol. 6, Issue 3, Pages 382-391, 2022.

- 22. Çevik, Z. A., Özsoy, K., & Erçetin, A. Metal eklemeli imalat ile üretilen 316l paslanmaz çeliğin mikro işlenmesinde kesme mesafesinin çapak genişliğine etkisi. International Journal of 3D Printing Technologies and Digital Industry, Vol. 6, Issue 2, Pages 338-346, 2022.
- 23. Mercado-Colmenero, J. M., La Rubia, M. D., Mata-Garcia, E., Rodriguez-Santiago, M., & Martin-Doñate, C. Experimental and numerical analysis for the mechanical characterization of petg polymers manufactured with fdm technology under pure uniaxial compression stress states for architectural applications. Polymers, Vol. 12, Issue 10, Pages 2202, 2020.
- 24. Özen, A., Abali, B. E., Völlmecke, C., Gerstel, J., & Auhl, D. Exploring the role of manufacturing parameters on microstructure and mechanical properties in fused deposition modeling (FDM) using PETG. Applied Composite Materials, Vol. 28 Issue 6, Pages 1799-1828, 2021.

- 25. Kechagias, J. D., & Vidakis, N. Parametric optimization of material extrusion 3D printing process: an assessment of Box-Behnken vs. full-factorial experimental approach. The International Journal of Advanced Manufacturing Technology, Vol. 121, Issue 5, Pages 3163-3172, 2022.
- 26. Alzyod, H., & Ficzere, P. Optimizing fused filament fabrication process parameters for quality enhancement of PA12 parts using numerical modeling and taguchi method. Heliyon, Vol. 9 Issue 3, 2023



ULUSLARARASI 3B YAZICI TEKNOLOJİLERİ VE DİJİTAL ENDÜSTRİ DERGİSİ

INTERNATIONAL JOURNAL OF 3D PRINTING TECHNOLOGIES AND DIGITAL INDUSTRY

ISSN:2602-3350 (Online)

URL: https://dergipark.org.tr/ij3dptdi

BODE: A BOUNDARY AWARE DIFFERENTIAL EVOLUTION BASED HYBRID OVERSAMPLING TECHNIQUE FOR IMBALANCED DATA CLASSIFICATION

Yazarlar (Authors): Muhammed Abdulhamid Karabiyik **D**

Bu makaleye şu şekilde atıfta bulunabilirsiniz (To cite to this article): Karabiyik M. A., "Bode: A Boundary Aware Differential Evolution Based Hybrid Oversampling Technique for Imbalanced Data Classification" Int. J. of 3D Printing Tech. Dig. Ind., 9(2): 320-330, (2025).

DOI: 10.46519/ij3dptdi.1703106

Araştırma Makale/ Research Article

Erişim Linki: (To link to this article): https://dergipark.org.tr/en/pub/ij3dptdi/archive

BODE: A BOUNDARY AWARE DIFFERENTIAL EVOLUTION BASED HYBRID OVERSAMPLING TECHNIQUE FOR IMBALANCED DATA CLASSIFICATION

Muhammed Abdulhamid Karabiyika D*

^aNiğde Ömer Halidemir University, Bor Vocational School, Computer Techologies Department, TURKEY

* Corresponding Author: abdulhamidkarabiyik@ohu.edu.tr

(Received: 20.05.25; Revised: 11.07.25; Accepted: 27.07.25)

ABSTRACT

Class imbalance presents a persistent challenge in supervised learning, often degrading classifier performance on underrepresented classes. This study introduces BODE, a hybrid oversampling method that combines boundary-aware instance selection, differential evolution-based perturbation, and density-constrained filtering. By targeting critical minority instances near decision boundaries, BODE generates diverse yet structurally valid synthetic samples. Experiments on 44 benchmark datasets using k-NN, Decision Tree, and SVM classifiers demonstrate that BODE consistently outperforms eleven widely used oversampling methods. Evaluated solely using the AUC metric, BODE achieves the highest average performance across all classifiers, with 28, 33, and 26 dataset-level wins, respectively. These results confirm BODE's robustness and generalization capability, particularly in challenging scenarios involving overlapping or sparse decision regions.

Keywords: Imbalanced Learning, Oversampling, Differential Evolution, Decision Boundary.

1. INTRODUCTION

In many real-world classification problems, the distribution of classes is highly imbalanced, with the minority class significantly underrepresented [1]. This imbalance often leads to biased models that perform well on the majority class while failing to detect rare but critical minority instances. Such failures are especially detrimental in domains like medical diagnosis, fraud detection, and fault prediction, where accurate identification of minority cases is essential for minimizing risk and ensuring reliable decision-making [2–4].

To mitigate the impact of class imbalance, various oversampling techniques have been proposed, with SMOTE and its variants being among the most widely adopted. These methods generate synthetic samples to augment the minority class, aiming to balance the dataset without discarding valuable majority information [5]. However, most interpolation-based approaches fail to preserve the decision boundaries and often generate overlapping or noisy samples, which may degrade classifier performance rather than improve it.

have Recent studies explored more sophisticated strategies, such as boundaryaware sampling and evolutionary algorithms, to improve synthetic sample quality. Boundaryfocused methods aim to reinforce critical regions near decision boundaries, while Differential Evolution (DE) offers a robust framework for generating diverse informative samples. Yet, these approaches are typically applied in isolation, and the lack of integration between boundary sensitivity and adaptive generation limits their overall effectiveness [6–9].

To overcome these limitations, BODE introduces a hybrid oversampling strategy that integrates boundary-aware instance selection with Differential Evolution-based synthetic sample generation. The method begins by detecting minority instances near decision boundaries through a k-nearest neighbors analysis. Controlled perturbations are then applied to these critical points using evolutionary operations, generating synthetic samples that are both diverse and well-positioned. This design enhances the distinction

between classes while reducing the risk of noise and redundancy.

The effectiveness of BODE has been validated through extensive experiments conducted on 44 benchmark datasets from the KEEL repository. Performance was evaluated using the Area Under the ROC Curve (AUC) metric, which is well-suited for imbalanced classification tasks. Across multiple classifiers, including k-Nearest Neighbors, Decision Trees, and Support Vector Machines, BODE consistently outperformed a range of established oversampling techniques, demonstrating its robustness and superior boundary modeling capability.

2. RELATED WORK

Synthetic Minority Oversampling Technique (SMOTE) and its variants have been widely used to address class imbalance by generating minority class samples interpolation. Extensions such as Borderline-SMOTE, Safe-Level-SMOTE, and ADASYN aim to refine sample generation by focusing on boundary regions, local density, or instance difficulty [10-12]. However, these methods often suffer from overlapping synthetic instances and fail to adequately capture complex decision boundaries. To address such limitations, filtering-based methods SMOTE-ENN and SMOTE-TomekLinks have been proposed, yet they still rely on static interpolation rules that limit adaptability in highly imbalanced or noisy datasets [13-14].

To improve flexibility and diversity in synthetic sample generation, evolutionary algorithms such as DE have been incorporated into oversampling frameworks. DE-based methods like DEBOHID have shown promise by exploring the feature space in an adaptive manner [9]. Other hybrid approaches, including swarm intelligence, genetic algorithms, and cluster-guided sampling, attempt to balance diversity and representativeness. However, most of these methods either ignore decision boundary awareness or lack mechanisms to constrain synthetic instances within meaningful regions. This creates a gap for methods that integrate evolutionary generation with explicit boundary sensitivity — a gap that BODE aims to fill.

3. PROPOSED METHOD

Imbalanced datasets often suffer from insufficient representation of minority class patterns, especially in regions close to decision boundaries. Conventional oversampling methods generate synthetic samples based on uniform strategies that disregard local data geometry or class overlap. This may lead to the creation of redundant or misleading samples that fail to improve classification performance.

To address these challenges, the proposed method BODE combines two complementary strategies: (1) the use of DE to generate diverse synthetic samples, and (2) the application of a density-aware boundary constraint to ensure the reliability of those samples. This hybrid approach prioritizes borderline regions while filtering out unsafe or noisy generations. The core components of BODE are presented in the following subsections.

3.1. Synthetic Sample Generation Via Differential Evolution

To generate diverse and informative synthetic samples, BODE employs DE, a population-based optimization algorithm. For each selected borderline minority instance x_{target} three distinct minority samples x_{r1}, x_{r2}, x_{r3} are randomly selected to construct a mutant vector using the DE/rand/1 strategy, as defined in Equation 1:

$$v = x_{r1} + F \cdot (x_{r2} - x_{r3}) \tag{1}$$

Here, $F \in (0,1)$ is a mutation factor that controls the amplification of the differential variation [15]. The resulting mutant vector v is then combined with the target instance x_{target} using a binomial crossover to produce a trial vector uuu, as shown in Equation 2:

$$x_{trial}(j) = \begin{cases} v[j] & if \ rand_j < CR \\ x_i[j] & otherwise \end{cases}$$
 (2)

In this expression, CR represents the crossover rate, and $rand_j$ is a uniformly distributed random number generated independently for each feature dimension j. The resulting trial vector v serves as a candidate synthetic sample. This mechanism introduces controlled diversity while preserving the structural coherence of the minority class [16].

In our implementation, we used a mutation factor F of 0.5 and a crossover rate CR of 0.9, which are commonly adopted values for maintaining a balance between exploration and exploitation in the evolutionary search process [Reference]. The population size was set to 50, ensuring sufficient diversity introducing excessive computational These parameter settings were kept constant across all datasets to maintain consistency and reproducibility of the results. Sensitivity analyses confirmed that these values provided stable and robust performance across various data distributions[17].

3.2. Step-by-Step Execution Of BODE

The BODE algorithm operates through a sequence of procedures that ensure synthetic samples are generated in informative and safe regions of the minority class distribution.

The process begins with identifying the structural center of the minority class. Kernel Density Estimation (KDE) is applied to approximate the densest region of minority samples [18]. Based on this estimation, a circular boundary is drawn around the computed center to define a safe generation area. This approach helps prevent sample creation in sparse or unreliable regions. The overall structure and the defined boundary are illustrated in Figure 1.

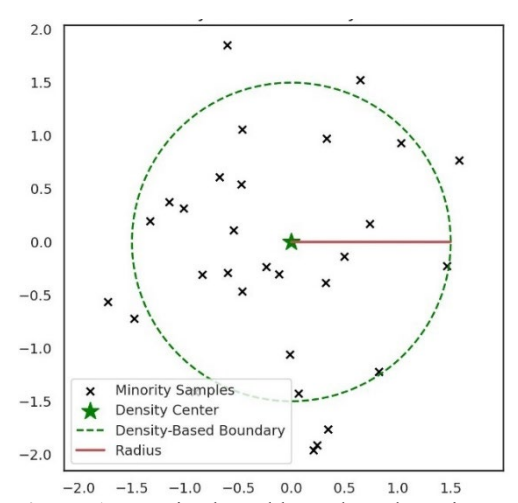


Figure 1. Density-based boundary detection on minority class samples. The central region is identified using KDE, and a circular boundary is drawn around the estimated density center to define a safe area for synthetic sample generation.

Following boundary construction, synthetic samples are generated using the DE strategy

described in Section 3.1. For each selected minority instance, a new sample is created through mutation and crossover operations involving neighboring instances. This mechanism introduces diversity while preserving class consistency. The sample generation process is visualized in Figure 2.

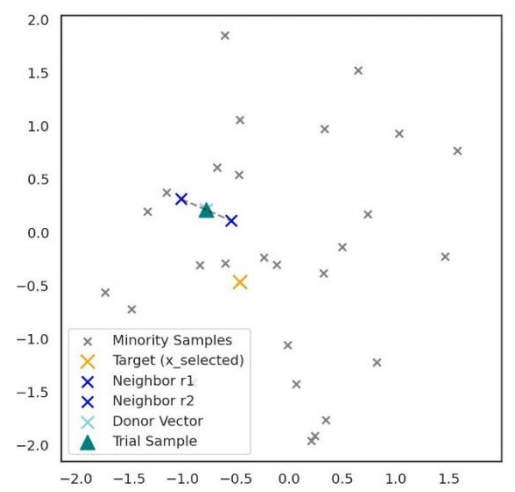


Figure 2. Synthetic sample generation using Differential Evolution. A target instance and three random neighbors are selected from the minority class, and a trial sample is generated through mutation and crossover operations.

Once candidate samples are produced, each one is validated based on its location relative to the previously defined boundary. Samples falling inside the safe zone are accepted, while those located outside are rejected to minimize the risk of noise or class overlap. The acceptance and rejection of synthetic instances are illustrated in Figure 3.

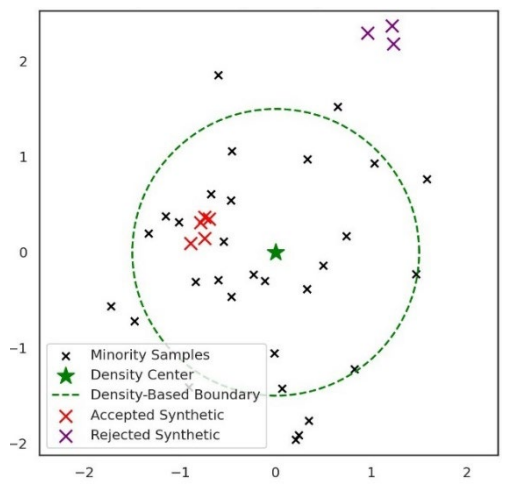


Figure 3. Validation of synthetic samples based on the boundary constraint. Samples generated inside the safe region are accepted, while those outsides are rejected to preserve class consistency and prevent noise.

4. EXPERIMENTAL EVALUATION

To evaluate the performance of BODE, experiments were conducted on a collection of benchmark imbalanced datasets obtained from the KEEL repository [19]. These datasets span a wide range of domains and vary significantly in size, dimensionality, and class distribution. Each dataset presents a binary classification problem in which the minority class is underrepresented to varying degrees.

The degree of class imbalance in each dataset is quantified using the imbalance ratio (IR), defined as the ratio of majority to minority class instances. A higher IR indicates a more severe imbalance, making the classification task more challenging.

A complete list of the datasets used in the experiments, along with their number of instances, features, and imbalance ratios, is provided in Table 1.

Table 1. Overview of the 44 Benchmark Datasets Used in the Experiments

		Total	Feature	Minority Class	Majority Class	Imbalance
No	Dataset Name	Samples	S	%	%	Ratio
1	ecoli0137vs26	281	7	2.49	97.51	39.15
2	shuttle0vs4	1829	9	6.72	93.28	13.87
3	yeastB1vs7	459	7	6.53	93.47	14.3
4	shuttle2vs4	129	9	4.65	95.35	20.5
5	glass016vs2	192	9	8.85	91.15	10.29
6	glass016vs5	184	9	4.89	95.11	19.44
7	pageblocks13vs4	472	10	5.93	94.07	15.85
8	yeast05679vs4	528	8	9.66	90.34	9.35
9	yeast1289vs7	947	8	3.16	96.84	30.5
10	yeast1458vs7	693	8	4.33	95.67	22.1
11	yeast2vs4	514	8	9.92	90.08	9.08
12	Ecoli4	336	7	6.74	93.26	13.84
13	Yeast4	1484	8	3.43	96.57	28.41
14	Vowel0	988	13	9.01	90.99	10.1
15	Yeast2vs8	482	8	4.15	95.85	23.1
16	Glass4	214	9	6.07	93.93	15.47
17	Glass5	214	9	4.2	95.8	22.81
18	Glass2	214	9	7.94	92.06	11.59
19	Yeast5	1484	8	2.96	97.04	32.78
20	Yeast6	1484	8	2.49	97.51	39.16
21	abalone19	4174	8	0.77	99.23	128.87
22	abalone918	731	8	5.75	94.25	16.4
23	cleveland0vs4	177	13	7.34	92.66	12.61
24	ecoli01vs235	244	7	2.86	97.14	9.16
25	ecoli01vs5	240	7	2.91	97.09	11
26	ecoli0146vs5	280	7	2.5	97.5	13
27	ecoli0147vs2356	336	7	2.08	97.92	10.58
28	ecoli0147vs56	332	7	2.1	97.9	12.28
29	ecoli0234vs5	202	7	3.46	96.54	9.1
30	ecoli0267vs35	224	7	3.12	96.88	9.18
31	ecoli034vs5	300	7	2.33	97.67	9
32	ecoli0346vs5	205	7	3.41	96.59	9.25
33	ecoli0347vs56	257	7	2.72	97.28	9.28
34	ecoli046vs5	203	7	3.44	96.56	9.15
35	ecoli067vs35	222	7	3.15	96.85	9.09
36	ecoli067vs5	220	7	3.18	96.82	10
37	glass0146vs2	205	9	4.39	95.61	11.05
38	glass015vs2	172	9	5.23	94.77	9.11

39	glass04vs5	92	9	9.78	90.22	9.22
40	glass06vs5	108	9	8.33	91.67	11
41	led7digit02456789vs	443	7	1.58	98.42	10.97
42	yeast0359vs78	506	8	9.8	90.2	9.12
43	yeast0256vs3789	1004	8	9.86	90.14	9.14
44	yeast02579vs368	1004	8	9.86	90.14	9.14

Three widely used classification algorithms were employed to assess the impact of oversampling: k-Nearest Neighbors (k-NN), Decision Tree (DT), and Support Vector Machine (SVM) [20–22]. These classifiers were selected due to their distinct learning mechanisms and frequent use in imbalanced learning literature. k-NN serves as a distancebased non-parametric method, DT provides a rule-based approach sensitive to data structure, and SVM offers a margin-maximizing framework that is particularly relevant for highdimensional and imbalanced data. diversity allows for a comprehensive evaluation of BODE's effectiveness across different classification paradigms.

Model performance was evaluated using the AUC, which measures a classifier's ability to discriminate between positive (minority) and negative (majority) classes. AUC is a threshold-independent metric that reflects overall ranking quality and is particularly useful for evaluating classifiers on imbalanced datasets [23].

In simplified binary classification settings, AUC can be estimated using the following relationship, shown in Equation 3:

$$AUC = \frac{1 + TPrate - FPrate}{2}$$
 (3)

where TPR is the true positive rate and FPR is the false positive rate. This formulation captures the trade-off between sensitivity and specificity, providing a robust evaluation criterion when class distributions are skewed. For this reason, AUC was used as the sole performance metric in all experimental comparisons.

In this study, the performance of the proposed BODE method was compared against a diverse set of baseline oversampling techniques. The Original setting, where no oversampling was applied, served as a control to assess the impact of sample generation. SMOTE, the most widely used synthetic sampling method, and its two

hybrid extensions—SMOTE-TomekLinks (Sand SMOTE-ENN (S-ENN)—were included to represent noise reduction and boundary-cleaning strategies. Borderline-SMOTE1 (Border1) and Borderline-SMOTE2 (Border2) were selected for their emphasis on generating samples near decision boundaries. Safe-Level SMOTE and ADASYN were included as density-sensitive methods, which adjust the location or frequency of generated samples based on local minority instance distributions. In addition, SMOTE-RSB (S-RSB) was chosen for its relative safe boundary enhancement, and DEBOHID, an evolutionary oversampling technique, was included as a recent alternative leveraging directional perturbation. This comprehensive set of eleven methods enabled a robust comparison across traditional, boundary-focused, density-aware, and evolutionary oversampling paradigms.

5. RESULTS AND DISCUSSION

This section presents a comparative analysis of the proposed BODE method against ten widely used oversampling techniques. The evaluation was conducted using three different classifiers: k-Nearest Neighbors (k-NN), Decision Tree (DT), and Support Vector Machine (SVM). The performance of each method was assessed using the AUC metric, which provides a robust, threshold-independent measure of classification quality in imbalanced settings. Detailed results are reported in Tables 2, 3, and 4, corresponding to the outcomes obtained with k-NN, DT, and SVM, respectively. In each table, the bestperforming oversampling method for each dataset is highlighted in bold, allowing for a quick visual comparison of model effectiveness across multiple settings.

According to the results reported in Table 2, the BODE method demonstrates strong and consistent performance when used with the k-Nearest Neighbors (k-NN) classifier. It achieves the highest AUC score in 28 out of 44 datasets, making it the most frequently successful oversampling technique in this

setting. In addition to its high win count, BODE also obtains the highest average AUC score of 0.8613, outperforming all baseline methods across the board.

Classical oversampling techniques such as SMOTE and ADASYN yield relatively lower and less stable results, particularly on datasets or overlapping decision with complex boundaries. Similarly, boundary-focused approaches like Borderline-SMOTE1 SMOTE-TomekLinks show competitive performance in certain cases but fail to match BODE's consistency across diverse scenarios. The k-NN classifier, being highly sensitive to neighborhood structure, significantly from BODE's ability to generate boundary-aware and noise-filtered synthetic samples. These results confirm that BODE is particularly well-suited for nearest-neighborbased learning under class imbalance.

The results in Table 3 further emphasize the effectiveness of BODE when used with the Decision Tree (DT) classifier. BODE achieves the highest AUC score in 33 out of 44 datasets, clearly outperforming all other oversampling methods in terms of win count. Additionally, it attains the highest average AUC value of 0.8625, reinforcing its robustness and adaptability across a wide variety of data distributions.

Compared to traditional techniques such as SMOTE, ADASYN, and Safe-Level SMOTE, BODE exhibits significantly better consistency, especially on datasets with complex or noisy structures. Even advanced methods like DEBOHID, which employs evolutionary strategies, fall behind BODE in both accuracy and frequency of top performance. The success of BODE in the DT setting can be attributed to its density-aware generation mechanism, which helps preserve the structural purity required for optimal tree-based splitting. These findings suggest that BODE is particularly effective in scenarios where decision trees are sensitive to sample quality near class boundaries.

As shown in Table 4, the proposed BODE method also performs strongly when evaluated with the Support Vector Machine (SVM) classifier. It achieves the highest AUC score in 26 out of 44 datasets, demonstrating its consistent effectiveness across a range of

imbalanced scenarios. With an average AUC of 0.8559, BODE outperforms all other oversampling techniques, including those specifically designed for boundary enhancement.

Although methods such as Borderline-SMOTE1. SMOTE-RSB. and DEBOHID exhibit competitive performance in certain datasets, they fail to match BODE's overall balance between accuracy and consistency. The margin-maximizing nature of SVM particularly benefits from BODE's strategy of generating synthetic samples near informative decision boundaries while avoiding noisy or overlapping regions. These results confirm that BODE not only performs well across diverse data distributions but also adapts effectively to fundamentally different classifiers with decision-making mechanisms.

Across all three classifiers—k-NN, Decision Tree, and SVM—BODE consistently demonstrates superior performance. It achieves the highest average AUC and the greatest number of dataset-level wins in each setting: 28/44, 33/44, and 26/44, respectively. This highlights BODE's robustness and adaptability across different classification paradigms.

By combining boundary-aware instance selection, evolutionary sample generation, and density-based filtering, BODE generates high-quality synthetic samples near informative boundaries while minimizing noise. Unlike conventional or purely evolutionary methods, it balances diversity with structural reliability. These results confirm BODE's effectiveness as a general-purpose oversampling method for imbalanced data problems.

Table 2. The mean of the AUC results with the kNN classifier of all methods

Dataset Name	et Name Original		Original SMOTE		S-TL		S-1	ENN	Boı	rder1	Bor	rder2	Safe	elevel	ADASYN		S-RSB		DEB	DEBOHID		ODE
	Mean	Std. Dev	. Mean	Std. Dev.	Mean	Std. Dev.	Mean	Std. Dev.	Mean	Std. Dev.	Mean	Std. Dev.	Mean	Std. Dev.	. Mean	Std. Dev.	Mean	Std. Dev	. Mean	Std. Dev.	Mean	Std. Dev.
ecoli0137vs26	0.8500	0.2236	0.8154	0.2066	0.8118	0.2040	0.8136	0.2039	0.8318	0.2113	0.8391	0.2171	0.8172	0.2064	0.8191	0.2074	0.8581	0.2069	0.8227	0.2042	0.8391	0.2172
shuttle0vs4	0.9960	0.0089	0.9960	0.0089	0.9960	0.0089	0.9960	0.0089	0.9960	0.0089	0.9960	0.0089	0.9951	0.0085	0.9951	0.0085	0.9960	0.0089	0.9960	0.0089	0.9960	0.0089
yeastB1vs7	0.5167	0.0373	0.7156	0.0948	0.6943	0.0698	0.7040	0.0553	0.6417	0.1355	0.6545	0.1146	0.6683	0.0682	0.7121	0.0635	0.7086	0.1150	0.7408	0.1338	0.7050	0.0768
shuttle2vs4	0.6000	0.2236	0.9960	0.0089	1.0000	0.0000	1.0000	0.0000	1.0000	0.0000	1.0000	0.0000	0.9673	0.0374	0.9960	0.0089	1.0000	0.0000	1.0000	0.0000	1.0000	0.0000
glass016vs2	0.5552	0.0763	0.6686	0.0924	0.6369	0.1310	0.6655	0.1356	0.6893	0.1372	0.6760	0.0540	0.6848	0.1500	0.6493	0.0744	0.6940	0.1342	0.6810	0.0992	0.7198	0.1567
glass016vs5	0.7386	0.1821	0.9686	0.0156	0.9157	0.1246	0.9186	0.1186	0.9771	0.0078	0.8714	0.1310	0.9457	0.0120	0.9600	0.0256	0.9243	0.1140	0.9243	0.1140	0.9786	0.0189
pageblocks13vs4	0.8076	0.0998	0.9383	0.0435	0.9250	0.0735	0.9416	0.0372	0.9351	0.0514	0.9351	0.0542	0.9047	0.0306	0.9360	0.0426	0.9106	0.0436	0.9317	0.0446	0.9475	0.0563
yeast05679vs4	0.6667	0.0879	0.8096	0.0607	0.8033	0.0636	0.8138	0.0597	0.8028	0.0684	0.8049	0.1017	0.7974	0.0631	0.8065	0.0554	0.7996	0.0706	0.8313	0.0453	0.8349	0.0572
yeast1289vs7	0.4995	0.0012	0.6322	0.1270	0.6923	0.0973	0.6972	0.0899	0.6107	0.1022	0.5481	0.0323	0.6256	0.0996	0.6617	0.1127	0.6557	0.1047	0.6404	0.0759	0.6073	0.0876
yeast1458vs7	0.4992	0.0017	0.6771	0.0744	0.6824	0.0786	0.6354	0.0658	0.5487	0.0927	0.5032	0.0424	0.6279	0.0682	0.6233	0.1105	0.6430	0.0394	0.6983	0.0658	0.6670	0.0975
yeast2vs4	0.8195	0.0452	0.8898	0.0449	0.9055	0.0149	0.8974	0.0553	0.8915	0.0397	0.8725	0.0497	0.8736	0.0230	0.8969	0.0372	0.8709	0.0538	0.8985	0.0306	0.9225	0.0459
Ecoli4	0.8484	0.1366	0.8965	0.0711	0.8965	0.0779	0.8997	0.0722	0.8905	0.0532	0.8905	0.0577	0.8870	0.0749	0.8870	0.0696	0.9215	0.0795	0.9060	0.0756	0.9425	0.0700
Yeast4	0.5741	0.0508	0.7959	0.0818	0.8238	0.0497	0.8087	0.0920	0.7401	0.0946	0.7554	0.0716	0.8224	0.0494	0.8069	0.0916	0.8069	0.0654	0.8252	0.0825	0.8112	0.0910
Vowel0	0.9772	0.0299	0.9978	0.0023	0.9994	0.0012	0.9994	0.0012	0.9994	0.0012	0.9994	0.0012	0.9783	0.0240	0.9911	0.0042	0.9961	0.0042	0.9994	0.0012	1.0000	0.0000
Yeast2vs8	0.7739	0.1033	0.8295	0.1159	0.8176	0.1172	0.8241	0.1175	0.7502	0.1134	0.7653	0.1094	0.7970	0.1604	0.8372	0.1015	0.8198	0.1258	0.7872	0.1432	0.8271	0.1332
Glass4	0.7808	0.1421	0.9001	0.0938	0.9001	0.0986	0.9051	0.1011	0.8917	0.1127	0.8942	0.1144	0.8704	0.1158	0.9052	0.1088	0.9151	0.1000	0.9226	0.1050	0.9363	0.1084
Glass5	0.6951	0.2080	0.9537	0.0338	0.9585	0.0281	0.9537	0.0200	0.8780	0.2125	0.9256	0.1268	0.9268	0.0414	0.9463	0.0318	0.9659	0.0291	0.8756	0.1212	0.8902	0.2187
Glass2	0.4848	0.0166	0.7948	0.0538	0.7562	0.1384	0.7688	0.1236	0.7001	0.0778	0.6756	0.0734	0.7437	0.0752	0.8029	0.1067	0.7763	0.1079	0.7174	0.0963	0.8021	0.0661
Yeast5	0.8497	0.0627	0.9663	0.0240	0.9649	0.0232	0.9663	0.0241	0.9510	0.0290	0.9500	0.0307	0.9757	0.0055	0.9653	0.0236	0.9656	0.0236	0.9674	0.0261	0.9782	0.0238
Yeast6	0.7387	0.1097	0.8736	0.0738	0.8705	0.0748	0.8705	0.0759	0.8566	0.1053	0.8719	0.1083	0.8749	0.0744	0.8708	0.0765	0.8698	0.0786	0.8367	0.0758	0.8708	0.0653
abalone19	0.5000	0.0000	0.5865	0.0702	0.5982	0.0350	0.5817	0.0697	0.6129	0.1051	0.5458	0.0579	0.5939	0.0727	0.5855	0.0707	0.5637	0.1063	0.5734	0.0942	0.6780	0.1199
abalone918	0.5681	0.0606	0.7720	0.1107	0.7675	0.1124	0.7703	0.1271	0.7355	0.1403	0.6616	0.1363	0.7663	0.1008	0.7800	0.1155	0.8212	0.1101	0.7815	0.1171	0.8574	0.0919
cleveland0vs4	0.4937	0.0086	0.5935	0.2184	0.5621	0.1891	0.5845	0.2056	0.6089	0.2395	0.6247	0.2318	0.5986	0.2418	0.5373	0.1542	0.5499	0.1602	0.6916		0.5592	0.1836
ecoli01vs235	0.8300	0.0671	0.8964	0.0475	0.8468	0.1016	0.8941	0.0354	0.8386	0.0707	0.8386	0.0712	0.8450	0.0529	0.8645	0.0811	0.8223	0.1158	0.9036	0.0829	0.9001	0.1017
ecoli01vs5	0.9000	0.1046	0.9045	0.0743	0.8977	0.0705	0.9000	0.0743	0.8932	0.1037	0.8886		0.8909	0.0756	0.8614	0.1011	0.9045	0.0790	0.9159	0.0721	0.9170	0.0709
ecoli0146vs5	0.8981	0.1023	0.9038	0.0978	0.9000	0.1012	0.9058	0.1025	0.8942	0.1008	0.8923	0.1014	0.8962	0.1039	0.8904	0.0977	0.9019	0.0967	0.9173	0.1083	0.9187	0.1094
ecoli0147vs2356	0.8467	0.0298	0.8712	0.0235	0.8696	0.0261	0.8760	0.0603	0.8821	0.0630	0.9020	0.0477	0.8329	0.0582	0.8598	0.0206	0.8612	0.0499	0.9122	0.0572	0.8957	0.0492
ecoli0147vs56	0.8384	0.1509	0.8875	0.0457	0.8711	0.0356	0.8728	0.0452	0.9037	0.0407	0.9069	0.0389	0.8825	0.0388	0.8744	0.0478	0.8776	0.0413	0.8923	0.0429	0.9273	0.0560
ecoli0234vs5	0.8944	0.1449	0.8975	0.1135	0.8975	0.1088	0.9031	0.1098	0.8890	0.1400	0.8890	0.1400	0.8920	0.1135	0.8561	0.1478	0.9031	0.1141	0.9113	0.1088	0.9105	0.1198
ecoli0267vs35	0.7875	0.0599	0.8679	0.0595	0.8654	0.0579	0.8654	0.0537	0.8501	0.1106	0.8452	0.1111	0.8079	0.1169	0.8531	0.0583	0.8778	0.0756	0.8728	0.0976	0.9276	0.0608
ecoli034vs5	0.8750	0.1250	0.9028	0.1215	0.8944	0.1189	0.9028	0.1133	0.8944	0.1105	0.8917	0.1073	0.8750	0.1035	0.8583	0.1109	0.8972	0.1165	0.9139	0.1184	0.9153	0.1176
ecoli0346vs5	0.8750	0.0884	0.9061	0.0647	0.8980	0.0683	0.9088	0.0670	0.9223	0.0711	0.9196	0.0736	0.8845	0.0526	0.8318	0.0873	0.9088	0.0724	0.9142	0.0676	0.9209	0.0724
ecoli0347vs56	0.8757	0.1337	0.8768	0.1243	0.8768	0.1241	0.8833	0.1210	0.9006	0.1370	0.9006	0.1364	0.8725	0.1175	0.8618	0.1237	0.8769	0.1283	0.9055	0.1271	0.9232	0.1380
ecoli046vs5	0.9000	0.1046	0.9060	0.0972	0.9032	0.0945	0.9061	0.1052	0.8919	0.0952	0.8891	0.0960	0.8868	0.0970	0.8788	0.0970	0.9060	0.1083	0.9142	0.1034	0.9209	0.1123
ecoli067vs35	0.8350	0.1799	0.8975	0.1257	0.8600	0.1210	0.8900	0.1285	0.8300	0.1671	0.8475	0.1664	0.8100	0.1701	0.8800	0.1220	0.8875	0.1259	0.8825	0.1653	0.9135	0.1406
ecoli067vs5	0.8475	0.0548	0.8525	0.0511	0.8575	0.0641	0.8375	0.0606	0.9000	0.0696	0.8975	0.0736	0.8550	0.0338	0.8675	0.0429	0.8675	0.0665	0.8925	0.0699	0.9056	0.0631
glass0146vs2	0.5118	0.0635	0.7807	0.1095	0.7367	0.0557	0.7166	0.0967	0.6809	0.1697	0.6883	0.0640	0.7464	0.0855	0.7087	0.1009	0.7246	0.0005	0.7326	0.1059	0.7422	0.0986
glass015vs2	0.5269	0.0794	0.7427	0.1188	0.7298	0.1439	0.7608	0.1432	0.6462	0.1913	0.6202	0.1343	0.7220	0.1469	0.7427	0.1271	0.7382	0.1258	0.7153	0.1100	0.7691	0.1226
glass04vs5	0.8500	0.0754	0.7427	0.0558	0.7238	0.0521	0.7608	0.0520	0.0402	0.0278	0.0202	0.0520	0.7220	0.0792	0.7427	0.0558	0.7562	0.0558	0.9820	0.0165	1.0000	0.1220
glass06vs5	0.7450	0.1771	0.9750	0.0350	0.9850	0.0321	0.9850	0.0320	0.9350	0.0278	0.8900	0.0320	0.9597	0.0772	0.9697	0.0338	0.9297	0.0330	0.9800	0.0209	0.9875	0.0000
8	1 0.5393	0.0360	0.6386	0.0230	0.6491	0.0137	0.98576	0.0137	0.5881	0.1161	0.5856	0.1399	0.5494	0.0221	0.6361	0.0208	0.6230	0.1150	0.6621	0.0209	0.6671	0.0123
veast0359vs78	0.6390	0.0660	0.0380	0.1080	0.7406	0.1037	0.7303	0.0389	0.7076	0.1200	0.7007	0.1271	0.7273	0.0510	0.0301	0.1080	0.0230	0.1103	0.7425	0.0944	0.7517	0.0823
yeast0256vs3789	0.7624	0.0553	0.7781	0.0384	0.7759	0.0402	0.7944	0.0393	0.7643	0.0368	0.7787	0.0302	0.7698	0.0643	0.7303	0.0732	0.7283	0.0431	0.7423	0.0603	0.7963	0.0503
yeast02579vs368	0.7624	0.0333	0.7781	0.0481	0.7739	0.0480	0.7944	0.0492	0.7643	0.0368	0.7787	0.0302	0.7698	0.0043	0.7798	0.0438	0.7787	0.0084	0.7894	0.0003	0.7903	0.0370
-	0.7389	0.0200	0.9133	0.0190	0.9010	0.0209	0.8467	0.0510	0.8232	0.0239	0.8971	0.0323	0.8933	0.0273	0.8324	0.0200	0.8387	0.0121	0.8476	0.0224	0.9202	0.0207
Average Winner / Total	1/44		0.8449 4/44		3/44		0.846 / 4/44		3/44		3/44		1/44		1/44		4/44		5/44		28/44	
Winner / Total	1/44		4/44		3/44		4/44		3/44		3/44		1/44		1/44		4/44		3/44		20/44	

Table 3. The mean of the AUC results with the DT classifier of all methods

Dataset Name	Original SN		SMOTE S-TL		S-1	ENN	Border1		Bor	der2	Safelevel		ADASYN		S-RSB		DEBOHID		В	ODE		
	Mean	Std. Dev.	Mean	Std. Dev.	Mean	Std. Dev.	Mean	Std. Dev.	Mean	Std. Dev.	Mean	Std. Dev.	Mean	Std. Dev.	. Mean	Std. Dev.	Mean	Std. Dev.	Mean	Std. Dev.	Mean	Std. Dev.
ecoli0137vs26	0.8427	0.2202	0.6818	0.2097	0.7709	0.2104	0.7781	0.2085	0.8427	0.2201	0.7409	0.2501	0.7154	0.2424	0.5800	0.1318	0.6336	0.2197	0.7390	0.2413	0.8391	0.2172
shuttle0vs4	1.0000	0.0000	0.9997	0.0007	1.0000	0.0000	1.0000	0.0000	1.0000	0.0000	1.0000	0.0000	0.9991	0.0013	0.9997	0.0007	0.9997	0.0007	0.9997	0.0007	0.9960	0.0089
yeastB1vs7	0.7100	0.0598	0.5797	0.1179	0.6123	0.0395	0.6844	0.1094	0.6220	0.0738	0.6101	0.0952	0.6459	0.1101	0.6572	0.1111	0.6681	0.0908	0.6383	0.0837	0.7050	0.0768
shuttle2vs4	0.9500	0.1118	0.9918	0.0112	0.9960	0.0089	1.0000	0.0000	0.9500	0.1118	1.0000	0.0000	0.9298	0.1148	0.9960	0.0089	1.0000	0.0000	1.0000	0.0000	1.0000	0.0000
glass016vs2	0.5548	0.0870	0.6226	0.0625	0.6195	0.1147	0.6421	0.0849	0.5290	0.1101	0.6017	0.1073	0.5819	0.1423	0.6367	0.0834	0.7345	0.1074	0.6071	0.1146	0.7198	0.1567
glass016vs5	0.8329	0.2299	0.8300	0.2274	0.9329	0.1267	0.8629	0.2588	0.8386	0.2341	0.9386	0.1216	0.8129	0.2366	0.8686	0.1607	0.9214	0.1050	0.8443	0.2229	0.9786	0.0189
pageblocks13vs4	0.9955	0.0062	0.9475	0.0528	0.9755	0.0372	0.9565	0.0472	0.9978	0.0050	0.9600	0.0501	0.9653	0.0444	0.9354	0.0769	0.9630	0.0443	0.9978	0.0050	0.9978	0.0047
yeast05679vs4	0.6540	0.1137	0.8094	0.0649	0.7585	0.0782	0.7751	0.0911	0.7019	0.1039	0.6821	0.0965	0.7572	0.0493	0.7104	0.1095	0.7441	0.0664	0.7304	0.0918	0.8349	0.0572
yeast1289vs7	0.6353		0.6118		0.6348	0.1083	0.5870	0.1092	0.5793	0.0459	0.6096	0.0756	0.5856	0.0393	0.6274	0.0998	0.6026	0.0652	0.6389	0.0693	0.6073	0.0876
yeast1458vs7	0.5259	0.0515	0.5025	0.0489	0.5117	0.0660	0.4949	0.0760	0.5448	0.0515	0.5061	0.0401	0.5769	0.0963	0.5783	0.1019	0.5518	0.1001	0.6087	0.1307	0.6670	0.0975
yeast2vs4	0.8475	0.0782	0.8428		0.8652	0.0550	0.9016	0.0415	0.8353	0.0746	0.8324	0.0693	0.8759	0.0333	0.8369	0.0696	0.8876		0.8347	0.0298	0.9225	0.0459
Ecoli4	0.8624	0.1484	0.8608	0.0806	0.8592	0.1174	0.8278	0.1031	0.8389	0.0971	0.8203	0.0717	0.7997	0.1318	0.8263	0.1374	0.8810	0.1380	0.8389	0.0945	0.9425	0.0700
Yeast4	0.6484	0.0943	0.6965	0.0482	0.7558	0.0767	0.6944	0.0648	0.6754	0.0689	0.7030		0.7162	0.1070	0.6712	0.0331	0.6975	0.1122	0.7138	0.1019	0.8112	0.0910
Vowel0	0.9422	0.0513	0.9444	0.0358	0.9727	0.0158	0.9633	0.0430	0.9039	0.0888	0.9533	0.0245	0.9483	0.0441	0.9655	0.0280	0.9589	0.0218	0.9561	0.0449	1.0000	0.0000
Yeast2vs8	0.7696		0.7545	0.1322	0.7773	0.1287	0.8066	0.1393	0.7402	0.0924	0.7870	0.1077	0.7796	0.1700	0.7100	0.1638	0.7730	0.1438	0.7762	0.1376	0.8271	0.1332
Glass4	0.8567	0.1852	0.8984	0.0954	0.8818	0.1107	0.9392	0.0878	0.8450	0.1570	0.9067	0.1138	0.9051	0.1011	0.8460	0.1670	0.8917	0.1159	0.9350	0.1036	0.9363	0.1084
Glass5	0.8427		0.9183	0.0004	0.9110	0.0990	0.9207	0.1035	0.8451	0.1370	0.7854	0.2611	0.8037	0.2097	0.9280	0.1070	0.8659	0.1139	0.8976	0.2223	0.8902	0.1004
Glass2	0.5376	0.2100	0.6904	0.0508	0.6060	0.0770	0.7132	0.1720	0.6052	0.1301	0.6058	0.1100	0.6429	0.1250	0.6965	0.1013	0.8035	0.2155	0.7390	0.2223	0.8021	0.0661
Yeast5	0.8201	0.1418	0.8521	0.0308	0.8847	0.0272	0.7132	0.1720	0.8337	0.1301	0.8309	0.1100	0.0429	0.1230	0.8885	0.1092	0.8632	0.0268	0.7390	0.0351	0.8021	0.0001
Yeast6	0.6823	0.0802	0.8321	0.0370	0.7936	0.0272	0.9070	0.1203	0.7506	0.1079	0.7649	0.0340	0.9281	0.1415	0.8883	0.0019	0.8032	0.0208	0.7633	0.0403	0.8708	0.0238
abalone 19	0.4978		0.5513	0.0682	0.5308	0.0738	0.5341	0.0746	0.4888	0.0091	0.5087	0.0302	0.5153	0.0408 0.1253	0.5358 0.7202	0.0744	0.5283	0.0428	0.5938	0.0431	0.6780	0.1199
abalone918	0.6911	0.1521		0.1052	0.7340		0.7151	0.1001	0.6837 0.8906	0.1687	0.7274	0.1249					0.7411	0.1400	0.7508	0.1189 0.0764	0.8574	0.0919
cleveland0vs4	0.7888		0.7198			0.0695	0.6833	0.0759		0.1506	0.7416		0.8282	0.0980	0.6561	0.1256	0.7489	0.1535	0.7139		0.5592	0.1836
ecoli01vs235	0.8114		0.7709		0.8959	0.0704	0.8173	0.1216	0.8136	0.1613	0.8632	0.0950	0.7932	0.1072	0.7936	0.0562	0.8045	0.0641	0.8155	0.1431	0.9001	0.1017
ecoli01vs5	0.8636		0.8250	0.1021	0.8159		0.8795	0.0915	0.8636	0.1139	0.8614		0.8750	0.1134	0.7682	0.1780	0.8727	0.0517	0.8864	0.0927	0.9170	0.0709
ecoli0146vs5	0.7308	0.1967	0.7981	0.1544	0.8481		0.8692	0.1473	0.7904	0.1427	0.8308	0.1021	0.7846	0.1363	0.8731	0.1198	0.8558	0.1207	0.8750	0.1534	0.9187	0.1094
ecoli0147vs2356	0.8219		0.8174	0.0934	0.8642	0.0578	0.8674	0.0651	0.8071	0.0512	0.8236	0.1525	0.8146	0.0822	0.8293	0.1345	0.8475	0.0668	0.8524	0.0741	0.8957	0.0492
ecoli0147vs56	0.7886	0.1277	0.8324		0.7993	0.1255	0.8122	0.0440	0.8654	0.0858	0.8854	0.0789	0.7923	0.0905	0.8393	0.0921	0.8392	0.0703	0.8837	0.0653	0.9273	0.0560
ecoli0234vs5	0.7806	0.0624	0.8834		0.8892	0.1177	0.8862	0.1098	0.8584	0.1456	0.8195	0.1104	0.8202	0.1222	0.8724	0.1055	0.8562	0.1613	0.8501	0.1262	0.9105	0.1198
ecoli0267vs35	0.7952	0.1090	0.8577		0.7903	0.1283	0.8254	0.1190	0.8078	0.1134	0.8078	0.1165	0.7879	0.1150	0.7754	0.1159	0.8080	0.1132	0.8304	0.1096	0.9276	0.0608
ecoli034vs5	0.8056	0.1562	0.8278		0.8667	0.1405	0.8500	0.1308	0.7889	0.1387	0.8111	0.1429	0.8500	0.1143	0.8667	0.1004	0.8972	0.1193	0.8611	0.0997	0.9153	0.1176
ecoli0346vs5	0.8392	0.1103	0.8676	0.0400	0.8703	0.0448	0.8730	0.0376	0.8446	0.1072	0.8419		0.8568	0.0720	0.8345	0.0994	0.9041	0.0433	0.8507	0.0802	0.9209	0.0724
ecoli0347vs56	0.7692		0.8476	0.1544	0.8611	0.1636	0.8675	0.1527	0.8470	0.1480	0.8449	0.1583	0.8325	0.1489	0.8454	0.1115	0.9077	0.0520	0.8834	0.0819	0.9232	0.1380
ecoli046vs5	0.8141	0.1134	0.8119		0.8508	0.1151	0.8591	0.0984	0.8336	0.1333	0.8586	0.1290	0.8592	0.1569	0.8924	0.0917	0.8592	0.0863	0.8782	0.0960	0.9209	0.1123
ecoli067vs35	0.8550		0.8175		0.8125	0.1589	0.8300	0.1619	0.7850	0.1791	0.8275	0.1726	0.8250	0.1635	0.8100	0.1638	0.8225	0.1662	0.8625	0.1556	0.9135	0.1406
ecoli067vs5	0.7700	0.2082	0.8775	0.0681	0.8375	0.0935	0.8900	0.0389	0.8025	0.1857	0.8600	0.0807	0.8650	0.0698	0.8650	0.0907	0.8300	0.1095	0.8275	0.1210	0.9056	0.0631
glass0146vs2	0.6120	0.1301	0.7539	0.1298	0.7685	0.1266	0.6757	0.0980	0.5793	0.1159	0.5492	0.0786	0.6751	0.1282	0.7346	0.0326	0.7137	0.0888	0.8137	0.1057	0.7422	0.0986
glass015vs2	0.5914	0.1430	0.6309	0.2545	0.6796	0.2202	0.7207	0.1659	0.6933	0.0960	0.6419	0.1742	0.6519	0.1706	0.7022	0.1723	0.7304	0.1323	0.6785	0.1960	0.7691	0.1226
glass04vs5	0.9941	0.0132	0.9401	0.0462	0.9761	0.0247	0.9577	0.0268	0.9941	0.0132	0.9938	0.0140	0.9632	0.0336	0.9574	0.0353	0.9463	0.0237	0.9941	0.0132	1.0000	0.0000
glass06vs5	0.9350	0.1055	0.9550	0.0671	0.9647	0.0518	0.9597	0.0517	0.9450	0.1095	0.9897	0.0141	0.9287	0.0354	0.9545	0.0372	0.9800	0.0274	0.9950	0.0112	0.9875	0.0125
led7digit02456789vs1	0.8788	0.0740	0.8869	0.0969	0.8808	0.0985	0.8372	0.0810	0.8955	0.0878	0.8931	0.0847	0.8871	0.0443	0.8958	0.0819	0.8689	0.0812	0.9088	0.0725	0.6671	0.0823
yeast0359vs78	0.6804	0.0428	0.5998	0.0760	0.6479	0.0539	0.6365	0.0756	0.6072	0.0399	0.6638	0.1051	0.7268	0.0884	0.6009	0.0225	0.6410	0.0461	0.6534	0.0714	0.7517	0.0363
yeast0256vs3789	0.7483	0.0280	0.7252	0.0735	0.7402	0.0548	0.7718	0.0262	0.7159	0.0470	0.7056	0.0473	0.7644	0.0563	0.7394	0.0503	0.7193	0.0504	0.7619	0.0731	0.7963	0.0570
yeast02579vs368	0.8715	0.0286	0.8963	0.0421	0.9090	0.0410	0.9168	0.0372	0.8696	0.0190	0.8782	0.0438	0.8910	0.0242	0.8918	0.0460	0.8854	0.0322	0.8724	0.0398	0.9202	0.0267
Average	0.7783		0.7984		0.8111		0.8136		0.7852		0.7924		0.7987		0.7951		0.8147		0.8194		0.8625	
Winner / Total	2/44		0/44		1/44		3/44		3/44		2/44		0/44		1/44		3/44		6/44		33/44	

Table 4. The mean of the AUC results with the SVM classifier of all methods

Mary 18 Mary	Dataset Name	Original		SM	OTE	S-	-TL	S-	ENN	Bo	rder1	Boi	rder2	Safe	elevel	ADASYN		S-RSB		DEBOHID		BODE	
Semithfield 1,000 1,000 1,000 1,000 0,000		Mean	Std. Dev.	Mean	Std. Dev.	Mean	Std. Dev.	Mean	Std. Dev.	Mean	Std. Dev.	Mean	Std. Dev.	Mean	Std. Dev.	Mean	Std. Dev.	Mean	Std. Dev.	Mean	Std. Dev.	Mean	Std. Dev.
yess pss 1,000 0,000 0,76 0,	ecoli0137vs26	0.8500	0.2236	0.7935	0.1959	0.7935	0.1959	0.7971	0.2007	0.8263	0.2118	0.8244	0.2159	0.8327	0.2164	0.7917	0.1949	0.8398	0.2056	0.8172	0.1993		0.0723
Semiglacy 1.00 0.	shuttle0vs4	1.0000	0.0000	1.0000	0.0000	0.9960	0.0089	1.0000	0.0000	1.0000	0.0000	1.0000	0.0000	0.9991	0.0013	0.9994	0.0008	0.9997	0.0007	1.0000	0.0000	1.0000	0.0000
Passellonges 1,000	yeastB1vs7	0.5000	0.0000	0.7636	0.0825	0.7543	0.0799	0.7419	0.0479	0.6718	0.1150	0.6707	0.1165	0.7733	0.0670	0.7651	0.0690	0.7605	0.0587	0.7384	0.0482	0.7797	0.0489
Final Purpose Final Purpos	shuttle2vs4	1.0000	0.0000	0.9793	0.0361	1.0000	0.0000	1.0000	0.0000	1.0000	0.0000	1.0000	0.0000	0.9470	0.0556	0.9795	0.0292	1.0000	0.0000	1.0000	0.0000	1.0000	0.0000
Puge-like-lik-lik-lik-lik-lik-lik-lik-lik-lik-lik	glass016vs2	0.5000	0.0000	0.5171	0.1412	0.5407	0.1310	0.5352	0.1023	0.6281	0.1235	0.5979	0.0616	0.5138	0.1022	0.5221	0.1280	0.6293	0.0724	0.6157	0.1116	0.5650	0.0993
Seesing Series S	glass016vs5	0.4971	0.0064	0.9486	0.0163	0.9486	0.0217	0.9514	0.0163	0.9800	0.0128	0.9629	0.0278	0.9314	0.0156	0.9514	0.0163	0.9486	0.0128	0.9686	0.0156	0.9171	0.0626
Franchist Sample	pageblocks13vs4	0.4728	0.1333	0.4090	0.1235	0.4840	0.2333	0.2948	0.1355	0.4604	0.1287	0.4606	0.0641	0.3069	0.1815	0.3565	0.0655	0.3934	0.2353	0.6004	0.1689	0.6071	0.0983
Frank 1.5 km 1.6 km 1	yeast05679vs4	0.5000	0.0000	0.7865	0.0830	0.7912	0.0612	0.7854	0.0822	0.7943	0.0847	0.7953	0.0862	0.7944	0.0639	0.7829	0.0592	0.7844	0.0803	0.7838	0.0918	0.8412	0.0594
Seast-Paris	yeast1289vs7	0.5000	0.0000	0.7189	0.0528	0.7263	0.0390	0.6910	0.0378	0.6762	0.0682	0.6757	0.0690	0.7064	0.0532	0.7123	0.0496	0.6946	0.0269	0.6921	0.0343	0.7583	0.0722
Feelifie	yeast1458vs7	0.5000	0.0000	0.6343	0.0519	0.6146	0.0482	0.6357	0.0500	0.6308	0.0662	0.6081	0.0743	0.6328	0.0556	0.6146	0.0433	0.6388	0.0524	0.6333	0.0797	0.6348	0.0961
Very New	yeast2vs4	0.6691	0.1163	0.8964	0.0331	0.8953	0.0349	0.8907	0.0326	0.8896	0.0293	0.8874	0.0280	0.8885	0.0351	0.8677	0.0253	0.8864	0.0350	0.8805	0.0193	0.9104	0.0272
Versich No. 989 0.0645 0.9699 0.079 0.9790 0.0790	Ecoli4	0.5750	0.0685	0.9716	0.0119	0.9402	0.0505	0.9668	0.0103	0.9342	0.0616	0.9295	0.0612	0.9541	0.0206	0.9102	0.0549	0.9620	0.0153	0.9576	0.0526	0.9921	0.0001
Part No. Part No.	Yeast4	0.5000	0.0000	0.8434	0.0217	0.8265	0.0348	0.8338	0.0336	0.8251	0.0300	0.8223	0.0310	0.8286	0.0314	0.8212	0.0355	0.8131	0.0328	0.8104	0.0294	0.8724	0.0330
Clases	Vowel0	0.8950	0.0645	0.9699	0.0077	0.9700	0.0095	0.9705	0.0093	0.9200	0.0367	0.9244	0.0560	0.9505	0.0150	0.9616	0.0170	0.9649	0.0080	0.9683	0.0274	0.9828	0.0146
Class	Yeast2vs8	0.7739	0.1033	0.7664	0.0960	0.7653	0.0948	0.7664	0.0960	0.7065	0.1244	0.7141	0.1159	0.7739	0.1033	0.7394	0.0523	0.7631	0.0971	0.7718	0.1023	0.8532	0.0620
Class Cla	Glass4	0.5592	0.0993	0.9101	0.1041	0.8977	0.1047	0.9027	0.1076	0.9226	0.1042	0.9176	0.1013	0.8704	0.1091	0.9002	0.1123	0.9002	0.1060	0.9101	0.1052	0.8871	0.1705
Yeas16 0.5000 0.0000 0.9635 0.0064 0.9622 0.0057 0.0048 0.8787 0.0048 0.8787 0.0048 0.8787 0.0049 0.8787 0.0049 0.8787 0.0049 0.8787 0.0049 0.8787 0.0049 0.8787 0.0049 0.8787 0.0049 0.8787 0.0049 0.8787 0.0049 0.8787 0.0049 0.00459 0.0059 0.0049 0.0059 0.0049 0.0059 0.0049 0.0059 0.0049 0.0059 0.0049 0.0059 0.004	Glass5	0.5000	0.0000	0.9366	0.0218	0.9366	0.0200	0.9439	0.0185	0.9732	0.0316	0.9561	0.0222	0.9366	0.0200	0.9463	0.0204	0.9415	0.0235	0.9683	0.0329	0.9000	0.0802
Part	Glass2	0.5000	0.0000	0.6155	0.1537	0.6777	0.0396	0.6309	0.1197	0.6050	0.2247	0.5880	0.2053	0.6546	0.0812	0.6803	0.0239	0.6212	0.1475	0.6085	0.1486	0.6241	0.1046
Part	Yeast5	0.5000	0.0000	0.9635	0.0066	0.9622	0.0055	0.9642	0.0066	0.9667	0.0033	0.9660	0.0038	0.9608	0.0044	0.9608	0.0068	0.9625	0.0062	0.9635	0.0032	0.9842	0.0048
Part	Yeast6	0.5000	0.0000	0.8730	0.0694	0.8723	0.0694	0.8737	0.0694	0.8791	0.0928	0.8777	0.0922	0.8730	0.0706	0.8628	0.0739	0.8870	0.0574	0.8820	0.0702	0.9180	0.0826
CheckelandOve4 C.7478 C.7172 C.	abalone19	0.5000	0.0000	0.7453	0.0889	0.7601	0.0679	0.7623	0.0659	0.6914	0.1140	0.6963	0.1528	0.7821	0.0451	0.7786	0.0642	0.7826	0.0869	0.7894	0.0607	0.7719	0.0778
California Cal	abalone918	0.5000	0.0000	0.8581	0.0429	0.8545	0.0419	0.8493	0.0481	0.8833	0.0728	0.8760	0.0769	0.8174	0.0391	0.8530	0.0414	0.8727	0.0360	0.8761	0.0444	0.7814	0.0552
Colio Coli	cleveland0vs4	0.7478	0.2172	0.9167	0.0557	0.9167	0.0568	0.9166	0.0655	0.7947	0.1655	0.8426	0.1102	0.8950	0.0652	0.9314	0.0279	0.8735	0.0600	0.9260	0.0645	0.9769	0.0227
	ecoli01vs235	0.8359	0.1670	0.8777	0.0981	0.8732	0.0931	0.8845	0.1032	0.8468	0.1525	0.8673	0.1092	0.8555	0.0873	0.8255	0.1379	0.8732	0.0931	0.8918	0.1027	0.9161	0.0937
Coli	ecoli01vs5	0.8364	0.1112	0.8591	0.0993	0.8341	0.1239	0.8614	0.0976	0.8864	0.1057	0.8568	0.1257	0.8614	0.1033	0.8068	0.1288	0.8364	0.1267	0.8750	0.1038	0.9170	0.1046
	ecoli0146vs5	0.8635	0.1516	0.8885	0.0956	0.8712	0.0939	0.8519	0.0914	0.8808	0.1595	0.8769	0.1533	0.8769	0.0960	0.8423	0.0614	0.8827	0.1014	0.8981	0.1083	0.8731	0.1360
	ecoli0147vs2356	0.8267	0.0538	0.8812	0.0710	0.8645	0.1066	0.8661	0.0554	0.8555	0.0470	0.8539	0.0428	0.8796	0.0774	0.8228	0.0509	0.8929	0.0740	0.8658	0.0681	0.9154	0.0621
$ \begin{array}{c ccccccccccccccccccccccccccccccccccc$	ecoli0147vs56	0.8719	0.0863	0.8812	0.0229	0.8730	0.0704	0.8530	0.0498	0.8821	0.0712	0.9021	0.0793	0.9012	0.0376	0.8054	0.0760	0.8779	0.0513	0.8775	0.0608	0.9276	0.0777
ccli034vs5	ecoli0234vs5	0.8667	0.0933	0.8891	0.1135	0.8810	0.1133	0.8946	0.1109	0.8806	0.1032	0.9029	0.1134	0.8920	0.1154	0.8204	0.1016	0.8865	0.1108	0.9002	0.1112	0.8729	0.1708
Cocilio346vs5 0.8696 0.8838 0.8899 0.0650 0.8926 0.0616 0.8676 0.0324 0.8588 0.0947 0.8888 0.0947 0.8899 0.0549 0.0820 0.0820 0.0820 0.0871 0.0909 0.0977 0.0872 0.0971 0.0872 0.0971 0.0872 0.0971 0.0872 0.0971 0.0872 0.0971 0.0872 0.0971 0.0872 0.0972 0.0872 0.0972 0.0872 0.0972 0.0872 0.0972 0.0872 0.0972 0.0872 0.0972 0.0872 0.0972 0.0872 0.0972 0.0872 0.0972 0.0872 0.0	ecoli0267vs35	0.8526	0.1062	0.8304	0.1198	0.8108	0.1403	0.8604	0.1075	0.8353	0.1020	0.8155	0.1074	0.8507	0.1347	0.8137	0.0904	0.8883	0.0928	0.8379	0.1127	0.8644	0.1467
Colio347vs56 0.8935 0.0746 0.8947 0.0691 0.8883 0.0719 0.8925 0.0752 0.9007 0.0805 0.8985 0.0885 0.0885 0.0885 0.0885 0.0885 0.8885 0.1160 0.8883 0.1111 0.8897 0.1143 0.8892 0.1084 0.8809 0.1103 0.8951 0.1158 0.8291 0.0886 0.8788 0.1077 0.9032 0.1170 0.8988 0.1270 0.001607vs35 0.8525 0.1357 0.8525 0.1357 0.8525 0.8525 0.8525 0.8525 0.8525 0.8525 0.8525 0.8525 0.8855 0.8855 0.2094 0.8895 0.2094 0.8809 0.2098 0.8809 0.2097 0.8800 0.2097 0.8800 0.1090 0.8855 0.1588 0.8700 0.1624 0.8463 0.2455 0.8000 0.0000	ecoli034vs5	0.8611	0.1361	0.8611	0.1593	0.8639	0.1606	0.8639	0.1588	0.9333	0.0794	0.9000	0.1160	0.8611	0.1614	0.8111	0.1109	0.8611	0.1593	0.8722	0.1650	0.9014	0.1103
Colio347vs56 0.8935 0.0746 0.8947 0.0691 0.8883 0.0719 0.8925 0.0752 0.9007 0.0805 0.8985 0.0886 0.0887 0.0886 0.0887 0.0886 0.0887 0.8896 0.1160 0.8843 0.1111 0.8897 0.1143 0.8892 0.1084 0.8809 0.1103 0.8951 0.1158 0.8291 0.0886 0.8788 0.1077 0.9032 0.1170 0.8988 0.1270 0.001607vs35 0.8255 0.1357 0.8525 0.2032 0.8650 0.1555 0.8525 0.8525 0.2045 0.8850 0.2045	ecoli0346vs5	0.8696	0.0838	0.8899	0.0650	0.8926	0.0616	0.8676	0.0324	0.8588	0.0947	0.8588	0.0947	0.8899	0.0549	0.7993	0.0727	0.8872	0.0674	0.9088	0.0724	0.8608	0.1327
Coclio67vs35 Coccolio67vs35 Coccolio67vs35 Coccolio67vs5 Coccolio67v		0.8935	0.0746	0.8947	0.0691	0.8883	0.0719	0.8925	0.0752	0.9007	0.0805	0.8985	0.0846	0.9040	0.0820	0.8651	0.0741	0.9019	0.0843	0.9099	0.0777	0.9215	0.1371
coli667vs5 0.8425 0.1357 0.8525 0.0675 0.8400 0.0693 0.8425 0.0785 0.08425 0.0840 0.0850 0.0875 0.8400 0.0825 0.08825	ecoli046vs5	0.8696	0.0887	0.8896	0.1160	0.8843	0.1111	0.8897	0.1143	0.8892	0.1088	0.8809	0.1103	0.8951	0.1158	0.8291	0.0886	0.8788	0.1077	0.9032	0.1170	0.8988	0.1270
$\begin{array}{cccccccccccccccccccccccccccccccccccc$	ecoli067vs35	0.8525	0.2160	0.8425	0.2032	0.8650	0.1555	0.8525	0.2045	0.8350	0.2094	0.8000	0.2008	0.8400	0.2057	0.8000	0.1970	0.8325	0.1538	0.8700	0.1624	0.8463	0.2455
$\begin{array}{cccccccccccccccccccccccccccccccccccc$	ecoli067vs5	0.8425	0.1357	0.8525	0.0675	0.8350	0.0757	0.8400	0.0693	0.8825	0.0535	0.8475	0.0768	0.8650	0.0912	0.7800	0.0942	0.8475	0.0681	0.8775	0.0548	0.8825	0.1084
glassO4vs5 0.8500 0.1369 0.9445 0.0518 0.9449 0.0465 0.9449 0.0465 0.9449 0.0465 0.9816 0.0278 0.9816 0.0278 0.9816 0.0278 0.0360 0.9816 0.0278 0.0360 0.9816 0.0278 0.0360 0.9816 0.0278 0.0360 0.9816 0.0278 0.0360 0.036	glass0146vs2	0.5000	0.0000	0.6067	0.0504	0.6237	0.0759	0.6227	0.0571	0.6277	0.0588	0.6785	0.0687	0.6013	0.0511	0.6174	0.0473	0.6306	0.0881	0.6052	0.0591	0.6459	0.0819
glassO4vs5	glass015vs2	0.5000	0.0000	0.5126	0.0685	0.5094	0.1494	0.5320	0.0304	0.4927	0.1287	0.5261	0.1147	0.5191	0.0664	0.4868	0.1023	0.5132	0.1298	0.5000	0.0861	0.5610	0.0912
led7digitt02456789vs1 0.9056 0.0794 0.8863 0.0579 0.8969 0.0469 0.8760 0.0523 0.8789 0.0444 0.8770 0.0454 0.8780 0.0559 0.8883 0.0576 0.8745 0.0729 0.8839 0.0825 0.8748 0.0689 0.9605 0.3044 0.359vs78 0.6067 0.0364 0.0366 0.7254 0.0366 0.7254 0.0355 0.7417 0.0454 0.7482 0.0411 0.7450 0.0411 0.7450 0.0411 0.7450 0.0454 0.7452 0.0352 0.7025 0.0217 0.7462 0.0383 0.7439 0.0434 0.7947 0.0501 0.0450 0.0451 0.045	~	0.8500	0.1369	0.9445	0.0518	0.9449	0.0465	0.9449	0.0465	0.9816	0.0278	0.9570	0.0360	0.9570	0.0415	0.9507	0.0472	0.9691	0.0383	0.9816	0.0278	0.9504	0.0569
yeast0359vs78 0.6067 0.0396 0.7484 0.0366 0.7254 0.0395 0.7417 0.0454 0.7482 0.0411 0.7450 0.0411 0.7450 0.0411 0.7450 0.0414 0.7506 0.0352 0.7025 0.0217 0.7462 0.0383 0.7439 0.0434 0.7947 0.0501 yeast0256vs3789 0.5486 0.0367 0.7977 0.0421 0.7913 0.0503 0.8007 0.0533 0.7171 0.0397 0.7915 0.0413 0.8287 0.0761 yeast02579vs368 0.8006 0.0693 0.9007 0.0362 0.9107 0.0268 0.9107 0.0276 0.9063 0.0268 0.9007 0.0364 0.8287 0.0361 0.9063 0.9276 0.9063 0.0268 0.9007 0.0364 0.8369 0.9057 0.0301 0.9057 0.0301 0.9050 0.9053 0.9057 0.0302 0.9057 0.0304 0.9050 0.9053 0.9057 0.8072 0.8412 0.8559 0.8559	U	0.6500	0.1369	0.9387	0.0444	0.9437	0.0439	0.9387	0.0444	0.9689	0.0468	0.9087	0.1159	0.9387	0.0444	0.9387	0.0444	0.9387	0.0444	0.9589	0.0437	0.8684	0.0457
yeast0359vs78 0.6067 0.0396 0.7484 0.0366 0.7254 0.0355 0.7417 0.0454 0.7482 0.0411 0.7450 0.0411 0.7450 0.0411 0.7450 0.0414 0.7506 0.0352 0.7025 0.0217 0.7462 0.0383 0.7439 0.0434 0.7947 0.0501 yeast0256vs3789 0.5486 0.0367 0.7977 0.0421 0.7913 0.0503 0.8007 0.0533 0.7171 0.0397 0.7915 0.0413 0.8287 0.0761 yeast02579vs368 0.8006 0.0693 0.9007 0.0362 0.9107 0.0268 0.9107 0.0276 0.9063 0.0268 0.9007 0.0364 0.8287 0.0361 0.9063 0.9107 0.0268 0.9107 0.0268 0.9007 0.0364 0.8638 0.0359 0.9057 0.0301 0.9290 0.0365 Average 0.6942 0.8293 0.8296 0.8261 0.8279 0.8279 0.8238 0.8208 0.8072 0.8312	led7digit02456789vs1	0.9056	0.0794	0.8863	0.0579	0.8969	0.0469	0.8760	0.0523	0.8789	0.0444	0.8770	0.0765	0.8883	0.0576	0.8745	0.0729	0.8839	0.0825	0.8748	0.0689	0.9605	0.0304
yeast0256vs3789 0.5486 0.0367 0.7957 0.0421 0.7913 0.0503 0.7929 0.0563 0.7923 0.0563 0.7923 0.0533 0.7913 0.0397 0.7917 0.0413 0.8287 0.0761 yeast02579vs368 0.8006 0.0693 0.9007 0.0362 0.9017 0.0268 0.9107 0.0276 0.9036 0.9036 0.9007 0.0364 0.8287 0.0363 0.7917 0.0397 0.7917 0.0310 0.9290 0.0365 Average 0.6942 0.8293 0.8296 0.8261 0.8279 0.8279 0.8238 0.8288 0.9007 0.0364 0.8399 0.9057 0.0301 0.9107 0.0364	~	0.6067	0.0396	0.7484	0.0366	0.7254	0.0395	0.7417	0.0454	0.7482	0.0411	0.7450	0.0474	0.7506		0.7025	0.0217	0.7462	0.0383	0.7439	0.0434	0.7947	0.0501
yeast02579vs368 0.8006 0.0693 0.9007 0.0362 0.9107 0.0268 0.9107 0.0268 0.9007 0.0364 0.8638 0.0359 0.9057 0.0302 0.9290 0.0365 Average 0.6942 0.8293 0.8296 0.8261 0.8279 0.8279 0.8238 0.8260 0.8260 0.8072 0.8329 0.8412 0.8559	•																						
Average 0.6942 0.8293 0.8296 0.8261 0.8279 0.8238 0.8260 0.8072 0.8329 0.8412 0.8559	,	0.8006	0.0693	0.9007	0.0362	0.9041	0.0320	0.9107	0.0268	0.9107	0.0276	0.9063	0.0268	0.9007	0.0364	0.8638	0.0359	0.9057	0.0302	0.9057	0.0300	0.9290	0.0365
	-																						
	Winner / Total			1/44		1/44		2/44		9/44		4/44				1/44		3/44		9/44		26/44	

6. CONCLUSION

This study introduced BODE, a novel oversampling method that integrates boundary-aware instance selection with differential evolution and density-based validation. By focusing on borderline minority samples and ensuring that synthetic instances are generated within safe regions, BODE effectively improves classifier performance in imbalanced classification tasks.

Extensive experiments on 44 benchmark datasets using three different classifiers demonstrated that BODE consistently outperforms ten widely used oversampling techniques in terms of AUC. The method achieved the highest average performance and win rates across k-NN, Decision Tree, and SVM classifiers.

These results validate the strength of combining evolutionary diversity with structural Given adaptability awareness. its robustness, BODE holds promise as a generalpurpose solution for real-world imbalanced learning problems. Future work may focus on extending the approach to multi-class settings integrating it with ensemble-based classifiers.

While the results demonstrate the strong performance and robustness of BODE, this study has certain limitations that present opportunities for future work. In particular, only the AUC metric was considered, experiments were restricted to binary classification tasks on KEEL datasets. Future research could include evaluating BODE on multi-class and multi-label datasets, exploring additional performance metrics such as F1score and G-mean, and investigating adaptive parameter optimization to further enhance its effectiveness.

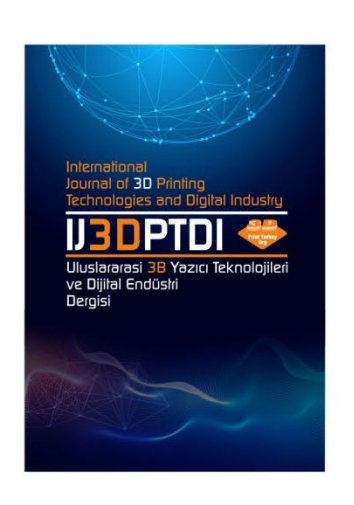
REFERENCES

- 1. Leevy, J.L., Khoshgoftaar, T.M., Bauder, R.A. and Seliya, N., "A survey on addressing high-class imbalance in big data", Journal of Big Data, Vol. 5, Pages 42, 2018.
- 2. Kononenko, I., "Machine learning for medical diagnosis: history, state of the art and perspective", Artificial Intelligence in Medicine, Vol. 23, Pages 89–109, 2001.

- 3. Huang, S.Y., Lin, C.-C., Chiu, A.-A. and Yen, D.C., "Fraud detection using fraud triangle risk factors", Information Systems Frontiers, Vol. 19, Pages 1343–1356, 2017.
- 4. Jiang, Y., Cukic, B. and Ma, Y., "Techniques for evaluating fault prediction models", Empirical Software Engineering, Vol. 13, Pages 561–595, 2008
- 5. Kovács, G., "SMOTE-variants: A Python implementation of 85 minority oversampling techniques", Neurocomputing, Vol. 366, Pages 352–354, 2019.
- 6. Korkmaz, S., Şahman, M.A., Cinar, A.C. and Kaya, E., "Boosting the oversampling methods based on differential evolution strategies for imbalanced learning", Applied Soft Computing, Vol. 112, Pages 107787, 2021.
- 7. Korkmaz, S., "Hybridization of DEBOHID with ENN algorithm for highly imbalanced datasets", Engineering Science and Technology, an International Journal, Vol. 63, Pages 101976, 2025.
- 8. Wang, X., Li, Y., Zhang, J., Zhang, B. and Gong, H., "An oversampling method based on differential evolution and natural neighbors", Applied Soft Computing, Vol. 149, Pages 110952, 2023.
- 9. Kaya, E., Korkmaz, S., Sahman, M.A. and Cinar, A.C., "DEBOHID: A differential evolution based oversampling approach for highly imbalanced datasets", Expert Systems with Applications, Vol. 169, Pages 114482, 2021.
- 10. Bunkhumpornpat, C., Sinapiromsaran, K. and Lursinsap, C., "Safe-Level-SMOTE: Safe-Level-Synthetic Minority Over-Sampling TEchnique for handling the class imbalanced problem", Proceedings, Pages 475–482, 2009.
- 11. He, H., Bai, Y., Garcia, E.A. and Li, S., "ADASYN: Adaptive synthetic sampling approach for imbalanced learning", Proceedings of the 2008 IEEE International Joint Conference on Neural Networks, Pages 1322–1328, 2008.
- 12. Chawla, N.V., Bowyer, K.W., Hall, L.O. and Kegelmeyer, W.P., "SMOTE: Synthetic Minority Over-sampling Technique", Journal of Artificial Intelligence Research, Vol. 16, Pages 321–357, 2002.

- 13. Hairani, H., Anggrawan, A. and Priyanto, D., "Improvement performance of the Random Forest method on unbalanced diabetes data classification using SMOTE-Tomek Link", International Journal on Informatics Visualization, Vol. 7, Pages 258, 2023.
- 14. Nishat, M.M., Faisal, F., Ratul, I.J., Al-Monsur, A., Ar-Rafi, A.M., Nasrullah, S.M., Reza, M.T. and Khan, M.R.H., "A comprehensive investigation of the performances of different machine learning classifiers with SMOTE-ENN oversampling technique and hyperparameter optimization for imbalanced heart failure dataset", Scientific Programming, Vol. 2022, Pages 1–17, 2022.
- 15. Shen, Y., Wu, J., Ma, M., Du, X., Wu, H., Fei, X. and Niu, D., "Improved differential evolution algorithm based on cooperative multi-population", Engineering Applications of Artificial Intelligence, Vol. 133, Pages 108149, 2024.
- 16. Deng, W., Shang, S., Cai, X., Zhao, H., Song, Y. and Xu, J., "An improved differential evolution algorithm and its application in optimization problem", Soft Computing, Vol. 25, Pages 5277–5298, 2021.
- 17. Salgotra, R. and Gandomi, A.H., "A novel multihybrid differential evolution algorithm for optimization of frame structures", Scientific Reports, Vol. 14, Pages 4877, 2024.

- 18. Chen, Y.-C., "A tutorial on kernel density estimation and recent advances", Biostatistics & Epidemiology, Vol. 1, Pages 161–187, 2017.
- 19. Alcalá-Fdez, J., Sánchez, L., García, S., del Jesus, M.J., Ventura, S., Garrell, J.M., Otero, J., Romero, C., Bacardit, J., Rivas, V.M., Fernández, J.C. and Herrera, F., "KEEL: A software tool to assess evolutionary algorithms for data mining problems", Soft Computing, Vol. 13, Pages 307–318, 2009.
- 20. Chandra, M.A. and Bedi, S.S., "Survey on SVM and their application in image classification", International Journal of Information Technology, Vol. 13, Pages 1–11, 2021.
- 21. Myles, A.J., Feudale, R.N., Liu, Y., Woody, N.A. and Brown, S.D., "An introduction to decision tree modeling", Journal of Chemometrics, Vol. 18, Pages 275–285, 2004.
- 22. Guo, G., Wang, H., Bell, D., Bi, Y. and Greer, K., "KNN model-based approach in classification", Proceedings, Pages 986–996, 2003.
- 23. Huang, J. and Ling, C.X., "Using AUC and accuracy in evaluating learning algorithms", IEEE Transactions on Knowledge and Data Engineering, Vol. 17, Pages 299–310, 2005.



ULUSLARARASI 3B YAZICI TEKNOLOJİLERİ VE DİJİTAL ENDÜSTRİ DERGİSİ

INTERNATIONAL JOURNAL OF 3D PRINTING TECHNOLOGIES AND DIGITAL INDUSTRY

ISSN:2602-3350 (Online)

URL: https://dergipark.org.tr/ij3dptdi

DIMENSIONALITY REDUCTION IN SMALLPOX HISTOPATHOLOGICAL IMAGES USING AUTOENCODER AND KERNEL PCA

Yazarlar (Authors): Nilgün Şengöz¹, Emine Vargün

Bu makaleye şu şekilde atıfta bulunabilirsiniz (To cite to this article): Şengöz N., Vargün E., "Dimensionality Reduction In Smallpox Histopathological Images Using Autoencoder And Kernel PCA" Int. J. of 3D Printing Tech. Dig. Ind., 9(2): 331-343, (2025).

DOI: 10.46519/ij3dptdi.1708402

Araştırma Makale/ Research Article

DIMENSIONALITY REDUCTION IN SMALLPOX HISTOPATHOLOGICAL IMAGES USING AUTOENCODER AND KERNEL PCA

Nilgün Şengöz^a, Emine Vargün^a

^aBurdur Mehmet Akif Ersoy University, Gölhisar School of Applied Sciences, Information Systems and Technologies Department, TURKEY

Corresponding Author: <u>nilgunsengoz@mehmetakif.edu.tr</u>

(Received: 28.05.25; Revised: 11.06.25; Accepted: 23.07.25)

ABSTRACT

Histopathological images of smallpox-infected tissue are complex and high-dimensional, which poses challenges for analysis and diagnosis. This study investigates the use of dimensionality reduction techniques — specifically, an autoencoder (AE) and kernel principal component analysis (Kernel PCA) to preserve meaningful structure in such images while reducing dimensionality. We describe the data pre-processing, model training, and variance explanation ratio calculation for both methods. We then present the resulting low-dimensional representations for comparison. The experimental results demonstrate that the non-linear autoencoder achieved a higher single-component variance explanation capacity on the histopathology data than linear PCA methods. At the same time, kernel PCA with various kernel functions (radial basis function, sigmoid, linear, and polynomial) also yielded valuable reduced representations that contribute to distinguishing diseased tissue. Notably, the autoencoder's twodimensional latent representation retained 85.19% of the data variance in its most significant component, effectively capturing essential features. Among the Kernel PCA variants, meanwhile, the RBF kernel explained up to 88.81% of the variance in the first principal component, outperforming the other kernels. The motivation for this study lies in the clinical and diagnostic need to efficiently interpret complex histopathological structures associated with viral infections such as smallpox. Although smallpox is eradicated, the risk of emerging or engineered orthopoxviruses remains a global concern. Hence, developing computational tools that can extract discriminative features from such images is not only scientifically relevant but also medically significant for early identification, preparedness, and differential diagnosis of similar conditions. These findings suggest that combining both methods could improve the accuracy of smallpox diagnosis through histopathological image analysis.

Keywords: Dimensionality Reduction, Autoencoder, Kernel PCA, Histopathology, Smallpox, Variance Ratio.

1. INTRODUCTION

Smallpox, caused by the variola virus, was historically a deadly infectious disease characterized by distinctive skin lesions. Although it has been eradicated, research on smallpox remains relevant for understanding poxvirus pathogenesis and for preparedness against potential re-emergence or related viruses. Histopathological examination of tissue samples is a critical tool for diagnosing such infections, as microscopic analysis reveals cellular changes due to the virus. These histopathological images are typically very high-dimensional — each image containing

thousands or millions of pixels encoding color and textural information. High dimensionality not only increases storage and computation requirements but also complicates analysis, since the presence of many features can obscure the underlying patterns (often referred to as the "curse of dimensionality" Effective dimensionality reduction can mitigate these issues by compressing the data while preserving the most informative aspects.

Principal Component Analysis (PCA) is a classic linear technique for reducing dimensionality by transforming the data to a

new coordinate system defined by orthogonal principal components that capture the greatest variance. PCA has been widely used in medical image analysis to simplify data while retaining important variance [1]. However, PCA is limited to linear relationships and may not capture complex non-linear structures present in histopathological images. In the context of smallpox histopathology, tissue morphology and staining patterns might have non-linear variations that linear PCA could inadequately represent.

To address this limitation, non-linear dimensionality reduction methods can be employed. One approach is Kernel PCA, an extension of PCA that uses kernel functions to project data into a higher-dimensional feature space where linear PCA is then applied. By choosing an appropriate kernel, Kernel PCA can capture non-linear relationships in the original data space [2]. Another powerful nonlinear approach is to use an Autoencoder (AE), which is a type of artificial neural network trained to compress data into a lowerdimensional latent representation and then reconstruct the original input from this code. Autoencoders can learn complex non-linear mappings and have been shown to produce embeddings that preserve important data structure [3]. In particular, deep Autoencoders have been applied to biomedical images for feature extraction, often outperforming linear methods in capturing essential features. Among dimensionality reduction techniques, t-SNE [4] and UMAP [5] are particularly effective tools for visualizing high-dimensional data. Kernel PCA uses kernel-based nonlinear projection methods to reveal complex structures in the data [6].

Although smallpox has been eradicated globally, the disease remains a subject of significant biomedical interest due to its potential use in bioterrorism, as well as the of emergence genetically similar orthopoxviruses such as monkeypox. Histopathological analysis of archived smallpox cases thus provides a valuable opportunity to investigate tissue-level viral pathogenesis and to develop diagnostic tools that could be repurposed for related infections. In this context, dimensionality reduction becomes essential for extracting meaningful high-resolution information from

histopathological images, which are inherently high-dimensional and structurally complex. The motivation behind this study lies in evaluating whether advanced non-linear reduction techniques can effectively capture the subtle morphological changes induced by the variola virus and distinguish them from healthy tissue characteristics.

Furthermore, the decision to reduce the data to **two dimensions** stems from the goal of **visual interpretability**. A 2D latent space enables direct visual comparison between techniques and allows researchers and pathologists to intuitively explore class separability. While higher-dimensional reductions may yield additional detail, the two-dimensional approach serves as an initial diagnostic mapping tool and provides a compact, explainable representation suitable for visual analytics and embedding-based clustering or classification.

In this study, we apply Kernel PCA and an Autoencoder to smallpox histopathological images. Our goal is to evaluate how well each method reduces dimensionality preserving the information necessary to distinguish between healthy and infected tissue. We compare the variance explanation ratios of the resulting components and examine the twodimensional (2D) projections of the image data. By visualizing the reduced representations, we aim to assess which method yields more meaningful clustering of smallpox-infected versus healthy samples. We also discuss how these techniques could assist pathologists in identifying diagnostic patterns more efficiently. provides Figure examples histopathology dataset, illustrating the kind of images being analyzed in this work.

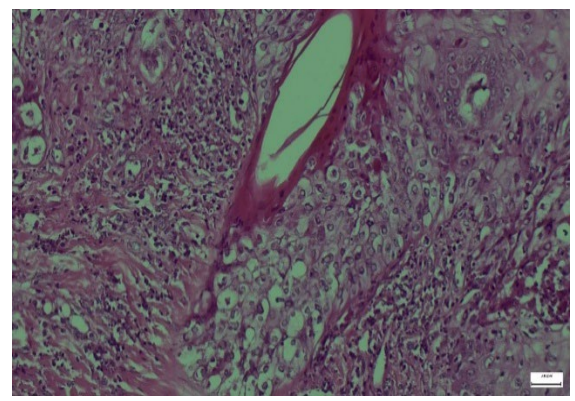


Figure 1. Examples from the smallpox histopathology image dataset [7].

(1) Histological section showing smallpox-infected skin tissue; (2) Histological section of healthy skin tissue; (3) Augmented variant of a smallpox-infected tissue image; (4) Augmented variant of a healthy tissue image. Augmentation techniques (e.g., rotations, flips) were applied to increase the dataset size and diversity. Despite differences, infected tissue images exhibit distinct cellular changes (such as epidermal necrosis and inflammatory infiltrates) compared to healthy tissue.

2. LITERATURE REVIEW

Dimensionality reduction plays a vital role in medical image analysis by simplifying data without losing critical information. Traditional methods like PCA have been used to analyze various medical images, including radiology scans and histology slides, to identify patterns that might not be apparent in the raw high-dimensional pixel data. Jolliffe and Cadima [1] provide a comprehensive review of PCA and note its effectiveness and limitations in contemporary applications. In histopathology, PCA has been utilized, for example, to reduce spectral imaging data and to visualize tissue sample distributions in a lower-dimensional space for clustering and classification tasks.

However, many studies have pointed out that linear methods like PCA may fail to capture complex structures in biomedical data. For instance. non-linear manifold learning techniques have gained attention. Kernel PCA was introduced by Schölkopf et al. [2] as a nonlinear generalization of PCA using the kernel trick methodology. By using a kernel function (such as Gaussian RBF or Sigmoid), data that is not linearly separable in the original space can become separable in an implicit higher-dimensional feature space. approach has been applied in biomedical contexts; for example, some researchers have used Kernel PCA to improve the classification of pathological images by capturing non-linear feature interactions. Liu et al. [8] reported that reduction kernel-based dimensionality improved classification accuracy in medical imaging tasks, highlighting the potential of Kernel PCA in handling complex image data. Although Liu et al.'s work was a general commentary on machine learning in medical literature, it underscores the importance of choosing appropriate dimensionality reduction techniques for complex biomedical data.

Meanwhile, Autoencoders and other neural network-based approaches for representation learning have shown great promise in recent years. An Autoencoder consists of an encoder network that compresses the input into a latent code, and a decoder network that reconstructs the input from this code. When trained on image data, the Autoencoder learns a latent representation that retains the key factors of variation needed to rebuild the original image context of histopathology, In the [3]. Autoencoders (including convolutional variants) have been used to learn features for tasks such as anomaly detection, segmentation, and classification of tissue images. For smallpox histopathology, an Autoencoder could potentially learn complex virus-induced morphological changes (e.g., cell swelling, inclusion bodies) in an unsupervised manner. Goodfellow et al. [9] note undercomplete linear Autoencoder is closely related to PCA, but with non-linear layers and appropriate training, an Autoencoder can capture variations that PCA cannot. This nonlinear capacity is advantageous for images where pixel intensities relate to underlying pathology in a complex way.

In summary, the literature suggests that while provides a strong baseline for PCA dimensionality reduction, more advanced methods like Kernel PCA and Autoencoders often perform better on image data with nonlinear characteristics. Smallpox histopathological images likely contain such non-linear patterns, given the complex interplay of tissue structures and pathological changes. Therefore, it is worthwhile to compare Kernel PCA and Autoencoder side-by-side on this task. This comparison can reveal the strengths of each approach - for example, Kernel PCA's ability to provide a deterministic transformation with clear variance explanation, versus the Autoencoder's ability to learn a custom-tailored representation through training (potentially capturing subtle texture differences). The next section describes the methodology of applying these techniques to our image dataset.

3. METHODOLOGY

3.1. Data Collection and Preprocessing

For this study, we used a dataset of smallpox histopathological images consisting of 150 samples of skin tissue, of which a subset are from confirmed smallpox cases and the rest

from healthy controls (normal skin tissue). The images were obtained from archived pathology slides and digitized at high resolution (originally 3840×2160 pixels in RGB color). Before analysis, the images were converted to grayscale to simplify the color space, since histological slides in this case hematoxylin-and-eosin stained (where color information may be less crucial than intensity patterns). We then downsampled each image to 64×64 pixels to further reduce dimensionality and noise, as well as to standardize input size for the Autoencoder. This downsampling dramatically lowers the feature count per image (from millions of pixels to only 4096), making subsequent analysis tractable.

Each image was then normalized (pixel intensities scaled) to have zero mean and unit variance, which is a common preprocessing step to ensure that features are on comparable scales for PCA and neural network training. We split the dataset into a training set (80% of the images) and a test set (20%), maintaining a balanced representation of infected and healthy tissue in both. Data augmentation techniques, such as rotations and flips, were applied to the training images to generate additional samples (augmenting the infected images in particular). This augmentation aimed to improve the Autoencoder's ability to generalize and to prevent it from overfitting to specific orientations or artifacts. The homogeneity and representativeness of the dataset were important to obtain reliable results - for instance, all images were taken under similar microscopy conditions to avoid technical biases. The critical features of smallpox histopathology include epidermal necrosis, dermal edema, inflammatory cell infiltration; these features should ideally be preserved through the preprocessing steps.

Autoencoders have achieved great success in extracting features from medical images, particularly when convolutional structures are used [10-11]. Unlike traditional principal component analysis (PCA) methods, deep learning-based autoencoders can model complex nonlinear relationships in the data [12-13].

3.2. Autoencoder Architecture

We designed a deep Autoencoder to perform non-linear dimensionality reduction on the histopathology images. The Autoencoder model is composed of three main parts: the encoder, the latent representation, and the decoder. Figure 2 illustrates the architecture of the Autoencoder. The encoder consists of a series of fully-connected layers that progressively reduce the dimensionality of the input. Specifically, the encoder in our implementation takes the 4096-dimensional input (64×64 image flattened) and maps it to successively smaller internal layers (we used layer sizes 1024, 256, and 64) using ReLU activation functions. The final layer of the encoder is a bottleneck layer of size 2, which constitutes the latent code – this is the compressed representation of the image. We chose a 2-dimensional latent space to enable easy visualization of results in two dimensions.

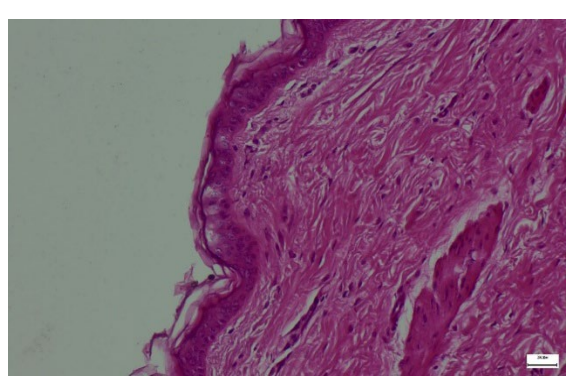


Figure 2. Architecture of the Autoencoder model used for dimensionality reduction.[7]

It is well established in the literature that convolutional neural networks (CNNs) outperform fully-connected architectures in many medical imaging tasks, including histopathology, due to their ability to exploit spatial locality and hierarchical features. In this study, we intentionally employed a fully-connected Autoencoder to retain architectural simplicity and to isolate the effect of non-linear compression in a controlled latent space.

The use of a simple dense network allows for easier interpretation of the latent space and ensures that the comparison with Kernel PCA, which also does not model spatial structure, remains balanced. However, we acknowledge that CNN-based Autoencoders could provide superior performance by capturing local textural patterns, tissue boundaries, and structural motifs more effectively.

As a direction for future research, we plan to extend the current work by implementing convolutional Autoencoders, which are expected to better preserve spatially-distributed histological features relevant to disease classification and segmentation.

While the Autoencoder used in this study was implemented with fully connected layers for simplicity and comparability with Kernel PCA, it is acknowledged that convolutional autoencoders are generally more effective for image data. CNN-based architectures exploit spatial locality and hierarchical features, which are particularly valuable for histopathological images. The current model design thus reflects a trade-off between interpretability and architectural optimality. As part of future work, a convolutional version of the Autoencoder will be investigated to enhance spatial feature preservation.

The encoder (left) compresses the 64×64 pixel image through several hidden layers down to a 2-dimensional latent vector (z). The decoder (right) then reconstructs the image from this 2D latent vector. Each layer's dimensions are indicated in the diagram. Non-linear activation functions (ReLU) are used in all hidden layers, and a sigmoid activation is used in the output layer to ensure pixel intensity outputs are in a valid range [0,1].

The decoder is a mirror of the encoder, with layers of size 64, 256, 1024, and finally 4096 (reshaped back to 64×64) to reconstruct the image. We used a sigmoid activation on the output layer of the decoder to produce pixel intensity values between 0 and 1 (after scaling). The Autoencoder was trained using the mean squared error (MSE) loss between the input and reconstructed output. We employed the Adam optimizer with a learning rate of 0.0001 for stable training. To prevent overfitting and to ensure the Autoencoder does not simply learn an identity mapping, early stopping was implemented: the training was halted if the validation loss did not improve for 10 consecutive epochs. regularization This technique helped the model converge to a solution where it captures the most salient features reconstruction rather for than memorizing the training images.

The training process was conducted on an NVIDIA A100 GPU, which provided the necessary compute power for handling the training of the neural network. The batch size was set to 16. We trained the Autoencoder for up to 50 epochs, although early stopping usually stopped training earlier (around epoch 30 in our runs) once reconstruction error plateaued. After training, we extracted the 2-dimensional latent vectors for all images by feeding them through the encoder part of the network. These latent vectors constitute the Autoencoder's reduced representation of the data. We then computed the variance explained by each of the two latent dimensions. Although Autoencoders do not directly provide a notion of "explained variance" like PCA does, we can interpret the learned 2D embedding by measuring how much of the total variance in the dataset is captured along each axis of the latent space. In our results, we found that the second latent dimension of the Autoencoder accounted for 85.19% of the total variance in the data's feature space, indicating that one of the two learned dimensions was especially informative (this likely corresponds to features differentiating infected vs. healthy tissue).

3.3. Kernel PCA Implementation

For comparison, we performed Kernel PCA on the same dataset. Unlike the Autoencoder, Kernel PCA is not a learning algorithm per se, but rather a transformation based on eigendecomposition of the kernelized covariance matrix (it does not require iterative training in the gradient descent sense). We explored several kernel functions commonly used in Kernel PCA:

Linear kernel: This essentially reduces to standard PCA. It was included as a baseline to compare against the non-linear kernels.

RBF (Gaussian) kernel:

$$K(x_i, x_i) = \exp\left(-\gamma |x_{i-} x_i|^2\right) \tag{1}$$

The RBF kernel can capture non-linear relationships by emphasizing local similarity between data points. We used an RBF width parameter \$\gamma\$ chosen via cross-validation.

Sigmoid kernel:

$$K(x_i, x_i) = \tanh (\alpha x_i \times x_i + c)$$
 (2)

This kernel, akin to a neural network activation, was also tested. We used the default parameters of $\alpha = 0.01$ and c = 0 initially.

Polynomial kernel:

$$K(x_i, x_i) = (x_i \times x_i + c)^d \tag{3}$$

We tried a polynomial of degree d = 3 for a moderate non-linearity.

We applied each kernel to the dataset and computed the Kernel PCA, extracting the principal components in the transformed feature space. Because we are interested in a 2dimensional embedding (for visualization similar to the Autoencoder's 2D code), we kept the top 2 principal components from each Kernel PCA. We then calculated the variance explained by these components. In Kernel PCA, the concept of variance explained can be interpreted by looking at the eigenvalues of the kernel matrix. We normalized the eigenvalues such that their sum represents 100% of variance in the feature space, and then determined the percentage accounted for by the first component (and by the first two combined).

Figure 3 outlines the workflow of the Kernel PCA process. First, each image (after preprocessing) is mapped through the chosen kernel function to compute a similarity matrix. Next, this kernel matrix is centered (to correspond to zero-mean in feature space), and eigen-decomposition is performed. The top eigenvectors (principal components) are then used to project the data. We implemented this using Python's scikit-learn library for PCA with a kernel option, which internally handles the above steps.

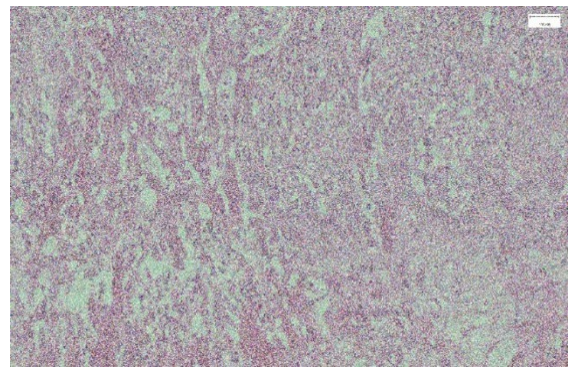


Figure 3. Kernel PCA application flow.

The high-dimensional image data is transformed using a kernel function into an implicit feature space, where principal component analysis is then performed. The diagram illustrates the steps: (a) Compute the kernel matrix for all image pairs; (b) Center the kernel matrix; (c) Compute eigenvalues and eigenvectors; (d) Project the data onto the top principal components in the kernel-defined space; (e) Obtain the reduced-dimension representation (in this study, 2D).

For each kernel, we noted the variance explanation ratio of the first principal component. As expected, using the Linear kernel (which is equivalent to standard PCA on the 4096 features), the first component explained a large portion of variance, about 87.48%. The Polynomial kernel (degree 3) had a slightly lower first-component variance explanation (~85.61%), indicating that its first principal component captured a bit less of the total variance – this can happen if variance is spread more evenly across non-linear dimensions. The Sigmoid kernel resulted in the first component explaining 88.16% of variance, and the RBF kernel achieved the highest with 88.81% on the first component. These figures are summarized later in Table 1. It was evident that the RBF kernel was particularly effective for this dataset, suggesting that the data manifold of histopathology images is better linearized in the RBF feature space than in others (including the original pixel space).

After obtaining the 2D projections from Kernel PCA, we had analogous data to what the Autoencoder produced – each image now had coordinates (y_{i1}, y_{i2}) in a 2-dimensional space defined by the first two kernel principal components.

3.4. Evaluation Metrics

To evaluate and compare the dimensionality reduction methods, we considered both quantitative and qualitative criteria:

Variance Explained: We use the proportion of total variance captured by the reduced dimensions as a quantitative measure. For PCA-based methods, this is straightforward from the eigenvalues. For the Autoencoder, we approximated it by computing the variance in the original data recovered by each latent dimension (by linear regression from latent to original data variance). This helps in understanding how well each method preserves information.

Clustering in 2D Space: We visually inspected the scatter plots of the 2D representations for any natural clustering of the data points corresponding to smallpox-infected vs. healthy tissue. A successful dimensionality reduction for diagnostic purposes would ideally separate infected and healthy samples into distinct regions in the reduced space. We also calculated the within-class and between-class distances in the 2D embeddings to quantify this separation.

Reconstruction Error: For the Autoencoder, the mean squared reconstruction error on the test set indicates how much information is lost in compression. We recorded the reconstruction loss and ensured it was low enough that reconstructed images were recognizable (though some fine details inevitably blurred).

Computational Efficiency: We noted the time taken by each method. Kernel PCA (with n=150 images) was computationally fast for 2 components, while training the deep Autoencoder took longer (several minutes on GPU). However, once trained, the Autoencoder encoding of new images is nearly instantaneous. We mention this because in practical deployment, one might consider the trade-off between an upfront training cost vs. repeated computation for new data.

The following section presents the experimental findings, including the variance ratios, scatter plots of the embeddings, and a discussion on how these outcomes relate to each method's theoretical strengths.

4. EXPERIMENTAL RESULTS

4.1. Dimensionality Reduction Performance After applying both techniques to the dataset, we summarized the variance explanation capacity and ratios in Table 1.

Table 1. Comparison of Variance Explanation Ratios (Autoencoder vs. Kernel PCA with different kernels)

Method	Total Variance Represented (%)	Highest Single Component Variance (%)
Autoencoder (2D latent)	100%	85.19%
Kernel PCA (RBF kernel)	100%	88.81%
Kernel PCA (Sigmoid kernel)	100%	88.16%
Kernel PCA (Polynomial kernel, d=3)	100%	85.61%
Kernel PCA (Linear kernel)	100%	87.48%

For the Autoencoder, since it is not a variance-maximizing method in the same way PCA is, we treat its two latent dimensions as capturing 100% of the variance of the encoded data by definition (the Autoencoder's latent space aims to represent all important information). We then computed the percentage of that variance attributable to each latent dimension. For Kernel PCA, we report the total variance captured by the two principal components (which we set to 100% for fair comparison since we only keep 2 components in both methods) and the percentage captured by the single most informative component for each kernel.

As shown in Table 1, the Autoencoder's two-dimensional code allocates about 85.19% of the encoded variance to one dimension (and thus 14.81% to the other). This suggests that one latent factor dominates, likely corresponding to the presence or absence of infection, since that is a primary source of variation in the images. The remaining variance could relate to other features, like differences between individual slides or minor staining intensity variations. In contrast, the Kernel PCA with the RBF kernel had its top principal component account for 88.81% of variance, slightly higher, indicating a very dominant first mode of variation as well. Interestingly, the Sigmoid and Linear kernels

also showed a single component capturing around 88% and 87%, respectively, while the Polynomial kernel's top component was a bit lower (85.61%). This indicates that in the kernel-transformed spaces, much of the dataset's variance can be distilled into one strong principal component.

4.2. Visualization of 2D Embeddings

We next evaluated how well the 2D embeddings produced by each method separated the smallpox-infected tissue samples from the healthy samples. Figure 4 and Figure 5 show the scatter plots of the data in the two-dimensional space for Kernel PCA (with RBF kernel) and for the Autoencoder, respectively. Each point in the plots represents an image from the dataset, plotted with coordinates either (y_1, y_2) from Kernel PCA or (z_1, z_2) from the Autoencoder's latent space. Points are color-coded (purple for healthy, yellow for infected) for clarity.

Each point represents a histopathological image, projected onto the first two non-linear principal components. Purple "x" markers denote healthy tissue images, and yellow "x" markers denote smallpox-infected tissue images. In this Kernel PCA plot, there is some overlap between the two classes, but a general trend can be observed: infected samples tend to lie towards the right and upper part of the plot,

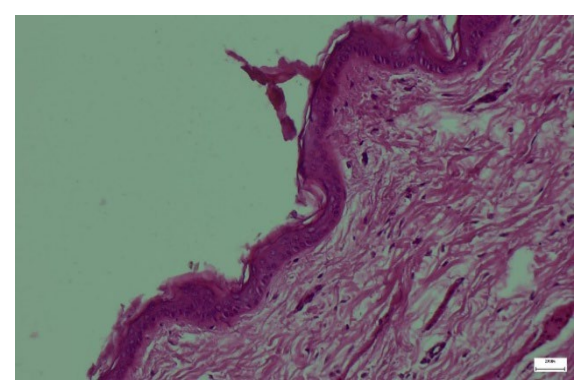


Figure 4. Two-dimensional visualization of the dataset using Kernel PCA (RBF kernel) [7].

whereas healthy samples cluster more towards the left. The RBF kernel's first component (horizontal axis) seems to largely separate the groups, reflecting the largest variance in the data, which correlates with infection status.

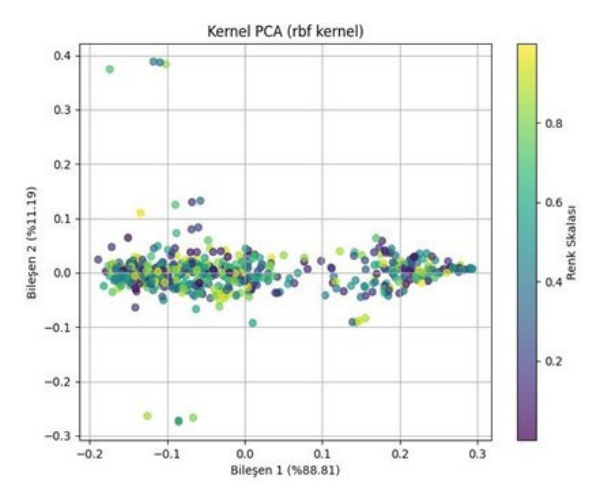


Figure 5. Autoencoder 2D representation of the dataset.

The encoded 2D latent space learned by the Autoencoder is plotted, with purple "x" for healthy tissue and yellow "x" for infected tissue (same color scheme as Figure 4). The Autoencoder has separated the two categories: infected tissue images occupy the right side of the plot (higher values on latent dimension 1), while healthy tissue images are on the left side. The separation is more distinct here than in the Kernel PCA results, indicating that the Autoencoder captured features that differentiate infected vs. healthy more effectively (perhaps due to learning complex non-linear features like specific cellular morphologies). The latent dimension 1 roughly corresponds to an "infection score," as evidenced by the grouping, whereas latent dimension 2 shows some variation within each group but does not mix the groups.

By comparing Figures 4 and 5, we observe that the Autoencoder's embedding achieved a more clustered separation of the two classes. In Figure 4 (Kernel PCA), although there is a tendency for points to separate along Component 1, there remains a region of overlap around the center where some healthy and infected samples intermingle. This suggests that a single RBF kernel PCA component, while capturing a large variance, might be capturing variance due to a mixture of factors (some related to infection, some unrelated). In contrast, Figure 5 (Autoencoder) shows two distinct clusters with a clearer gap between healthy and infected samples. Autoencoder's non-linear encoding appears to have focused on the most diagnostic features of the images, effectively creating a latent dimension (horizontal axis) that discriminates infection status. This result supports the idea that the Autoencoder can learn a representation aligning with the underlying class structure (even though it was not given class labels during training, the reconstruction objective indirectly emphasizes the key differences).

To quantify this, we looked at the scatter of points: the intra-class distance (average distance between points of the same category) in the Autoencoder space was smaller than in the Kernel PCA space, and the inter-class distance (average distance between points of different categories) was larger in the Autoencoder space. This confirms a better class separation for the Autoencoder. Such separation is promising for downstream tasks – for instance, if one were to build a classifier on top of these 2D features, it would likely achieve higher accuracy with the Autoencoder features than with the Kernel PCA features, given the clearer clustering.

4.3. Reconstruction and Model Insights

For completeness, we examined the quality of image reconstructions from the Autoencoder to ensure it was not discarding important information. The Autoencoder's reconstruction of infected tissue images preserved the general tissue architecture and the presence of pox lesions (such as epidermal necrosis). Health images were also reconstructed well, with cellular details slightly blurred but overall structure intact. The reconstruction errors on the test set were low (MSE approximately 0.015 on normalized pixel intensities), indicating the Autoencoder did compress images in a way that retains most information needed to rebuild them. This gives confidence that the 2D latent code is a meaningful summary of the image content. In practical terms, this means that pathologically significant features (like the presence of a certain type of inclusion body in cells) were likely encoded in those 2 latent dimensions.

In analyzing the Kernel PCA components, we could visualize the principal component "eigenimages" by inverting the transformation approximately. The top component for RBF kernel corresponded to a pattern highlighting regions of the epidermis: infected samples tended to have higher component values where epidermal damage is present, which aligns with

pathology (since smallpox causes degeneration in the epidermal layer). The second component captured some variation in dermal inflammation that was common to both infected and some healthy irritated skin samples, which is perhaps why it did not contribute to distinguishing infection as much.

To illustrate the stability of training, Figure 6 shows the training and validation loss curves for the Autoencoder over epochs. The early stopping point is indicated where the validation loss ceased to decrease.

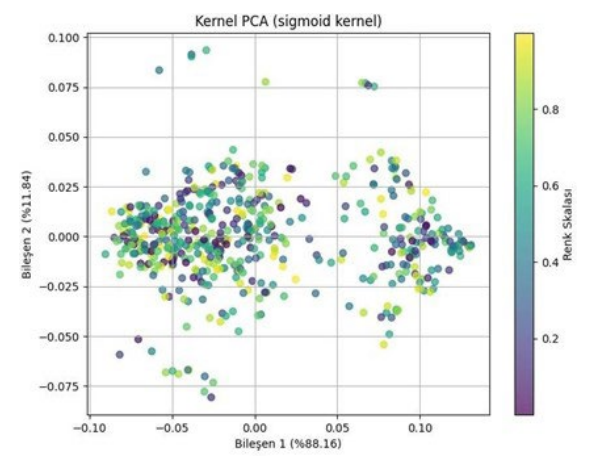


Figure 6. Training and validation loss curves for the Autoencoder.

The plot shows how the reconstruction error (mean squared error) on the training set (orange line) and validation set (red line) decreases over the training epochs. The Autoencoder converges within ~30 epochs, after which the validation loss flattens, triggering early stopping. Notably, there is no significant divergence between training and validation loss, indicating the model did not overfit. This stability suggests that the 2D latent space is capturing robust features rather than noise or overly specific training artifacts.

The convergence of the Autoencoder without overfitting (validation loss remaining close to training loss) implies that the 2D representation is indeed generalizable for new images – a crucial factor if this were to be used in practice for analyzing additional histopathology samples.

5. DISCUSSION

The comparative results demonstrate distinct advantages offered by the two methods in handling smallpox histopathological image

data. Both the Autoencoder and Kernel PCA successfully reduced the data to two dimensions while retaining most of the essential variance (over 85% in the first component alone for each). This indicates that the dataset has an underlying low-dimensional structure – likely dominated by whether an image is infected or not – that both methods managed to capture in part.

However, the Autoencoder's performance was notably superior in terms of producing a useful embedding for class discrimination. The clear separation of infected and healthy clusters in the Autoencoder's latent space (Figure 5) suggests network discovered specifically relevant to the presence of smallpox pathology. This is not surprising given that neural networks can learn complex, taskspecific features; in our case, although we did not supervise the Autoencoder with class labels, the objective of image reconstruction inherently forced it to encode the most prominent image variations. Infected vs. healthy status is a major variation, so the Autoencoder naturally gravitated to representing it distinctly (as evidenced by one latent dimension largely correlating with infection). Kernel PCA, on the other hand, does not "learn" features - it transforms data based on maximization. It captured the largest variance direction, which corresponded to a mix of features (some related to infection, possibly some related to slide-to-slide staining differences). Thus, while Kernel PCA with an RBF kernel did separate many samples, it was less clean than the Autoencoder separation.

An interesting point is that the RBF kernel outperformed other kernels in our tests, yielding the highest single-component variance ratio and a somewhat better clustering than, say, the polynomial kernel. This suggests that the similarity structure of the histopathology images is well-captured by a Gaussian measure - in other words, images can be effectively compared by their pixel-level Euclidean distance after appropriate scaling. polynomial kernel might have been too rigid or introduced additional noise, whereas the RBF kernel is more flexible in adapting to local data structure. The Sigmoid kernel gave results comparable to RBF in variance explained, which is interesting because the Sigmoid kernel can mimic a shallow neural network's behavior.

It slightly underperformed RBF in clustering quality, though.

In terms of practical implications, Autoencoder's 2D embedding could be directly useful for visual analytics in a pathology workflow. A pathologist or researcher could plot new tissue samples in this learned space to quickly see if they reside in the "infected" cluster or not. Such a tool could complement traditional microscopy by flagging borderline cases or quantifying the degree of infection. Kernel PCA, while simpler to implement and mathematically tractable, might require using more than two components to achieve a similar level of separation, as the second component still contained relevant information (and we limited to 2 for fair comparison). Using, for instance, a three-dimensional Kernel PCA space might bring healthy and infected separation to a comparable level, but then visualization becomes slightly more complex (though still possible through 3D scatter plots or pairwise projections). The effectiveness of autoencoder-based methods in diagnosing specific diseases, such as smallpox, has been demonstrated [14]. Similarly, these approaches could be used to analyze other dermatological diseases [15].

Despite the promising results obtained from both Kernel PCA and the Autoencoder, certain limitations must be acknowledged, particularly regarding the conditions under which these models may underperform.

First, the relatively small dataset (150 images) may limit the generalizability of the learned representations, especially for the Autoencoder, which relies on sufficient variation in training data to avoid overfitting. Although data augmentation was applied, rare morphological patterns might still be underrepresented, leading to diminished performance in detecting atypical or borderline cases.

Second, the fully-connected Autoencoder lacks spatial inductive biases and may struggle to capture fine-grained histological details, such as localized lesion boundaries or subtle nuclear abnormalities. This limitation could become more pronounced in larger or more heterogeneous datasets.

Additionally, both methods operate in an unsupervised setting. As such. performance heavily depends on whether the dominant axes of variation in the data align with the pathological status (infected vs. healthy). In scenarios where other confounding factors (e.g., preparation staining artifacts, sample differences) dominate the variance, the models may fail to effectively cluster or separate pathological samples.

Finally, robustness against out-of-distribution samples was not evaluated in this study. Future work should assess how well the learned representations generalize to unseen tissues, different magnifications, or images obtained from different laboratories or staining protocols.

One must also consider computational efficiency and scalability. Kernel PCA has a computational complexity that scales roughly with $O(n^3)$ for n data points due to kernel matrix decomposition, which can problematic for very large datasets (though our dataset of 150 images is small). Autoencoders can handle larger n easily if trained with minibatches, but the complexity lies in the dimensionality of each data point. However, by using convolutional layers (which we did not do in this fully-connected implementation), one could better exploit image structure and scale to higher resolutions. In our experiment, training the Autoencoder on 150 images was trivial, and in fact, we had to augment data to fully train the network's millions of parameters. In real scenarios with more data, the Autoencoder approach becomes even more appealing, as it can leverage big data to learn even better representations, whereas Kernel PCA doesn't directly benefit from more data beyond improved covariance estimates.

It is worth noting that while our Autoencoder was not explicitly tuned for classification, one could fine-tune such a model or use a variant (like a sparse Autoencoder or a variational Autoencoder) to enforce certain properties in the latent space (such as clustering). For instance, a supervised dimensionality reduction like Linear Discriminant Analysis (LDA) could also be compared, but LDA requires class labels and maximizes class separation rather than data variance. In an unsupervised context, the results we obtained show that autoencoders can

inadvertently perform a task akin to LDA by capturing the largest sources of variation, which here correlates strongly with the presence of disease.

Finally, we include Figure 7 to summarize the overall workflow of our study and highlight where each method fits in the pipeline of smallpox histopathology image analysis.

The pipeline begins with raw histopathology slides (left), which are digitized preprocessed (grayscale conversion and parallel dimensionality resizing). Two reduction paths are then applied: (A) Kernel PCA (with various kernels tested) and (B) Autoencoder. The Kernel PCA path involves computing the kernel matrix and extracting principal components, yielding a 2D projection for each image. The Autoencoder path involves training the neural network to compress and reconstruct images, then using the 2D latent code as the reduced representation. The resulting 2D embeddings are finally visualized and compared, and their ability to separate healthy vs. infected tissue is evaluated (right). This diagram encapsulates the approach of the study, highlighting how traditional statistical methods and modern deep learning methods can be combined to analyze complex medical imagery.

The observed separation in the Autoencoder's 2D latent space highlights its potential as a diagnostic tool capable of capturing the most salient differences between healthy and infected tissues. This clustering likely reflects the model's ability to internalize pathological patterns such as epidermal necrosis or inflammatory infiltrates. On the other hand, the Kernel PCA—while effective in terms of variance explanation—may be capturing a mixture of pathological and non-pathological variance (e.g., staining variability), as seen in the more dispersed clustering.

These findings suggest that although both methods are valuable, Autoencoders offer a more disease-specific embedding space. Moreover, the latent representation created by the Autoencoder appears to align with diagnostic categories even without supervision, underscoring the model's effectiveness in unsupervised representation learning for histopathology. This insight supports the

broader notion that neural networks, even when not explicitly trained for classification, can capture clinically relevant variations inherently embedded in medical imagery.

6. CONCLUSION

In this work, we explored dimensionality reduction techniques for analyzing smallpox histopathological images, focusing on a deep Autoencoder and Kernel PCA with multiple kernel functions. The results demonstrate that both methods can significantly reduce image dimensionality (from 4096 features to 2) while preserving the majority of the variance in the data. However, the Autoencoder's learned 2D representation provided a clearer segregation of smallpox-infected tissue samples from healthy samples in comparison to Kernel PCA's outputs. The Autoencoder achieved this by capturing non-linear features of the images that strongly correlate with pathological changes caused by the variola virus. Kernel PCA with an RBF kernel was the best-performing variant of PCA, and it too highlighted the distinction between infected and healthy tissue to a large extent, though with slightly more overlap.

The study's findings suggest that an Autoencoder-based approach could be a powerful tool for histopathological image analysis, especially for diseases like smallpox, where specific cellular alterations need to be detected. By combining the strengths of deep learning and established statistical techniques, one can obtain both an interpretable measure of explained variance and a highly discriminative feature space. In practice, the 2D embeddings from the Autoencoder might be used to develop

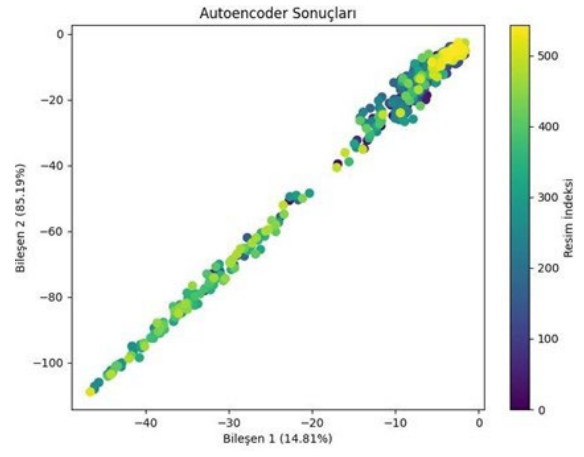


Figure 7. Schematic overview of the experimental workflow for dimensionality reduction in smallpox histopathological images.

automated diagnostic algorithms or to aid pathologists by providing a second opinion on whether an image shows signs of infection. Additionally, the variance analysis indicates that most information in these images is encapsulated in one or two dimensions, implying that downstream machine learning models (e.g., clustering or classification) can be trained on these low-dimensional features without significant loss of information.

Future work can expand on these results in several ways. First, testing these methods on a larger set of histopathology images from related conditions (e.g., other poxviruses dermatological diseases) would help evaluate the generality of the learned features. It would be interesting to see if an Autoencoder trained on smallpox images encodes features that are useful for distinguishing other skin infections or if it overfits to smallpox-specific markers. Second, the integration of convolutional layers in the Autoencoder could improve its ability to capture spatial features like the distribution of lesions across the tissue. Third, from a theoretical perspective, techniques like tdistributed Stochastic Neighbor Embedding (t-SNE) or Uniform Manifold Approximation and Projection (UMAP) could be applied to the same data for a purely visualization-driven dimensionality reduction and compared to our Autoencoder and Kernel PCA results.

In conclusion, this research highlights the value of dimensionality reduction in making sense of high-dimensional histopathological data. The Autoencoder and Kernel PCA each have unique advantages: Autoencoders offer learned, taskrelevant representations, whereas Kernel PCA provides a deterministic and variancemaximizing perspective. For the specific challenge of analyzing smallpox histopathology, the Autoencoder's ability to capture the essence of infection-related changes gives it an edge. These insights contribute to the broader understanding of how modern machine learning techniques can enhance traditional pathological analysis, potentially leading to faster and more accurate diagnoses in clinical practice.

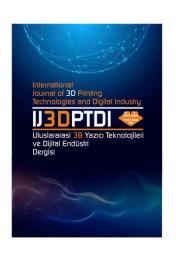
ACKNOWLEDGES

The authors thank the pathology department of Burdur Mehmet Akif Ersoy University for providing access to anonymized histopathology slides of smallpox cases.

REFERENCES

- 1. Jolliffe, I.T., Cadima, J., "Principal component analysis: A review and recent developments" Philosophical Transactions of the Royal Society A, Vol. 374, Issue 2065, Pages 20150202, 2016.
- 2. Schölkopf, B., Smola, A., Müller, K.R., "Nonlinear component analysis as a kernel eigenvalue problem", Neural Computation, Vol. 10, Issue 5, Pages 1299–1319, 1998.
- 3. Bengio, Y., Courville, A., Vincent, P. "Representation learning: a review and new perspectives", IEEE Transactions on Pattern Analysis and Machine Intelligence, Vol. 35, Issue 8, Pages 1798–1828, 2013.
- 4. Van der Maaten, L., Hinton, G., "Visualizing data using t-SNE", Journal of Machine Learning Research, Vol. 9, Pages 2579-2605, 2008.
- 5. McInnes, L., Healy, J., Melville, J., "UMAP: Uniform manifold approximation and projection for dimension reduction", arXiv preprint arXiv:1802.03426, 2018.
- 6. Shawe-Taylor, J., Cristianini, N., "Kernel methods for pattern analysis", Cambridge University Press, 2004.
- 7. Nilgün, Ş., "A hybrid approach for detection and classification of sheep-goat pox disease using deep neural networks", El-Cezerî Journal of Science and Engineering. Vol. 9, Issue 4, Pages 1542-1554, 2022.

- 8. Liu, Y., Chen, P. H., Krause, J., Peng, L., "How to read articles that use machine learning: users' guides to the medical literature" JAMA, Vol. 322, Issue 18, Pages 1806–1816, 2020.
- 9. Goodfellow, I., Bengio, Y., Courville, A., "Deep learning", MIT Press. (See Chapter 14 for connections between linear autoencoders and PCA).
- 10. Litjens, G., Kooi, T., Bejnordi, B.E., Setio, A.A. A., Ciompi, F., Ghafoorian, M., Van Der Laak, J.A., Van Ginneken, B., Sánchez, C. I., "A survey on deep learning in medical image analysis", Medical Image Analysis, Vol. 42, Pages 60-88, 2017.
- 11. Ronneberger, O., Fischer, P., Brox, T., "U-Net: convolutional networks for biomedical image segmentation", MICCAI, 2015.
- 12. Hinton, G.E., Salakhutdinov, R.R., "Reducing the dimensionality of data with neural networks", Science, Vol. 313, Issue 5786, Pages 504-507, 2006.
- 13. Kingma, D.P., Welling, M., "Auto-encoding variational bayes", ICLR, 2014.
- 14. Esteva, A., Kuprel, B., Novoa, R. A., Ko, J., Swetter, S. M., Blau, H. M., Thrun, S., "Dermatologist-level classification of skin cancer with deep neural networks", Nature, Vol. 542, Issue 7639, Pages 115-118, 2017.
- 15. Cruz-Roa, A., Basavanhally, A., González, F., Gilmore, H., Feldman, M., Ganesan, S., Shih, N., Tomaszewski, J., Madabhushi, A., "Automatic detection of invasive ductal carcinoma in whole slide images with convolutional neural networks", Medical Imaging 2014", Digital Pathology, Pages 9041, 2014.



ULUSLARARASI 3B YAZICI TEKNOLOJİLERİ VE DİJİTAL ENDÜSTRİ DERGİSİ

INTERNATIONAL JOURNAL OF 3D PRINTING TECHNOLOGIES AND DIGITAL INDUSTRY

ISSN:2602-3350 (Online)

URL: https://dergipark.org.tr/ij3dptdi

DETECTION OF ARTIFICIAL DISCONTINUITIES LOCATED IN DIFFERENT LOCATIONS IN PLA SPECIMENS MANUFACTURED WITH MEX AT DIFFERENT LAYER THICKNESSES BY ULTRASONIC INSPECTION

Yazarlar (Authors): Alperen Doğru +

Bu makaleye şu şekilde atıfta bulunabilirsiniz (To cite to this article): Doğru A., "Detection of Artificial Discontinuities Located in Different Locations in PLA Specimens Manufactured with MEX at Different Layer Thicknesses by Ultrasonic Inspection" Int. J. of 3D Printing Tech. Dig. Ind., 9(2): 344-351, (2025).

DOI: 10.46519/ij3dptdi.1737913

Araştırma Makale/ Research Article

Erişim Linki: (To link to this article): https://dergipark.org.tr/en/pub/ij3dptdi/archive

DETECTION OF ARTIFICIAL DISCONTINUITIES LOCATED IN DIFFERENT LOCATIONS IN PLA SPECIMENS MANUFACTURED WITH MEX AT DIFFERENT LAYER THICKNESSES BY ULTRASONIC INSPECTION

Alperen Doğru^a

^a Ege University, Aviation HVS, Aircraft Technology, TURKEY

* Corresponding Author: <u>alperen.dogru@ege.edu.tr</u>

(Received: 08.07.25; Revised: 06.08.25; Accepted: 15.08.25)

ABSTRACT

PLA (polylactic acid) is the most commonly used polymer in material extrusion-based additive manufacturing (MEX), which is one of the most innovative methods in the production of polymers. Its biodegradability, availability, and low cost drive its widespread use. Due to the nature of additive manufacturing, some discontinuities tend to occur in the production of polymer materials. Discontinuities such as junction problems between layers, voids, and solidification of extruded polymers occur between the production of layers. Non-destructive testing methods can be used to detect these discontinuities. Ultrasonic testing, a volumetric Non-destructive testing method, is well-suited to detect such discontinuities. This study evaluates how layer thickness influences ultrasonic detection of discontinuities in MEX-produced PLA specimens. 0.1 mm, 0.2 mm, and 0.4 mm layer thicknesses of PLA specimens, each of which has artificial discontinuities (holes) placed at different depths and locations, were analyzed by the ultrasonic inspection technique. In the experimental studies, sound waves were sent to the specimens, and the reflected echoes were evaluated. Results show that layer thickness alters echo amplitude and the positional accuracy of detected discontinuities. In specimens with a layer thickness of 0.1 mm, the detection of discontinuities was clearer, while in specimens with a layer thickness of 0.4 mm, the sound echoes were more scattered, negatively affecting the measurement accuracy. These findings clarify how manufacturing parameters shape Non-destructive testing effectiveness in additive manufacturing and hold practical implications for industry.

Keywords: PLA, Non-Destructive Testing, Additive Manufacturing, Polymers

1. INTRODUCTION

Additive manufacturing (AM) technologies enable fast, cost-effective production of geometries [1]. Today, complex technologies, which are at the forefront of industrial production processes with their advantages such as design flexibility, costeffectiveness, and rapid prototyping, are creating a significant transformation in the manufacturing world [2-3]. One such method, extrusion-based material additive manufacturing (MEX), enables the creation of three-dimensional structures polymer-based materials [4-5].

Polylactic acid (PLA), one of the most commonly used polymers in production with

MEX, is preferred due to its biodegradable structure, renewable source, low melting temperature, and good dimensional stability. These properties make **PLA** both environmentally friendly and suitable for processing. In the production process with MEX, production parameters directly affect the mechanical properties of the parts. The parts produced with MEX exhibit anisotropic properties and lower mechanical properties along the Z-axis. Layer thickness, one of the production parameters, is a critical parameter that directly affects the surface quality, mechanical properties, and internal structural homogeneity of the part. Numerous studies in the literature have examined the impact of these parameters on material performance [6–10]. On the other hand, in the MEX method, discontinuities such as voids, separations, and extrusion layering, which may occur in the internal structure depending on the production process, can negatively affect the reliability of the part [4-5]. Detecting these discontinuities and investigating the effects of production parameters on discontinuity detection are open topics for research [11-18]. Production parameters primarily affect manufacturability production and MEX can cause discontinuities[19]. Nozzle temperature, printing speed, extrusion speed, and layer thickness affect part quality [20-21]. In their study, Zanjanijam et al. stated that the production quality of PEEK specimens produced with MEX varied depending on nozzle temperature, printing speed, and layer thickness[22]. Triyono et al, examined how porosity nozzle diameter affects MEX-printed PLA [23]. Sandhu et al investigated the effect of printing parameters on the dimensional stability of PLA specimens in MEX production and determined the process parameters that cause shrinkage [24]. Allum et al. have stated that low extrusion negatively affects the mechanical properties in production with MEX and causes void formation [25]. Gardner et al. have stated that internal stresses generated during interlayer adhesion during production in acrylonitrile butadiene styrene (ABS) specimens cause delamination [26]. Studies have shown that many different can occur discontinuities depending on production parameters and the polymer preferred for production. Detecting these discontinuities is critical for the reliability of products manufactured with MEX and enables the expansion of the application area. The detectability of defects is also one of the issues that needs to be investigated.

Non-destructive testing (NDT) methods are used as effective tools for detecting discontinuities without compromising the structural integrity of materials [18,27]. Among the volumetric inspection methods included in NDT, ultrasonic testing stands out due to its high resolution and ability to detect discontinuities within materials [28].

Fayanzbakhsh et al. detected interlayer voids in PLA specimens produced with MEX using high-frequency phased array ultrasonic testing and investigated their effect on mechanical properties [29]. Butt et al investigated the effect of production parameters on the mechanical properties of graphene-reinforced PLA specimens using ultrasonic sound transmission [30]. To our knowledge, no prior work quantifies how printing parameters or defect location affect ultrasonic detectability in MEX parts.

The layered structure of parts produced using MEX can affect the propagation and reflection of sound waves, thereby limiting detection performance. The effect of layer thicknesses on the propagation of sound waves and the detection of discontinuities is a topic that requires further investigation. In this study, the focus is on detecting artificial discontinuities placed in PLA specimens produced with different layer thicknesses using the MEX method through ultrasonic testing.

2. MATERIALS AND METHODS

2.1. Materials

Ultrafuse Natural PLA filament (BASF) was used. The filament density was 1248 kg/m³, the melting temperature (T_m) was 151 °C (ISO 11357-3) and the glass transition temperature (T_g) value was 61 °C (ISO 11357-2) [31]. The mechanical properties of the specimens produced in the flat (XY) plane, as specified by the manufacturer of the PLA filament, are presented in Table 1.

Table 1. PLA Filament Mechanical Properties[31]

Properties	Value	Standard
Tensile Strength (MPa)	34.7	ISO 527
Elongation at Break (%)	4.2	ISO 527
Young Modulus (MPa)	2308	ISO 527
Flexural Strength (MPa)	98	ISO 178
Flexural Modulus (MPa)	1860	ISO 178
Flexural Strain at Break	4.8	ISO 178
(%)		
Impact Strength Charpy -	2.5	ISO 179-2
notched (kJ/m²)		

2.2. Production and Design

Hole-containing specimens were printed to assess NDT detection performance in PLA specimens produced with MEX. In this context, $15 \times 20 \times 80$ mm rectangular prisms with 5-mm-diameter holes were produced in three different layer thicknesses, as shown in Figure 1. Figure 2 shows the discontinuity-free region and 5-mm holes in three positions. A 5-mm-diameter was determined to accurately detect discontinuities with the ultrasonic sensor used.

Holes of 3 different depths were created to detect discontinuities at different depths. Three different positionings were made to examine the effect of depth on discontinuity detection. Specimens were modelled in the Autodesk Fusion 360 computer-aided design program (CAD). The CURA computer-aided manufacturing (CAM) software was used for the production parameters.

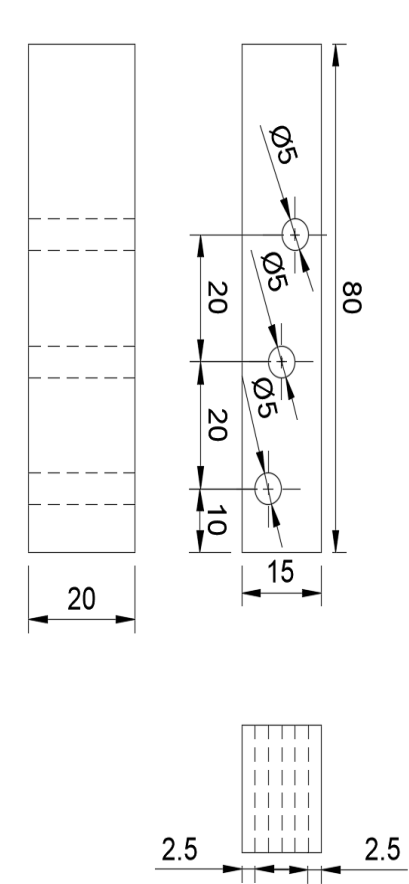


Figure 1. Drawings of PLA Specimens produced with MEX

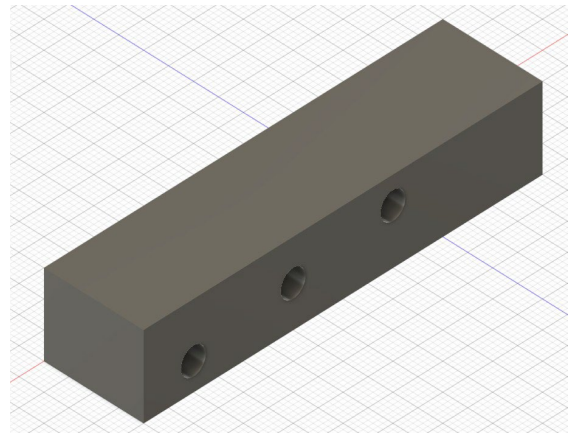


Figure 2. 3D Image of Specimens

The specimens were produced using an Ultimaker Model 3 MEX device with a 0.4 mm diameter Ultimaker Printcore AA nozzle. The fixed parameters used for production are given in Table 2. All specimens were printed with fixed settings except for layer thickness (0.1, 0.2, 0.4 mm).

Table 2. Fixed MEX Production Parameters

Parameters	Value
Nozzle Temperature (°C)	210
Bed Temperature(°C)	60
Bed Material	Glass
Print Speed (mm/s)	60
Infill Degree (°)	0
Infill Percent (%)	100

Each layer was produced parallel to the long side of the specimens in the direction shown in Figure 3 (a) (infill degree). Images of rectangular prisms produced in different layer thicknesses and with a 5-mm-diameter hole are shown in Figure 3 (b). The 5-mm-diameter hole is positioned to represent an artificial discontinuity—the specimens were produced in three different layer thicknesses.

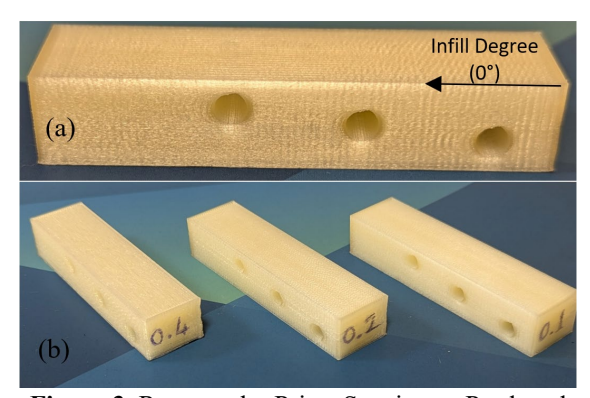


Figure 3. Rectangular Prism Specimens Produced

2.3. Testing

Ultrasonic testing, an NDT technique, was used to determine discontinuities and examine the effect of layer thickness on discontinuity detection.

The detection performance of discontinuities in rectangular prism pieces with 5-mm-diameter artificial holes produced at different layer thicknesses and located in different areas was carried out using ultrasonic testing. The Tru-test brand Digital Ultrasonic Flaw Detector device was used for ultrasonic testing. Because polymers have low acoustic impedance, a low-frequency probe was selected. Therefore,

the BD-412 model from Tru-Sonics with a 4 MHz frequency and 12 mm crystal size ceramic-coated vertical probe was used in the tests. Figure 4 illustrates the device and probe.



Figure 4. Ultrasonic testing device and probe used

3. RESULTS AND DISCUSSION

PLA specimens designed in the shape of a rectangular prism measuring $15 \times 20 \times 80$ mm and containing three circular holes with a diameter of 5 mm placed in different positions to represent artificial discontinuities were produced using additive manufacturing with three different layer thicknesses of 0.1 mm, 0.2

mm and 0.4 mm and tested using an ultrasonic inspection method. In addition to the three holes in different positions, one near the bottom surface, one at mid-height, and one near the top surface, each specimen with a different layer thickness also included an area without any internal discontinuities as a reference for ultrasonic inspection.

Figure 5 presents ultrasonic signals from specimens printed at three-layer thicknesses, each with three 5-mm holes. The horizontal axis shows the depth (mm) at which the reflected sound echo signals were received. The vertical axis shows the intensity of the sound signal. The rightmost graphs correspond to the discontinuity-free region. The images of the signals obtained from the holes near the surface, middle, and bottom regions are shared from left to right. The tests were performed at 11 dB, with an 8 mm delayed signal, and signals below 29% filtered out.

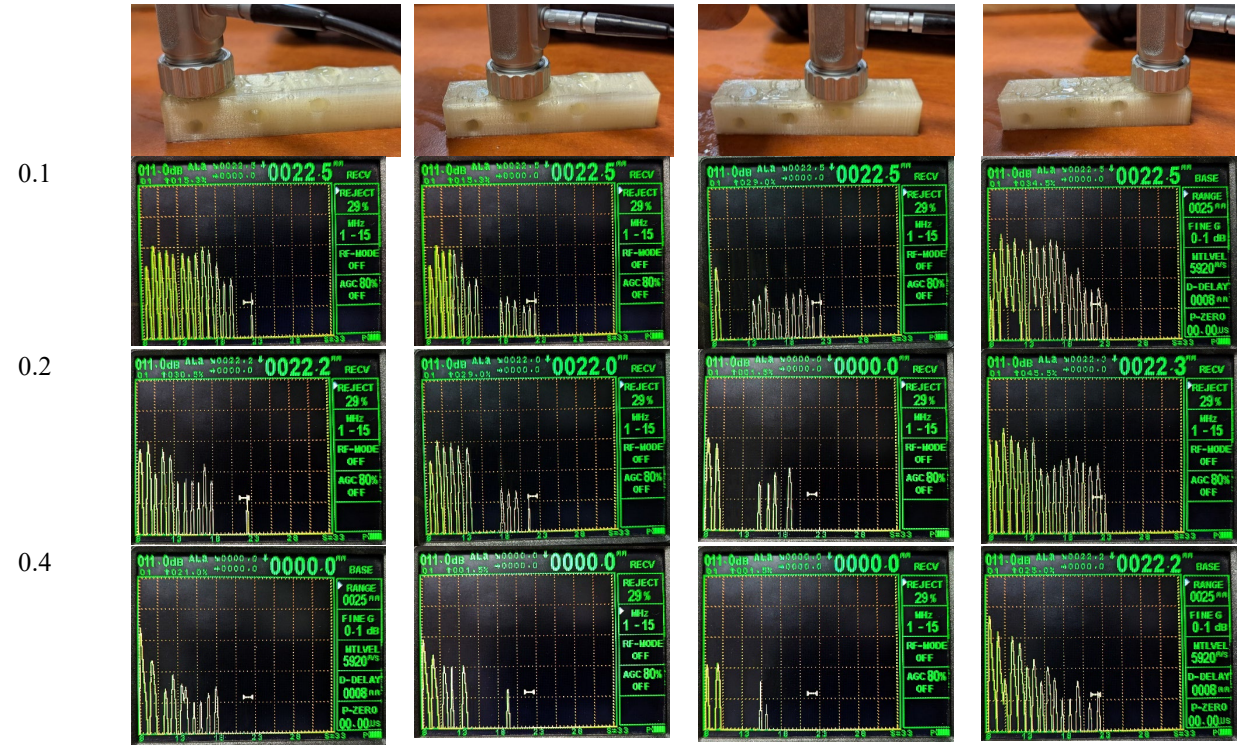


Figure 5. Ultrasonic test graphs of discontinuous and discontinuity-free regions of specimens

Signals from discontinuity-free regions showed the highest echo amplitudes in 0.1 mm layers. In addition to high resolution, the echo signals were clearly distinguished. Signals from the regions between each layer were detected at a specific frequency. The homogeneous internal structure of the material provided good communication, and minimal signal attenuation was observed. Compared to specimens with a layer thickness of 0.1 mm, a decrease in signal amplitude was observed in specimens with a layer thickness of 0.2 mm. Although the first signals were strong, the clarity of the successive echoes decreased slightly. The interlayer

bonding surfaces have scattered the signal to some extent. In specimens with a layer thickness of 0.4 mm, the echo height has decreased significantly, and the signal attenuation is more pronounced. The echo signals are more widespread and scattered. Bonding interfaces in thicker layers significantly disrupt wave propagation. This likely reflects increased refraction at thicker layer interfaces, which redirects and attenuates waves.

Echoes from sound regions were highly sensitive layer thickness; acoustic to heterogeneity increased as thickness rose. It has been observed that scattering and attenuation in sound wave propagation increase significantly with an increase in layer thickness. Echo intensity and clarity decreased with increasing layer thickness. The sound waves did not deviate much when passing through thick layers within the material, so the sound echoes were dispersed. Despite the presence of more bonding surfaces and environmental changes in low-layer thicknesses, it has been observed that sound is transmitted smoothly between layers in these regions. This situation can be explained by the fact that the dimensional tolerances of production are better at low layer thicknesses.

In the specimen with a layer thickness of 0.1 mm, the signal amplitudes obtained from all hole positions were high, and the echoes were intense. The sound waves echoed clearly, with minimal signal loss. In specimens with a layer thickness of 0.2 mm, the signal amplitude was observed to decrease and the echoes were observed to be less frequent. In addition, when the dimensions of the measured artificial discontinuity were compared, the dimensional results were more accurate in specimens with a layer thickness of 0.2 mm. In comparison, the dimensions of artificial discontinuity were lower in specimens with a layer thickness of 0.1 mm. For bottom-surface defects, the signal drop began at 19.5 mm for 0.1-mm layers. Considering an 8 mm signal delay, this corresponds to a depth of approximately 11.5 mm. In specimens with 0.2 mm and 0.4 mm layer thickness, the signal discontinuity for the region near the bottom surface starts at 18 mm. Again, considering the 8 mm signal delay, this indicates that the discontinuity begins at a depth of 10 mm. Accordingly, spatial accuracy was higher for 0.2 and 0.4 mm layers. This may stem

from the greater number of interfaces in thinner layers. The large number of echoes created by the increased number of layer interface surfaces resulted in a smaller discontinuity image. As the layer thickness increased, the echo gap associated with the artificial discontinuity widened. The closest measurements were observed at a layer thickness of 0.2 mm, while a smaller discontinuity size was observed in specimens with a layer thickness of 0.1 mm. In specimens with a layer thickness of 0.4 mm, the echoes obtained after the discontinuity were measured from deeper regions, and therefore a larger discontinuity size was observed in specimens with a layer thickness of 0.4 mm.

When the ultrasonic sound signals obtained from the artificial discontinuity located near the upper surface were examined, the error location was detected in all specimens. In the specimen with a layer thickness of 0.1 mm, the sound echoes could continue to the back surface within the material, but in the specimens with layer thicknesses of 0.2 and 0.4 mm, only a small amount of echo was received from the region after the artificial discontinuity. The effect created by the artificial discontinuity on the upper surface prevented the sound waves from reaching the lower layers. Therefore, the proximity of the discontinuity to the upper surface prevented the sound waves from advancing to the lower region. This effect became more pronounced with the increase in layer thickness and made it more difficult to detect the echoes. The discontinuity in the middle region was observed in all three specimens with different layer thicknesses, but in the specimen with a 0.4 mm layer thickness, sound waves could not reach the lower surface of the specimen. This situation was observed in all artificial discontinuities in the specimen with a 0.4 mm layer thickness.

Overall, ultrasonic transmission degraded as layer thickness increased. While signals were received in specimens with a layer thickness of 0.1 mm, almost no echo was measured in specimens with a layer thickness of 0.4 mm in areas containing discontinuities. These results highlight how internal architecture governs detectability: thicker layers absorbed more energy, masking echoes.

According to the experimental results of the study, an increase in layer thickness directly

affects the detectability of discontinuities by ultrasonic examination. In specimens with a layer thickness of 0.1 mm, the location of discontinuities could be determined more clearly thanks to the sound transmission advantage provided by the smoother and more homogeneous structure. The discontinuity size was measured more clearly in specimens with a layer thickness of 0.2 mm. However, this situation is affected by the location of the discontinuity. In contrast, in specimens with a layer thickness of 0.4 mm, the scattering and reflection of sound waves increased, making it difficult to interpret the echoes.

4. CONCLUSIONS

In this study, the capability and sensitivity of ultrasonic testing techniques in detecting artificial internal discontinuities at various depths in PLA components produced with MEX were evaluated. Comparing signals from defect-free and defective regions allowed us to isolate the effects of depth and layer thickness on detection. A comparative evaluation of ultrasonic signals corresponding to different discontinuity locations and printing parameters is presented. Signal characteristics—amplitude, intensity, and attenuation—were analysed to assess detectability and resolution. The effect of production parameters, particularly layer thickness, on signal clarity and discontinuity visibility is also discussed in detail.

Ultrasonic detectability decreased markedly with increasing layer thickness. It was observed that discontinuities were more clearly detected in specimens with a layer thickness of 0.1 mm, where holes in the middle position could be detected more reliably than others, but discontinuity dimensions were more clearly measured in specimens with a layer thickness of 0.2 mm. In addition, it has been found that discontinuities located near the bottom surface are more difficult to detect due to the signals travelling longer distances, which leads to increased attenuation.

This work systematically demonstrates layer-thickness effects on ultrasonic inspection performance in MEX-printed PLA. The findings indicate that lower layer thicknesses provide an advantage in terms of more successful detection of discontinuities. Future work should examine other printing parameters and materials to generalise these findings.

REFERENCES

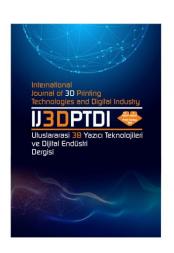
- 1. Thomas, D.S.; Gilbert, S.W., "Costs and Cost Effectiveness of Additive Manufacturing A Literature Review and Discussion.", 10-89, NIST Special Publication, Washington, 2014.
- 2. Khan, L.S.; Yousaf, G.A.; Hussain, I. "3D Printing Techniques: Transforming Manufacturing with Precision and Sustainability." International Journal of Multidisciplinary Sciences and Arts, Vol.3, Issue 3, 2024.
- 3. Zhou, L.; Miller, J.; Vezza, J.; Mayster, M.; Raffay, M.; Justice, Q.; Al Tamimi, Z.; Hansotte, G.; Sunkara, L.D.; Bernat, J. "Additive Manufacturing: A Comprehensive Review." Sensors, Vol.24, Issue 9, Page 2668-2024, 2024.
- 4. Khan, I.; Barsoum, I.; Abas, M.; Al Rashid, A.; Koç, M.; Tariq, M. "A Review of Extrusion-Based Additive Manufacturing of Multi-Materials-Based Polymeric Laminated Structures." Composite Structures, Vol.349-350, Issue 118490, 2024.
- 5. Jasik, K.; Lucjan', L.; Zek, L.; Kluczy'nski, J.; Kluczy'nski, K. "Additive Manufacturing of Metals Using the MEX Method: Process Characteristics and Performance Properties—A Review." Materials, Vol. 18, Issue 12, Page 2744, 2025.
- 6. Bacak, S.; Özkavak, H.V.; Tatlı, M. "FDM Yöntemi ile Üretilen PLA Numunelerin Çekme Özelliklerine İşlem Parametrelerinin Etkisinin İncelenmesi" Mühendislik Bilimleri ve Tasarım Dergisi, Vol.9, Issue 1, Page 209–216, 2021.
- 7. Bacak, S.; Özkavak, H.V.; Sofu, M.M. "Comparison of Mechanical Properties of 3D-Printed Specimens Manufactured Via FDM with Various Inner Geometries" Journal of the Institute of Science and Technology, Vol.11, Issue 2, Pages 1444–1454, 2021.
- 8. Camargo, J.C.; Machado, Á.R.; Almeida, E.C.; Silva, E.F.M.S. "Mechanical Properties of PLA-Graphene Filament for FDM 3D Printing" International Journal of Advanced Manufacturing Technology, Vol.103, Pages 2423–2443, 2019.
- 9. García Plaza, E.; Núñez López, P.J.; Caminero Torija, M.Á.; Chacón Muñoz, J.M. "Analysis of PLA Geometric Properties Processed by FFF Additive Manufacturing: Effects of Process Parameters and Plate-Extruder Precision Motion" Polymers, Vol.11, Issue 10, Pages 1581, 2019.

- 10. Erdaş, M.U.; Yıldız, B.S.; Yıldız, A.R. "Experimental Analysis of the Effects of Different Production Directions on the Mechanical Characteristics of ABS, PLA, and PETG Materials Produced by FDM" Materials Testing, Vol.66, Issue 2, Pages 198–206, 2024.
- 11. Kechagias, J.; Chaidas, D.; Vidakis, N.; Salonitis, K.; Vaxevanidis, N.M. "Key Parameters Controlling Surface Quality and Dimensional Accuracy: A Critical Review of FFF Process." Materials and Manufacturing Processes, Vol.37, Issue 9, Pages 963–984, 2022.
- 12. Gonabadi, H.; Yadav, A.; Bull, S.J. "The Effect of Processing Parameters on the Mechanical Characteristics of PLA Produced by a 3D FFF Printer." International Journal of Advanced Manufacturing Technology, Vol.111, Pages 695–709, 2020.
- 13. Ameri, B.; Taheri-Behrooz, F.; Aliha, M.R.M. "Evaluation of the Geometrical Discontinuity Effect on Mixed-Mode I/II Fracture Load of FDM 3D-Printed Parts." Theoretical and Applied Fracture Mechanics, Vol.113, Issue 102953, 2021.
- 14. Doğru, A.; Sözen, A.; Neşer, G.; Seydibeyoğlu, M.Ö. "Numerical and Experimental Investigation of The Effect of Delamination Defect at Materials Of Polyethylene Terephthalate (PET) Produced By Additive Manufacturing on Flexural Resistance." International Journal of 3D Printing Technologies and Digital Industry, Vol.6, Issue 3, Pages 382–391, 2022.
- 15. Havva, Y.; Özdemir, N.; Sözen, A.; Demir, M.; Doğru, A.; Seki, Y.; Özdemir, H.N. "Production of Waste Jute Doped PLA (Polylactic Acid) Filament for FFF: Effect of Pulverization." International Journal of 3D Printing Technologies and Digital Industry, Vol.7, Issue 1, Pages 124–128, 2023.
- 16. Doğru, A.; İrez A.B., "The microstructural evolution of material extrusion based additive manufacturing of polyetheretherketone under different printing conditions and application in a spinal implant." Polymer Engineering & Science, Vol.64, Issue 11, Pages 5486–5502, 2024.
- 17. Doğru, A.; Kaçak, M.; Seydibeyoğlu, M.Ö. "Examination of Mechanical Properties of Fasteners Produced with PET and PLA Materials in Extrusion-Based Additive Manufacturing Method." International Journal of 3D Printing Technologies and Digital Industry, Vol.8, Issue 3, Pages 407–415, 2024.

- 18. Baechle-Clayton, M.; Loos, E.; Taheri, M.; Taheri, H. "Failures and Flaws in Fused Deposition Modeling (FDM) Additively Manufactured Polymers and Composites." Journal of Composites Science, Vol.6, Issue 7, Pages 202, 2022.
- 19. Alo, O.A.; Mauchline, D.; Otunniyi, I.O. "3D-Printed Functional Polymers and Nanocomposites: Defects Characterization and Product Quality Improvement." Advanced Engineering Materials, Vol.24, Issue 10, 2022.
- 20. Attalla, R.; Ling, C.; Selvaganapathy, P. "Fabrication and Characterization of Gels with Integrated Channels Using 3D Printing with Microfluidic Nozzle for Tissue Engineering Applications." Biomed Microdevices, Vol.18, Issue 1, Pages 1–12, 2016.
- 21. Pérez, B.; Nykvist, H.; Brøgger, A.F.; Larsen, M.B.; Falkeborg, M.F. "Impact of Macronutrients Printability and 3D-Printer Parameters on 3D-Food Printing: A Review." Food Chemistry, Vol.287, Pages 249–257, 2019.
- 22. Zanjanijam, A.R.; Major, I.; Lyons, J.G.; Lafont, U.; Devine, D.M. "Fused Filament Fabrication of PEEK: A Review of Process-Structure-Property Relationships." Polymers, Vol.12, Issue 8, Pages 1665, 2020.
- 23. Triyono, J.; Sukanto, H.; Saputra, R.M.; Smaradhana, D.F. "The Effect of Nozzle Hole Diameter of 3D Printing on Porosity and Tensile Strength Parts Using Polylactic Acid Material." Open Engineering, Vol.10, Issue 1, Pages 762–768, 2020.
- 24. Sandhu, K.; Singh, S.; Prakash, C. "Analysis of Angular Shrinkage of Fused Filament Fabricated Poly-Lactic-Acid Prints and Its Relationship with Other Process Parameters." IOP Conference Series: Materials Science and Engineering, Vol.561, Issue 012058, 2019.
- 25. Allum, J.; Moetazedian, A.; Gleadall, A.; Mitchell, N.; Marinopoulos, T.; McAdam, I.; Li, S.; Silberschmidt, V. V. "Extra-Wide Deposition in Extrusion Additive Manufacturing: A New Convention for Improved Interlayer Mechanical Performance." Additive Manufacturing, Vol.61, Issue 5, 2023.
- 26. Gardner, J.M.; Hunt, K.A.; Ebel, A.B.; Rose, E.S.; Zylich, S.C.; Jensen, B.D.; Wise, K.E.; Siochi, E.J.; Sauti, G. "Machines as Craftsmen: Localized Parameter Setting Optimization for Fused Filament Fabrication 3D Printing." Advanced Materials Technologies, Vol.4, Issue 3, 2019.

- 27. Inês Silva, M.; Malitckii, E.; Santos, T.G.; Vilaça, P. "Review of Conventional and Advanced Non-Destructive Testing Techniques for Detection and Characterization of Small-Scale Defects." Progress in Materials Science, Vol.138, Issue 101155, 2023.
- 28. Gupta, M.; Khan, M.A.; Butola, R.; Singari, R.M. "Advances in Applications of Non-Destructive Testing (NDT): A Review." Advances in Materials and Processing Technologies, Vol.8, Isssue 4, Pages 2286–2307, 2022.
- 29. Fayazbakhsh, K.; Honarvar, F.; Amini, H.; Varvani-Farahani, A. "High Frequency Phased Array Ultrasonic Testing of Thermoplastic Tensile Specimens Manufactured by Fused Filament Fabrication with Embedded Defects." Additive Manufacturing, Vol.47, 2021.

- 30. Butt, J.; Bhaskar, R.; Mohaghegh, V. "Non-Destructive and Destructive Testing to Analyse the Effects of Processing Parameters on the Tensile and Flexural Properties of FFF-Printed Graphene-Enhanced PLA." Journal of Composites Science, Vol.6, Issue 5, Page 148, 2022.
- 31. BASF 3D Printing Solutions BV Sales@basf-3dps.Com Www.Basf-3dps.Com General Information.



ULUSLARARASI 3B YAZICI TEKNOLOJİLERİ VE DİJİTAL ENDÜSTRİ DERGİSİ

INTERNATIONAL JOURNAL OF 3D PRINTING TECHNOLOGIES AND DIGITAL INDUSTRY

ISSN:2602-3350 (Online)

URL: https://dergipark.org.tr/ij3dptdi

PREDICTION PERFORMANCE OF DECISION TREE INDUCERS ON AUGMENTED BACILLUS CEREUS GROWTH DATA

Yazarlar (Authors): Hamit Armağan •

Bu makaleye şu şekilde atıfta bulunabilirsiniz (To cite to this article): Armağan H., "Prediction Performance of Decision Tree Inducers on Augmented Bacillus Cereus Growth Data" Int. J. of 3D Printing Tech. Dig. Ind., 9(2): 352-362, (2025).

DOI: 10.46519/ij3dptdi.1726410

Araştırma Makale/ Research Article

PREDICTION PERFORMANCE OF DECISION TREE INDUCERS ON AUGMENTED BACILLUS CEREUS GROWTH DATA

Hamit Armağan^a

^aInformatics Department, Suleyman Demirel University, Türkiye

* Corresponding Author: hamitarmagan@sdu.edu.tr

(Received: 25.06.25; Revised: 09.08.25; Accepted: 15.08.25)

ABSTRACT

Accurate prediction of microbial growth is of great importance in critical areas such as food safety and environmental sciences. In this study, a hybrid of mathematical methods and machine learning-based approaches are used to model the growth dynamics of foodborne pathogen *Bacillus cereus*. Since the use of mathematical models alone does not sufficiently cover the non-linear data structure of bacterial systems, better results are obtained when hybrids are used together with machine learning methods. We examine the results of five different tree-based models for predicting the growth of Bacillus cereus, namely Fine Tree, Medium Tree, Coarse Tree, Ensemble Boosted Trees and Ensemble Bagged Trees. We evaluate each model with performance metrics such as Root Mean Square Error (RMSE), Mean Square Error (MSE), R² and Mean Absolute Error (MAE). The results show that the Ensemble Bagged Trees model performs the best, with a validation RMSE of 0.0094 and an R² value of 0.9995. Also, the Fine Tree model has an R² value of 0.9990. In general, ensemble methods offer significant advantages in prediction accuracy.

Keywords: Data Augmentation, Machine Learning, Microbial Growth Prediction, Tree-Based Models

1. INTRODUCTION

Accurate prediction of microbial growth is crucial across disciplines such as food safety, agriculture, and environmental sciences. Bacillus cereus, a significant foodborne pathogen, poses serious health risks due to its ability to produce enterotoxins that cause gastrointestinal illness [1-2]. Understanding its growth under various environmental conditions is essential for effective risk mitigation. Key aspects include:

- o Food safety relevance: Accurate modeling of B. cereus growth is critical to prevent foodborne outbreaks and ensure consumer protection [3-4].
- o Agricultural impact: Microbial dynamics influence crop health and soil quality, affecting agricultural productivity [5-6].
- Environmental significance: Modeling microbial behavior contributes to understanding ecological interactions and managing microbial risks [7-8].

Recent studies emphasize the integration of modeling techniques to address the multifactorial and complex nature of microbial growth [9-10]. Historically, microbial growth has been described using mathematical models, which are typically based on simplified assumptions regarding environmental conditions [11]. However, these models present several limitations [12-13]:

- Limited complexity: Classical models often fail to capture the nonlinear and dynamic interactions inherent in biological systems [14-15].
- o Low adaptability: Their static structures hinder generalization across diverse environmental conditions or food matrices [16].
- O Decreased accuracy: These models struggle to accurately reflect the effects of rapid or synergistic changes on microbial behavior [17].
- O Data limitations: Traditional models are generally trained on limited and homogeneous datasets, which impedes their

ability to represent extensive and variable realworld data [18].

- O Complex influence of environmental factors: Factors such as temperature, pH, and humidity interact in variable and combined ways that classical models do not fully represent [1,19].
- O Challenges in parameter estimation: Determining model parameters is often difficult, and inaccurate estimations adversely affect model performance [14].
- O Insufficient model flexibility: The ability of the model to rapidly adapt to environmental or experimental changes is limited [15].
- O Neglect of biological diversity: Variations in growth characteristics among different strains or species are inadequately accounted for in classical models [3,14].

These limitations impede accurate and reliable predictions of microbial growth, thereby complicating risk management and decision-support processes.

The aim of this study is to enhance the accuracy of predicting Bacillus cereus microbial growth dynamics and to improve the generalizability of modeling approaches. To achieve this, an integrative framework combining mathematical modeling with machine learning techniques has been developed to more effectively capture the complex, nonlinear, and dynamic interactions inherent in biological systems. In particular, decision tree-based and ensemble methods have been employed to increase model robustness and predictive reliability across diverse datasets and environmental conditions. Additionally, polynomial regression techniques have been utilized to model higher-order functional while data relationships, augmentation strategies have expanded the diversity and size of the training dataset. Through this integrative approach, the study seeks to provide more accurate and reliable predictions of Bacillus cereus growth under various real-world scenarios, thereby contributing development of effective decision-support tools in food safety, agricultural productivity, and environmental risk management.

2. MATERIAL and METHOD

2.1. Bacterial Strain and Culture Conditions In this study, Bacillus cereus was employed as the model bacterial strain. The initial cultivation and preparation steps were conducted under controlled and sterile conditions to ensure experimental reliability:

- O Bacillus cereus colonies were grown on petri dishes containing Nutrient Agar and incubated at 37 °C for 24 hours to allow colony formation. Two to three distinct colonies were then selected and transferred to sterile tubes containing Nutrient Broth.
- O The selected colonies were vortexed vigorously to produce a homogeneous suspension, which was subsequently incubated overnight at 37 °C with shaking at 130 rpm to promote optimal growth and obtain sufficient cell density.
- O After incubation, the optical density at 660 nm (OD₆₆₀) was measured using a UV spectrophotometer to assess the bacterial growth level and confirm suitability for further experimentation.
- O Two milliliters of the overnight culture were inoculated into 50 mL of fresh Nutrient Broth in sterile 250 mL Erlenmeyer flasks and incubated at 37 °C with shaking at 130 rpm. All procedures were performed aseptically to prevent contamination.
- O Inoculations were conducted in triplicate to ensure data reproducibility. The initial OD₆₆₀ was recorded, followed by hourly measurements to monitor the growth kinetics of Bacillus cereus, as OD₆₆₀ is a standard indicator for bacterial cell density while minimizing interference from the culture medium [17].

2.2. Data Augmentation with Polynomial Regression Model

In study the growth rate of Bacillus cereus is a fourth-order polynomial regression model was developed to characterize the growth dynamics of *Bacillus cereus* based on systematically collected experimental data:

Table 1. Summary of Bacillus cereus Growth Data, Augmentation Method, and Model Performance Metrics (Statistical metrics between measured data and augmented data)

	(Statistical metrics between measured data and augmented data)
Description	Details
Initial Dataset	9 data points including time, temperature, and bacterial count, collected under controlled
IIIIIai Daiasei	laboratory conditions to construct the initial growth model.
Method	Data augmentation was performed using a Polynomial Regression Model to expand the
Method	dataset and enhance model robustness.
E 1.1D.44	Dataset increased to 401 data points to improve model precision and generalizability,
Expanded Dataset	capturing environmental influences on bacterial growth more comprehensively.
	- Sum of Squared Errors (SSE): 0.0082
Model	- Root Mean Square Error (RMSE): 0.0452
Performance	- Coefficient of Determination (R ²): 0.9951
Metrics	- Adjusted R ² : 0.9901
	- Degrees of Freedom for Error (DFE): 4

time Bacillus cereus Bacillus cereus time Metrics (observed) (observed) (augmented) (augmented) 0 0.054 0.038 min 0 8 8 1.187 1.201 max 4 4 0.741 0.754 mean 2.738 2.318 0.455 0.403 std dev 9 401 9 count 401

The dataset metrics indicate that the observed time values range from a minimum of 0 to a maximum of 8, with a mean of 4 and a standard deviation of 2.738, based on 9 data points. After augmentation, the time values retain the same minimum and maximum (0 and 8, respectively) and mean of 4, while the standard deviation slightly decreases to 2.318 across 401 data points. For Bacillus bacterial counts, the observed values span from 0.054 to 1.187 with a mean of 0.741 and a standard deviation of 0.455 based on 9 observations. The augmented Bacillus counts range from 0.038 to 1.201, with a mean of 0.754 and a standard deviation of 0.403 over 401 data points.

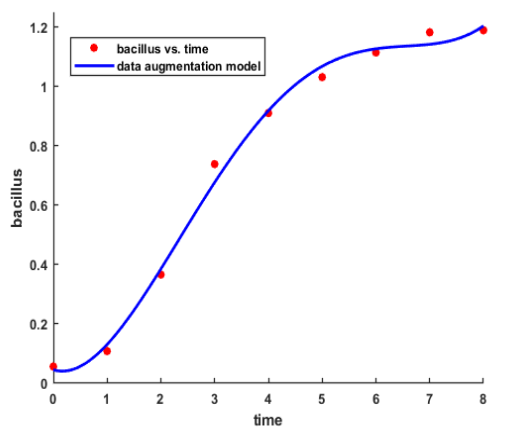


Figure 1. Measured data and augmented data

Figure 1 illustrates the original measured values of *Bacillus cereus* growth alongside the synthetically generated data obtained through

data augmentation techniques. The augmented data extends the range and density of the dataset, enhancing the model's ability to generalize and improving prediction performance across varying conditions.

2.3. Tree-Based Machine Learning Models

The dataset consisted of 401 observations in total. Of these, 341 samples (~85%) were used for model training and validation via 5-fold cross-validation, while 60 samples (~15%) were reserved for independent testing. We use five different machine learning models to model the growth dynamics of Bacillus cereus: Fine Tree, Medium Tree, Coarse Tree, Ensemble Boosted Trees and Ensemble Bagged Trees. We choose each model for its distinct algorithmic advantages in capturing non-linear relationships and patterns in the dataset as follows in Figure 2:

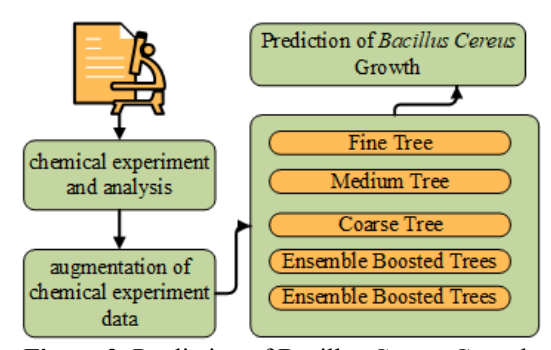


Figure 2. Prediction of Bacillus Cereus Growth with Machine Learning Based Models

Table 2 presents a comparative overview of five tree-based machine learning models used to

predict the growth dynamics of Bacillus cereus, highlighting their structural complexity, key characteristics, overfitting risks, and optimal use cases. Each model offers distinct advantages in capturing non-linear patterns within the dataset, depending on its algorithmic design. While simpler models such as the Coarse Tree generalize well on linearly separable and lowdimensional data, more complex models like the Fine Tree and ensemble methods provide improved accuracy on intricate, non-linear datasets. Ensemble Boosted Trees and Ensemble Bagged Trees, in particular, demonstrate enhanced predictive performance by reducing bias and variance, respectively. Therefore, selecting the appropriate model requires careful consideration of both the data characteristics and the desired balance between model complexity and generalization capability.

The hyperparameters of the decision tree—based regression models employed in this study played a decisive role in determining model complexity, generalization capacity, and predictive accuracy. The Fine Tree model was configured with high complexity, using the Mean Squared Error (MSE) as the split criterion, a minimum parent node size (MinParent) of 10, a minimum leaf size (MinLeaf) of 4, and a maximum number of splits

(MaxSplits) of 340. All predictor variables were considered for splitting (NVarToSample = all), and pruning was enabled with the MSE as the pruning criterion. The Medium Tree model was designed with MinParent set to 24 and MinLeaf set to 12, achieving a balanced trade-off between complexity and generalization. The Coarse Tree model, with MinParent set to 72 and MinLeaf set to 36, generated fewer branches, resulting in a simpler structure with higher generalization capability but reduced capacity to capture intricate relationships. Among the ensemble approaches, the Ensemble Bagged Trees model utilized 30 weak learners (NLearn = 30) with bootstrap aggregation (bagging) and a learning rate of 1.0, combining the independently trained trees through averaging. The Ensemble Boosted Trees model also used 30 weak learners but adopted a sequential improvement strategy via the LSBoost method with a learning rate of 0.1, whereby each subsequent tree was fitted to reduce the residual errors of its predecessor. These hyperparameter configurations contributed to the superior predictive performance of high-complexity tree structures and ensemble methods, particularly in terms of accuracy and generalization, compared with single decision tree models.

Table 2. Tree-Based Machine Learning Models for Bacillus cereus Growth

	1 11010 21 1100	Basea Machine Bearing Models for Bacinas e	ereas crema	*
Model	Model Complexity	Key Characteristics	Overfitting Risk	Best Use Case
Fine Tree Model	High	Produces deep, complex trees; captures subtle interactions between time and environmental factors.	High	Nonlinear, Complex datasets
Medium Tree Model	Moderate	Balances complexity and performance; reduces risk of overfitting while maintaining sufficient predictive power.	Medium	Moderately complex datasets
Coarse Tree Model	Low	Simple and shallow structure; generalizes well; less prone to overfitting in simpler datasets.	Low	Small, Linearly separable datasets
Ensemble Boosted Trees s	High (with equential depth)	Sequentially corrects errors of prior models; reduces bias and improves prediction accuracy on complex datasets.	Medium	Complex, Nonlinear datasets
Ensemble Bagged Trees	Moderate to High	Uses bootstrap samples; trees trained independently; final prediction is average of individual predictions; reduces variance.	Low	Nonlinear, Noisy datasets

3. RESULTS AND DISCUSSIONS

The results of this study reveal notable differences in accuracy and error metrics between various tree-based models in predicting the target variable. The Ensemble Bagged Trees model, which has the highest overall accuracy

among the tested models, calculate an RMSE of 0.009377553 in the validation set and an RMSE of 0.006517267 in the test set, as well as an R² value of 0.999465892 in the model validation set and 0.999725126 in the test set in Table 3.

T 11 4 T		1 1	1		1
Table 3. Tree	regression	models	error and	lapproximation	values

Model	Type	RMSE	MSE	R ²	MAE	Pearson Correlation (r)
Fine Tree	Validation	0.01399	0.00019	0.99881	0.00947	0.9993
The free	Test	0.01239	0.00015	0.99900	0.00937	0.9993
Medium Tree	Validation	0.03084	0.00095	0.99422	0.02055	0.9975
Medium Tree	Test	0.02493	0.00062	0.99597	0.01728	0.9973
Coarse Tree	Validation	0.06947	0.00482	0.97068	0.05083	0.9856
	Test	0.05610	0.00314	0.97962	0.03899	0.9830
Ensemble Boosted Trees	Validation	0.03593	0.00129	0.99215	0.03102	0.9922
Ensemble Boosted Trees	Test	0.03459	0.00119	0.99225	0.03002	0.9922
Ensemble Bagged Trees	Validation	0.00937	0.00008	0.99946	0.00606	0.9997
	Test	0.00651	0.00004	0.99972	0.00453	0.3997

The RMSE values of the Fine Tree model are 0.013993197 in the validation set and 0.012392232 in the test set. The calculated R^2 values are 0.998810721 for the validation set and 0.999006194 for the test set. These values

indicate that the model has a high capacity to capture variability in the data. These findings show that the Fine Tree model is effective in terms of low error metrics while providing high accuracy in Figure 3.

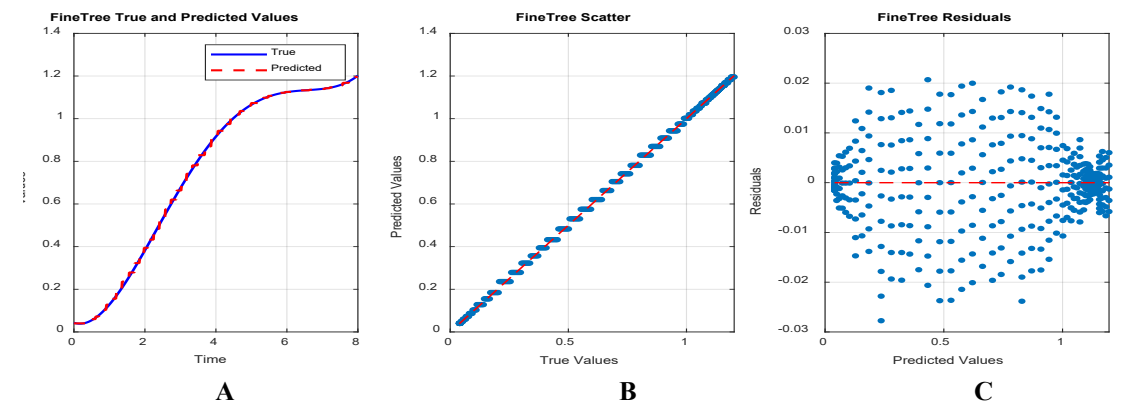


Figure 3. Fine Tree model analysis. (A) Fine Tree model true and predicted values. (B) Fine Tree model scatter. (C) Fine Tree model residuals.

The RMSE values of the Ensemble Boosted Trees model are 0.035932635 in the validation set and 0.034597338 in the test set. The R² values of the model are calculated as 0.992157982 for

the validation set and 0.992253812 for the test set in Figure 4.

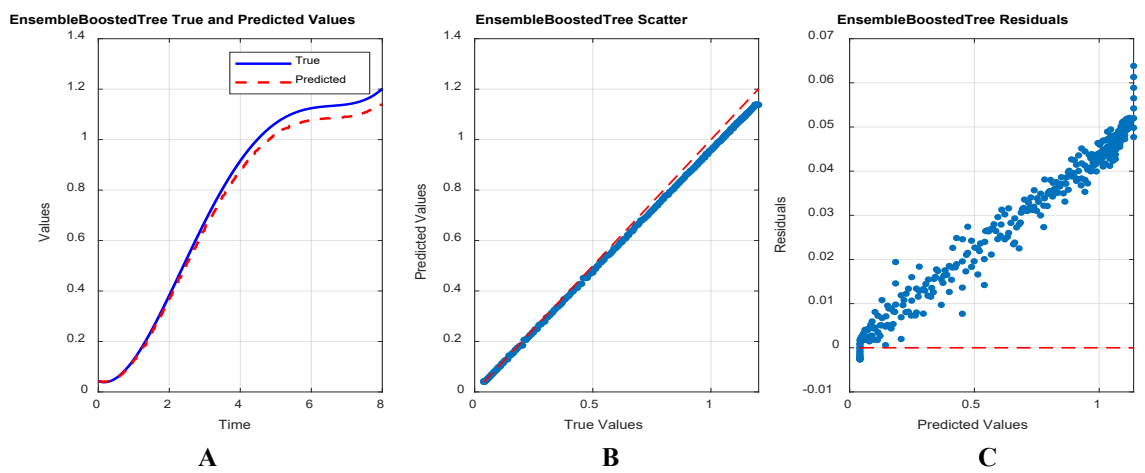


Figure 4. Ensemble Boosted Tree model analysis. (a) Ensemble Boosted Tree model true and predicted values. (B) Ensemble Boosted Tree model scatter. (C) Ensemble Boosted Tree model residuals.

The root mean square error (RMSE) values of the Coarse Tree model are 0.069470298 in the validation set and 0.056109042 in the test set. The R² values are 0.970687826 for the validation

set and 0.979626371 for the test set, indicating that the model does not adequately capture the complexity of the data compared to ensemble methods in Figure 5.

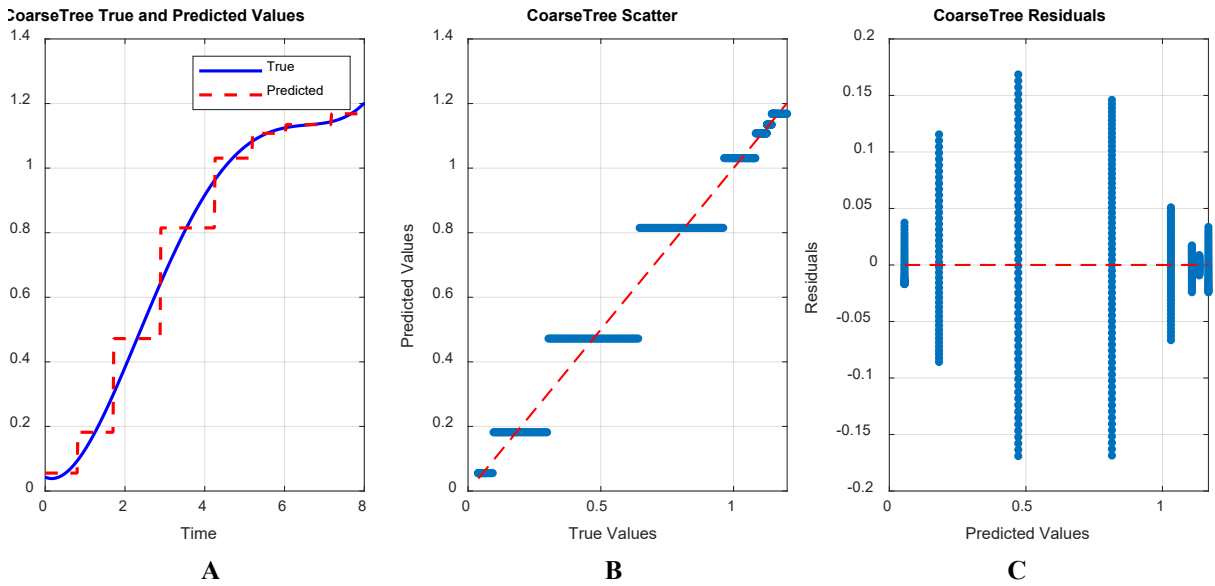


Figure 5. Coarse Tree model analysis. (A) Coarse Tree model true and predicted values. (B) Coarse Tree model scatter. (C) Coarse Tree model residuals.

The Medium Tree model performs moderately well with a validation RMSE of 0.030842445 and a test RMSE of 0.024931828. The R² values of 0.994222402 for the validation set and 0.995977362 for the test set provide a satisfactory level of accuracy, but not as high as

the levels observed in the most effective models. The higher error values compare to other models such as Fine Tree or Bagged Trees suggest that this model may tend to overfit or underfit more complex approaches in Figure 6.

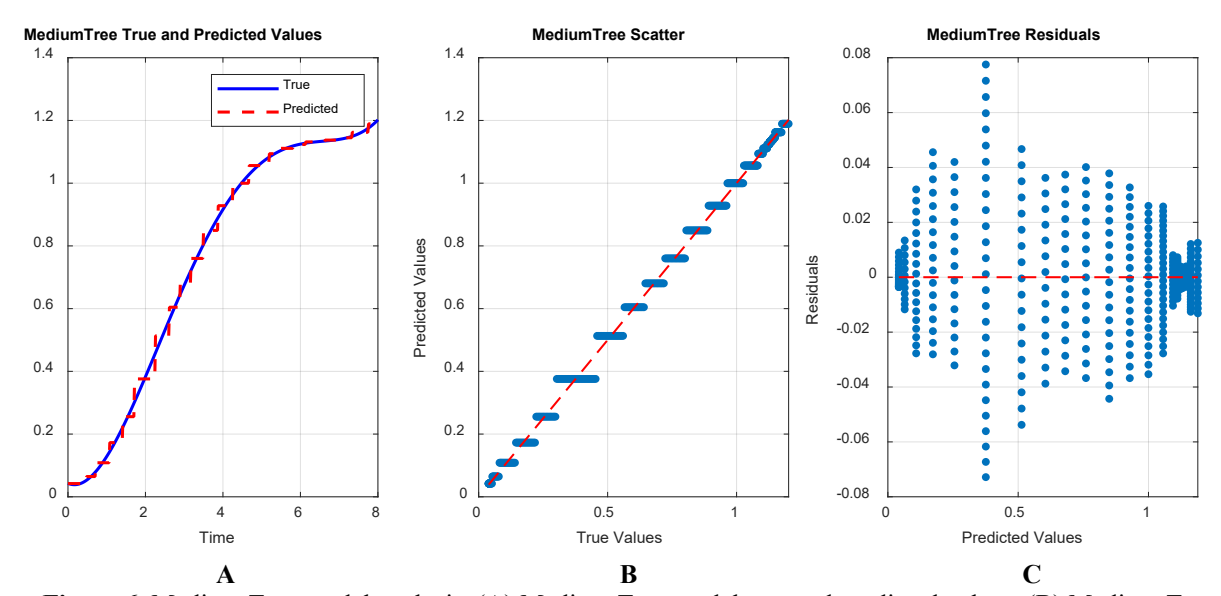


Figure 6. Medium Tree model analysis. (A) Medium Tree model true and predicted values. (B) Medium Tree model scatter. (C) Medium Tree model residuals.

The results show that ensemble methods, especially the Ensemble Bagged Trees model, surpass single tree models in terms of prediction accuracy and generalization. The high R² values and low RMSE and MSE values of the best performing models show their effectiveness in

reducing prediction errors. These results demonstrate the sensitivity of ensemble techniques in tree-based modeling and show that the combination of multiple models can significantly improve the robustness and accuracy of predictions in Figure 7.

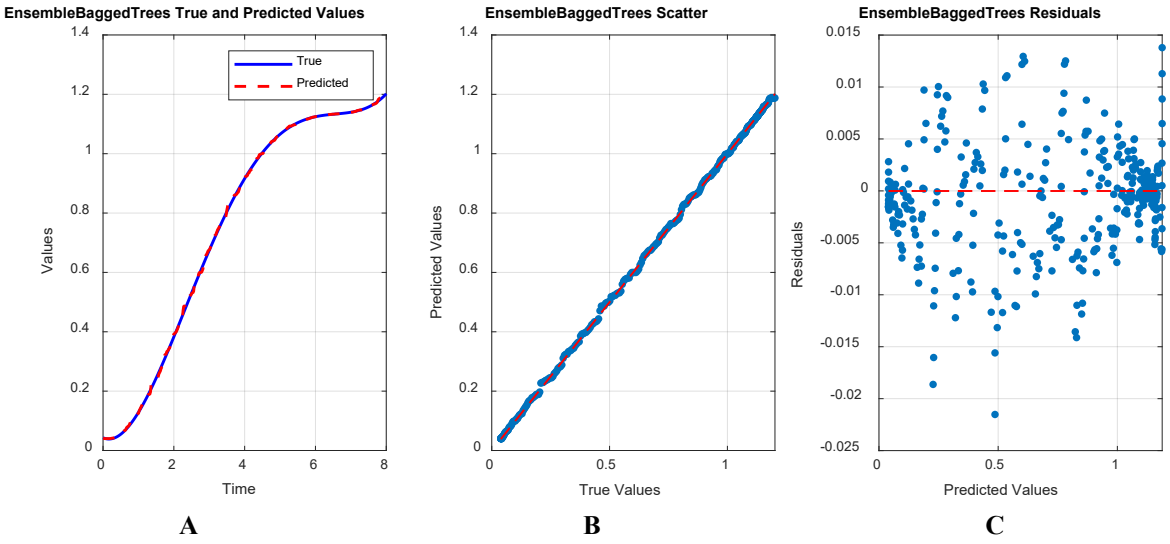


Figure 7. Ensemble Bagged Trees model analysis. (Left) Ensemble Bagged Trees model true and predicted values. (Center) Ensemble Bagged Trees model scatter. (Right) Ensemble Bagged Trees model residuals.

Table 4. Scatter Plot and Residual Plot Analyses

Model	Scatter Plot Interpretation	Residual Plot Interpretation
Fine Tree	Points closely aligned along y = x line. Very strong fit.	Residuals around ±0.01, randomly distributed.
Medium Tree	Slight dispersion around y = x line, but overall good fit.	Residuals between ±0.02-±0.03, slight deviation observed.
Coarse Tree	Points more spread out, weaker fit.	Residuals up to ± 0.05 , systematic patterns present.
Ensemble Bagged Trees	Almost perfect alignment along $y = x$ line.	Very small residuals (~±0.005), random distribution.
Ensemble Boosted Trees	Good overall, slight deviations.	Residuals around ± 0.03 , slight pattern possible.

Table 4 provides a qualitative interpretation of the scatter and residual plots for each machine learning model applied to predict $Bacillus\ cereus$ growth. Models such as Fine Tree and Ensemble Bagged Trees exhibit strong predictive performance, as indicated by the close alignment of predicted values along the y = x line and minimal, randomly distributed residuals. Medium Tree and Ensemble Boosted Trees show

moderate fit quality, with slightly larger residuals and minor deviations or patterns. In contrast, the Coarse Tree model demonstrates limited predictive capability, evidenced by a greater spread in the scatter plot and systematic residual patterns. These observations underscore the importance of visual diagnostics in evaluating model accuracy and generalization behavior.

Table 5. Paired t-Test Results (Hypotheses: H0: No difference between observed and predicted values. H1:

There is	s a uniterence of	etween observed and predicted values.)
Model	p-Value	Statistical Conclusion
Fine Tree	0.078	No significant difference (H0 accepted)
Medium Tree	0.043	Significant difference (H0 rejected)
Coarse Tree	0.015	Significant difference (H0 rejected)
Ensemble Bagged Trees	0.312	No significant difference (H0 accepted)
Ensemble Boosted Trees	0.051	Borderline, generally considered no significant difference

Fine Tree and Ensemble Bagged Trees show no statistical difference from the observed data, indicating excellent model fitting. Medium Tree and Coarse Tree demonstrate statistically significant differences, suggesting weaker model fitting (Table 5).

Studying the growth rate of Bacillus cereus is critical to understanding microbial kinetics. Stacked plot is used as a visual tool to show

different growth rates over time. This graph combines data obtained at different time intervals into a layered structure to more clearly show the change in growth rate over each period in Figure 8. By examining how Bacillus cereus grows under specific conditions, the stacked plot provides a comparative graph of multiple models at once.

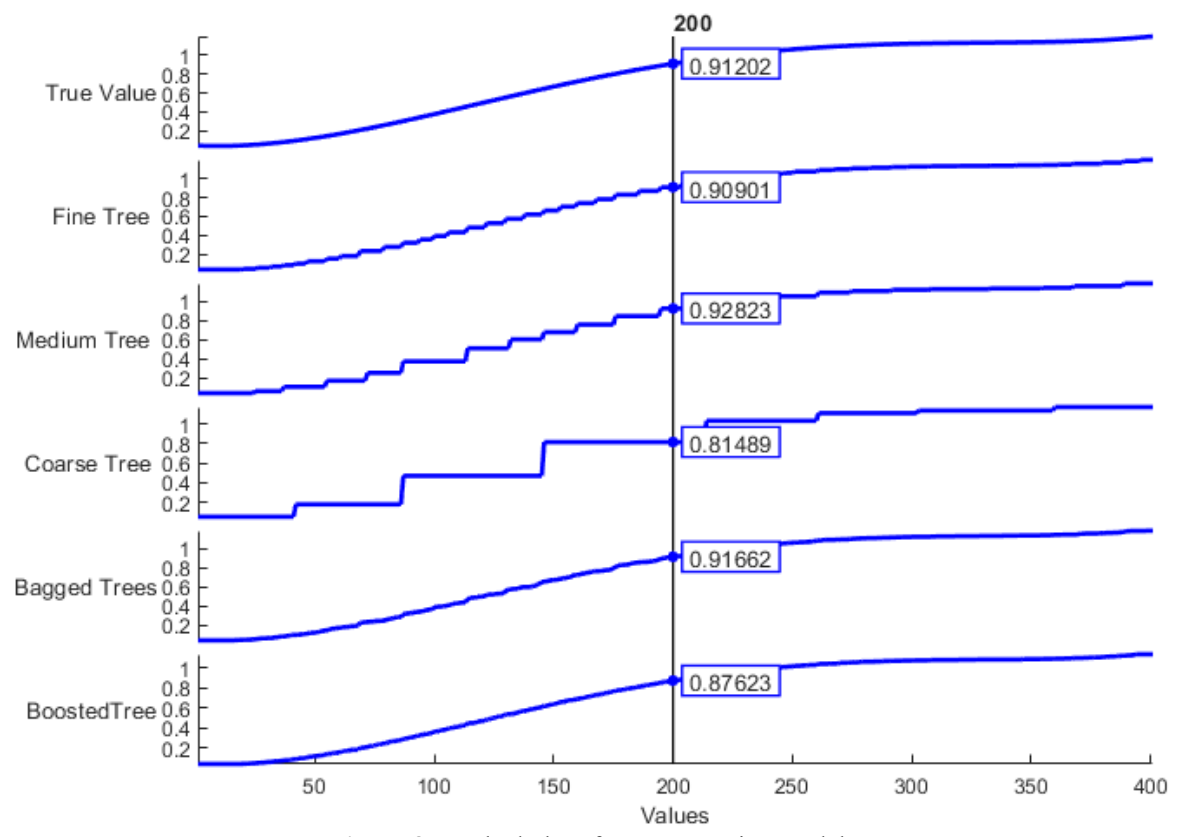


Figure 8. Stacked plot of Tree regression models

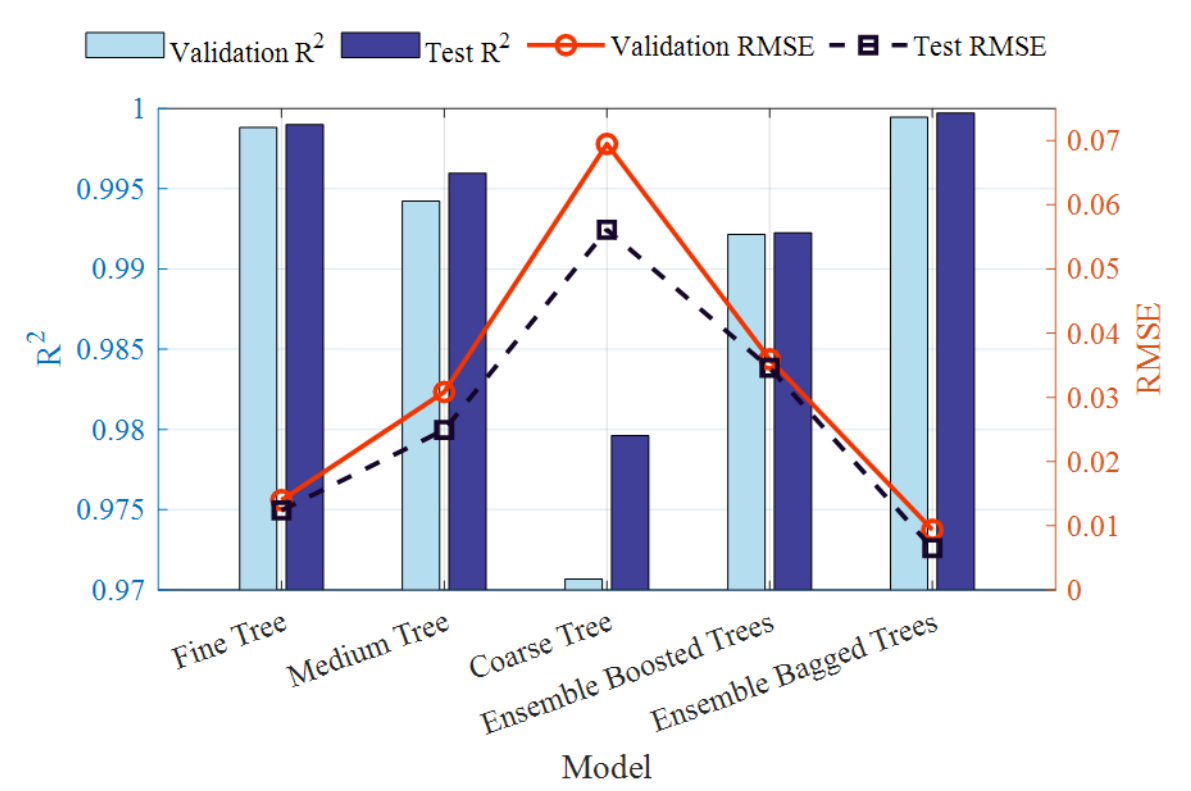


Figure 9. Comparison of tree-based regression models.

In the dual-axis comparative plot, the bars on the left axis represent the coefficient of determination (R2) for the validation and test sets, while the lines on the right axis illustrate the Root Mean Squared Error (RMSE) values for the same datasets. The results indicate that the Ensemble Bagged Trees model achieved the highest predictive accuracy, with R² values of 0.99946 (validation) and 0.99972 (test), accompanied by the lowest RMSE values of 0.00937 and 0.00651, respectively. The Fine Tree model also demonstrated performance, attaining high R2 values of 0.99881 (validation) and 0.99900 (test) with correspondingly low RMSE values of 0.01399 and 0.01239. The Medium Tree model exhibited a balanced yet comparatively lower accuracy, with R2 values of 0.99422 and 0.99597, and RMSE values of 0.03084 and 0.02493 for validation and test sets, respectively. The Ensemble Boosted Trees model achieved moderate performance, with R² values around 0.992 and RMSE values of approximately 0.036 (validation) and 0.034 (test). In contrast, the Coarse Tree model produced the lowest predictive performance, with R² values of 0.97068 (validation) and 0.97962 (test), and the highest RMSE values of 0.06947 and 0.05610, indicating limited

suitability for modeling complex datasets. Overall, the combination of near-perfect R² values and minimal RMSE highlights the Ensemble Bagged Trees model as the most effective predictive approach among all evaluated models.

4. CONCLUSION

In this study, the predictive performance of various tree-based machine learning models was evaluated using statistical metrics. Key findings are summarized as follows:

- o Ensemble models, particularly Ensemble Bagged Trees and Ensemble Boosted Trees, outperformed single decision tree algorithms by yielding lower RMSE and higher R² values, indicating superior accuracy and generalizability across complex datasets. These models effectively reduce prediction error by integrating the outputs of multiple decision trees.
- O Single decision tree models, such as Fine Tree and Medium Tree, demonstrated moderate performance. While they provided acceptable results, their predictive power was consistently lower than that of ensemble models, especially in terms of robustness and error minimization.

O The Coarse Tree model, due to its simplistic structure, achieved the lowest performance, with higher error rates and a poorer fit to the data, making it less suitable for modeling datasets with complex relationships.

The results of this study show that ensemble techniques, especially bagging and boosting, are highly effective in improving the accuracy of forecasting models. These methods offer sensitive approaches for applications where precision and reliability are critical.

Acknowledgments

The author would like to express their sincere gratitude to Ulaş YAMANCI (Süleyman Demirel University, Department of Statistics) and Selmihan Şahin ABDULMAJEED (Süleyman Demirel University, Department of Chemistry) for their valuable contributions and insightful support throughout the study.

Competing Interests

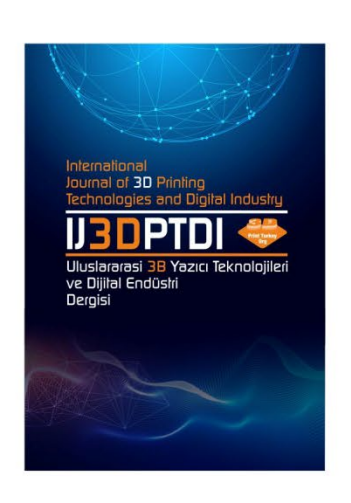
The authors declare that they have no conflict of interest.

REFERENCES

- 1. Rizki, W.M., Ratih, D.H., Harsi, D.K., "Comparison of Predictive Growth Models for Bacillus Cereus in Cooked and Fried Rice During Storage", The Annals of the University Dunarea De Jos of Galati. Fascicle VI Food Technology, Vol. 46, Issue 2, Pages 89-103, 2022.
- 2. Ellouze, M., Buss Da Silva, N., Rouzeau-Szynalski, K., Coisne, L., Cantergiani, F., Baranyi, J., "Modeling Bacillus cereus Growth and Cereulide Formation in Cereal, Dairy, Meat, Vegetable-Based Food and Culture Medium", Frontiers in Microbiology, Vol. 12, Article 639546, 2021.
- 3. Buss da Silva, N., Baranyi, J., Carciofi, B.A.M., Ellouze, M., "From Culture-Medium-Based Models to Applications to Food: Predicting the Growth of B. cereus in Reconstituted Infant Formulae", Frontiers in Microbiology, Vol. 8, Article 1799, 2017.
- 4. Bursová, Š., Haruštiaková, D., Necidová, L., Krobotová, E., Mlejnková, Z., Tkáč, M., Stojanová, K., Golian, J., "Evaluation of Bacillus cereus growth in cooked rice", The Journal of Microbiology, Biotechnology and Food Sciences, Vol. 14, Issue 1, Article e10985, 2024.

- 5. Ahmad, M.M., Azoddein, A.M., Olalere, O.A., Isa, S., "A Predictive Batch Culture Growth and Biosynthesis for Bacillus cereus (ATCC 14579) using Response Surface Methodology", Journal of Environmental Bioremediation and Toxicology, Vol. 5, Issue 2, Pages 40-45, 2022.
- 6. Juneja, V.K., Golden, C.E., Mishra, A., Harrison, M., Mohr, T.B., "Predictive model for growth of Bacillus cereus at temperatures applicable to cooling of cooked pasta", Journal of Food Science, Vol. 84, Issue 3, Pages 590-598, 2019.
- 7. Valik, L., Görner, F., Laukova, D., "Growth dynamics of Bacillus cereus and shelf-life of pasteurized milk", Czech Journal of Food Sciences, Vol. 21, Issue 6, Pages 195-202, 2003.
- 8. Choi, M.-S., Kim, J.Y., Jeon, E.B., Park, S.Y., "Predictive growth models of Bacillus cereus on dried laver Pyropia pseudolinearis as a function of storage temperature", Korean Journal of Fisheries and Aquatic Sciences, Vol. 53, Issue 5, Pages 699-706, 2020.
- 9. Jiang, Y.N., Luo, J., Huang, D., Liu, Y., Li, D., "Machine learning advances in microbiology: A review of methods and applications", Frontiers in Microbiology, Vol. 13, Article 925454, 2022.
- 10. Romana, A.S., "A Comparative Study of Different Machine Learning Algorithms for Disease Prediction", International Journal of Advanced Research in Computer Science and Software Engineering, Vol. 7, Issue 7, Pages 172, 2017.
- 11. Atolia, E., Cesar, S., Arjes, H.A., Rajendram, M., Shi, H., Knapp, B.D., Khare, S., Aranda-Díaz, A., Lenski, R.E., Huang, K.C., "Environmental and physiological factors affecting high-throughput measurements of bacterial growth", mBio, Vol. 11, Issue 5, Article e01378-20, 2020.
- 12. Eckart, L., Eckart, S., Enke, M., "A brief comparative study of the potentialities and limitations of machine-learning algorithms and statistical techniques", E3S Web of Conferences, Vol. 266, Article 02001, 2021.
- 13. Weller, D., Love, T., Wiedmann, M., "Interpretability versus accuracy: A comparison of machine learning models built using different algorithms, performance measures, and features to predict E. coli levels in agricultural water", Frontiers in Artificial Intelligence, Vol. 4, Article 628441, 2021.

- 14. Chorin, E., Thuault, D., Cléret, J.J., Bourgeois, C.M., "Modelling Bacillus cereus growth", International Journal of Food Microbiology, Vol. 38, Issues 2-3, Pages 229-234, 1997.
- 15. Ince, V., Bader-El-Den, M., Arabikhan, F., Sari, O.F., "Machine Learning for Bacterial Growth Prediction and Examination of Bacterial Impact on Growth", Proceedings of the 2024 IEEE 12th International Conference on Intelligent Systems (IS), Pages 1-6, 2024.
- 16. Kowalik, J., Lobacz, A., Zulewska, J., Dec, B., "Analysis and mathematical modelling of the behaviour of Escherichia coli in the mascarpone cheese during cold storage", International Journal of Food Science and Technology, Vol. 53, Issue 6, Pages 1541–1548, 2018.
- 17. Martinez-Rios, V., Gkogka, E., Dalgaard, P., "Predicting growth of Listeria monocytogenes at dynamic conditions during manufacturing, ripening and storage of cheese Evaluation and application of models", Food Microbiology, Vol. 92, Pages 1–12, 2020.
- 18. Stavropoulou, E., Bezirtzoglou, E., "Predictive modeling of microbial behavior in food", Foods, Vol. 8, Issue 12, Pages 1-16, 2019.
- 19. Baranyi, J., Buss da Silva, N., Ellouze, M., "Rethinking tertiary models: relationships between growth parameters of Bacillus cereus strains", Frontiers in Food Microbiology, Vol. 8, Article 1890, 2017.



ULUSLARARASI 3B YAZICI TEKNOLOJİLERİ VE DİJİTAL ENDÜSTRİ DERGİSİ

INTERNATIONAL JOURNAL OF 3D PRINTING TECHNOLOGIES AND DIGITAL INDUSTRY

ISSN:2602-3350 (Online)

URL: https://dergipark.org.tr/ij3dptdi

TASARIM EĞİTİMİNDE YAPAY ZEKÂ UYGULAMALARININ SOYUTLAMA VE YORUMLAMA EŞLİĞİNDE KULLANIMININ YARATICILIĞA ETKİSİ: ENDÜSTRİYEL TASARIM STÜDYO DENEYİMİ

THE EFFECT OF THE USE OF AI APPLICATIONS IN DESIGN EDUCATION WITH ABSTRACTION AND INTERPRETATION ON CREATIVITY: INDUSTRIAL DESIGN STUDIO EXPERIENCE

Yazarlar (Authors): Mahmut Celaleddin Kaleli®*

Bu makaleye şu şekilde atıfta bulunabilirsiniz (To cite to this article): Kaleli M. C., "Tasarım Eğitiminde Yapay Zekâ Uygulamalarının Soyutlama ve Yorumlama Eşliğinde Kullanımının Yaratıcılığa Etkisi: Endüstriyel Tasarım Stüdyo Deneyimi" Int. J. of 3D Printing Tech. Dig. Ind., 9(2): 363-394, (2025).

DOI: 10.46519/ij3dptdi.1713122

Araştırma Makale/ Research Article

Erişim Linki: (To link to this article): https://dergipark.org.tr/en/pub/ij3dptdi/archive

TASARIM EĞİTİMİNDE YAPAY ZEKÂ UYGULAMALARININ SOYUTLAMA VE YORUMLAMA EŞLİĞİNDE KULLANIMININ YARATICILIĞA ETKİSİ: ENDÜSTRİYEL TASARIM STÜDYO DENEYİMİ

Mahmut Celaleddin Kaleli^a **

^aSelçuk Üniversitesi, Güzel Sanatlar Fakültesi, Endüstriyel Tasarım Bölümü, TÜRKİYE

*Sorumlu Yazar: celaleddinkaleli@selcuk.edu.tr

(Geliş/Received: 03.06.25; Düzeltme/Revised: 03.07.25; Kabul/Accepted: 08.08.25)

ÖZ

Yapay zekâ kullanımının endüstriyel tasarım süreçlerine dâhil edilmesinin, öğrencilerin yaratıcı düşünme bağlamında tıkanıklık yaşadıkları biçim yaratma süreçlerinde yeni olanaklar sağlayabileceği değerlendirilmektedir. Bu çalışmanın amacı, üçüncü sınıf endüstriyel tasarım öğrencilerini YZ uygulamalarıyla tanıştırarak ve YZ kullanımını teşvik ederek endüstriyel tasarım stüdyo deneyimini yaratıcı düşünme bağlamında daha ileri bir noktaya taşımaktır. Ancak yapay zekâ uygulamalarının endüstriyel tasarım alanındaki ilk kullanım denemelerinde disiplinin karakterine uymayacak "kitch" tasarım çıktıları ürettiği gözlemlendi. YZ ile ilk karşılaşmada yaşanan erken olumsuzlukların, soyutlama ve yorumlama gibi disiplinin geleneksel yöntemleriyle paralel şekilde kullanılarak aşılabileceği öngörülmektedir. Stüdyo dersinde endüstriyel tasarım geliştirme süreçlerinin daha sistematik bir şekilde ele alınabilmesi için çalışma yöntemi, analiz aşaması, YZ aşaması ve sentez aşaması olarak üç aşamada yapılandırıldı. Veri toplama süreci marka ve ürün incelemelerini içeren analiz aşamasının bir parçasıdır. YZ aşaması uygulamaların proje süreçlerine doğrudan uygulanarak elde edilen ilk çıktıların değerlendirildiği ikinci aşamadır. Sentez aşamasıysa ilk iki aşamada elde edilen verilerin sentezlenerek, soyutlanarak yorumlandığı ve yaratıcı düşünme becerisinin nihai ürün tasarımlarında somutlaşarak ortaya çıktığı üçüncü aşamadır. Bu aşamalarda elde edilen sonuçların ve araştırmacıya ait gözlemlerin öğrenci deneyimleriyle kıyaslanabilmesi ve de çapraz biçimde yorumlanabilmesi için araştırmacının görüslerini yansıtmasını ve elde ettiği bulguları yorumlamasını mümkün kılan nitel arastırma yöntemlerinden yararlanılmıştır. Bu araştırmanın sonucunda endüstriyel tasarım proje/stüdyo derslerinde YZ kullanımının bir taraftan öğrencilerin zaman yönetimine ve yaratıcılıklarına katkı sunarak tasarım aşamalarının birçok yerinde kolaylaştırıcı bir role sahip olduğu görülürken diğer taraftan da onları tembelleştirerek ve kolaya alıştırarak bazı tasarım melekelerini köreltme riski taşıdığı ortaya çıkmıştır. Sonuç olarak bu çalışma endüstriyel tasarım eğitiminde YZ kullanımının yaratıcı düşünme becerilerini tetikleyen bir katalizör olarak kullanımına yönelik farkındalık oluşturması ve bu konuda eğitimcileri cesaretlendirmesi açısından özgün bir çalısma olarak sunulmustur.

Anahtar Kelimeler: Yapay Zekâ, Yaratıcı Düşünme, Soyutlama, Endüstriyel Tasarım.

THE EFFECT OF THE USE OF AI APPLICATIONS IN DESIGN EDUCATION WITH ABSTRACTION AND INTERPRETATION ON CREATIVITY: INDUSTRIAL DESIGN STUDIO EXPERIENCE

ABSTRACT

It is evaluated that incorporating artificial intelligence into industrial design processes can offer new possibilities in the creation of forms, particularly in contexts where students experience congestion in their creative thinking. This study aims to take the industrial design studio experience to a higher level by introducing third-year industrial design students to ai applications and encouraging the use of ai.

However, in the initial attempts to utilise ai applications in the field of industrial design, it was observed that they produced "kitch" design outputs that did not align with the discipline's character. It is envisioned that the early negativity experienced in the first encounter with ai can be mitigated by using it in conjunction with traditional methods of the discipline, such as abstraction and interpretation. To address industrial design development processes more systematically in the studio course, the working method was structured into three phases: analysis, ai, and synthesis. Data collection is a key component of the analysis phase, which encompasses brand and product reviews. The ai phase is the second phase, where the first outputs obtained by directly applying the applications to the project processes are evaluated. The synthesis stage is the third stage in which the data obtained in the first two stages are synthesised, abstracted and interpreted, and creative thinking skills are embodied in the final product designs. To facilitate comparison and interpretation of the results obtained in these stages and the researcher's observations with the students' experiences, qualitative research methods were employed, which enable the researcher to reflect on their views and interpret the findings. As a result of this research, it has been revealed that the use of AI in industrial design project/studio courses, on the one hand, plays a facilitating role in many parts of the design stages by contributing to students' time management and creativity, but on the other hand, it carries the risk of dulling some design skills by making them lazy and accustomed to ease. All in all, this study presents an original contribution to raising awareness about the use of ai as a catalyst for developing creative thinking skills in industrial design education, and to encouraging educators in this regard.

Keywords: Artificial Intelligence, Creative Thinking, Abstraction, Industrial Design.

1. GİRİS

1.1. Bağlam ve Faaliyet Alanı

Literatürden derlenen veriler etrafında yapay zekâ, insana özgü zekâ gerektiren görevleri yerine getirebilmek için insan zekâsını taklit etmeve odaklanan bir disiplin özetlenebilir [1-2]. Calısmanın kalanında "yapay zekâ" terimi "YZ" şeklinde kısaltılarak kullanılacaktır. 1950'li yıllardan bu yana YZ'nın bir alt disiplini olarak değerlendirilen makine öğrenimi başta olmak üzere çok farklı alanlarda YZ ile ilgili birçok araştırma ve çalışma yapılmıştır. Ağırlıklı olarak yüksek miktarda verileri hafizasında tutarak süratle bunları analiz etme, sınıflandırma, mukayese etme, mantık yürütme ve çıktı üretme becerilerini insana benzer bir şekilde yapmaya yaklaşması uzun yıllar almıştır.

Bu alandaki ilerleme hızı günümüzde geçmişe kıyasla oldukça yükselmiştir. Bunun sebebi ilk olarak YZ alanlarında kullanılan mikroişlemci ve ekran kartlarının daha az enerjiyle, daha az ısınarak çok daha yüksek bir işlem gücüne ulasması olarak gösterilebilir. Ayrıca YZ alanında yapılan çalışmalar neticesinde bu alanda yüksek bir bilgi ve deneyim birikmesi de süreci hızlandıran faktörler arasında sayılabilir. Bu sürec hızını sürekli arttırarak devam Günümüze gelindiğinde etmektedir. bilgisayarların YZ yardımıyla öğrenme ve dayanarak fotoğrafları üretme becerisine

gerçekçi bir şekilde düzenleyebilen, değiştirebilen, farklı görseller ve üç boyutlu modeller üzerinde eğitilebilen, girilen yazılı metinleri anlayabilen, talep edilen görselleri modelleyerek iki boyutlu, üç boyutlu çıktılar ve hatta videolar üretebilen uygulamalar geliştirilmiştir.

Bu uygulamalar endüstriyel tasarım, mimarlık, iç mimarlık, peyzaj mimarisi, grafik tasarımı, moda tasarımı, seramik-cam sanatları, resim ve heykel gibi birçok alanda kullanılabilmektedir. Bu uygulamalara 2019 yılından itibaren geliştirilen rastgele çizimleri yorumlayarak manzara resmine dönüstüren "Nvidia Canvas" serbest eskiz çalışmalarını yorumlayarak ürün tasarımlarına dönüstürebilen Vizkom, girilen metinleri yorumlayarak görseller yaratabilen Middiourney, Dall-E ve Stable Diffusion gibi programlar örnek olarak verilebilir. Grafik tasarımı disiplininde yapılan bir araştırma YZ uygulamalarından yararlanan örneklemlerin, kullanmayanlardan, yaratıcılık bağlamında çok daha başarılı sonuçlara ulaşabildiğini göstermektedir [3].

Endüstriyel tasarım bölümünde verilen proje/stüdyo dersleri, henüz aday konumunda olan öğrencileri endüstriyel tasarımcıya dönüştüren bölümün temel dersleridir. Bu dersler profesyonel hayattaki tasarım ofislerinde icra edilen bir ürünü sıfır

noktasından başlayarak tasarlamanın. geliştirmenin ya da var olan bir ürün üzerinde iyileştirmeler yapmanın bir simülasyonu olarak değerlendirilebilir. Proje/stüdyo derslerinde öğrenciler profesyonel tasarım hayatında yaşanan problemlerin benzerleriyle yüze geldikleri karsılasırlar. Yüz problemlerin çözüm yollarını ararken dersi yürüten tasarım hocası onlara rehberlik eder. Bahsi geçen tasarım problemlerinden birisi de öğrencilerin biçim yaratmada yasadıkları varatıcılıkla ilgili problemlerdir. Bu derslerin icrasında öğrenciler bir taraftan da güncel tasarım ve üretim uygulamalarıyla tanışma ve deneyimleyerek onları öğrenme vakalarlar. Proje/stüdyo derslerinde tıpkı profesyonel hayatta olduğu gibi endüstriyel yolla seri olarak üretilecek bir tasarlanırken belirli adımlardan oluşan bir süreç takip edilir. Bu süreçlerle ilgili tasarım metodolojisi bağlamında ilk çalışmalardan bu yana pek çok model sunulmuştur [4-6]. Bu modellerin önemli kısımlarından birisi de varatıcı düsünme melekelerinin voğun bir şekilde ortaya çıktığı, ürünlerin dış formlarının yaratıldığı seçenek üretme ve seçenek arıtma kısımlarıdır. Öğrenciler proje stüdyo dersinde aldıkları brief doğrultusunda ilk olarak mevcut ürünleri ve alandaki bilgileri araştırırlar ve proje yürütücüsüne sunarlar.

Daha sonra elde ettikleri bilgiler ve veriler doğrultusunda ürünlerini tasarlamaya başlarlar. Diğer bir ifadevle araştırmalarını ürünleştirmeye çalışırlar. Süreç boyunca çalışmalarını proje yürütücüsüne hem sözel olarak hem de serbest eskiz cizimleriyle ve bilgisayar destekli tasarım programlarını kullanarak gösterirler. Ancak öğrencilerin zihinlerindeki tasarım bağlamında sözel olarak modelleyerek anlattıklarıyla çizerek ve görselleştirdikleri proje çıktıları her zaman paralellik arz etmeyebilir ya da birbirlerini desteklemeyebilir.

Tasarımın iletişim yönünü tıkayan bu durumun genellikle öğrencilerin serbest el çizimi ve bilgisayar destekli tasarım programlarını kullanma becerilerini proje/stüdyo derslerini almaya başladıkları dönemlere kadar yeterince geliştirmemelerinden kaynaklandığı, nitel araştırma yöntemleriyle desteklenen araştırmalarda gözlemlenmektedir [7]. Öğrencilerin endüstriyel tasarımın gerektirdiği donanıma yeterince sahip olamamaları biçim

yaratma konusunda tıkanıklık yaşamalarına ve zamanı etkili kullanamamalarına da neden olabilmektedir. Bu makale YZ kullanımının öğrencilerin yaratıcı düşünme ve görselleştirme becerileri gerektiren endüstriyel tasarım proje dersi üzerindeki etkilerini incelemektedir.

1.2. Araştırma Soruları

Çalışmaya rehberlik etmesi ve çalışmanın sınırlarının çizilmesi amacıyla bazı araştırma soruları oluşturuldu. Bu araştırmada aşağıdaki sorulara yanıt aranmaktadır:

- 1. Proje/stüdyo derslerinde ürün tasarımlarının dış formları tasarlanırken, tasarım problemleri tespit edilirken ve çözülmeye çalışılırken YZ'dan nasıl yararlanılabilir?
- 2. YZ kullanımının yaratıcılık, zaman yönetimi ve çalışma motivasyonu bağlamında olumlu ve olumsuz etkileri nelerdir?
- 3. YZ kullanımında yaşanan olumsuzluklar nasıl giderilebilir?
- 4. YZ tasarım öğrencileri tarafından hem olumlu hem de olumsuz taraflarına bakan yönleri itibarı ile nasıl algılanmaktadır?

1.3. Calışmanın Amacı

Bu çalışmanın amacı örnek bir vaka analizi üzerinden endüstriyel tasarım proje/stüdyo derslerinde öğrencileri YZ uygulamalarıyla tanıştırarak dersleri öğrencilerin yaratıcılıkları bağlamında daha etkili hale getirmekti. Ancak bu amaçla teşvik edilen öğrenci çalışmalarının erken çıktılarında bazı olumsuzluklarla karşılaşıldı. Bu olumsuzluklardan bazıları sunlardır:

- 1. İlk olumsuzluk, verilen proje brifine yönelik yapılan YZ destekli çalışmalarda endüstriyel tasarım disiplini açısından kabul edilemeyecek "kitch" çıktılar üretilmesi oldu. ("Kitch" kavramı çalışmanın literatür kısmında detaylandırılacaktır.)
- 2. Ayrıca YZ destekli üretilen erken çıktılarda ürünlerin insanın antropometrik yapısına uygun olmadığı ve ergonomi standartlarını karşılayamadığı belirlendi.
- 3. YZ destekli tasarlanan ürünlerin üretim yöntemleri açısından ideal bir şekilde çözümlenemediği gözlemlendi.

Dolayısıyla bu çalışmanın güncellenmiş amacı yukarıda anlatılan olumsuzlukların çözümünde disiplinin kendi yöntemlerinin çalışmaya dâhil edilerek bu olumsuzlukların aşılabileceğini ve nihai amaca ulaşabileceğini göstermektir.

2. LİTERATÜR

2.1. Endüstriyel Tasarım Disiplini ve Eğitimi Bağlamında Yaratıcı Düşünme Becerileri: Soyutlama ve Yorumlama

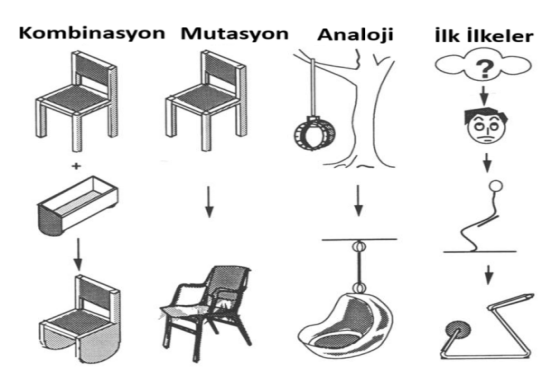
Endüstriyel tasarım, ürünün kullanımından ya görüntüsünden kaynaklanan, olunmayan durumları, arzu edilen ve mutlu olunan durumlara çevirmeyi amaçlayan bir problem çözme faaliyetidir. Tasarım süreçleri hazır bulunan bilgi ve deneyimlerden yola çıkılarak yeni bilgiler ve anlayıslar üretmek yoluyla değişik tasarımlar yapmayı amaçlar [8-9]. Endüstriyel tasarım disiplininde takip edilen süreçler mutlak bir hiyerarşiye bağlı olmadan yapılan çalışmalarla ilerler [10]. Endüstriyel tasarım süreçlerine estetik ya da işlevsel bir gereksinimden kavnaklanan tasarım idrak problemlerinin edilmesi için incelenmesiyle baslanır. Ardından kavramsal çalışmalar, somut ifadeler ve detaylı tasarımlarla tasarım süreçleri sürdürülür [11]. Endüstriyel tasarım süreçlerinde tasarımcıların ya da tasarım öğrencilerinin, yaratıcılık içeren her düşüncesine tekrar geri dönüp bakmak ve süreçlerde bunları değerlendirebilmek için kalıcı hale getirmesi gerekir. Bunun için kullanımlarından etkili bir fayda sağlamak için yetkinleşmeyi gerektiren serbest çizimleri, maket ve model yapımı, bilgisayar destekli tasarım programları, üç boyutlu yazıcıların kullanımı, ileri render programları gibi araçlar örnek olarak verilebilir.

Etraflıca düşünme, idrak etme, mukayese etme öğrenme, çalışma motivasyonu ve karşılıklı iletişim endüstriyel tasarım disiplinindeki yaratıcılıkla ilişkili süreçlerin bilişsel ve duyusal bileşenlerini oluşturur [12]. Amabile, üç temel bileşenin bir araya gelerek tasarım öğrencilerindeki bireysel yaratıcılığı ortaya çıkardığını bildirir. Bu bileşenler şunlardır: mesleki uzmanlaşma, yaratıcı becerilerin ortaya çıkması için gerekli olan tasarım yetenekleri ve çalışma motivasyonu [13].



Şekil 1. Amabile'ye göre yaratıcılığı ortaya çıkaran temel bileşenler [13].

Mimarlık, iç mimarlık, endüstriyel tasarım, şehir ve bölge planlama, peyzaj mimarlığı ve grafik tasarımı gibi tasarım disiplinlerinin eğitiminde farklı düşünme biçimlerini ve yaratıcılığı geliştirmek için çok farklı metotlar önerilmiştir. Nigel Cross bu yöntemleri kombinasyon, mutasyon ve analoji ve temel prensipler olarak derlemektedir. Cross bu metotları kullanarak bünyesinde yaratıcı düşünceyi barındıran tasarımların geliştirilebileceğini savunmaktadır [14].



Şekil 2. Nigel Cros'un savunduğu kombinasyon, mutasyon, analoji ve temel ilkeleri gösteren örnekler [14]

Çağrışımlar geçmiş deneyimlerimizden elde ettiğimiz anılardan hareket ederek farklı duyularımıza hitap eden kavramsal temsilleri birbirlerine bağlamaktadır [15]. Örneğin bir havlama sesi duyduğumuzda bir köpeğin sesi zihnimizde belirebilir ya da bir gül resmine baktığımızda zihnimiz bize gülün kokusunu hatırlatabilir. Bar, çağrışım kavramını çağrışımlar, analojiler ve tahminler olmak üzere üç ana unsur üzerinden açıklamaktadır.

Çağrışımlar sürekli tekerrür eden insan hafızasındaki örneklerin zihinde birikmesiyle oluşur. Analoji ise hafızamıza kaydettiğimiz deneyimler ve bilgilerden sonra karşılaştığımız veni bilgiler arasında benzetme yoluyla örüntüler kurmamıza aracılık eder. Tahmin etme yoluyla da, karşılaştığımız yeni bilginin hafızamızdaki bilgilerden hangisine benzediğini bulmaya çalışırız [16]. Burada Analoii kavramına baktığımızda tarafından "ortak bazı yönleri bulunan iki kavram arasında benzetme ve örnekseme" olarak tanımlandığını görürüz [17].

Buradan hareketle ortak noktalar inşa etmek istediğimiz iki olgu arasında aktarma yapma eylemine "Analojide bulunma" diyebiliriz. Örneğin "şimdiye çoktan uyumuştur bizim tavuk" dediğimizde tanıdığımız birisine tavuk diyerek tavukların erken uyumlarına göndermede bulunmuş ve o kimseyi tavuğa benzeterek analojide bulunmuş oluruz.

Bu çalışmada bir fiil olarak kullandığımız "eğretilemek" ise "analojide bulunma ile yakın

anlamdadır. Bu çalışma boyunca "eğretileme" terimi kaynak ya da iletici durumundaki dilsel, olgunun görsel veya işitsel bir hedef konumundaki baska bir olguya atıfta bulunmasına isaret edecektir. Eğretileme; bir nesneyi ya da olguyu baska bir nesne ya da olguya yaslanarak görmek, daha iyi bilinen bir bölgeden, daha az bilinen bir bölgeye bilgi taşımak demektir [18]. Endüstriyel tasarım alanında eğretileme yapıldığında benzetme yaparak bir anlam ve ifade bir olgu ya da nesneden yeni yaptığımız ürüne transfer edilir. Böylece yeni tasarımla benzetilen olgu arasında akrabalık ilişkisi kurulmuş olur.

Tasarım disiplinlerinde yaratıcılığı geliştirmek için analoji ve eğretileme kavramları farklı şekillerde önerilmekte ve kullanılmaktadır. Örneğin Janine Benyus tasarım problemlerinin çözümünde doğadan analojide bulunulmasını önermektedir. Benyus'a göre insanlar herhangi bir tasarım yaparken doğada neyin gerçekten işe yaradığını ve neyin kalıcı olduğunu görebilmek için doğadaki biçimlere, süreçlere ve ekosistemlere bakmalıdır [19].



Sekil 3. Doğadan analojide bulunularak tasarlanan endüstriyel ürün tasarımından örnekler [20-23]

Yaratıcılığı geliştirmek için kullanılan analoji yöntemlerinden birisi de retro tasarımdır. Geçmişte üretildiği halde kült olmuş ve geniş kitleler tarafından kabul görmüş "vintage" ya da günümüzün "retro" ürünlerin modern cizgileriyle veniden soyutlanarak tasarlanmasıyla doğan retro tasarımlar ürün tasarımında yaratıcılık bağlamında bir çözüm olarak kullanılmaktadır. Retro tasarımlar, dijital öncesi çağın nostaljik yönlerini ele alarak önceki dönemlerin ruhunu yakalamayı ve tanıdığımız, sevdiğimiz insanlarla iletişim kurmanın retro bir yolunu sunabilir. Çünkü bazı

insanlar günümüz teknolojilerinin rahatlığını takdir ettiği halde önceki dönemlerin analog denevimlerini özleyebilmekteler [24]. Hatıralarımızla ilintili nostaljik deneyimlerimizi teknolojiye kaptırdığımızdan dolayı kaybettiklerimizi geri kazanmak için retro ve vintage havası taşıyan yeni ürünlere meyleden bir tüketici eğilimi ortaya çıkabilir. Aşağıda retro ve vintage ürünlerden analojide bulunularak ve soyutlanarak tasarlanmış endüstriyel tasarım örneği görmektesiniz. Burada 1970'lerin tasarım dilini modasını temsil eden nostaljik televizyondan modern bir

bilgisayar monitörüne biçim dili transferi yapılmıştır. Aynı şekilde eskiye ait olan bir radyo kasasından modern bir bilgisayar kasasına ve de eski nesli temsil eden bir daktilodan modern bir bilgisayar klavyesine biçim dili transferi yapılarak nostalji esintileri taşıyan, kadim olanı yad ederken modernlikten de taviz vermeyen bir tasarım diline ulaşılmaya çalışılmıştır.

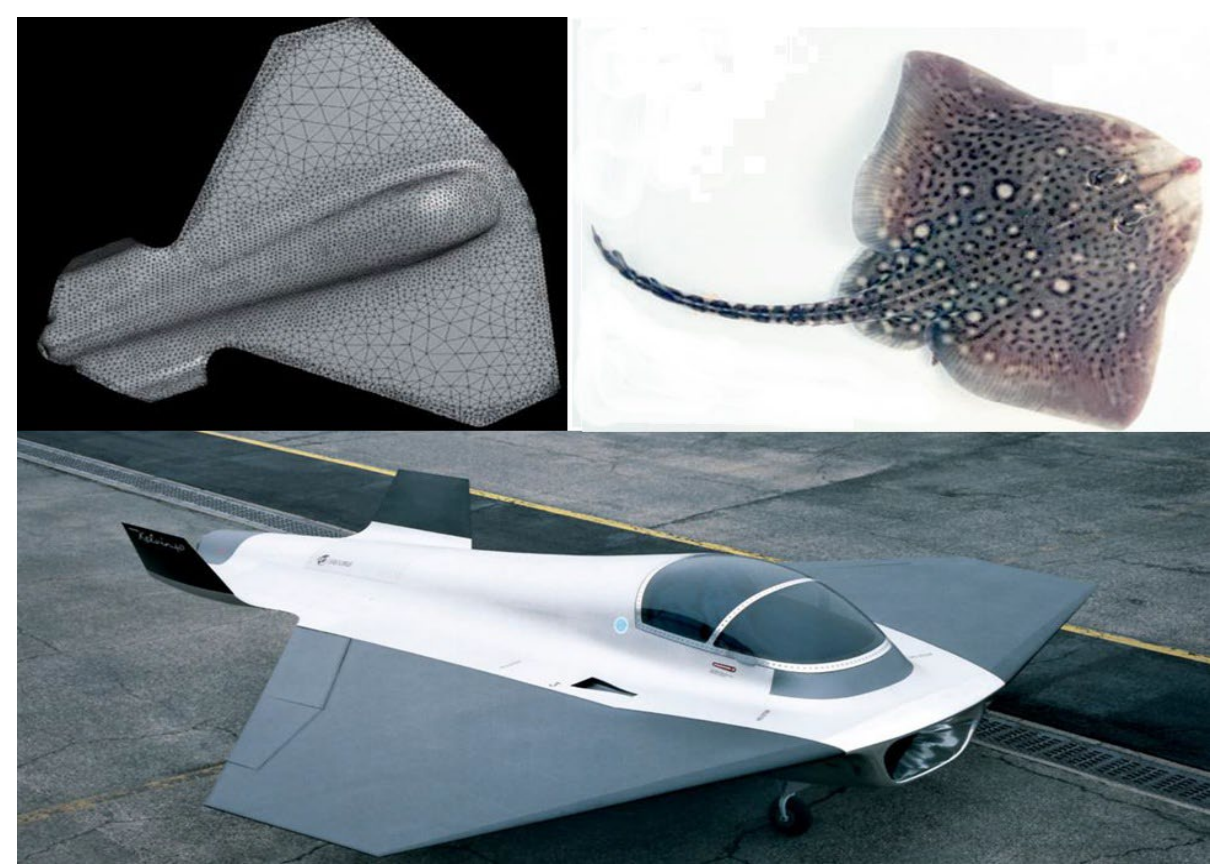


Şekil 4. Shultzeworks endüstriyel tasarım stüdyosu tarafından tasarlanan Philco Pc'de vintage ürünler soyutlanarak retro bir tasarıma ulaşılmış [25].

Prof. Dr. Oğuz Bayrakçı endüstriyel tasarım disiplininde eğretileme ve analoji eylemlerinin başarıya ulaşması için iki temel şart öne sürer [26]. Bunlardan ilki analojinin kaynak olarak kullanacağı olgu ya da kavram ile analoji aktarımının yapılacağı ürün tasarımı arasındaki anlambilimsel iliski doğru bir kurulmalıdır. İkincisi ise ürün tasarımında analoji yapılırken kaynak olarak kullanılan olgu olduğu gibi aktarılmamalı bunun yerine gereksiz ayrıntılar çıkarılarak analoji gerçekleştirilmelidir. Diğer bir deyişle mutlaka soyutlanmalıdır. Eğer bu iki şart sağlanırsa yeni ürün tasarımının yaratıcılık bağlamında avangart ve ikonik tasarım olma şansı artar.

Burada avangart tasarım kendi tarzını benzersiz ve ilk olarak ortaya koyarak öncü haline gelen tasarım anlamında kullanılmaktadır. İkonik tasarım ise kendine has tarzıyla kendi benzerleri içinden sıyrılarak ve hafızalarda yer edinerek sembollesen ürün tasarımları kullanılmaktadır. Eğer bu iki sarttan birisi ya da her ikisi de yerine getirilemezse bu tasarım "kitch" tasarım durumuna düşme riski taşır. Burada "kitch" kavramı adi, ucuz ya da bayat anlamlarına gelen bir Fransızca sözcüktür. Bu kavramların daha iyi anlaşılabilmesi için hem avangart ve ikonik tasarımlardan hem de kitch tasarımlardan örnek verilmesi uygun görüldü.

Örneğin endüstri tasarımcısı Marc Newson tarafından tasarlanan "Kelvin 40" isimli uçak tasarımına bakıldığında bu uçağın vatoz balığından esinlenerek ve analojide bulunularak tasarlandığı görülür. İlk olarak vatoz balığı yüzgeç yerine kanatlı bir yapıda yaratılmıştır ve suyun içerisinde âdeta uçarak ilerler. "Kelvin 40" da bir uçak olarak tasarlandığı için biçimişlev ilişkisi açısından anlambilimsel bağıntının doğru bir şekilde kurulduğu söylenebilir. İkinci olarak da "Kelvin 40" tasarlanırken uçağı doğrudan ilgilendirmeyen vatoz balığına ait biçimsel özelliklerin soyutlanarak tasarımına aktarıldığı gözlenmektedir. Vatoz balığının gözleri ya da kuyruk kısmı elenmiş, kanat yapıları ise sadeleştirilerek taşınmıştır.



Şekil 5. Endüstri tasarımcısı Marc Newson tarafından Vatoz balığından analojide bulunularak tasarlanan Kelvin 40 isimli uçak tasarımı [27].

Diğer taraftan aşağıdaki görselde sunulan bilgisayar faresine bakıldığında Mercedes marka bir otomobilden analojide bulunularak tasarlandığını görebiliriz. Ancak bir otomobil ile bilgisayar kullanımı arasında mantıklı bir kavramsal bağıntı bulunmamaktadır. Ayrıca bulunulurken analojide biçimin hiçbir soyutlama yapılmadan olduğu gibi alıntılandığı görülmektedir. Örneğin bilgisayar kullanımıyla hiçbir ilgisi bulunmayan otomobilin tekerleri ve farları aynen bilgisayar faresi tasarımına taşınmıştır. Dolayısıyla bu bilgisayar faresi "kitch" tasarım olarak adlandırılabilir.

Diğer resme bakıldığında ise yine aynı şekilde aralarında anlambilimsel hiçbir örüntü olmayan bir çizgi roman karakteri olan Mickey Mouse kullanılarak soyutlanmaksızın iletişim aracı olarak telefon tasarlandığı görülüyor. Buradaki eğretilemede de hem anlam bilimsel bağıntı kurulmadığı hem de soyutlama işlemi yapılmadığı için bu Mickey Mouse'lu telefonu da kitch bir ürün tasarımı olarak değerlendirmek mümkündür.



Şekil 6. Anlambilimsel örüntü olmaksızın ve soyutlama yapılmadan analojide bulunularak tasarlanan kitch ürün örnekleri [28-29].

Çalışmanın bu noktasında soyutlama kavramına ve önemine daha yakından bakılması faydalı Tasarım disiplinlerinde başarılı olacaktır. tasarımların yapılabilmesi icin tasarım problemlerinin doğasının incelenmesi, idrak edilmesi ve doğru bir sekilde tanımlanmasına ihtiyaç duyulur. Burada soyutlama yöntemi nedenlerin ve sonuçların doğasını etraflıca anlamaya önemli bir katkı sunar. Soyutlama hem biçimsel hem de işlevsel açıdan tasarım problemleriyle ilgili en önemli bilgilere ulaştırır çünkü somut veriler tasarımcılara sadece biçime yönelik yüzeysel bir gerçeklik sunabilir [30]. Soyutlamak, tasarımların veya kavramların gerekli ve öz olan kısımlarını gereksiz detaylardan ayırt etmeye yardım eder [31]. Hegel'e göre soyutlama, görünür hale gelme sürecinde olduğu halde henüz tam görünür hale gelerek aşikâr olamamış varlığa dair bilginin gerçekliğini temsil etmektedir [32]. Bir teknik olarak bicimsel soyutlama, tasarımcılar süreçlerinin tarafından tasarım erken aşamalarında çevreye dair bilgileri toplamak, biçimsel eskiz araştırmaları yaparak tasarım fikirlerine ulaşmak ve ürün tasarımlarını gerekli olmavan detavlardan kurtarmak kullanılmaktadır [31]. Bu nedenle soyutlama eyleminin yaratıcı düşünme becerilerinin ortaya çıkmasında bir katalizör ya da tetikleyici olarak işlev gördüğü söylenebilir. Tasarım süreçleri içerisinde bir ürün yaratılırken tasarımın uygulanabilir olması için sadece soyut düzlemde çalışmak yerine soyut ve somut arasında bir gel git yaşanması gerekir. Nihayetinde tasarımcılar soyut çalışmalar eşliğinde giderek somutlaşan bir ürün tasarımı gelistirmek için soyut ve somut arasındaki yaratıcı düsünme döngüde melekelerini geliştirirler [31].

2.2. YZ ve Endüstriyel Tasarım Eğitimi Alanındaki Kullanım Olanakları

bilgisayar Yapılan destekli çalışmalar teknolojide yaşanan hızlı gelişmelerle birlikte tasarım, mimarlık ve sanat disiplinleri de dâhil olmak üzere birçok alanda destekleyici araçlara dönüşmüştür. Ancak insana ait olan yaratıcı düşünme ve farklı bakış açıları bir araç olarak kullanılan teknolojiden ve diğer yardımcı araçlardan daha önemlidir [33]. Literatür taraması yapıldığında YZ uygulamalarının endüstriyel tasarım, moda tasarımı, iletişim tasarımı, grafik tasarımı, iç mimarlık, mimarlık gibi görsel ağırlıklı disiplinlerde kullanımına dair yapılmış hem akademik hem de pratiğe

yönelik çalışmalarla karşılaşılmaktadır. Bunlara ilk olarak YZ uygulamalarının mimarlık disiplinleri için önemli bir şans olduğunu ve disiplinin gözden kaçan kısımlarını yakalayarak daha etkili ve çeşitli sonuçlara ulaşılmasını sağladığını iddia eden Chaillou'nun çalışması örnek verilebilir [34].

Peyzaj mimarlığı ve iç mimarlık disiplinlerinde kullanılmak üzere özelleştirilerek geliştirilmiş YZ uygulamalarıyla da karşılaşılabilir. Örneğin Visualize AI, Interior AI, Spacely AI, Homevisualiser AI, REimagine home gibi YZ uygulamaları bilgisayar ortamına yüklenen hem iç hem de dış mekân mimarisine dönük fotoğrafları arzu edilen tasarım stillerine uygun olarak yeniden tasarlayabilmektedir. Örneğin bahsi geçen YZ uygulamaları, yüklediğiniz dijital görseldeki bir oturma odası tasarımını Victoria dönemi, Destill, Japonizm, Art Neuvo vb. pek çok tasarım üslubuna ve trendine göre yeniden çizebilmektedir.

Literatürde YZ'nın tasarım disiplinleri üzerindeki olumlu ve olumsuz tesirlerinin hangisinin ağır bastığının incelendiği çalısmalar da bulunmaktadır. Bu çalışmalardan birisi de Radhakrishan tarafından 2023'te yazılan ve "Is Midjourney-AI New Anti-Hero of Architectural Imagination and Creativity?" başlığını taşıyan makaledir. Burada Radhakrishan, Midjourney vb. YZ uygulamalarının mimarlık açısından olumsuz tesirlerinin ağırlıkta olduğunun söylenemeyeceğini ancak doğru kullanılmaması halinde olumsuz tesirlerinin çıkabileceğini belirtiyor öne [35]. Radhakrishan'a göre YZ ile elde edilen çıktılar insan yorumuna ve müdahalesine ihtiyaç duymakta ve yaratıcı düşünmeyi henüz tam olarak otomatik hale getirememektedir. Paniker mimarlık disiplininde eğitim öğrencilerin bazılarının tasarım süreçlerindeki tasarım olasılıklarını görsel hale getirmekte zorlandığını, bu tür öğrenciler için YZ'nın varatici düşünme bağlamında yardımcı olabileceğini söylüyor [36].

YZ uygulamaları grafik tasarımı alanında da etkili bir şekilde kullanılmaktadır. Grafik tasarımcılarının süreç içerisinde harcadıkları zamanı düşürmekte ve tasarım olasılıklarını genişleterek yaratıcı düşünme becerilerini beslemektedir [37].

Grafik tasarımı disiplinlerinin yan dalları olarak değerlendirilebilecek haberler için görsel tasarımlar hazırlama, logo tasarımları, web sayfalarının tasarlanması, fotoğraflar üzerinde çeşitli düzenlemeler yapılması gibi çeşitli grafik YZdisiplinlerinde uygulamalarından yararlanılmaktadır. Bu YZ uygulamalarına Opal örnek olarak verilebilir. Opal yazılı olarak girilen bir metni genel olarak idrak ederek o metnin içeriğine uygun görseller hazırlamakta genellikle iletişim tasarımı alanında kullanılmaktadır. Liu ve arkadasları tarafından 2022 yılında yapılan bir çalışmada Opal YZ uygulamasından yararlanan örneklem grubunun kullanmayan guruptan çok daha fazla sayıda kullanılabilir sonuca ulaştığı gözlemlenmiştir [3].

disiplinler için özellesmis Belirli YZkullanımlarıyla moda ve tekstil tasarımı disiplinde de karşılaşılmaktadır. Bunlara The New Black, Fashion Q, Ablo, Zemu, Cala, Stilist ve TeeAI gibi moda ve tekstil tasarımı için özel olarak geliştirilmiş YZ uygulamaları örnek olarak verilebilir. Bu uygulamalar yüklenen fotoğraflardaki moda stilini anlayarak tasarımcının çizdiği kıyafetlerle arakesit oluşturabilmekte, farklı moda çizgilerini ve stillerini bir araya getirterek yeni ve yaratıcı kıyafet tasarımları yapabilmektedir. Ayrıca bir cinsiyet için tasarlanmış bir kıyafeti karşı cins için yorumlayabilmekte, bir kıyafeti taşıyan bir modelden ödünç alarak farklı etnisite ve cinsiyetteki modellerin üstüne giydirebilmektedir. Bu uygulamalardan Fashion Q adlı YZ uygulaması Jeon ve arkadasları tarafından 2021 yılında yapılan bir çalışmada 10 moda ve tekstil tasarımı uzmanına kullandırılarak gözlemlendi. Gözlem sonunda Fashion Q YZ uygulamasının farklı ve yaratıcı düşünme becerilerini tetiklediği için yaratıcı tasarım süreçlerine yardımcı olduğu iddia edildi [38]. Endüstriyel tasarım alanında yaratıcı düsünme biçimlerine destek olmak üzere YZ'dan önce üretken tasarım uygulamaları geliştirildi. Üretken tasarım uygulamalarına yönelik çalışmalar izlendiğinde 1980 öncesine kadar geriye gitmektedir [39]. Üretken tasarım uvgulamalarının ilk örneklerinde karmasık tasarım strüktürlerinin çözümlenmesiydi. Daha sonraları tasarım çalışmalarının yaratıcılık bağlamındaki araştırmalarında destekleyici olarak gelişimini sürdürdü [40].

Üretken tasarım uygulamalarıyla yapılan tasarım calısmalarında. klasik tasarım metodolojileriyle kıyaslandığında hem nitelik hem de nicelik bakımından daha zengin ve etkili tasarım alternatiflerine ulasılmaktadır. Bu alternatifler endüstriyel ürünlerin ya da bu ürünleri oluşturan parçaların ağırlıklarının azaltılmasında, performanslarının geliştirilmesinde, daha uzun ömürlü olmalarında, bicimsel yaratıcılıkta, gereksinimlere göre özelleştirilmelerinde ortaya çıkabilmektedir [41].

3. YÖNTEM

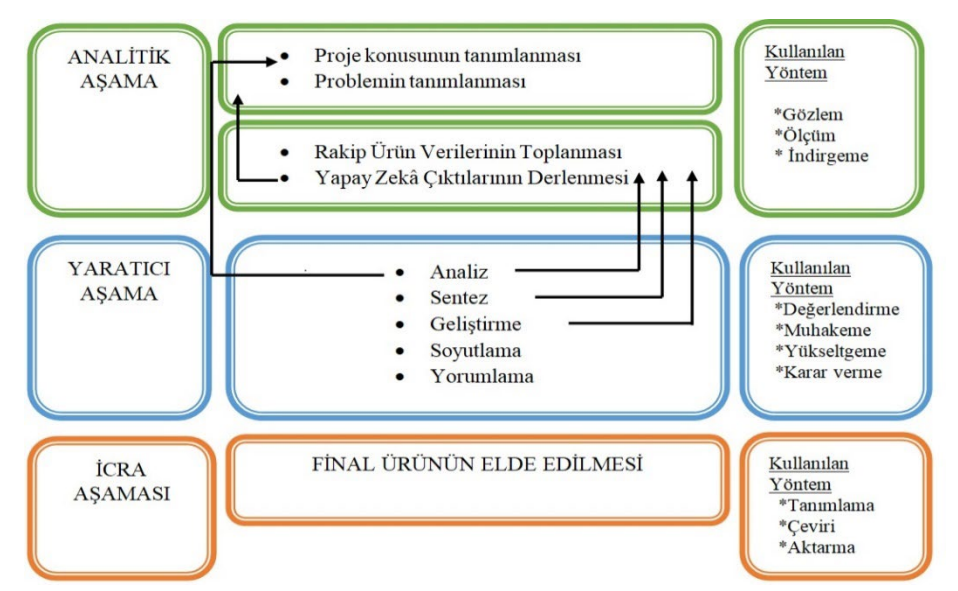
Bu çalışmada başlıca iki yöntem kullanılmıştır. İlk olarak YZ kullanılarak elde edilen tasarım çıktılarında karşılaşılan olumsuzluklar ve zorlukların aşılmasında kullanılan Cross ve Archer tarafından geliştirilen "Cross ve Archer Tasarım Süreçleri Yöntemi" dir. İkinci olarak ise araştırmacının proje süreçlerinde YZ kullanımının öğrencilerin ve proje çıktılarının üzerinde edindiği gözlemlerin öğrencilerin kişisel deneyimleriyle kontrol ve mukayese edilebilmesini mümkün kılan nitel araştırma yöntemlerinden yarı yapılandırılmış yüz yüze görüşme yöntemidir.

3.1. Cross ve Archer Tasarım Süreçleri Yöntemi

Bu makale, endüstriyel tasarım eğitiminde öğrencilerin yaratıcı düşünmeyi gerektiren proje süreçlerinde tıkanıklık yaşadıkları adımlarda YZ kullanımını teşvik ederken karşılaşılan olumsuzlukları gidermek için YZ çıktılarını soyutlayarak ve veniden yorumlayarak bir tasarım yöntemi geliştirme fikrine odaklanmaktadır. Günümüzde birçok bilim, disiplin, eğitim ve mesleği yoğun bir şekilde etkileyen YZ alanındaki gelişmelerin endüstriyel tasarım disiplinine ve bu disiplinin eğitimine doğru bir şekilde entegre edilmesi mesleğin gelisimi ve çağa doğru bir sekilde ayak uydurabilmesi için oldukça önemlidir. Bu nedenle endüstriyel tasarım proje/stüdyo dersi kapsamında YZ uygulamalarıyla elde edilen sonuçların disiplinin gereksinim ve karakteriyle uyumlu hale getirilebilmesi için bir model gelistirilmistir. Bu model kendisine Archer ve Cross tarafından geliştirilen bir modeli örnek almaktadır. Bu model endüstriyel tasarım eğitiminde kullanılarak YZ uygulamalarına dayalı bir tasarım süreci incelenmeye çalışılmıştır. Tasarım süreci, bu süreçte kullanılan donanım ve yöntemlerden oluşan

eylem sırası olarak tanımlanmaktadır. Bu süreci etkili bir şekilde desteklemek için adımlar doğru bir şekilde atılmalıdır [5]. Geri bildirime dayalı olarak çalışan yaratıcı aşamada analiz, sentez ve geliştirme süreçleri bulunmaktadır. Bu aşamada YZ tarafından üretilen çıktıların

disiplinin karakteri ve gereksinimleriyle örtüşmeyen tarafları soyutlama, yorumlama ve yeniden tasarlama yoluyla tekrar ele alınır. Cross ve Archer tarafından önerilen tasarım süreçleri "analitik", "yaratıcı" ve "icra" olmak üzere üç ana başlıktan oluşmaktadır. [8-14].



Şekil 7. Çalışmada kullanılan endüstriyel tasarım süreçleri

Endüstriyel Tasarım Stüdyo Süreci

Selçuk Üniversitesi Güzel Sanatlar Fakültesi Endüstriyel Tasarım Bölümünde 2023 yılının güz yarıyılında kendisi de bir endüstri tasarımcısı olan Dr. Öğretim Üyesi Mahmut Celaleddin Kaleli'nin idaresinde yürütülen Endüstriyel Tasarım 3 dersinde üçüncü sınıf öğrencileri tarafından tasarlanan endüstriyel ürünler vaka analizi olarak sunulmaktadır. Daha önce de belirtildiği gibi bu çalışmanın ilk amacı öğrencileri YZ uygulamalarıyla tanıştırarak proje/stüdyo derslerini daha etkili hale getirecek bir strateji geliştirmekti.

Özellikle ürünlerin dıs formlarının yaratılmasında öğrencilerin yaratıcı düşünme bağlamında yaşadıkları zorlukları ve tıkanıklıkları aşabilmek için YZuygulamalarının eğitim bilimsel bir araç olarak kullanılabileceği değerlendirildi. Ancak YZ uygulamalarıyla yapılan ilk denemelerde YZ'nın endüstriyel tasarımın karakteriyle "kitch" örtüsmeven cıktılar ürettiği gözlemlendi. Ayrıca üretilen YZ çıktıları ergonomi ve endüstriyel üretim yöntemleriyle celisebilmekteydi.

Yaşanan erken zorlukların endüstriyel tasarım disiplininin yaratıcı düşünmeyle ilintili soyutlama, eğretileme, yorumlama, ödünç

alma, yeniden tasarlama gibi yöntemleriyle aşılabileceği değerlendirildi. Bu amaçla yukarıda da anlatılan Cross ve Archer'ın önerdiği tasarım yöntemlerinden yararlanılarak bir metot geliştirildi ve uygulandı.

İlk olarak eğitim varıvılı basında Endüstrivel Tasarım 3 dersi kapsamında verilen briefte öğrencilerden elektrikli ev aleti üretmeyen ünlü bir firma eğer elektrikli mutfak aletleri verseydi üretmeye karar nasıl ürünler tasarlanabilirdi sorusuna cevap aramaları istendi. Bu bağlamda öğrencilerden elektrikli ev aletleri üretmeyen ancak belirli bir tasarım felsefesine ve küresel capta tanınırlığa sahip olan bir firma ve de mutfakta kullanılan üç adet elektrikli alet seçmeleri istendi. Daha sonra seçilen firmanın tasarım felsefesine uygun olarak sömestr içerisinde üç adet elektrikli mutfak aleti tasarlamaları talep edildi. Calısmanın ilk adımı analitik calısma aşamasıydı.

Bu aşamada öğrenciler ilk önce seçtikleri elektrikli ev aleti üretmeyen farklı sektörlerdeki firmaların tasarım felsefesini analiz edebilmek için kendi hizmet alanlarında ürettikleri ürünlerin biçim dillerini incelediler. Ardından kendilerine proje konusu olarak sunulan

elektrikli mutfak aletlerinden tasarlamak istedikleri ürünlerin işlevsel açıdan piyasadaki müstakbel rakiplerini incelediler. Bu aşamanın ardından "Chat GPT" ve "Midjourney" YZ uygulamalarına "seçilen elektrikli mutfak aleti üretmeyen firma kendi tasarım felsefesine uyan öğrencinin seçtiği bir mutfak aleti üretseydi bu ürünlerin tasarımı nasıl olurdu?" sorusu yöneltilerek çıktılar elde edildi. Burada 2023 yılında sınırlıda olsa gerçekçi render kalitesini ücretsiz kullanıma sunduklarından ve metinden görsel olusturmada öncü olduklarından "Chat GPT" ve "Midjourney" YZ uygulamaları tercih edildi. Sonucta üç küme seklinde gerekli veriler derlenerek analiz aşaması tamamlandı. Bu üç küme özetle şu şekilde oluştu:

- 1. Öğrenci tarafından seçilen, elektrikli mutfak aleti üretmeyen, uluslararası tanınırlığı ve kendine özgü tasarım felsefesi olan markanın ürünleri incelenerek elde edilen veriler.
- 2. Öğrencilerin yarıyıl içinde tasarlamak üzere seçtiği üç adet elektrikli mutfak aletinin piyasadaki müstakbel rakiplerini inceleyerek elde ettikleri tasarım problemlerine dair veriler.

3. YZ tarafından üretilen veriler.

Verilerin toplanmasının ardından tasarım öğrencileri endüstriyel tasarım 3 dersinin stüdyo kültürü ortamında markalara, rakip ürünlere ve YZ çıktılarına dair bulgularını ve ön bilgilerini kendi aralarında ve dersin yürütücüsüyle tartışarak bilgi alışverişinde bulundular. Böylece tasarım sürecinin analiz asaması tamamlanmıs oldu. Tasarım sürecinin varatici asamasına geçildiğinde verilen yönergelerle YZtarafından. tasarlanan ürünlerin endüstriyel tasarım disiplininin karakteri ve gereksinimleriyle uyuşmayan kısımlarıyla faydalı ve etkili bulunan kısımları tekrar incelendi. Tasarım disiplinlerinde yaratıcı düşünmeyi destekleyen eğretileme, ödünç alma, benzetme, soyutlama, ayıklama, yorumlama, sadeleştirme gibi eylemler uygulanarak gerçekleştirilen çalışmalarla alternatif tasarımlara ulaşıldı.

Böylece tasarım sürecinin yaratıcı aşaması tamamlanmış oldu. Uygulama aşamasında elde edilen alternatif tasarım modelleri arıtılarak seçenekler teke düşürüldü. Bu aşamada seçeneklerin en iyi tarafları bir araya getirilerek nihai tasarımlara yaklaşıldı. Daha sonra endüstriyel üretim yöntemlerine, ergonomi

standartlarına ve doğru biçim işlev ilişkisine uygun detaylı tasarımlar yapılarak uygulama aşaması tamamlandı.

3.2. Nitel Araştırma Yöntemi: Yarı Yapılandırılmış Yüz Yüze Görüşme ve Tematik Analiz

Tasarım süreçlerinde YZ uygulamalarının kullanılmasının öğrenciler üzerindeki olumlu olumsuz etkilerini arastırmacının gözlemlerine paralel olarak inceleyebilmek için nitel arastırma vöntemlerinden yapılandırılmış yüz yüze görüşme ve tematik analiz yöntemlerinden yararlanılmıştır. Çalışmanın bu kısmında öğrencilerin kendi deneyimleri üzerinden YZ'ya dair algıları ve konmaya düşünceleri ortaya çalışıldı. Calısmanın nitel arastırma kısmındaki örneklem evrenini 2023 yılının güz döneminde Endüstriyel Tasarım 3 proje/stüdyo dersini alan Üniversitesi Endüstriyel Tasarım Bölümü öğrencileri arasından gönüllü olarak öğrenci oluşturmaktadır. seçilen 10 öğrencilerin seciminde amaclı örneklem seçimlerinden birisi olan aşırı örneklem seçimi tercih edilmistir. Dolayısıyla bu arastırmaya dâhil edilen öğrenciler akranlarına oranla YZ'yı daha etkili olarak kullandıkları değerlendirilen öğrencilerden oluşmaktadır. Aşırı ve aykırı durumlar, bireyler ya da olgular normallerine göre çok daha zengin bir veri ortaya koyabilir ve araştırma problemini derinlemesine ve çok boyutlu bir sekilde idrak etmemizi kolaylaştırabilir [42]. Amaçlı örneklem secimlerinde örneklemin büyüklüğünü araştırmada elde edilen bulgular belirler. Asıl hedefin mümkün olduğu kadar farklı bilgi ve bulguya ulaşma olduğu koşullarda analiz edilen son örneklemlerden elde edilen bulguların yeni bilgiler getirmediği görüldüğünde örneklem sayısının yeterli büyüklüğe ulaşmış olduğu anlaşılır [43]. Bu çalışmada örneklem grubunu olusturacak öğrenci sayısı çalısmanın gidisatına göre belirlendi. Katılımcıların sayısı 5'e ulaştığında gelen verilerin kendisini tekrar etmeye başladığı, 8'e ulaştığındaysa yeni veri gelmemeye başladığı gözlemlendi.

Bu nedenle örneklem evreni 10 tasarım öğrencisiyle sınırlandırıldı. Örneklem evreni 6 erkek ve 4 kız öğrenciden oluşmaktadır. Yapılan görüşmelerde öğrencilere yöneltilen sorular çalışmanın sonunda yer alan ekler kısmında sunuldu. En temelde bu soruların içeriğini YZ kullanımının öğrenciler ve

projeleri üzerindeki olumlu ve olumsuz etkilerini desifreve vönelik aravıslar oluşturmaktadır. Nitel araştırmalarda kullanılan yöntemlerden birisi de mecaz kullanımıdır. Mecazlar özellikle nasıl ve niçin sorularıyla birlikte kullanıldığında normal betimlemelere göre daha zengin ve derin anlayışlara ulaşmamızı sağlayan bir anlam ve ifade gücüne sahiptir. Ayrıca analiz edilmeleri sınıflandırılmaları diğer nitel yöntemlere göre daha kolaydır [42]. Bu nedenle görüşmelerin sonunda katılımcılara YZ'yı insan ve insan dısı varlıklara benzetmelerini talep eden sorular da soruldu. Genel olarak bu sorularla öğrencilerin YZ'ya dair algılarının ve düşüncelerinin en gerçekçi fotoğrafı çekilmeye çalışıldı. Yüz yüze yapılan görüşmeler öğrencilerin müsaadeleriyle cep telefonunun ses kayıt özelliği kullanılarak kavdedildi. Kavdedilen sesler daha sonra metne geçirildi. Metinler defalarca okunarak dikkatlice "in vivo" olarak kodlamalar yapıldı. Tematik kodlama, elde edilen verilerden çalışmanın amacına yönelik kesitler elde etmek icin verilerin cesitli kısımlarına sembolik kısaltmalar yapmaktır [44]. "In vivo" olarak bahsedilen ise kodlamalar yapılırken mümkün olduğunca katılımcıların ifadelerinin aynen kullanılmasıdır [45]. Son olarak oluşturulan kodlar kategorize edilerek tematik analiz gerçekleştirildi. Eğer katılımcının kullandığı anlamlı ifadeleri aynen kullanmak mümkün olmazsa arastırmacı katılımcının ifadelerine en yakın anlama gelecek ifadeleri seçerek kullanabilir [46].

4. BULGULAR

4.1. YZ Kullanımıyla Edinilen Tasarımların Cross ve Archer Tasarım Süreçleri Yöntemiyle Yeniden Tasarlanmasıyla Ulaşılan Bulgular

Calışmada ilk olarak öğrencilere "İmage FX", "ChatGPT" "Middjourney" ve örnek kullanımlar esliğinde uygulamaları gösterildi. Elde ettikleri YZ çıktılarındaki olumsuzlukları giderebilmeleri için tasarımda eğretileme. yorumlama ve soyutlama kavramlarının aşamaları özgün ve yaratıcı süreçlerinde öğrencilere tasarım calısıldı. Öğrenciler YZ kazandırılmava

uygulamalarıyla elde ettikleri görsel çıktılara yaratıcı düşünme becerilerini geliştirmek için yorumlama soyutlama, eğretileme ve eylemlerini uyguladılar. Bu eylemler endüstriyel tasarımda öğrencilere özgün ve yaratıcı düşünme becerileri kazandırmayı amaçlamaktadır. YZ uygulamalarının yaratıcı evlemlerle paralel sekilde kullanılması geleneksel, alışılmış tasarım yöntemlerini izlemekten ziyade, kullanıcıların benzersiz tasarım gereksinimlerine YZ uygulamaları gibi güncel teknolojilerle vanıt veren essiz, yaratıcı tasarımlar gelistirmelerine yardımcı olmaktadır. Calısmanın ilk asamasında öğrencilerin elde ettiği YZ çıktılarının çeşitli alternatiflerle uygunluğu belirtilmiş ve seçilen YZ çıktılarının soyutlama, eğretileme ve yorumlama aşamalarına geçilmiştir. Soyutlama, eğretileme ve yorumlama yapılırken Prof. Dr. Oğuz Bayrakçı'nın ürün semantiğinde iletisimsel önerileri temel alınmıstır. Calısma YZ uygulamaları tarafından tasarlanan ürünlerdeki tasarım problemlerinin değerlendirilmesi, analizi vorumlanarak veniden tasarlanmasına dayanmaktadır. Öğrencilerin YZ çıktılarından yararlanarak ve onlara tasarım disiplinlerinin yöntemleriyle müdahale ederek gerçekleştirdikleri ürün tasarımları stüdyo/proje dersi kapsamında tartışılmış ve yorumlanmıştır. YZ'nın ürettiği ürün tasarımlarında biçimsel ve oransal değişimler, dönüşümler yaşanmıştır. cıktılarının tasarım disiplinlerivle uzlaşmayan kısımları elenerek, yol gösterici nitelikteki tarafları kullanılarak eşsiz, yaratıcı nitelikte ürün tasarımlarına ulasılmıştır. Böylece tasarım sürecinde YZ yardımıyla nihai ürüne ulaşılırken soyutlama, eğretileme ve yorumlama önemli bir rol oynamaktadır. YZ soyutlanmasında cıktılarının yorumlanmasında yaratıcı düsünme kavramı kopya olmayan, kendine özgü düşünme biçimleriyle ilişkilendirilmektedir. Bu çalışma da öğrencilerin benzersiz sonuçlar elde ettiğini göstermektedir. Bu durum tasarımcıların yaratıcılığında YZ gibi güncel teknolojilerin bazı handikaplarına rağmen öğrencilerin yaratıcı düşünme becerilerinin gelişiminde oldukça etkili olabileceğini göstermektedir.



Şekil 8. 3.Sınıf Öğrencisi Arif Kemal Söylemez'in "Porche" Otomobil Firması İçin Tasarladığı Kahve Yapma, Ekmek Kızartma ve Tost Makinesi Tasarımları



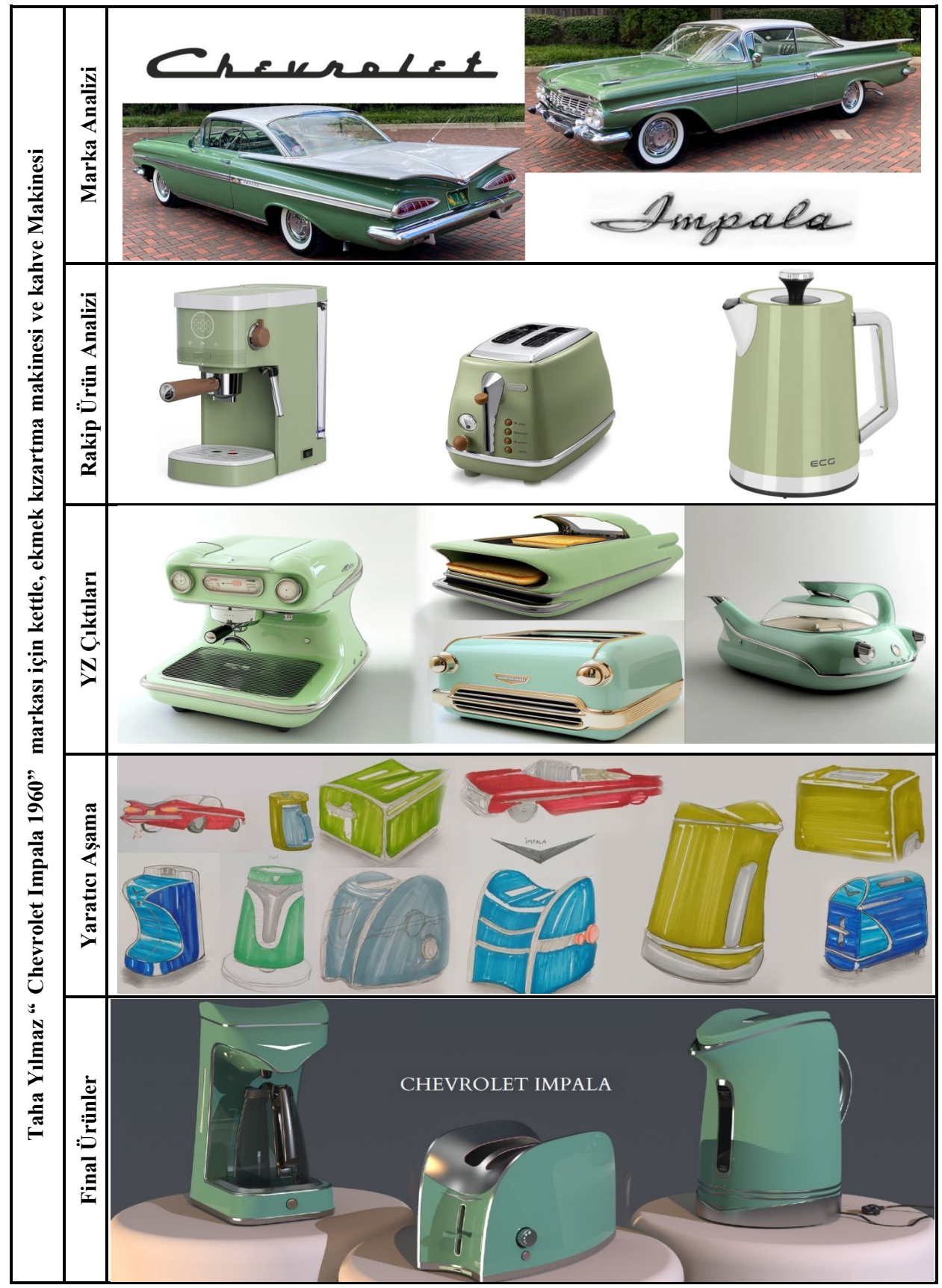
Şekil 9. 3. sınıf öğrencisi Kübra Sepetçi'nin "Volkswagen Beetle" otomobil firması İçin tasarladığı Airfry, Kettle ve Ekmek kızartma makinesi tasarımları.



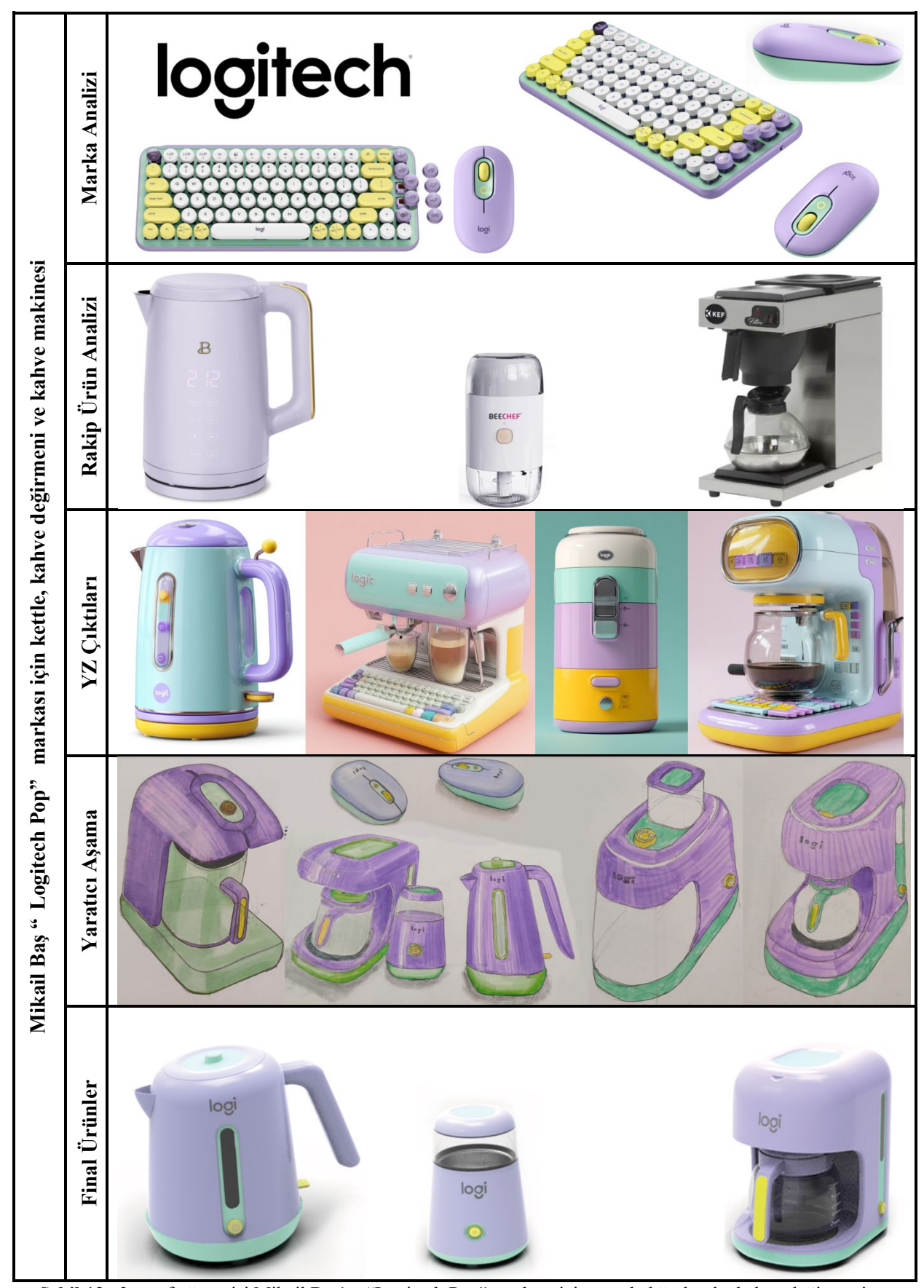
Şekil 10. 3. sınıf öğrencisi Özge Yılmaz'ın "Vespa" motosiklet firması İçin tasarladığı Pamuk şeker yapma, Smoothie Blender ve Mısır patlatma makinesi tasarımları.



Şekil 11. 3. sınıf öğrencisi Betül Tümen'in "Sony Play Station 5" markası için tasarladığı, smoothie blender, tost makinesi ve kahve makinesi tasarımları.



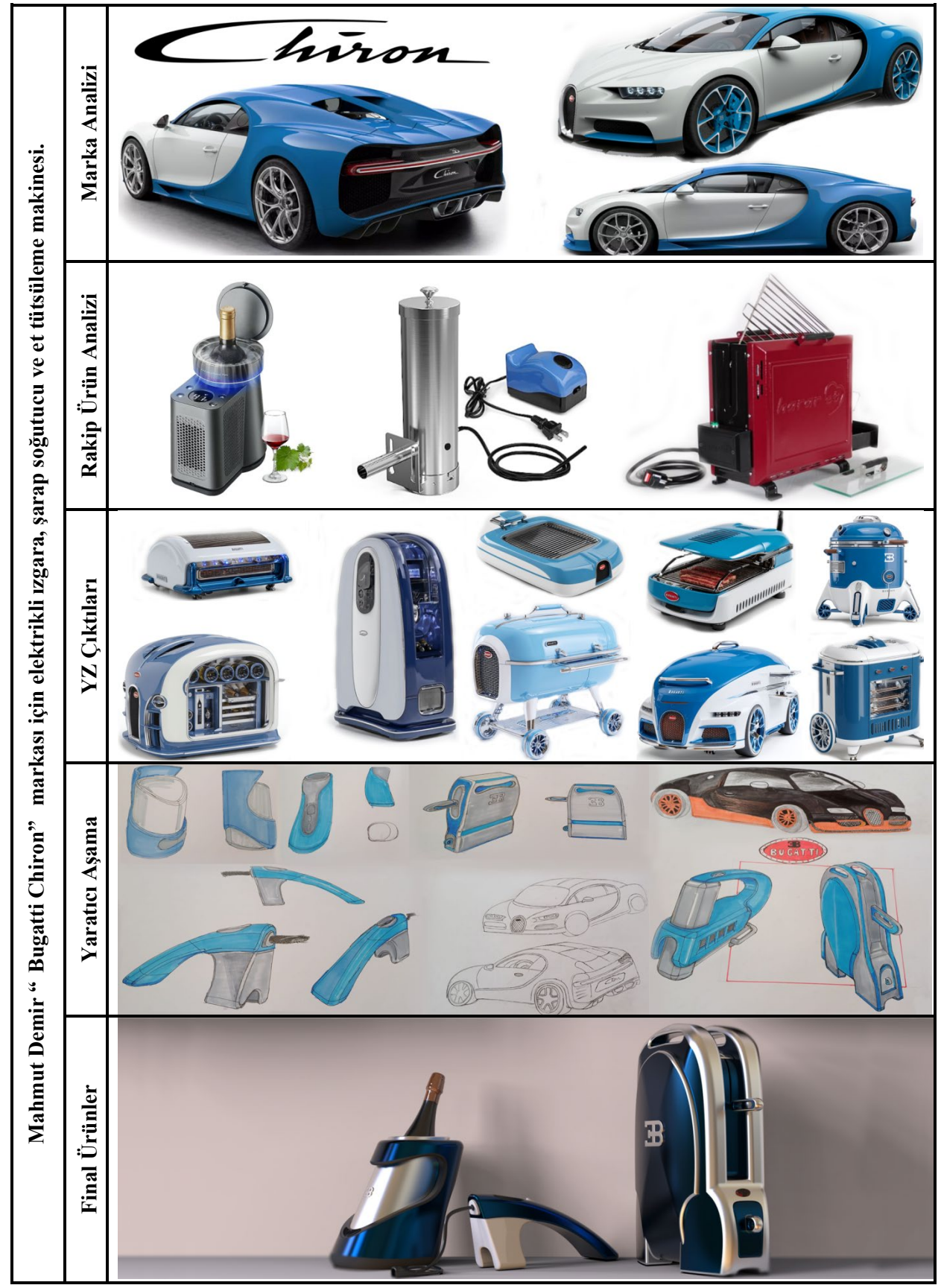
Şekil 12. 3. sınıf öğrencisi Taha Yılmaz'ın "Chevrolet Impala" markası için tasarladığı, kettle, ekmek kızartma ve kahve makinesi tasarımları.



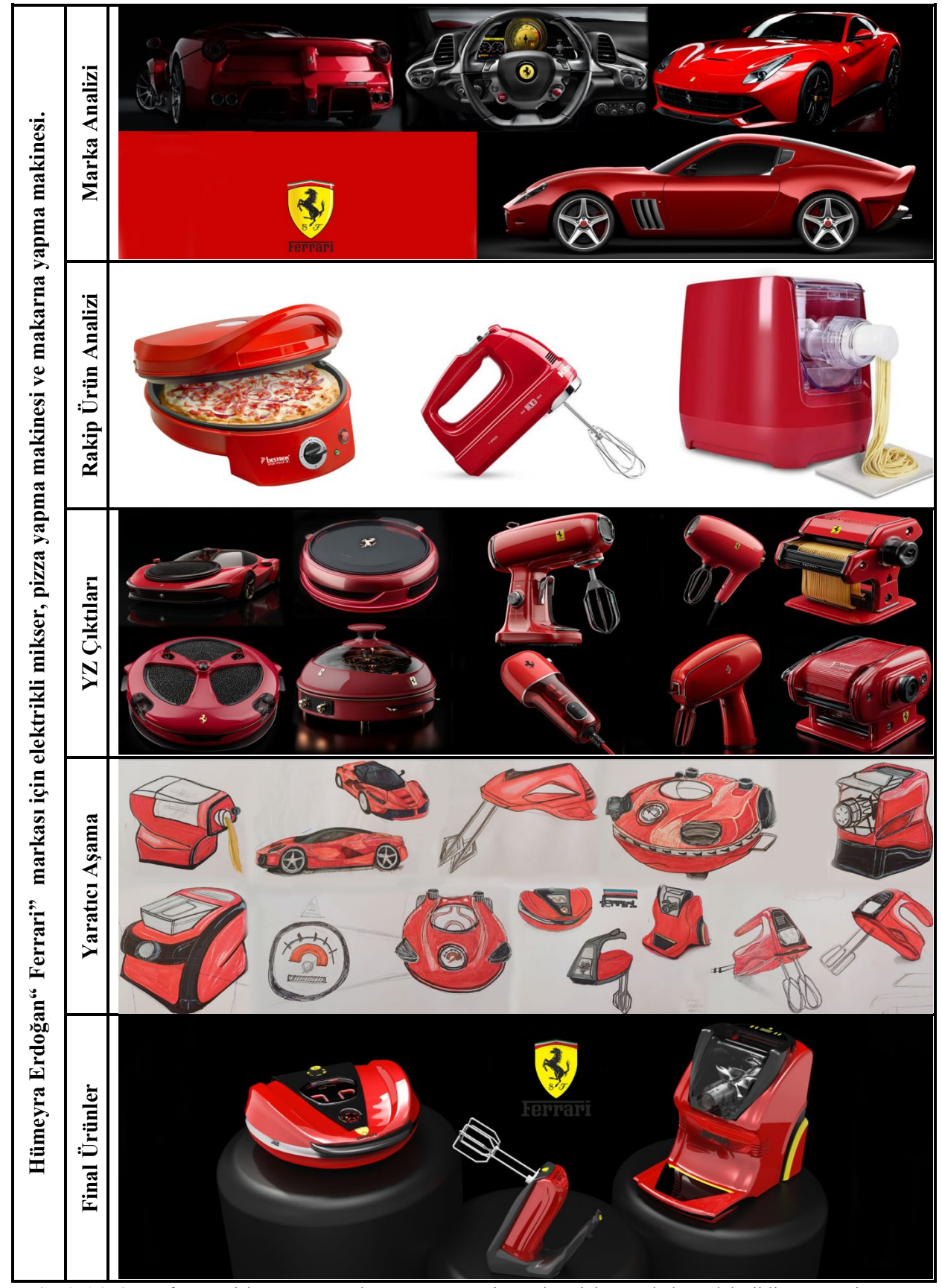
Şekil 13. 3. sınıf öğrencisi Mikail Baş'ın "Logitech Pop" markası için tasarladığı, kettle, kahve değirmeni ve kahve makinesi tasarımları.



Şekil 14. 3. sınıf öğrencisi Riwa Braika'nın "Msi" markası için tasarladığı, kettle, ekmek kızartma makinesi ve smothie blender tasarımları.



Şekil 15. 3. sınıf öğrencisi Mahmut Demir'in "Bugatti Chiron" markası için tasarladığı, şarap soğutucu, elektrikli ızgara ve et tütsüleme makinesi.



Şekil 16. 3. sınıf öğrencisi Hümeyra Erdoğan'ın "Ferrari" markası için tasarladığı, elektrikli çırpıcı, pizza yapma makinesi ve makarna yapma makinesi.



Şekil 17. 3. sınıf öğrencisi Mahmut Yıldız'ın "Kärcher" markası için tasarladığı, airfryer, kahve değirmeni ve filtre kahve yapma makinesi.

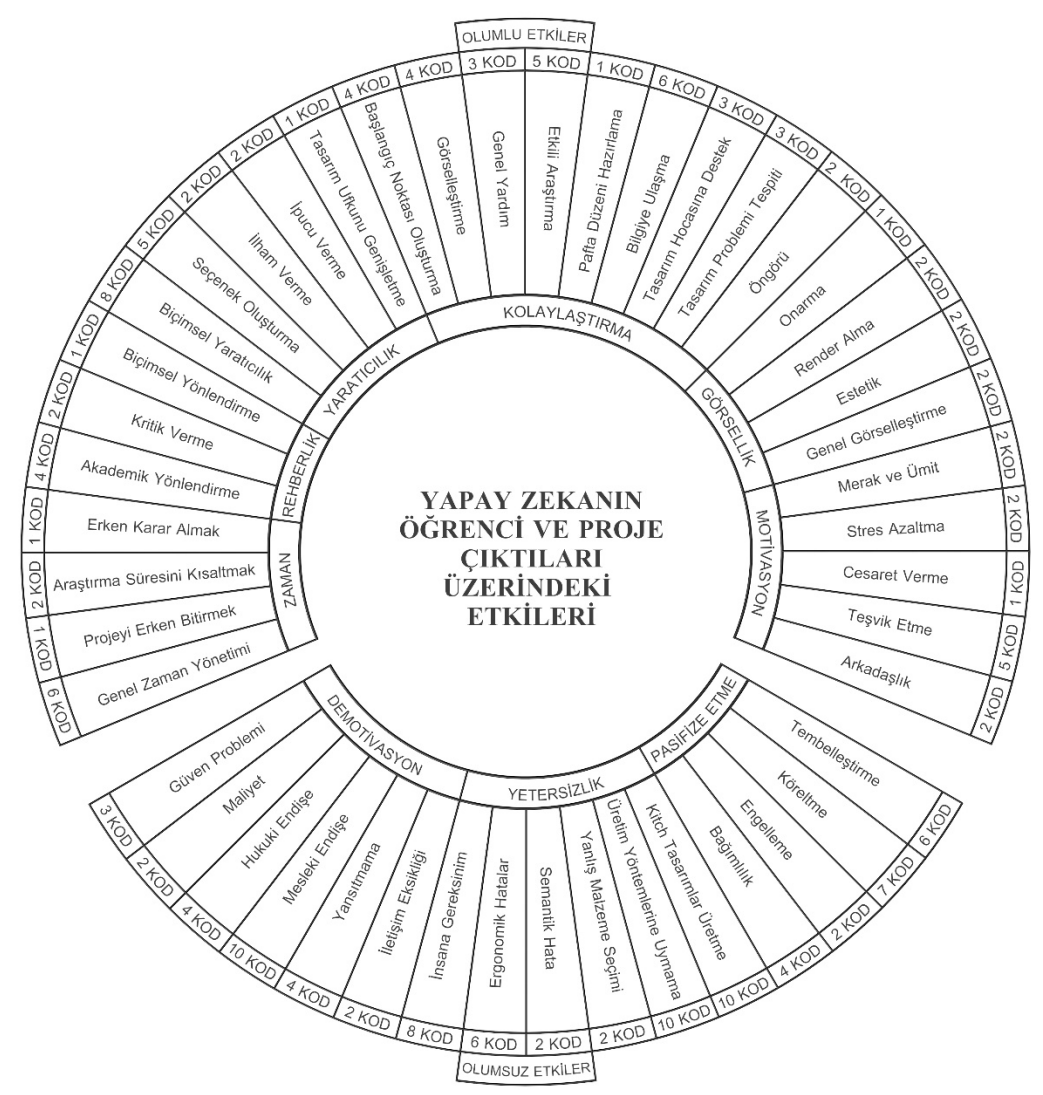
4.2. Yarı Yapılandırılmış Yüz Yüze Görüşme ve Tematik Analizle Elde Edilen Bulgular

Calışmanın bu kısmı nitel araștırma tekniklerinde kullanılan tematik analiz metodu ve nitel arastırma yöntemlerinin araçlarıyla yapılan deşifreleri ihtiva etmektedir. Bu inceleme yüz yüze yapılan görüşmelerde tutulan ses kayıtlarının ilk olarak metne geçirilmesi ve ardından da tematik kodlamaya tabi tutularak elde edilen veriler baslıca iki içermektedir. Bunlardan ilki uygulamalarının tasarım öğrencileri ve proje çıktıları üzerindeki etkileriyle ilgili bulgular ortaya koymaya yönelik sınıflandırma, diğer bir manada indirgeme; bir diğeri ise sözü edilen etkileri görünür kılmaya dönük indirgeme sonucu desifre edilen bulguları yorumlama adımlarıdır. Yöntemin uygulanmasında ilk güz yılının sömestrinde olarak 2023 "Endüstriyel Tasarım 3" proje/stüdyo dersini almış olan ve amaçlı örneklem yöntemiyle seçilmiş olan 10 öğrenciyle yapılan yarı yapılandırılmış görüşmeler cep telefonu aracıvla kavıt altına alınmıstır. Kavıt altına alınan bu görüşmeler daha sonra metne geçirilmiş ve daha sonra tematik analiz uygulanarak 167 adet koda indirgenmiştir. Elde edilen tematik kodlar ifade ettikleri anlam yakınlıkları bakımından gruplandırılmış ve 30'u olumlu 16'sı olumsuz etkileri içerecek şekilde ortak bir isim altında birleştirilerek toplam 46 adet kategoriye indirgenmiştir. Bu kategoriler ise en temel düzeyde baktıkları yönler itibarıyla gruplandırılarak 6'sı olumlu 3'ü olumsuz olmak üzere toplam 9 adet temaya indirgenmiştir. Kodlar röportajların yazıya geçirilmis halinin defalarca gözden geçirilerek analiz edilmesi neticesinde nihai haline gelmis, aralarında mantıksal örüntüler, mana açısından yakınlıklar ve baktıkları yönler itibarıyla kendi içlerinde ilişkilendirilerek iki aşamaya düşürülmüş ve böylece önce kategorilere sonra da temalara ulasılmıstır. Kodların okuyucular tarafından kontrol edilebilmesi, çalışmanın ekler kısmında bulunan kod listelerinin incelenmesiyle mümkün hale gelmektedir. Kodların her birisi hangi katılımcının görüşme kayıtlarına ait olduğunu işaret eden bir harf ve katılımcının görüşme kayıtlarında kaçıncı sırada olduğunu gösteren düzenli bir koordinat sistemiyle izlenebilmektedir.

Mesela ilk röportaj yapılan "A" örnekleminin röportaj kayıtlarında ilk sırada bulunan "AYNI İŞİ DAHA AZ ZAMANDA YAPMAK" kodu "A1" bu sistem icerisinde koduyla gösterilmiştir. Görüşülen son örneklem olan "K" örnekleminin "YZ İNSAN DÜSÜNEMEDİĞİ İCİN TAM BİR EĞİTİMCİ ÖĞRENCİYE GİBİ **DUYGUYU** AKTARAMAYABİLİR" ise "K17" olarak gösterilmistir. Bu sayede kodların çalısmanın bütün bölümlerinde takip edilmesi mümkün kılınmıştır. Çalışmada kodları metin kısmında listelemenin makalenin seyrine zarar vereceği değerlendirildiği için 167 adet kod makalenin metin kısmına yerleştirilmemiş, liste şeklinde ve örneklemlere dağıtılmış şekilde "https:// archive.org/details/celaleddin-kaleli-yapayzeka-makalesi-kodlar" konulmuştur.

Kategoriler, kodlar ile temalar arasında bir ara adım olarak değerlendirilmektedir. Kategoriler ilk olarak birebir aynı olan, çok yakın anlama gelen ya da anlam kökleri yönüyle aynı yöne bakan 167 kodun sınıflandırılarak 46 adet kategoriye indirgenmesi sonucunda elde edildi. Literatürde "taksonomi" olarak adlandırılan bu nitel araştırma tekniği araştırmacının elde ettiği veriler arasında benzerlik örüntüleri kurmasına dayanan sübjektif bir değerlendirme, akıl ve mantık yürütme eylemi olarak değerlendirilmektedir [42].

Bazı kodların aynı anda birden daha fazla kategoriye yerleştirilebileceği tahmin edilmiş, ancak bu bir sorun olarak değerlendirilmemiştir. Çünkü indirgemenin asamalarında daha sonraki zaten kategoriye veya aynı temaya yerleşecekleri öngörülmüstür. Bu noktada arastırmacı tarafından mantık yürütme yoluyla önceden elde edilen kategoriler arasında yakın yönlere bakan ve benzer mana köklerine sahip olanlar tekrar bir araya getirilerek 9 ana temaya ulaşılmıştır. Şekil 6.2'de araştırmaya katılan uvgulamalarının öğrencilerin YZsüreçlerine dâhil edildiği takdirde yaratıcı düşünme becerilerine ve proje çıktılarına nasıl yansıyacağına dair düşünceleri tematik analize tabi tutularak çark seklinde görsellestirilmistir. Bu görselde yüz yüze yapılan görüşmelerden elde edilen kodların kod sayılarıyla birlikte hangi kategorilere ve temalara dâhil oldukları gösterilmektedir.



Şekil 18. Katılımcıların YZ'nın öğrenci ve proje çıktıları üzerindeki etkilerine dair algı ve düşüncelerine yönelik bulguları; kategoriler, temalar ve kod sayılarıyla birlikte gösteren çark biçimindeki şekil.

Temalara ve kapsadıkları kategorilere bakılacak olursa "ZAMAN" teması YZ uygulamalarının proje gelistirmenin bütün süreçlerinde zaman tasarrufu sağlayarak birçok işi daha kısa sürelerde bitirmeye isaret etmekte ve "Genel Zaman Yönetimi", "Projeyi Erken Bitirmek", "Araştırma Süresini Kısaltmak" ve "Erken Karar Almak" kategorilerini içermektedir. "REHBERLİK" teması YZ uygulamalarının proje geliştirme süreçlerinde bir tasarım hocası rolüne bürünerek öğrencileri yönlendirebilmesine işaret ederek "Akademik Yönlendirme", "Kritik Verme" ve "Biçimsel Yönlendirme" kategorilerini içermektedir.

"YARATICILIK" teması YZ uygulamalarının öğrencilerin normalde kendi yaratıcılıklarıyla düşünebilecekleri, tasarlayabilecekleri biçimsel ve işlevsel olguların yelpazesini genişleterek daha zengin hale gelmesine olan katkılarına

etmektedir. Bu tema "Biçimsel isaret Yaratıcılık", "Seçenek Oluşturma", "İlham Verme", "İpucu Verme" ve "Tasarım Ufkunu Genisletme" kategorilerini içermektedir. "KOLAYLAŞTIRMA" teması uygulamalarının proje süreçlerinde kullanılmasının süreçlerde karşılaşılan tüm zorluklar üzerindeki kolaylaştırıcı, yardımcı olma işlevine işaret etmektedir.

Bu tema "Başlangıç Noktası Oluşturma", "Görselleştirme", "Genel Yardım", "Etkili Araștırma", "Pafta Düzeni "Bilgiye Ulaşma", "Tasarım Hocasına Destek", Tasarım Problemi Tespiti" ve "Öngörü" temalarını icermektedir. "GÖRSELLESTİRME" teması YZuygulamalarının görselleştirme becerilerine güzellestirme odaklanarak "Onarma", "Render Alma", "Estetik", "Genel Görselleştirme" kategorilerini içermektedir. "MOTİVASYON" teması YZ'nın öğrencileri tasarım yapma ve ders çalışma yönünde motive etmesine olan katkılarına odaklanmaktadır. Bu tema "Merak ve Ümit", "Stres Azaltma", "Cesaret Verme", "Teşvik Etme" ve "Arkadaşlık" kategorilerinden oluşmaktadır.

YZ uygulamalarının öğrenciler ve proje çıktıları üzerindeki olumsuz etkilerine yönelik veriler ise temelde 3 tema içerisinde kümelendi. "PASİFİZE ETME" teması uygulamalarının da bilinçsiz asırı ya kullanımının öğrencilerin tasarım becerilerini geriletmesi ve öğrencileri tembelliğe itmesine odaklanmaktadır. Bu tema "Tembelleştirme", "Köreltme", "Engelleme" ve "Bağımlılık" oluşmaktadır. kategorilerinden "YETERSİZLİK" teması YZ uygulamalarının endüstrivel tasarım ürettiği çıktılarının disiplinin karakteriyle çeliştiği, yetersiz kaldığı ve sıkça hata yaptığı noktalara işaret etmektedir. Bu tema "Kitch Tasarımlar Üretme", "Üretim Yöntemlerine Uymama", "Yanlış Malzeme "Semantik Hata", "Ergonomik Seçimi", Hatalar", "İnsana Gereksinim" kategorilerini içermektedir. "DEMOTİVASYON" teması YZ uygulamalarının tasarım öğrencilerinin motivasyonları üzerindeki olumsuz etkilerine odaklanmaktadır. Bu tema "Güven Problemi", "Maliyet", "Hukuki Endişe", "Mesleki Endişe" "Yansıtmama" kategorilerinden oluşmaktadır.

4.3. Katılımcıların YZ Eğretilemelerine Yönelik Verdiği Bulgular

Einstein: Einstein'ın fizik tarihini değiştirerek dünya üzerinde büyük bir etkisi oldu. YZ da tıpkı Einstein gibi dünyayı dönüştürüyor.

Mariana Çukuru: Mariana Çukuru'nun sadece belli bir derinliğine kadar inebiliyoruz; henüz en dip noktasını keşfetmiş değiliz. Şu ana kadar binlerce canlı keşfedildi ama belki de hâlâ milyonlarca bilinmeyen tür var.

YZ da aynı şekilde; gelişmeye devam ettikçe, bize daha derin ve detaylı bilgiler sunacak. Şu an teknolojimiz Mariana Çukuru'nun dibine inmek için yeterli değil, tıpkı YZ'nında henüz tam potansiyeline ulaşmamış olması gibi. Ama ileride, onunla birlikte çok daha büyük keşifler yapabiliriz.

Tiyatrocu: Gerçeği tam yansıtmaması, rolden role girişi bana tiyatrocuları anımsatıyor.

Büyücü Küresi: Büyücüler aradıkları şeyleri çağırmak ve gizli bilgilere vakıf olmak için kürelerini kullanıyorlar.

Örümcek: Gizemli ve ürkütücü varlıklar oldukları için YZ örümceklere benziyor.

Yalnız İnsan: YZ yalnız yaşarken, kendi başına sürekli bir şeyler öğrenen ama ne yapacağı belli olmayan insana benziyor.

Otoban: Dünyayı sarmış, sayesinde her yere ulaşabildiğimiz otobana benziyor.

Ustabaşı: Fabrikadaki ustabaşılar işlerin başında durur, işçileri koordine eder, onlara işi öğretir ve işlerin daha kaliteli ve hızlı çıkmasını sağlar. YZ da insanları hem eğiterek hem de yönlendirerek insanların işlerini daha kısa zamanda ve daha kaliteli yapmasını sağladığı için fabrikadaki ustabaşına benziyor.

Taksi Şoförü: Arabayı çok iyi kullanabilen ve şehrin her yerini bildiği için istediğin yere seni hızlıca götürebilen bir taksi şoförüne benziyor.

Çita: Çita gideceği yere diğer hayvanlardan daha hızlı gider. YZ da diğer yöntemlerle yapılacak işi daha hızlı bir şekilde yapar.

Baykuş: Baykuş bilgeliği ve zamanı temsil eder. YZ da bilgiyi hızlı bir şekilde size sunar.

Alâeddin'in Sihirli Lambası: Kendisini kullandığınız zaman içinden çıkan cin dile benden ne dilersen diye sorar ve isteklerinizi hemen yerine getirir. YZ da kendisini kullandığınızda öğrenmek istediğiniz şeyleri size hemen öğretir.

Psikolog: Psikolog benim anlattıklarımı çözümleyerek bana geri anlatarak bana bilgi veriyor. Bu nedenle psikolog olabilir.

Kâşif Dora'nın Çantası: Kâşif Dora isimli çizgi filimde kahramanımızın sihirli bir çantası vardı. O an neye ihtiyacı varsa o çıkıyordu içinden. YZ da o anda neye ihtiyacımız varsa içinden o çıkıyor.

Sherlock Holmes: Hızlı ve analitik düşünebilen bir karakter olduğu için YZ'yı Sherlock Holmes'e benzetebilirim.

Cin Çağırma Tahtası: Cinleri çağırarak bilmediklerimizi sorduğumuz cin çağırma tahtasına (OİJUA) benziyor. Tehlikeli olabilir ve söyledikleri ne kadar doğru emin olamayız.

Peygamber: Etrafındaki insanların tıkanıklık yaşadıklarında ya da kararsız kaldıklarında ona danıstıkları bir insan.

Akıllı Buzdolabı: İçinde her malzemenin olduğu buzdolabına benziyor. Buzdolabı yiyecekleri ve malzemeleri taze tutar ve korur. İçindeki malzemeleri ya doğrudan kullanırız ya da onları kullanarak farklı yemekler yapabiliriz. YZ da içindeki bilgileri bozulmadan tutuyor.

İstediğimiz malzemeleri her an sunabiliyor. YZ öyle bir buzdolabı ki bize bilmediğimiz tarifleri de öğretiyor.

Eğitilmesi Gereken Zeki Köle: Tam olarak bizim değil ama yine de bizim emirlerimizi yerine getiren zeki bir köle. Bu köle ancak verdiğimiz referanslar kadar emirlerimizi yerine getirebiliyor. Ancak emirlerimizi daha iyi yerine getirebilmesi için iş yaptıracağımız alanda onu eğitmemiz gerekiyor.

Mantar: Olmadık yerlerde biten ve her ortamda kendisini yetiştirebilen mantarlar olabilir. Çünkü YZ da kendisini eğitebiliyor.

Antrenör: Başkalarından öğrendikleriyle bizi eğitirken bizden de bir şeyler öğrenerek onu da başkalarına öğreten bir antrenöre benziyor.

Güneş: Karanlık geceye doğduğunda ışığıyla aydınlatan, bize ilham veren güneşe benziyor.

Karmaşık Asansör: Sadece kendisini kullanmayı bilenleri yukarı taşıyabilen bir asansöre benziyor. Kullanmayı bilmiyorsanız yerinizde sayarsınız. Yanlış kullanırsanız sizi aşağıya da götürebilir.

Zeki ve Çalışkan bir Çırak: Zeki, çalışkan bir çırağa benziyor. Çok çalışkan olduğu için çok üretiyor, çok iş yapıyor. Ancak deneyimsiz olduğu için yaptığı işlerde sık hata da yapıyor. Onun bir usta tarafından eğitilmesi gerekiyor.

Bilim Kurgu Kitabı: Geçmişi ve geleceği gösterebilen, farklı dünyaları görmemizi sağlayan bir bilim kurgu kitabına benziyor.

5. SONUC VE DEĞERLENDİRMELER

YZuygulamalarını endüstriyel tasarım proje/stüdyo derslerine entegre ederek yaratıcılık ve özgünlük bağlamında öğrencilerin yaşadıkları tıkanıklıkları gidermeye yardımcı olabilecek yeni yaklaşımlara ulaşabilmeyi amaçlayan bu çalışmada YZ uygulamalarının hem olumlu hem de olumsuz taraflarıyla karşılaşıldı. Çalışmanın nihayete erdirileceği bu bölümde ilk olarak YZ uygulamalarının proje süreclerine edilmesi entegre sonrası gözlemlenen olumlu bulgular özetlenecek. İkinci olarak olumsuz tarafları paylaşılacak. Üçüncü olarak olumsuz taraflarını elemek için uvgulanan yöntemin sonuçları konulacaktır. Ardından araştırmaya katılan örneklem gurubuna yaptırılan YZ'ya yönelik eğretilemeler yorumlanacaktır. Sonuç kısmının bölümünde ise çalışmanın kısıtları belirtilecek ve literatüre nasıl katkı sağladığı belirtilerek çalışma sonlandırılacak.

5.1. YZ Uygulamalarının Proje/Stüdyo Dersine Uygulanması Sırasında Ve Sonrasında Gözlemlenen Olumlu Sonuçlar

- 1. YZ uygulamalarının proje geliştirme süreçlerine entegre edilmesinin öğrencilerin merak ve ümit duygularını harekete geçirerek çalışma motivasyonlarını arttırdığı gözlemlendi (A20, H23).
- 2. YZ'nın derslerde yaratıcılığı destekleyen biomimicry, retro tasarım, kurgusal tasarım v.b esinlenme kaynaklarına değerli bir seçenek eklediği değerlendirilmektedir. Kısa sürede çok sayıda alternatif üreterek zengin bir kaynak sağlayabildiği görülmüştür. Bu durumda yaratıcılığı geliştirerek öğrencilerin yaratıcılık noktasında yaşadıkları tıkanıklığı gidermeye vardımcı olmustur (C8, C15, D7, H6, J11). YZ tarafından üretilen zengin seçenek kümesini olusturan çıktılar genellikle öğrencilerin normalde düşünemeyecekleri ya da akıllarına gelecek unsurlar içerdiği için yaratıcılıklarına katkı sunmaktadır (A11, B5, D11, E2, E17, G7, K7).
- 3. Öğrenciler genellikle proje süreçlerinde araştırma aşamasından sonra kendi projelerini geliştirmeye nasıl başlayacakları noktasında sıkıntı yaşarlar. YZ uygulamalarının öğrencilere yorumlayabilecekleri, eleştirebilecekleri ve esinlenebilecekleri eşsiz bir başlangıç noktası sunduğu görülmektedir (B13, D1, E14, F5, H1, B13).
- 4. Bu çalışmada bilgisayar destekli tasarım programlarına istenilen düzeyde hâkim olmayan öğrencilerin bile YZ uygulamalarına hızla adapte olabildikleri gözlemlendi.
- 5, ChatGPT YZ uygulamasının proje süreçlerinin araştırma kısımlarında doğru bir şekilde kullanımının, konvansiyonel arama motorlarına kıyasla araştırmaları, daha kısa sürede ve daha derli toplu bir şeklide elde etmelerini sağladığı gözlemlendi.

Bu durumun öğrencilerin zaman yönetimine olumlu katkı sunduğu gözlemlendi (A1, B6, H2, J7, K3, A3, G2). YZ uygulamalarının öğrencilerin isabetli kararlarını daha erken almalarını ve yanlış kararlarından daha erken dönmelerini sağlayarak zaman yönetimine katkı sunduğu gözlemlendi (E12). YZ'nın araştırma süreçlerinde bilgiyi amaca yönelik ayrıştırabildiği, sadece yararlanılabilecek

kısımlarını derleyerek ve düzenleyerek verebildiği, öğrencilerin bilgi kirliliği içinde kaybolmasını engellediği gözlemlendi (A10, E1, E13, F1, K8). Bu durumun öğrencilerin araştırmalarını sadece daha kısa zamanda yapmalarını sağlamakla kalmayıp araştırmayı çok daha etkili ve yaralı bir şekilde kurgulanmasını sağladığı değerlendirilmektedir.

- 6. Endüstriyel tasarım disiplininin önemli süreçlerinden birisi olan müstakbel rakip ürünlerdeki tasarım problemlerinin tespiti YZ olmaksızın büyük ölçüde öğrencinin o ürünü kullanma firsatı yakalamasına ve gözlem gücüne bağlıydı. Ancak YZ'nın internet ağlarını tarayarak ürünlerin kullanıcı yorumlarına erişerek onları derleyebildiği için problem tespitini kolaylaştırdığı değerlendirilmektedir (H3, J10, K2).
- 7. Tasarım öğrencilerinin proje yürütücülerine ulaşamadıkları durumlarda öğrencileri akademik ve biçimsel olarak yönlendirebildiği, araştırmalarını kurgulayabildiği ve bir tasarım hocası gibi proje kritiği verebildiğine yönelik elde edildi. Bu durumun veriler uygulamalarının bir tasarım hocası rolünü üstlenerek hocanın üstündeki yükü hafiflettiği değerlendirilmektedir (D2, H13, J5, H21, G1, G4, H5, B14, C16, D15). YZ'nın öğrencilerin projeleriyle baş başa kaldıkları durumlarda yalnızlık duygusunu azalttığı, onlara bir ekip arkadaşı olduğu hissi verdiği, stresini azalttığı ve öğrencileri cesaretlendirdiği gözlemlendi (D9, D8, C5, B9, B8, E15, F1, G4, H7, G11).
- 8. YZ uygulamalarının ürün tasarımı yapmanın dışında öğrencilerin bizzat tasarladıkları ürünleri de render programlarına göre daha etkili bir şekilde verilen promptlarla istenilen mekânlarda görselleştirerek, render alabildikleri gözlemlendi. Bu durumun öğrencilerin çalışma motivasyonlarına olumlu katkı sunduğu değerlendirilmektedir. (A15, F6, J6).
- 5.2. YZ Uygulamalarının Proje/Stüdyo Dersine Uygulanması Sırasında Ve Sonrasında Gözlemlenen Olumsuz Sonuçlar

 1. YZ uygulamalarından "ChatGPT", "Midjourney" ve "Image fx" ile yapılan erken denemelerde bu uygulamalara metin olarak proje brifinde belirtilen talepler doğrultusunda soru soruldu. Bu soru: "X firması (elektrikli

- mutfak aleti üretmeyen) eğer elektrikli mutfak aletlerinden Y ürününü üretmek için kendi tasarım felsefesi ve tasarım çizgilerini yansıtan bir ürün tasarlayacak olsaydı nasıl ürünler ortaya çıkardı?" Cevap olarak endüstriyel tasarım disiplininin karakteriyle uzlaşmayacak "kitch" ürünler ürettiği gözlemlendi (A15, B7, C11, E19, G9, G10, H10, H19, J16, K12).
- 2. YZ uygulamalarının tasarladığı ürünlerin ergonomik, antropometrik standartlara ve kullanılabilirliğe aykırı olabileceği gözlemlendi (A19, B11, D12, G8, J15, K9).
- 3. YZ uygulamalarının tasarladığı ürünlerde malzeme ve üretim yöntemleriyle çelişebilecek tasarımlar ortaya çıktığı da gözlemlendi (A16, H17, A17, B2, B12, C12, D13, H11, H16, H18, J17, K10).
- 4. YZ uygulamalarının görselleştirme açısından bazen ve bazı öğrencilere göre mükemmel çıktılar üretmesinin öğrencilerin bazı zamanlarda YZ'yı rakip olarak algılamalarına ve mesleki gelecekleri açısından endişe duymalarına neden olduğu da gözlemlendi (A8, A23, B15, C7, D16, C6, F7, G14, J18, K4).
- 5. Tasarım öğrencilerinin proje süreçlerinde YZ kullanımının tasarım hukuku, fikrî mülkiyet ve sınai haklar konusunda sorun çıkarmasına dair hukuki endişeler taşıdıklarına dair veriler elde edildi (A24, K14, G15, K13). YZ kullanımının hukuki sorun teşkil etmemesi için hangi sınırlar ve çerçeveler içerisinde kullanılması gerektiğine dair öğrencilerin kaygılı oldukları gözlemlendi.
- 6. YZ uygulamalarına fazla bağımlı kalmanın öğrenciler ekip ve gurup çalışmalarından uzaklaştırabileceği, öğrencileri aşırı bireyselleştirebileceği ve öğrenciler arasındaki iletişime zarar verebileceği endişesine dair veriler elde edildi.
- 7. YZ tarafından üretilen tasarım çıktılarının öğrencilerin bireysel tasarım üsluplarına uymadığı, kendi tarzlarını yansıtmadığı için motivasyon düşüşü ve tıkanıklık yaşadıklarına dair görüşlerle de karşılaşıldı (A4, A6, G5). Ancak bu durumun doğru promt girmemeyle alakalı olabileceği de değerlendirilmektedir.
- 8. YZ uygulamalarına ücretsiz erişimin çok sınırlı olmasının ve erişim ücretlerinin yüksek

olmasının öğrencileri ümitsizliğe sevk ederek onları olumsuz yönde etkilediği gözlemlendi (C17, E16).

- 9. YZ uygulamalarına fazla bağımlı kalmanın öğrencileri tembelliğe sürükleyebileceği, öğrencilerde ertelemeyi alışkanlık haline getirebileceği, yapacağı işleri son dakikaya bırakmalarına neden olabileceği gözlemlendi (C13, F2, F3, G3, H20, K15).
- 10. YZ kullanımının öğrencileri düşünce tembelliğine ittiği için yaratıcı melekelerine zarara verebileceği ve öğrencilerin tasarım ve araştırma becerilerini köreltebileceğine dair veriler elde edildi (A12, A13, C9, C14, E18, J12, A21).
- 11. Öğrenci psikolojisi açısından hazır ve kolay sonuçlara eğilimli olan öğrencilerin tasarım açısından olgunlaşmamış olduğu halde sırf iyi göründüğü için YZ uygulamalarının erken çıktılarını kendi emeklerini katmadan çabucak benimsemeye çalıştıkları da gözlemlendi. Bu durumun yaratıcılıklarını olumsuz etkileyebileceği değerlendirildi.

5.3. YZ Kullanımında Karşılaşılan Problemler ve Zorlukların Giderilmesi Amacıyla Kullanılan Yöntemin Değerlendirilmesi

YZ'nın proje süreçlerine entegre edilme denemelerinde karşılaşılan olumsuzlukları ve zorlukları aşabilmek için endüstriyel tasarım disiplininin yaratıcılığı teşvik eden yöntemleri olan soyutlama, yorumlama, kıyaslama, yeniden tasarlama gibi eylemler Cross ve Archer tarafından geliştirilen yaratıcı tasarım metodolojisiyle birlikte YZ çıktılarına uygulanılarak yeni ürünler tasarlandı Bunun nihayetinde ise aşağıdaki sonuçlara ulaşıldı.

- 1. YZ uygulamalarının tasarladığı ürün çıktılarında karşılaşılan kitch unsurlar soyutlanarak ürün tasarımlarından çıkarıldı. Ürünlerin biçim ve işlev uyumu böylece korunarak YZ uygulamalarından yararlanılmış oldu.
- 2. YZ ile elde edilen ürün tasarımlarındaki ergonomik ve antropometrik sıkıntılar doğru ölçeklendirme ve tasarım çizgisini koruma şartıyla yeniden çizilerek kullanılabilirlik standartları tekrar yakalandı.

- 3. YZ ile elde edilen ürün tasarımlarında üretim yöntemleriyle çelişen kısımlar bulunmaktaydı. Birleşme çizgisi olmadan oluşturulan ve plastik ile metal enjeksiyon kalıplarından çıkamayacak geometrilerdeki ürün parçaları yeniden montajlanarak birleştirilecek şekilde biçim dilleri muhafaza edilerek yeniden çizildi. Böylece YZ uygulamalarının ürettiği tasarımlar yeniden revize edilerek tasarlanırken üretim yöntemlerine uygun hale getirildi.
- 4. Yaratıcı endüstriyel tasarım süreçlerinin YZ çıktılarına uygulanması, öğrencilere tamamen YZ'ya yaslanmak ve ona güvenmek ya da ondan ürkmek yerine onu sadece yararlanılması gereken kullanışlı bir araç olduğunu da göstererek eğitim sürecine katkı sunmuştur.

5.4. YZ'ya Yönelik Yapılan Eğretilemelerin Yorumlanması

Bu bölümde katılımcıların YZ hakkındaki algıları ve düşünceleri kullandıkları mecaz ifadeler ve eğretilemeler üzerinden deşifre edilmeye çalışılacaktır.

Öğretmen rolü: Katılımcılardan gelen "Peygamber", "Antrenör" "Ustabaşı" ve benzetmeleri olarak YZ'nın öğretmen "Antrenör" algılandığını göstermektedir. YZ'nın baskalarından benzetmesi öğrendiklerini bize öğretmesine işaret ederken "Ustabaşı" benzetmesiyse YZ'nın bizi bir eğitirken taraftan diğer taraftan da yönlendirerek çabuk isleri ve kaliteli yapmamızı sağladığına işaret etmektedir.

Eğitime muhtaç ve hizmetle mükellef olması:

"Eğitilmesi Gereken Zeki Köle", "Zeki ve Çalışkan Çırak" benzetmeleri YZ'nın belirli görevleri daha iyi yapabilmesi için özel eğitime ihtiyacını gösterir. Bu benzetmeler YZ'nın insanlara hizmet ve itaatle mükellef olmalarına yönelik bir algıyı da vurgular. Çalışkan çırak ifadesi aynı zamanda henüz tam eğitilmemiş YZ uygulamalarının çok sayıda çıktı verebilmesine rağmen sık hata yapabilmesine de atıfta bulunuyor.

Kendisini eğitebilmesi: "Mantar" benzetmesi ekilmediği ve sulanmadığı halde kendiliğinden çıkarak büyümesine atıfta bulunarak YZ'nın kendisini eğitebilmesine işaret etmektedir. Ayrıca "yalnız yaşayan insan" benzetmesi de YZ'nın kendisini eğitebileceğine ve yetebileceğine yönelik algıyı gösteriyor.

Kullanıcıya göre şekillenmesi: "Psikolog" benzetmesi psikologların hastalarını dinleyerek onları çözümlemesi ve onların mizacına göre şekillenerek onları bilgilendirmesi üzerinden YZ'nın kullanıcılara göre şekillendiğine yönelik bir algıya isaret etmektedir. başka bir katılımcıdan gelen karmaşık asansör benzetmesi de YZ'nın kendisini kullanan kişinin idrak seviyesine göre şekillenerek yararlı ya da zararlı olabileceği algısına işaret etmektedir. Karmasık asansörün kendisini bilincli ve beceriklice kullanabilen yolcularını yukarı taşıdığı, kendisini kullanamayanları yerinde saydırdığı, yanlış kullananlarıysa aşağı indirdiği gibi YZ'yı bilinçli ve beceriklice kullananları yukarı taşıyabilmesine, kendisini kullanamayanlarla yanlış kullananları ya yerinde saydırmasına ya da yeteneklerini körelterek aşağı çekebilmesine dair algılara isaret etmektedir.

Kuşatma ve bağıntı rolü: Bir katılımcıdan gelen "otoban" benzetmesi YZ'nın dünyayı kuşatmasını vurgular. Otobanların dünyadaki tüm şehirleri bir birine bağlaması üzerinden YZ da bilgileri birbirine bağlar. Ayrıca otobanların tali yollardan daha hızlı ulaşım sağlaması da YZ'nın diğer araçlardan daha hızlı olmasına göndermede bulunuyor. Benzer şekilde "Taksi şoförü" benzetmesi de taksi şoförlerinin şehri iyi bildikleri için yolcuyu istediği yere hızlıca ulaştırması gibi YZ'nın kullanıcıları istedikleri bilgiye hızlıca ulaştırmalarına işaret etmektedir.

Analitik Düşünebilme: Bir kullanıcıdan gelen "Sherlock Holmes" benzetmesi bu kurgusal karakterin hızlı ve analitik bir şekilde düşünebilme becerisi üzerinden YZ'nın da benzer becerilere sahip olduğuna dair bir kanıyı ortaya koymaktadır.

Hız: Bir katılımcıdan gelen çita benzetmesi çitaların diğer canlılardan daha hızlı koşabilmelerine gönderme yaparak YZ'nın diğer araçlara göre çok daha hızlı çalışabilmesine işaret etmektedir.

Dünyayı değiştirme: Katılımcılardan gelen Hz. Muhammet, Einstein ve Newton benzetmeleri peygamberlerin ve önemli bilim insanlarının dünyayı değiştirme, etkileme, dönüştürmeleri üzerinden YZ'nın dünyayı değiştirme ve etkilemesine dair algılara sahip olduklarına işaret etmektedir.

Dilekleri yerine getirme: Bir katılımcıdan gelen Alâeddin'in Sihirli Lambasından çıkan cin benzetmesi YZ'nın insanların öğrenmeyi diledikleri bilgileri onlara sunarak dilekleri yerine getirmesine işaret etmektedir. Bu arada Alâeddin'in Sihirli Lambasından ancak 3 dilekte bulunulabilmesi de YZ maliyetine ve sınırlı kullanıma isaret edebilir.

Geçmişi, geleceği ve görünmeyeni gösterme: "Güneş", "büyücü küresi", "OİJUA cin çağırma tahtası" gibi metaforlar karanlıkta kalan, uzaklarda bulunan, normalde zor erişilebilecek bilgileri aydınlığa çıkararak aşikâr kılan bir özelliğine göndermede bulunmaktadır. Ayrıca büyücü küresiyle birlikte başka bir katılımcıdan gelen "bilim kurgu kitabı" metaforu geçmişi, geleceği ve farklı dünyaları göstermesi ve hayal dünyamızı ve yaratıcılığımızı tetiklemesiyle YZ'nın bu özelliklerine de isaret etmektedir.

Gizem, ürkütücülük ve şüphe: "Ağıyla birlikte örümcek" metaforu ve yukarıda bahsedilen "büyücü küresi" ile "OİJUA cin çağırma tahtası" YZ'nın gizemli ve ürkütücü taraflarını vurgulamaktadır. Bu arada cin çağırma tahtasının tehlikeli olabilmesi ve gelen cinin yalan söyleme olasılığı üzerinden YZ'nın tehlikeli ve şüpheli olma ihtimaline yönelik algıları ortaya konmaktadır. Tiyatrocu metaforu da tiyatrocuların gerçeği tam yansıtmaması üzerinden şüphe algısına gönderme yapmaktadır.

Sonsuz bilgiyi muhafaza edebilme: "Kâşif Dora'nın çantası" ve "Akıllı Buzdolabı" metaforları, YZ'nın ne zaman neye ihtiyacımız olsa onu bize sunabilmesinin yanı sıra ihtiyacımız olan sonsuz bilgiyi muhafaza edebilmesine işaret etmektedir.

Buzdolabının akıllı olması malzemeyi sadece sunmakla kalmayıp yemek tarifi yapabilmesine göndermede bulunarak YZ'nın bilgiyi nasıl kullanabileceğimizi öğretmesine işaret etmektedir.

5.5. Araştırmanın Kısıtları

Bu araştırmada da birçok çalışmada olduğu gibi bazı kısıtlar bulunmaktadır. Öncelikle bu çalışma sadece Selçuk Üniversitesi Endüstriyel Tasarım 3 dersi kapsamında yürütülmüş ve öğrencilere tasarım rehberliği sadece bu makalenin yazarı tarafından sunulmuştur. Diğer üniversitelerin endüstriyel tasarım bölümlerinin

de iştirakiyle yapılacak ve birçok tasarım hocasının kendine özgü deneyimleri ve becerileriyle katılacakları YZ ve yaratıcılık odaklı çalışmalarla daha zengin ve güvenilir sonuçlar ortaya çıkarılabilir. Ayrıca bu çalışmanın gerçekleştirildiği tarihte Midjourney YZ uygulaması ücretsiz olarak tek bir Google hesabına günde sadece üç çıktı alınmasına izin veriyordu. Bu durumda öğrenciler ek Google hesapları açarak ancak belli sürelerde ve sınırlı bir YZ uygulamasına erişebiliyordu. Bu da kısıtlı zamanda ancak sınırlı sayıda YZ tasarımlarına ulaşabilmeyi mümkün kıldı.

Ek finansman destekleriyle öğrencilere ve eğitimcilere sınırsız ve farklı YZ uygulamalarına ulaşmalarını sağlayabilecek konuyla ilgili çalışmalar da daha etkili ve güvenilir sonuçlara ulaşmayı mümkün kılabilir.

5.6. Araştırmanın Literatüre Katkıları

Bu çalışmadan daha önce YZ uygulamalarının tasarım disiplinlerine uvgulanmasına vönelik yapılmış İrem Elal & Hüseyin Özkal Özsoy'un ve de Radhakrishan'ının çalışmalarında YZ uygulamalarının öğrencilerin yaratıcılık, heyecan, merak ve çalışma motivasyonlarına etkisi incelenmişti [35-47]. Bu çalışma ise kendinden önceki çalışmalara ek olarak YZ uygulamalarıyla elde edilen endüstriyel ürün tasarımlarındaki handikaplara Nigel Cross ve Archer'ın önerdiği tasarım metodolojisi örnek alınarak yaklaşılmış ve YZ uygulamalarının eksik ve hatalı kısımlarının giderilmesine yönelik olumlu sonuçlar elde ederek literatüre önemli bir katkıda bulunmuştur.

Ayrıca araştırmacının kendi gözlem ve değerlendirmelerinin öğrencilerin görüşleriyle paralel bir şekilde değerlendirilmesi ve çapraz şekilde okunması bir taraftan araştırmacının gözlemlerini kontrol edebilmesine olanak sağlarken diğer taraftan da gözünden kaçan unsurları yakalamasını mümkün kılmıştır. Arastırmada kullanılan YZ'ya vönelik eğretileme çalışması tasarım öğrencilerinin YZ'yı algılama biçimlerine ve YZ ile ilgili düşüncelerine mecaz anlatımın gücünden yararlanarak önemli deşifreler sağlamıştır. Sonuc olarak YZ uygulamaları gelisen bilgisayar donanımları, biriken deneyimler ve insan tarafından eğitilmeye halen devam edilmesi suretiyle gelişimini hızını arttırarak sürdürmektedir. Yakın gelecekte bu çalışmanın konusu olan handikap ve olumsuz tarafları

giderilebilir. Bu nedenle YZ'ya hem tasarım eğitimcilerinin hem de öğrencilerinin hazır olması gerektiği değerlendirilmektedir.

KAYNAKLAR

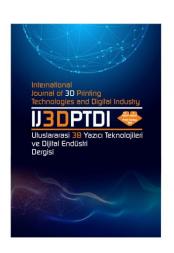
- 1. Rich, E., "Artifical Intelligence". McGraw-Hill Press. Newyork, 1983.
- 2. McCarthy J. Minsky M.L., Rochester N., Shannon C.E., "A Proposal fort the Dartmouth Summer Research Project on Artificial Intelligence, Dartmouth College in Hanover, New Hampshire, 1955.
- 3. Liu, V., Qiao, H., Chilton, L., "Opal: Multimodal Image Generation for New Illustration". UIST '22: Proceedings of the 35th Annual ACM Symposium on User Interface Software and Technology, 73, Pages 1-17, Oregon, 2022.
- 4. Polya, G., "How to solve it", Doubleday Anchor Books, Newyork, 1957.
- 5. Lawson, B., Dorst, K., "Design expertise", Architectural Press, London, 2009.
- 6. Curry, T., "A Theoretical Basis for Recommending the Use of Design Methodologies as Teaching Strategies in the Design Studio", Design Studies, Vol. 35, Issue 6, Pages 632-646, 2014.
- 7. Kaleli, M. C., "Tasarım Eğitiminde Proje Yürütücülerinin Davranışlarının Stüdyo Kültüründe Öğrencilerin Çalışma Motivasyonlarına ve Yaratıcılıklarına Etkisi Üzerine Bir Araştırma", Doktora Tezi, Mimar Sinan Güzel Sanatlar Üniversitesi, Fen Bilimleri Enstitüsü, İstanbul, 2019.
- 8. Archer, L. B., "Systematic Method for Designers", The Design Council, London, 1965.
- 9. Simon, H. A., "The Sciences of the Artificial", (First Edition), MIT Press, Cambridge, 1969.
- 10. Heskett, J., "Design: A very short introduction", Oxford University Press, Oxford, 2005.
- 11. Howard, T. J., Culley, S. J., and Dekoninck, E., "Describing the creative design process by integration of engineering design and cognitive psychology literature", Design Studies, Vol 29, Issue 2, Pages 160-180, 2008.
- 12. Gülen, E., "Gaining Pre-Project Competence in Industrial Design Undergraduate Programme: A Review on the Example of MSGSU", Phd Thesis, Mimar Sinan Fine Arts University, Institute of Science and Technology, İstanbul, 2019.

- 13. Amabile, T. M., "Motivating Creativity in Organizations: On Doing What You Love and Loving What You Do", California Management Review, Vol. 40, Issue 1, Pages 39-58, 1997.
- 14. Cross, N., "Descriptive models of creative design: application to an example", Design Studies, Vol. 18, Issue 4, Pages 427-440, 1997.
- 15. Alacı E. T., "The Effect of Visual Data Scanning on Pinterest on Creative Thinking in Conceptual Design Process: A Review on Experienced and Inexperienced Designers", Master's Thesis, İstanbul Technical University, Institute of Science and Technology, İstanbul, 2019.
- 16. Bar, M., "The Proactive Brain: Using Analogies and Associations to Generate Predictions", Trends in Cognitive Sciences, Vol. 11, Issue 7, Pages 280-289, 2007.
- 17. "Türk Dil Kurumu Sözlükleri", www.tdk.gov.tr, Temmuz 1, 2025.
- 18. Burke, K., "A Grammar of Motives and A Rhetoric of Motives", University of California Press, 1945
- 19. Benyus, J. M., "Biomimicry: Innovation Inspired by Nature", Harper Collins Books, Newyork, 1997.
- 20. "Filcowa pufa / Felt pouf", https://mieszkacpieknie.blogspot.com/2014/02/filcowa-pufa-felt-pouf.html, Temmuz 1, 2025.
- 21. "Mercedes Benz Bionic Car", https://en.wikipedia.org/wiki/Mercedes-Benz Bionic, Temmuz 1, 2025.
- 22. "ekoIQ yeşil iş yeşil yaşam", https://www.ekoiq.com/termit-yalicapkini-vedigerleri-biyomimikri/, Temmuz 1, 2025.
- 23. "Monografias", https://www.monografias.com/trabajos-pdf5/biomimetica-tecnologia-partir-naturaleza/biomimetica-tecnologia-partir-naturaleza Temmuz 1, 2025.
- 24. Mathewson, A., "New Analogue-Design In The Post Digital Age", Master Thesis, International Hellenic University, Thessaloniki, 2020.
- 25. "schultze works design studio", https://www.schultzeworks.com/, Temmuz 1, 2025.
- 26. Bayrakçı, O., "Çağdaş İletişim Kuramları Açısından Tasarımda İletişimsel Modeller", Mimar Sinan Üniversitesi Yayınları, İstanbul, 2004.

- 27. "Marc Newson", https://marc-newson.com/kelvin40, Temmuz 1, 2025.
- 28. "SURUGA-YA During MEGA SALE", https://www.suruga-ya.com/en/product/508692433, Temmuz 1, 2025.
- 29. "Vintage Disney Mickey Mouse Telephone AT&T Design line Phone 1990's", https://www.ebay.com/itm/167348235453?chn=ps &mkevt=1&mkcid=28&google_free_listing_action =view item, Temmuz 1, 2025.
- 30. Hançerlioğlu, O., "Felsefe ansiklopedisi kavramlar ve akımlar", Remzi Kitapevi, 1993.
- 31. Nezor, S., "Mimarlık eğitimi ve soyutlama", Master Thesis, Karadeniz Technical University, Trabzon, 2011.
- 32. Hegel, G. W. F., "Estetik-Güzel Sanatlar Üzerine Dersler Cilt 1", Çeviri Editörleri: Hünler, H., Altuğ, T., Payel Yayınları, İstanbul, 2012.
- 33. Sezer, N., "The Effects of Technological Developments on the Artist and Artwork in the Design and Production Phase", International Art Symposium, Page 485-498, Muğla, 2015.
- 34. Chaillou, S., "AI + Architecture: Towards a New Approach", Master Thesis, Harvard University, Graduate School of Design, Cambridge, 2019.
- 35. Radhakrishnan, M., "Is MidJourney-Ai the New Anti-Hero of Architectural Imagery & Creativity?", Global Scientific Journals, Vol. 11, Issue 1, Pages 94-104, 2023.
- 36. Panicker, S., "AI-Inflected Art/Architecture: Who (or rather, what) is the artist/architect?" Blueprint September, Vol. 3, Issue 2, Pages 15–36.
- 37. Ergün A., "Effects of Artificial Intelligence on Art", Master Thesis, Istanbul Arel University, Institute of Social Sciences, Graphic Design, İstanbul, 2019.
- 38. Jeon, Y., Shih, P. & Han, K., "Fashion Q: An Al-Driven Creativity Support Tool for Facilitating Ideation in Fashion Design", Proceedings of the 2021 CHI Conference on Human Factors in Computing Systems, Pages 1-26, Yokohama, 2021.
- 39. Armağan Y., "Artificial Intelligence in Furniture Design: An Evaluation on Design and R&D Centers", Master Thesis, Hacettepe University Institute of Fine Arts Department of Interior Architecture and Environmental Design, Ankara, 2019.

- 40. Soddu, C., "Generative Design: A swimmer in a natural sea frame", Generative Art International Conference, Milan, 2006.
- 41. McKnight, M., "Generative Design: What it is? How is it being used? Why it's a game changer", KnE Engineering, Vol. 2, Issue 2, Pages 176–181, 2017.
- 42. Yıldırım, A., Şimşek, H., "Sosyal Bilimlerde Nitel Araştırma Yöntemleri", Seçkin Yayın Evi, Ankara, 2016.
- 43. Lincoln, Y. S., Guba, E. G., "Naturalistic Inquiry", Sage Publications, London, 1985.
- 44. Merriam, S., B., "Nitel Araştırma, Desen ve Uygulama için Bir Rehber", Çeviri Editörü: Selahattin Turan, Nobel Kitap, Ankara, 2013.

- 45. Robson, C., "Real World Research", Wiley Publications, New Jersey, 2011.
- 46. Strauss, A., Corbin, J., "Basics of qualitative research", Sage Publications, Newbury, 1990.
- 47. Elal, İ., and Özsoy, H. Ö., "Investigating The Effects of Using Artificial Intelligence in The Conceptual Design Phase of The Industrial Design Process", Gazi University Journal of Science Part B: Art Humanities Design and Planning, Vol. 12, Issue 2, Pages 255-276, 2024.



ULUSLARARASI 3B YAZICI TEKNOLOJİLERİ VE DİJİTAL ENDÜSTRİ DERGİSİ

INTERNATIONAL JOURNAL OF 3D PRINTING TECHNOLOGIES AND DIGITAL INDUSTRY

ISSN:2602-3350 (Online)

URL: https://dergipark.org.tr/ij3dptdi

WIND TURBINE POWER PREDICTION USING MACHINE LEARNING MODELS: A CASE STUDY WITH REAL FARM DATA

Yazarlar (Authors): Abdullah Fatih Hocu¹, Gul Fatma Turker¹

Bu makaleye şu şekilde atıfta bulunabilirsiniz (To cite to this article): Hocu A.F., Turker G. F., "Wind Turbine Power Prediction Using Machine Learning Models: A Case Study with Real Farm Data" Int. J. of 3D Printing Tech. Dig. Ind., 9(2): 395-404, (2025).

DOI: 10.46519/ij3dptdi.1629937

Araştırma Makale/ Research Article

WIND TURBINE POWER PREDICTION USING MACHINE LEARNING MODELS: A CASE STUDY WITH REAL FARM DATA

Abdullah Fatih Hocu^a, Gul Fatma Turker^a

^aSuleyman Demirel University, Engineering and Natural Science Faculty, Computer Engineering Department, TURKEY

* Corresponding Author: <u>gulturker@sdu.edu.tr</u>

(Received: 30.01.25; Revised: 14.04.25; Accepted: 29.07.25)

ABSTRACT

The power generated from wind turbines is of critical importance as one of the fundamental components of sustainable and renewable energy systems. However, the complex and nonlinear nature of wind flow and the influence of interconnected factors make turbine power estimation significantly difficult. This study aims to evaluate the performance of different forecasting models using real-time data obtained from wind turbines and to determine the most effective model for wind power generation. The analyses are performed based on performance metrics that measure the agreement between the predicted and actual values. The study results reveal that the Decision Tree Regressor model provides the highest accuracy with 0.998 R² value and low error rates (RMSE: 0.151, MAE: 0.036) and that tree-based models are more effective in wind power estimation. These models, trained using large datasets, offer significant potential in terms of increasing power grid stability and ensuring the optimization of wind farms. The study shows that advanced methods used in turbine power estimation are an effective tool for optimizing renewable energy use by contributing to sustainable energy targets.

Keywords: Artificial Intelligence, Bigdata, Prediction, Renewable Energy, Sustainability

1. INTRODUCTION

Renewable energy has become a cornerstone of global efforts to combat climate change and reduce dependence on fossil fuels. Among these energy sources, wind energy has attracted attention due to its scalability and potential to generate significant amounts of energy without carbon emissions [1]. However, the inherent characteristics of wind, such as variability and discontinuity, make it difficult to accurately predict energy outputs, which creates critical challenges for integration into energy grids and system stability [2].

To address these challenges, various forecasting methods have been developed over the years. Traditional methods have been based on physical models and statistical analyses. For example, methods such as Autoregressive Integrated Moving Average (ARIMA) and Kalman filtering have tried to predict wind power based on historical data [3]. Numerical Weather Prediction (NWP) based physical models have improved forecast accuracy by

simulating the effects of meteorological conditions [2]. Nonetheless, these conventional models fall short in capturing the complex and nonlinear behavior of wind dynamics [4].

In light of these limitations, recent years have witnessed a shift towards more data-driven approaches. The advent of Machine Learning (ML) and Deep Learning (DL) has ushered in a new era in wind power forecasting. Deep learning algorithms such as Convolutional Neural Network (CNN) and Long Short-Term Memory (LSTM) have shown superior performance in capturing temporal and spatial dependencies in wind turbine data [5]. Hybrid approaches have improved prediction accuracy, especially with techniques such as the combination of Discrete Wavelet Transform (DWT) and LSTM [6]. Recently, meta-heuristic methods such as Sparrow Search Algorithm (SSA) have been used in wind power forecasts and have significantly improved the forecast accuracy [7]. In addition, hybrid ARIMA-LSTM models have shown high performance

by capturing short- and long-term dependencies [8].

Despite these advancements, some challenges remain. The limited availability of high-quality data and the difficulty of generalizing models across different geographical regions limit the applicability of wind power forecasts [9]. Furthermore, errors in the accuracy of NWP models lead to performance degradation in short-term forecasts [10]. To mitigate these issues, hybrid strategies combining learningbased models with optimization techniques have been proposed. For example, performance improvement has been achieved by combining Teaching Learning Based Optimization (TLBO) algorithms with deep learning models [2]. addition. Variational Decomposition (VMD) and Gated Recurrent Unit (GRU) based models offer higher accuracy, especially in short-term forecasts [11].

Another important approach to improving forecasting performance is the effective use of turbine-level data. The utilization of turbine-level data is critical in improving forecast accuracy. These approaches have been improved by the development of hierarchical models that effectively utilize turbine-level information [12]. For example, new methods utilizing turbine-level information have led to improvements in probabilistic wind power forecasts [6,13].

In summary, while substantial progress has been made in the field of wind power forecasting, several persistent challenges remain to be addressed. Achieving high forecasting accuracy is essential not only for ensuring grid stability but also for the efficient integration of renewable energy into the power system. However, limitations such as the low quality and availability of data, regional and climatic variability, and the inherent constraints of traditional prediction models continue to hinder progress in this domain. The literature highlights that overcoming these challenges requires the development of more robust. adaptive and generalizable, approaches. Therefore, there is a pressing need for novel methods that can enhance model performance, accommodate diverse operating environments, and contribute to the reliable use of wind energy in sustainable power systems. In this study, the

performance of various machine learning algorithms are compared using real-time data at the turbine level and an effective prediction model is developed. In the second section, information about the comprehensive dataset is given, and the details of the machine learning algorithms applied after pre-processing steps, with evaluation parameters, presented. In the third section, experimental results are presented and the models are compared. In the results section, the accuracy of the developed forecasting model and its contribution to power grid stability are discussed. In addition, the limitations of the study are evaluated and suggestions for future studies are presented.

2. MATERIAL AND METHODS

2.1. Data Source

In this study, real-time data were obtained from a wind farm located in the Denizli region of Turkey, where the energy production values of three turbines, each with three blades and a capacity of 3.4 MW (3400 kWp), were monitored for one year. The site has an elevation of 1618 meters and a hub height of 79.5 m. The dataset, comprising 526,221 rows and 22 columns, was collected between January 1 and December 31, 2024, with minute-level sampling recorded daily from an actual wind turbine in the region. These data enables the estimation of wind energy production over time. These dataset columns contain various measurements that track in detail the performance and operating parameters of a wind turbine. Parameters such as time data, device identifier, active power, wind speed, nacelle orientation, operating status, current and voltage values, frequency, reactive power, fault codes, rotor and generator rotational speeds, ambient temperature, hydraulic system pressure and total amount of energy supplied to the grid are used to monitor the instantaneous and performance. cumulative characteristics and operating conditions of the turbine.

The dataset used in this study was obtained in real-time from an industrial-scale wind turbine site. It encompasses electrical, mechanical, and environmental variables measured under actual operational conditions. This enhances both the practical relevance of the study and its contribution to sustainable energy systems. Table 1 provides detailed descriptions of the

dataset variables, including operational, environmental, and electrical parameters collected from wind turbines.

Table 1. Description of the wind turbine dataset variables

variables.			
Data Column	Description		
	Timestamp of the		
time	record (UTC)		
	Unique identifier		
	assigned to each wind		
device id	turbine		
	Active power output of		
active_power	the turbine (kW)		
active_power	Wind speed at the		
wind_speed	turbine location (m/s)		
wilia_speed	Nacelle (turbine head)		
1:4:			
yaw_direction	direction (degrees)		
	Operational		
	status/state of the		
wt_operationstate	turbine		
	Phase V current value		
current_v	(Amps)		
	Phase U current value		
current_u	(Amps)		
	Phase W current value		
current_w	(Amps)		
_	Phase V voltage value		
voltage_v	(Volts)		
8 =	Phase U voltage value		
voltage_u	(Volts)		
	Phase W voltage value		
voltage_w	(Volts)		
voitage_w	Frequency of the		
	generated electricity		
frequency	(Hz)		
requericy	Reactive power output		
ranativa namar	of the turbine (VAR)		
reactive_power			
	Error codes, if any,		
1	detected during		
error_code	operation		
	Rotor rotational speed		
	(Revolutions Per		
rotor_rpm	Minute)		
	Generator rotational		
generator_rpm	speed (RPM)		
	Ambient temperature		
ambie_tmp	near the turbine (°C)		
	Hydraulic system		
hyd_press	pressure		
. _	Total energy exported		
active energy export	to the electrical grid		
_ 6/_ 1	Active energy		
	difference between		
	consecutive		
eac	measurements		
	incubal citionity		

The dataset used in the prediction algorithm includes electrical, mechanical, and

environmental variables collected at the turbine level. Among these, electrical parameters-particularly current and voltage-played a decisive role in prediction performance, significantly enhancing model accuracy by providing strong predictive power.

2.2. Data Preprocessing

The performance and accuracy of wind turbine forecasting models can be significantly affected by missing or inaccurate data in the dataset. Such errors are usually caused by missing values, inconsistent data entries or irregularities in the dataset. In this study, a comprehensive data preprocessing process was implemented to improve the quality of the dataset and ensure the reliability of the prediction models.

Firstly, K-Nearest Neighbours (KNN), Linear Interpolation and Mode Interpolation methods were used to fill the missing data. These methods provided a statistically consistent filling of missing values. In addition, redundant and repetitive columns (redundant features) in the dataset were identified and removed. In order to create a data structure suitable for time series analysis, new features derived from the 'time' column were created. These features include 'hour', 'day', 'month', 'year', 'day name'. These inferences allowed the model to learn temporal dynamics better.

In order to increase the generalization capability of the dataset and to prevent overfitting of the model, cross-validation method was applied. In addition, normalization was performed to eliminate the scale differences between the features and to increase the convergence speed of the model. These steps made the dataset suitable for machine learning models. In addition, statistical analyses were performed on input features and power. This process contributed to eliminating inconsistencies in the dataset and increasing model accuracy.

Feature Engineering: Feature extraction is the process of creating numerical features from raw data that can be used in machine learning models. The number of input features can be very large and many of them may have low correlation with the target variables. Feature selection methods are a critical step to improve model performance, reduce training time and improve the interpretability of models [14].

In this study, new features are derived to better model wind turbine performance and improve prediction accuracy. These features include energy exchange ratio (active energy / reactive energy), rotor and generator speed ratio, current unbalance (standard deviation of currents), voltage unbalance (standard deviation of voltages) and power efficiency (active power / wind speed). These derived characteristics better reflect the dynamic behavior of the system, strengthening the predictive capability of the model and enabling a more effective analysis of critical parameters related to power generation.

2.3. Machine Learning

Within the scope of machine learning, various regression-based machine learning models are applied in this study for the prediction of wind turbine data. These models aim to estimate the dependent variable based on independent features using learning algorithms [15]. In the study, nine machine learning models were trained according to the characteristics of the dataset and the results were analyzed. The data were divided into 80% for training the model and 20% for testing.

Among the models, Decision Tree Regressor, based on decision trees, stands out with its capacity to make fast and effective predictions by branching the data [14]. XGBoost Regressor, a more advanced algorithm, provides high accuracy and performance by using the gradient boosting method [16]. Similarly, Gradient Boosting Regressor aims to reduce the error by successively optimizing a set of weak predictors.

Furthermore, the Extra Tree Regressor model offers greater generalization capacity by using randomized decision tree principles [14,17]. K-Neighbors Regressor offers a simple and efficient approach, basing predictions on the values of the KNN. Linear Regression, a more basic model, makes predictions assuming a linear relationship between the target and independent variables. However, this model may have limitations on non-linear datasets. In addition, more sophisticated models such as Ridge, Elastic Net and Lasso try to avoid overfitting by using regularization techniques [18-20]. This process has enabled the identification of the most suitable algorithms for wind turbine forecasting models.

2.4. Performance Metrics of the Model

Error metrics used to evaluate the performance of machine learning algorithms play a critical role in measuring how well the model fits with real values and its generalization capability. These metrics help to evaluate the effectiveness and reliability of the model by determining its predictive accuracy and predictive power.

Mean Absolute Error (MAE) is a metric used to determine how close the predictions are to the true values and evaluates the average error of the predictions. This metric is calculated by Eq. 1 [21].

$$MAE = \sqrt{\frac{1}{n} \sum_{j=1}^{n} \left| Z_j - \hat{Z}_j \right|} \tag{1}$$

Root Mean Square Error (RMSE) measures the magnitude of deviations of the model's predictions from the true values; it indicates how well the predicted values agree with the true observations and is a metric reflecting the error rate. To compare the prediction accuracy of different models, RMSE is calculated by Eq. 2 [21-22].

RMSE
$$\sqrt{\frac{1}{n}\sum_{j=1}^{n}(Z_j - \hat{Z}_j)^2}$$
 (2)

R-squared (R^2) is a measure of how well a model fits the data; high values indicate the explanatory power of the model. Eq. 3 [23].

$$R^{2}=1-\frac{\sum_{j=1}^{n}(Z_{j}-\hat{Z}_{j})^{2}}{\sum_{j=1}^{n}(Z_{j}-\hat{Z}_{j})}$$
(3)

Mean Squared Error (MSE) is a widely used evaluation metric that quantifies the average of the squared differences between predicted and actual values. It provides a measure of how close the regression model's predictions are to the true outcomes. The MSE is calculated by Eq. 4.

$$MSE = \frac{1}{m} \sum_{j=1}^{m} \left(Z_j - \hat{Z}_j \right)^2 \tag{4}$$

3. EXPERIMENTAL FINDINGS

In this study, the power generation performance and operating dynamics of the wind turbines are analyzed in detail using annual real-time data obtained from the wind farm. The analyses of the monthly energy production values reveal that the turbines provide a high stability in energy production throughout the year, and these findings are presented in detail in Figure 1. From January to December, the total energy production ranged between 2.5x10¹² kWh and 3.0x10¹² kWh, with a slight increase in production in the last quarter of the year (October, November, December). This increase can be attributed to the increase in wind speeds during this period of the year. However, the generation remained relatively constant during

the summer months (June, July, August), indicating that the system operates continuously and efficiently despite the seasonal variations in wind speed. The results show that wind turbines provide a reliable contribution to the energy needs in the region.

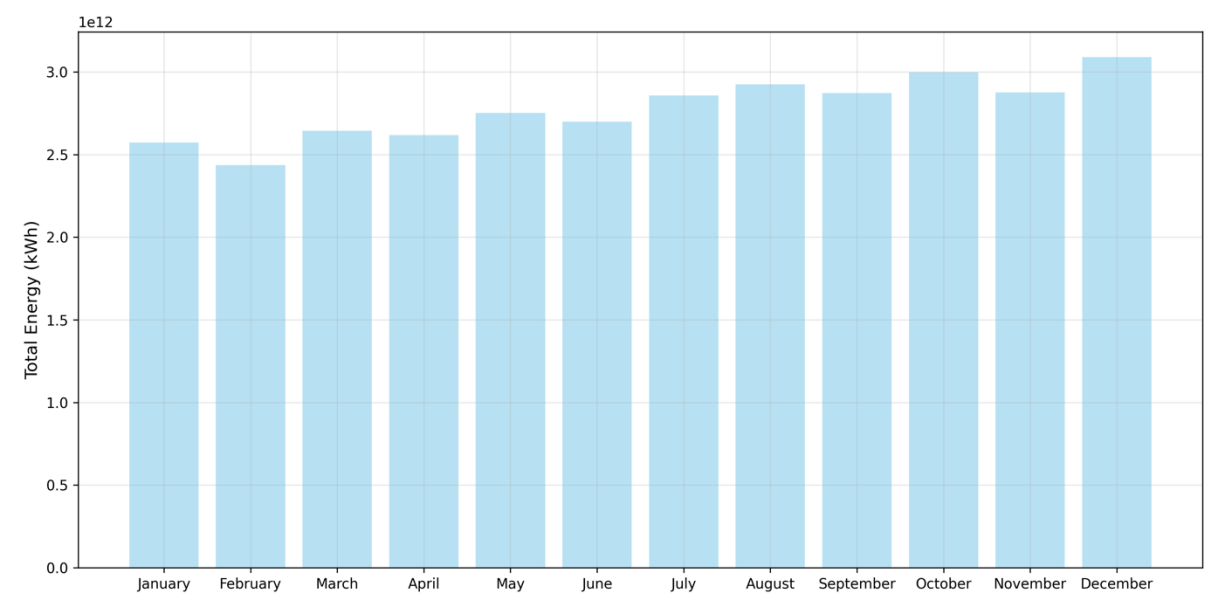


Figure 1. Total montly energy production.

Figure 2 illustrates the importance of various input features in predicting active power output, based on the linear regression coefficients. The results clearly underscore the dominant role of electrical current variables in the model's predictive performance. Among all variables, three-phase current values (current w, current v, current u) exhibited the highest regression coefficients. While current w and current v contributed positively, current u presented a strong negative coefficient, likely reflecting phase-specific imbalances in the system.

The differences between the phases are due to asymmetric loading and instantaneous power regulation in the system. In real wind turbine data, the contribution of each phase to the active power is not equal due to factors such as rotor position, wind direction and inverter operating characteristics. The higher effect observed especially in the W phase can be associated with the situations where this phase carries more current under load or that phase transmits more

energy at the inverter output. Such imbalances are commonly observed in field operations.

Voltage components (voltage v and voltage w) also had a moderate yet positive influence on the model output, indicating their supplementary role in power estimation. Conversely, mechanical indicators such as wind speed and rotor RPM, although theoretically significant and highly correlated with active power, showed relatively lower predictive power within the linear regression model. This suggests that for short-term forecasting, electrical signals provide more direct and immediate predictive value than mechanical inputs.

Environmental parameters such as ambient temperature and hydraulic pressure contributed minimally, offering only limited explanatory power related to operational efficiency. Similarly, frequency and reactive power had negligible influence, indicating their minor role in determining active power within this context.

Overall, the integration of highly impactful electrical variables, particularly current and voltage, substantially enhanced the model's prediction accuracy. These findings reinforce the superiority of electrical parameters over mechanical and environmental variables for short-term active power forecasting in wind energy systems.

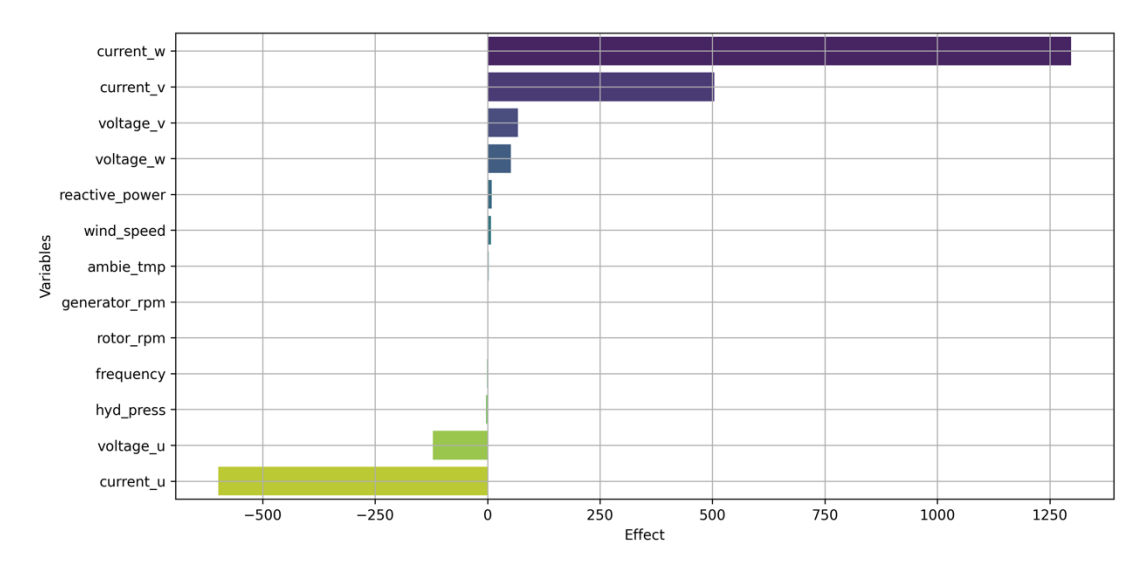


Figure 2. The impact of variables on active power based on linear regression coefficients.

The correlation matrix illustrates the interdependencies among various wind turbine parameters. A very strong positive correlation was observed between active power and current in phases U, V, and W (r = 1.0), indicating that electrical current directly determines active power generation. Additionally, rotor RPM and generator RPM also showed a strong correlation with active power (r = 0.83), underlining the importance of mechanical rotation in energy conversion. Interestingly, voltage values (U, V,

W) displayed weaker correlations with active power (ranging from 0.16 to 0.25), and frequency showed an even lower correlation (r = 0.042). These findings reinforce that mechanical dynamics such as rotor speed, along with electrical current, are the dominant factors in power production, whereas voltage and frequency play a comparatively limited role.

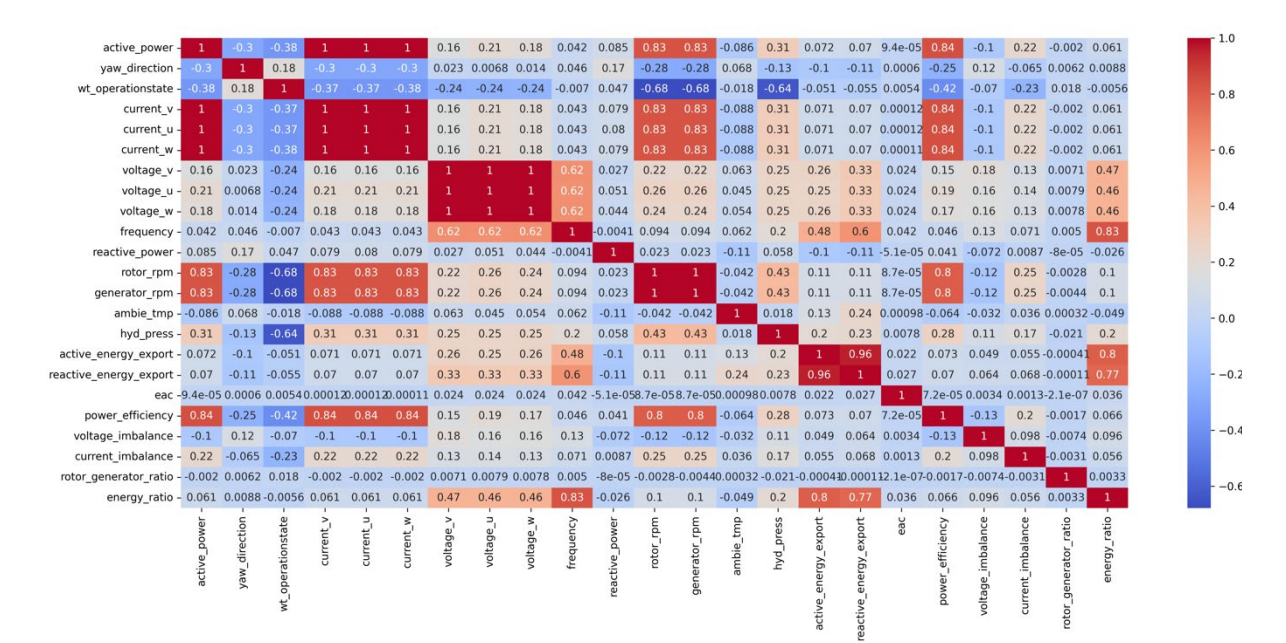


Figure 3. Wind farm parameter correlation matrix.

In this study, various machine learning models were applied to predict energy production using real-time farm data obtained from wind turbines and the performances of these models are comprehensively given in Table 2 with metrics such as accuracy (R²), error rates (RMSE, MAE).

It compares the performance of various machine learning algorithms in predicting wind turbine energy production. Decision Tree Regressor showed the highest performance with R² value of 0.998, RMSE 0.151 and MAE 0.036, and provided the most accurate predictions by providing a very good fit to the data. XGBoost Regressor and Extra Tree Regressor provided an accuracy close to Decision Tree with R² values of 0.995 and 0.989, respectively, and were among the reliable models with low error rates. Gradient Boosting Regressor provided an acceptable accuracy with R² value of 0.962, but was considered a less effective model due to higher RMSE and MAE values. K-Neighbors Regressor showed a moderate performance with R² value of 0.912. However, Linear Regression and Ridge models had low accuracy with R2 values of 0.806, and their high error rates showed that they could not capture the data complexity sufficiently. Elastic Net and Lasso models had the lowest accuracy with R2 values

of 0.734 and 0.729, and they exhibited poor performance with high error rates.

Table 2. Machine learning regression model results for wind power prediction.

for wind power prediction.			
ML Regression	R_Squared	RMSE	MAE
Algorithms			
DecisionTree	0.998	0.151	0.036
XGBoost	0.995	0.256	0.114
ExtraTree	0.989	0.390	0.086
GradientBoosting	0.962	0.740	0.433
Kneighbours	0.912	1.126	0.746
Linear	0.806	1.679	1.123
Ridge	0.806	1.679	1.123
ElasticNet	0.734	1.965	1.235
Lasso	0.729	1.983	1.235

Figure 4 compares the agreement between predicted and actual values of different machine learning models. The analysis revealed that tree-based models provide the highest accuracy in energy production estimation by better capturing complex data relationships. While these models provide effective and reliable results in wind energy estimation, it was observed that simple models cannot adequately represent the data complexity and therefore exhibit lower performance. This clearly shows that complex and optimized algorithms provide more reliable results in wind power estimation.

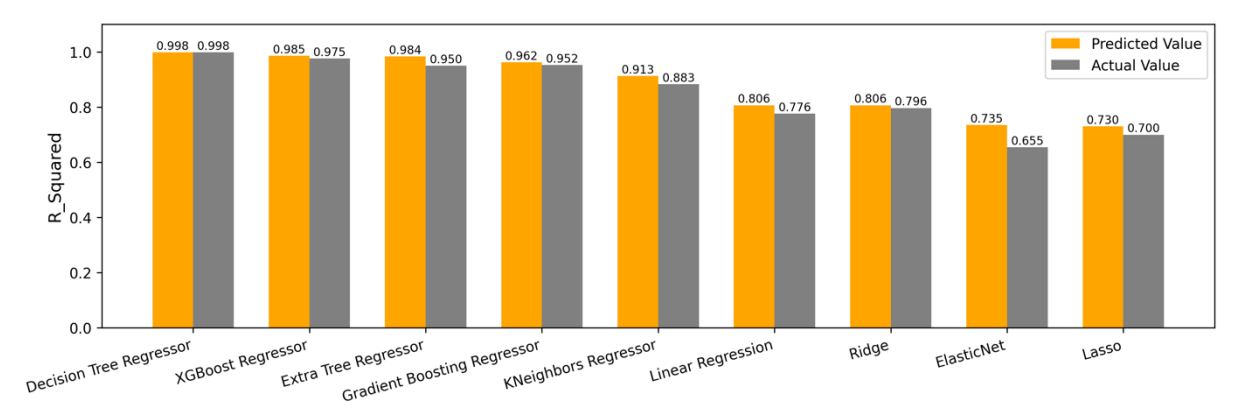


Figure 4. Predicted and actual values of the machine learning models of R² score.

The accuracy of the models developed within the scope of the study was tested not only on the turbine data used for training, but also on the data of a different turbine located in the same region. This validation process is critical to evaluate the generalization capacity of the models and to determine the consistency of performance on new data. The results revealed that the Decision Tree Regressor model provided a high fit ($R^2 = 0.998$) in both the training and validation phases. This finding proves that the model is not limited to a specific turbine, but can also make effective predictions with data obtained from different turbines in the same region.

This approach emphasizes model development process that ensures consistency within regional differences and increases the potential for the model to be used in real-world applications. It also demonstrates the critical importance of region-specific turbine data on forecast performance. In the future, performing similar validation processes on turbines in different regions can further strengthen the generalization capacity of the model and provide a solid foundation for wider applications. In this context, it is aimed to provide more reliable and sustainable solutions in renewable energy systems.

3.1. Discussion

This study evaluates the effectiveness of machine learning algorithms in wind power forecasting using real-time data from wind turbines. The analysis revealed that the Decision Tree Regressor model achieved superior performance with high accuracy (R² = 0.998), effectively modeling complex and nonlinear relationships. These findings are consistent with previous research, which

highlights the effectiveness of tree-based models in wind energy forecasting.

Traditional physical and statistical methods often fall short in modelling regional and meteorological variability. In contrast, machine learning and artificial intelligence-based approaches offer strong potential to address these challenges. Particularly, hybrid models and transfer learning techniques have shown notable improvements in forecast accuracy [24]. However, this study demonstrates that even with simple models and high-quality turbine-level data, competitive results can be achieved.

Some limitations should be considered. The dataset covers only a specific region and time frame, which may restrict the generalization of the findings to other geographic and climatic conditions. The quality and representativeness of turbine data significantly influence prediction accuracy. Therefore, the use of larger and more diverse datasets, along with adaptation strategies such as transfer learning, will be critical for enhancing the generalization capacity of forecasting models.

Future research could focus on the integration of hybrid model architectures and metaheuristic optimization techniques to improve robustness and scalability. Additionally, the explainable development of forecasting systems, such as transformer-based models enhanced with attention mechanisms, may enhance both the transparency and usability of prediction tools. Ultimately, such innovative approaches can support the reliable integration of renewable energy into power grids and contribute to the achievement of sustainable energy goals.

4. RESULTS

This study investigates the applicability of machine learning algorithms for wind power forecasting using real-time data from wind turbines. Among the tested models, the Decision Tree Regressor yielded the highest accuracy ($R^2 = 0.998$) and the lowest error metrics (RMSE: 0.151, MAE: 0.036), demonstrating its robustness in capturing complex data patterns. In contrast, linear models such as Linear Regression and Ridge showed limited performance, failing to adequately model the nonlinearities inherent in wind energy data. The findings highlight the suitability of tree-based models for wind power forecasting and their potential to enhance grid stability and support the sustainable integration of wind energy into power systems. By leveraging turbine-level data, machine learning approaches offer accurate and scalable solutions for modern energy management.

REFERENCES

- 1. Lu, H., Zhang, L., Tian, C., Niu, T., & Wei, W., "Volatility index prediction based on a hybrid deep learning system with multi-objective optimization and mode decomposition", Energy Conversion and Management, Vol. 323, Pages 119155, 2024.
- 2. Sulaiman, M. H., & Mustaffa, Z., "Enhancing wind power forecasting accuracy with hybrid deep learning and teaching-learning-based optimization", Cleaner Energy Systems, Vol. 9, Pages 100139, 2024
- 3. Tian, L., & Wei, Z., "Integration of VMD and neuro-fuzzy systems for wind speed analysis", Energy Conversion and Management, Vol. 323, Pages 119155, 2025.
- 4. Mehmood, Z., & Wang, Z., "Wind turbine energy forecasting using real wind farm's measurement data and performance of gene expression programming analytical model in comparison to traditional algorithms", International Journal of Green Energy, Vol. 22, Issue 2, Pages 414–431, 2025.
- 5. Bashir, T., Wang, H., Tahir, M. F., & Zhang, Y., "Short-term electricity load forecasting using hybrid prophet-LSTM model optimized by BPNN", Renewable Energy, Vol. 239, Pages 122055, 2025.
- 6. Gilbert, A., & Huang, L., "Hierarchical approaches for turbine-level wind power forecasting", Renewable Energy, Vol. 167, Pages 119155, 2020.

- 7. Shao, L., Huang, W., Liu, H., & Li, J., "Study of wind power prediction in ELM based on improved SSA", IEEJ Transactions on Electrical and Electronic Engineering, 2025.
- 8. AlShafeey, M., & Csaki, C., "Adaptive machine learning for forecasting in wind energy", Heliyon, Vol. 10, Pages e34807, 2024.
- 9. Ukoba, K., Odebiyi, A., & Oghenevwogaga, J., "Harnessing machine learning for sustainable futures: Advancements in renewable energy and climate change mitigation", Bulletin of the National Research Centre, Vol. 48, Pages 99, 2024.
- 10. Yang, M., Guo, Y., Huang, T., & Zhang, W., "Power prediction considering NWP wind speed error tolerability", Applied Energy, Vol. 377, Pages 124720, 2025.
- 11. Liu, Z., Guo, H., Zhang, Y., & Zuo, Z., "A comprehensive review of wind power prediction based on machine learning", Energies, Vol. 18, Issue 350, 2025.
- 12. Mokarram, M., et al., "Adaptability of forecasting models across geographies", Sustainable Energy Technologies and Assessments, Vol. 54, Pages 104070, 2025.
- 13. Chen, X., Han, B., Wang, X., Zhao, J., Yang, W., & Yang, Z., "Machine learning methods in weather and climate applications: A survey", Applied Energy, Vol. 13, Pages 12019, 2021.
- 14. Ahmad, M. W., Reynolds, J., & Rezgui, Y., "Predictive modelling for solar thermal energy systems: A comparison of support vector regression, random forest, extra trees and regression trees", Journal of Cleaner Production, Vol. 203, Pages 810-821, 2018.
- 15. Panda, S. K., & Mohanty, S. N., "Time series forecasting and modeling of food demand supply chain based on regressors analysis", IEEE Access, Vol. 11, Pages 42679-42700, 2023.
- 16. Velthoen, J., Dombry, C., Cai, J. J., & Engelke, S., "Gradient boosting for extreme quantile regression", Extremes, Vol. 26, Issue 4, Pages 639-667, 2023.
- 17. Geurts, P., Ernst, D., & Wehenkel, L., "Extremely randomized trees", Machine Learnig, Vol. 63, Pages 3-42, 2006.
- 18. He, H. J., Zhang, C., Bian, X., An, J., Wang, Y., Ou, X., & Kamruzzaman, M., "Improved prediction of vitamin C and reducing sugar content in sweetpotatoes using hyperspectral imaging and

- LARS-enhanced LASSO variable selection", Journal of Food Composition and Analysis, Vol. 132, Pages 106350, 2024.
- 19. Ranstam, J., & Cook, J. A., "LASSO regression", Journal of British Surgery, Vol. 105, Issue 10, Pages 1348-1348, 2018.
- 20. Diebold, F. X., & Shin, M., "Machine learning for regularized survey forecast combination: Partially-egalitarian lasso and its derivatives", International Journal of Forecasting, Vol. 35, Issue 4, Pages 1679-1691, 2019.
- 21. Nayak, J., Vakula, K., Dinesh, P., Naik, B., & Pelusi, D., "Intelligent food processing: Journey from artificial neural network to deep learning", Computer Science Review, Vol. 38, Pages 100297, 2020.

- 22. Khan, M. I. H., Sablani, S. S., Nayak, R., & Gu, Y., "Machine learning-based modeling in food processing applications: State of the art", Comprehensive Reviews in Food Science and Food Safety, Vol. 21, Issue 2, Pages 1409-1438, 2022.
- 23. Chicco, D., Warrens, M. J., & Jurman, G., "The coefficient of determination R-squared is more informative than SMAPE, MAE, MAPE, MSE and RMSE in regression analysis evaluation", PeerJ Computer Science, Vol. 7, Pages e623, 2021.
- 24. Abdel-Aty, A.-H., et al., "Boosting wind turbine performance with advanced smart power prediction", Alexandria Engineering Journal, Vol. 96, Pages 58–71, 2024.